NASA TECHNICAL MEMORANDUM

NASA TM X-64726

LARGE SPACE TELESCOPE PHASE A FINAL REPORT

Volume V – Support Systems Module

By Program Development

December 15, 1972

NASA

George C. Marshall Space Flight Center
Marshall Space Flight Center, Alabama

MSFC - Form 3190 (Rev June 1971)

DOCUMENT CONTENTS

TECHNICAL REPORT STANDARD TITLE PAGE

1. REPORT NO.	2. GOVERNMENT ACCESSION NO.	3. RECIPIENT'S CATALOG NO.
TM X- 64726		

4. TITLE AND SUBTITLE	5. REPORT DATE
Large Space Telescope Phase A Final Report Volume V — Support Systems Module	December 15, 1972 6. PERFORMING ORGANIZATION CODE
7. AUTHOR(S)	8. PERFORMING ORGANIZATION REPORT #
By Program Development	
9. PERFORMING ORGANIZATION NAME AND ADDRESS	10. WORK UNIT NO.
George C. Marshall Space Flight Center Marshall Space Flight Center, Alabama 35812	11. CONTRACT OR GRANT NO.
	13. TYPE OF REPORT & PERIOD COVERED
12. SPONSORING AGENCY NAME AND ADDRESS	Technical Memorandum
National Aeronautics and Space Administration Washington, D.C. 20546	14. SPONSORING AGENCY CODE

15. SUPPLEMENTARY NOTES

Prepared by Program Development

16. ABSTRACT

This document is a report of the Phase A study of the Large Space Telescope (LST). The study defines an LST concept based on the broad mission guidelines provided by the Office of Space Science (OSS), the scientific requirements developed by OSS with the scientific community, and an understanding of long range NASA planning current at the time the study was performed.

The LST is an unmanned astronomical observatory facility, consisting of an optical telescope assembly (OTA), scientific instrument package (SIP), and a support systems module (SSM). The report consists of five volumes: Volume I is an executive summary, Volume II is a summary of the entire report, and Volumes III, IV, and V contain the analyses and conceptual designs of the OTA, SIP, and SSM, respectively. The report describes the constraints and trade off analyses that were performed to arrive at a reference design for each system and for the overall LST configuration.

The LST will be launched into low earth orbit by the Space Shuttle and operated for 10 to 15 years. The Shuttle will also be used to maintain the LST and to update the scientific instrument complement. Several maintenance modes have been investigated, including on-orbit pressurization of the SSM to provide a shirtsleeve environment for maintenance, and earth return of the LST.

The LST will provide the scientific community with several fundamentally unique capabilities which will permit the acquisition of new and important observational data. Its location in space permits observations over the entire spectrum from about 100 nm to the far infrared.

A low cost design approach was followed in the Phase A study. This resulted in the use of standard spacecraft hardware, the provision for maintenance at the black box level, growth potential in systems designs, and the sharing of Shuttle maintenance flights with other payloads.

17. KEY WORDS	18. DISTRIBUTION STATEMENT
Large Space Telescope Scientific Satellite Astronomy Payload High Resolution Astronomy Faint Object Detection Conceptual Satellite Design Shuttle Maintenance Spacecraft	STAR Announcement Erich E. Goerner, Director Preliminary Design Office

19. SECURITY CLASSIF. (of this report)	20. SECURITY CLASSIF. (of this page)	21. NO. OF PAGES	22. PRICE
Unclassified	Unclassified	696	NTIS

LIST OF ACRONYMS

A/D	analog to digital
ACN	Ascension Island (tracking station)
ACS	attitude control system
AFO	Announcement for Flight Opportunity
AGC	automatic gain control
AGO	Santiago, Chili (tracking station)
ALU	arithmetic logic unit
AM	airlock module
AOS	acquisition of signal
APP	antenna position programmer
ASCS	attitude sensing and control system
ASR	automatic send/receive
ASTAM	automated system test and monitor
ATM	Apollo Telescope Mount
ATS	Applications Technology Satellite
AVE	Mojave, California (tracking station)
BDA	Bermuda (tracking station)
BECO	Teledyne-Brown Engineering Company
BER	bit error rate
BITE	built-in test equipment
BOL	beginning of life
BOM	basic operating module
BUR	Johannesburg, South Africa (tracking station)
C&DH	communications and data handling

LIST OF ACRONYMS (Continued)

C&DHS	communications and data handling system
C&W	caution and warning
CAM	computer address matrix
CCD	charge couple device
CCS	contamination control system
CDR	critical design review
CG, C.G.	center of gravity
CMG	control moment gyro
CMOS	complementary metal oxide semiconductor
CPU	central processor unit
CRO	Carnarvon (tracking station)
CSS	coarse sun sensor
CTU	command and telemetry unit
CYI	Canary Islands (tracking station)
D/A	digital to analog
DAU	data acquisition unit
DDT&E	design, development, test, and engineering
DEA	drive electronics assembly
DG	double gimbal
DGCMG	double gimbal CMG
DOD	depth of discharge
DPA	digital processor assembly
DSIF	Deep Space Instrumentation Facility
DTPL	domain tip propogation logic

LIST OF ACRONYMS (Continued)

DTU	data transmission unit
ECA	electrical control assembly
EC/LSS	environmental control/life support system
EDS	electrical distribution subsystem
EDU	electrical distribution unit
EIRP	effective isotropic radiated power
EM, em	electromagnet; engineering model
EMC	electromagnetic control
EMI	electromagnetic interference
EOL	end of life
EOM	end of mission
EPS	electrical power subsystem
ERTS	Earth Resources Technology Satellite
ESE	electrical support equipment
ETC	Engineering Training Center, Greenbelt, Maryland
EVA	extravehicular activity
EVLSS	extravehicular life support system
FGS	fine guidance system
FHST	fixed-head star tracker
FM	frequency modulated
FMEA	failure mode effects analysis
FOV	field of view
FRUSA	flexible, rollup solar array
FST	fixed star tracker

LIST OF ACRONYMS (Continued)

GAC	Grumman Aerospace Corporation
GDN	ground data network
GDSX	Goldstone (tracking station)
GESE	ground electrical support equipment
ghu	gyro hang-up
GMT	Greenwich mean time
GRARR	Goddard range and range rate
GSE	ground support equipment
GSFC	Goddard Space Flight Center
GST	gimbaled star tracker
GWM	Guam (tracking station)
HAW	Hawaii (tracking station)
HEAO	High Energy Astronomy Observatory
HEPA	high efficiency particulate air
HPI	high performance insulation
HSK	Honeysuckle Creek, Australia (tracking station)
I/O	input/output
I. D.	inside diameter
IESE	in-space electrical support equipment
IOCC	integrated operations control console
IOP	in the orbit plane
ISA	interstage adapter; interface systems adapter
IVA	intravehicular activity
LCP	left circular polarized
LOHARR	Lockheed heat rate program
LOS	line of sight

LIST OF ACRONYMS (Continued)

LSI	large scale integration
LST	Large Space Telescope
MAC	maximum allowable concentration
MAD	Madrid, Spain (tracking station)
MCC	mission control center
MCF	Mating/Checkout Facility
MIB	minimum impulse bit
MIL	Merritt Island, Florida (tracking station)
MMS	micrometeoroid shell
MNOS	metal nitride oxide silicon
MOJAVE	tracking station at Barstow
MOS/LSI	metal oxide semiconductor/large-scale integrated
MSFC	Marshall Space Flight Center
MSFN	Manned Space Flight Network
MSS	magnetometer sensing system
MT	magnetic torquer
MTBF	mean time between failures
MTE	magnetic torquer electronics
MTF	modulation transfer function
MTS	magnetic torquing system
MTU	magnetic tape unit
NASCOM	National Aeronautics and Space Administration Communications Network
NASO	National Astronomical Space Observatory
NDRO	nondestructive readout
NEA	noise equivalent angle

LIST OF ACRONYMS (Continued)

NFL	St. John's, Newfoundland (tracking station)
OAAR	other activities as required
OAO	Orbiting Astronomical Observatory
OAS	Orbit Adjust Stage
OMS	orbit maneuvering system
OOC	observatory operation center
ORRX	Orroral Valley (tracking station)
OSR	optical solar reflector
OTA	optical telescope assembly
OWS	Orbital Workshop
PCM	phase change material; pulse code modulator
PCS	peripheral communication system
PCU	power converter unit
PDR	preliminary design review
PEP	perpendicular to the ecliptic plane
PGA	pressure garment assembly
PM	pulse modulated
POP	perpendicular to the orbit plane
PRR	preliminary requirements review
PSD	power spectral density
PSK	phase shift keyed
PSU	power switch unit
QUI	Quito, Equador (tracking station)
R&D	research and development
RAM	research applications module (studies); reference alignment mode

LIST OF ACRONYMS (Continued)

RBV	return beam vidicon
RCD	remote command decoder
RCP	right circular polarized
RCS	reaction control system
REC	recurring costs
RF	radio frequency
RFI	radio frequency interference
RGA	reference gyro assembly
ROM	read-only-memory
ROS, ROSMAN	tracking station at Rosman, North Carolina
RSDP	remote site data processer
RTV	room temperature vulcanizing
RW	reaction wheel
SAA	South Atlantic anomaly
SBU	sensor buffer unit
SCAMA	switching, conferencing, and monitoring arrangement
SEC	secondary electron conduction
SFP	solicitation for proposal
SG	single gimbal
SGCMG	single gimbal CMG
SI	science instrument
SIP	scientific instrument package
SIT	silicon intensified target
SMS	secondary mirror sensor
SPD	solar power distributor

LIST OF ACRONYMS (Continued)

SPEH	special purpose equipment handler
SPF	single-point failure
SPG	single-point ground
SSM	support systems module
SSP	Space Station prototype
STADAN	Space Tracking and Data Acquisition Network
STDN	Spaceflight Tracking and Data Network
2-SPEED	two scissored pair ensemble explicit distribution
TA	transfer assembly
TACS	thrust attitude control system
TAN	Tananarive, Malagasy Republic (tracking station)
TBC	The Boeing Company
TCS	thermal control system
TDRS	tracking and data relay satellite (network)
TEX	Corpus Christi, Texas (tracking station)
TMR	triple modular redundancy
TOOMBA	tracking station at Cooby Creek
TRW	TRW Systems, Incorporated
TTY	teletypewriter
TWT	traveling wave tube
ULA	Fairbanks, Alaska (tracking station)
UPD	update buffer
USB	unified S-band
USBE	unified S-band equipment
VAB	Vertical Assembly Building
VGP	vehicle ground point

LIST OF ACRONYMS (Concluded)

VPM	variable permanent magnet
W-R	Wolf-Rayet
WASS	wide angle sun sensor
WFE	wavefront error
WNK	Winkfield, United Kingdon (tracking station)
XPDR	transponder

INTRODUCTION

The Large Space Telescope (LST) concept identified in this Phase A report defines a spacecraft composed basically of three major parts. These are shown in Figure 1 as:

1. The optical telescope assembly (OTA).
2. The scientific instrument package (SIP).
3. The support systems module (SSM).

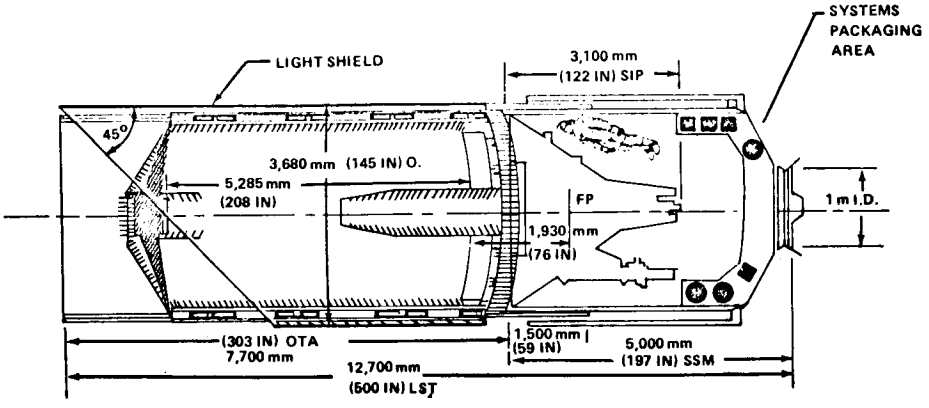

Figure 1. LST configuration.

The OTA and the SIP were studied under contract by Itek Optical Systems Division, Lexington, Mass., and by Kollsman Instrument Corporation, Long Island, N.Y., and are covered in more detail in Volume III (OTA) and Volume IV (SIP) of this report.

Two launch vehicles were considered. The primary one is the Space Shuttle to inject the LST into its 611-kilometer, 28.5-degree-inclination, circular operational orbit. The alternate one is an expendable Titan launch vehicle. In this latter case a "kick stage" was necessary to obtain required vehicle performance and to trim orbit injection inaccuracies. The Titan IIIE

with Orbit Adjust Stage (OAS) for the kick stage was selected as the alternate launch vehicle in this study since this was the current High Energy Astronomy Observatory (HEAO) launch configuration at the time the study was made. A performance analysis and comparison of various Titan/kick stage configurations are given in Volume III, Chapter III of this report.

This volume documents work done in an in-house Marshall Space Flight Center (MSFC) study to define the SSM. The SSM interfaces structurally with the OTA and provides the OTA and the SIP with electrical power, communications and data handling, environmental control, coarse attitude sensing and control, launch vehicle structural and electrical interface, and a docking structure for on-orbit servicing or retrieval by the Space Shuttle.

The SSM consists of the following systems:

1. Structures.
2. Thermal control.
3. Electrical.
4. Communications and data handling.
5. Attitude control.

These systems and the design analyses made to define them are described in detail in this documentation.

A number of alternate designs and approaches were considered in each of the systems areas. Trades were conducted among these alternatives and a viable reference design was made for the purpose of demonstrating LST feasibility in this Phase A study. The reference design, the rationale for the choice, and the indepth analysis which substantiate concept feasibility are all described in considerable detail in the following chapters. Discussions of the maintainability and reliability concepts and analyses which were conducted in support of the systems design are also included. Cost-effective approaches to long mission lifetimes, which are made possible by utilization of the unique capabilities of the Space Shuttle, are treated. Contamination protection during Shuttle manned maintenance operations was also studied; the results of the study are in the Appendix of this volume.

CHAPTER I. CONFIGURATION AND SYSTEM DESIGN

TABLE OF CONTENTS

LIST OF ILLUSTRATIONS

LIST OF TABLES

CHAPTER I. CONFIGURATION AND SYSTEM DESIGN

A. Reference Design Configuration

The support systems module (SSM) is a mostly cylindrical structure with a total length of 5000 mm (197 in.) and an inside diameter (I.D.) of 3300 mm (130 in.) (Fig. I-1). The aft end of the SSM is a shallow cone ending in a standard androgynous docking assembly with four projecting ears and a 1015 mm (40 in.) diameter opening. Both the cylindrical and the conical portion are provided with a bumper for protection against micrometeoroids. For the same purpose, a nonpressurizable cover closes the docking port opening. That cover is removable to allow access when required. A ring of 4270 mm (168 in.) diameter stiffens the cylinder/cone intersection.

The SSM assembly is joined to the optical telescope assembly (OTA) at the primary ring, while the OTA meteoroid shield is attached to the SSM at an interface located 1.5 m (59.0 in.) aft of the primary ring in order to isolate the primary mirror from the influence of the long meteoroid shield and sun shade.

The large space telescope (LST) is separated from the orbit adjust stage (OAS) by a "super zip" joint slightly forward of the docking plane. The solar arrays are located near the aft end of the cylinder. Each consists of two wings which fold forward and are articulated to wrap around the cylindrical portion of the SSM. The location of the solar arrays determines the orientation of the separation planes of the Titan shroud. The latter has a dynamic envelope (Fig. I-2) which is elliptical in cross section and must be oriented in such a way that the major axis of its ellipse goes through the masts of the solar arrays.

Two launch modes are considered in this study. The primary mode is the Space Shuttle and the alternate is the Titan IIIE/OAS launch vehicle. The Shuttle will retrieve the spacecraft; therefore, the structural system is required to satisfy the criteria of both of these launch modes. The attach points for Shuttle launch and retrieval are located at the primary OTA ring just forward of the SSM, and on the ring located at the intersection of cylindrical and conical portions of the SSM. In the case of a Titan launch, a payload adapter assembly will be provided which connects spacecraft and shroud to the OAS kick stage.

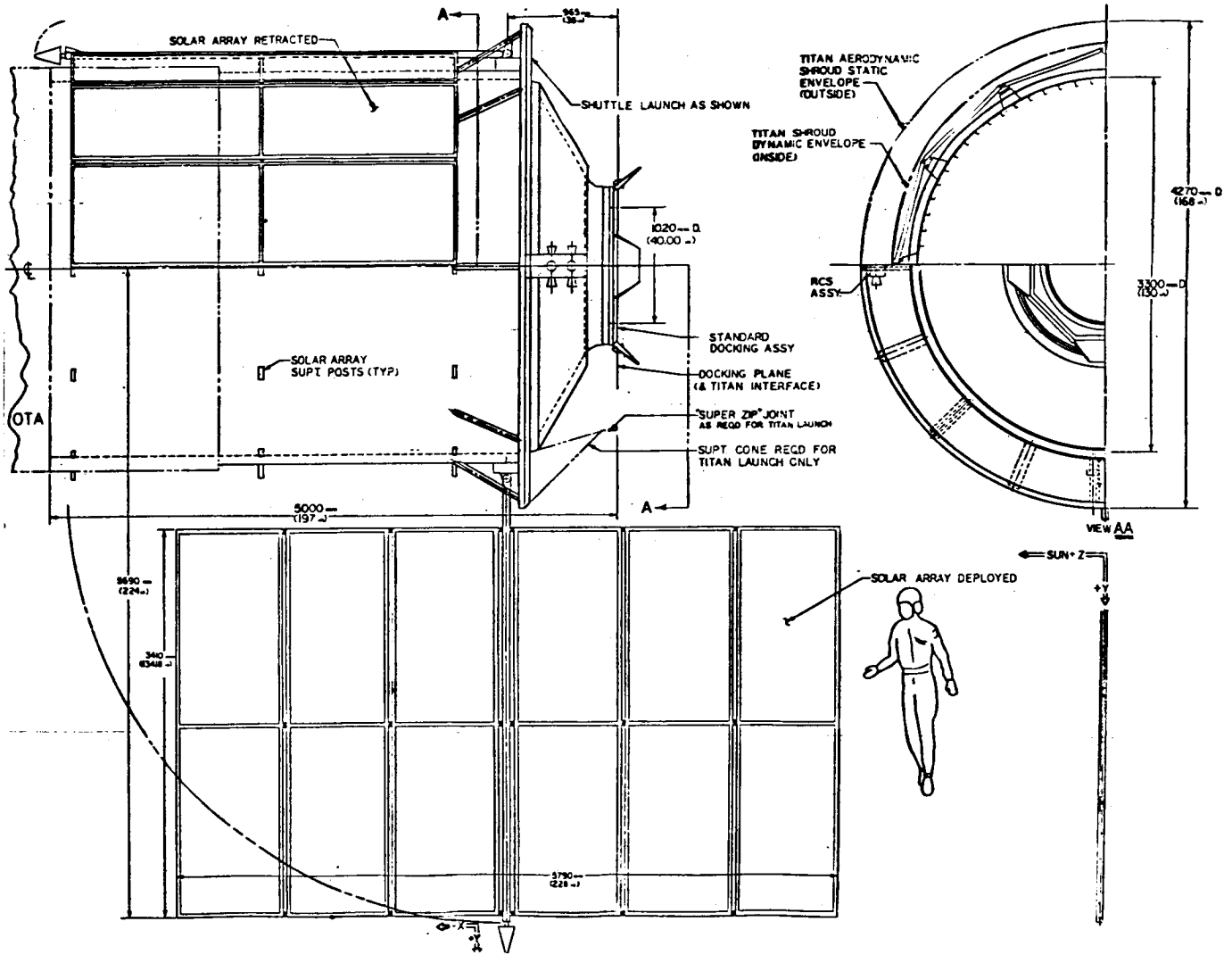

Figure I-1. Support systems module (SSM) reference design.

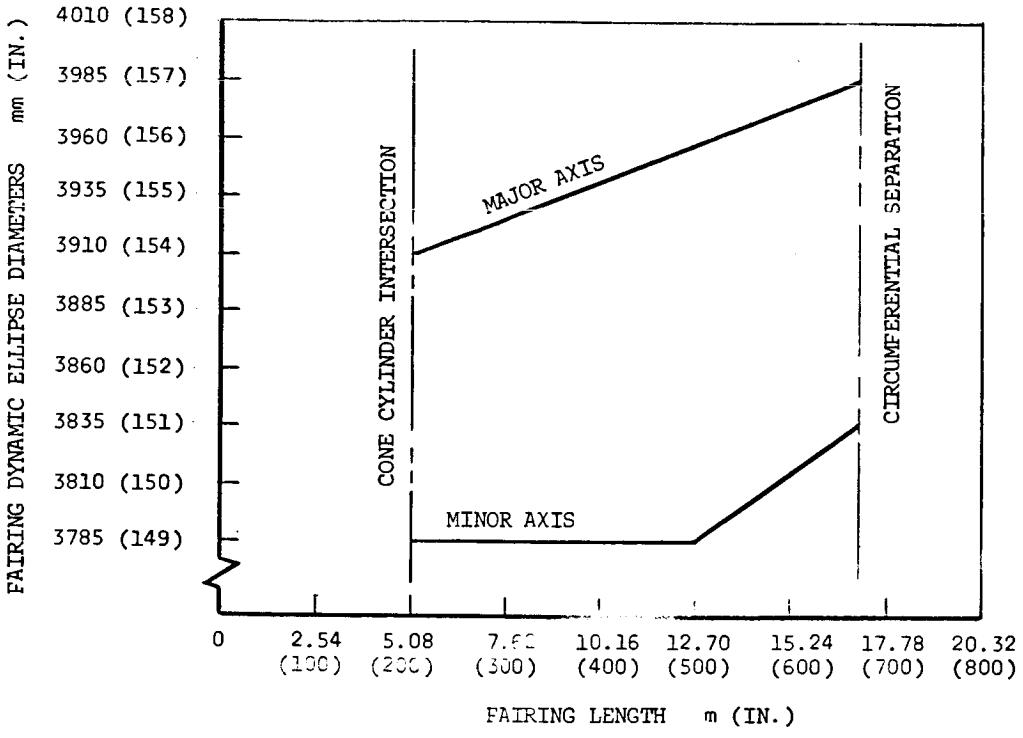

Figure I-2. Titan fairing dynamic envelope.

B. Design Details

The SSM is an aluminum structure which can be manufactured using standard aerospace methods. The cylindrical portion consists of a stiffened shell which is surrounded by a meteoroid shield. The shell [3300 mm I. D. (130 in. I.D.)] is part of the pressure vessel which allows pressurized maintenance and serves as a carrier for all loads and moments as required. Stiffening rings on the outside are deep enough to support the meteoroid shield which consists of a thin aluminum sheet that, for thermal reasons, has an external thermal barrier coating and internal High Performance Insulation (HPI) covering. The thermal shield and meteoroid bumper cover about two-thirds of the length of the SSM. The forward third is protected by the meteoroid shield of the OTA, which extends down over the SSM. The HPI extends to the systems compartment. Provisions are made for disconnecting the OTA meteoroid shield from the SSM in case disassembly becomes necessary. Brackets are provided on the outside of the pressure shell to support the solar array panels during launch, docking, and reentry.

The shallow cone at the aft end is an unstiffened sheet metal structure. Its connection to the docking structure is not clearly defined because the docking structure itself lacks sufficient definition; however, the influence of this uncertainty on the layout is negligibly small. A deep flanged ring is located at the cylinder/cone intersection and is braced with tubular members at eight equally spaced locations (Fig. I-3, Detail A). The ring provides support for the solar arrays, provides a mounting fitting for LST support in the Shuttle payload bay (Fig. I-4), serves as stiffening ring at the joint between cylinder and cone when the SSM is pressurized, and supports the aerodynamic fairing for the alternate Titan launch.

The details of the structure are shown in Figure I-3 where the cross section of the cylindrical shell is shown in Detail C. The inner shell in this cross section is the stringer-stiffened, load carrying structure. The thickness of this shell was determined to be 1.46 mm (0.058 in.) which will satisfy the requirements of both load carrying and meteoroid protection.

The maximum panel compressive and shear loads were used to determine the stringer spacing of 32.9 mm (5.43 in.) and the Z-stringer size of 25.4 × 38.1 × 1.27 mm (1.00 × 1.50 × 0.05 in.). The 50.8 × 25.4 × 3.18 mm (2.00 × 1.00 × 0.125 in.) channel ring frames were spaced 830 mm (32.8 in.) apart to prevent the cylinder from failing from general instability. Both the stringer and ring frame size and spacing prevent the pressure skin from buckling under load. The 12 equally spaced longerons shown in the detail are provided for subsystem equipment mounting.

Two 1500 mm (59.0 in.) long shear posts were installed on the cylinder at the Shuttle attachment points. These posts help to distribute the large concentrated Shuttle launch or retrieval load in the shell.

The outer shell is 0.5 mm (0.020 in.) thick and serves as the thermal shield as well as the meteoroid bumper. It is spaced 63.5 mm (2.50 in.) from the pressure shell by the 50.8 × 25.4 × 3.18 mm (2.00 × 1.00 × 0.125 in.) channel ring and 12.7 mm (0.500 in.) thermally insulated standoffs. This shell and the pressure shell with the space between constitutes the two-sheet meteoroid protection system.

C. System Arrangement

The systems are arranged as shown in Figure I-5. Components are coded by number as noted in the Master Equipment List (Table I-1). The philosophy behind the arrangement was to place as many of the smaller

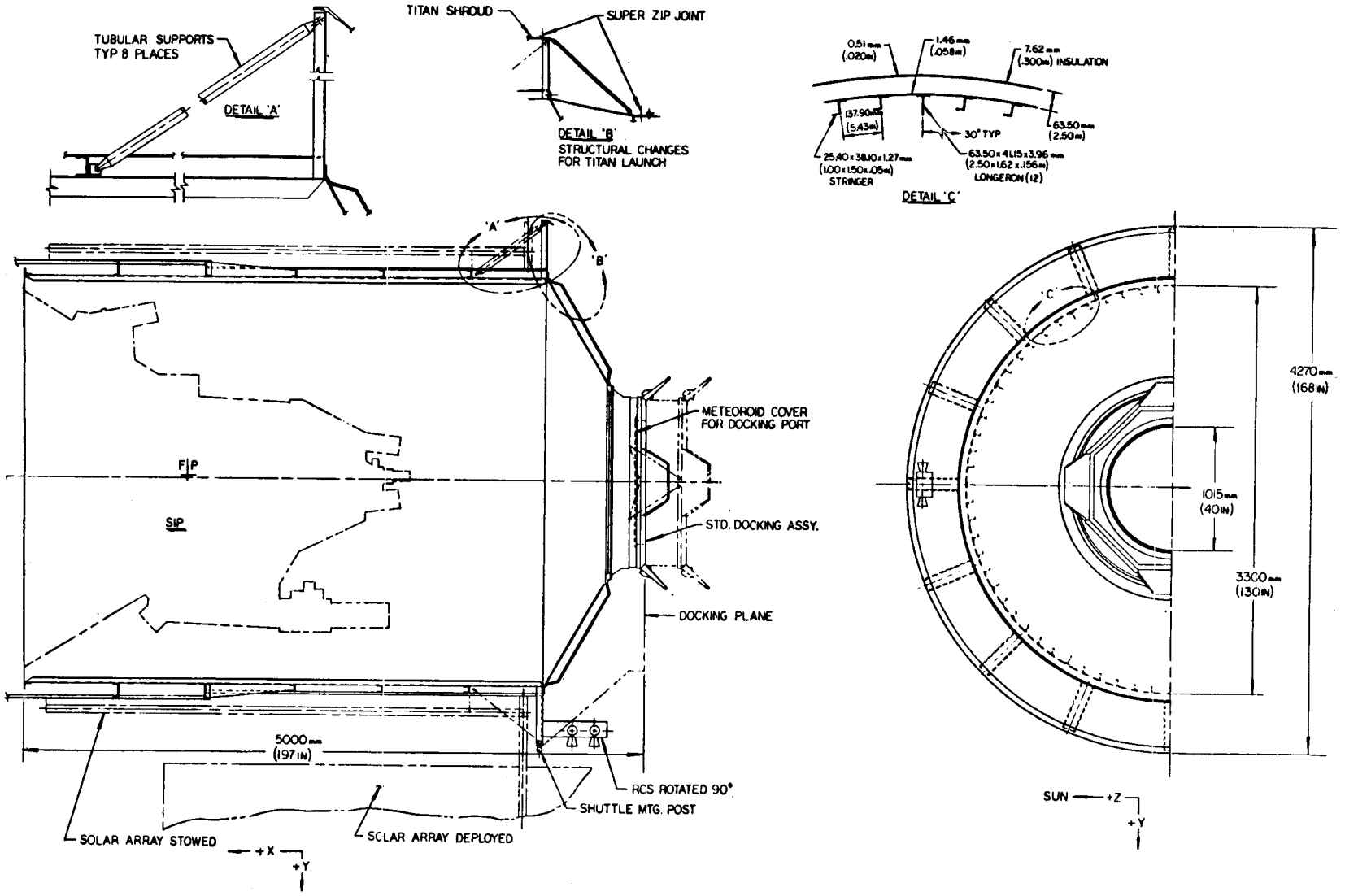

Figure I-3. SSM reference design longitudinal cross section.

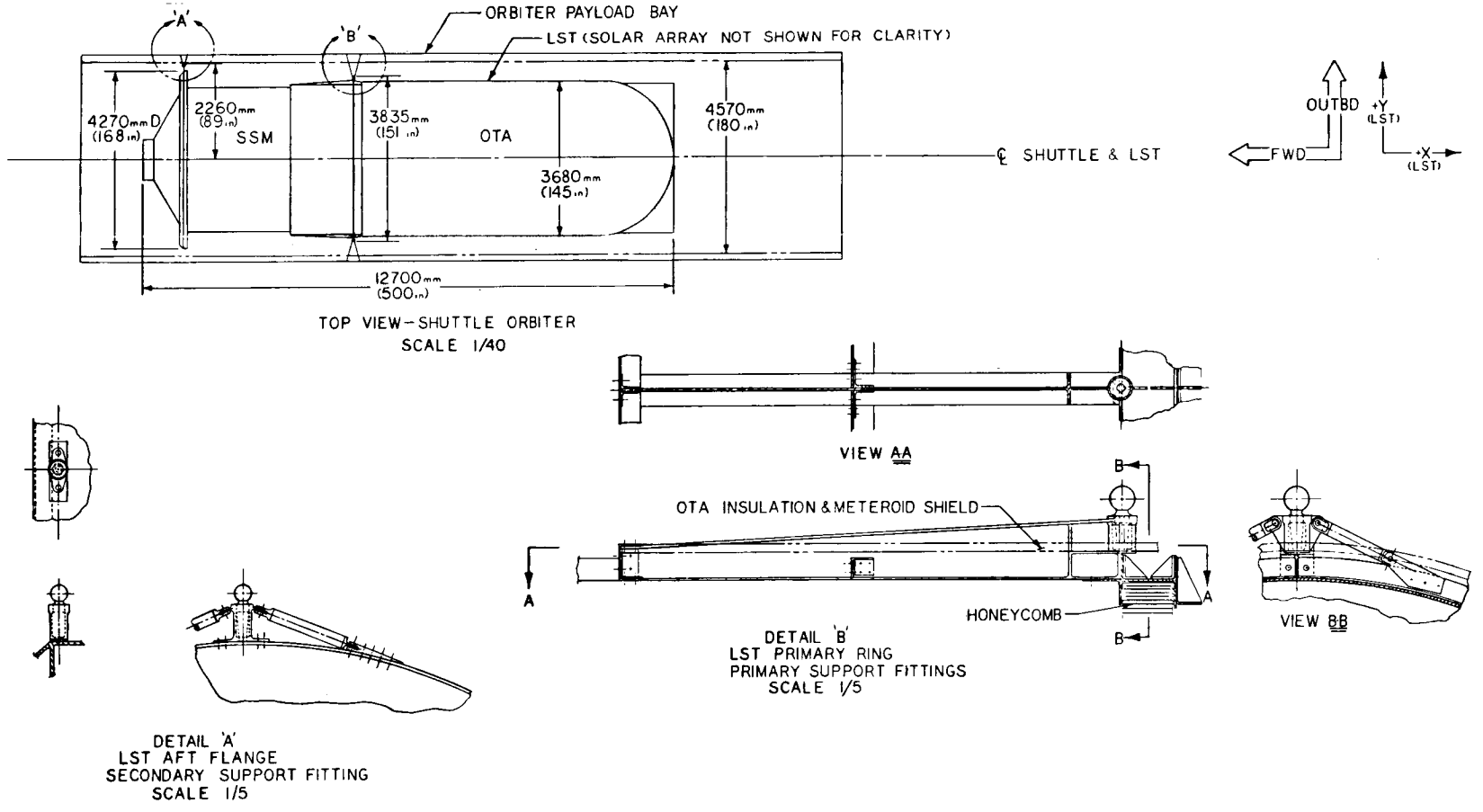

Figure I-4. LST support in payload bay.

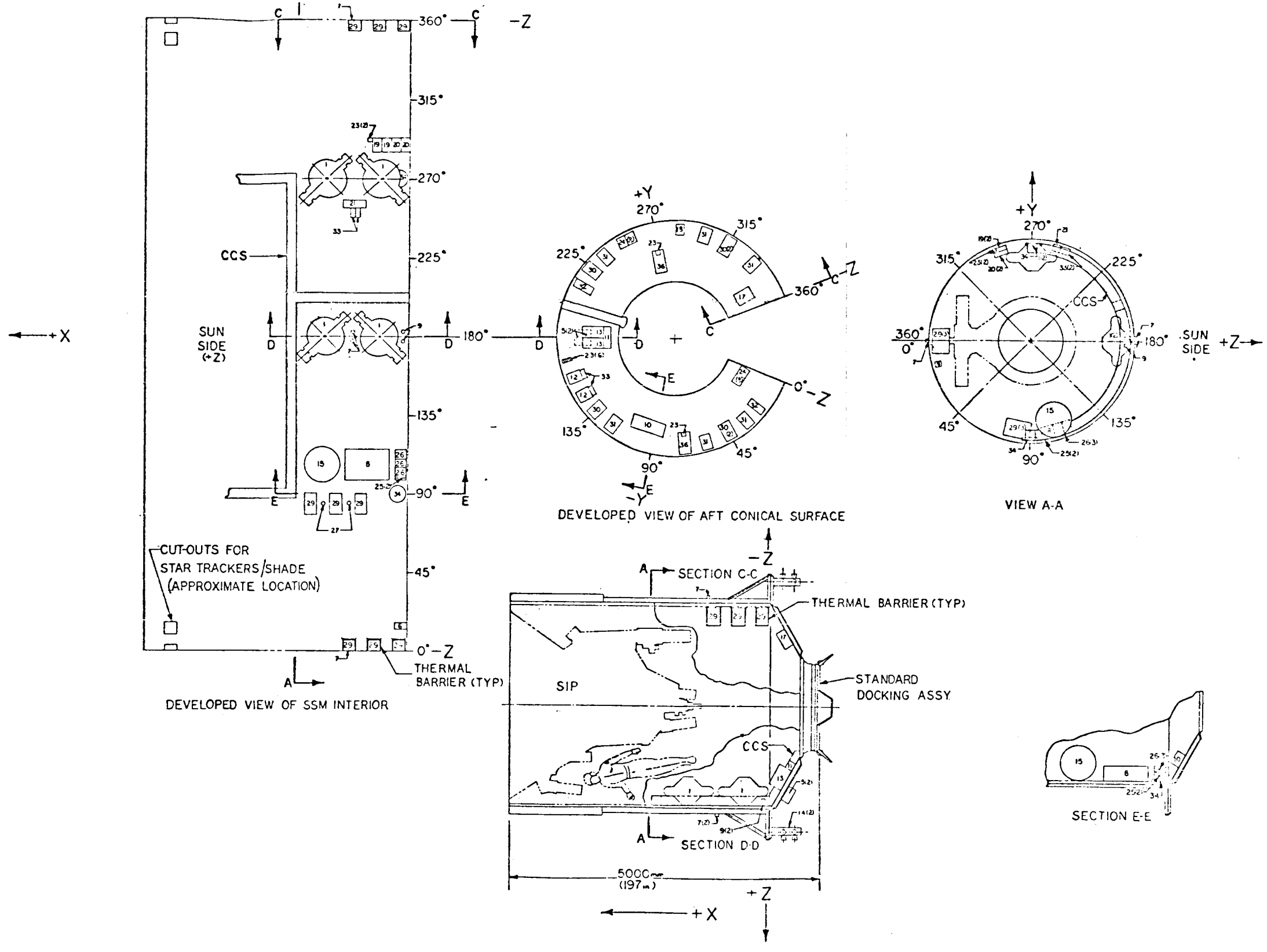

Figure I-5. SSM subsystems layout.

components as possible on the shallow aft cone inner surface, thus providing maximum clearance for the scientific instrument package (SIP). The remaining components that were too large or that had high operating temperatures, were arranged into four longitudinal rows. These rows were located mostly aft of the SIP and were offset in the circumferential direction from the large SIP components that require astronaut maintenance. The batteries, the most temperature critical subsystems, were placed on the antisun side, whereas the control moment gyros (CMGs), with higher allowable temperatures, were placed on the sun side. Some items such as the reaction control system (RCS) tank and related equipment are thermally inactive and will operate satisfactorily in any location within the SSM. These items were located near the items with which they interact. Thermal output is not necessarily a function of size; thus, a "volume balanced" arrangement is not required.

The fixed head star trackers are mounted on the SIP truss and view space through flat windows in the pressure shell. Respective openings are cut into the meteoroid bumpers. The windows are arranged perpendicular to the viewing direction of each star tracker and have sealed mounts so that they do not interfere with the pressurization of the SSM.

In the present arrangement, the star trackers' views are blocked when the solar arrays are in their folded position. This could be eliminated by cutouts in solar panels, if desired. A small increase in panel length would compensate for the area lost because of the cutouts.

Out of the Contamination Control System (CCS) only the major ducts, filters, and instrumentation are included in the SSM. These are indicated in Figure I-5. The fans are located in the Shuttle support volume. Specific details of the CCS are presented in the Appendix of Chapter VII of this volume.

As discussed elsewhere, preliminary analyses of the reference design arrangement show that all systems meet their respective thermal requirements, and that there is adequate clearance for astronaut maintenance for all components within the SSM.

D. Spacecraft Attachment to the Launch Vehicle

A statically determinate four-point scheme which is shown in Figure I-4 was used to support the spacecraft in the Shuttle. A schematic of the attachment at the spacecraft main ring is depicted in Figure I-6.

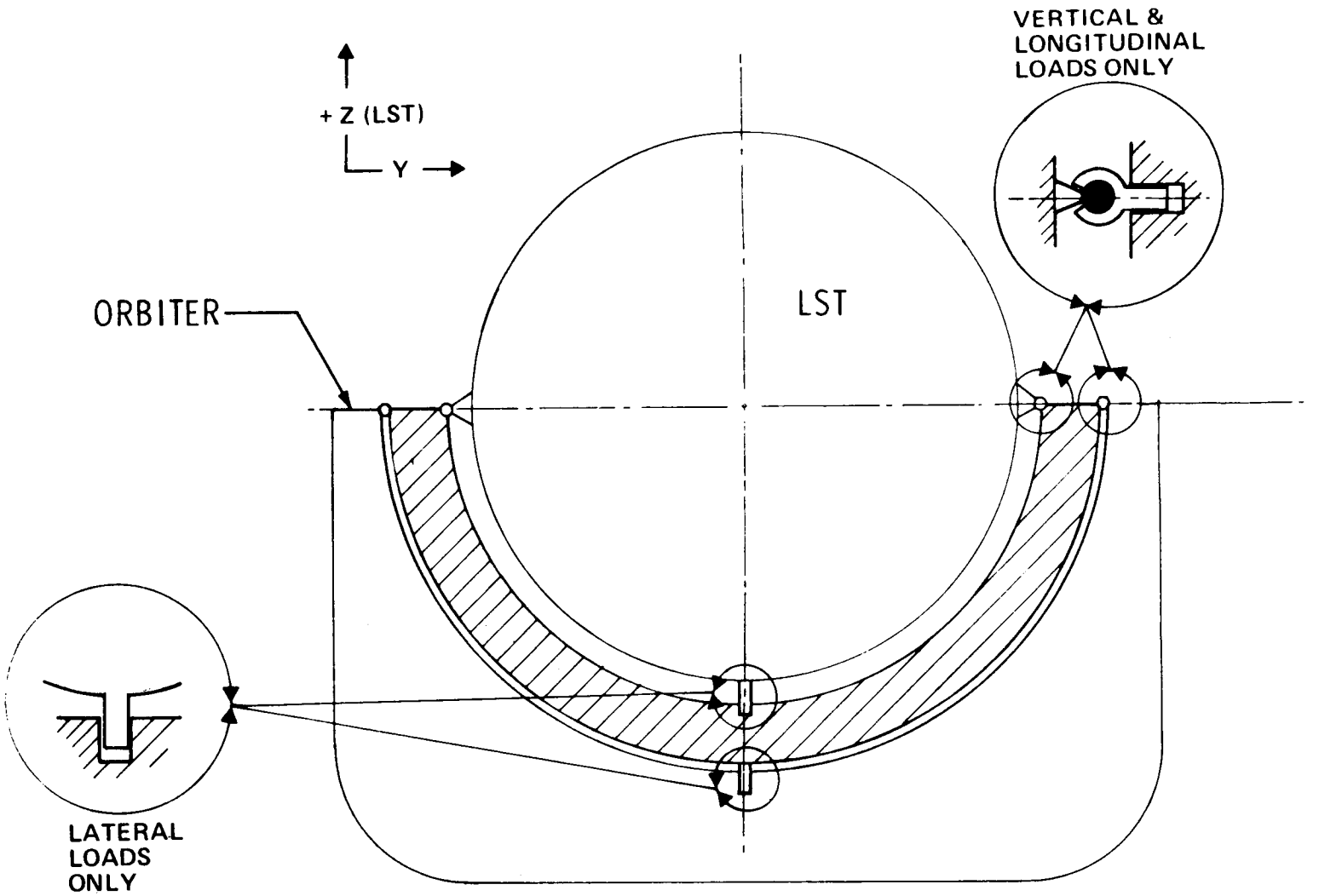

Figure I-6. Attachment of spacecraft to Shuttle.

The attach point on the large aft ring of the SSM takes loads along the Shuttle vertical axis only, while the points in the yaw plane on the OTA main ring take vertical and longitudinal loads. The third point on the main ring in the vertical plane takes loads along the lateral axis only. All of the attachments are designed so that moments are not transmitted to the LST from the Shuttle. Thus, with this attachment arrangement, the LST structural system will be completely relieved from loads induced by structural deflections of the Shuttle during flight.

The SSM structure with its shear post was designed to withstand concentrated attachment interface loads. The OTA primary ring was checked for the Shuttle launch loads; it was found to be adequate and required only local modification to allow installation of the attach fittings.

For the Titan launch, a 4.3 mm (0.17 in.) thick conical adapter, which is shown in Figure I-3, Detail B, is provided to attach the spacecraft to the OAS kick stage.

TABLE I-1. MASTER EQUIPMENT LIST

Ident. No.	System Component	No. of Units Required	No. of Units Provided	Unit Power (W)	Total Power (W)	Unit Heat Dissipated (W)	Size		Unit Mass (Weight)		Total Mass (Weight)		Allowable Operating Temperature (°C)
							mm	in.	kg	lb	kg	lb	
	SUPPORT SYSTEMS MODULE												
	Attitude Control												
1	CMGs and Digital Electronics Assembly[a]	3	4	17 (pt.) 22.5 (slew)	68 (pt.) 90 (slew)	17	1019X775X584	40.1X30.5X23	80.9	178	323.6	712	0 to 57
2	Magnetic Torquer[b,c]	6	6	2.5	15	–	51DX1905	2DX75	23.5	52	141	310	-18 to 54
3	Fixed Star Tracker (FST)[a,d]	2	3	5	10	5	114X114X406	4.5X4.5X16	5.5	12	16.4	36	-35 to 70
3	FST Shades[a]	2	3	0	0	–		18X12 Diag.	1.6	3.5	4.8	10.5	
4	Reference Gyro Assembly[a,d,e]	x	1	36	36	36	444X173X152	17.5X6.8X6	10.45	23	10.45	23	0 to 57
5	3-Axis Magnetometer[f]	1	2	2	2	2	127X127X254	5X5X10	3	6.5	5.9	13	-35 to 70
6	Magnetic Torquer Electronics[c]	1[y]	1	5	5	5	203X102X102	8X4X4	2.3	5	2.3	5	-18 to 54
7	Coarse Sun Sensors[a,g]	1	5	0	0	–	48DX41	1.9DX1.6	0.1	0.2	0.4	0.8	-84 to 51
8	Lines, Valves, and Regulator Set[h]			–	–	–	711X508X178	28X20X7	44	96.7	44	96.7	
11	Digital Processor Assembly[a,i]	1	1	16	16	16	107X130X366	4.2X5.1X14.4	6.2	13.7	6.2	13.7	-55 to 71
12	Transfer Assembly[j]	1	2	26.5	26.5	26.5	152X203X246	6X8X9.7	4.7	10.3	9.4	20.6	-55 to 71
13	RCS Electronics[c]	1	2	11[bb]	0[bb]	–	229X356X178	9X14X7	7.3	16	14.5	32	-55 to 71
14	RCS Thruster Module[k]	2	4	–	–	–	274X127X160	10.8X5X6.3	2	4.5	8.2	18	TBD
15	RCS Tank[l]	1	1	–	–	–	Sphere:576D	22.66	32.4	71.3	32.4	71.3	-18 to 54
15	GN_2	–	–	–	–	–			19.5	43	19.5	43	
	Totals				178.5						639	1405.6	
	Electrical												
29	Batteries[j]	3	6	–	–	21	406X279X178	16X11X7	22.4	49.3	134.4	296	+5 to 10
30	Chargers[m]	3	6	0.33	2	6	305X203X152	12X8X6	6.8	15	40.9	90	-18 to 52
31	Regulators[m]	3	6	–	–	23	279X203X127	11X8X5	3.5	7.8	21.4	47	-18 to 52
32	Solar Power Distributor[c]	2	2	5	10	10	325X165X152	12.8X6.5X6	5.5	12	10.9	24	-18 to 52
33	Electrical Distribution Units[c,j]	4	8	2.5	20	3	152X102X76	6X4X3	1.1	2.5	9.1	20	-18 to 52
34	Solar Panel Mechanisms[c]												TBD
	Boom Deployment	2	2						48.2	106	96.4	212	
	Panel Deployment	2	2						10.0	22	20.0	44	
	Wing Orientation	2	2	2	4	2							
35	Solar Panels[c]	12	12	–	–	–	3370X927X10	133X36.5X0.38	15.1	33.3	186.4	410	≤100
36	Electrical Control Assembly[c]	1	2	5	10	6	356X203X203	14X8X8	7.3	16	14.5	32	-18 to 52
37	Cabling and Connect[c]	–	–	–	–	43					113.6	250	
	Subtotals				46						647.6	1425	
	Preinstalled (Inactive) Equipment for Manned Support and Maintenance[c]												
	Lighting	8	8	30	Supplied						9.1	20	-10 to 50
	Caution and Warning Cable	1	1	10	From						4.5	10	-10 to 50
	Headset Receptacle	3	3	–	Orbiter						4.5	10	-10 to 50
	ECLS Electrical Provisions	–	–	–							2.3	5	-10 to 50
	Cable and Test Accessories	–	–	–							18.2	40	-10 to 50
	Subtotals										38.6	85	
	Totals				46						686.2	1510	
	Communications and Data Management												
9	Communications and Data Handling Switch[n]	1	2	–	–	–	51DX105	2DX4	0.5	1	0.9	2	-18 to 60
10	Apollo Transponder[c]	1[y]	1	16	5.3[cc]	5.3[cc]	565X229X152	22.2X9X6	14.5	32	14.5	32	-18 to 60
16	Antenna[a]	1	2	–	–	–	Cone: 76DX245H	3DX10H	0.9	2	1.8	4	-18 to 60
17	ERTS Transponder[a]	1[y]	1	28	9.3[cc]	9.3[cc]	203X152X330	8X6X13	10.9	24	10.9	24	-18 to 60
18	PSK Demodulator[j]	1[y]	1	4	4	4	184X140X89	7.25X5.5X3.5	0.9	2	0.9	2	-18 to 60
19	Data Control Unit[j]	1	2	3	3	1.5	152X229X71	6X9X2.8	1.8	4	3.6	8	-18 to 60
20	Format Generators[j,o]	1	2	4	4	4	152X229X152	6X9X5.6	1.8	4	3.6	8	-18 to 60
21	Command Processor and Memory[j]	1[y]	1	16	16	16	107X130X366	4.2X5.1X14.4	6.2	13.7	6.2	13.7	-18 to 60
23	Digital Acquisition Unit[a]	14	28	1.34	1.34	–	71X71X25	2.8X2.8X1	0.1	0.25	3.2	7	-18 to 60
24	Remote Command Decoders[a]	8	16	1.4	22.4	1.4	152X229X71	6X9X2.8	0.4	0.8	5.8	12.8	-18 to 60
25	Tape Control[a]	1	2	1	1	1	157X185X41	6.2X7.3X1.6	1.4	3	2.7	6	-18 to 60
26	Tape Recorders[p]	z	3	12 rec. 24 P.B.	20	20[dd]	246X203X147	9.7X8X5.8	5.5	12	16.4	36	-18 to 60
27	Clock[j]	1[y]	1	1.7	1.7	1.7	56DX114H	2.2DX4.5H	0.5	1	0.5	1	-18 to 60
	Totals				88.0						71.0	156.5	
	Thermal Control												
	Insulation on SSM External[m]		–		–	–					11.0	24.2	
	Internal[m]		–		–	–					3.3	7.3	
	Louvers – In SSM[j]		–		–	–					5.6	12.3	
	Paint – On SSM[c]		–		–	–					46.9	103.2	
	Strip Heaters – In SSM[a]				–	–					5.5	12.1	
	Total										72.3	159.1	
	Contamination Control 10 000/100 000 System												
	Ducting[q]	–	50 ft 15 250 mm	–	–	–	152X152X0.5	6X6X0.02	0.001/ mm	0.57/ft	13.2	29	
	Misc. Fittings[q,r]	–	–	–	–	–					1.8	4	
	Quick Disconnect Joint[q,s]	–	1	–	–	–	610DX76L	24DX3L	2.3	5	2.3	5	
	HEPA Filters[q,t]	–	6	–	–	–	305X305X152	12X12X6	1.4	3	8.2	18	
	HEPA Filters[q,u]	–	2	–	–	–	356X356X152	14X14X6	1.8	4	3.6	8	
	Total										29.1	64	
	SSM Structure												
	Docking Port Equipment (Mech., Port, and Environment Protection Cover)	–	–	–	–	–	–		199	437	199	437	
	Shroud Adaptor (Only for Titan launch)	–	–	–	–	–	–	–	251	553	251	553	
	Cylindrical Wall												
	Primary Load-Carrying Shell	–	–	–	–	–	–	–	–	–	332	731	
	Ring Frames	–	6	–	–	–	–	–	21.7	47.8	130	287	
	Longerons	–	12	–	–	–	–	–	5.8	12.8	70	154	
	Shear Posts	–	2	–	–	–	–	–	3	6	6	12	
	Mounting Brackets, etc.	–	–	–	–	–	–	–	–	–	23	50	
	Meteroid and Thermal Shield	–	–	–	–	–	–	–	–	–	74	163	
	Total										1085	2387	
	Grand Total For SSM				312.5						2582.6	5682.2	
	OPTICAL TELESCOPE ASSEMBLY												
	Structure												
	Metering Truss[ff]	–	–	–	–	–					402.79	888.16	
	SIP Primary Structure	–	–	–	–	–					149.96	330.66	
	Meteoroid Shield	–	–	–	–	–					531.16	1171.2	
	Baffles	–	–	–	–	–					291.56	643.55	
	Electronics Structure	–	4	–	–	–			4.94	10.9	19.75	43.62	
	Aperture Door Assembly	–	–	–	–	–					98.55	217.3	
	Light Shield	–	–	–	–	–					343.58	757.6	
	Pressure Bulkhead Door	–	–	–	–	–					48.03	105.9	
	SIP Contamination Cover	–	–	–	–	–					165.62	365.19	
	Total										2051.0	4523	
	Thermal Control												
	Insulation (Passive)	–	–	–	–	–					78.97	174.12	
	Primary Mirror Thermal System	–	–		306	306					14.07	31.02	
	Secondary Mirror Thermal System	–	–		40	40					9.38	20.68	
	Paint/Coatings	–	–	–	–						(Included in Structure)		
	Total				346						102.4	226	
	Optics												
	Primary Mirror	–	1	–	–				2001.2	4412.65	2001.2	4412.65	
	Secondary Mirror	–	1	–	–				40.03	88.27	40.03	88.27	
	Focal Plane and Fold Optics	–	–	–	–				–	–	40.0	88.2	
	Total										2081.2	4589	
	Performance Control												
	Fine Guidance Assembly	–	1		110	110			116.48	256.83	116.48	256.83	
	Figure Sensor	–	1		0	0			17.36	38.29	17.36	38.29	
	Focus Sensor	–	1		1	1			12.66	27.92	12.66	27.92	
	Decenter Sensor	–	2		1	0.5			8.05	17.75	16.1	35.5	
	Angle Sensor	–	2		1	0.5			4.42	9.75	8.84	19.5	
	Diagnostics	–	–		10	10					23.56	52.0	
	Secondary Mirror Alignment												

Part 2

Actuators	–	6		2	0.3			10.98	24.19	65.86	145.13	
Primary Mirror Force Transducers	–	24		0	0			0.72	1.58	17.23	38	
Secondary Mirror Tracking Actuators	–	1		30	30			29.55	65.15	29.44	65.15	
Total				155						307.5	678.32	
Data Management												
Data Acquiaition	–	1						2.13	4.7	2.13	4.7	
Command Decoders	–	1						1.04	2.3	1.04	2.3	
	Electronics are Included in Each Appropriate System or Assembly[aa]											
Total										3.2	7	
Power Distribution												
Electrical Distribution	–	1	–	–	3			2.27	5.0	2.27	5.0	
Power Conditioner Control	–		–	–								
Cabling	–	–	–	–	15					31.75	70	
Total										34	75	
OTA Total				501						4579.3	10 098	

SCIENTIFIC INSTRUMENT PACKAGE

Item	FOV	Operating Range (nm)	Resolution	Image Tube Size (mm)	Location	Mass kg (lb)	Power W (Avg)	Remarks
			Airy Disc Dia					
Field Cameras								
f/12 Image Tube	4.7 arc min	115-550	5.6	50X50	Radial	68.7 (152)	34	
Filter Wheel	–			–	Radial	2.3 (5)	2	3 Positions
f/96 Image Tube	35 arc sec	115-300	1.5	50X50	Radial	67.2 (148)	36	
Filter Wheel	–	–			Radial			3 Positions (mass and power included in f/96 magnifier)
f/96 Image Tube	35 arc sec	160-600	1.5	50X50	Radial	67.2 (148)	36	
Filter Wheel					Radial			3 Positions (mass and power included in f/96 magnifier)
f/96 Image Tube	35 arc sec	500-1100	1.5	50X50	Radial	67.2 (148)	37	
Filter Wheel					Radial			3 Positions (mass and power included in f/96 magnifier)
f/96 Magnifier and Housing					Axial	15.5 (34)		
f/96 Camera Selection Assembly					Axial	21.9 (47.9)	2	
			Spectral Resolution $\lambda/\Delta\lambda$					
High Spectral Resolution Spectrographs								
Echelle Spectrograph	0.05-0.2X2 sec	110-180	$4.5X10^4$	25X25	Axial	62.4 (137.6)	16	3 Slit Sizes: 0.05X1.0 arc sec 0.1X0.1 arc sec 2.0 arc sec dia
Echelle Spectrograph	0.05-0.2X2 sec	180-350	$3.0X10^4$	25X25	Axial	62.4 (137.6)	16	3 Slit Sizes: Same as above
Faint Object Spectrographs								
Czerny-Turner (Gratings A and B)	0.05-0.1X10 sec	A-110-160 B-160-220	A. $1.25X10^3$ B. $1.75X10^3$	25X25	Axial	64.2 (141.5)	17	3 Slit Sizes: 1X15 arc sec 15X15 arc sec Other
Wadsworth (Dichronic Mirror)	0.05-0.1X10 sec	220-350 350-660	A. $1.23X10^3$ B. $0.75X10^3$	25X25	Radial	49.2 (108.3)	17.5	3 Slit Sizes } Same as above 3 Slit Sizes }
Slit Mechanism					Radial			(mass and power in inst.)
Czerny-Turner	0.05-0.1X10 sec	650-1μ	$1.5X10^3$	25X25	Radial	47.6 (104.8)	17.5	3 Slit Sizes: Same as above
Slit Mechanism					Radial			(mass and power in inst.)
Fourier Interferometer	2.5-5.0 sec dia	1μ-5μ	$3.3X10^4$	25X25	Radial	50.0 (110.5)	10.0	2 Circular FOV openings
Slit Jaw Camera Assembly	13 sec	115-550			Radial	47.7 (105.2)	20	
Contingency Equipment[v]						36.9(81.3)	25	
Support Equipment								
Collimating Mirrors and Axial Spectrograph Selector					Axial	7.0(17.4)	2.5	
Axial Spectrograph Slit Selector Mechanism and Calibration Source Assembly					Axial	4.8(10.5)	3.5	Serves 2 Echelles and F.O. Spectrographs
Support Electronics and Cabling						38.1 (84.0)	22	
Scientific Instrument Controller[v]					Radial	6.2 (13.7)	16	
Scientific Data Link Control Logic[v]					Radial	2.3 (5.0)	2	
Thermal Control Paint[v]						12.3 (27)	–	
Strip Heaters[v]						10.4 (23)	ee	
Secondary SIP Structure						189.3 (418.3)		
Thermo-Electro Devices (10 units)							80	Only needed for very faint sources (28th Magnitude) 50 Watts per tube max.
Totals						1000.8 (2208.6)	412.0[w]	

a. HEAO component
b. Mounted on OTA
c. New design (existing technology)
d. Mounted on OTA main ring
e. Nine watts per gyro
f. Existing component of OAO
g. Electronics in transfer assembly
h. Existing component of Agena, Satellite Control Section, and others
i. Software special for LST
j. HEAO commonality possible if HEAO or LST concept is changed slightly
k. Existing component of Agena thruster cluster
l. Existing component of Lockheed Satellite Control Section backup RCS
m. Existing component of ATM Skylab
n. Existing commercial component
o. Includes two PCM encoders, six ROMs
p. Existing component of Gemini
q. Existing component
r. Duct work support straps, etc.
s. Plug-in for air supply
t. Cabin manifold; 150 CFM capacity
u. SIP inlet; 200 CFM capacity
v. Not included in list of instruments in Volume IV
w. Based on earlier estimates; power used in estimating overall power requirements was 500W
x. Six gyros per assembly (3 required)
y. Internally redundant
z. One active in record, one active in playback (P.B.) during contact
aa. Power included in SSM electrical system.
bb. Duty cycle is very small Used only in emergency
cc. On during ground contact only. Max ground contact estimated to be 33.3 percent
dd. One unit active normally; second unit during ground contact. A max of 33.3 percent was assumed contact time
ee. Heaters are on when some instruments are off; therefore, no additional power is required
ff. Includes main ring and pressure bulkhead

CHAPTER II. STRUCTURES

TABLE OF CONTENTS

LIST OF ILLUSTRATIONS

LIST OF ILLUSTRATIONS (Continued)

LIST OF ILLUSTRATIONS (Concluded)

LIST OF TABLES

CHAPTER II. STRUCTURES

A. Introduction

The structural system of the LST spacecraft, which is shown in Figure II-1, consists of two major assemblies: the optical telescope assembly (OTA), and the support systems module (SSM).

The SSM assembly is joined to the OTA assembly at the primary ring, while the OTA meteoroid shield is attached to the SSM at an interface located 1.5 m (59.0 in.) aft of the primary ring. This 1.5 m length of SSM structure is considered to be a transition section and is designed to help distribute the large mirror load that is concentrated in that area during launch or retrieval. It also isolates the primary mirror from the influence of the long meteoroid shield and sun shade.

Two launch modes are considered in this study. The primary mode is Space Shuttle and the alternate is the Titan IIID/OAS launch vehicle. Since the Shuttle will retrieve the spacecraft, the structural system is required to satisfy the criteria of both of these launch modes.

B. SSM Assembly

The SSM primary load-carrying structure consists of the pressure shell with its stiffeners, longerons, and ring frames, and, in the case of a Titan launch, a payload adapter assembly which attaches the spacecraft and shroud to the OAS kick stage. The remaining structural components are not subject to overall spacecraft launch loads but they do provide the protection system, the closeout structure required to allow pressurization, and the support for subsystem components of the spacecraft.

1. Design Criteria. The SSM structural assembly was designed for the limit load requirements of both the Shuttle and Titan launch. The limit load factors in the axial, pitch, and yaw directions and the launch phases considered are as follows:

1. Titan Launch.

   a. +6.0 g axial, +1.5 g pitch.

TABLE II-1. SSM STRUCTURAL MASS SUMMARY

Items	Mass, kg (Wt., lb)
Cylindrical Wall[a]	
Primary Load-Carrying Shell	332 (731)
Ringframes (6)	130 (287)
Longerons (12)	70 (154)
Shear Posts (2)	6 (12)
Mounting Brackets, etc.	23 (50)
Meteoroid and Thermal Shield	74 (163)
Total	635 (1397)
Docking Port	199 (437)
Shroud Adapter (only for Titan-launch) and Support Structure	251 (553)
Total (Titan Launch)	1085 (2387)
Total (Shuttle Launch)	834 (1834)

a. The load-carrying structural components are designed for the requirements of both Titan and Shuttle launches.

C. Solar Cell Substrate and Support Structure Analysis

A structural analysis of the LST solar array substrate and support structure was made to ensure that the structure has adequate stiffness to preclude the solar array motion coupling with the spacecraft motion, particularly during fine pointing. The analysis is also intended to assess the deflection and stress levels caused by vehicle acceleration.

The solar cell panels are subject to launch vibration environments as well as the launch loads for the Shuttle and Titan. Launch vibration environments are given in References II-1 and II-2 and the Shuttle and Titan launch loads were given in Section 1 (Design Criteria). The panels can be well supported in their stowed position during the launch; therefore, it was assumed that these loading conditions were not critical and they were not analyzed.

1. Structural Description. The structure analyzed was a 3400 mm (134.18 in.) by 5800 mm (228 in.) array consisting of 12 rectangular honeycomb panels which are 930 mm (36.65 in.) by 1700 mm (67.09 in.). The edges of the panels are closed out with lightweight framing members which also carry the system of hinges that join the panels. The line of hinges on the longitudinal centerline of the array that lock it in the deployed position is shown in Figure II-2. These hinges were considered to be rigid members in the analysis. The entire array is cantilevered from the SSM structure by a 430 mm (17.0 in.) articulated beryllium boom. Further details of the substrate and support structure can be seen in Chapter IV of this volume..

The honeycomb sandwich panel is 9.5 mm (0.375 in.) thick and has 7075-T6 aluminum alloy facing sheets that are 0.25 mm (0.10 in.) thick. The panel core is 36.8 kg/m^3 (2.3 lb/ft^3) 5052 aluminum alloy honeycomb with a 6.4 mm (0.25 in.) cell size. The framing members and hinges are made of aluminum alloy.

2. Static Analysis. A uniformly distributed mass of 364 kg/m^2 (51.6×10^{-4} lb/in.^{2}) of panel surface was assumed for the structure in the analysis. This distribution represents the total mass of the solar cells, dielectrics, adhesives, and paints that make up the solar cell module assemblies and the mass of the substrate panel adhesives.

With this mass distribution and an acceleration of 1.0 g normal to the array surface, the static analysis yields a maximum tip deflection of 605 mm (23.8 in.). The maximum stress in the honeycomb panel is less than 27.6 MN/m^2 (4000 lb/in.^{2}). Although the deflection and stress levels are acceptable values, the 1.0 g load is much larger than any load that will be encountered in space when the solar array is deployed. The results can be proportioned to the actual imposed load to obtain the actual deflection and stresses. It is apparent, however, that little or no strength and deflection problems will arise with this solar array structure.

3. Dynamic Analysis. The natural frequencies and their corresponding mode shapes were calculated for the array. These data were also used to corroborate the input to the dynamic response analysis discussed later in this chapter.

The first 10 natural frequencies are listed in Table II-2 and the undeformed shape of the solar array is shown in Figure II-3. The mode shapes at the listed natural frequencies are shown in Figure II-4 through II-13. The deflections plotted are normalized to the maximum computed deflection.

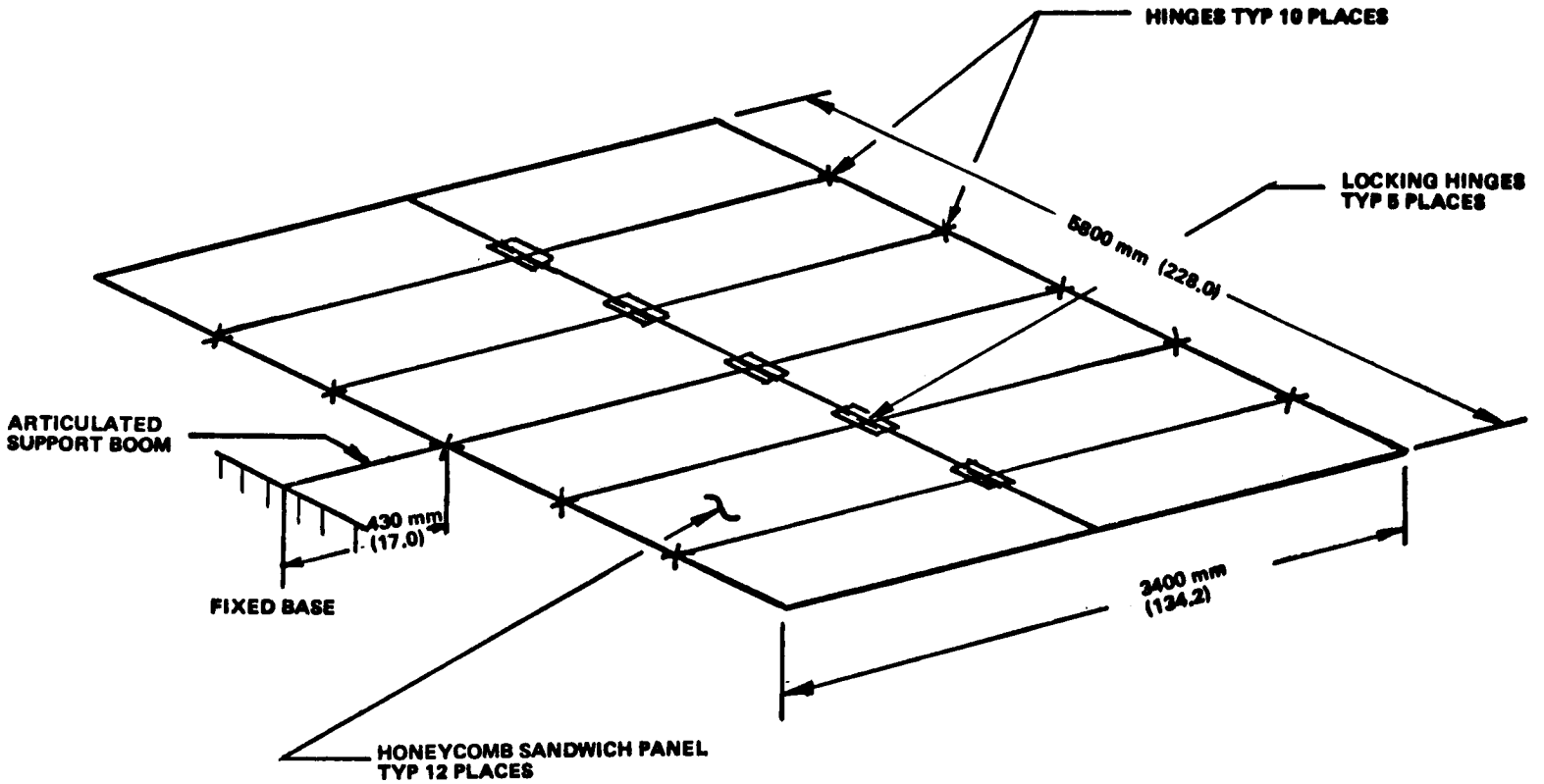

Figure II-2. Geometry of solar cell array.

TABLE II-2. NATURAL FREQUENCIES OF THE SOLAR ARRAY

Mode	Frequency (Hz)
1	0.68
2	0.75
3	2.43
4	3.00
5	4.50
6	5.46
7	5.85
8	7.61
9	7.67
10	8.39

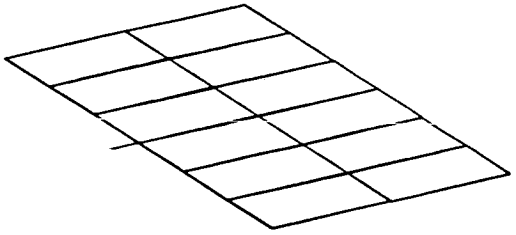

Figure II-3. Undeformed shape of solar panel.

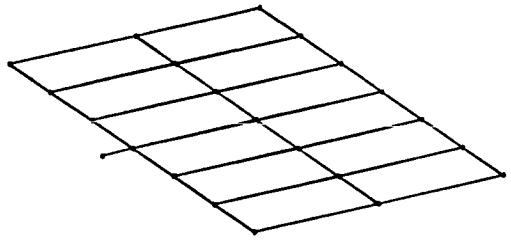

Figure II-4. First mode shape of solar panel.

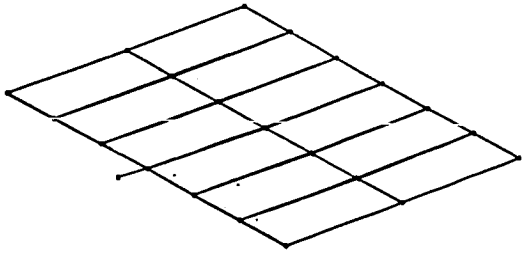

Figure II-5. Second mode shape of solar panel.

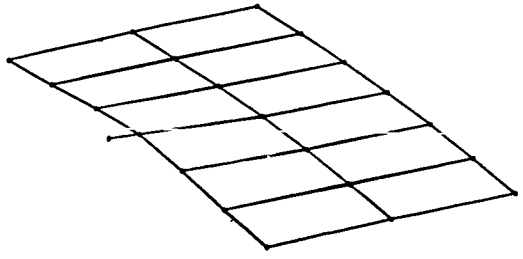

Figure II-6. Third mode shape of solar panel.

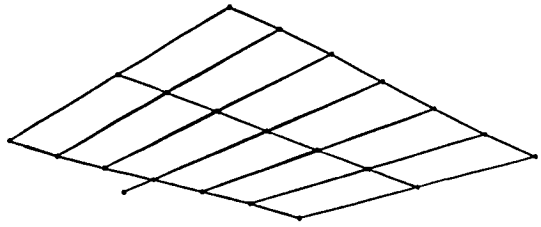

Figure II-7. Fourth mode shape of solar panel.

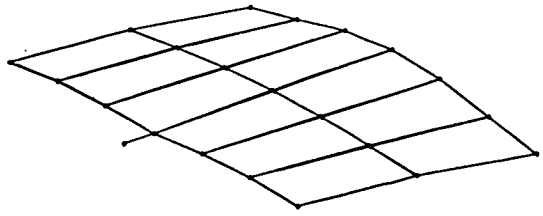

Figure II-8. Fifth mode shape of solar panel.

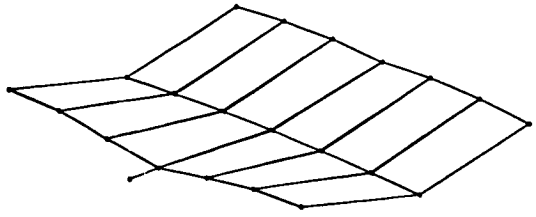

Figure II-9. Sixth mode shape of solar panel.

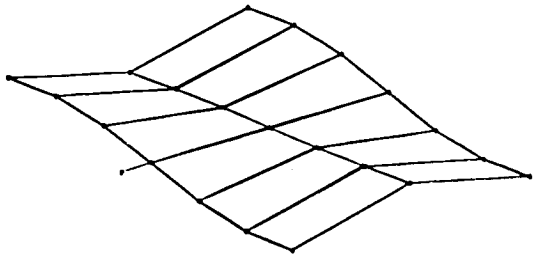

Figure II-10. Seventh mode shape of solar panel.

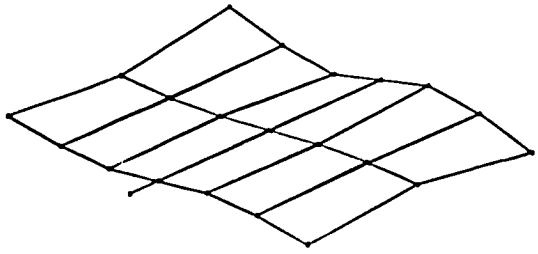

Figure II-11. Eighth mode shape of solar panel.

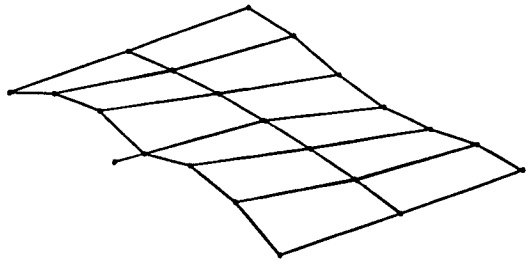

Figure II-12. Ninth mode shape of solar panel.

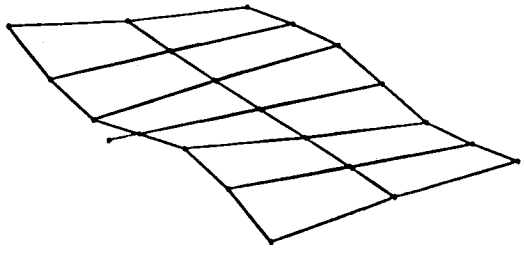

Figure II-13. Tenth mode shape of solar panel.

The acceleration response of the outermost tip of the array to a 1.0 g sinusoidal load was also calculated and the results are plotted in Figure II-14. In summary, the solar array substrate, support structure, and overall configuration are adequate since all of their requirements are easily fulfilled. The configuration also allows design leeway for any problems that may arise as the depth of the design and analysis progresses.

D. Structural System Analysis

1. Dynamic Characteristics. To make an evaluation of on-orbit performance such as the resultant pointing error due to structural vibration excited by the eccentric forces of the CMGs, it is necessary to know the dynamic response characteristics of the system. As the first step toward obtaining the response characteristics, the natural frequencies and their corresponding mode shapes should be calculated for the deployed LST. The frequency range of possible disturbing forces or moments will dictate the number of natural frequencies required in the frequency response analysis.

a. Model Description. An idealized, discrete element, dynamic model of the LST reference design was constructed, as shown in Figure II-15. The LST design is represented by 30 lumped masses, interconnected by 29 massless elastic bar elements. Except for masses 3, 4, and 6, each mass in the model is free to move along and to rotate about the three principal axes used to define the motion of the spacecraft. Masses 3, 4, and 6 are related to the solar panel and are constrained so that the elastic deformation of the support ring is neglected. This assumes that the bar members between masses 3 and 4, and 3 and 6 are infinitely rigid. The motion of the LST is represented by the 168 independent coordinates; 162 coordinates define the elastic motion and 6 coordinates define the rigid-body motion of the spacecraft.

As shown in Figure II-15, the light shield is extended from the meteoroid shield and is supported, with meteoroid shield and main light baffle, by the SSM at node 12. The primary mirror (mass 16) and the scientific instrument package (SIP) (mass 15) are connected to the primary ring at node 14. Two solar panels are extended outward from node 3. The main body of the spacecraft consists of the SSM and the metering truss. The coordinate locations of each mass as measured from an origin at the center of the docking port are shown in Table II-3.

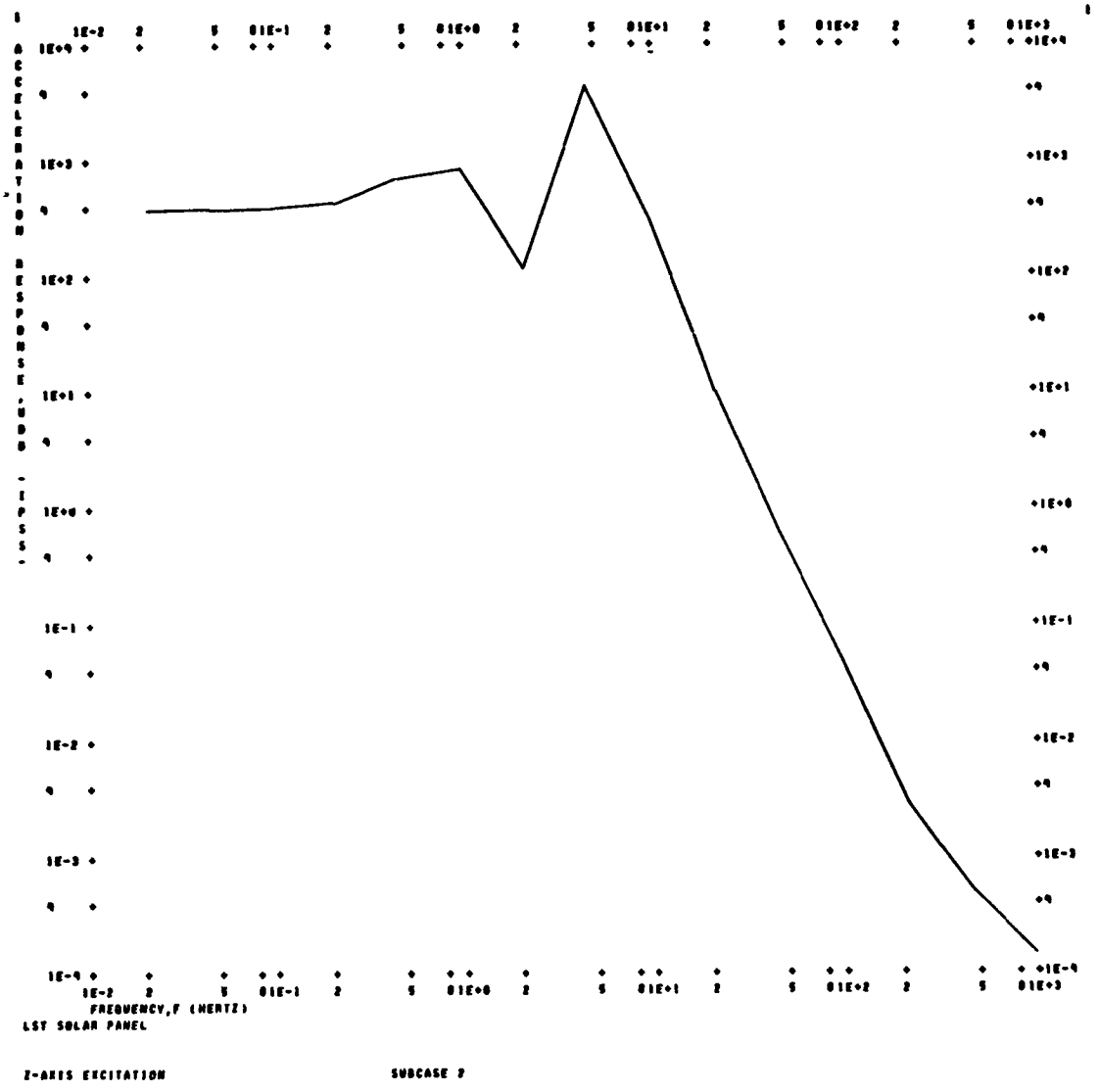

Figure II-14. Maximum solar panel acceleration response due to 1.0 g sinusoidal acceleration.

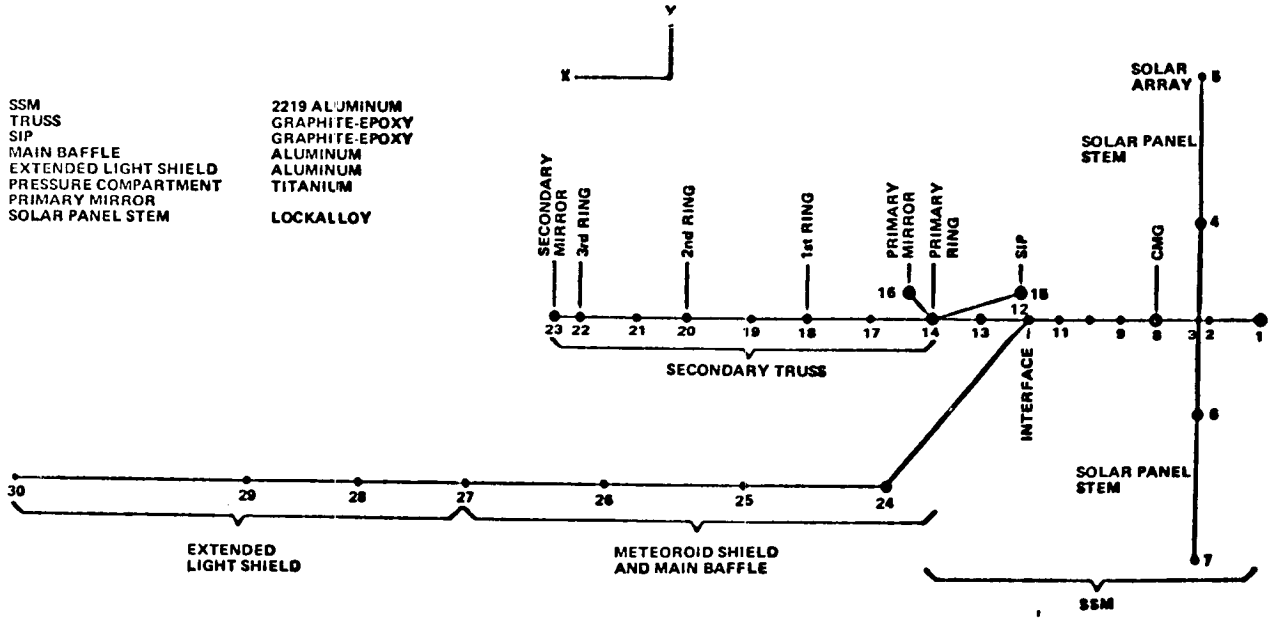

Figure II-15. Dynamic model of LST design reference.

TABLE II-3. COORDINATES OF LUMPED MASS LOCATIONS OF LST DESIGN REFERENCE

Mass	X		Y		Z	
	mm	in.	mm	in.	mm	in.
1	0	0	0	0	0	0
2	813	32.0	0	0	0	0
3	965	38.0	0	0	0	0
4	965	38.0	1524	60.0	0	0
5	965	38.0	3810	150.0	0	0
6	965	38.0	-1524	-60.0	0	0
7	965	38.0	-3810	-150.0	0	0
8	1 651	65.0	0	0	0	0
9	2 197	86.5	0	0	0	0
10	2 667	105.0	0	0	0	0
11	3 137	123.5	0	0	0	0
12	3 607	142.0	0	0	0	0
13	4 356	171.5	0	0	0	0
14	5 105	201.0	0	0	0	0
15	3 683	145.0	0	0	0	0
16	5 474	215.5	0	0	0	0
17	6 073	239.1	0	0	0	0
18	7 038	277.1	0	0	0	0
19	7 930	312.2	0	0	0	0
20	8 821	347.3	0	0	0	0
21	9 713	382.4	0	0	0	0
22	10 605	417.5	0	0	0	0
23	10 996	432.9	0	0	0	0
24	5 804	228.5	0	0	0	0
25	8 001	315.0	0	0	0	0
26	10 198	401.5	0	0	0	0
27	12 395	488.0	0	0	0	0
28	14 148	577.0	0	0	0	0
29	15 900	626.0	0	0	0	0
30	19 583	771.0	0	0	0	0

The inertial properties of each mass have been computed and are shown in Table II-4. Except for masses 4, 5, 6, and 7, which represent the solar arrays, the mass moment of inertia about the Z-axis of each mass is equal to that about its Y-axis. For masses 4, 5, 6, and 7, the mass moment of inertia about the Z-axis of each mass is equal to that about the X-axis. The mass moments of inertia for each mass except those for the solar arrays were computed by assuming axisymmetric distribution about the X-axis and uniform distribution within each bar element. The total mass is 7642 kg (16 812 lb), which is the earlier estimate of the deployed LST mass excluding the 251 kg (553 lb) shroud adapter.

The structural properties of the connecting bar members of the dynamic model are shown in Table II-5. These members are finite structural elements which possess extensional, shear, and bending stiffnesses.

For the stringer stiffened cylindrical shells, e. g., meteoroid shield and SSM, the stringers were smeared and equivalent monocoque shell thicknesses ($\bar{t}$) were computed. The area moments of inertia were then computed on the basis of equivalent thicknesses ($\bar{t}$). For the metering truss, actual areas of strut members were used in the computation of the total bar cross-sectional area and the area moments of inertia.

The shear correction factor, k, for a cylindrical shell is given in Reference II-3. For the cylindrical truss, the shear correction factor is estimated to be 0. 45 by trial and error, i. e., comparing the natural frequencies of the equivalent cantilever beam and the cantilever truss supported by the primary ring.

b. Natural Frequencies. To locate the peak values in the frequency response spectra, the natural frequencies and their corresponding mode shapes were calculated. These natural frequencies were input to the response amplitude computation.

Table II-6 shows the first 25 natural frequencies and their mode shape characteristics. The first 10 modes are dominated by the motions of the solar arrays. Modes 17 through 22 are main body bending modes. Except for the extensional and torsional modes, the natural frequencies appear as pairs with slight differences because of the effect of the solar arrays.

TABLE II-4. INERTIAL PROPERTIES OF LST DESIGN REFERENCE DYNAMIC MODEL

Mass Point	Mass[a]		I_x[b]		I_y[b]	
	kg	lbf-sec^2/in.	kg-m^2	lbf-in. sec^2	kg-m^2	lbf-in. sec^2
1	19.322	1.324	33.95	3 606	18.04	1 916
2	26.342	1.805	71.80	7 626	35.90	3 813
3	17.498	1.199	47.70	5 066	24.10	2 560
4	2.831	0.194	0.0188	2	0.0188	2
5	7.560	0.518	7.22	767	19.67	2 089
6	2.831	0.194	0.0188	2	0.0188	2
7	7.560	0.518	7.22	767	19.67	2 089
8	52.641	3.607	143.49	15 240	73.41	7 797
9	7.749	0.531	21.12	2 244	10.73	1 140
10	7.166	0.491	19.53	2 074	9.90	1 051
11	7.166	0.491	19.53	2 074	9.90	1 051
12	14.930	1.023	58.50	6 213	31.97	3 396
13	11.223	0.769	30.59	3 249	15.99	1 698
14	65.031	4.456	177.27	18 827	88.63	9 413
15	88.221	6.045	72.58	7 709	102.31	10 866
16	177.434	12.158	212.98	22 620	106.49	11 310
17	0.482	0.033	1.53	162	0.96	102
18	1.620	0.111	5.12	544	3.22	342
19	0.482	0.033	1.53	162	0.96	102
20	1.620	0.111	5.12	544	3.21	341
21	0.482	0.033	1.53	162	0.96	102
22	2.087	0.143	6.60	701	3.30	350
23	7.297	0.500	0.76	81	0.38	40
24	18.126	1.242	57.30	6 086	35.94	3 817
25	21.730	1.489	68.70	7 296	43.09	4 576
26	22.139	1.517	69.97	7 431	43.88	4 660
27	15.032	1.030	50.98	5 414	31.03	3 296
28	11.909	0.816	40.38	4 289	23.81	2 529
29	13.952	0.956	47.31	5 025	33.07	3 512
30	3.021	0.207	10.24	1 088	8.87	933

a. Total mass = 7642 kg (43.544 lb-sec^2/in. or 16 812 lb mass).

b. I_x and I_y are the mass moments of inertia about X- and Y-axis, respectively.

TABLE II-5. STRUCTURAL PROPERTIES OF LST DESIGN REFERENCE DYNAMIC MODEL

Member		Area		I_y[b]		I_x[b]		E[c]			
From	To	mm^2	$in.^2$	mm^4	$in.^4$	mm^4	$in.^4$	GN/m^2	10^6 $lb/in.^2$	ν[c]	k[c]
4	5	583	0.904	32.24×10^{-8}	0.7746	16.12×10^{-8}	0.3873	198.0	28.7	0.300	0.50
6	7										
3[a]	4										
3[a]	6										
1	2										
2	3										
3	8										
8	9										
9	10	28 723	44.52	3.91×10^{-2}	94 040	7.83×10^{-2}	188 080	72.4	10.5	0.312	0.50
10	11										
11	12										
12	13										
13	14										
14	15	790	1.225	1.36×10^{-4}	327.8	2.73×10^{-4}	655.6	303.4	44.0	0.224[d]	0.45
14	16	238	0.369	1.90×10^{-4}	456.0	3.79×10^{-4}	912.0	144.8	21.0	0.300	0.50
14	17										
17	18										
18	19										
19	20	1 011	1.567	2.53×10^{-3}	6 089	5.03×10^{-3}	12 080	303.4	44.0	0.224[d]	0.45
20	21										
21	22										
22	23										
12	24										
24	25										
25	26	16.458	25.51	2.80×10^{-2}	67 161	5.59×10^{-2}	134 322	303	44.0	0.224[d]	0.5
26	27										
27	28	11 755	18.22	2.00×10^{-2}	47 969	3.99×10^{-2}	95 938	72.4	10.5	0.312	0.5
28	29										
29	30	5 877	9.11	9.98×10^{-3}	23 985	2.00×10^{-2}	47 969	72.4	10.5	0.312	0.45

a. Multipoint constraints were used to simulate rigid-body motion of the ring frame.
b. I_x and I_y are area moments of inertia about X- and Y-axis, respectively.
c. E is the modulus of elasticity, ν the Poisson's ratio, and k the shear correction factor.
d. Equivalent Poisson's ratio.

TABLE II-6. DEPLOYED LST NATURAL FREQUENCY SUMMARY

Mode	Frequency (Hz)	Mode Shape Characteristics
1	0.92	Solar panel symmetrical bending — X-axis
2	0.93	Solar panel antisymmetrical bending — X-axis
3	1.07	Solar panel antisymmetrical torsional
4	1.08	Solar panel symmetrical torsional
5	1.26	Solar panel symmetrical bending — Z-axis
6	1.33	Solar panel antisymmetrical bending — Z-axis
7	3.61	Solar panel antisymmetrical bending — X-axis
8	3.62	Solar panel symmetrical bending — X-axis
9	4.91	Solar panel symmetrical bending — Z-axis
10	4.92	Solar panel antisymmetrical bending — Z-axis
11	15.88	Primary mirror bending — Y-axis
12	15.91	Primary mirror bending — Z-axis
13	19.30	SIP bending — Y-axis
14	19.51	SIP bending — Z-axis
15	25.06	SIP torsional
16	27.60	SIP torsional
17	29.02	Metering truss bending — Y-axis
18	29.07	Metering truss bending — Z-axis
19	33.83	Metering truss bending — Y-axis
20	33.96	Metering truss bending — Z-axis
21	38.14	Metering truss bending — Y-axis
22	38.16	Metering truss bending — Z-axis
23	38.21	Primary mirror extensional
24	49.28	Light shield bending — Y-axis
25	49.70	Light shield bending — Z-axis

2. Frequency Response. The translational frequency response of the LST along the Y- and Z-axis and the rotational response about these axes were computed with the NASTRAN computer program when the system was excited at the CMG location with a sinusodial force of 4.448 N (1.0 lb) amplitude and a moment of 1.356 N-m (1.0 ft-lb) amplitude. The computed outputs were plotted by the computer's plotter.

The structural damping factor used in the computation is 0.01. This is equivalent to 0.5 percent of the critical damping coefficient at resonances, i.e., when the excitation frequency coincides with each natural frequency.

Figures II-16 through II-19 show the deflections along the Y-axis and rotations about the Z-axis of the primary and secondary mirrors when they are excited by a sinusoidal force with a 4.448 N (1.0 lb) amplitude acting along the Y-axis of the CMG. Because of axisymmetry, there are no deflections along the Z-axis or rotations about the Y-axis from the force applied along the Y-axis.

Figures II-20 through II-23 show the deflections along the Y-axis and rotations about the Z-axis of the primary and secondary mirrors when they are excited by a sinusoidal moment with a 1.356 N-m (1.0 ft-lb) amplitude acting about the Z-axis of the CMG.

Figures II-24 through II-27 give the deflections along the Z-axis and rotations about the Y-axis of the primary and secondary mirrors when they are excited by a sinusoidal force with a 4.448 N (1.0 lb) amplitude acting along the Z-axis of the CMG.

Figures II-28 through II-31 show the deflections along the Z-axis and rotations about Y-axis of the primary and secondary mirror when they are excited by a sinusoidal moment with 1.356 N-m (1.0 ft-lb) amplitude acting about the Y-axis of the CMG.

The phase shifts associated with all response amplitudes shown in Figures II-16 through II-31 are also included. These phase shifts are given in degrees, the deflection amplitudes are given in multiples of 25.4 mm and inches, and the rotations are in radians.

An examination of all frequency response plots (Figures II-16 through II-31) indicates that the dynamic deflections from any disturbance at CMG location are certainly not structurally significant by themselves; however, effects on the pointing error due to structural vibrations may be significant and these are evaluated and presented in Chapter VI of this volume.

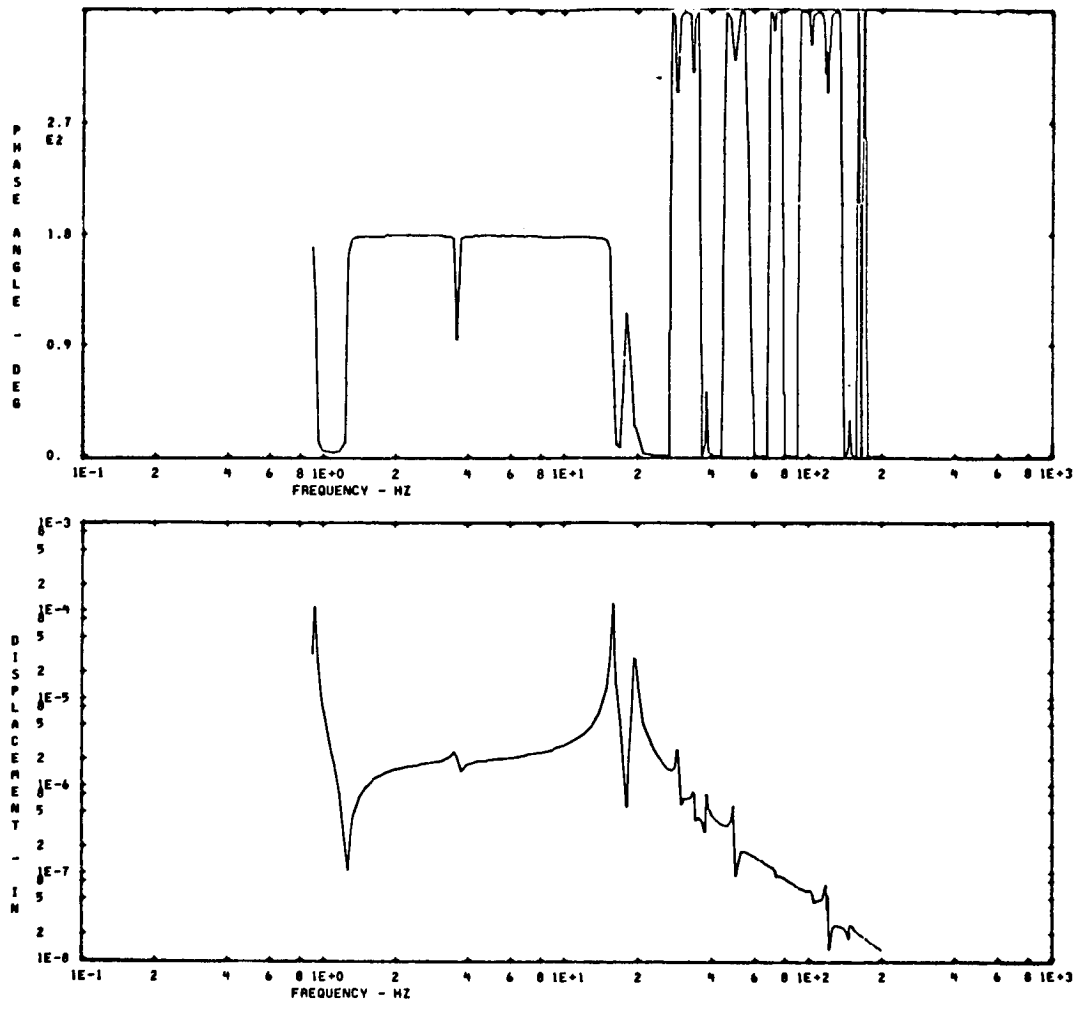

Figure II-16. Primary mirror deflection along Y-axis due to a sinusoidal force with 4.448 N (1.0 lb) amplitude acting along Y-axis at CMG.

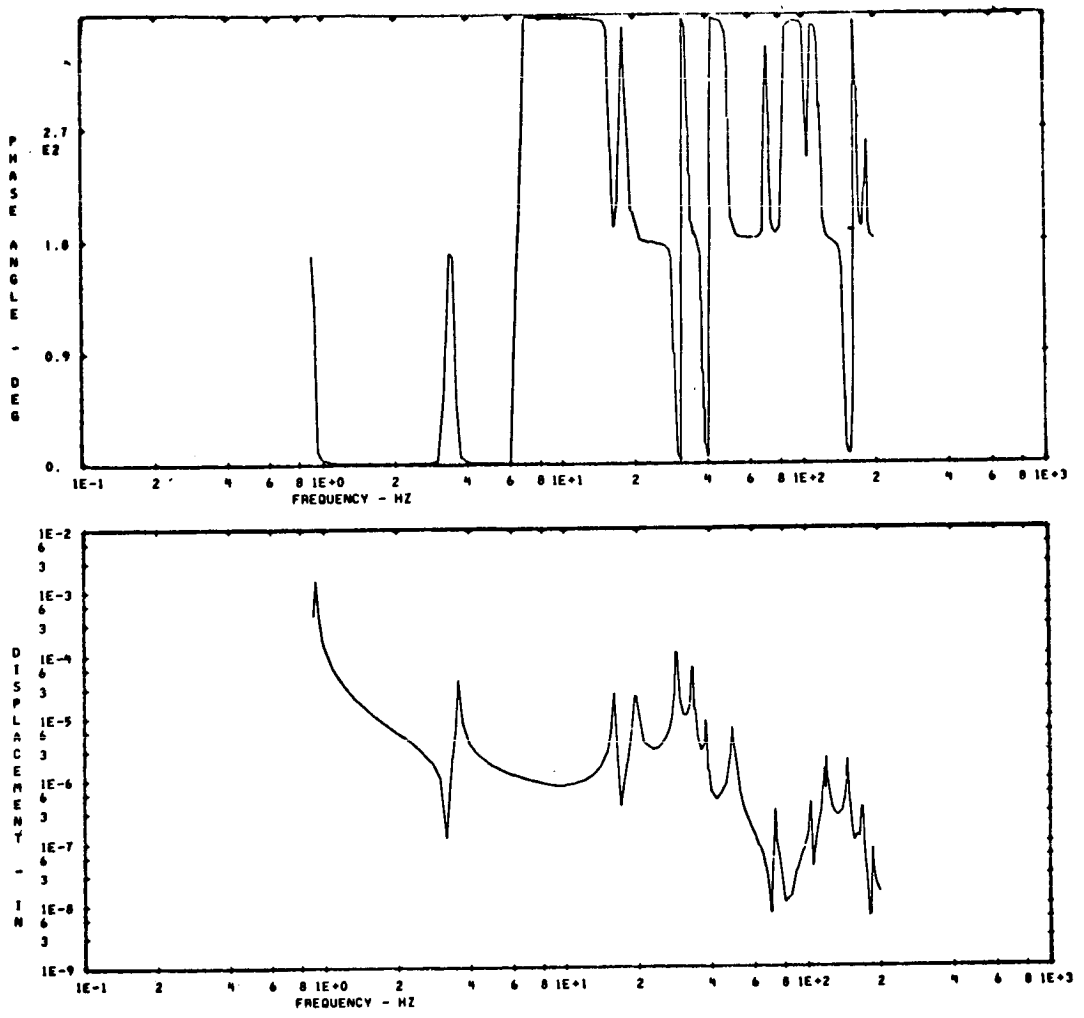

Figure II-17. Secondary mirror deflection along Y-axis due to a sinusoidal force with 4.448 N (1.0 lb) amplitude acting along Y-axis at CMG.

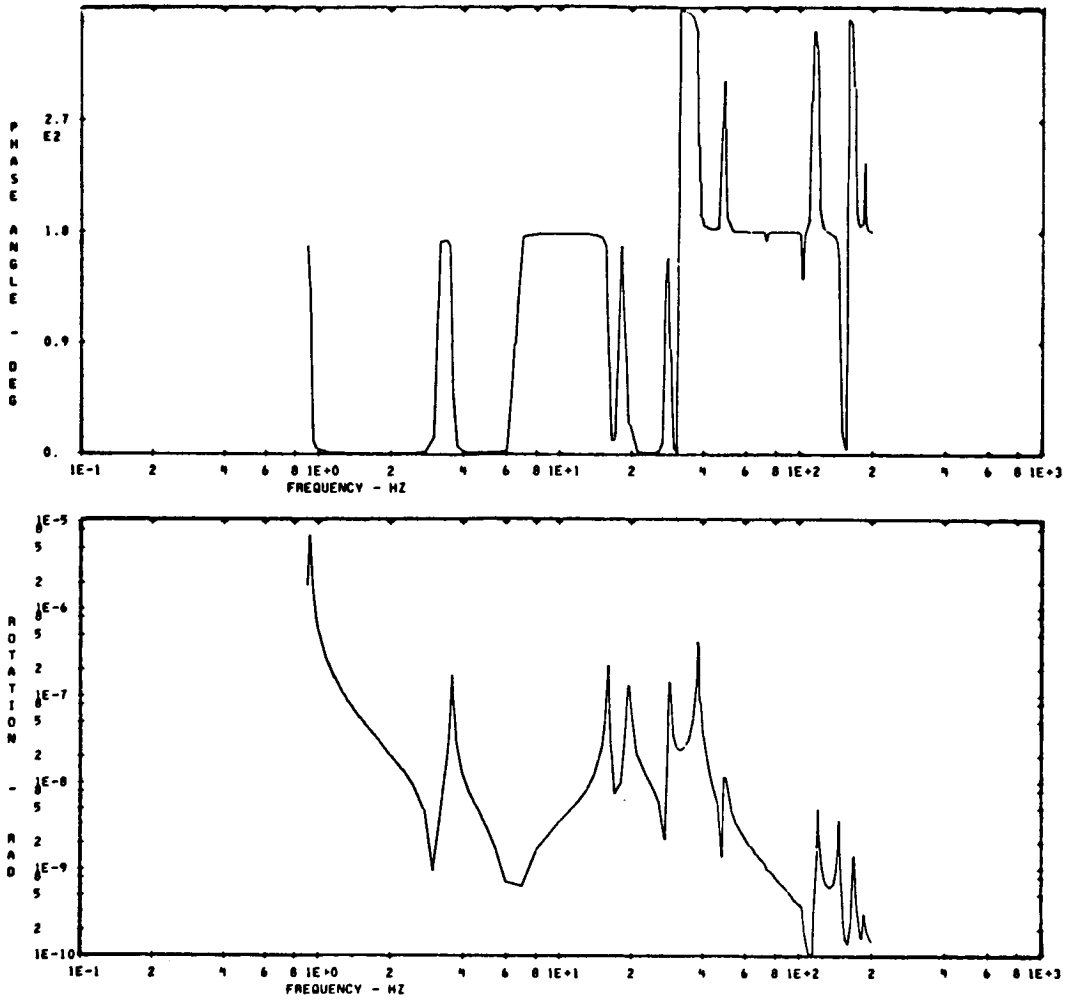

Figure II-18. Primary mirror rotation about Z-axis due to a sinusoidal force with 4.448 N (1.0 lb) amplitude acting along Y-axis at CMG.

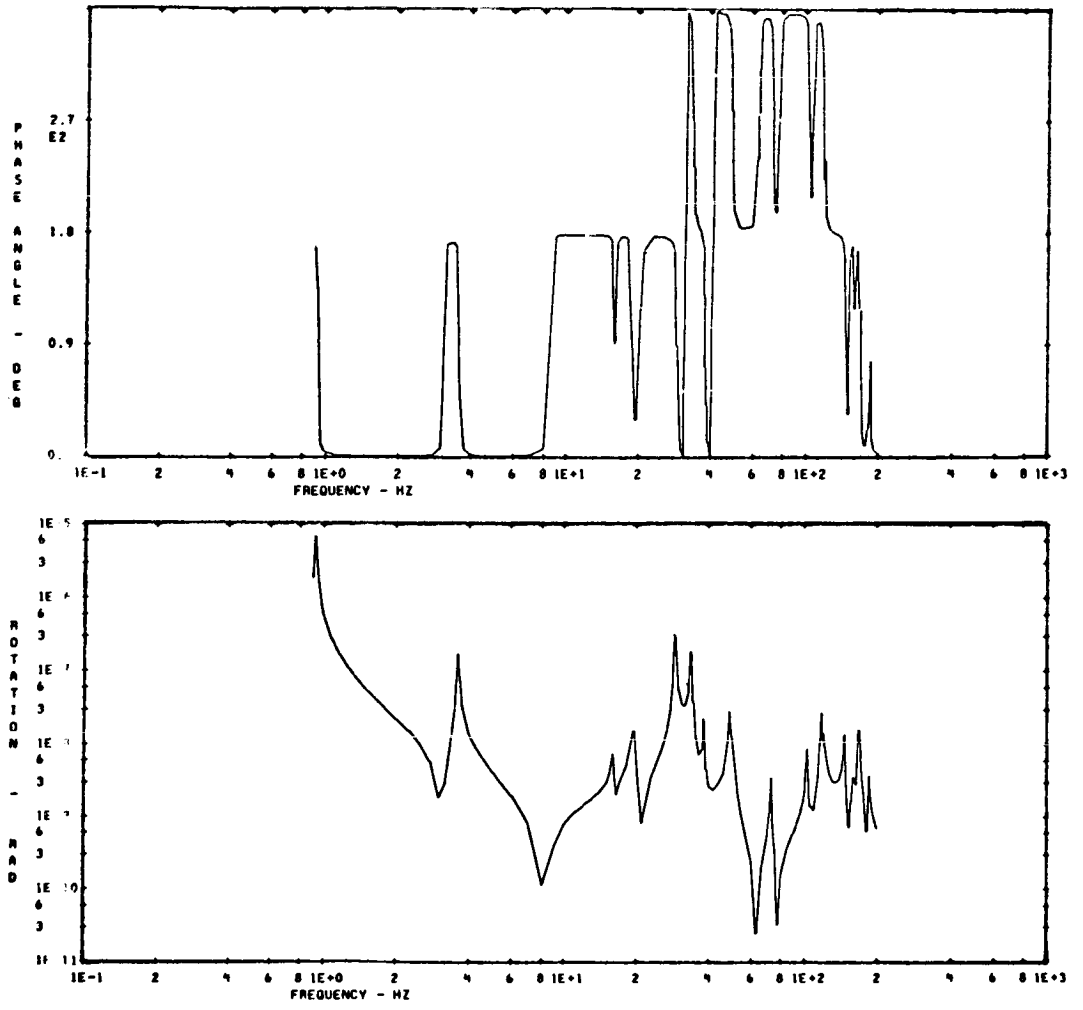

Figure II-19. Secondary mirror rotation about Z-axis due to a sinusoidal force with 4.448 N (1.0 lb) amplitude acting along Y-axis at CMG.

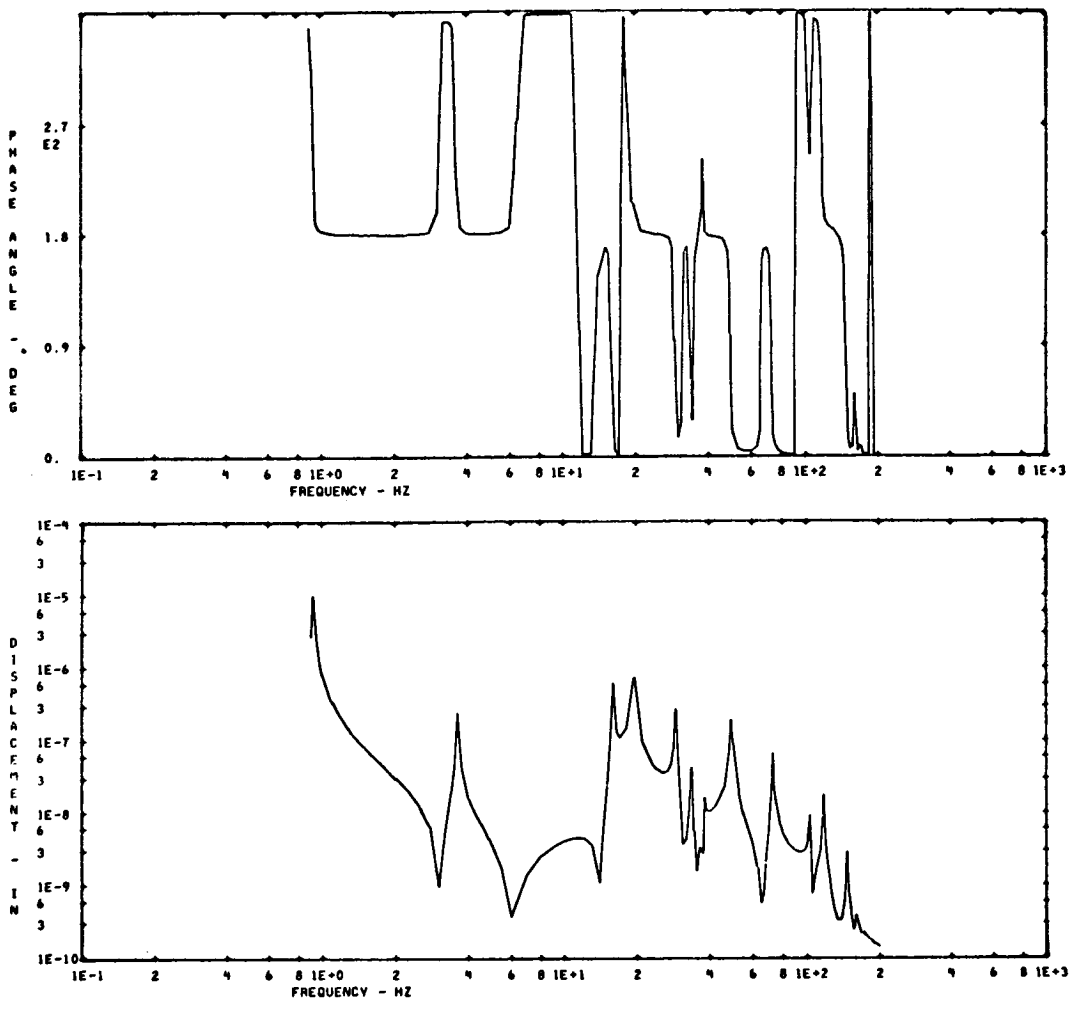

Figure II-20. Primary mirror deflection along Y-axis due to a sinusoidal moment with 1.356 N-m (1.0 ft-lb) amplitude acting about Z-axis at CMG.

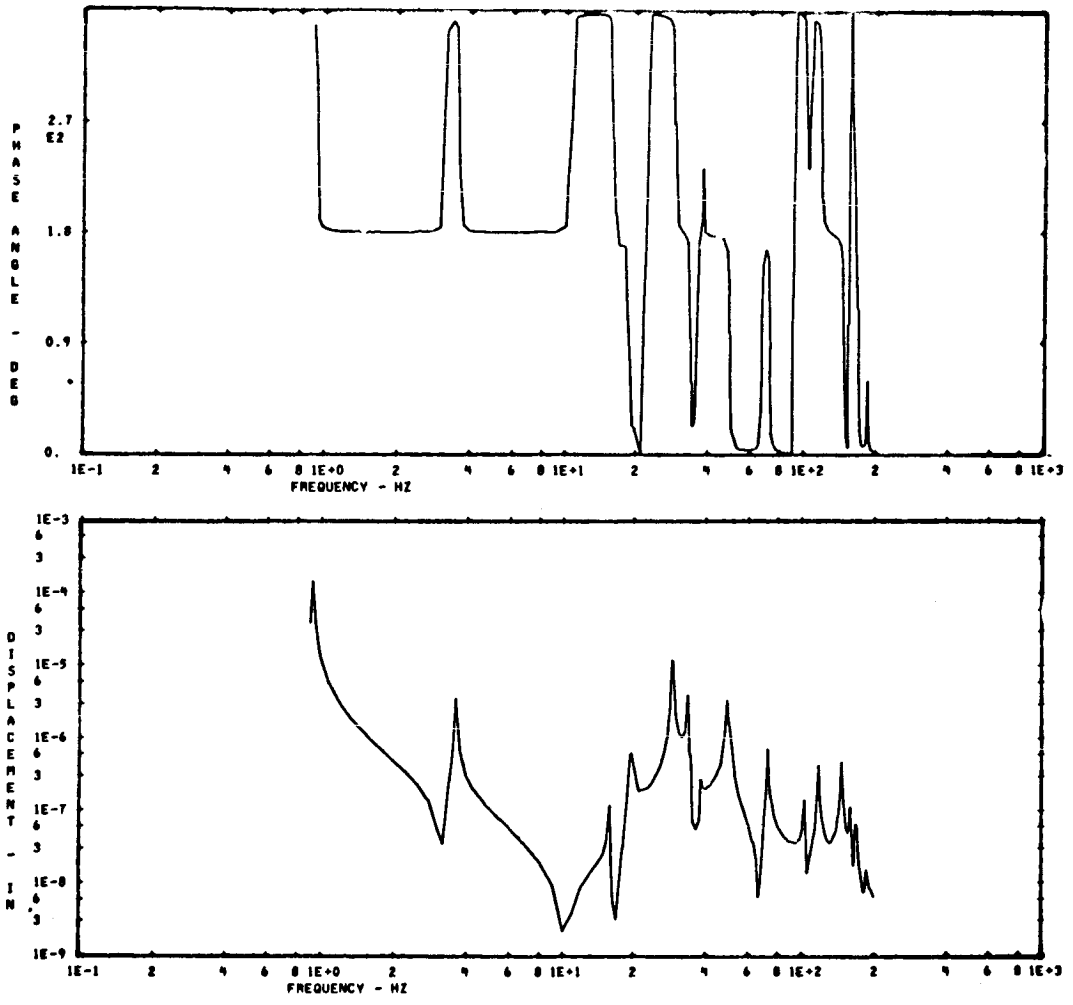

Figure II-21. Secondary mirror deflection along Y-axis due to a sinusoidal moment with 1.356 N-m (1.0 ft-lb) amplitude acting about Z-axis at CMG.

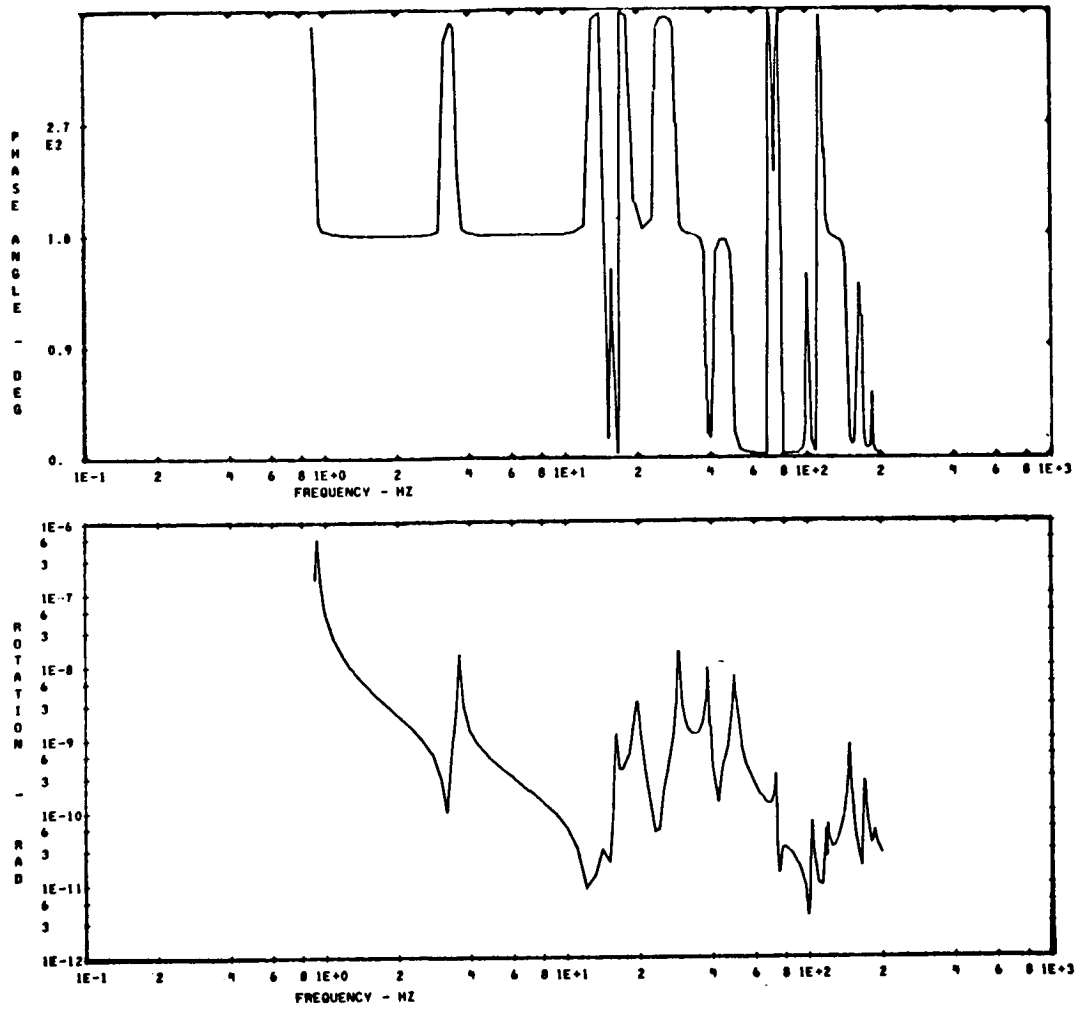

Figure II-22. Primary mirror rotation about Z-axis due to a sinusoidal moment with 1.356 N-m (1.0 ft-lb) amplitude acting about Z-axis at CMG.

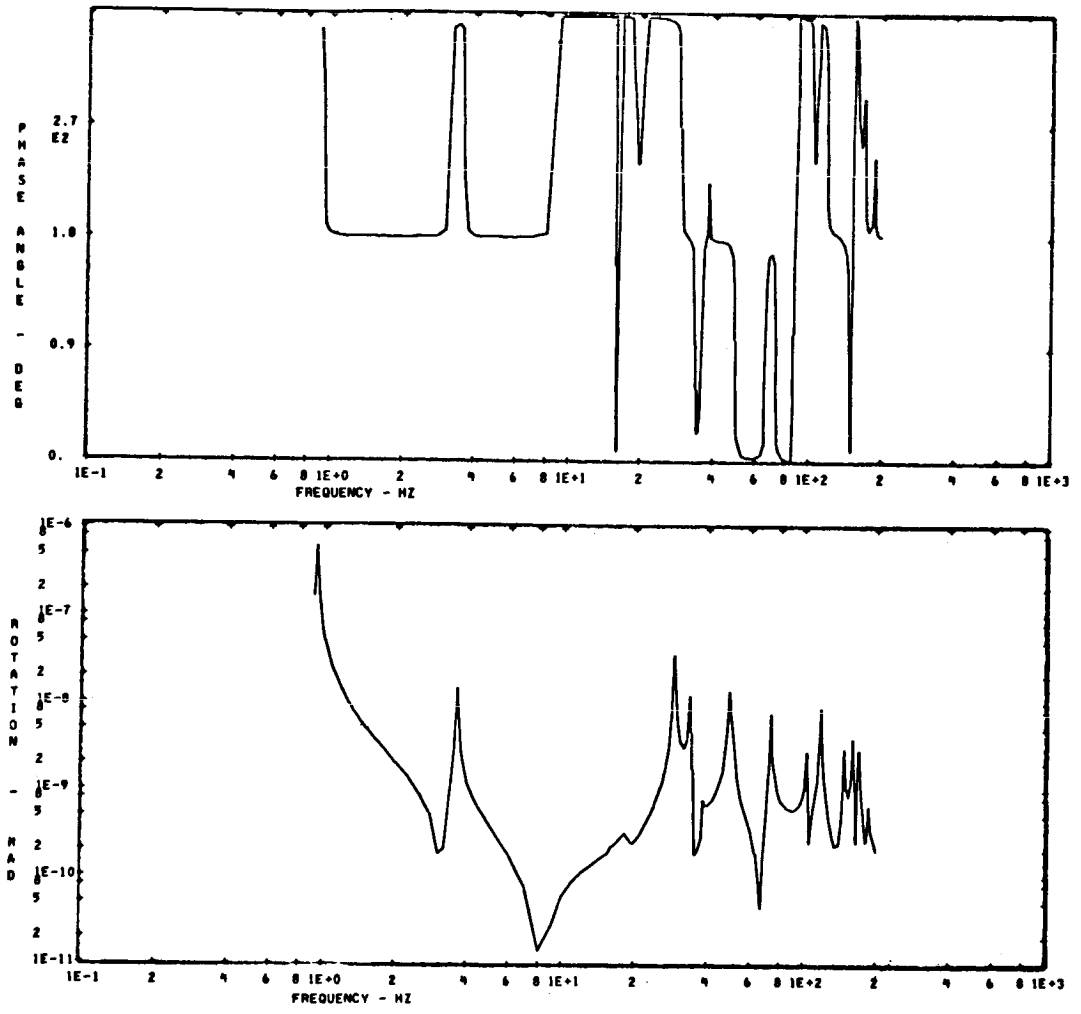

Figure II-23. Secondary mirror rotation about Z-axis due to a sinusoidal moment with 1.356 N-m (1.0 ft-lb) amplitude acting about Z-axis at CMG.

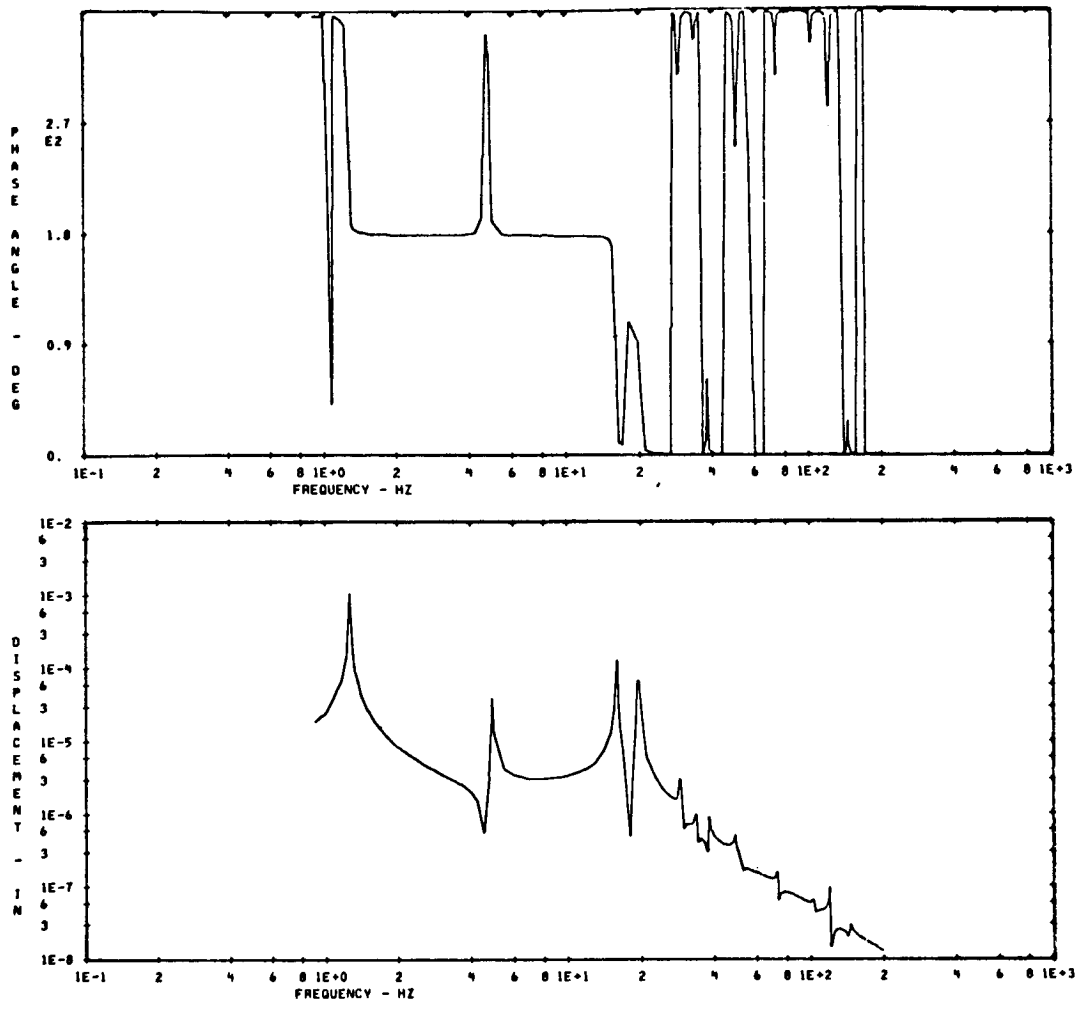

Figure II-24. Primary mirror deflection along Z-axis due to a sinusoidal force with 4.448 N (1.0 lb) amplitude acting along Z-axis at CMG.

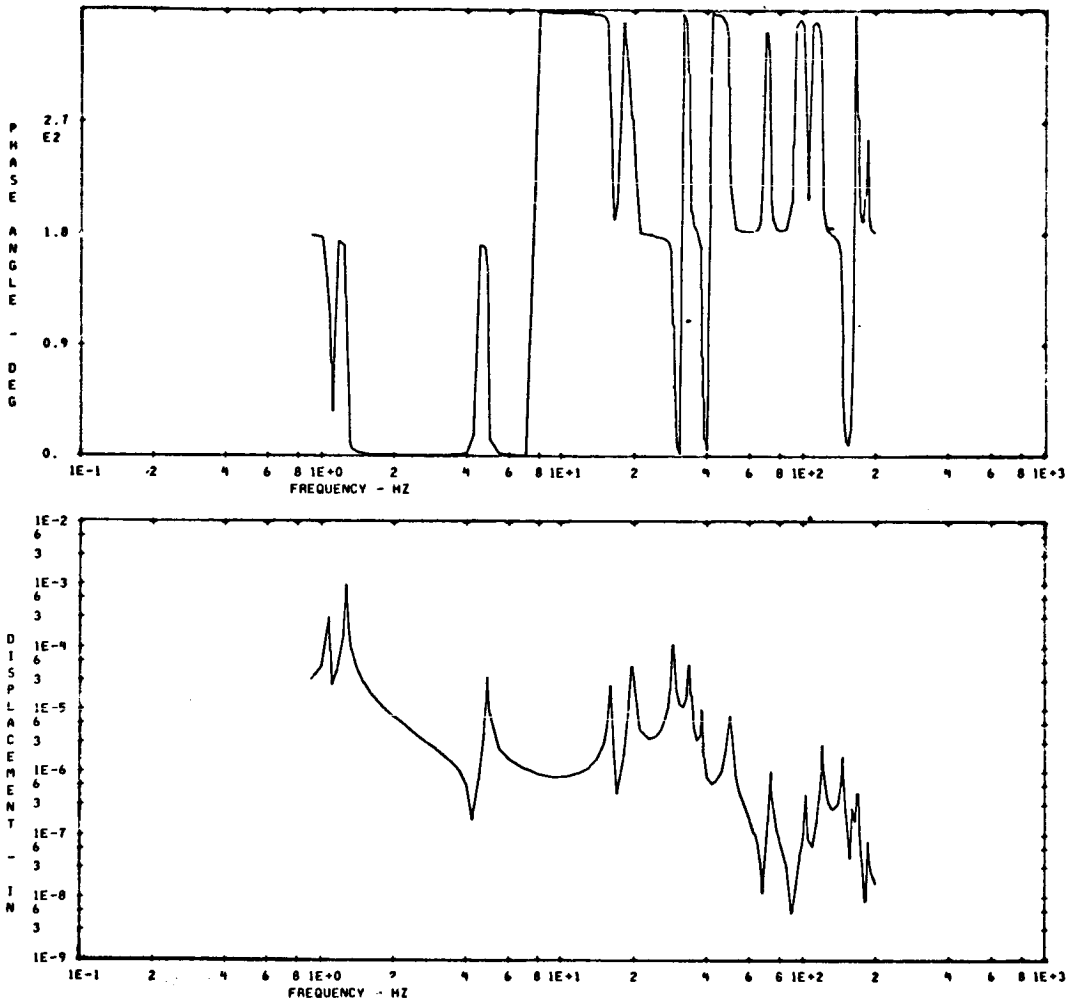

Figure II-25. Secondary mirror deflection along Z-axis due to a sinusoidal force with 4.448 N (1.0 lb) amplitude acting along Z-axis at CMG.

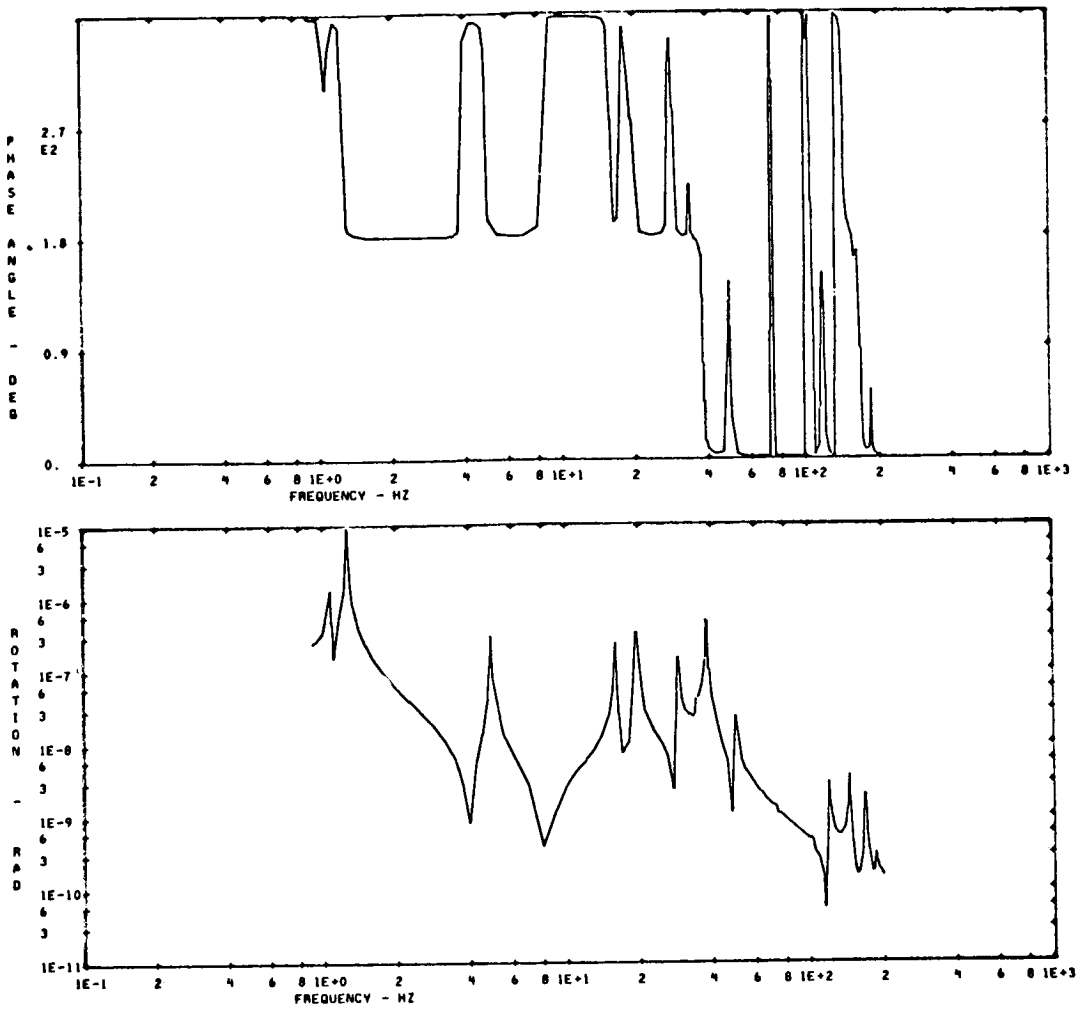

Figure II-26. Primary mirror rotation about Y-axis due to a sinusoidal force with 4.448 N (1.0 lb) amplitude acting along Z-axis at CMG.

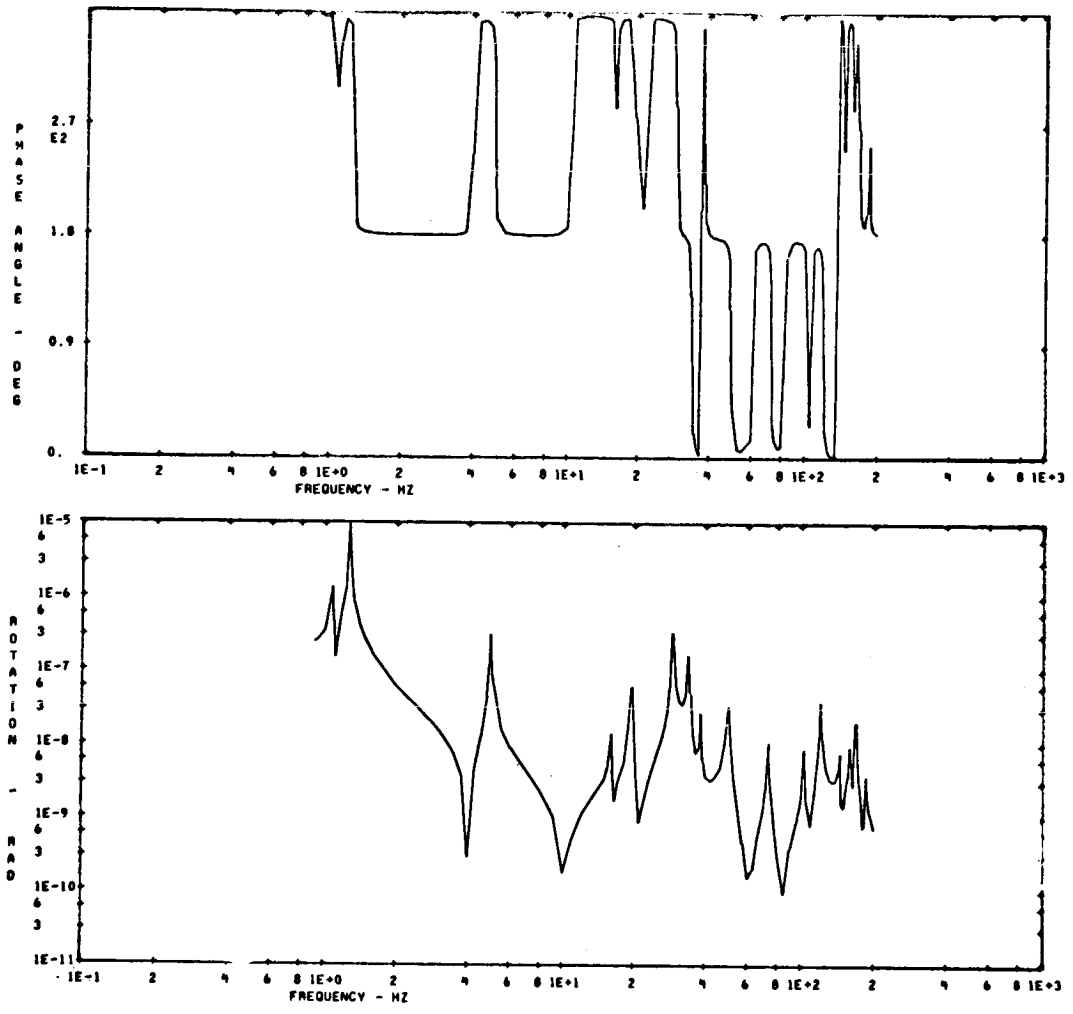

Figure II-27. Secondary mirror rotation about Y-axis due to a sinusoidal force with 4. 448 N (1. 0 lb) amplitude acting along Z-axis at CMG.

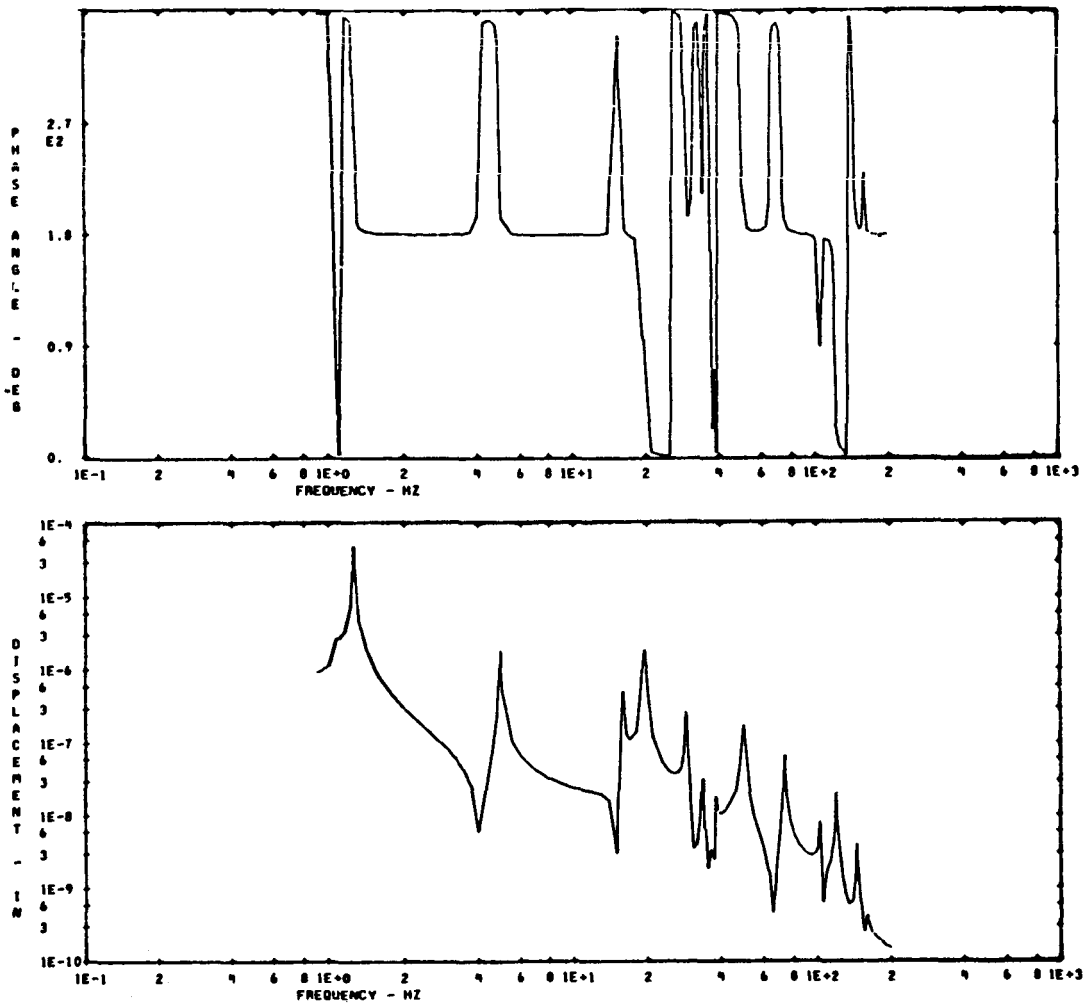

Figure II-28. Primary mirror deflection along Z-axis due to a sinusoidal moment with 1.356 N-m (1.0 ft-lb) amplitude acting about Y-axis at CMG.

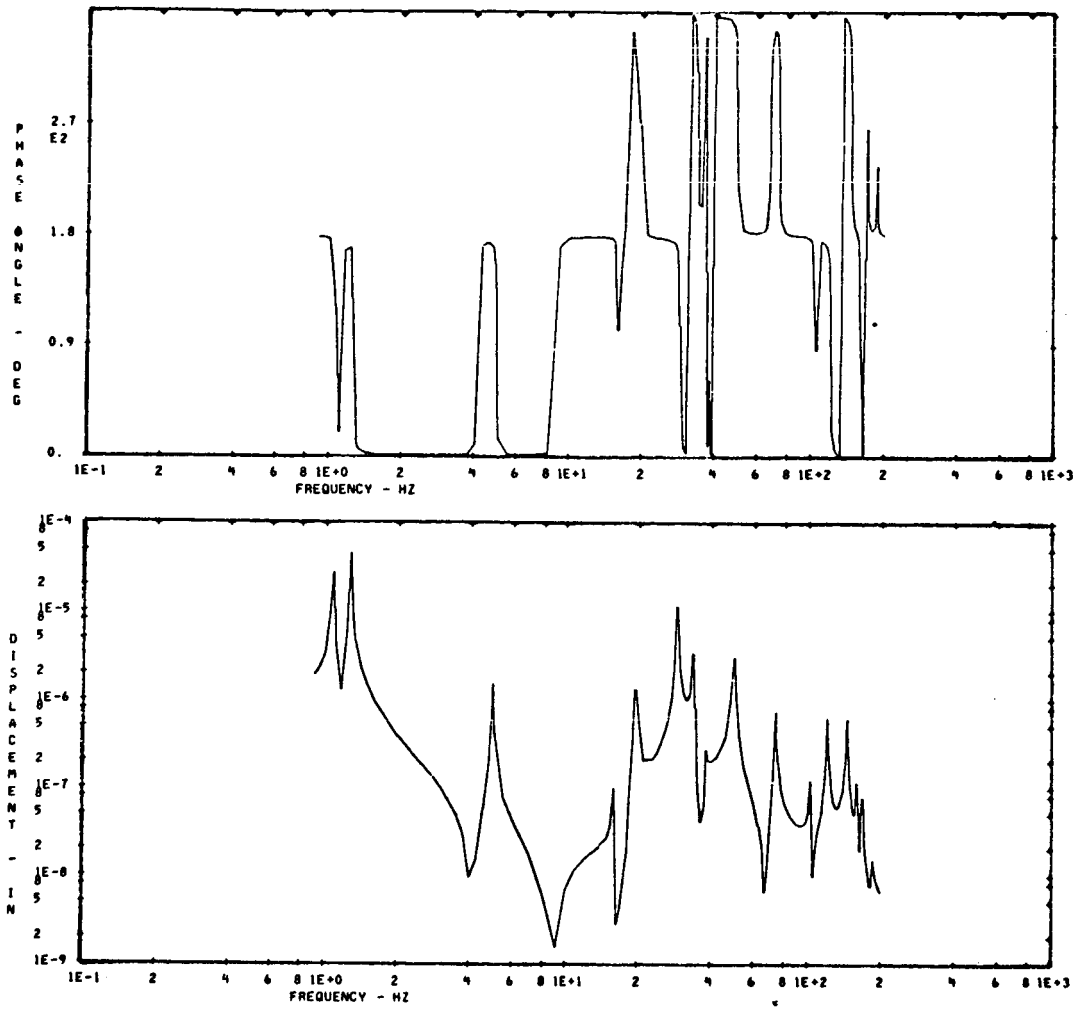

Figure II-29. Secondary mirror deflection along Z-axis due to a sinusoidal moment with 1.356 N-m (1.0 ft-lb) amplitude acting about Y-axis at CMG.

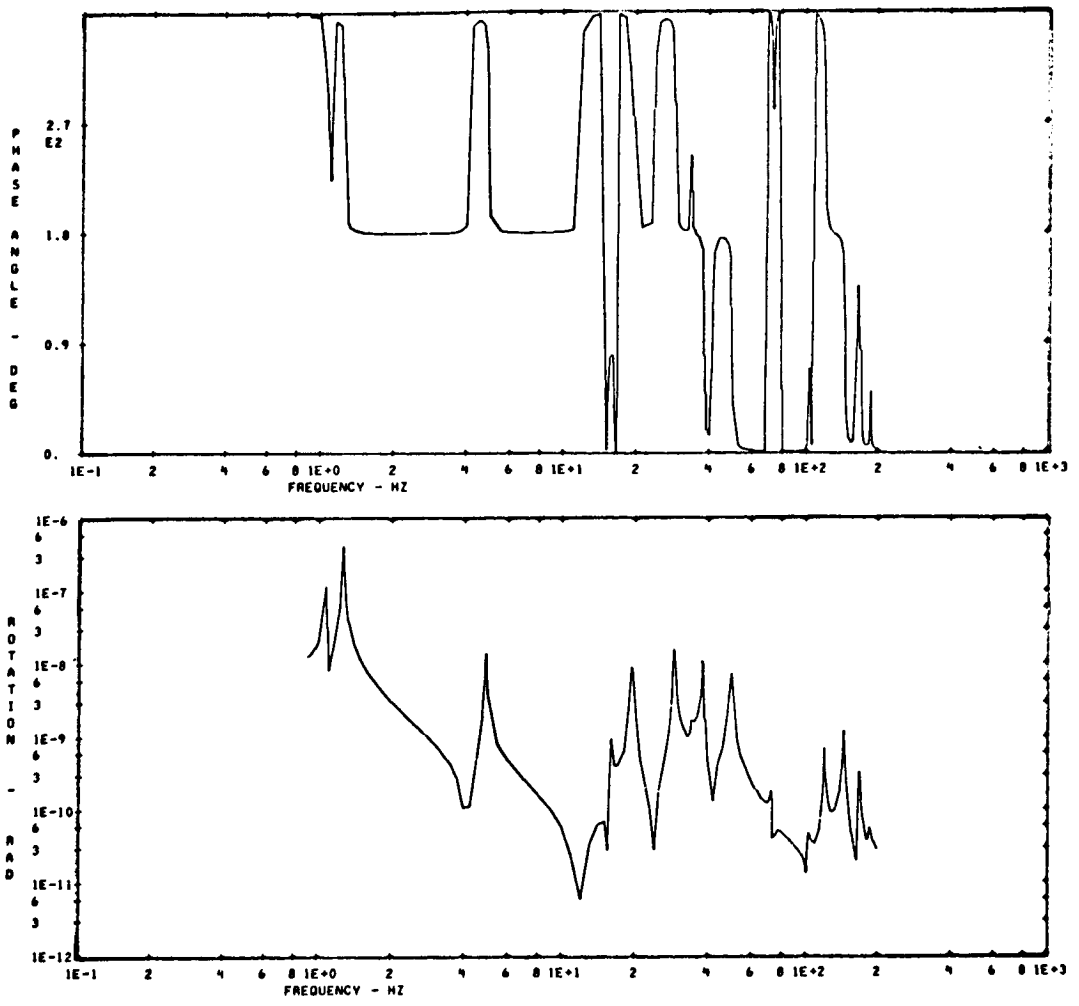

Figure II-30. Primary mirror rotation about Y-axis due to a sinusoidal moment with 1.356 N-m (1.0 ft-lb) amplitude acting about Y-axis at CMG.

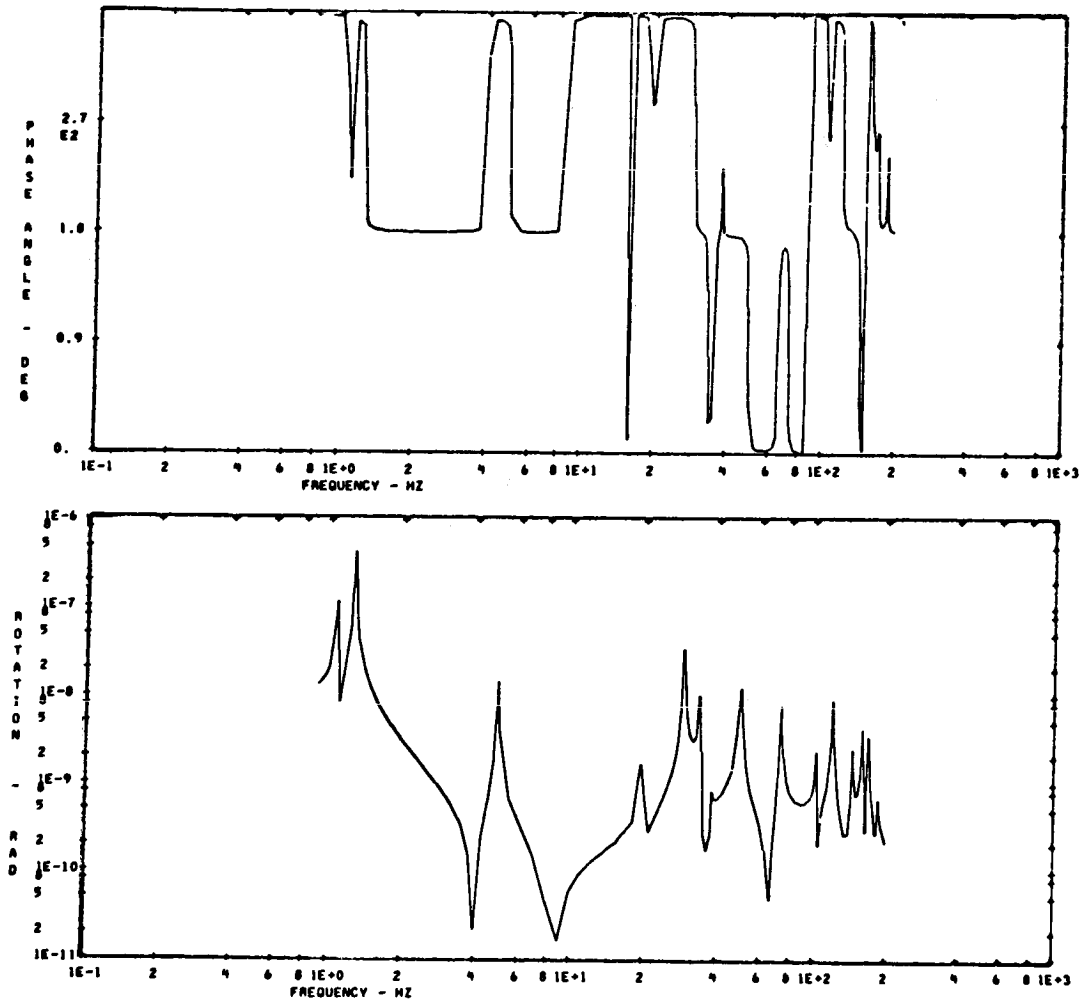

Figure II-31. Secondary mirror rotation about Y-axis due to a sinusoidal moment with 1.356 N-m (1.0 ft-lb) amplitude acting about Y-axis at CMG.

References

II-1. Manned Spacecraft Center: Space Shuttle Baseline Accommodations for Payloads. Payload Engineering Office, Future Programs Division, Engineering and Development Directorate, June 27, 1972.

II-2. Martin Marietta Corporation: Titan Payload User's Guide.

II-3. Roark, R. J.: Formulas for Stress and Strain. Fourth Ed. McGraw-Hill Book Company, 1965.

CHAPTER III. THERMAL CONTROL SYSTEM

TABLE OF CONTENTS

LIST OF ILLUSTRATIONS

LIST OF ILLUSTRATIONS (Concluded)

LIST OF TABLES

CHAPTER III. THERMAL CONTROL SYSTEM

A. Introduction and Description

The thermal control system (TCS) of the support systems module maintains the SIP and the electronic equipment within required limits with margin through all mission phases. The design philosophy is identical to that used on HEAO.

Temperature control is achieved by establishing a heat balance between the absorbed radiation (solar, albedo, and earth), internal heat dissipation, and emitted energy. High efficiency multilayer insulation, thermal covers, and coatings minimize the effect of large variations in incident radiation caused by changes in orbital parameters or LST orientation.

Components, such as the batteries, that experience large variations in internal heat dissipation during an orbit are placed in thermally independent modules. Their heat balance is closely controlled with separate louvers, radiating surfaces, cold plates, and heaters.

A small amount of thermal control heater power is provided to certain components that may require a warmer environment than provided by adjacent equipment. Commandable standby heaters are also placed on major heat dissipating system equipment to maintain a constant Observatory heat dissipation should it be necessary to turn off units for extended periods of time. The standby heaters do not impose an additional power load since they use power made available when components are turned off.

The LST-SSM heat emitted is regulated by the thermophysical characteristics of the external surfaces. Orbital excursions are also attenuated by these controlled surfaces. The surfaces are designed to maintain the Observatory thermal balance under long-term orbital, seasonal, and orientation conditions, as well as providing flexibility to respond to changes in thermal requirements during development.

During transient eclipse and short-term, off-point modes, the thermal inertia of the LST greatly facilitates temperature control. The thermal inertia also serves to maintain temperature control during short-term boost and transfer orbit conditions when incident heating and internal heat dissipation conditions are not within long-term orbital design values.

B. Hardware Description

The items described below represent the total SSM thermal control hardware deliverables. Table III-1 contains a listing of the SSM TCS hardware with corresponding descriptions and performance characteristics.

1. Louvers. Each SSM louver assembly (similar to that used on HEAO) consists of four separate blades. Each louver assembly is placed on the battery baseplate external surface viewing the pressure shell. Bimetallic actuators sense the local battery baseplate temperature and provide the torque to rotate the louver blades. The bimetallic springs are thermally coupled to the baseplate by anchoring the frame to the baseplate, painting the bimetal, isolating the louvers with fiberglass shafts, and insulating the actuator housing.

2. Insulations. The insulation installation techniques are similar to those used for other spacecraft. The 24-layer aluminized Mylar insulation is constructed as shown on Table III-1. All the blankets are made in sections to fit around the spacecraft between the pressure shell and the micrometeoroid shield. Venting occurs through the gaps and perforations in each layer. The perforations are staggered to avoid radiation heat loss.

A thermal barrier is maintained between the SIP and the SSM compartments by a polished aluminum sheet having the polished surface facing the SIP. This sheet was used in place of a thermal blanket to eliminate the need for an insulation purge due to moisture contamination during manned maintenance.

3. Paint. Zinc orthotitanate (Zn_2TiO_4), a high emittance white paint, was chosen as the design reference for the SSM external surface. Table III-2 shows a list of surface finishes considered. Zn_2TiO_4 was chosen because of its low α/ϵ ratio and low degradation alpha value of 0.005 per year. This paint is one of many being tested on the Skylab program. As a backup to the Zn_2TiO_4, a mosaic of optical solar reflectors (OSR) and white paint could be used.

4. Heaters. The heaters are standard flexible strip heaters that can be bonded to a conducting surface with a low outgassing RTV adhesive. The heaters are available in wattages from 1 to 10 at 28V. Heaters are enabled by command, after which turn-on is controlled automatically by a standard snap-acting thermoswitch. The number, size, and setting for the heaters are to be determined.

TABLE III-1. SSM THERMAL CONTROL HARDWARE DESCRIPTION

ITEM	DESCRIPTION	LOCATION	AREA (m^2)	MASS (Kg)	PERFORMANCE
LOUVER UNITS	0.5m x 0.33m - FOUR BLADE UNIT ONE PER BATTERY (1.12m^2 BATTERY) 6 TOTAL, SIZED TO HANDLE 35W (MAX) ORBITAL AVERAGE BATTERY HEAT DISSIPATION AT 10°C	-Z, +Y, AND -Y AXIS ON PRESSURE SHELL SURFACE, FOR EACH BATTERY BASE PLATE.	6.72	5.6	ϵ OPEN = 0.7 AT 14°C ϵ CLOSED = 0.22 AT 6°C
EXTERNAL SURFACE INSULATION	24 LAYERS OF ALUMINIZED MYLAR: (1) - 1 MIL COVER SHEET ALUMINIZED SIDE FACES INWARD (22) - ¼ MIL CRINKLED FILLER SHEETS - ALUMINIZED SIDE FACES INWARD[a] WITH 4-1/8" DIA. VENT HOLES PER SQ. FT. (1) - 1 MIL INNER COVER SHEET - ALUMINIZED SIDE FACES INWARD	OUTSIDE OF THE PRESSURE SHELL OVER THE AREA USED TO DUMP HEAT FROM SIP	29.0	11.0	$\frac{K}{\Delta X} = 0.009 \frac{W}{m^2\ °C}$
INTERNAL INSULATION	POLISHED ALUMINUM SHEET	COVERING ALL ELECTRONIC EQUIPMENT SO SIP IS NOT AFFECTED BY SSM	6.0	3.3	ϵ = 0.04 SURFACE FACING SIP
PAINT	Zn_2 Ti 0_4 (ZINC ORTHOTITANATE)[b]	OUTSIDE COVER OF MICROMETEOROID SHELL INSIDE PRESSURE SHELL	39.1	16.0	α = 0.120 ϵ = 0.92
	HIGH EMITTANCE WHITE		38.0	15.1	$\epsilon = 0.85^2$
	BLACK	INSIDE MICRO-METEOROID SHIELD	39.0	15.8	$\epsilon = 0.85^2$
HEATERS	THERMOSTATICALLY CONTROLLED RESISTANCE TYPE PT-4-B-13004	AS REQUIRED	4.0	5.5	≈250W

a. RECOMMENDED MATERIALS TO MEET NASA ATM 50M02442 (LOW OUTGASSING SPECIFICATION).
b. THIS IS A NEW PAINT. RESEARCH TEST DATA α DEGRADES 0.005/YR WILL BE A TEST PAINT ON SKYLAB.

TABLE III-2. THERMAL CONTROL COATINGS CONSIDERED

COATING	a	ϵ	a/ϵ	UV DEGRADATION RESISTANCE	HANDLING EASE
S-13G	0.19	0.91	0.21	POOR	GOOD
Z-93	0.18	0.87	0.20	FAIR	POOR
ALZAK	0.15	0.75	0.20	FAIR	GOOD
OSR	0.05 TO 0.1	0.70 TO 0.80	0.06 TO 0.15	EXCELLENT	POOR TO FAIR
GSFC 101	0.19	0.91	0.21	POOR	GOOD
TiO_2	0.22	0.91	0.24	POOR	GOOD
$Zn_2\ TiO_4$	0.12	0.92	0.13	Δa = 0.005/YR GOOD	GOOD

C. Requirements Versus Capabilities

The requirements imposed on the SSM thermal control system are expressed in terms of the allowable temperature ranges of the electronic equipment, as follows (see also guidelines in Volume II, Chapter IV):

Component	Allowable Temperature Range (°C)
Communications Equipment	-10 to 50
Data Handling Equipment	-18 to 60
Attitude Control Equipment	-10 to 55
Solar Cells	Less than 100
Batteries	5 to 15
Other Electrical Power Components	-18 to 50

Six vehicle orientations that were considered in the thermal analysis are shown in Figure III-1. The reliability requirement for the thermal control system was 0.95 for 1 year.

The baseline thermal control design fulfills all the design requirements imposed by the various vehicle environments. The environmental data shown in Table III-3 were used in all subsequent thermal calculations. The heat load contingency allowed for growth was 700 watts in the SSM (100 percent) and 200 watts (50 percent) in the SIP.

D. Design Substantiation

1. Thermal Analysis of Support Systems Module. Work summarized in this section is the result of a thermal control study performed on the design reference configuration. The objective of this study was to determine whether proposed locations and mounting techniques were suitable to keep the system components within their required operating temperature range.

CASE I -- ORBITAL ANGLE β = 52° SPACECRAFT LONGITUDINAL AXIS PARALLEL TO SUN	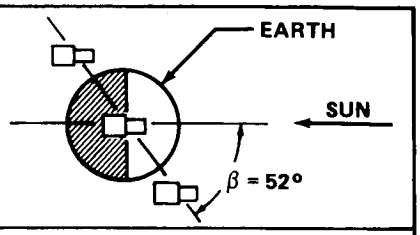
CASE II -- ORBITAL ANGLE β = 52° SPACECRAFT LONGITUDINAL AXIS PERPENDICULAR TO SUN	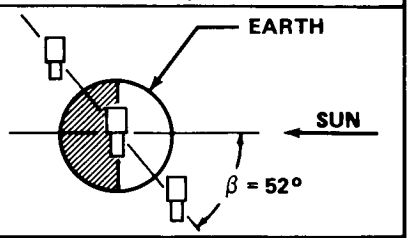
CASE III -- ORBITAL ANGLE β = 52° SPACECRAFT LONGITUDINAL AXIS INCLINED 45° TO SUN	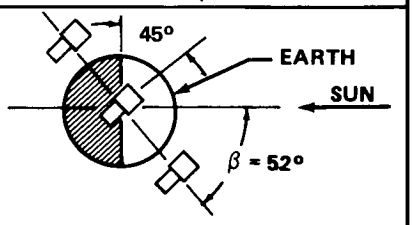
CASE IV -- ORBITAL ANGLE β = 0° SPACECRAFT LONGITUDINAL AXIS PARALLEL TO SUN	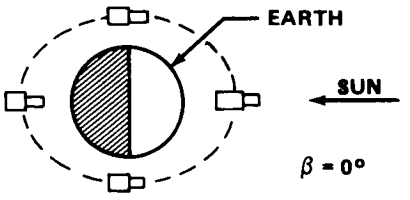
CASE V -- ORBITAL ANGLE β = 0° SPACECRAFT LONGITUDINAL AXIS PERPENDICULAR TO SUN	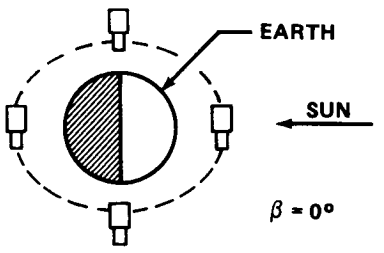
CASE VI -- ORBITAL ANGLE β = 0° SPACECRAFT LONGITUDINAL AXIS INCLINED 45° TO SUN	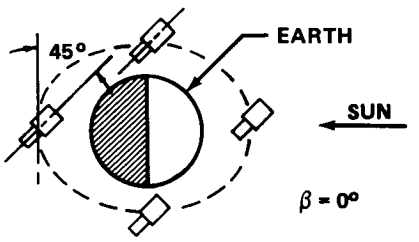

Figure III-1. Spacecraft orbits/orientations considered in thermal analysis.

TABLE III-3. ENVIRONMENTAL DATA USED IN ANALYSIS

MISSION PHASE	PRELAUNCH SHUTTLE	SHUTTLE OPERATIONS			ORBITAL OPERATIONS		
		ASCENT	ORBIT	DESCENT	SCAN[b]	OFF POINT[c]	OFF POINT[d]
1. AMBIENT[a] TEMPERATURES							
MAXIMUM (°C)	36	65.5	65.5	93.3	-12.8	-12.8	-12.8
NOMINAL (°C)	21				--	--	--
MINIMUM (°C)	-1	4.4	-73.3	-73.3	-273	-273	-273
2. SOLAR HEATING[a]							
MAXIMUM (W/m^2)	946				1400	1400	1400
NOMINAL (W/m^2)	473				1353	1353	1353
MINIMUM (W/m^2)	0				1309	1309	1309
3. ALBEDO[a]							
3 MAXIMUM (W/m^2)	–				650	650	650
NOMINAL (W/m^2)	–				406	406	406
-3 MINIMUM (W/m^2)	–				162	162	162
4. EARTH EMISSION							
3 MAXIMUM (W/m^2)	–				298	298	298
NOMINAL (W/m^2)	–				237	237	237
-3 MINIMUM (W/m^2)	–				176	176	176
5. OBSERVATORY ORIENTATION WITH SUN (ANGLE BETWEEN +Z AXIS AND SUN VECTOR)							
MAXIMUM (DEG)	180	–	–	–	--	45	180
NOMINAL (DEG)	--				--	--	--
MINIMUM (DEG)	0				0	0	0
6. ORBIT ALTITUDE CIRCULAR (KM)	0	0	611	0	611	611	611
7. ORBIT PERIOD (MIN)	0	0	96.9	0	96.9	96.9	96.9

a. SOLAR, ALBEDO, & EARTH EMISSION NOMINAL AND 3 σ VALUES OBTAINED FROM NASA TM X-64627
b. SCAN +Z AXIS POINTED AT SUN (LONG TERM)
c. OFF POINT +Z AXIS POINTED 45 DEG FROM SUN (LONG TERM)
d. OFF POINT +Z AXIS POINTED UP TO 180 DEG FROM SUN (SHORT TERM)

Passive thermal control consisting of insulation and thermal control coatings is utilized as much as possible. Because of the variation in the spacecraft external environment (due to changes in orbit and spacecraft orientations), resistance heaters are required for some components. These components must be mounted so they will not exceed their maximum limits during peak environmental heating. With this condition satisfied, some components would go below their minimum operating limit during a cold orbit or spacecraft orientation. For this reason, heaters and/or louvers are required.

a. Guidelines and Assumptions. The following guidelines and assumptions were used in performing this analysis:

1. Thermal Properties of Materials and Surfaces:

a. Aluminum — $K = 166 \frac{J}{\text{sec m } ^\circ K}$, $C_p = 0.881 \frac{J}{g\ ^\circ K}$, $\rho = 2.706 \frac{g}{cm^3}$.

b. Multilayered Insulation — $K_\perp = 8.65 \times 10^{-5} \frac{J}{\text{sec m } ^\circ K}$, $C_p = 1.25 \frac{J}{g\ ^\circ K}$, $\rho = 0.040 \frac{g}{cm^3}$, $K_\parallel = 0.0519 \frac{J}{\text{sec m } ^\circ K}$.

c. Meteoroid Shield (external) $\alpha = 0.135$,[1] $\epsilon = 0.92$.
(internal) $\epsilon = 0.5$.

d. Pressure Wall (both sides) $\epsilon = 0.5$.

2. Orbit:

a. Circular at an Altitude of 611 km.

b. 28.5 Degrees Inclination to the Equator.

b. Analytical Approach. The SSM component layout utilized in this analysis is presented in Figure III-2. The component identification numbers are given in the Master Equipment List in Chapter I of this volume. This layout was selected to meet structural, contamination control and thermal requirements. Components located on the aft conical pressure shell are separated from the internal environment by a polished aluminum sheet.

1. Accounts for 3 years worth of degradation.

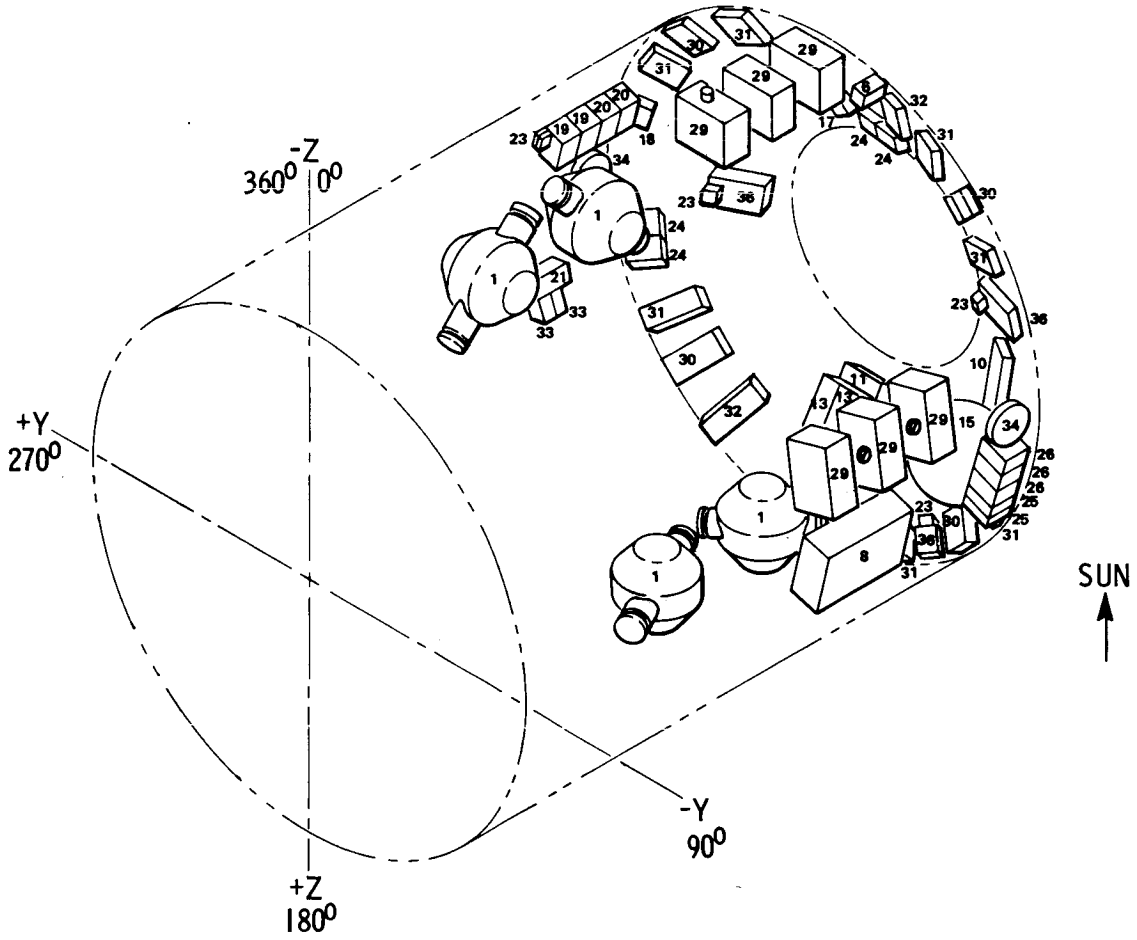

Figure III-2. SSM component layout.

Components located on the cylindrical pressure wall are covered in the same manner. The remaining wall area is left as thermal control surface for the SIP components. Figure III-3 presents the nodal layout utilized to determine the external heating rates. The Lockheed heat rate program (LOHARP) was used to perform the calculations.

Thermal response of the SSM components to the environmental heating rates and the internal heat sources was evaluated through utilization of the SINDA digital computer program. The thermal model was composed of 65 nodes. Each component or closely packed group of components was designated as a node and attached to the longerons adjacent to the pressure shell. Components with little or no heat output were insulated from the pressure shell. Heat

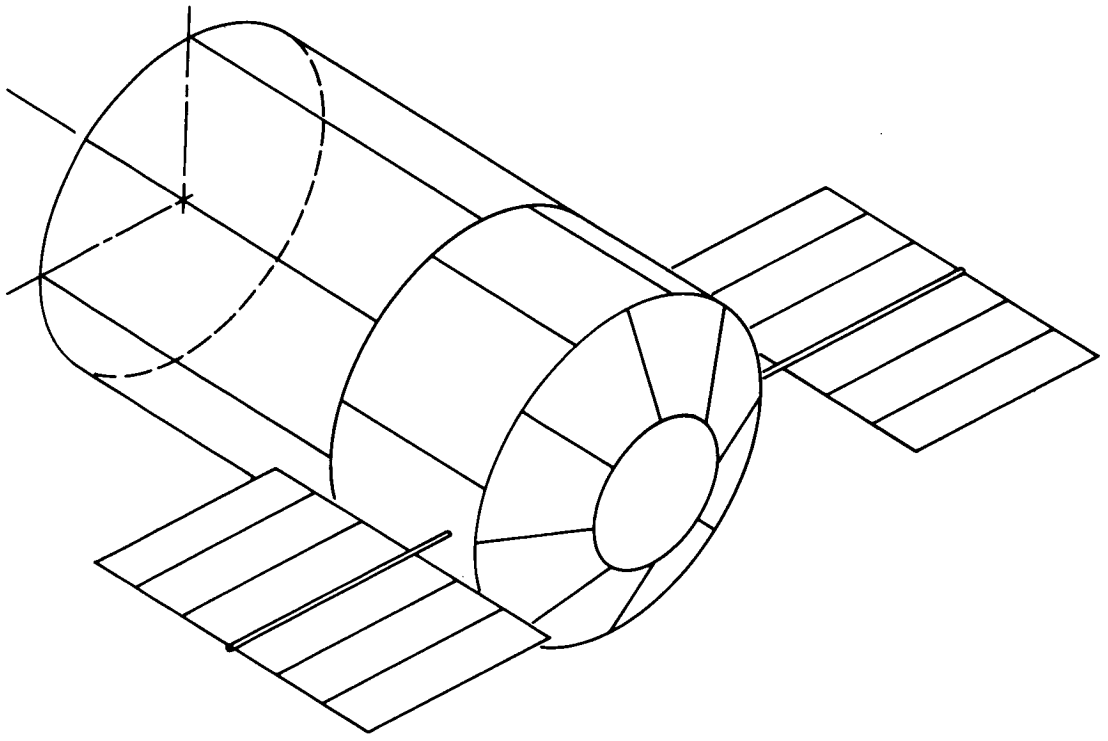

Figure III-3. Nodal model used to determine external surface heat rates.

was rejected from the components by way of conduction through the mounting brackets and radiation to the pressure wall. Emissivity of the component external surface was varied based on the heat dissipation rate and the radiating area. The average heat dissipation rate and size that was input for each component is presented in Table III-4. With the exception of the batteries, all SSM components have a wide temperature operating range. Therefore, more care must be taken in thermal control design for the batteries. For this analysis, a combination of conduction and radiation that gave acceptable results was (1) a cross-sectional area of 32 cm^2 of aluminum used to connect the battery to the pressure wall with a 5 cm conducting path and (2) surface emissivity of 0.5. Two basic vehicle orientations were investigated, one where the LST longitudinal axis is perpendicular to the solar vector and one where the longitudinal axis is parallel to the solar vector. Beta angles of 52 and 0 degrees were considered.

c. Results and Conclusions. The resulting quasi-steady state component temperatures are given in Table III-5. Although the meteoroid shield and pressure shell experience large temperature excursions during an orbit, the components have enough mass and the heat transfer path is such

TABLE III-4. SSM COMPONENT SIZE AND HEAT DISSIPATION

IDENT. NO.	ITEM	NO. USED	DIMENSIONS (mm)	TOTAL THERMAL HEAT DISSIPATED (W)
1	CONTROL MOMENT GYRO AND DRIVE ELECTRONICS ASSEMBLY	4	1019 x 775 x 584	68
2	MAGNETIC TORQUER	6	51d x 1905	15*
3	STAR TRACKER	3	114 x 114 x 406	10*
4	REFERENCE GYRO ASSEMBLY	1	444 x 173 x 152	36*
5	MAGNETOMETER	2	127 x 127 x 254	2*
6	MAGNETIC TORQUER ELECTRONICS	1	203 x 102 x 102	5
7	COARSE SUN SENSOR	5	48d x 41	—
8	RCS LINES, REGULATOR, ETC.	1	711 x 508 x 178	—
9	COMMUNICATION AND DATA HANDLING SWITCH	2	51d x 105	—
10	TRANSPONDER (APOLLO)	1	565 x 229 x 152	5.3
11	DIGITAL PROCESSOR ASSEMBLY	1	107 x 130 x 366	16
12	TRANSFER ASSEMBLY	2	152 x 203 x 246	26.5
13	RCS ELECTRONICS	2	229 x 356 x 178	—
14	RCS TRANSFER MODULE	4	—	—
15	RCS TANK	1	576d SPHERE	—
16	ANTENNA	2	76d x 254h	—
17	TRANSPONDER (ERTS)	1	203 x 152 x 330	9.3
18	BASELINE UNIT	1	184 x 140 x 89	4
19	DATA CONTROL UNIT	2	152 x 229 x 71	3
20	FORMAT GENERATOR	2	152 x 229 x 152	4

TABLE III-4. (Concluded)

IDENT. NO.	ITEM	NO. USED	DIMENSIONS (mm)	TOTAL THERMAL HEAT DISSIPATED (W)
21	COMMAND PROCESSOR & MEMORY	1	107 x 130 x 366	16
22	DELETED			
23	DATA ACQUISITION UNIT	28	71 x 71 x 25	1.34
24	REMOTE DECODER	16	152 x 229 x 71	22.4
25	TAPE CONTROL UNIT	2	157 x 185 x 41	1
26	TAPE RECORDER	3	246 x 203 x 147	20
27	CLOCK	1	56d x 114h	1.7
28	DELETED			
29	BATTERY	6	406 x 279 x 178	151
30	CHARGER	6	305 x 203 x 152	36
31	REGULATOR	6	279 x 203 x 127	150
32	SOLAR POWER DISTRIBUTION	2	325 x 165 x 152	40
33	ELECTRIC DISTRIBUTION UNITS (2 LOCATED IN SIP, 2 IN OTA)	8	152 x 102 x 76	20
34	SOLAR PANEL MECHANISM	2	—	4
35	SOLAR PANEL	12	3370 x 927 x 10	—
36	ELECTRICAL CONTROL ASSEMBLY	2	356 x 203 x 203	24
37	CABLING	—	—	43

TABLE III-5. SSM COMPONENT TEMPERATURES

I.D. NO.	ITEM	AVERAGE POWER	TEMPERATURE °C			
			⊥		∥	
			$\beta = 52^{o}$	$\beta = 0$	$\beta = 52^{o}$	$\beta = 0$
1	CMG'S & DRIVE ELECTRONICS ASSY (CMG & DEA)	WATTS 68 (PT) 90 (SLEW)	35.5 23	32 21	10.5 20	10.4 18.7
6	MAGNETIC TORQUER ELECT. (MTE)	5	28	32.6	28	28.7
8	RCS ELECTRONICS	0	-5.5	-8.5	-8	-9.6
11	DIGITAL PROCESSOR ASSY. (DPA)	16	-2	-5.3	3	1.0
15	RCS TANK	0	-5.5	-.3	-5.5	-5.2
17	TRANSPONDER	9.3	-0.5	2	15.5	12
18	BASEBAND UNIT	4	-13	-9	12	7
19	DATA CONTROL UNIT	3	12	9.9	9	7.3
20	FORMAT GENERATOR	7	12	9.9	9	7.3
21	COMMAND PROCESSOR AND MEMORY	16	-6	-9.5	-10	-13.4
23	ELECTRIC CONT. ASSY.	24	19	19	32	29.1
24	REMOTE DECODERS	22.4	17 18	17 19.2	26 31	23.3 28.2
25 26	TAPE RECORDERS & TAPE CONTROL UNIT	21	9	7	6	4.1
29	BATTERIES	27	1.5 13.0	8 11	5.5 10.5	3.0 8.4
30	CHARGERS	36	-3 34 33 3	0 32.8 28.8 3.8	16.5 46.5 46.0 21.5	13 42.5 42.6 17
31	REGULATORS	150	23 27 24.5 28	25 27 22.7 28.8	34 34 31 38	31.7 31.5 29.8 35.5
32	SOLAR POWER DISTRIBUTOR	20	26	24	31.5	29.3
34	SOLAR PANEL MECH.	4	10.5	9.5	9.5	8
34	SOLAR PANEL DEPLOYMENT MECH.	4	4	2.5	1.5	0.4
36	DATA ACQUISITION UNIT (DAU)	1.34	10 12.0	5 9.9	21 9	16 7.3
37	TRANSFER ASSEMBLY (TA)	21.5	25.5	23.5	30	28.6

that these excursions are dampened out. Therefore the temperature remains essentially constant after stabilization for an orbit and spacecraft orientation. Orbital temperature histories for the batteries and CMGs are shown in Figures III-4 and III-5, respectively. The batteries located on the antisolar side operated at 3.5°C lower than the minimum limit. This can be corrected by increasing the emissivity or conducting path to the pressure shell. This close temperature tolerance dictates a requirement for louvers and heaters for the batteries. Louvers can control the temperature by acting as a buffer in the radiating path. No electrical power is required for the louvers; therefore, they are desirable for the primary method of control. However, mesh-type resistance heaters are required as a backup system in case of louver failure. These louvers should be the normally open type so that they would go to the open position in the failure mode.

It is concluded that, based on the assumptions used, the current placement of the SSM components within the spacecraft is acceptable and the radiating area is more than enough to dissipate the waste heat.

2. Thermal Analysis of SSM/SIP Interface

a. Design Reference Configuration. Orbital transient analyses were performed to predict the orbital temperature excursions of the SIP and to determine the required insulation thickness on the SSM pressure shell. A schematic of the analytical model is shown in Figure III-6. It was assumed that the spacecraft was oriented with the longitudinal axis perpendicular to the solar vector and in an orbit oriented to produce maximum sun time. Transient temperatures were calculated throughout an orbit. Results are presented in Figures III-7 and III-8. These curves represent temperatures of the SIP, pressure shell, insulation, and meteoroid shield along a radial line.

Results of the analyses show that a passive system is feasible and that a maximum heat load of 600 watts could be dissipated by this design. If the wattage were increased above this value, the insulation thickness would have to be decreased to the point where the instrument temperatures would vary out of limits.

b. Alternative Concepts. An alternate to the reference design approach to provide SSM/SIP thermal control was studied. The fluid loop system shown in Figure III-9 was considered. The basic operating temperature of the SIP was assumed to be $20 \pm 4°C$. The temperature at which the heat energy is removed at the SIP surface is determined by the efficiencies of the conductive and convective heat transport mechanisms in series. A double

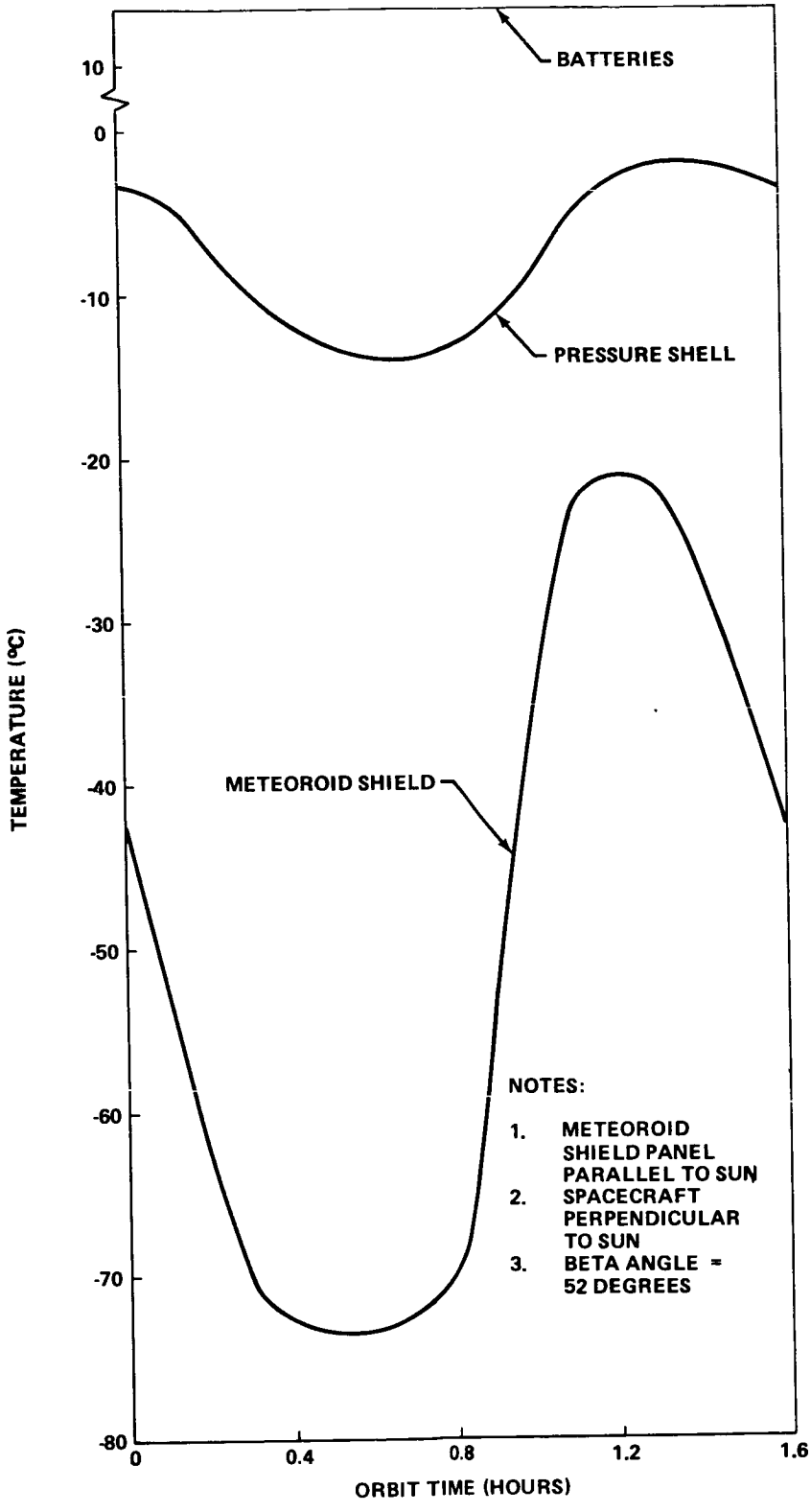

Figure III-4. Typical temperature distribution from component through walls of spacecraft.

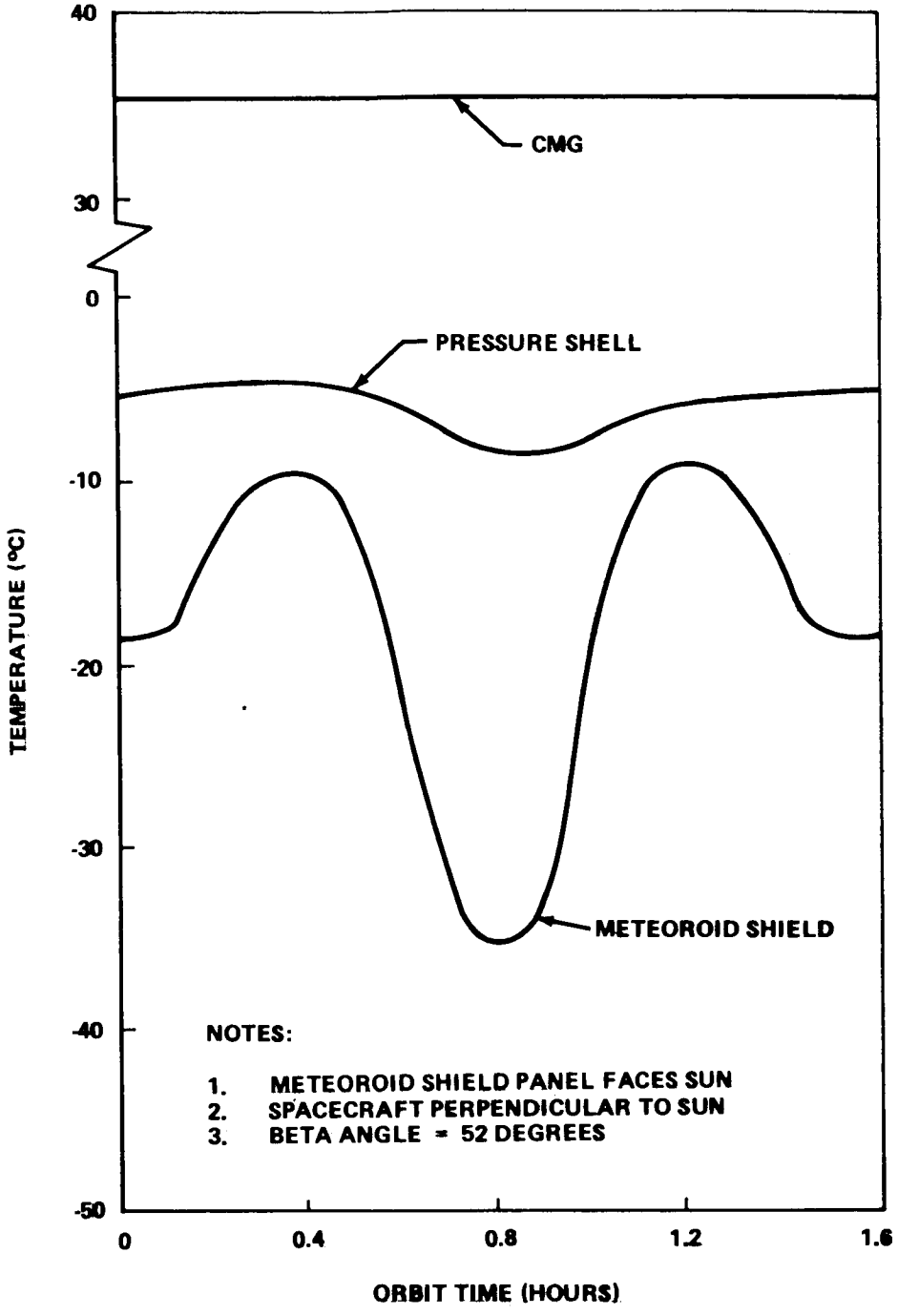

Figure III-5. Temperature distribution from CMG to meteoroid shield.

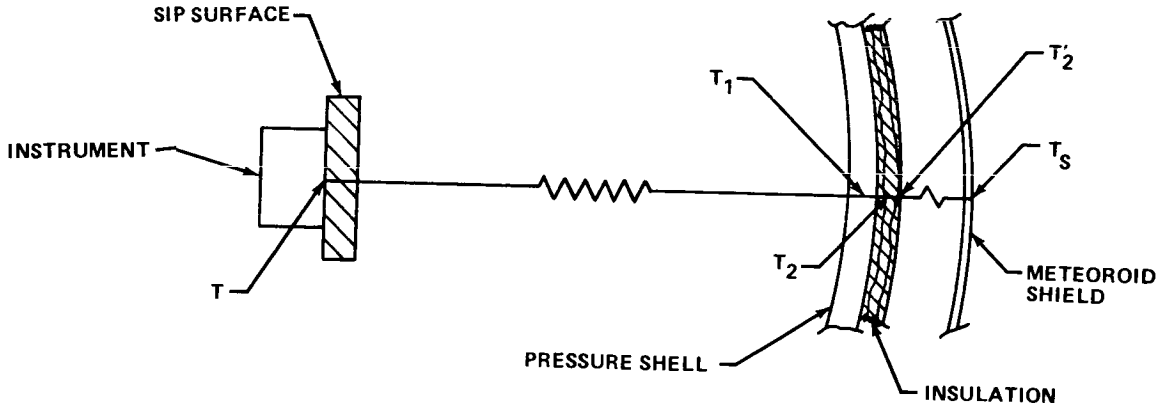

Figure III-6. Thermal model of SSM/SIP interface.

loop system was considered because of the nontoxicity requirements of the shirt-sleeve working environment provided within the SSM during manned occupancy. No toxic working fluids, such as the common refrigerants, can be permitted to pass through the manned environment. Therefore, water was selected as the working fluid for the internal loop. Freon 21 was selected for the external loop to prevent freezing in the radiator during periods of low environmental heating and/or low internal heat loads. A bypass valve will be required at each cold plate to precisely control the temperatures of the different components. A temperature sensor on the critical component will feed back a signal to control a valve which will vary the flow of the refrigerant through the cold plate. A similar bypass arrangement will be provided in the external loop to control the inlet temperature of the liquid/liquid heat exchanger under varying heat loads and orbital heat fluxes. Lower reliability, the possibility of telescope fine pointing interference from moving fluids and rotating pumps, greater contamination potential, difficulty in maintenance, and cost led to the rejection of this system.

Another alternate SIP thermal control system considered was variable control heat pipes. In these pipes the temperature of the heat source is related directly to the internal vapor pressure of the heat pipe and the available surface area of the condensing region. Thus by controlling the vapor pressure of the heat pipe with a predetermined volume of injected noncondensible gas, the heat pipe temperature is controlled. Theoretically, the reliability of the heat pipe system should be better than that of the active loop system, but the lack of previously demonstrated flight systems employing variable control heat pipes led to the rejection of this system for the SIP.

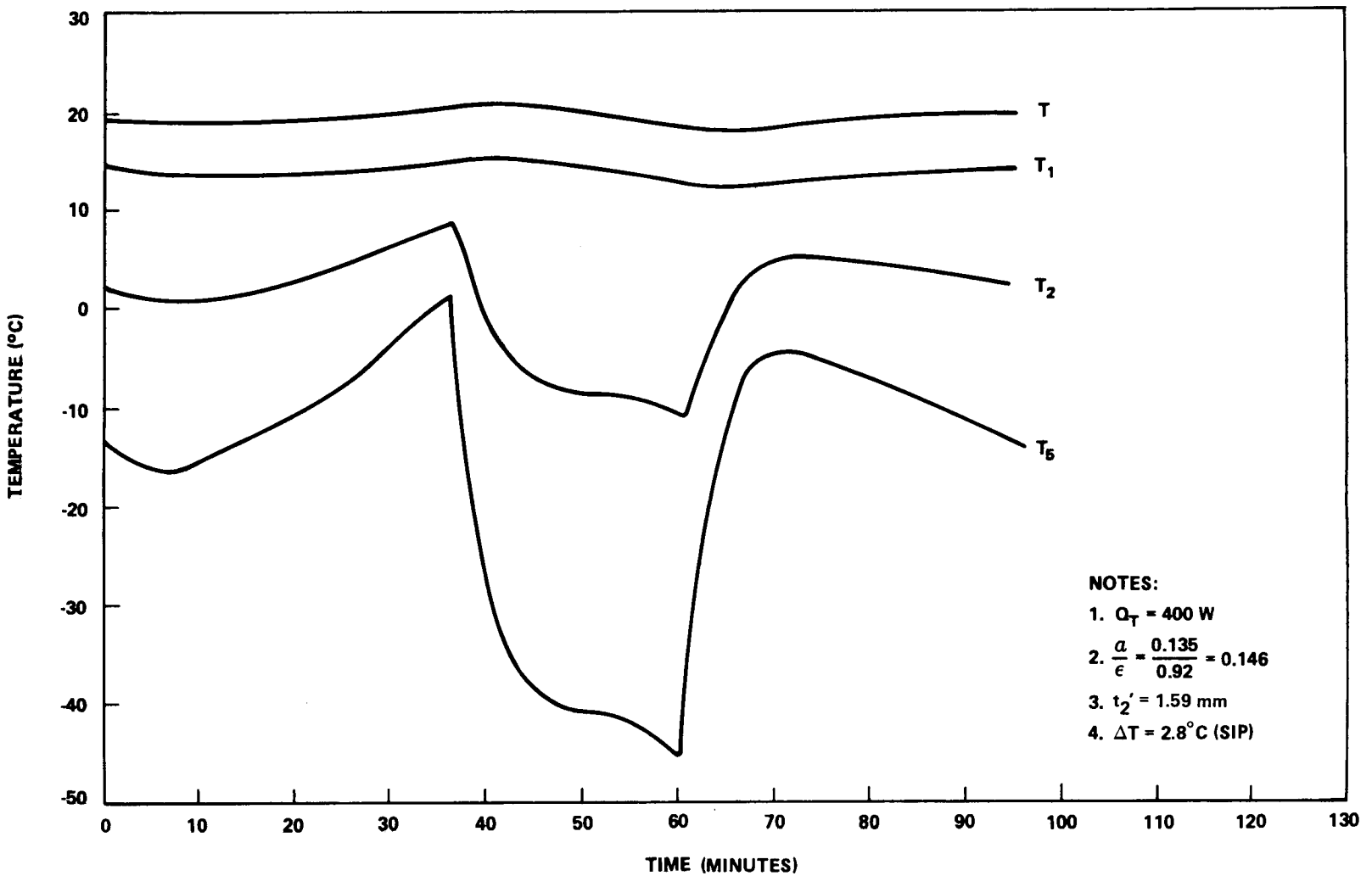

Figure III-7. Absorbed heat flux and temperature variations through an orbit (+Z).

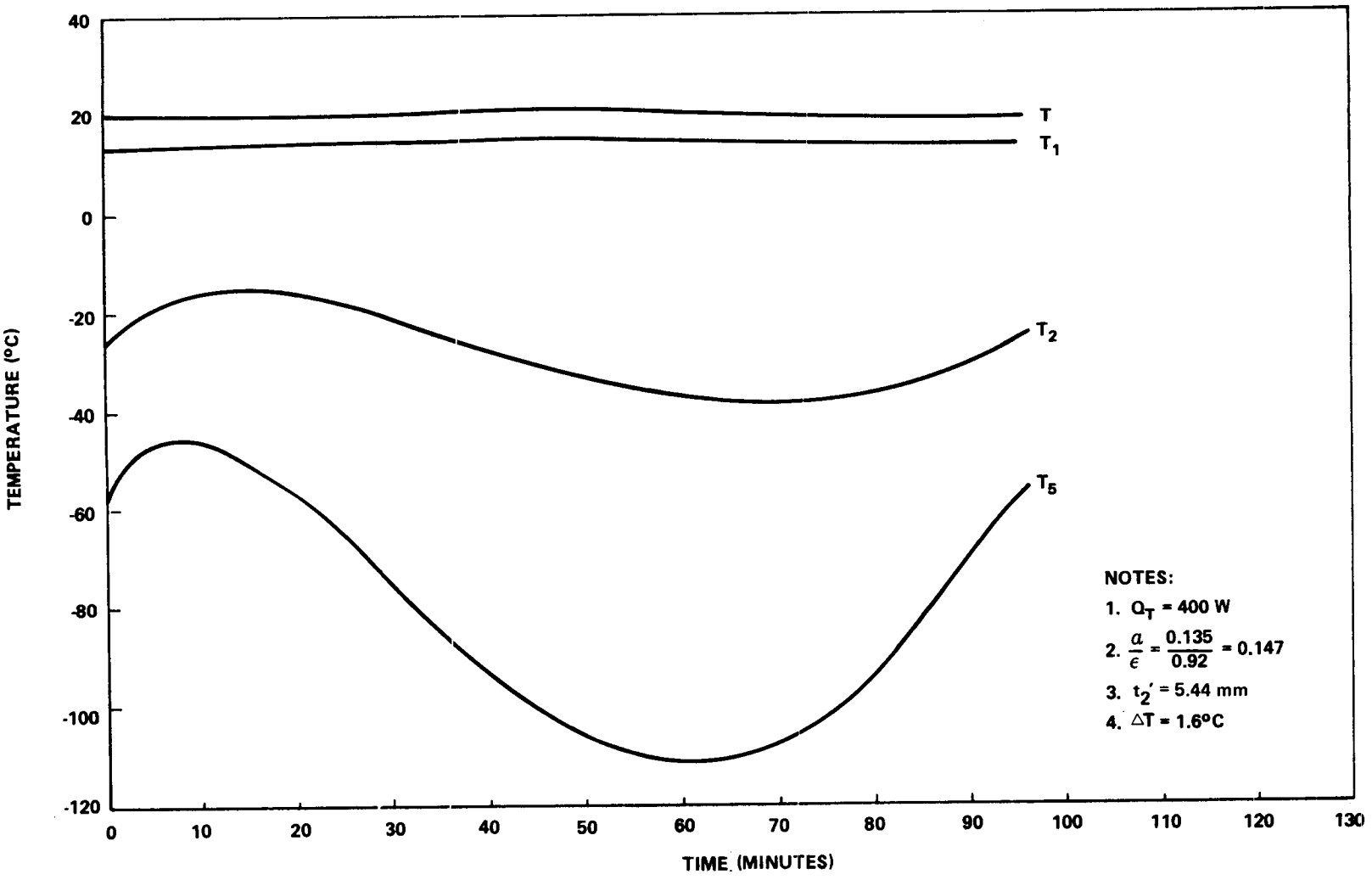

Figure III-8. Absorbed heat flux and temperature variations through an orbit (-Z).

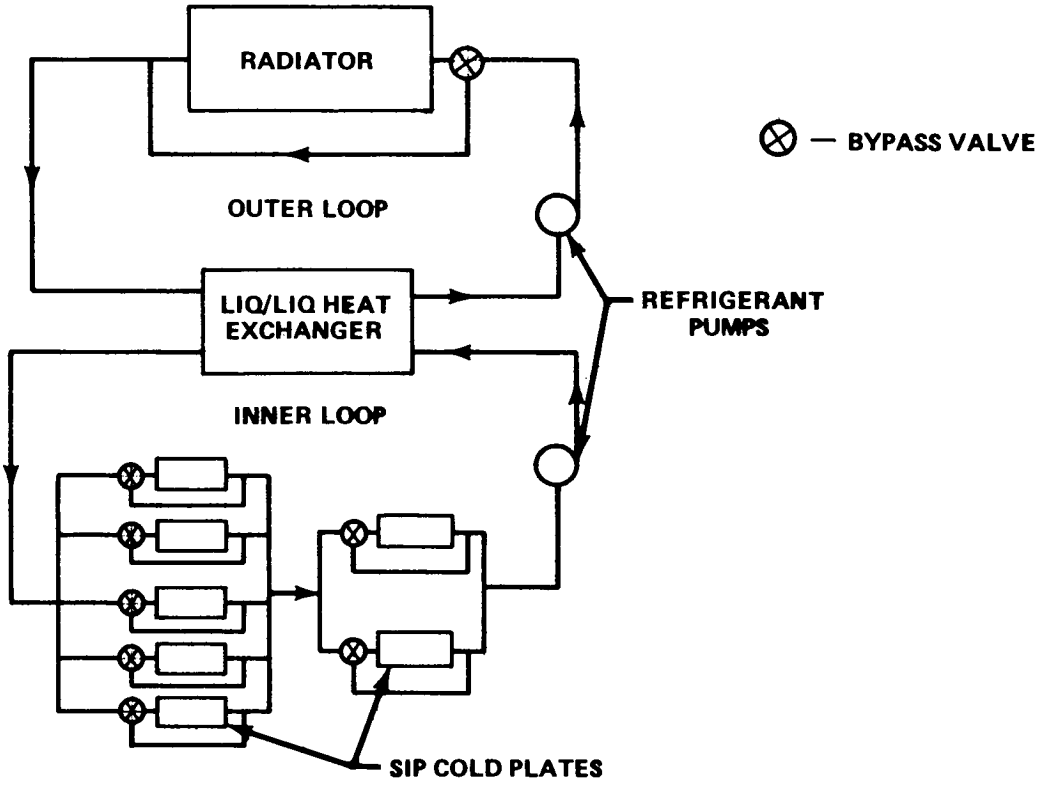

Figure III-9. Schematic of alternate thermal control system for SIP components.

3. Miscellaneous Considerations

a. Manned Occupancy. Unscheduled maintenance will probably be performed before the end of the second year and as required thereafter. Since the maintenance is to be performed in a shirt-sleeve environment, the SSM will be pressure-sealed. The astronaut must not be exposed to either an excessively hot or cold wall. Also, existence of a cold wall must be avoided to prevent condensation from the cabin atmosphere, which will be supplied from the attached service spacecraft.

In order to dock, the solar cells will have to be retracted and wrapped around the vehicle as in the launch condition. Because of the high solar absorptivity ($\alpha = 0.78$), the temperature on the sun side was 20°C and on the antisun side it was 10°C. This is well above the dew point temperature, so no condensate will form. For the aft conical section, 250 watts will have to be supplied to maintain equipment temperature above the dew point.

b. Component Access for Maintenance. When performing maintenance on the scientific instruments or the subsystems, it will be necessary to remove the thermal covering over the subsystem components and SIP components. Each component can be attached so that when the panel is opened, it can be easily removed.

c. Launch Thermal Environment. A prelaunch purge is necessary to remove the heat absorbed from the environment and added to components being energized during testing. The LST may be launched, returned to earth, and relaunched by the Space Shuttle. The Shuttle apparently will present no thermal problem from ascent aerodynamic heating if 2.5 cm of microquartz (56 kg/m^3) insulation is installed inside the cargo bay walls. Under this condition the cargo bay temperature will peak at approximately 41°C during ascent; this will not result in overheating of the subsystems. The Shuttle ascent heating phase lasts for less than 5 minutes.

The effects of the Titan III launch environment on the LST thermal response have not been evaluated. However, it is expected that the utilization of protective insulation inside the shroud walls will maintain the LST components within their respective temperature limits.

4. Solar Arrays

a. Guidelines and Assumptions. The following guidelines and assumptions were used in performing this analysis:

1. Orbit:

   a. Circular at an Altitude of 611 km.

   b. 28.5 Degrees Inclination to the Equator.

2. Solar Absorptivity and Infrared Emissivity.

   a. Solar Cells — 0.78 and 0.82, respectively.

   b. Antisolar Side of Solar Panels — 0.35 and 0.87.

   c. Spacecraft External Surfaces Over SSM — 0.135 and 0.92.

3. Environmental Heat Source Constants.

a. As Given Previously (Table III-3).

The analysis was performed utilizing the following three orbit and spacecraft orientation combinations:

1. Beta angle of 52 degrees with the spacecraft longitudinal axis perpendicular to the solar vector.

2. Beta angle of 0 degrees with the spacecraft longitudinal axis perpendicular to solar vector.

3. Beta angle of 52 degrees with the spacecraft longitudinal axis parallel to the solar vector.

b. Analytical Approach. A transient orbital thermal analysis was performed on the solar cell array design for the LST. The nodal model used to perform these calculations is presented in Figure III-10. All the spacecraft surfaces seen by the solar panels were included in the model so that reflection and reradiation effects would be considered. With a passive thermal control system the external spacecraft skin must act as a radiator; therefore, for these analyses, one kilowatt of heat (representing the component heat dissipation requirement) was dissipated from the nodes representing the meteoroid shield covering the SSM.

c. Results. The predicted temperature histories of the solar panels for three different orbit/spacecraft orientations are presented in Figures III-11, III-12, and III-13. The two curves on each graph represent one node near the spacecraft body and one on the outer edge. In Figures III-11 and III-12, the curves which represent the parallel and perpendicular spacecraft orientations at β = 52 degrees show that the orientation of the spacecraft has little effect on the solar panel temperature. Figure III-13 represents the β = 0 degree case and shows that, although the spacecraft is exposed to the sun for a shorter length of time, the temperature is 7.2°C higher at one point than in the cases where β = 52 degrees. This results from the fact that in the β = 0 degree orbit there is a point where the spacecraft is directly between the sun and earth. At this location, the maximum albedo and planetshine radiation strikes the backside of the solar panels causing the temperature increase. For the β = 52 degrees cases, the backside temperature remained approximately 5.6°C lower than the side facing the sun. For the β = 0 degree case, the backside temperature varies from 0.5 to 4.5°C lower than the side facing the sun.

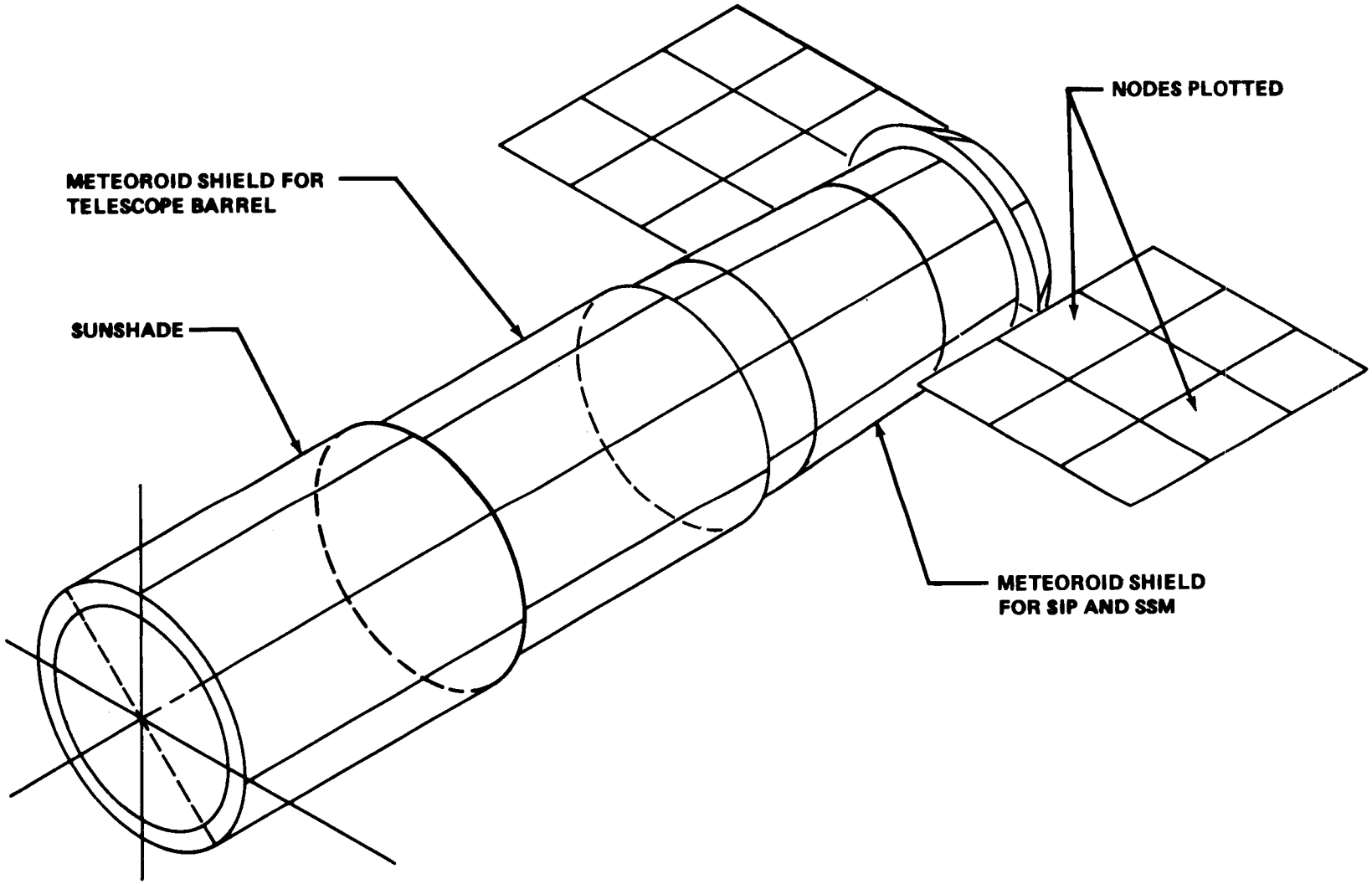

Figure III-10. Nodal layout of thermal model used in analysis.

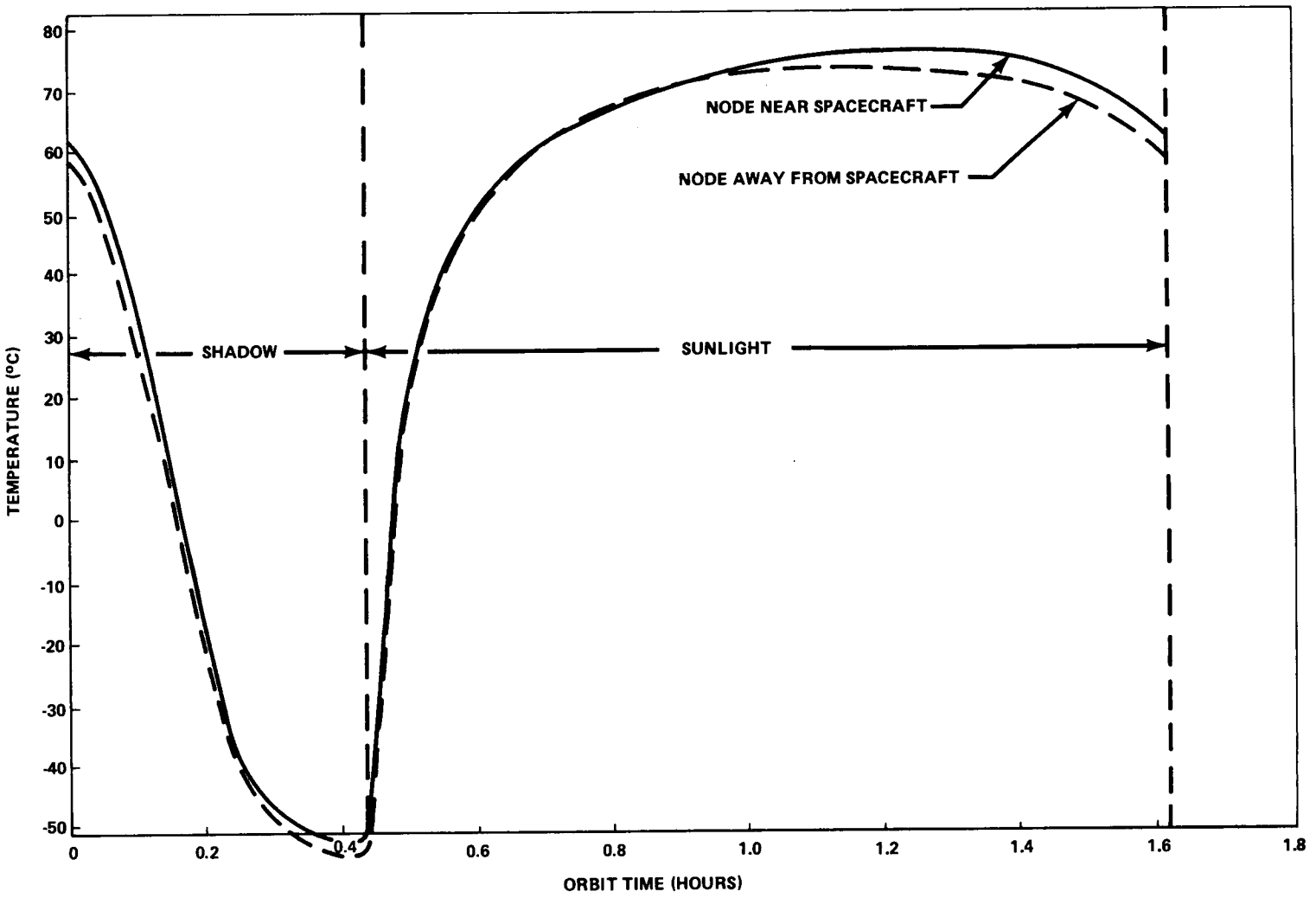

Figure III-11. Solar panel temperature throughout an orbit with β = 52 degrees and spacecraft longitudinal axis perpendicular to solar vector.

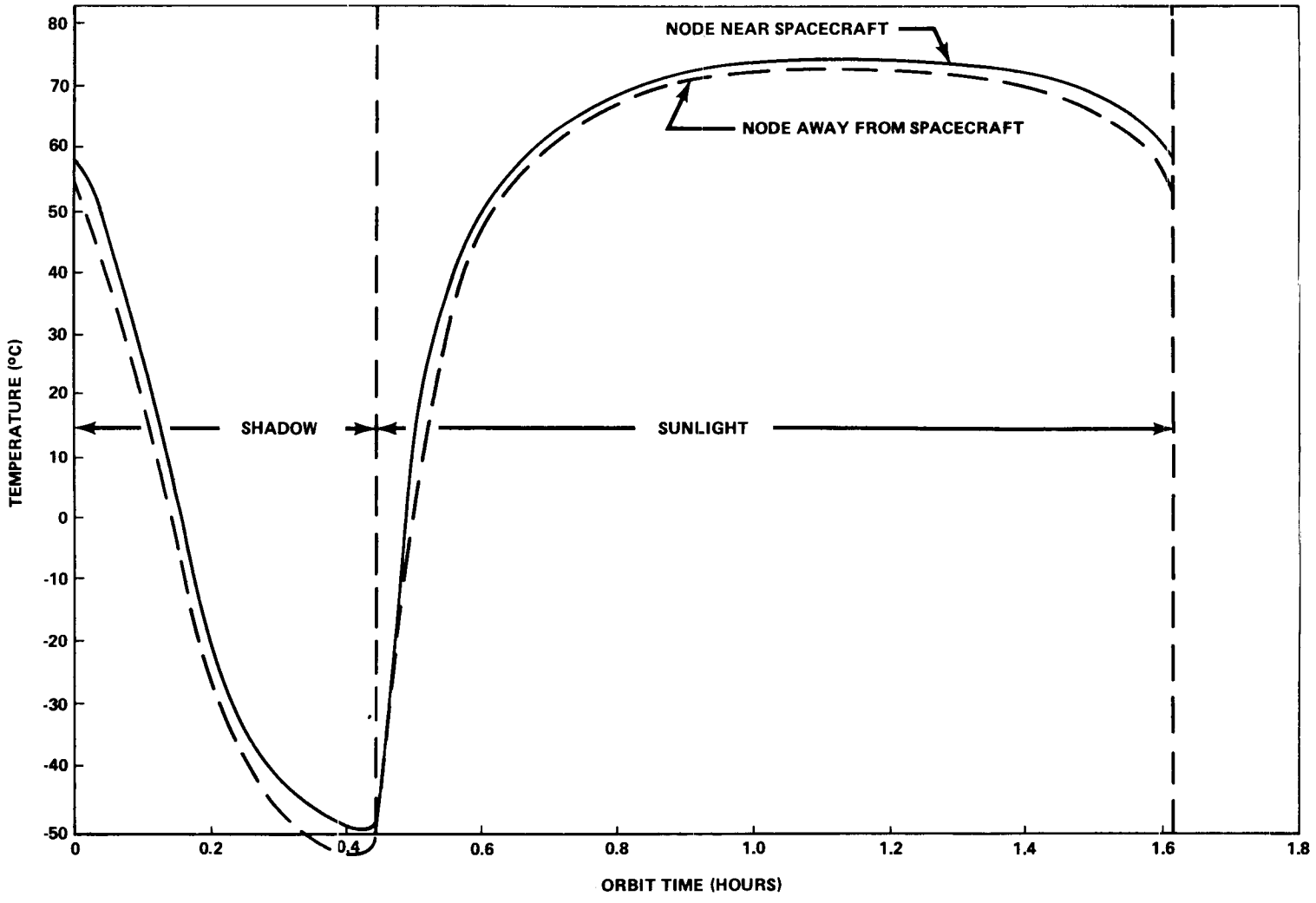

Figure III-12. Solar panel temperature throughout an orbit with β = 52 degrees and spacecraft longitudinal axis parallel to solar vector.

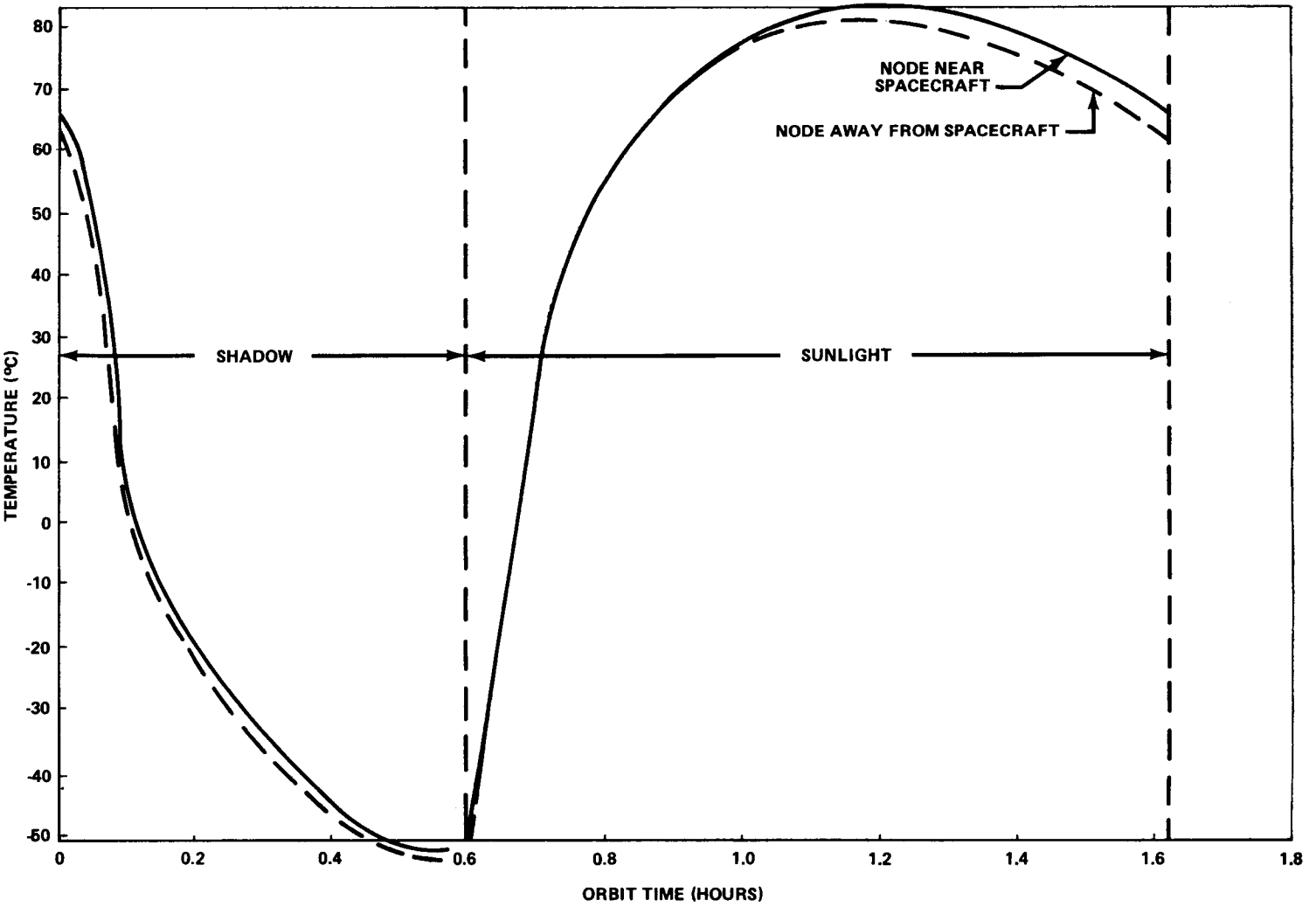

Figure III-13. Solar panel temperature throughout an orbit with β = 0 degrees and the spacecraft longitudinal axis perpendicular to solar vector.

The predicted solar panel temperature histories presented in Figures III-11 through III-13 are conservatively high because the maximum environmental heat source constants were used. With these conservative results, the maximum predicted temperature was 17°C below the prescribed upper limit of 100°C.

d. Analysis of Solar Panels Incorporating Phase Change Materials. Preliminary analysis of the proposed LST solar panel design resulted in establishment of solar cell temperature cycling between -52°C and 83°C. The cells can operate within this range, but the extreme cycling reduces service life because of the constant expansion and contraction that takes place. This thermal cycling can be greatly reduced by the incorporation of a phase change material (PCM). The resulting tradeoff is the cost, contamination, and mass penalty versus the amount of temperature cycle dampening desired.

A PCM has the unique ability to absorb and liberate large quantities of heat without appreciable temperature change by utilizing the heat of fusion of the material as a very large heat sink. For this application a thermal model was constructed representing the solar panels with a PCM encapsulated in the honeycomb substrate. The PCM selected was lithium nitrate trihydrate ($LiNO_3 \cdot 3H_2O$) because of its solid/liquid phase change temperature (32.7°C) and latent heat of fusion (390 827 J/kg).

The model was analyzed in a 611 km circular orbit at $\beta = 52$ degrees. Two cases were run utilizing different amounts of PCM: 1.9 kg/m^2 and 2.5 kg/m^2, or a total of 68 kg and 90.7 kg, respectively. The predicted solar panel temperature histories for the two cases are presented in comparison with conventional solar panel temperatures in Figure III-14. The effect is obvious: With a mass penalty of 90.7 kg, the solar panel temperature variation can be held within a range of 43°C.

5. Reliability. A study was performed by Federal Electric Corporation to examine reliability characteristics of TCS in the conceptual phase of design.[2] From the literature surveyed, it seems that very little concern has been displayed about reliability of TCS. From this study it can be seen that reliability considerations in the conceptual design phase are feasible for TCS. There needs to be an effort to accumulate failure data, particularly wearout data, on TCS elements.

---

2. Results of this study are presented in Federal Electric Corporation Report No. 1412-195-72, Aug. 4, 1972.

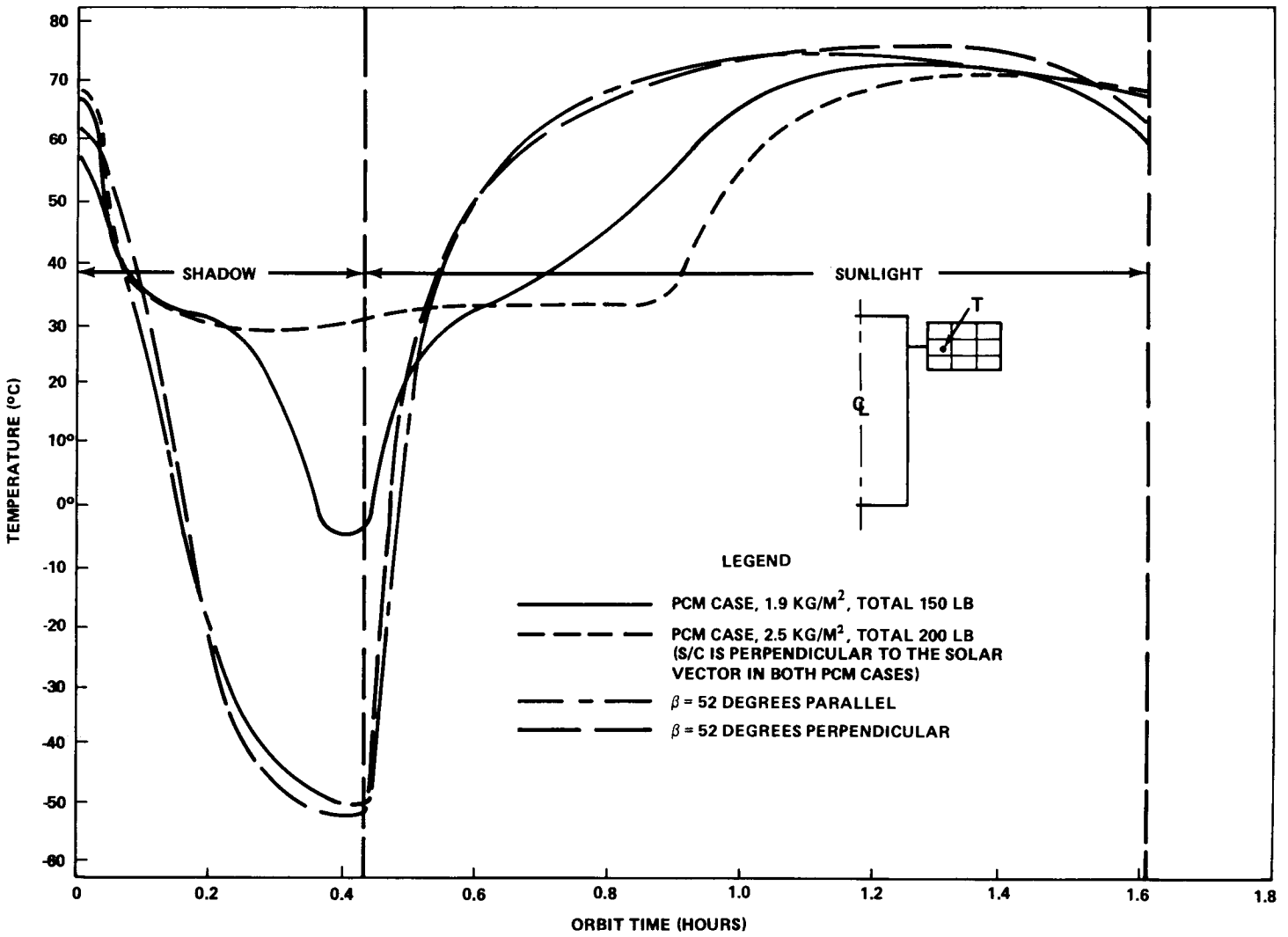

Figure III-14. LST solar panel temperature history throughout an orbit with and without a phase change material encapsulated in the honeycomb panel substrate.

The passive LST concept for thermal control is the most promising from a reliability viewpoint. Redundancy at a system level, if the functional requirements can be met, is a promising approach to enhancing overall TCS reliability.

Bibliography

Newby, T. S.: Lockheed (140 Node) Orbital Heat Rate Program. Contractor Report No. CR-59281, October 1966.

Smith, J. P.: Systems Improved Numerical Differencing Analyzer. TRW Report No. 14690-H001-R0-00, April 1971.

Federal Electric Corporation: Thermal Control System Reliability Study. Report No. 1412-195-72, August 1972.

Winn, T. L.: Preliminary Analysis of Thermal Shield Requirements for the Shuttle Orbiter Cargo Bay. Teledyne Brown Engineering Summary Report ASD-PD-1425, October 1971.

CHAPTER IV. ELECTRICAL SYSTEM

TABLE OF CONTENTS

TABLE OF CONTENTS (Continued)

TABLE OF CONTENTS (Continued)

TABLE OF CONTENTS (Concluded)

LIST OF ILLUSTRATIONS

LIST OF ILLUSTRATIONS (Concluded)

LIST OF TABLES

equipment shall be rated for at least 150 percent of the highest average determined. Power is to be delivered efficiently to the loads at a voltage of 28 ± 2 percent Vdc.

d. Life. The system design and hardware concepts shall assure that the power and functional requirements are satisfied throughout the 5 year mission. Refurbishment will be accomplished by replacement of failed or degraded components during on-orbit maintenance. The minimum maintenance interval is to be determined on a cost basis. Presently, an estimate of 2 years is being used for the minimum life of components.

e. Reliability. The electrical system shall have a sufficiently high reliability so that the reliability for the SSM will be 0.95 for 1 year. With maintenance, the system shall have adequate reliability to sustain the 5 year mission.

f. Protection. Reliable design methods and devices shall be used to protect the system integrity and to assure a cost-effective mission. The system design and implementation will assure:

1. Single point failures will not degrade system performance.

2. Protection against credible faults that could jeopardize the mission.

3. Transients and/or electromagnetic interference (EMI) will not affect operational reliability, accuracy of controls, or quality of data.

4. Transient suppression is provided as needed for critical networks. In general, transients having 10 μsec pulse widths shall not exceed ±50 volts.

g. Technology and Commonality. Maximum use of flight proven concepts and components is ground ruled for low cost and development risk. Unless they are cost effective, innovations are to be avoided. Use of adequate, existing specifications and documentation is also desired for low cost.

h. Environment. The electrical system shall be compatible with environmental conditions to be determined for the mission and with those specified for a Shuttle launch and for the alternate Titan launch. The maximum solar array temperature shall be limited to 100°C by design. Battery temperature shall be closely controlled within the range of 5°C to 15°C.

i. Mass. The system mass must be compatible with the spacecraft limits and allocations. No mass constraints have been allocated to the electrical system. Assembly mass shall be consistent with safe, easy handling and maintenance concepts. Special approval will be required for assemblies exceeding 45 kg.

j. Orbital Parameters. The electrical system shall be capable of satisfactory performance and self-sustained operation in the 611 km circular orbit with a 28.5 degree inclination. Possible variations due to launch date shall be accommodated.

k. Pointing. The solar array shall not constrain vehicle pointing. The vehicle X-axis may be pointed to any location on the celestial sphere; except that, it will not be directed to within 45 degrees of the sun. Short-term allowances are made for 15 degree cone angles toward the moon and earth. The system will have adequate power to sustain the vehicle for two operating modes. The normal operating mode is three-axis stabilized with roll position unconstrained by experiment requirements. The special mode shall be permissible for one to three orbits per month. In the special mode, the roll position will be constrained by the experiment. Further coordination with scientific investigators is required to determine minimum acceptable time and degree of roll.

l. Launch Vehicle. The system shall be compatible with the Shuttle system and operations. It will satisfy the electrical interfaces to be established for prelaunch, launch, and orbital operations.

m. Alternate Launch Vehicle. The electrical system will also be compatible with the requirements and constraints of the alternate Titan launch site and vehicle. The design shall permit easy adaptation without major modification. Add-on modification kits are permissible for interface adaptation.

n. Location. To the extent possible, the major part of the electrical system shall be located within the SSM section of the LST. The SSM will provide the necessary services and interfaces for the OTA/SIP. External interfaces will be located around the docking port in accordance with interface documents to be supplied by the Shuttle system. The solar array will be located only on the SSM.

o. Configuration. The electrical systems will be compatible with the cylindrical configuration and dimensions of the SSM. The solar array shall be compatible with launch vehicle constraints and the envelope specified for the

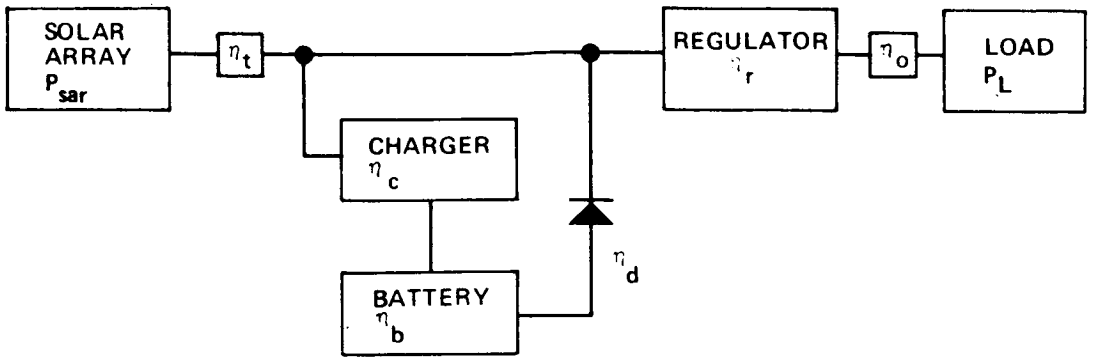

Titan shroud. The electrical system equipment shall be modularized with features that permit easy access, handling, installation, and maintenance.

2. Electrical Load Requirements. Based on preliminary studies of the LST, an orbital average load of 1500 watts was set as the reference for electrical power design studies. The minimum peak load of 2250 watts selected was 150 percent of the design average load. It represented a conservative rating considering that the highest maximum previously determined was 1750 watts. Experience has shown that a margin between 10 percent and 25 percent should be included in the design load to account for probable changes that occur between Phase A and the final vehicle requirements. The margin depends on engineering judgment of system design maturity and practicality of requirements.

The load requirements described here represent the results of further iterations made during this study. Load requirements were solicited from the various SSM subsystem designers and from the OTA and SIP study results. All loads are given in terms of 28 Vdc equivalent power. Conversion to different voltages or to ac will be accomplished within the system requiring the conversion. The individual loads for the subsystems are given as the average requirement at the load terminals, exclusive of system losses. These figures are considered more accurate than maximum or peak power requirements, which are dependent on combinations of subsystems and coincidence of loads that can occur in a random manner. Preliminary estimates of load combinations were used to develop the power profile to be shown.

Because the design concepts for OTA and SIP are in their infancy, it is difficult to make accurate load and operational predictions. The low confidence in these requirements should be compensated by a larger margin. Since the SSM systems are based on previous designs, the requirements of most of the elements have been verified. Thus, a higher confidence and a lower margin may be attributed to the SSM loads.

The size of the EPS is also sensitive to load variations that may occur as a function of occultation and sunlight periods of the orbit. Such variations depend on operational and sequencing concepts which have not been well defined. To emphasize the need for good load definition — broken down at least to averages for occultation and sunlight periods — parametric performance curves are given in Sections C.2 and F.1 to show the effect of dark-to-light load ratios and the solar array and batteries.

a. Power for Attitude Control. The equipment within the attitude control system (ACS) that requires electrical power is identified in Table IV-1; the unit power ratings, typical average power, and potential peaks are also given. The components of the ACS with appreciable peaks are the CMGs, the magnetic torquers, and the gyros. The reaction control subsystem (RCS) could represent a significant current peak. (The RCS requirements are mentioned here because they were combined with the ACS in this study.) Requirements are the same for either the Shuttle or Titan launch vehicles.

TABLE IV-1. POWER REQUIREMENTS FOR ATTITUDE CONTROL SYSTEM

EQUIPMENT	AVERAGE UNIT POWER, WATTS	ACTIVE UNITS	MAXIMUM POWER, WATTS	DUTY[d] CYCLE, %	AVERAGE TOTAL POWER, WATTS
STAR TRACKERS	5	2	10	100	10
REFERENCE GYROS[a]	9	4	36	100	36
MAGNETOMETERS	2	1	2	100	2
CMG AND DEA[b]	17	4	90	76	68[e]
MAGNETIC TORQUER	2.5	6	30	50	15
MTE	5	1	5	100	5
DIGITAL PROCESSOR	16	1	16	100	16
TRANSFER ASSEMBLY	26.5	1	26.5	100	26.5
RCS ELECTRONICS[c]	11	1	11	S	0
			TOTAL AVERAGE POWER		178.5

a. STARTING POWER IS 72 WATTS FOR REFERENCE GYRO ASSEMBLY.
b. CMG SPINUP POWER IS APPROXIMATELY 135 WATTS EACH, PEAK. SPINUP IS PROGRAMMED OVER SEVERAL HOURS.
c. RCS IS NOT NORMALLY USED. RCS ELECTRONICS WOULD BE ACTIVE OCCASIONALLY FOR SYSTEM MONITORING.
d. "S" DENOTES "SELDOM USED."
e. 90 WATTS MAXIMUM FOR SLEWING. HAPPENS EVERY EXPERIMENT PERIOD. DUTY CYCLE IS EQUIVALENT.

The largest peaks for CMGs and gyros occur at initial startup aboard the Shuttle. Since these assemblies are individually controlled, startup can be programmed to avoid large peaks. After initial peaks, the load tapers off as the speed increases; approximately 8 hours is expected for warmup and starting of a CMG system. The reference gyro assembly requires less than an hour. Once stabilized, CMG operating power is constant. Small peak loads, lasting for a few minutes, occur when slew maneuvers are commanded.

A typical power profile for the magnetic torquers is approximately a sinusoidal variation from 0 to 30 watts over a period of an orbit.

Presently the RCS represents an emergency backup to the ACS and may be required for rendezvous and docking with the orbiter. It was assumed that RCS operation was not required during normal LST orbital operations; therefore, it would have minor influence on the average power. The electronics associated with RCS instrumentation requires 11 watts and this source was included in the ACS power budget. Superposition of potential peaks for RCS valves and thrusters with other electrical loads was not considered typical. If used during rendezvous and docking, the peaks would occur when the SIP and most of the OTA equipment would not be operating.

b. Communications and Data Handling (C&DH) Loads. The power requirements determined for the C&DH components are tabulated in Table IV-2. In general, most of the redundant items will be dormant and require no power. Of the online equipment, only the transmitters, the data acquisition units (DAUs), and tape recorders were considered to be cyclic loads. Both transmitter and recorder requirements depend on the LST contacts with ground tracking stations. An average of 34 minutes contact time per orbit was used to determine the average power allocation. For the power profile, it was assumed that 4 contacts per orbit occur, each lasting 8.5 minutes. During most of the orbit, one tape recorder is operating in the record mode and standby power is supplied to the transmitters. Over a ground station, full transmitter power is supplied. One recorder operates in a record mode while the second recorder is operating in the playback mode.

Fourteen of the 28 DAUs are active but operate in a continuous off-on sequence in accordance with the data sampling rate. The duty cycle for any unit is approximately 7.2 percent; however, the maximum power is that of the one unit energized at any instant.

TABLE IV-2. POWER REQUIREMENTS FOR COMMUNICATION AND DATA HANDLING SYSTEM

EQUIPMENT	AVERAGE UNIT POWER, WATTS	ACTIVE UNITS	MAXIMUM POWER, WATTS	DUTY [c] CYCLE, %	AVERAGE TOTAL POWER, WATTS
APOLLO TRANSPONDER	5.3	1	16	33	5.3
ERTS TRANSPONDER	9.3	1	28	33	9.3
FORMAT GENERATOR	4	1	4	100	4
COMMAND PROCESSOR	16	1	16	100	16
REMOTE DECODER	1.4	16	22.4	100	22.4
TAPE RECORDER [a]	12	1	24	33	20
CLOCK	1.7	1	1.7	100	1.7
TAPE CONTROL UNIT	1	1	1	100	1
DAU [b]	1.3	14	1.3	7.2	1.3
BASEBAND UNIT	4	1	4	100	4
DATA CONTROL UNIT	3	1	3	100	3
			TOTAL AVERAGE POWER		88.0

a. ONE TAPE RECORDER IS ALWAYS RECORDING; ONE IS ON PLAYBACK 33% OF THE ORBIT.
b. ONLY ONE OF THE 28 DAU IS ON AT ANY GIVEN TIME; THE DUTY CYCLE FOR EACH IS 7.2% THE SEQUENCE RATE.
c. AVERAGE TRANSMISSION TIME IS 33% OF AN ORBIT.

c. Thermal Control Loads. The major thermal control loads are included in the OTA/SIP requirements. The SSM thermal control is primarily passive. Strip heaters are provided for unusual conditions where system temperatures might become too low. Abnormal powering down and orientation conditions that might increase heater power were not considered typical. Therefore, an average power allocation was not given to SSM thermal control. Unusual thermal conditions may occur during maintenance operations with the orbiter. In this case power can be supplied from the orbiter, thus, it is not a direct imposition on the LST power sources.

d. Contamination Control System Load. During normal, self-sustained orbital operation of the LST, there are no power requirements for contamination control. It is anticipated that the power needed for contamination control, when the LST is aboard the orbiter or during orbital maintenance, will be supplied from power sources located in the orbiter. The contamination control average load was 874 watts with a 58 percent duty cycle (allowing 10 hours per day shutdown for rest periods) and, considering that 5 days is typical for a maintenance visit 61 kW-h of energy would be required for this load.

e. Electrical System Loads. The power required to operate system instrumentation and protection devices, array orientation mechanisms, deployment/retraction devices, and secondary distribution controls were considered as loads rather than losses. Distribution losses, EPS assembly effeciencies, main controls, and diode drops were determined on a system basis and are later considered as requirements to be satisfied.

The power for electrical systems loads is allocated by assemblies in Table IV-3. The allocation for the electrical distribution units included an average allotment for several 5-volt measuring reference supplies. Array deployment/retraction and orientation items represent the major peak loads. The deployment/retraction load has little influence on requirements because it only occurs at the beginning of the mission and for a Shuttle revisit. The orientation load peak of 100 watts may occur at random intervals depending on the experiment periods. Normally this peak will be a short duration; however, for design purposes, it was considered to last an average of 4 minutes per orbit.

f. OTA Power Requirements. Due to the preliminary design status of the OTA, the power requirements listed in Table IV-4 are considered preliminary estimates subject to some change. For preliminary design an average of 500 watts was allocated for the OTA. Most of the overall design margin obtained could also be allocated to the OTA, to the SIP, or to both.

As shown in Table IV-4, eight of the loads have either a random or cyclic nature. A negligible duty cycle is indicated for random loads such as the sun shade or aperture doors. These will have negligible influence on average power since they occur only a few times during the mission. Such loads can be scheduled in advance to avoid superimposing peaks on other peak requirements. The cyclic loads were considered to operate once per orbit. With the estimated 2 percent duty cycle, these loads have a minor effect on the average requirement.

TABLE IV-3. POWER REQUIREMENTS FOR ELECTRICAL SYSTEM

EQUIPMENT	AVERAGE UNIT POWER, WATTS	ACTIVE UNITS	MAXIMUM POWER, WATTS	DUTY [c] CYCLE, %	AVERAGE TOTAL POWER, WATTS
BATTERY CHARGERS	.5	6	3	67	2
SOLAR POWER DISTRIBUTORS	5	2	10	100	10
ELECTRICAL CONTROL ASSEMBLY	5	2	10	100	10
DEPLOYMENT MECHANISM [a]	67.5	2	135	S	0
ORIENTATION MECHANISM [b]	50	2	100	4	4
ELECTRICAL DISTRIBUTION UNIT	2.5	8	2.5	100	20
TOTAL AVERAGE POWER					46

a. NORMALLY OPERATES ONLY AT BEGINNING OF MISSION AND DURING MAINTENANCE OPERATION.
b. ASSUMES 4 MINUTES OPERATION PER ORBIT.
c. "S" DENOTES "SELDOM;" RESULTS IN AVERAGE ESSENTIALLY ZERO.

The electronics and fine guidance sensors were the only constant loads identified. The heater power for thermal control is also a variable load dependent on thermal conditions. However, the thermal loads are expected to change slowly.

g. SIP Power Requirements. The power requirements for the scientific instruments are given in Table IV-5. The requirements are considered preliminary estimates. Variation may result from later specific requirements that might affect instrument size and power.

TABLE IV-4. POWER REQUIREMENTS FOR OTA

EQUIPMENT	AVERAGE UNIT POWER, WATTS	ACTIVE UNITS	MAXIMUM POWER, WATTS	DUTY [b] CYCLE, %	AVERAGE TOTAL POWER, WATTS
FORCE ACTUATORS	10	3	20	5	0
SECONDARY MIRROR CONTROLS	25	3	75	2	2
APERTURE DOORS	30	1	30	S	0
SUNSHIELD	50	1	50	S	0
FINE GUIDANCE	110	1	110	100	110
FIGURE SENSOR	40	1	40	S	0
FOCUS SENSOR	1	1	40	2	1
DECENTER SENSOR	1	1	21	2	1
TILT SENSOR	1	1	21	2	1
HEATERS - PRI & SEC [a]	10/20	38	452	76	346
ELECTRONICS	40	1	40	100	40
			TOTAL AVERAGE POWER		501 [c]

a. NUMBER OF UNITS NOT GIVEN; DUTY CYCLE DEPENDS UPON ORBITAL CONDITIONS, POWER GIVEN IS BASED ON PRELIMINARY ASSUMPTIONS.
b. "S" DENOTES "SELDOM," TYPICALLY A FEW TIMES PER MISSION.
c. 500 WATTS WERE USED FOR THE PRELIMINARY DESIGN OF THE ELECTRICAL SYSTEM.

TABLE IV-5. POWER REQUIREMENTS FOR SIP
(SCIENTIFIC INSTRUMENT PACKAGE)

EQUIPMENT	AVERAGE UNIT POWER, WATTS	ACTIVE UNITS	MAXIMUM POWER, WATTS	DUTY CYCLE, %	AVERAGE TOTAL POWER, WATTS
F/12 CAMERAS	48	1	48	100	48
F/96 CAMERAS	48.6	3	145.8	100	145.8
FILTER WHEELS	1.7	1	1.7	100	1.7
ECHELLE SPECTROGRAPHS	20	2	40	100	40
FAINT OBJECT SPECTROGRAPHS	20	3	62	100	62
INTERFEROMETER	4	1	4	100	4
SLIT JAW CAMERA	20	1	20	100	20
SUPPORT EQUIPMENT	a	4	122.7	100	122.7
CONTINGENCY EQUIPMENT	a	—	25	100	25
				TOTAL AVERAGE POWER [b]	469.2

a. VARIOUS LOADS INVOLVED.
b. TOTAL SIP POWER IS CONSTANT; WHEN ANY EXPERIMENT IS OFF, HEATER POWER IS ADDED TO MAINTAIN PROPER THERMAL CONTROL.

As shown in Table IV-5, the loads are considered to be constant, having no significant peaks. This results from the concept that during a given experiment period, the heater power will be left on for the nonactive instruments. For extended inactive periods, it is permissible to turn the instruments and heaters off. However, considering that a typical experiment period may be 10 hours (6 orbits), these off periods would have little influence on the requirements needed for defining the power system. Averaging power requirements over periods greater than one orbit could lead to undersizing the system. Later thermal studies indicate that SIP power requirements may be reduced as much as 200 watts subsequently.

h. LST Power Profile. During the several iterations that were made of the power requirements, considerable fluctuations occurred. This is indicative of the conceptual status of the system and the changes in estimates that normally occur as the concepts mature. At one point, load profiles having sustained loads of 1750 watts were determined. Also, a difference of over 600 watts in maximum to minimum steady state loads was indicated. Following tradeoffs and optimization studies, considerable reductions in load requirements occurred. Better insight into system conditions and operational concepts resulted in smaller variations in the load profile. The trend has been to reduce the complications and anticipated life problems associated with a large number of high cyclic loads.

Power profiles were constructed from the latest load information described in the foregoing subsections. With some assumptions, typical operational sequences were defined, considering probable conditions and load combinations. A simplified timeline of the Shuttle launch and initial orbital operational phase is shown in Table IV-6. The table has been simplified to show only events that may affect power requirements.

A typical power profile for initial phases of the LST mission is shown in Figure IV-1. Shuttle interface documents indicate that the power sources within the orbiter can furnish the payload power identified. The profile also shows a limited segment of self-sustained orbital operations where the LST is free of the orbiter. The profile investigations were not intended to fix specific mission cases. Generalization of highest possible and probable load combinations were sought. Key letters on the profile are identified in Table IV-6.

i. Total Power Requirements Summary. The total power requirements, determined for the LST from the foregoing load information, is summarized in Table IV-7. The peak power requirement was determined from profile investigations. This peak is considerably less than the sum of the loads connected to the buses.

B. Reference System Summary

The LST electrical system is primarily located in the SSM, which can be pressurized for in-space maintenance and system updating. The electrical system consists of the electrical power subsystem and the electrical distribution subsystem. The EPS and the EDS are functionally interdependent — as a system they are self-sustained and provide the necessary power and distribution

TABLE IV-6. LST ELECTRICAL POWER TIMELINE FOR SHUTTLE LAUNCH AND INITIAL OPERATIONS

Time (hr:min)	Profile Key	Event
-72		LST Battery Test
-48		Combined Systems Check
-5		Transfer to Shuttle Power
+6	A	Circularize into 611 km
7:30		Open Bay and Erect LST
7:40		LST Distribution and Power Check
7:50	B	Start CMGs and Gyros
8:50	B	Deploy Light Shield
9:00		Limited SSM Checks
13:00	C	Thermal Heaters Coming On (Auto)
16:00		CMG Spinup Completed
23:00	D	ACS Checks with Orbiter
32:00	E	LST Solar Array Deploy/Retract Test
34:00	F	LST Communications/Data Handling Test
46:00	G	Verify ACS, C&DH Functions
47:00	H	Thermal, Power and Data Test
48:00		Verify Outgassing O.K.
48:30		Functional Checks on Instruments and Power Supplies
69:00	I	Preliminary Calibration and SSM Tests
96:00	J	Continue Preliminary Calibrations
144:00	K	Verify Release Readiness
144:10	K	LST on Internal Power
144:15	K	Disconnect Cables
144:50	K	Eject LST and Begin Stationkeeping
144:53		LST Under Ground Command
145:00	L	ACS Pointing Tests and Experiments
—	L	Max Peak Power Check
149:00		Exercise Subsystems and Check Experiments by RF Links
—	M	Normal Operating Peaks
150:00		LST Begins Normal Operations
—	N	Average Power Level

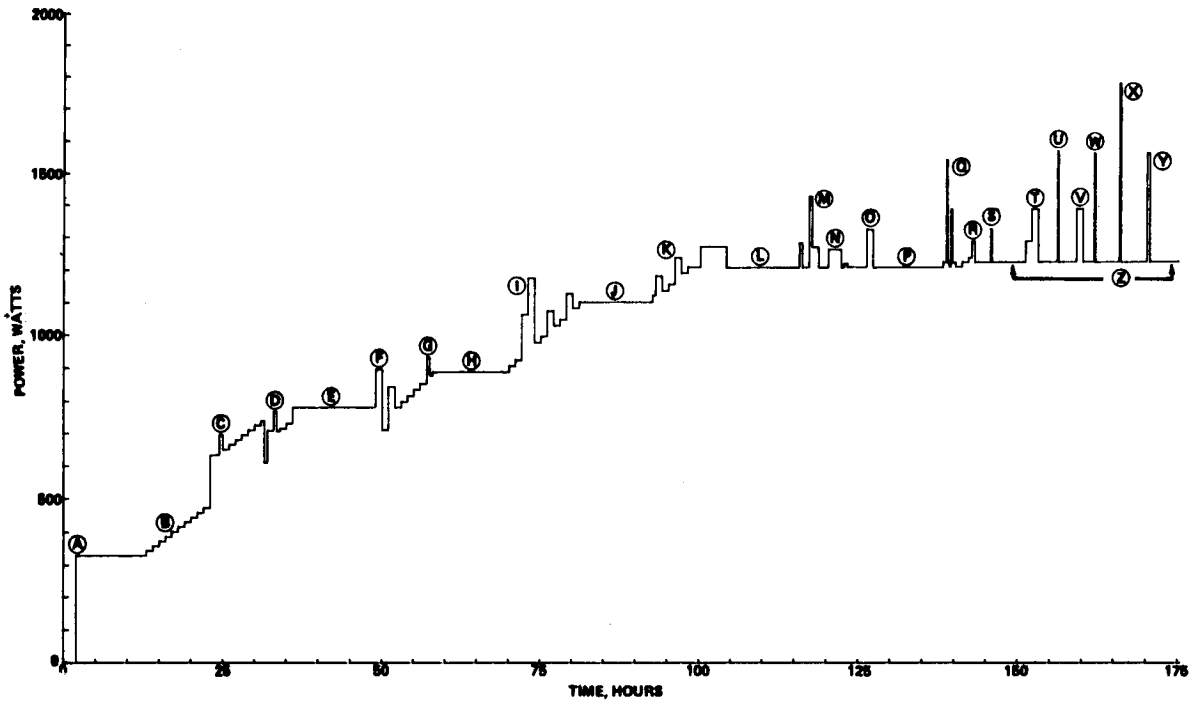

Figure IV-1. LST power profile for launch and orbital checkout.

TABLE IV-7. TOTAL AVERAGE LST SUBSYSTEM POWER REQUIREMENTS

SUBSYSTEM	AVERAGE POWER WATTS	MAXIMUM [b] PEAK POWER WATTS
ATTITUDE CONTROL AND SENSING	179	227
COMMUNICATIONS AND DATA HANDLING	88	127
ELECTRICAL SYSTEM	46	143
OPTICAL TELESCOPE ASSEMBLY	501	819
SCIENTIFIC INSTRUMENT PACKAGE [a]	469	469
TOTAL POWER	1283	1785

a. SIP POWER IS CONSTANT; HEATERS MAKE UP THERMAL DISSIPATION OF "OFF" INSTRUMENTS.
b. ASSUMES ALL NORMAL OPERATING PEAKS OCCUR SIMULTANEOUSLY.

services to operate the LST. These subsystems are composed of assemblies that house the devices and components required for generating, storing, and conditioning power and for controlling and protecting the distribution networks. The complement and characteristics of the major electrical equipment are given in Table IV-8.

TABLE IV-8. ELECTRICAL SYSTEM EQUIPMENT

Components	Quantity	Unit Dimensions (mm)	Total Mass (kg)	Average Thermal Load (Total) (W)
Active System				
Battery Assembly	6	406 × 279 × 178	134.4	126
Charger Assembly	6	305 × 203 × 152	40.9	36
Regulator Assembly	6	279 × 203 × 127	21.4	135
Solar Power Distribution	2	325 × 165 × 152	10.9	20
Electrical Control Assembly	2	356 × 203 × 203	14.5	24
Electrical Distribution Unit	8	152 × 102 × 76	9.1	24
Solar Panels	12	3370 × 927 × 10	186.4	—
Deployment Mechanism (Sets)	2	—	96.4	—
Orientation Mechanism and Electronics	2	200 Dia × 350	20.0	4
Cabling	—	—	113.6	43
Active System Total			647.6	412
Inactive Equipment For Maintenance				
Lights	8		9.1	120
Caution and Warning Assembly	1	Units Energized	4.5	10
Headset Receptacles	3	from IESE[b] in	4.5	—
ECLS[a] Provisions	—	Orbiter	2.3	—
Test Cables, Umbilicals, Etc.	—		18.2	—
Inactive Equipment Total			38.6	130

a. Environmental control and life support.
b. In-space electrical support equipment.

Automatic controls are provided to protect the system against many types of failures possible in the 5 year mission. Particular attention was given to avoiding catastrophic conditions that might impair the ability to recover and maintain the vehicle. Protection will favor those loads considered critical to survival. System operations are controllable from the ground via the interfaces with the command and data subsystems. Power management may be effected in response to the status and diagnostic information telemetered to the remote control stations.

The system has provisions for test and checkout operations on the ground. The external connectors are located on the aft end of the SSM to satisfy the interface requirements being established for in-space operations and maintenance with the Shuttle orbiter. Limited use of the same interfaces will satisfy the Shuttle launch phase requirements. In the event that the alternate launch vehicle is used, the system is designed for easy adaptation to the Titan-OAS system. Mounting space and additional distributor connectors will be provided to accommodate "add-on" Mod Kits consisting of small junction assemblies and adapter cables.

As assumed for Phase A, the three major elements of the LST — the SSM, the OTA, and the SIP — contain a section of the electrical system. The SSM provides the subsystems and electrical integration functions necessary to energize, operate, and control the LST and to retrieve the scientific information.

The electrical system configuration was primarily influenced by the configuration and electrical size of the LST, the 5 year mission, the high reliability needed, and the considerations given to cost and maintenance. As indicated, critical components and networks are made redundant because they determine the probability of mission success based on the practicality of in-space maintenance. Low cost rather than mass and performance optimization was of primary importance in the selection of design concepts. Except for special scientific items, existing technology has been used throughout. Space-proven assemblies have been used, in general, whenever it was determined that such have adequate capacity and electrical characteristics for the LST system. For the few cases where existing assemblies were not satisfactory, qualified subassemblies, modules, and designs were selected from such programs as HEAO, OAO, Skylab, ATM, Air Force programs, et al. Since very little of the reference hardware has been qualified for the life and reliability required for LST, maintenance is essential to achieve mission objectives, especially when components with known life limits are considered.

Studies were performed to use the unprecedented advantages provided for payloads by the Shuttle system. Based on preliminary information pertaining to the Shuttle support system and crew capabilities, the pressurized LST was the most practical, cost-effective approach. It minimized operational risks, provided the most extensive maintenance capabilities, and offered the best utilization of in-space time. Compared to other versions studied from an electrical standpoint, the pressurized concept tended to reduce mass, volume, and design complexity and permitted modularization for reliable service and selection of proven, low-cost assemblies. The reference electrical configuration and assembly concepts also appear to be consistent with minimum cost for test, spares, and logistics.

The assembly and cabling concepts of the system considered low cost design and fabrication methods consistent with modularization needed for ease of replacement and testing, and for reliable operations. To assure trouble-free operations, networks required only for launch or maintenance are kept independent, physically and electrically, to the extent possible. Assembly configurations were based on reliable operation, thermal compatibility, and features needed for maintenance. Reference to Figure I-5 and Table I-1 of Chapter I will show that the electrical equipment is located, with most of the SSM equipment, in the aft section of the SSM, around the circumference of the cylindrical module. The arrangement considered efficient cabling as well as access for maintenance. Special attention was given to locating temperature-sensitive items, such as the batteries. The batteries are located on the side of the vehicle that will normally face away from the sun. The thermal design will keep the batteries normally below 10°C and will maintain close temperature control, both of which are essential to reliable performance.

A simplified block diagram of the SSM electrical system is given in Figure IV-2. The electrical relationship of the major assemblies dedicated to power generation and distribution and to test and maintenance are shown. A more complete schematic is given in Section D of this chapter.

The power distribution networks are composed of two solar power distributors (SPDs), two electrical control assemblies (ECAs), eight remote electrical distribution units (EDUs), cabling, and interface devices. The SPDs centralize and control the power transmission network that primarily services the electrical power subsystem. Although the solar array is not redundant, it is modularized for protection and redundant wiring is provided to the SPDs. Each SPD receives power from one wing of the array. Either or both of the redundant primary buses may be energized. Control switching permits crossties between the buses of both SPDs.

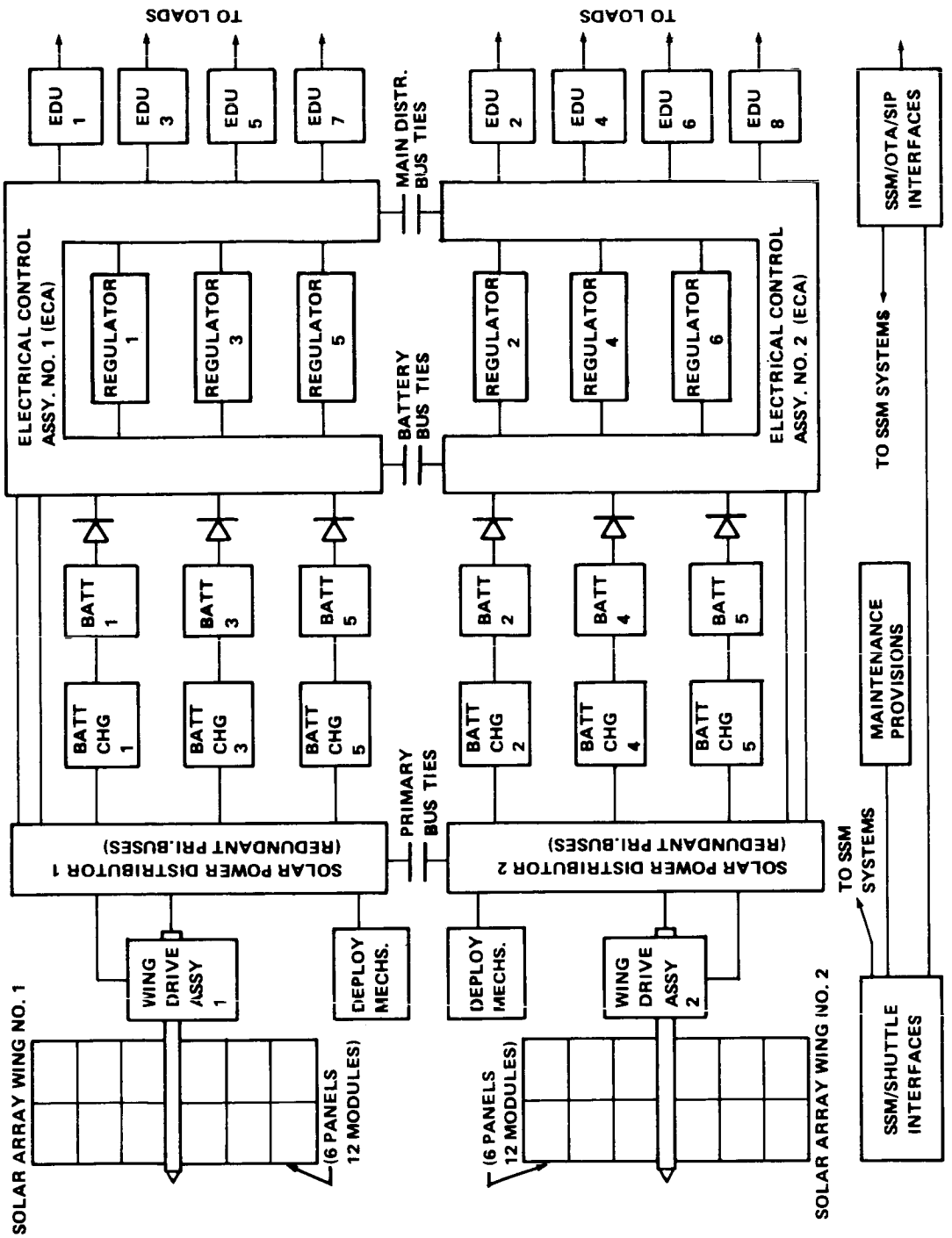

Figure IV-2. Reference electrical system.

The SPDs protect and control the transmission of primary power to the EPS assemblies and to the ECAs. Cabling from the external interface is provided to the SPDs for control and test purposes during ground, launch, and in-space maintenance operations. Although the SPDs have provisions to house a remote command decoder (RCD), they presently receive commands via the ECAs which have the RCDs allocated for electrical system functions.

Main distribution is centralized and controlled by the ECAs, which are redundant with each having the capacity to satisfy the requirements of the LST. The inputs to each ECA are redundant. They receive primary power from the SPDs, secondary power from the batteries, and regulated power from the regulators. Each ECA houses redundant buses which may be crosstied to the buses of the other ECA. Main distribution is protected with the ECAs and directed to the EDUs. The single-point grounding for the entire system is located in the ECAs.

The EDUs receive power from the ECAs and control and protect secondary distribution. These units are also redundant and are decentralized to provide for growth and versatility. They provide output adaptability for the OTA/SIP but simplify and maintain the interfaces to be established with the SSM. Electrical access from the OTA/SIP to the external interfaces is channeled through the EDUs.

The electrical power subsystem of the electrical system consists of two deployed, pivoted solar array wings; orientation, deployment/retraction assemblies; six battery charger assemblies; six regulator assemblies; and various sensors and control devices. With maintenance, the EPS is rated to deliver 1500 watts at 28 ± 2 percent Vdc throughout the mission. The functions and characteristics of the EPS equipment are described in the following section.

C. Electrical Power Subsystem

1. Summary. The EPS must furnish power to all the LST electrical loads and must satisfy system losses during orbital operations. If the alternate launch vehicle is used, the LST EPS must supply the necessary power during launch and subsequent phases of the mission. With maintenance, it must have the capability to sustain operations throughout the 5 year mission.

The reference EPS is designed for an orbital average power of 1500 watts at the 5 year, end-of-mission (EOM) conditions. Although the peak

capability of the equipment is greater, the EPS is rated for a peak power of 2700 watts to limit the discharge rate to half the rating of the combined batteries. As determined by the preliminary load analyses discussed in Section A.2, the LST requires an average power of 1283 watts and a peak power of 1785 watts. This gives a design margin of 217 watts and 915 watts for the average and maximum power, respectively. The system has an overall efficiency of 77.8 percent, including energy storage and distribution losses.

Except for its size and the features required for adaptation to the LST, the EPS is a conventional solar array, battery-type power system with output power conditioning to regulate system voltage at 28 Vdc ± 2 percent. Design and performance criteria determined for existing hardware modules and qualified components have been used for establishing the concepts and size of the system.

A centralized, series regulator configuration was selected because it simplified design and integration, it offered good performance and reliable service, and it was considered cost effective. This configuration was selected from four candidates subjected to tradeoff studies for the LST application. Similar research applications module (RAM) studies tend to confirm this selection. Decentralized concepts offer more versatility and isolation but require more hardware. The protection and versatility provided in the EDS permit incorporation of power conditioning in the remote EDUs, if required. The concept permits such changes later as the system design matures. For large loads, the central regulators can be bypassed to avoid additional conditioning losses.

Figure IV-3 is a diagram of the electrical power subsystem for LST.

2. Reference Configuration and Performance Requirements. Various EPS configurations were reduced to lumped parameter models for computer analysis of the design and performance requirements for the major elements of the subsystem. The preliminary considerations given these configurations and the rationale for selecting the reference design are discussed in Section F.1 of this chapter. A block diagram of the design reference EPS configuration is shown in Figure IV-4. The symbols and values used are defined in Table IV-9.

The voltage and load requirements established in Section A.2 are considered to be at the load terminals, exclusive of the distribution losses, η_o. The orbital average design load of 1500 watts provides a 217-watt design margin for growth and flexibility for updating the scientific instruments.

a. Power Conditioning Requirements. The average output rating of the power conditioning/regulator elements must satisfy the average design load and distribution losses. Therefore, the average rating must be 1530 watts. To assure that maximum loads and transients are safely handled, these elements should have a peak rating of at least 1.5 times the average, or 2295 watts. The output voltage should be slightly higher than the nominal 28 Vdc, and the regulation must be slightly better than the ±2 percent specified for the loads. Since the power conditioning assemblies receive power from the primary (solar array) buses during sunlight periods of the orbit and from the energy storage (battery) buses during occultation, the inputs must be compatible with both the battery and solar array voltages. The baseline EPS employs buck-boost regulators which permit the input voltage range to exceed the extreme range of 24 to 88 volts expected from the solar array-battery combination.

b. Energy Storage Requirements. The energy storage part of the EPS consists of batteries of rechargeable cells and their associated power conditioning assemblies designated as charger assemblies. Referring to Figure IV-4, the primary power available from the solar array is zero during occultation and the system load must be supplied from energy storage. The system efficiency when the batteries are discharged during occultation, η_{BD}, is given by

$$\eta_{BD} = \eta_o \eta_r \eta_d = 86.5 \text{ percent} \quad . \tag{1}$$

If the peak value of P_{Ld} is used with equation (1), the minimum power or current rating of the batteries is established.

Equation (2) defines the energy storage requirements E_D as a function of the occultation period, t_d; the average load during occultation, P_{Ld}; and the system losses involved:

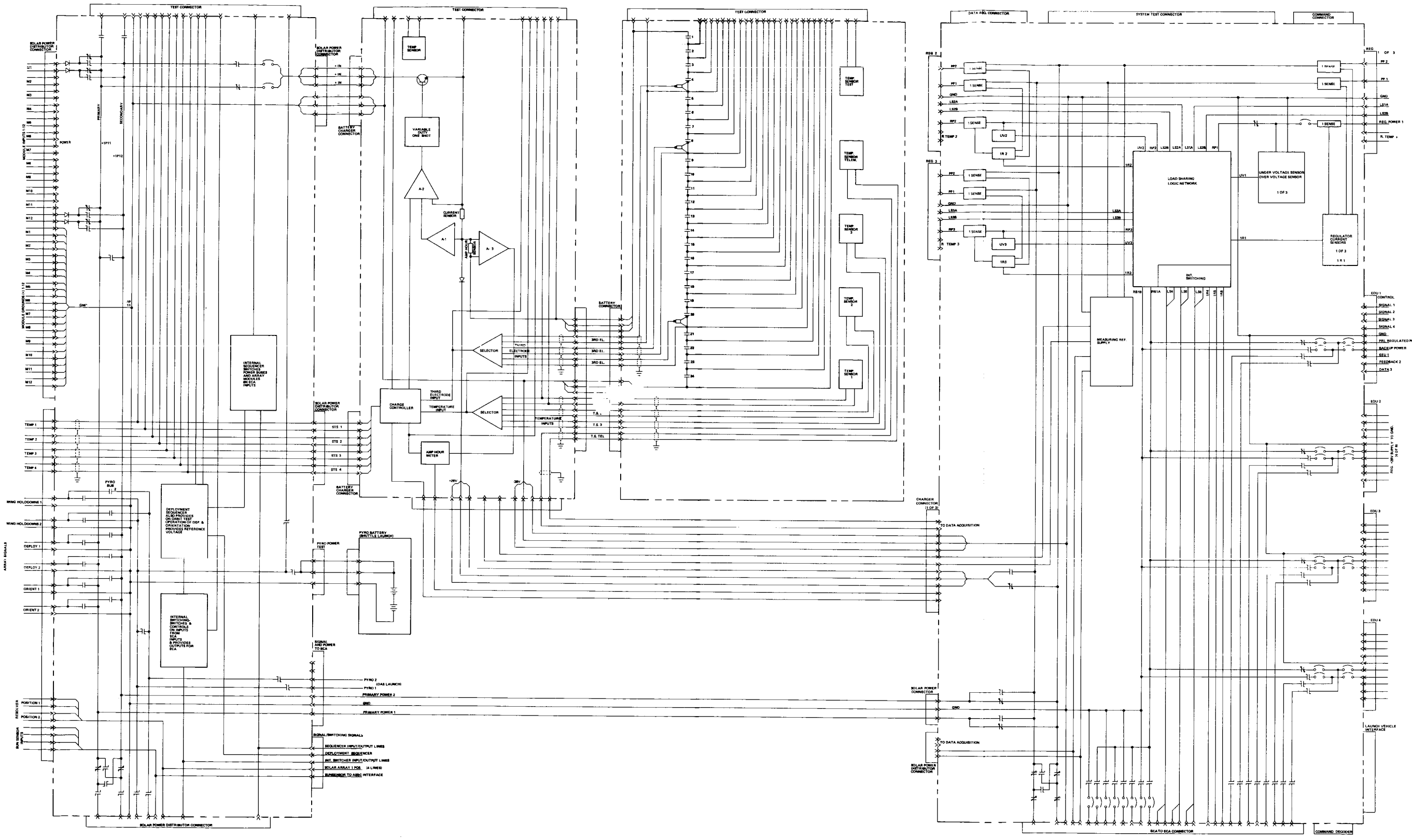

Figure IV-3. Electrical power subsystem schematic.

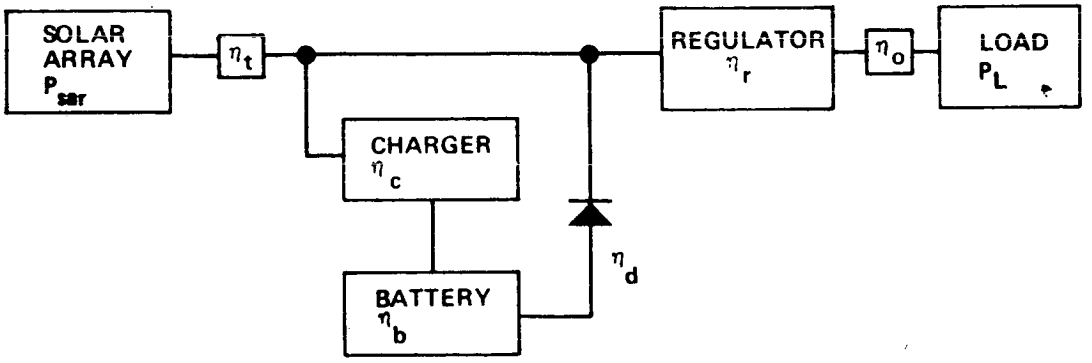

Figure IV-4. EPS configuration.

TABLE IV-9. EPS SYMBOLS AND DESIGN FACTORS

Symbol	Definition	Values	Unit
P_L	Orbital Average Load Required	1500	watts
P_{LS}	Average Load During Sunlight	See Note a	watts
P_{Ld}	Average Load During Darkness	See Note a	watts
J	Ratio of P_{Ld} to P_{LS}	See Note a	—
t_o	Orbital Period	1.615	hours
t_s	Sunlight Period (min)	1.021	hours
t_d	Occultation Period (Max)	0.592	hours
E_D	Energy Required During Occultation	TBD[b]	W-h
P_{SR}	Solar Array Power Required	TBD	watts
η_t	Solar Power Transmission Efficiency	98	%
η_c	Charger Efficiency	95	%
η_b	Battery Watt-Hour Efficiency	80	%
η_d	Battery to Regulator Line Efficiency	97	%
η_r	Regulator Efficiency	91	%
η_o	Output Distribution Efficiency	98	%
η_{ps}	Primary Power to Load Efficiency	87.4	%
η_{BD}	System Efficiency During t_d	86.5	%
η_{ES}	Efficiency of Energy Storage Loop	73.7	%
η_{EPS}	Overall System Efficiency	TBD	%
M_s	Performance Factor (P_{SR}/P_L)	TBD	%

a. Output power considered parametrically.
b. TBD — To be determined.

$$E_D = \frac{P_{Ld} \cdot t_d}{\eta_{BD}} \quad . \tag{2}$$

For the maximum occultation, a 1500 watt load requires 1024 watt-hours of energy.

Figure IV-5 shows the sensitivity of energy storage requirements to variations in P_{Ld} for the maximum and average occultation periods of the specified 611 km orbit. The importance of determining a good power profile on the basis of sunlight/dark periods is illustrated by Figure IV-6. The variation in energy storage requirements has been shown as a function of the ratio of load during occultation to the load during sunlight, with the restriction that the 1500 watt orbital average design load, P_L, be maintained constant. The average orbital load is defined by

$$P_L = \frac{P_{Ld} \cdot t_d + P_{LS} \cdot t_s}{t_o} \quad . \tag{3}$$

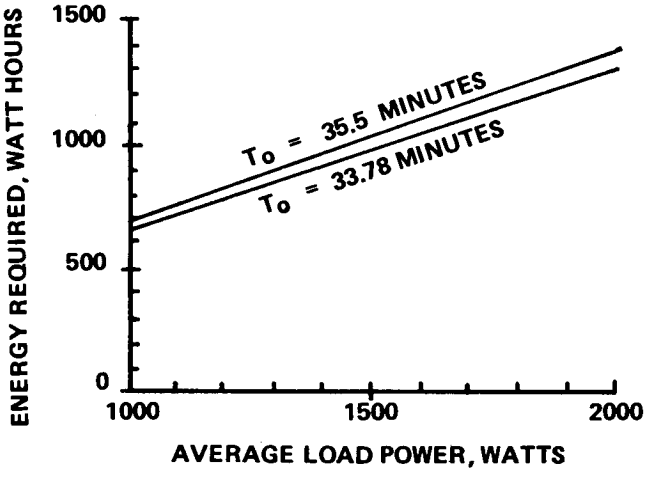

Figure IV-5. Energy required as a function of load and occultation.

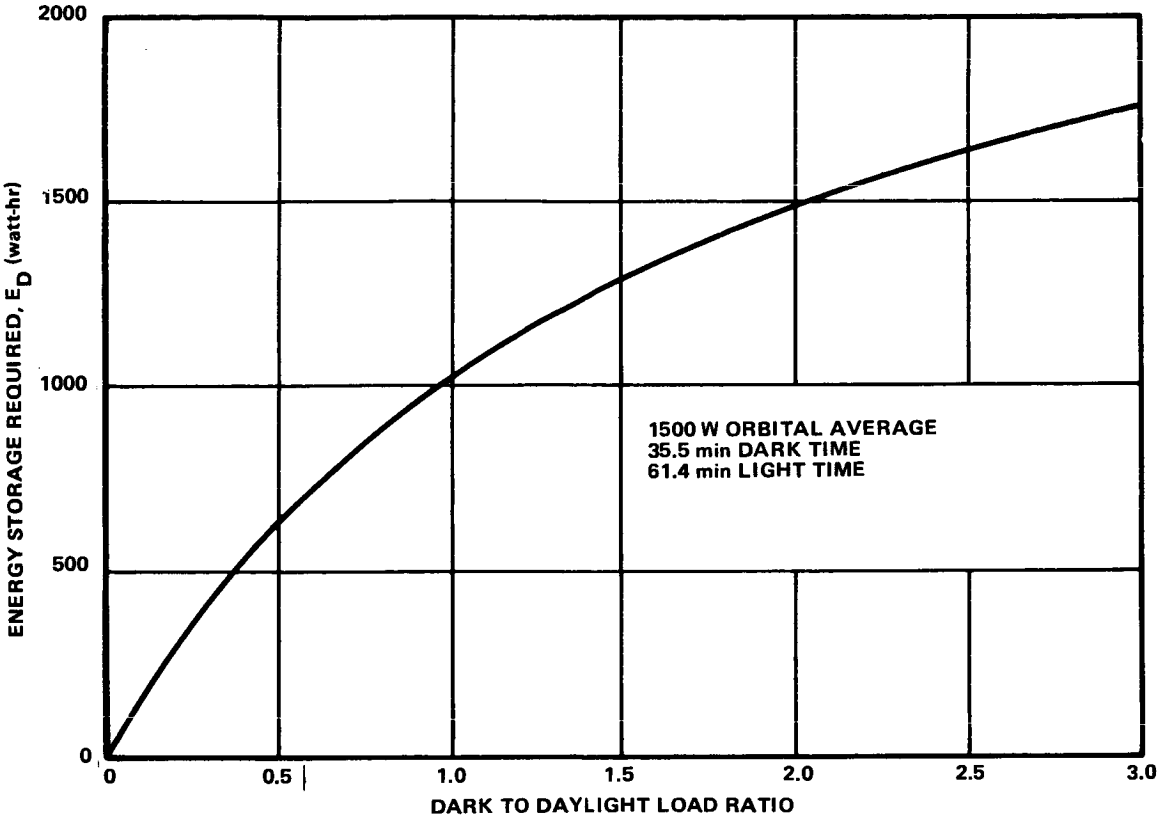

Figure IV-6. Energy storage versus dark to daylight load ratio.

c. Solar Array Requirements. During sunlight periods, the solar array must simultaneously furnish the system load, P_{LS}, satisfy system losses, and replace the battery energy used during the occultation period. The efficiency, η_{ps}, at which the system delivers power to the load is

$$\eta_{ps} = \eta_o \eta_r \eta_t = 87.4\% \quad . \tag{4}$$

The efficiency of the energy storage loop of the EPS is defined by

$$\eta_{ES} = \eta_d \eta_b \eta_c = 73.7\% \quad . \tag{5}$$

From Figure IV-4, the average solar array power required, P_{SR}, may be derived in terms of the sunlight load and the dark load as given by

$$P_{SR} = \frac{P_{LS}}{\eta_{ps}} + \frac{P_{Ld}\, t_d}{\eta_{ps}\, \eta_{ES}\, t_s} \quad . \tag{6}$$

Letting J equal the ratio, P_{Ld}/P_{LS}, and substituting equation (3) into equation (6), one can state the solar power required in terms of the orbital average load and the ratio of dark load to sunlight load as given by

$$P_{SR} = \frac{P_L\, t_o}{\eta_{ps}\, \eta_{ES}\, t_s} \quad \frac{\eta_{ES}\, t_s + J\, t_d}{t_s + J\, t_d} \quad . \tag{7}$$

For the selected baseline design conditions, $P_{SR} = 3054$ watts.

The solar array power required is shown as a function of load and occultation period in Figure IV-7. It is assumed that $P_L = P_{LS} = P_{Ld}$ (i.e., J = 1) for this plot.

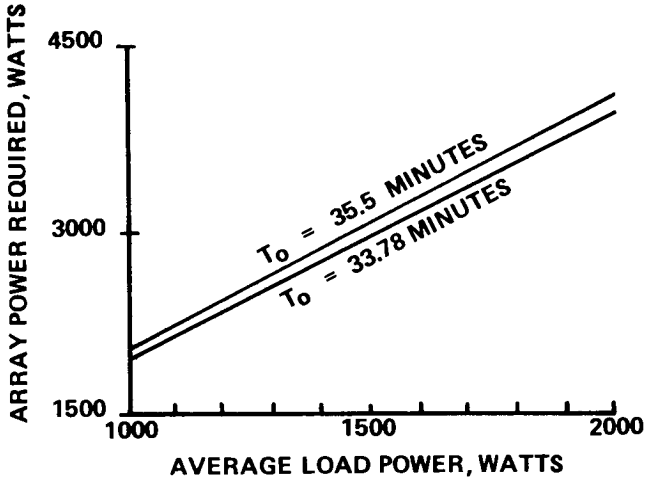

Figure IV-7. Array power required as a function of load and occultation.

The system performance factor, M_s, defined as the ratio of solar array power required to the orbital average load, is given by

$$M_s = \frac{P_{SR}}{P_L} \quad . \tag{8}$$

Since this factor indicates the size of the array needed, it has been plotted in Figure IV-8 against J, the ratio of occultation power to sunlight power, maintaining the orbital average load at 1500 watts. For the reference design conditions, $M_s = 2.04$. The total watt-hour efficiency of the system, η_{EPS}, is the total energy received by the load throughout the orbit divided by the solar array energy supplied. Combining equations (3) and (7), the total efficiency is determined by

$$\eta_{EPS} = \frac{\eta_{ps}\,\eta_{ES}\left(t_s + J\,t_d\right)}{\eta_{ES}\,t_s + J\,t_d} \quad . \tag{9}$$

For an average orbit and $J = 1$, the efficiency of the design reference EPS is 77.8 percent.

3. Reference Solar Array

a. Configuration and Stowage. Low cost and proven technology were of prime importance in the LST study. Within reasonable limits, weight was not a constraint; the Shuttle allows a liberal weight margin for the LST spacecraft. Conventional array construction was selected for the reference design because of the Titan alternate launch vehicle, although more advanced designs offer more advantages when Shuttle maintenance operations are considered. The alternate arrays considered are described in Section F.2. Although flexible arrays may be 10 to 15 percent more expensive at the present time, they are scheduled for several programs in the near future. Their increasing use could make them more economical than the rigid panel type by the time the LST detail design phase starts.

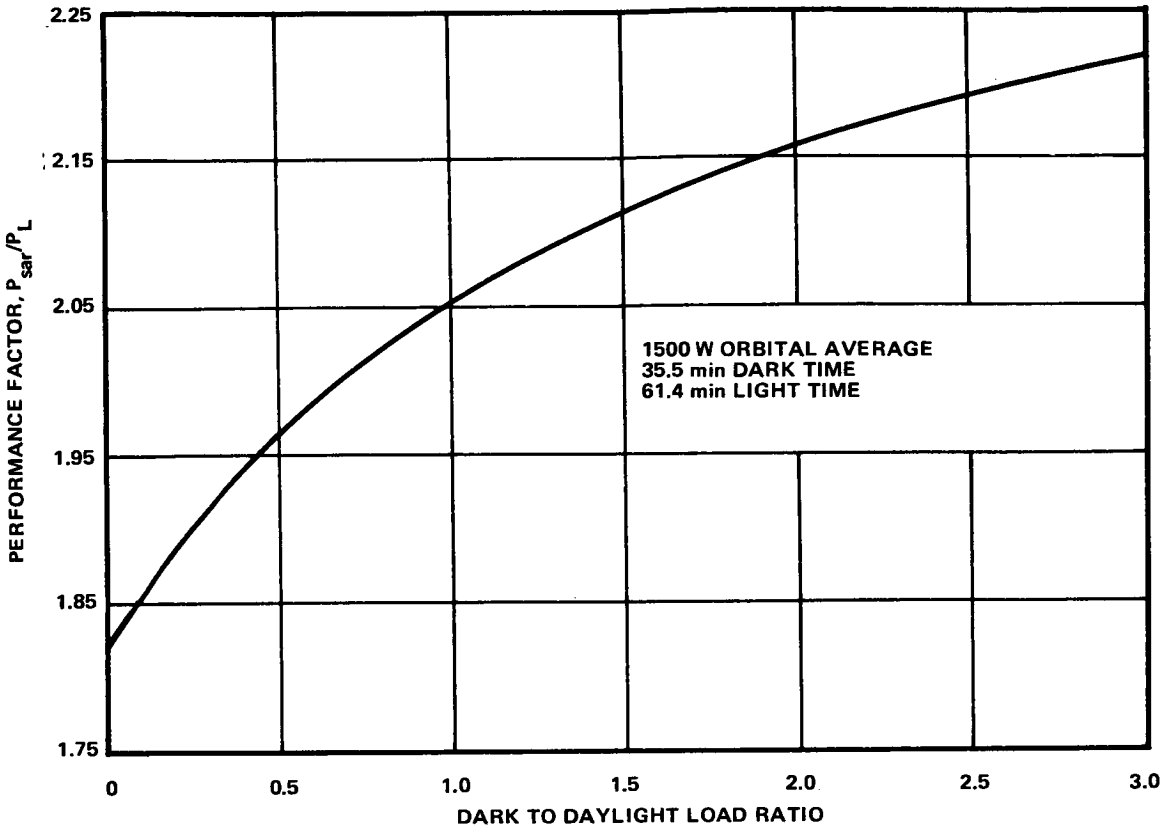

Figure IV-8. Performance factor versus dark to daylight load ratio.

Figure IV-9 shows the reference solar array deployed on the LST. As was shown in Section C.2, the design load of 1500 watts requires an EOM average power rating of 3054 watts at the design temperature of 63°C. With this requirement, an oriented array is necessary for the requisite array dimensions and the LST pointing constraints. The array consists of two deployable wings mounted on two booms as illustrated. Once deployed, the wings rotate about the Y-axis of the vehicle to achieve sun orientation for efficient use of the array.

The requirement for an alternate Titan launch vehicle was an important constraint upon the solar array design. The Titan IIIE shroud envelope limit of 374 cm diameter confines the stowage space so that a wrap-around configuration is needed. The array stowage and deployment concepts are shown in Figure IV-10. Although this configuration is somewhat heavier than a completely folded version, it is a simpler design, and deployment/retraction

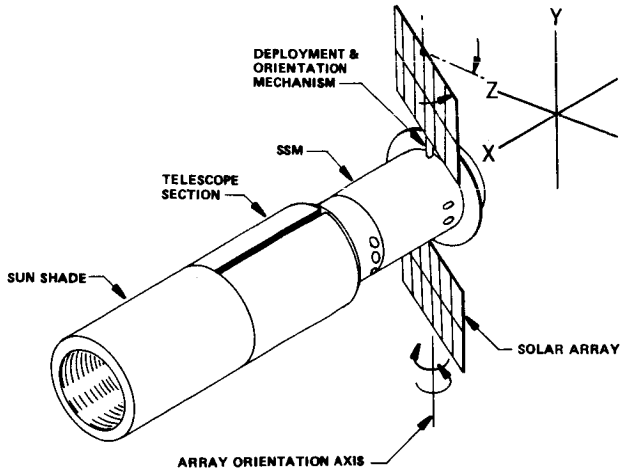

Figure IV-9. LST with deployed solar array.

reliability is higher. The folded version also would have required the SSM configuration to change. The cylinder would have to be flattened on two sides to accommodate array stowage. The stowage constraint does not apply for a Shuttle launch.

With the design reference concept, the array is near its maximum size with the constraint that it be mount only on the SSM. A slight increase in panel length is possible. The mounting ring structure (also resulting from the alternate launch requirement) provides bearing mounting for the cylindrical rotatable booms. These are required to support the wing assemblies which weigh 141.4 kg each. A second set of bearings is located within the orientation drive assembly inside the SSM. The boom locations on the aft end of the SSM offer thermal advantages for the spacecraft and minimize influence on the sensitive OTA structure.

Each wing consists of six hinged, rigid panels which become erect when the booms are deployed. Torsion rods provide the driving force. Each panel consists of two modules on which the solar cells and cover slides are mounted. The module substrates are aluminum honeycomb assemblies, similar to those used for HEAO and Skylab. The length and width of the modules were selected to fit the SSM tightly when the array is folded.

The wing dimensions shown in Figure IV-10 provide a total array area of 39.1 m^2. This size allows for the degradation predicted to result from 5 years of exposure to space radiation, ultraviolet radiation and

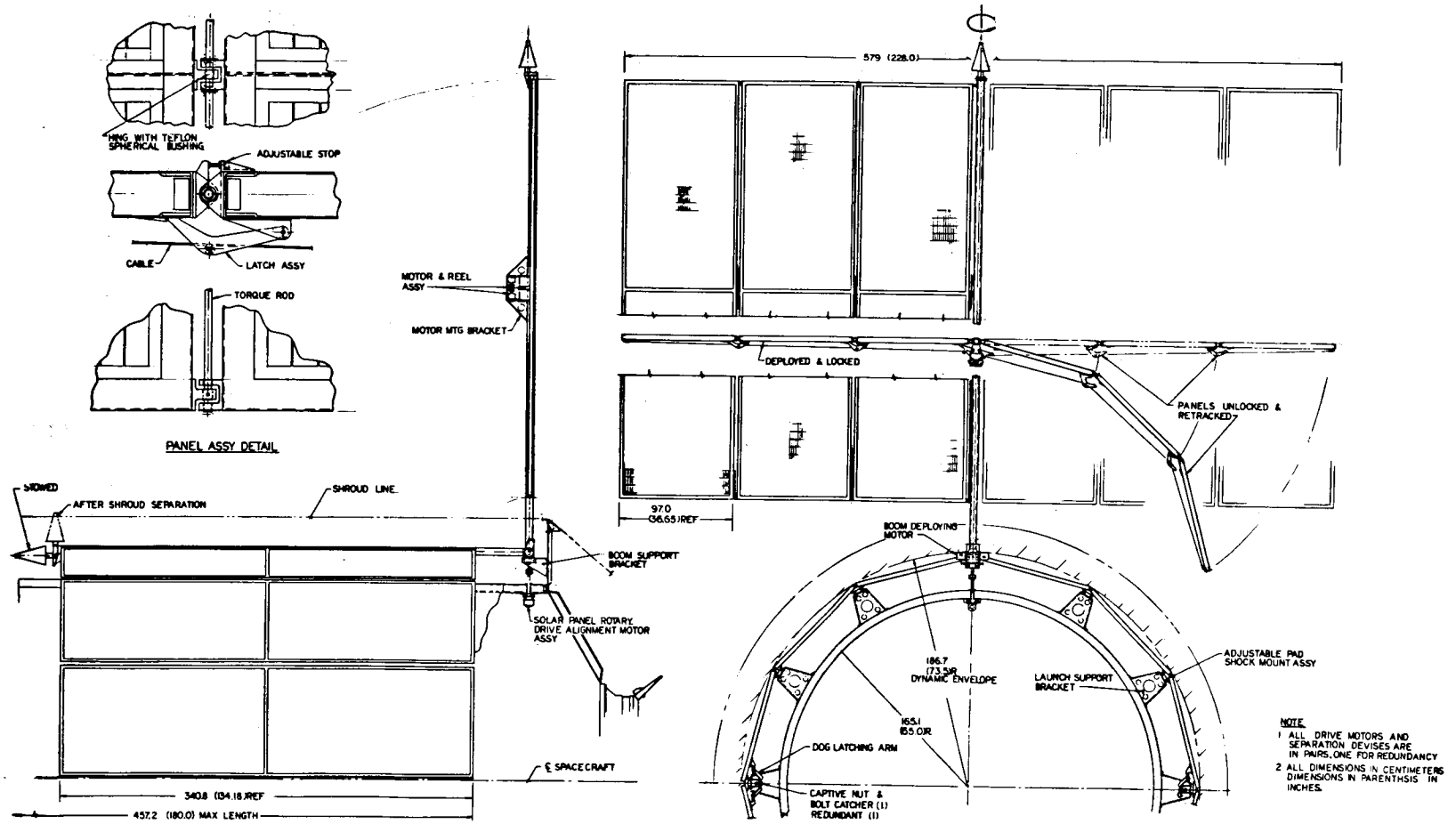

Figure IV-10. Reference solar array configuration.

micrometeorites. The 5 year design is necessary because the array is not suitable for easy in-space replacement. EVA would be required to replace or repair the array. As an assembly, it is too massive and unwieldy for a suited man to handle. However, the modules and mechanisms are designed so that they could be readily disconnected for replacement of individual components of the array. The Shuttle revisit capabilities permit smaller design margins and optimistic degradation predictions without undue risk to the mission.

b. Deployment/Retraction. During launch, the array panels are held against shock absorbing snubbers to prevent shock and vibration damage. Pyrotechnic separation bolts of the type to be used for the HEAO were tentatively selected because of the possible use of the alternate launch vehicle. Several such devices have been qualified and are considered applicable; selection will depend on detail design. These units have redundant firing squibs and would be connected to redundant switches and sources for firing. Separation joints are redundant (two in series) and each is held by a separate bolt. This assures that array separation will occur. Considering a Shuttle launch and maintenance, this is not a desirable approach. Powered mechanical latches should be investigated for array release. These should have the ability to automatically relatch the array when it is retracted for a Shuttle visit.

When the panels are free, the torsion rod linkages extend then into a planar configuration. The controlled wire cable can provide damping if necessary. Once erected, they are latched in this position. Proper sequencing is provided to initiate boom deployment after the panels are released. The motor-gear assembly at the boom hinge point is energized to rotate the boom outward 90 degrees. Redundant limit switches deenergize the motor when boom deployment is achieved. The current limiting motor-drive design offers additional protection. The motors are rated for continuous stall current should the limit switches fail. Deployment power can be turned off later by remote command.

The retraction requirement is not conventional and a unique design is required. This is one of the reasons the alternate flexible arrays were attractive. Analysis indicated that the deployed reference array is sturdy and rigid enough to withstand release and docking forces associated with Shuttle operations. Present docking concepts permit deployment of the array when it is attached to the Shuttle. The LST, with arrays deployed, is shown attached to the orbiter in Figure IV-11. In its worst position, the array has ample clearance, although rotation of it would provide greater clearance, if desired for docking operations.

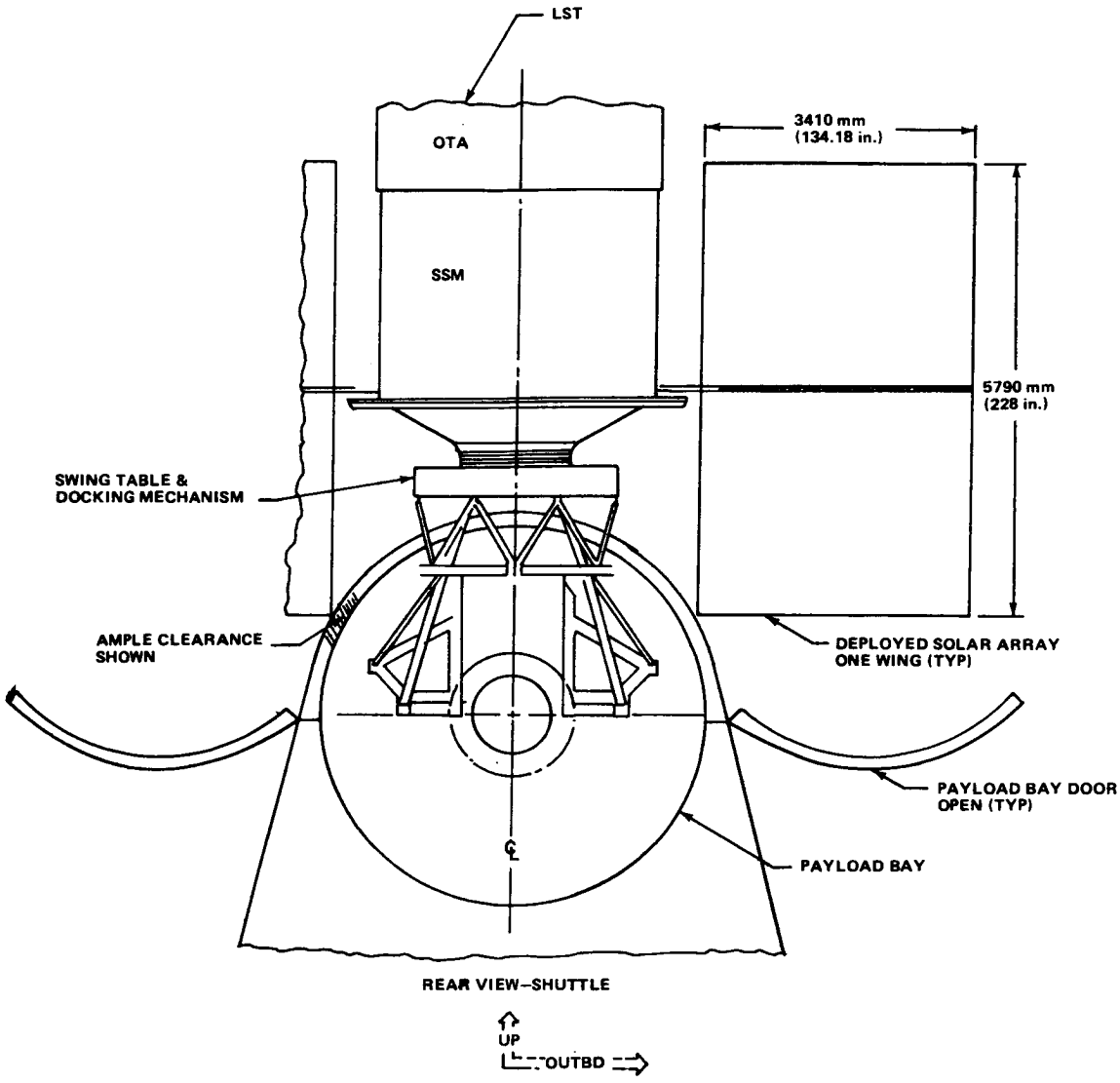

Figure IV-11. Array clearance with Shuttle.

However, to provide the capability to retrieve the LST into the payload bay, retraction mechanisms are included in the design. The deployment sequence is reversed for retraction. Upon command, the boom deployment motors are energized over separate lines provided for reverse operation. When the boom reaches the stops on the SSM, limit switches deenergize the

boom motors and energize the retraction motors. The retraction motor and cable linkages unlatch the wing panels and draw them back around the SSM mountings. Limit switches deactivate the retraction motors. All mechanisms are reversible and command overrides are provided for all switching operations.

c. Solar Cells and Coverslides. The LST application requires no unusual characteristics, exceptionally lightweight assemblies, or unique techniques that might incur high cost to satisfy stringent requirements. Based on previous solar cell and coverslide performance trade studies, and on historical cost information, the cells and coverslides were selected to obtain the most cost-effective array for the 5 year mission. Several sizes, thicknesses, and two-base resistivities were considered for N/P silicon cells. Glass and fused silica, several thicknesses, and several coatings were variations in coverslides considered. The cost per watt at the end of the reference mission was determined on the basis of fabricated assembly costs and long-term performance variations. For the typical coverslides considered, the selected 10 ohm-cm base resistivity was better beyond 3 years. Fabrication and breakage costs are higher for thin cells and coverslides. Unit cost is not a function of thickness, but of processing. The efficiency is higher for thicker cells, and is near maximum for 0.031 cm thickness. The cell size of 2×4 cm is becoming an industry standard because it is most economical for a given output. The thicker fused silica coverslides with blue filter were best for the LST mission because of lowered transmission losses and decreased overall degradation.

Typical characteristics for the coverslide selected for the LST array are listed in Table IV-10.

TABLE IV-10. COVERSLIDE CHARACTERISTICS

Name	Blue filter coverslide
Size	$4 \times 2 \times 0.031$ cm
Material	Fused silica
Manufacturer Type	Corning 7940
Filter Coating	Rejects below $0.410 \pm 0.015\ \mu$
Antireflection Coating	Less than 2% reflection
Transmission Loss	Less than 4% above $0.450\ \mu$

Characteristics and ratings of the reference solar cell are given in Table IV-11; they are specified at industry-standard conditions. Standard temperature is 28° ± 2°C, with illumination of 140 mW/cm^2. Power and efficiency ratings are based on total solar spectral energy incident on effective solar cell area. The incidence angle is within 1 degree of normal (90 degrees ± 1 degree).

TABLE IV-11. BARE SOLAR CELL CHARACTERISTICS

Type	Silicon N/P
Size	2 × 4 × 0.031 cm
Base Resistivity	10 ohm-cm
Contacts	Ag-Ti
Effective Area, Min	7.7 cm^2
Open Circuit Voltage	0.554 V
Short Circuit Current	285 mA
Max Power Voltage	0.442 V
Max Power Current	259 mA
Efficiency, Nominal	10.6%

Solar array construction incurs unavoidable losses in performance due to coverslide losses, contact and wiring resistance, and cell mismatching. Figure IV-12 shows the composite array degradation predicted over a period of 5 years for the reference design. Analysis of previous array performance in space and radiation test results show that both voltage and current decrease. The effect on cell current is much greater however. For the predicted space environment, the reference cell characteristics were adjusted for degradation to determine the EOM array performance. For the several factors that contribute to degradation, the equivalent power loss is given as a percent of initial power rating in Table IV-12.

Solar array performance is significantly affected by other factors — temperature, intensity, and angle of incidence. Array power is a function of the cosine of the angle of incidence. Since the array is to be normally oriented, no corrections were made for increased reflectance losses that occur when the incidence angle exceeds ~45 degrees. Thermal analyses were made to determine the array temperatures as a function of orbit cycles and extreme thermal cases expected for the mission. Array thermal characteristics and temperatures are discussed in Chapter III. The solar constant variations and temperature coefficients applicable to the reference design are given in Table IV-13.

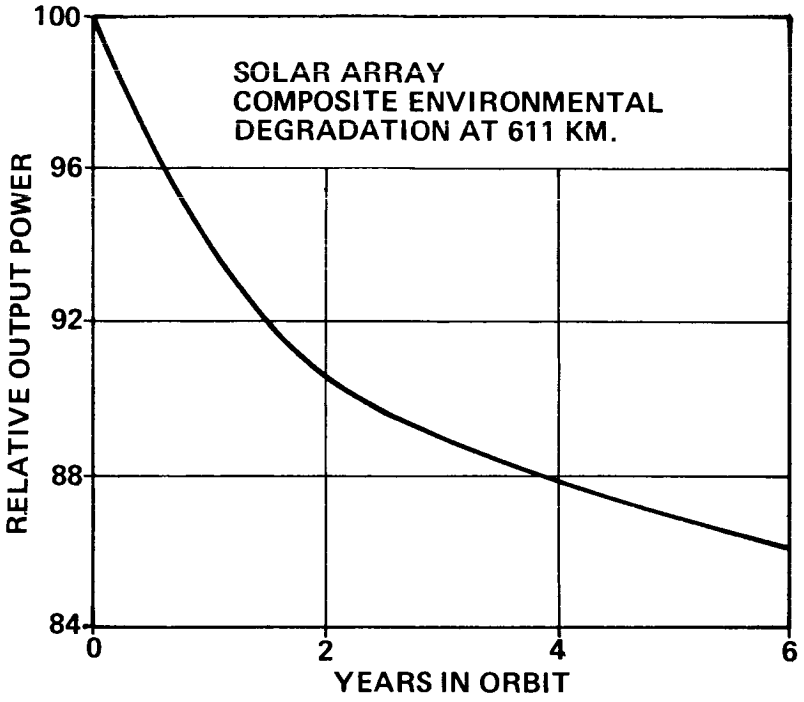

Figure IV-12. Solar array degradation.

TABLE IV-12. ARRAY DEGRADATION

Type of Degradation	Loss at 5 Years (%)
Coverslide (Fixed)	3.7
Radiation	10.5
UV Losses	0.7
Micrometeorite	1.5
Blocking Diodes	none
Transmission (Fixed)	2.0

TABLE IV-13. SOLAR ARRAY DESIGN FACTORS

Factor	Symbol	Value
Solar Constant	S	135.4 ± 1% mW/cm^2
Season Variations	ΔS	+3.43%, -3.26%
Max Temperature Range	T	-52°C to +83°C
Temperature Coefficients		
Short Circuit Current	K_{sc}	+0.037%/°C
Open Circuit Voltage	K_{oc}	-2.3 mV/°C
Max Power Voltage	K_{mV}	-2.2 mV/°C
Max Power	K_p	-0.51%/°C

d. Solar Cell Panels. Solar array design was iterated with performance studies to optimize the array design. Performance studies consisted of determining power, current, and voltage characteristics as a function of orbital parameters, temperature, intensity, incidence, and mission life for variations in panel design and cell layouts. Typical extreme and average values of the above parameters were used to assure that system requirements were satisfied. Design ratings and sensitivity data derived from the performance studies were then used to adapt the panel and module design to spacecraft and mission constraints and to the power requirements.

Details of the module design determined for the array are illustrated in Figure IV-13. Aluminum honeycomb, 0.953 cm thick, is used for the substrates. These have 0.025 cm face sheets. Micaply bonded to the substrates serves as insulation for the cells. The cells and coverslides are mounted on the insulated substrate using proven adhesives qualified for low outgassing characteristics. Proven flat laydown techniques, existing interconnects, and qualified connectors and wiring are used in the construction. Figure IV-14 shows a cross section of the solar cell module and identifies the material used.

The frame indicated in Figure IV-13 provides for attaching two modules to form a panel. Hinges with bearings are attached to two sides of the panel to permit linkage of the panels and for attachment to the boom that will support the wing assembly as indicated in Figure IV-10.

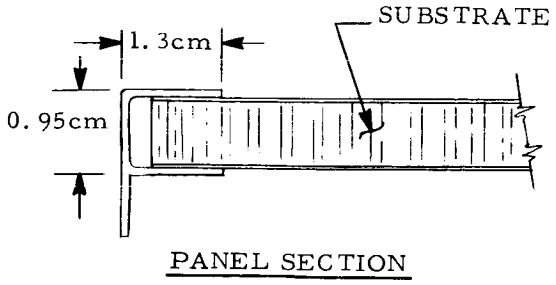

PANEL SECTION

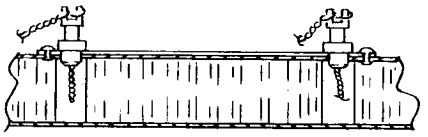

SLOTTED TERMINAL
INSULATED SWAGE MOUNTING

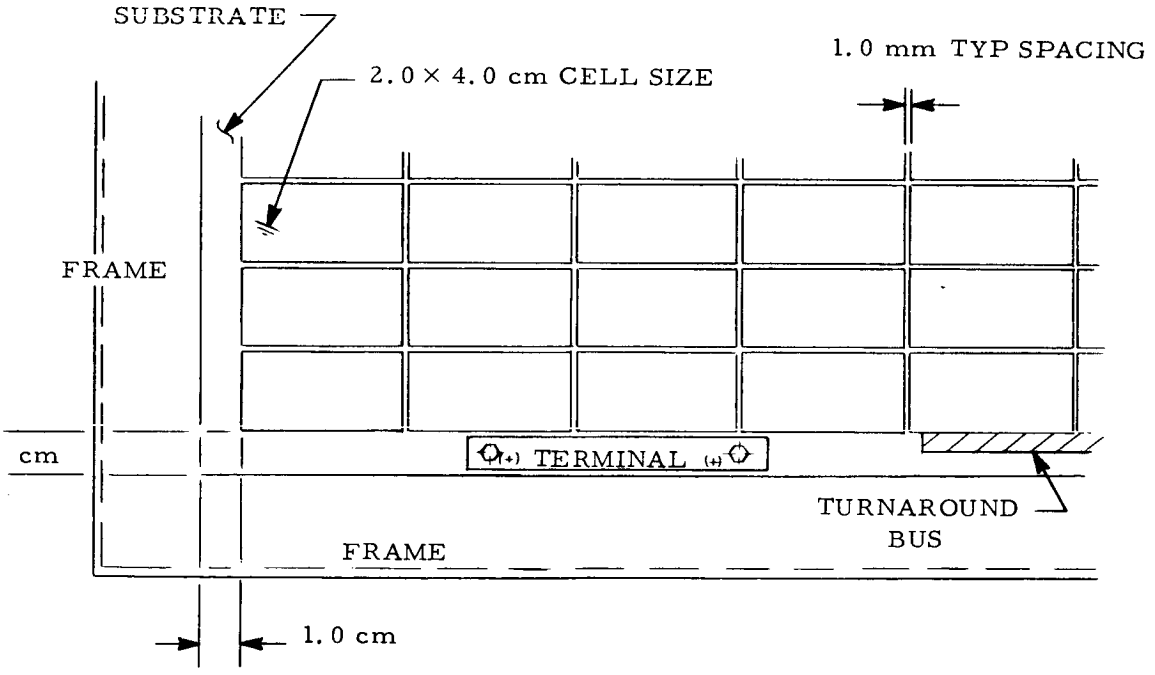

Figure IV-13. Module details.

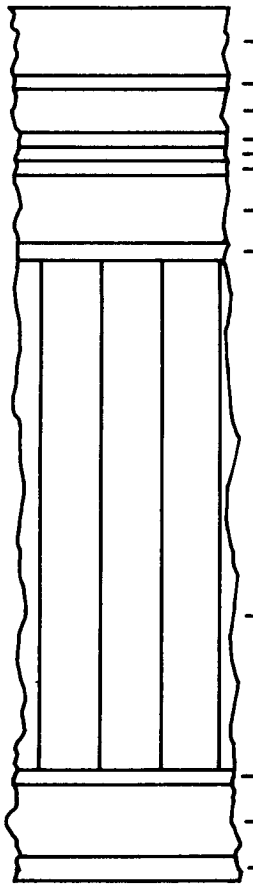

	THICKNESS mm	DENSITY 8m/cm^3	WEIGHT gm	MATERIAL
COVERSLIDE	.305	2.21	898	COR 7940
ADHESIVE 1	.076	1.05	107	SYL 182
SOLAR CELL	.305	2.46	999	SILICON
ADHESIVE 2	.076	1.06	108	SYL 140
DIELECTRIC	.076	1.08	131	MICAPLY
ADHESIVE 3	.076	1.10	133	EP-101
FACE SHEET	.254	2.88	1160	ALUMINUM
ADHESIVE 4	.432	1.73	823	HT-424
CORE	9.525	.0037	567	HONEYCOMB
ADHESIVE 4	.432	1.73	823	HT-424
FACE SHEET	.254	2.88	1160	ALUMINUM
PAINT	.203	2.75	887	S-136
TERMINALS AND MISCELLANEOUS			320	
TOTAL			8116	

Figure IV-14. LST solar array module cross section.

The panel configuration is illustrated in Figure IV-15. Two modules are shown fastened together to form the panel. A section of the solar cell arrangement for the panel assembly is also shown.

e. Orientation Requirements. Two degrees of freedom are required for the solar array to be oriented toward the sun while the telescope is fixed on a target star. One degree is provided by a roll maneuver of the spacecraft. The second degree is provided by mechanical rotation of the arrays about the Y-axis of the spacecraft.

Since the spacecraft telescope pointing excludes a 45-degree cone centered on the sun and the same side of the spacecraft is always oriented away from the sun, the solar panels are required to rotate only through 145 degrees about the Y-axis; continuous rotation is not required. Each time the spacecraft is reoriented to point the telescope to a new target star, the spacecraft is rolled about the spacecraft star line and the solar array is mechanically rotated about the Y-axis to point toward the sun. The arrays are not reoriented during an experiment exposure. The angular rate of rotation of the panels about the Y-axis will be about 8.7×10^{-3} rad/sec during each reorientation period. This allows the array reorientation to be completed within the period of one ground station contact.

An accuracy of ±4 degrees is adequate for the roll and gimbal angles. During off-nominal operations where the roll attitude of the spacecraft must be varied for experiment purposes, power system performance variations have been calculated. During a reorientation of the solar array, torques developed between the solar array and the spacecraft should be less than 6.8 N-m to keep spacecraft disturbances within reasonable limits. Commands to reposition the array about the Y-axis will be received from the command system. These commands will be absolute position, not error signals. Array position will be telemetered back to the ground, based on array shaft position from an encoder and from wide angle sun sensor outputs.

The drive motor must develop sufficient starting torque to overcome the inertial load presented by the solar array and the coulomb friction loads presented by the gear train and bearings. It must also overcome the spring resistance of the power transfer cables across the rotary joint. The starting torque for the motor is usually chosen from the range of 5 to 10 times the coulomb friction loads in a conservative design. The torque acting against the inertia of the array, causing it to accelerate, is the motor torque less the torque losses to bearing friction and power transfer cable windup spring resistance. For this design a peak motor starting torque to loss torque ratio

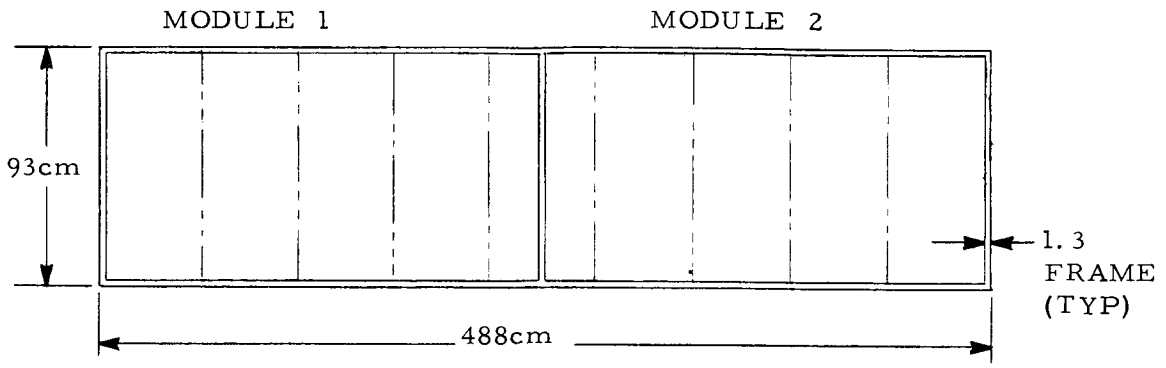

a) MODULE ARRANGEMENT ON EACH PANEL

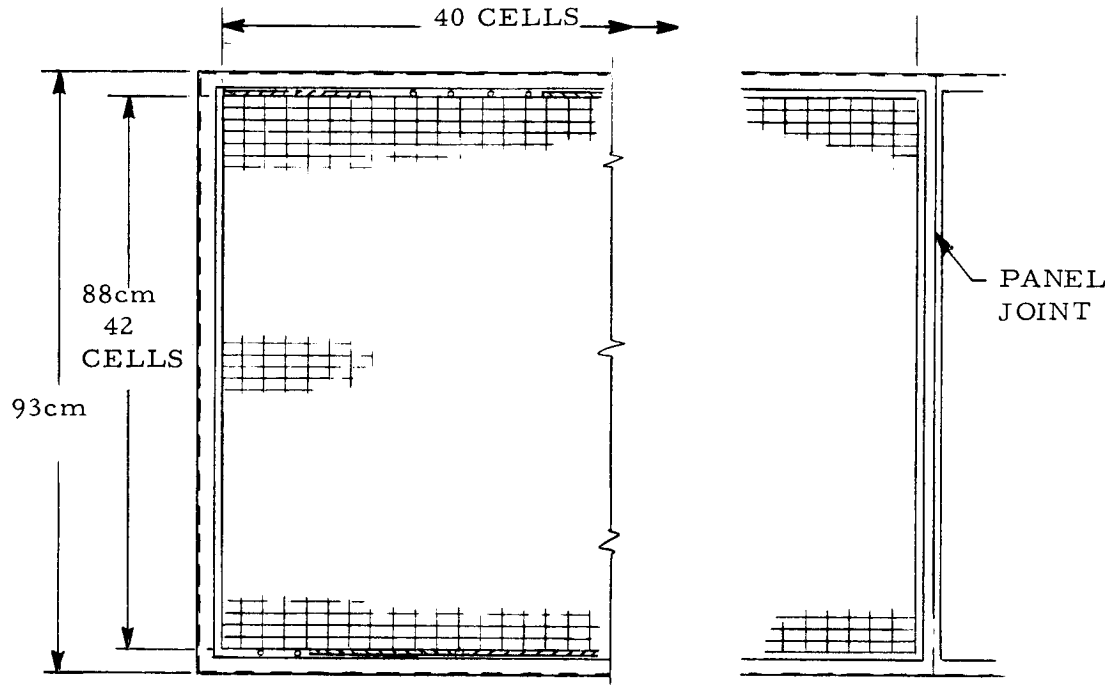

b) ARRANGEMENT OF CELLS IN EACH MODULE

Figure IV-15. Panel arrangement.

of 8.5 has been used. The peak torque less loss torque will act to accelerate the array. A check has been made to ensure that by using an on-off motor control, the forces developed will not damage the array or produce large control system disturbances.

For a journal bearing of a polyimide polymer sliding on stainless steel, the coefficient of friction is about 0.2 maximum. For two 5.08-cm diameter bearings preloaded at 22.2 N an additional 2.67-N load results from a maximum vehicle angular acceleration of 1.47×10^{-4} rad/sec^2. The coulomb friction load will be about 0.253 N-m. A 2.5 cm diameter polyimide/steel seal with a 44.5 N preload is used to allow removal of the motor from the inside of the pressurized container; therefore, an additional 0.113 N-m coulomb load will be incurred. The spring resistance of the power transfer cable is about 0.113 N-m. Therefore, the torque losses between the motor/gearhead and the array shaft total 0.479 N-m.

f. DC Stepper Motor Drive. A dc stepper motor drive is used to provide the 4.067 N-m to the output shaft, bearings, and seals. A 30:1 harmonic drive is provided to reduce the 15 degree steps of the stepper to increments of 0.5 degree. Assuming a conservative harmonic drive efficiency of 50 percent, the required stepper motor torque is about 0.282 N-m. If the efficiency of the harmonic drive is nearer 0.90 and the loss torques on the output shaft are 0.479 N-m, then up to 14.372 N-m of net torque would momentarily act as a disturbance on the spacecraft attitude when simultaneously reorienting the two solar array wings. The attitude system can hold against torques below 27.116 N-m. Although not provided for in the present design, rate feedback can be added to limit the net torque acting as a disturbance on the spacecraft attitude, if required. The load reflected by the solar array inertia into the drive assembly during a maximum spacecraft angular acceleration of 1.47×10^{-4} rad/sec^2 is about 0.068 N-m. For this angular acceleration, the drive assembly motor would not have to be energized. The friction of the journal bearings and seals would hold the array with respect to the spacecraft during maneuvers and during quiescent periods when experiments are being performed.

A layout of the required dc stepper motor, harmonic drive, encoder, bearings and seals is shown in Figure IV-16. This is packaged and seals are provided such that the assembly may be replaced from within the pressurized LST volume. The overall assembly is packaged within an envelope of 20 cm diameter × 35 cm length and has a mass of 10 kg. Redundant windings can be provided within the motor. A spring clutch/shock adsorber device is included to smooth the motor pulses and to slip if excessive external torque loads during ground operations are reflected back in through the output shaft. This is desired to protect the harmonic drive teeth from potential over-stress.

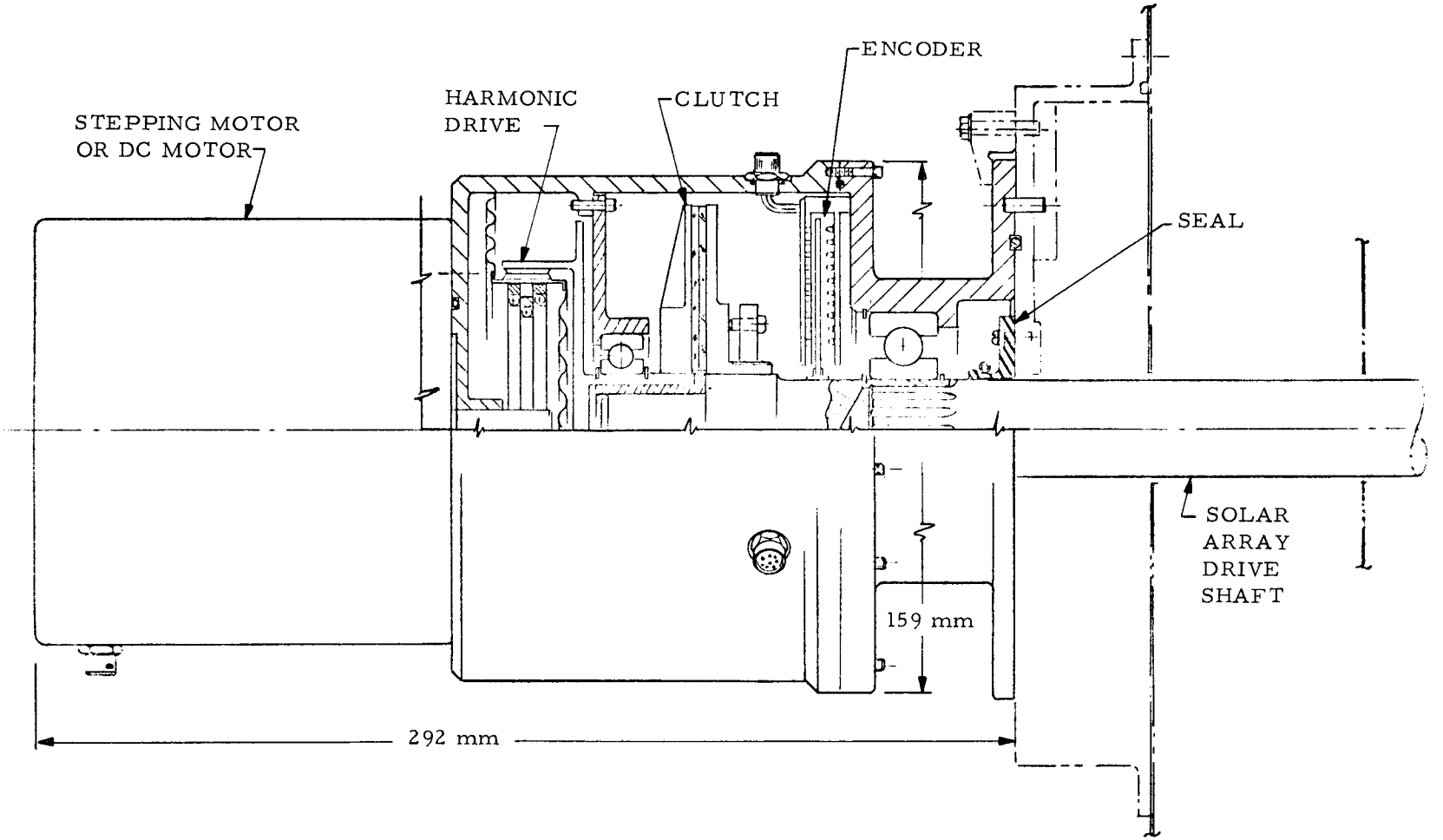

Figure IV-16. Orientation drive assembly with harmonic drive.

If the solar array drive assembly must be exchanged during maintenance, it can be removed while the SSM is pressurized. The shaft seal prevents excessive leakage during an exchange operation. If the shaft must be removed, it is done from outside the LST SSM and the motor is left mounted to the inside wall with the O-ring seals intact. The shaft and external bearing can then be removed also with the LST SSM pressurized.

A block diagram of the dc stepper motor control circuit is shown in Figure IV-17. Upon receiving the 8-bit position command from the command system, it is compared with the existing position of the array stored in the array position encoder. If a difference exists, a signal indicating clockwise or counterclockwise rotation is sent from the comparator to the stepper motor driver logic and a signal to start the one pulse per second pulse generator is sent from the comparator. The pulse generator output is sent to the stepper motor logic and driver which in turn energizes the stepper motor. When the solar array drive reaches the correct position, the position encoder output matches the position register output and the comparator output to the pulse generator is a stop signal.

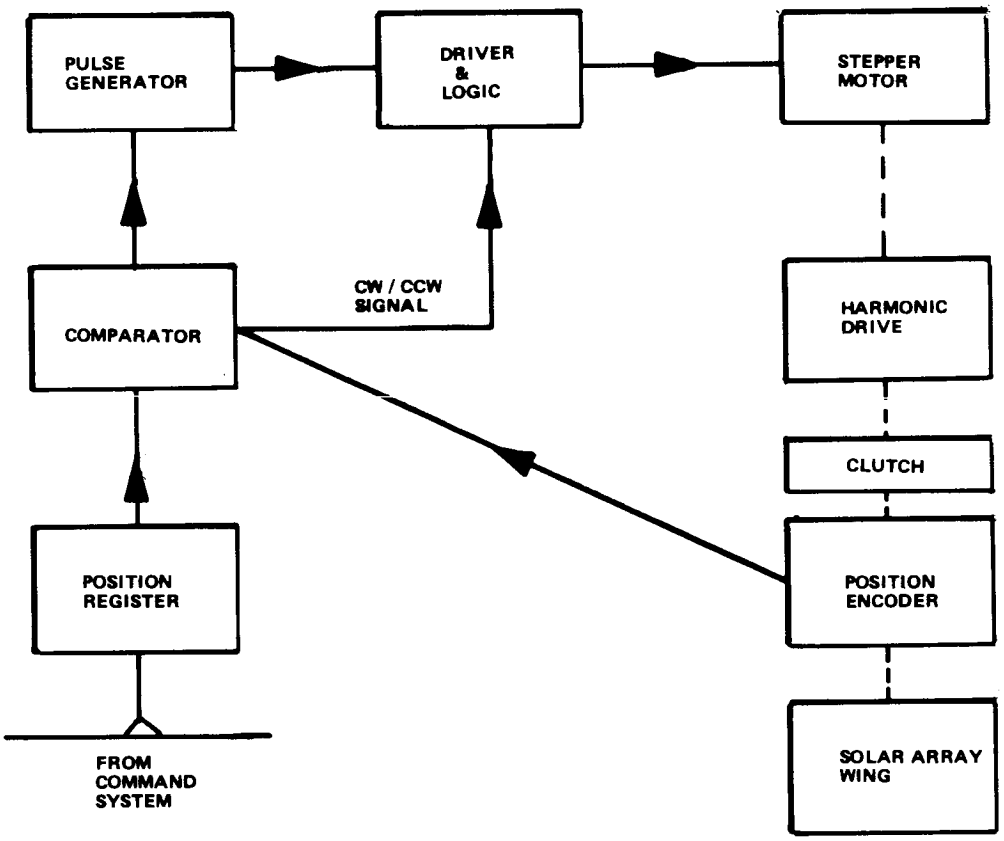

Figure IV-17. Orientation control circuit.

g. Array Performance. A computer program was developed to calculate and plot the solar array performance. Plots were made of current and voltage and voltage and power at the minimum, maximum, and average array temperatures. The results for the design reference array at the end of 5 years in space, at temperatures of +63°C, and 83°C, are shown in Figures IV-18 and IV-19. The array parameters are shown in each figure. The beginning-of-life (BOL) characteristics at 63°C are shown in Figure IV-20.

Performance calculations were made for a modification of the design reference array using phase change material (PCM) enclosed in the solar cell modules. The phase change material selected was lithium nitrate trihydrate — its heat of fusion absorbs heat conducted to it from the solar cells. The PCM will stay at a constant temperature until all of the mass has changed phase — in this case, to a liquid. This has the effect of maintaining the array at a cooler average temperature, thereby increasing the overall electrical power conversion efficiency. The output power variation over a typical sunlight period of the orbit is shown in Figure IV-21 for arrays with PCM compared to the performance of the reference design. The output of the reference array is higher initially but drops rapidly as the sunlight heats it. Those with PCM have lower initial power but maintain a more constant output because the solar heating has less effect on the cell temperature. The array with 68 kg of PCM had an average output equivalent to that of the reference design. With 91 kg of PCM, the array's average output was 6 percent higher than the reference design.

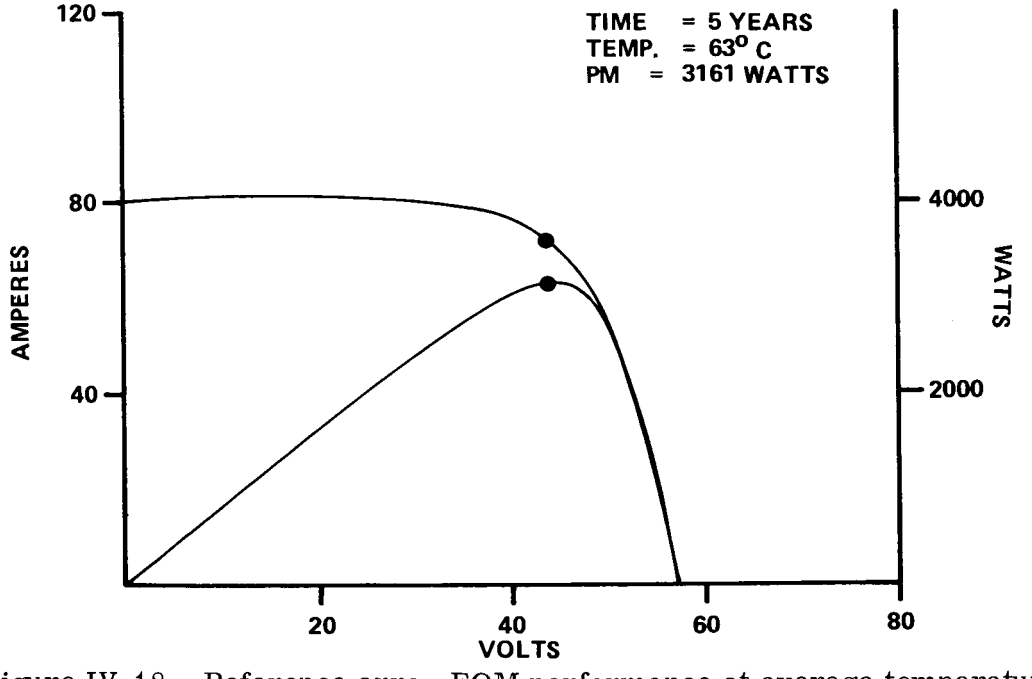

Figure IV-18. Reference array EOM performance at average temperature.

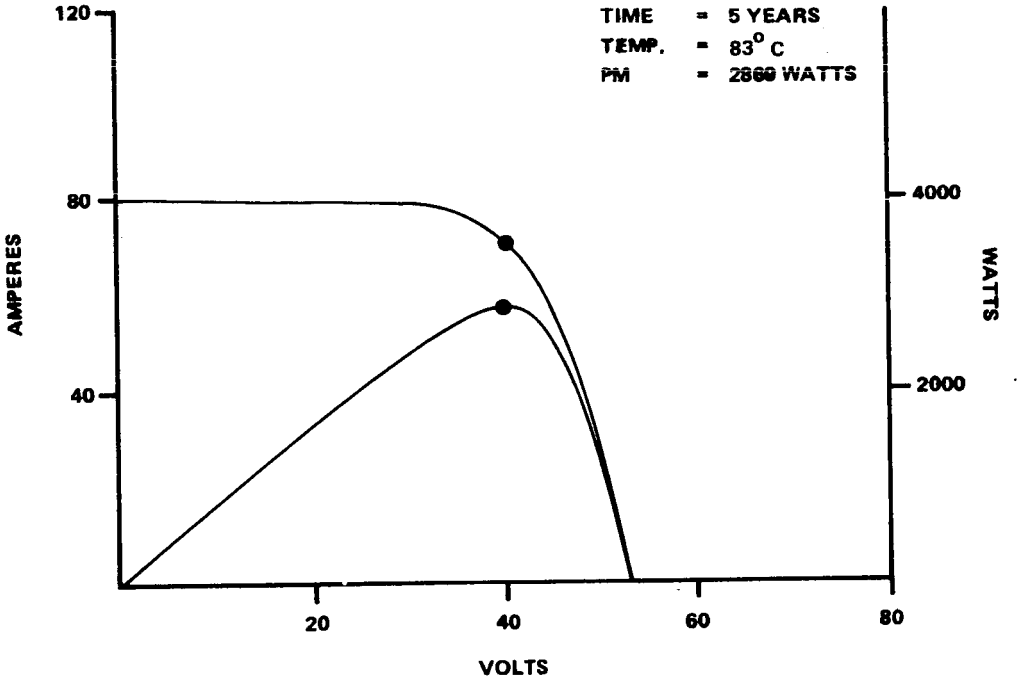

Figure IV-19. Reference array EOM performance at maximum temperature.

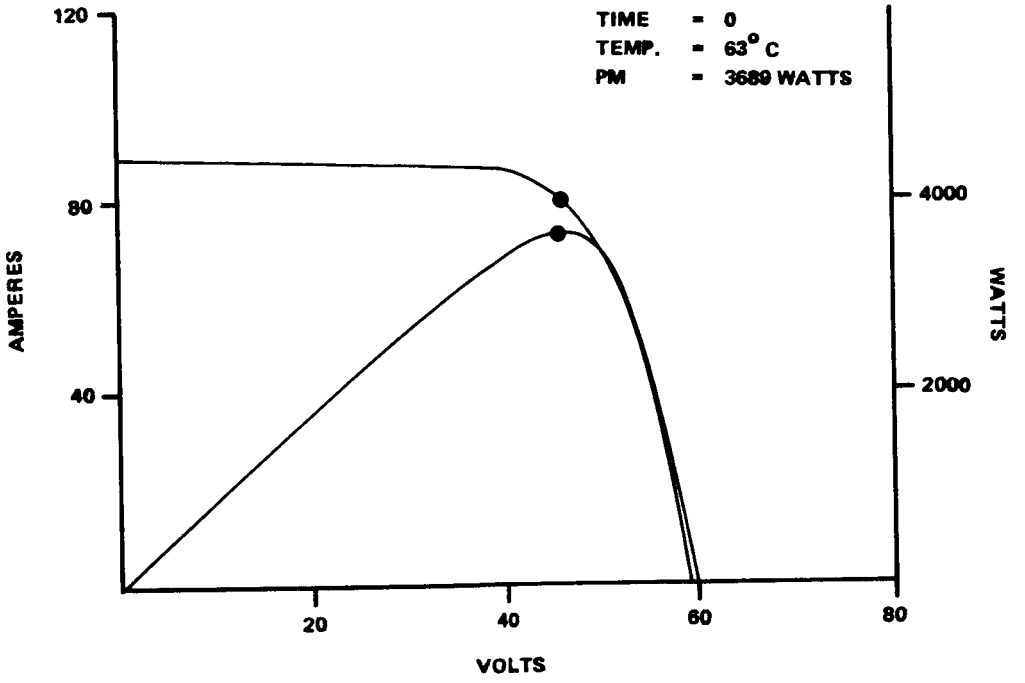

Figure IV-20. Reference array BOL performance.

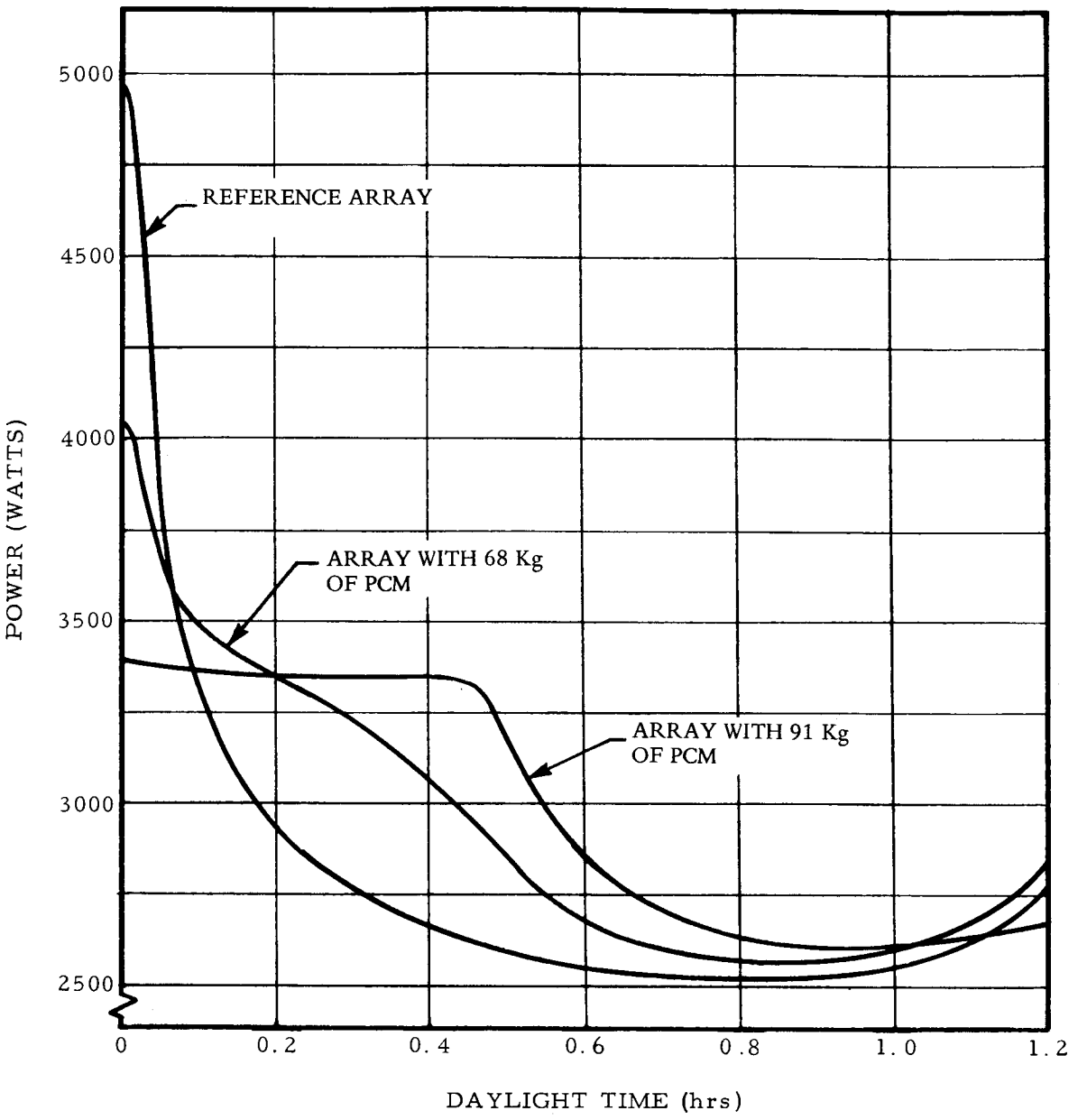

Figure IV-21. Array performance with and without PCM.

One of the major advantages of the PCM would be the increased reliability of cell interconnections because the thermal cycling stresses would be reduced significantly. Although power and reliability advantages are quite attractive if mass is no constraint, this approach was not considered further because considerable R&D would be required to make the concept practical for an array. The material is compatible with aluminum but whether or not it is compatible with array adhesives was not determined. Lithium nitrate trihydrate has been considered for other applications, but no experimental work has been devoted to solar panels. The containment of such material would be critical for an array and could lead to higher construction costs.

4. Energy Storage Subsystem. The energy storage subsystem must store energy during sunlight periods of the orbit and must furnish the LST with electrical power during occultation periods. It must supplement the solar array power occassionally during off-sun orientation cases and, if the alternate launch vehicle is used, it must power the LST during the initial launch phase of the mission. The energy storage subsystem must also provide means for conditioning and controlling energy storage and must accept array power only when not needed to sustain loads.

In Section F.1 it is shown that different EPS configurations have only a small effect on energy storage requirements. The influence of load, efficiency, occultation periods, temperature, and life are more significant. The requirement to accomplish off-sun roll maneuvers can be a design driver on capacity requirements, as discussed in Section C.6. Based on the 86.5 percent system efficiency when operating from batteries, the energy storage subsystem must deliver 1024 W-h of energy for each maximum occultation orbit. It must be capable of reliable performance for the temperature range of $10 \pm 5°C$ and for the mission duration with maintenance.

a. Subsystem Description. The energy storage subsystem consists of six nickel cadmium battery assemblies, six dedicated charger assemblies, and the associated sensors and controls needed to operate and protect the subsystem. Today's technology and conservative reliability data were used to size the subsystem and to predict performance. With the capability for in-space maintenance, LST system requirements can be met without the need for advanced technology.

Based on selection rationale and trades discussed later, a six-battery configuration was selected as a cost-effective, reliable approach compromising battery design and operational characteristics with system complexity, control, protection, and maintenance. Although further adjustments for energy required during off-sun pointing experiments may be necessary, 30-A-h cells and 24 cell assemblies were chosen to give the

subsystem a 5400 W-h energy rating. The normal operating mode, maximum occultations, and design load conditions would incur a depth of discharge (DOD) of 19 percent. The cycle life, DOD, and temperature relationship shown in Figure IV-22 indicates a 2.2 year life rating for the subsystem. Figure IV-22 was conservatively derived from available reliability test data. To maintain reliable performance, the maximum DOD during periodic off-sun pointing conditions should be limited to between 50 percent and 60 percent. The limit is dependent on system conditions and the age of the batteries.

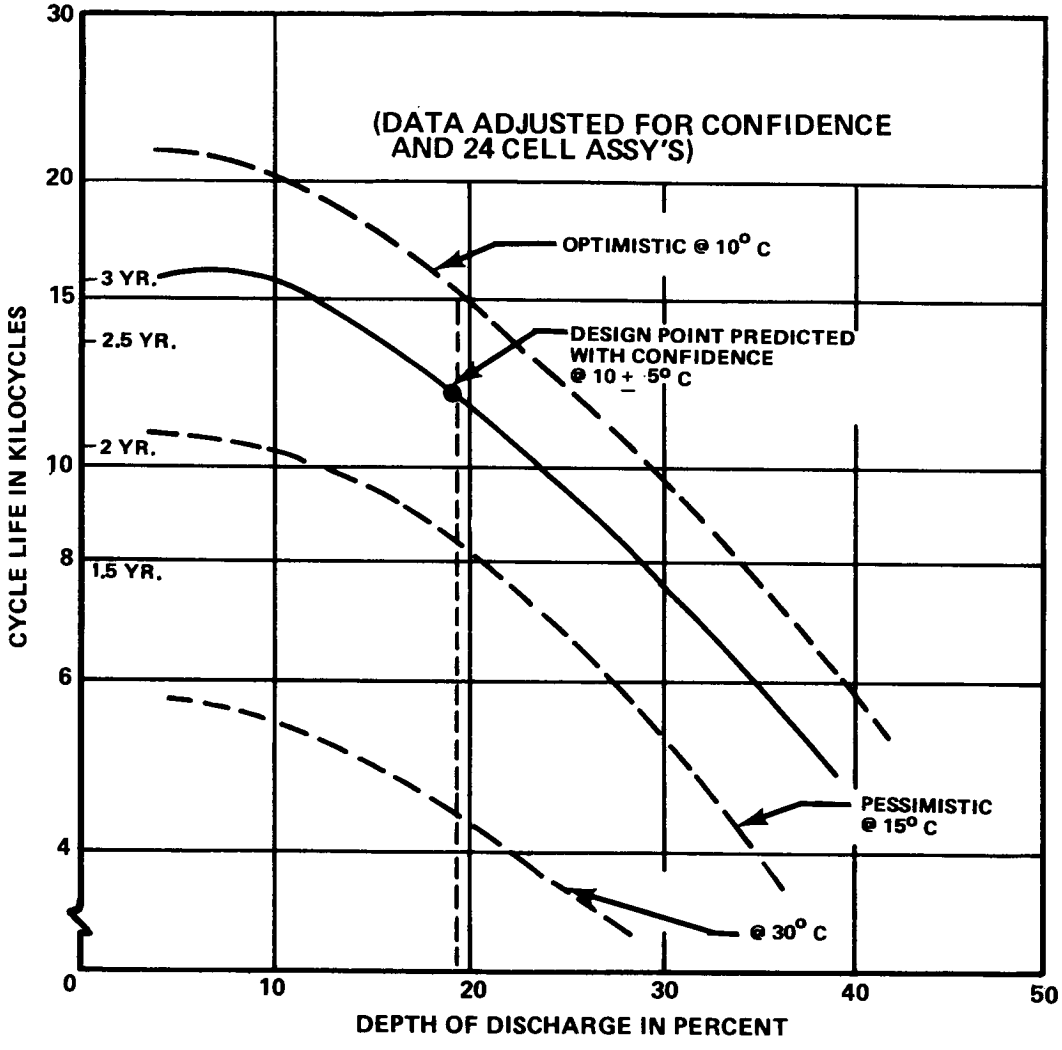

Figure IV-22. Battery life prediction.

All batteries will be energized and cycled during typical orbital operations because trickle charge/standby does not significantly improve life and it also conditions the battery to accept higher loads. The system controls permit batteries to be discharged in several parallel combinations, providing redundancy. Normally the system will be operated with three pairs of isolated batteries or two sections of three in parallel to guard against total power loss in the event of a load short. Remote command control of the energy storage subsystem allows other configurations for power management or fault isolation by controlling cross strapping of the four output buses located in the electrical control assemblies.

Each battery is protected against circulating or reverse current by diodes located in the output circuits. The input and output of the batteries are channeled through the dedicated chargers which monitor battery performance parameters continuously. Redundant lines are provided for all battery cabling. Overload and low voltage protection guards the integrity and avoids excessive over-pressurization of cells. In the event of abnormal system conditions, each battery may be isolated for diagnostics and special recharge conditioning. Should service faults occur that necessitate the removal of a battery from service, the redundancy and power management scheme permits continued system operations by increasing the DOD of the remaining assemblies. Although the life is affected by such conditions, the capacity and thermal design are adequate to sustain full load with three operating battery assemblies. Fault protection is established to always favor critical loads with a source of power.

The condition of each battery is monitored and controlled by a separate charger assembly. The chargers provide current and voltage instrumentation and receive temperature and third electrode signals from the batteries to assure reliable battery control. All battery instrumentation designated for telemetry is channeled through the chargers. Because of the long mission and to provide versatile power management and protection, ampere-hour meters have been included to provide better indication of battery conditions to the ground. The output of these meters can also provide redundant cutoff signals for charge termination.

Each of the six charger assemblies is redundantly connected to the primary solar power buses. Each charger demands primary bus power in accordance with the specific battery needs. Power tracking networks in the solar power distributors permit full utilization of array power available but assure that system loads are first satisfied before power is delivered to the chargers.

The chargers deliver variable current and voltage up to 36 Vdc to the batteries. The charger output is controlled by battery instrumentation to assure proper adaptation to battery characteristics and conditions. The chargers are designed to handle 700 watts to allow adequate recharge for abnormal conditions when several batteries are no longer in service. The chargers will furnish higher charge rates at the beginning of a sunlight period when the "cold" arrays deliver higher power. Normally the chargers will limit the charge rate to half the current rating of the battery.

Characteristics and ratings of the energy storage subsystem are summarized in Table IV-14.

TABLE IV-14. ENERGY STORAGE SUBSYSTEM CHARACTERISTICS AND RATINGS

Characteristic	Subsystem Rating
Batteries	
No. of Assemblies	6
Type	Sealed NiCd
Cell Rating	30 A-h
Temperature	10° ± 5°C
Average DOD	19%
Charger Assemblies	
No. of Assemblies	6
Type	Step Down Converter
Max Recharge Rating	4200 watts
Max Charge Voltage	36 Vdc
Total Subsystem	
Energy Capacity	5400 W-h
Average Power	2700 watts
Max Current	180 A
Output Voltage	24 to 31 Vdc
Input Voltage	38 to 88 Vdc
Efficiency	73.5%
Life	2.2 years
Mass	170 kg
Volume	177 500 cm^3

b. Battery Selection Rationale. Sealed, nickel cadmium (NiCd) batteries are considered the only feasible candidates to satisfy the electrochemical energy storage requirements for the LST low earth orbit mission. NiCd batteries possess the ruggedness, energy capacity, cycle life, and fast recharge characteristics best suited for such an application. Although the LST's 5 year mission would tax the technology, the in-space maintenance capabilities established for LST permit the use of existing technology.

Several preliminary battery designs were made using data obtained from several manufacturers. Numerous cell configurations are possible for the different A-h ratings considered; however, for a given size and style these differences had small influence on battery performance. Typical performance trades are briefly described in Section F.3. Also, several past programs were investigated for design and hardware applicable to LST.

Because of its electrical size and capacity requirements, the LST required larger cells to minimize system complexity and to ensure reliable performance. Of the NASA systems canvassed for applicable hardware, only the Skylab and ATM surpass the LST size. However, 30-A-h cells are scheduled for several programs, e.g., HEAO, Skylab, and Mariner. Larger cell ratings of one manufacture have been flown in several Air Force programs. None of the assemblies reviewed were exactly consistent with the LST system and maintenance concepts. Modification would probably cost as much as a new assembly since assemblies are not production line products. The HEAO battery was the closest candidate and its considered to be a satisfactory alternate for adaptation to the LST if necessary. This would incur a mass or performance penalty compared to the reference system but not enough to jeopardize system feasibility.

Several manufacturers have the competence and cell sizes needed for LST, although improvements are desirable. Historical cost investigations have shown that battery hardware has been a relatively low cost item.

Battery performance predictions for long missions are difficult because of the wide variations in test and reliability data. This subject is treated in Chapter VIII. Test results appear to be random in most cases, varying with the manufacturing line, the test lab, a large number of conditions imposed on tests. Type of failures also appear to be random, e.g., open circuits, short to case, overpressurization, loss of capacity, seal leakage, etc. Data correlating failures to design or fabrication processes are rare. Most of the existing data pertain to cell sizes of 20 A-h or less.

Typical cycle life curves published for NiCd cells, obtained by curve fitting techniques, usually apply to limited test samples showing better than average performance. If such data are to be used, conservatism is recommended because most of the raw data existing will not support these curves. Engineering judgment, as well as statistical analysis, is needed to adjust these curves for the application so that reliability can be predicted with confidence. Extrapolation is required for the number of cells in the assembly. The range and tolerances of other system conditions, such as temperature and loads, should be considered, especially, the range of charge and discharge rates possible. Finally, a margin commensurate with the wide dispersion in test data should be subtracted. Such adjustments are feasible because experience has shown that with the proper precautions and control of battery fabrications, handling, and testing, existing technology batteries can be made to perform for periods of 3 years or more. The curves previously shown in Figure IV-22 were adjusted in this manner.

A lower battery capacity (higher DOD) might be acceptable if large load variations and off-sun pointing were not anticipated. Later discussion of off-sun pointing will indicate that the reference system may not have sufficient capacity because the opinions of the scientific investigators as to the degree of roll and pointing converage essential will vary.

Considering performance and life requirements, available test and reliability data, and in-space maintenance, the following criteria are considered essential to the LST applications:

1. Use conservatively rated cells.

2. Keep the depth-of-discharge low.

3. Keep the temperature in the range of 5°C and 15°C.

4. Effect good control on manufacturing and acceptance.

5. Use matched cells and reliable charge control.

6. Assure that size, configuration, and installation features permit safe, easy handling, and replacement in space.

The reference battery is the only EPS component that might be considered unconventional; although, it is well within today's technology. Cylindrical cells were used extensively in early satellites but low weight or

convenient sizes were not available. The preference for rectangular assemblies led to the wide use of rectangular cells. Cell sizes and ratings, however, have not been standardized and there have been numerous configuration variations in cells or a given A-h rating. The reference battery is based on cost saving concepts investigated in recent low cost studies for future payloads. The basic cost saving criteria for these studies are briefly related to the battery design as follows:

1. Components (cells) should be common with commercial lines and compatible with production tooling. Commercial cells favor cylindrical models. Production tooling has been developed for the similar configurations.

2. Components must be rugged and as independent of assembly design and processes as possible. Pressure independence is offered by cylindrical cells and permits low weight assembly designs.

3. Standardized items should have good performance consistent with technology, should be conservatively rated to minimize testing, and should have versatility for a wide range of applications. The reference design permits adaptation for capacity ratings up to 50 A-h. Only the cell height needs to be changed and standard plates and separator added for higher ratings.

c. Reference Battery Assembly. Subsystem studies were made of existing assemblies and preliminary designs based on data from several battery manufacturers. Design trades indicated that the reference battery assembly, shown by Figure IV-23, offered a significant improvement in energy-to-weight ratio. The design was subjected to a detailed materials and weight analysis. Fabrication concepts and techniques were reviewed to establish that the assembly could be cost-effective, reliable, and consistent with standardization concepts. Further reductions in weight of housing are possible but the design was not iterated.

Since the assembly does not need to resist cell pressure, it can be a low weight casting of magnesium alloy with lightening holes. It is assembled in two parts. The bottom section has a standard size; it retains cell position and provides thermal dissipation. An upper part, not shown, would be used for larger cells; it would have the same length and width dimension, as the bottom to which it attaches. The housing protects cells, exposed terminal, and straps and provides for mounting of cover and connectors. To permit several capacity ratings, several top sections would be available where only the height varies to adapt for higher cells. The housing for the

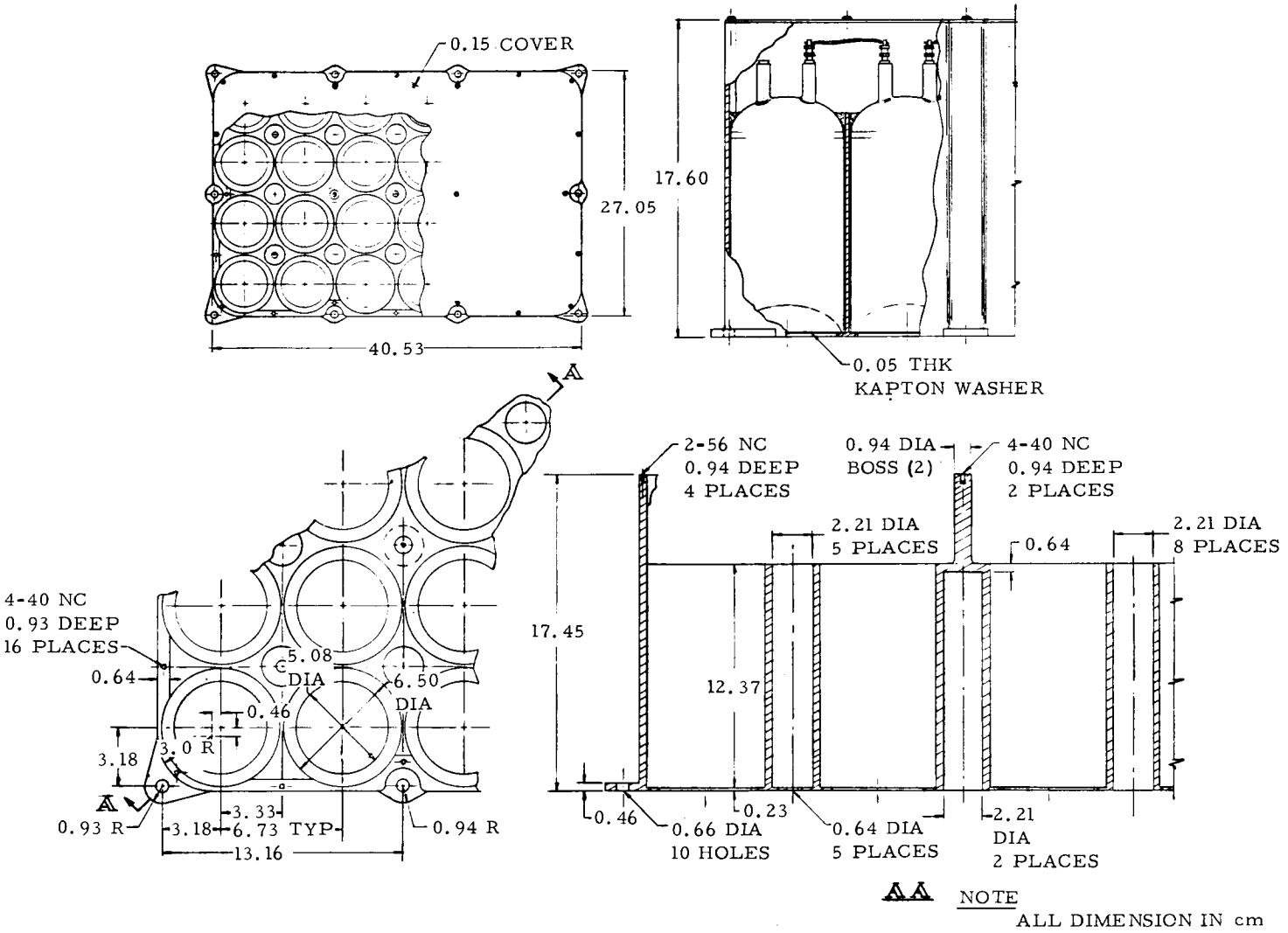

Figure IV-23. Reference battery assembly.

30 A-h assembly would have a mass of 6.27 kg and would occupy a volume of 17 500 cm^3. The mounting foot point would stay constant for cell ratings up to 50 A-h. Kapton cell insulation, adhesive for retaining cells, cell straps, and connectors add 1.43 kg. The 24 cells, rated for 30 A-h, have a mass of 14.7 kg. Thus, the total assembly has a mass of 22.4 kg, giving a specific energy of 40.1 W-h/kg.

The performance advantages are a result of the low mass cell construction and light assemblies and not on advance electrode performance. Standard tooling provides high strength, electroformed, nickel casings 0.15 mm thick. The safe, unconstrained operating pressure is more than 69 N/m^2 and is 5 times better than an equivalent rectangular cell. Each cell is hermetically sealed and all hardware, materials, and processes are standard. Only the cell length and number of plates are varied (four sizes should be adequate) for different capacity ratings if required. Table IV-15 shows cell parameters for four possible ratings. The specific energy of the battery increases when the larger cells are used. With 24 cells of the 30 A-h size, the assembly is nominally rated for 900 W-h at 30 Vdc. The conservative cell insulation used provides an insulation rating over twice the 500 volts normally specified.

The cells would be linked in series with flexible, copper-nickel straps suitable for brazing, welding, or bolting to the cells. The ends of the straps are solid tips that are compression welded to the braided center. The flexible straps assure that terminals and cell seals are not damaged from contraction/expansion over the most severe temperature range that a battery would incur. A recombination electrode is recommended for all cells. At least three cells in the assembly would have a control signal electrode to indicate oxygen pressure. The assembly includes three temperature sensors for charge control, one for telemetry, and one for hardware monitoring during ground, launch, and maintenance operations.

Standard system connectors are provided to connect the batteries into the system. The power input, output, and ground lines are redundant. Cables will be shielded from EMI. A separate, small instrumentation connector is recommended for connection to the chargers. A capped test connector (not used in the system) is provided for access to individual cells during conditioning, test, and maintenance of the battery.

TABLE IV-15. CELL DESIGN CHARACTERISTICS, HIGH-ENERGY NiCd CELLS

A-h Size	Dimensions (cm)			Volume (cm^3)	Volts (Avg Discharge)	Current, 1 hr Rate (A)	Weight (g)	Energy Density (W-h/cm^3)	Specific Energy (W-h/kg)
	Diam	Cylinder Length	Height with Terminals						
20	6.35	10.52	13.69	128.42	1.26	20	440	0.20	57.27
30	6.35	13.11	16.28	163.57	1.26	30	612	0.23	61.76
40	6.35	15.70	18.87	195.50	1.26	40	783	0.26	64.37
50	6.35	17.02	20.19	211.95	1.26	50	945	0.30	66.67

d. Battery Chargers. Each of the six battery assemblies will have a dedicated charger. The charger assemblies must track the changing charge/discharge characteristics of each associated battery and maintain them in good operational condition for a year. Each assembly will:

1. Monitor charge, discharge, and battery conditions.

2. Limit the charge voltage to 36 Vdc and provide output between 24 and 36 volts as needed.

3. Limit the charge current to less than 21 A and normally deliver an average current between 4 and 6 A.

4. Receive solar array power at voltage between 38 and 88 Vdc.

5. Be rated for 700 watts.

6. Sense primary bus voltage and avoid overloading the bus.

7. Terminate charge appropriately to avoid degradation and thermal burden.

8. Provide instrumentation for remote power management.

9. Be consistent with the system reliability and redundancy requirements.

The charger is a nonisolated, stepdown, static-switching converter, basically consisting of controlled semiconductor switches; magnetic, and electrostatic energy storage devices; and electronic control components. As indicated in Figure IV-24, power transistors are used to accomplish conversion and to control the output. Magnetic chokes and capacitors provide the necessary energy storage. Logic and amplifier circuitry, consisting of resistors, diodes, transistors, and capacitors, control the power switches in accordance with the input control signals received. Low-pass filter sections are provided to meet the system EMI and radio frequency interference (RFI) requirements.

The charger replenishes the energy drawn from the battery and furnishes additional power to compensate for the losses incurred by battery inefficiency. The output of the charger is a variable that is adapted to the battery characteristics.

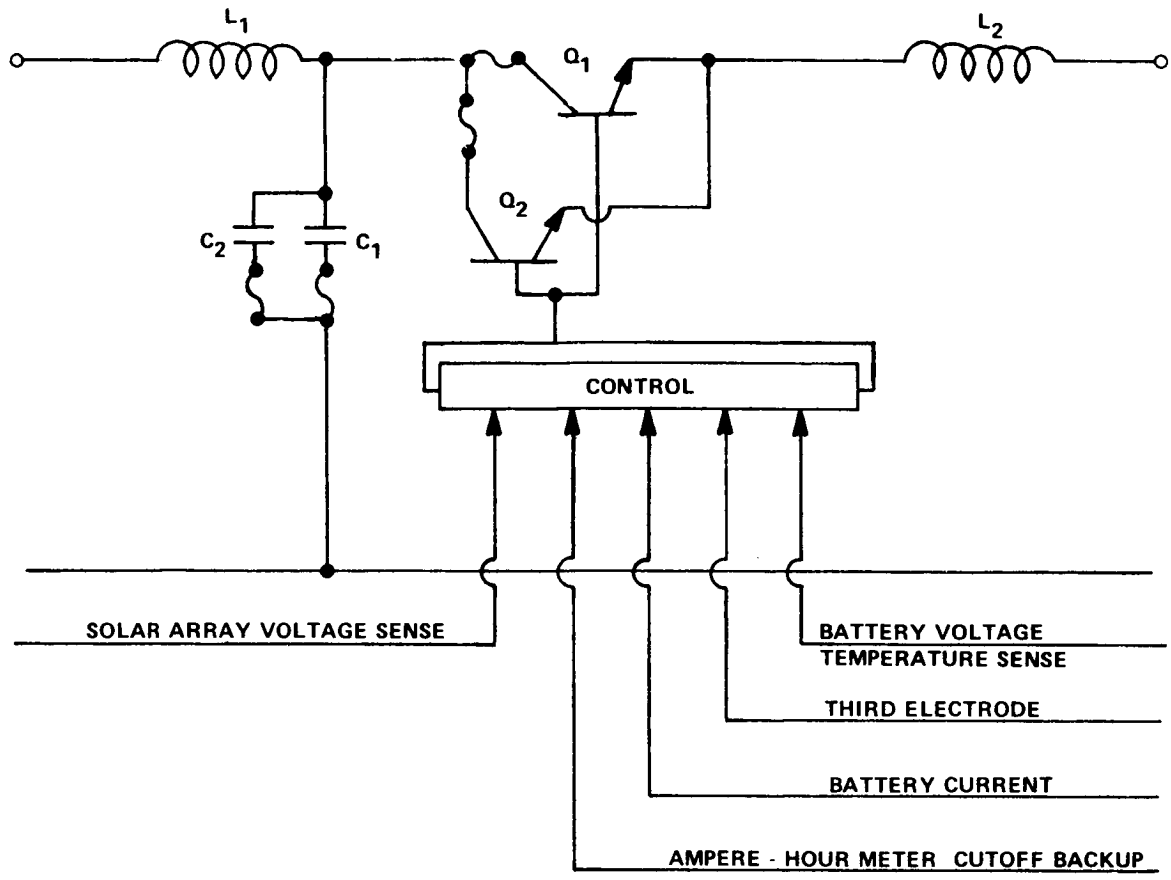

Figure IV-24. Battery charger simplified diagram.

The charger has a modified constant current and a constant voltage output characteristic which is adjusted by the control signals received. The control signals are received from internal and remote sensors. The battery current, voltage, and ampere-hours are monitored internally. Remote signals received are battery temperature and third electrode cell signals from the battery assembly, and signals from the V-I characteristics of the solar array bus from the solar power distributor.

Without array power tracking feedback, the charger would limit the initial charge current to about 21 A. High rates are permissible when the battery is discharged and when the battery temperature is in the proper range. Normally, with six batteries requiring charge, the peak power tracking feedback will limit the initial charger current for each battery to about 7 A when the array is cold. As the array heats and the power available

decreases, the charger will reduce the charge current so that the spacecraft loads are supplied first. The charge current is also reduced when the battery detectors indicate a reduction is needed. The current, voltage, and temperature are interdependent in this mode to adjust to the specific characteristics of the battery. When the temperature-dependent voltage reaches a preset level, the charge voltage drops 0.5 volt. The current is reduced and the charger operates in a constant voltage mode until cutoff is initiated by third electrode signals or redundantly by the ampere-hour detector.

The ampere-hour meter monitors the battery output and input during the entire charge-discharge cycle. When the output and the losses have been resupplied, the meter furnishes an output that is used to terminate the charge also. The ampere-hour meter also furnishes battery charge-discharge status information to the telemetry subsystem for transfer to the ground. This information enables control of batteries and chargers from the ground.

Recombination electrodes within the cells permit a high charge rate over a wide temperature range, and these electrodes avoid the hazard of hydrogen pressure buildup. These electrodes also enhance the characteristics of the third electrode. The charger, however, provides charge rate limiting or shutdown capabilities for abnormal battery conditions. Temperature limit sensors, in the battery, signal charge limits if the battery is too cold or charge termination if it is too hot.

A summary of the baseline battery charger characteristics is presented in Table IV-16.

TABLE IV-16. BATTERY CHARGER CHARACTERISTICS

Input Voltage	
Equipment Rated (Open Circuit)	125 Vdc
Normal from Solar Array	38-88 Vdc
Output Current	
Normal Operation (Max)	22 A
Input Power (Max)	750 watts
Output Voltage	24-36 Vdc
Efficiency	95% at Full Load
Thermal Dissipation	9 watts
Size	31 × 20 × 15 cm
Mass	6.8 kg
Ambient Temperature Range	25°C to 100°C

5. Regulator Assemblies. Six buck-boost regulators are provided to regulate the 24 to 36 Vdc input from the batteries and the 37.5 to 88 Vdc input from the solar array to the 28 ± 2 percent Vdc output provided to the loads. The solar panels supply the battery chargers and the regulators in parallel; the regulators have priority on the power. Excess power above that required by day loads is used to charge the batteries. The regulators use a buck-boost switching circuit to provide regulated voltage to the load buses. Each regulator has a power capability of 700 watts. Six are connected into the system so that any three are capable of powering the spacecraft. Any one of the regulators will carry those critical loads required for spacecraft survival. Each regulator assembly has redundant inputs and outputs so that from one to six may be paralleled, upon command, to a primary bus and/or to redundant distribution buses.

A simplified schematic of the regulator is shown in Figure IV-25. Critical components are redundant, fuse protected, and self-clearing. Each assembly is current-limiting and provides inherent overload protections for itself and for the power source. Internal and external voltage and current sensing provisions provide redundancy, permit adaptable regulation characteristics, and allow for external load sharing control.

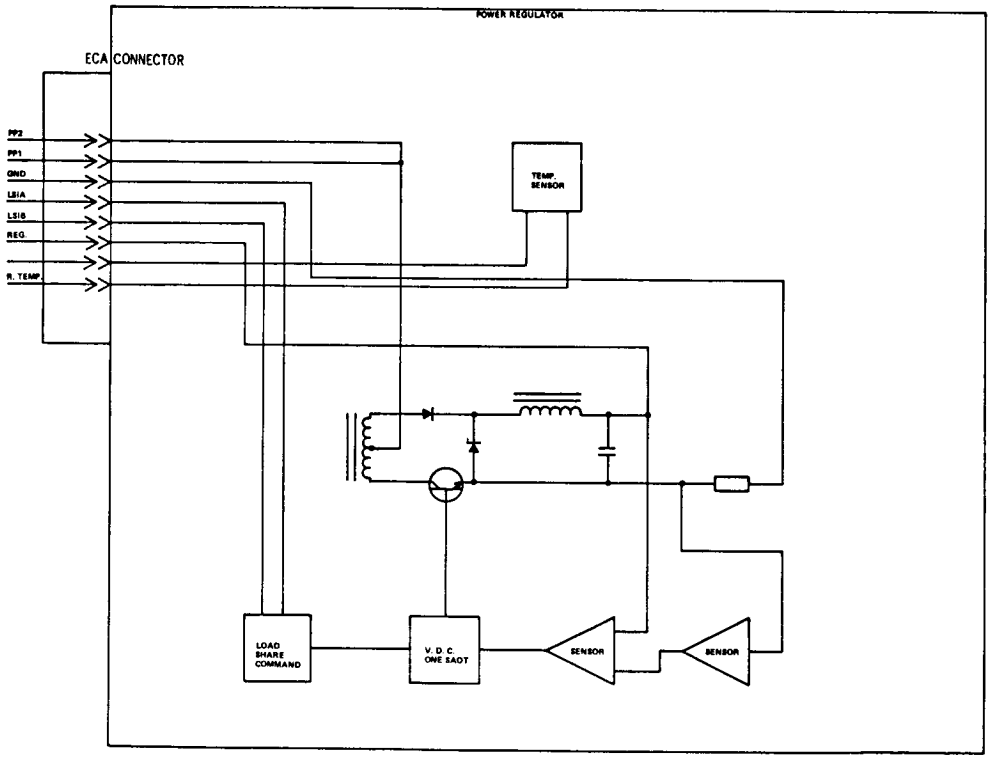

Figure IV-25. Regulator simplified diagram.

A prime requirement is that the regulator have the capability of parallel operation and have the ability to share the load and maintain output voltage regulation. Power division within the regulator is accomplished by a combination of voltage sensors and current limiters. Each regulator has a current limiting sensor to limit its maximum power output capability or its share of full load power. Voltage sensing and load share control signals are developed within the ECA and supplied as input to each regulator.

The electrical control assemblies (ECAs) will contain the current sensors and logic circuits required to develop load sharing control signals for each of the six voltage regulators. The regulators are designed to have a voltage drop of 0.5 volts between no load and full load when operating without any external control signal. One regulator feeding a bus, common to other regulators, operates as a master and is allowed to operate without a feedback control signal. The current output of this regulator is compared with other regulators feeding the common output bus. A signal increasing or decreasing the pulse rate and/or pulse width of each slave regulator is provided to adjust its current to match that being provided by the master. The regulator acting as the master can be changed by ground command. It is automatically switched if the high/low voltage monitor registers a large out-of-voltage tolerance condition. Regulator characteristics are summarized in Table IV-17.

TABLE IV-17. REGULATOR ASSEMBLY CHARACTERISTICS AND RATINGS

Input Voltage (Equipment Rating)	22-125 Vdc
Normal From Batteries	24-36 Vdc
From Solar Array	38-88 Vdc
Voltage Slope	0.02 V/A
Output Power	700 watts
Efficiency	90% Min at Full Load
Assembly Size	279 × 203 × 127 mm
Assembly Mass	3.5 kg
Thermal Dissipation	25 watts
Maximum Ambient Temperature	100°C

6. EPS Capabilities for Polarimetry Experiments. Polarimetry experiments may require the LST to roll about its X-axis from a sun-oriented position. The power from the array will be reduced when this roll occurs due to shadowing and the increase of the angle of incidence, the angle between the sunline and the normal to the array. This constraint could be eliminated with another degree of freedom on the array, but this would incur additional complexity and cost. Therefore, the reference EPS capabilities to sustain operations during off-sun roll maneuvers have been evaluated on the basis that the batteries will be required to furnish additional energy when the solar array power becomes limited. Additional battery capacity can be added if the baseline does not satisfy the scientific requirements. The cost of an additional battery would be less than $10 000, much lower than array costs. The weight and internal volume penalties, however, would be considerably higher.

The effect of a vehicle roll command on the power available from the solar array has been analyzed with respect to that available when the array is oriented. When oriented, the array power is P_s. Following an off-sun roll maneuver, neglecting shadowing, reflectance, etc., the array power P_s' is reduced by the increase in incidence angle γ in accordance with

$$P_s' = P_s \cos \gamma \quad . \tag{10}$$

To determine the variation due to angle of incidence, consider X_v, Y_v, Z_v to be the standard, vehicle-fixed orthogonal coordinate system. The longitudinal axis X_v must point to the celestial target. The solar array rotates about Y_v; therefore, a unit vector normal to the array, $\bar{n}$, remains in the X_v-Z_v plane and has no Y_v component. Letting ψ signify the degree of rotation of $\bar{n}$ about Y_v, measured from X_v, the normal vector is described as

$$\bar{n} = \cos \psi + j0 - k \sin \psi \quad . \tag{11}$$

A sun-oriented coordinate system, X_s, Y_s, Z_s, centered at the vehicle is then established as a reference with X_s pointing toward the sun. The unit solar vector, $\bar{s}$, is then coincident with X_s. The initial relationship of the vehicle and sun-oriented coordinate systems is illustrated in Figure IV-26. X_v points at a target θ degrees from the sunline $\bar{s}$. Y_s and Z_s have been rotated about X_s so that Y_s and Y_v are coincident, a condition necessary for orientation.

The vector normal to the array may be defined in terms of solar coordinates by multiplying by H, the transformation between X_v, Y_v, Z_v and X_s, Y_s, Z_s coordinates

$$\bar{n}_s = H\bar{n}$$

$$\bar{n}_s = \cos\psi \cos\theta + \sin\psi \sin\theta \quad . \tag{12}$$

The sunline vector, $\bar{s}$, in the same coordinate system is

$$\bar{s} = 1 + j0 + k0 \quad . \tag{13}$$

The dot product, $\bar{n}_s \cdot \bar{s}$, of equations (12) and (13) yields the cosine of the incidence angle:

$$\cos\gamma = \cos\psi \cos\theta + \sin\psi \sin\theta \quad . \tag{14}$$

Making $\psi = \theta$ for the initial vehicle position of Figure IV-26 orients the array to the sun since equation (14) reduces to

$$\cos\gamma = \cos^2\theta + \sin^2\theta = 1 \quad . \tag{15}$$

Two cases are considered for array orientation following a vehicle roll about the X_v-axis from the foregoing initial position. Case 1 assumes that the array position with respect to the vehicle (or angle ψ) remains fixed. Case 2 considers a reorientation of the array after roll to optimize the angle of incidence.

1. Case 1 — Letting X_v', Y_v', Z_v' represent the vehicle coordinates after a roll of ϕ degrees from the initial position, the new vehicle position with respect to solar coordinate reference is as shown in Figure IV-27. X_v' still points to the target θ degree from the sunline, but $\bar{s}$ is no longer perpendicular to Y_v; also, $\bar{n}'$ is not coincident with $\bar{s}$. Using G as the transformation between the X_v, Y_v, Z_v and the X_v', Y_v', Z_v' coordinate systems, the solar vector, equation (13), is transformed into the new vehicle coordinates:

$$\bar{s}_v' = GH\,\bar{s}$$

$$s_v' = \cos\theta + j\sin\theta\sin\phi + k\sin\theta\cos\phi \quad . \tag{16}$$

Since ψ was fixed, $\bar{n}' = \bar{n}$ of equation (11) and the cosine of the incidence angle is then determined by the dot product of $\bar{s}_v'$ and $\bar{n}'$:

$$\cos\gamma = \cos\theta\cos\psi + \sin\theta\sin\psi\cos\phi \quad .$$

Since the initial value, $\psi = \theta$, is held constant,

$$\cos\gamma = \cos^2\theta + \sin^2\theta\cos\phi \quad . \tag{17}$$

The cosine of the incident angle determined by equation (17) is plotted as a solid line curve against the pointing angle, θ, for several roll angles, ϕ, in Figure IV-28. Referring to equation (10), Figure IV-28 also indicates the percent of solar array power available compared to that available when the array is sun oriented.

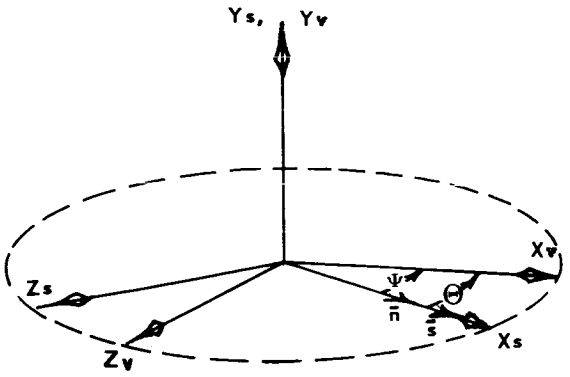

Figure IV-26. Initial oriented position of LST coordinates related to sun coordinates.

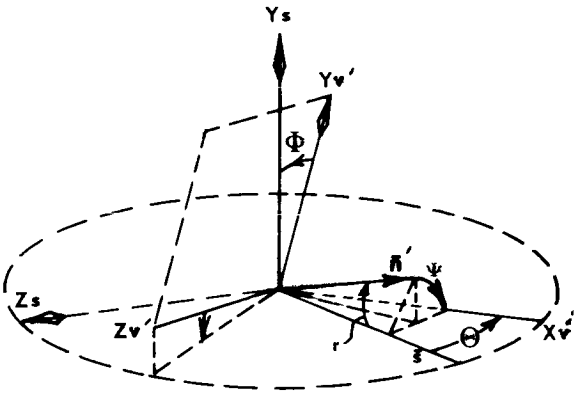

Figure IV-27. LST coordinate position after roll maneuver.

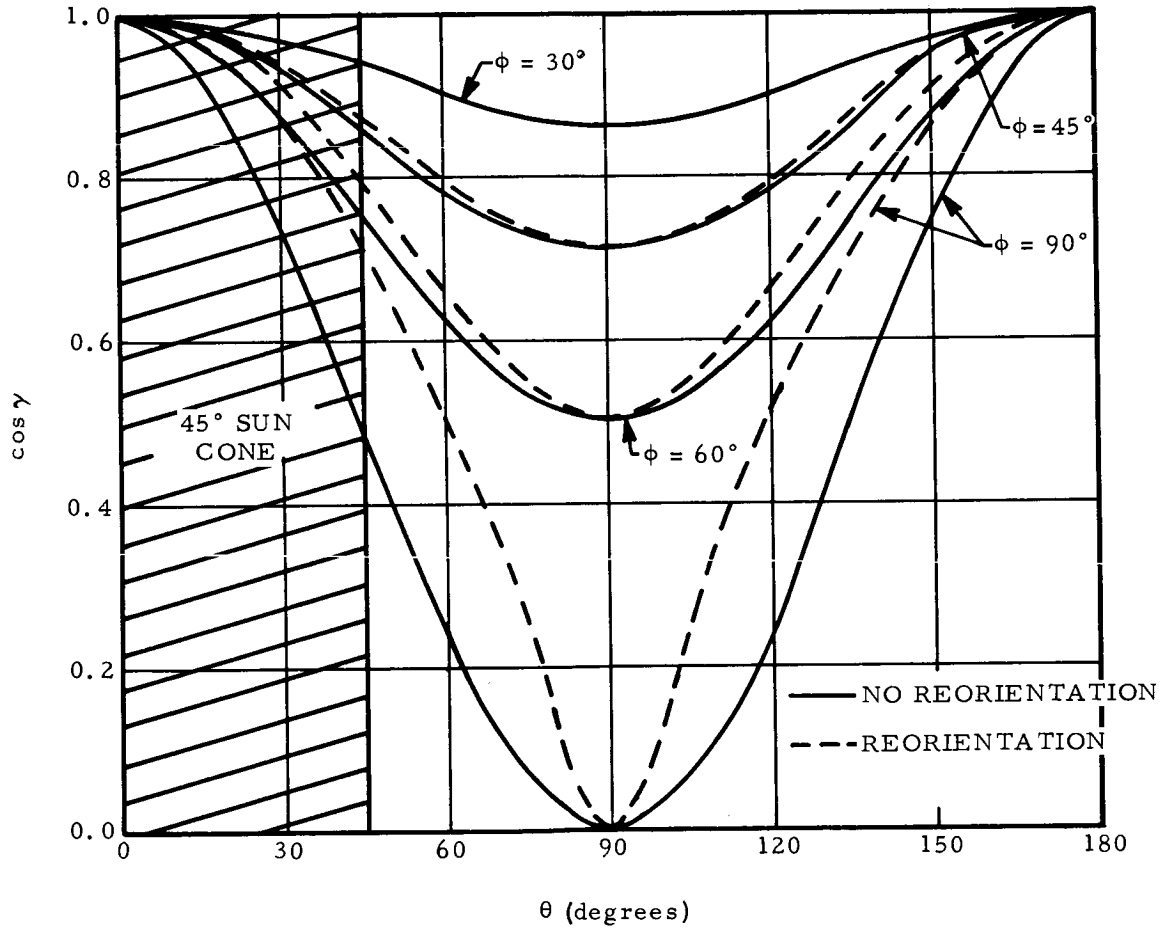

Figure IV-28. Cosine of angle of incidence, γ, as a function of θ with ϕ as a parameter.

2. Case 2 — The sun vector described by equation (16) of Case 1 is the same for Case 2. If the array is reoriented after roll (i.e., ψ is changed), the minimum incident angle or the highest power is obtained when the array normal vector $\bar{n}'$ is along the intersection of the s_v'-Y_v' plane and the X_v'-Z_v' plane. Letting Y_v' be a unit vector, the optimum direction for $\bar{n}'$ is obtained by determining a normal to plane s_v'-Y_v' and then finding the vector normal to the above normal and to Y_v'. This is expressed in terms of cross products of s_v' and Y_v' as follows:

$$\bar{n}' = \frac{Y_v' \times \left(S_v' \times Y_v'\right)}{\left|Y_v' \times \left(S_v' \times Y_v'\right)\right|}$$

$$\bar{n}' = \frac{\cos\theta + j\,0 + k \sin\theta \cos\phi}{\sqrt{\cos^2\theta + \sin^2\theta \cos^2\phi}} \quad . \tag{18}$$

The largest value for the cosine of the incident angle is then determined from equation (16) and (18):

$$\cos\gamma = \bar{s}_v' \cdot \bar{n}' = \frac{\cos^2\theta + \sin^2\theta \cos^2\phi}{\sqrt{\cos^2\theta + \sin^2\phi \cos^2\phi}} \quad . \tag{19}$$

The array orientation angle, ψ, necessary to satisfy equation (19) is given by

$$\psi = \cos^{-1}\left(\frac{\cos\theta}{\sqrt{\cos^2\theta + \sin^2\theta \cos^2\phi}}\right) \quad . \tag{20}$$

Optimum values of $\cos\gamma$ are also plotted as dashed line curves in Figure IV-28. The greatest improvement occurs when the roll angle, ϕ, is ±90 degrees except when θ is ±90 degrees. When both θ and ϕ are are 90 degrees, the normal to the array remains perpendicular to the sunline regardless of the value of the array rotation angle, ψ. As indicated the array

power can vary between the maximum oriented power (i.e., P_s = 3054 watts) and zero when $\cos \gamma = 0$ for the $\theta = \phi = 90$ degree case.

Battery Limits. When the array power becomes limited, the number of off-sun orbits that the EPS can sustain is determined by the battery capacity installed and the DOD that can be safely allowed for short periods of time. Modifying the energy balance equations for limited solar array power, the energy storage requirements are detemined for the same conditions considered in the solar array Cases 1 and 2 above.

Using the power available from the array, P_s', given by equation (10), the power available for the chargers is

$$P_c = P_s' \eta_t - P_L(s)/\eta_R/\eta_o \quad . \tag{21}$$

If $P_c > 0$, the energy required of the battery occurs during darkness only, as given by

$$E_D = \frac{P_{L(D)}\, t_d}{\eta_{BD}} \quad . \tag{22}$$

The energy replaced during sunlight periods is

$$E_R = P_c \eta_c \eta_b t_s \quad .$$

Thus for N orbits off-sun, the energy required of the battery when $E_D > E_R$ is,

$$E_N = (N + 1)\, E_D - N\, E_R \tag{23}$$

when $E_R \geq E_D$,

$$E_N = E_D \quad . \tag{24}$$

If in equation (21) $P_c \leq 0$, energy is not replaced by the array, and the battery must supplement the power required by the load during sunlight. The energy required of the battery then becomes,

$$E_N = (N + 1)\, E_D + N \left[\frac{P_{L(S)}}{\eta_{BD}} - P_S' \frac{\eta_T}{\eta_d} \right] t_s \quad . \tag{25}$$

The energy required using equations (23), (24), and (25), depending on the solar array power available in equation (19) and the E_D to E_R relationships, is shown in Figures IV-29 and IV-30. The installed battery capacity needed to satisfy any of the conditions determined by the above equations can be found by dividing E_N by a safe depth of discharge (DOD). A maximum DOD of 50 percent is recommended when the battery life exceeds 5 or 6 months. If batteries can be replaced on a yearly basis, a DOD of 60 percent could be permitted for the first 6 months of each year as long as such cycles occur only once or twice per month. The energy available from the baseline batteries, having a 5400 W-h capacity, for 50 percent DOD is indicated as dashed lines on Figures IV-29 and IV-30.

For a roll angle, ϕ, of 45 degrees as shown in Figure IV-30, the spacecraft can view any object for one or two orbits and if the object is within approximately 60 degrees of the sun or antisunline it can be viewed for three orbits without discharging a 5400 W-h battery greater than 50 percent depth of discharge. From Figure IV-29, it can be seen that a roll angle of 90 degrees greatly increases the energy required if the object is not near the ecliptic plane.

Figures IV-31 and IV-32 are for the same conditions except that the beginning of life solar array power was used. The extra array power reduces the energy requirement for the 45 degree roll case so that three orbits at any θ can be viewed. The 90 degree roll case is improved but, if θ is near 90 degrees, the improvement is small or zero.

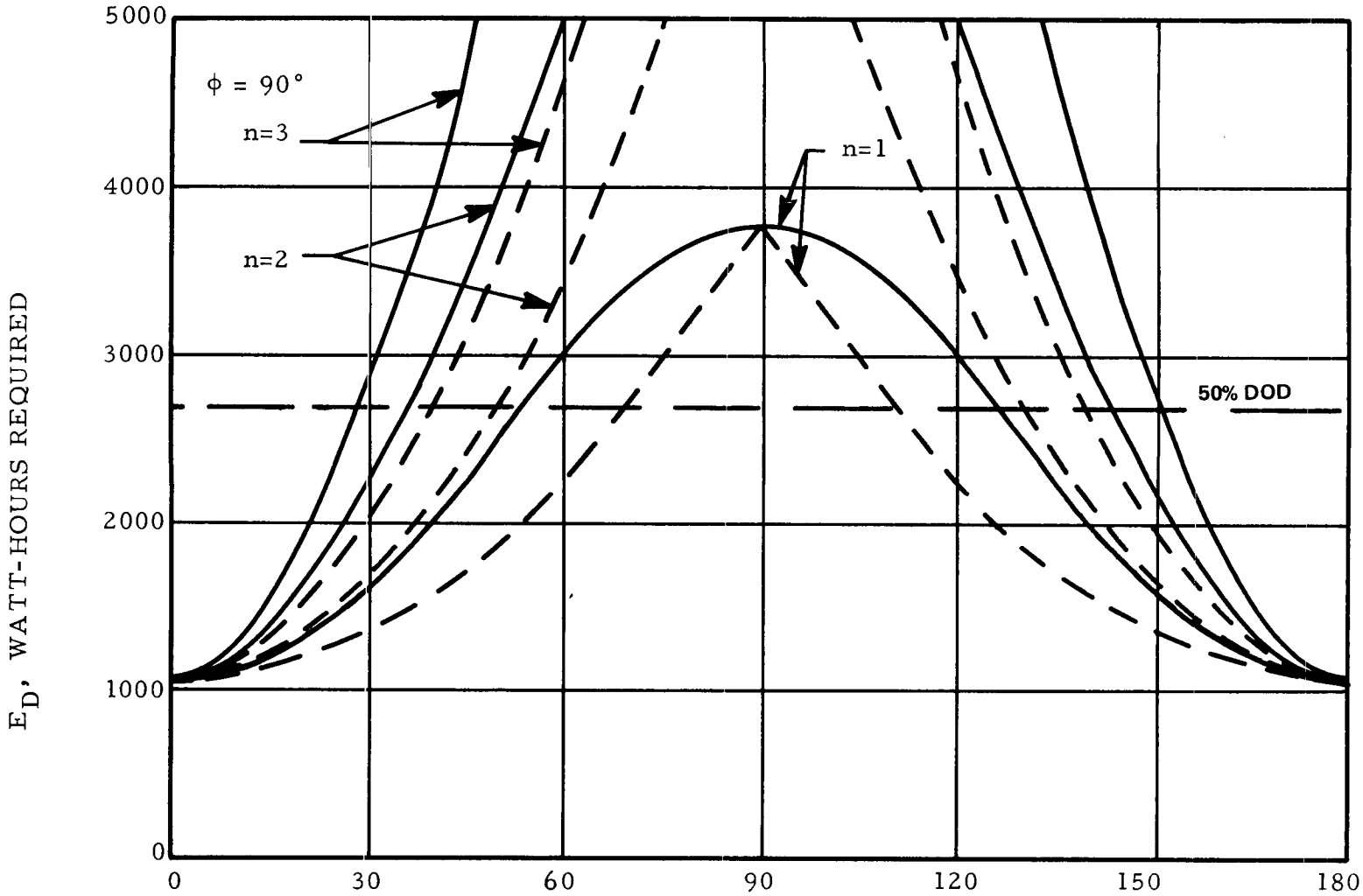

Figure IV-29. Energy required with ϕ = 90 degrees and end of life solar array.

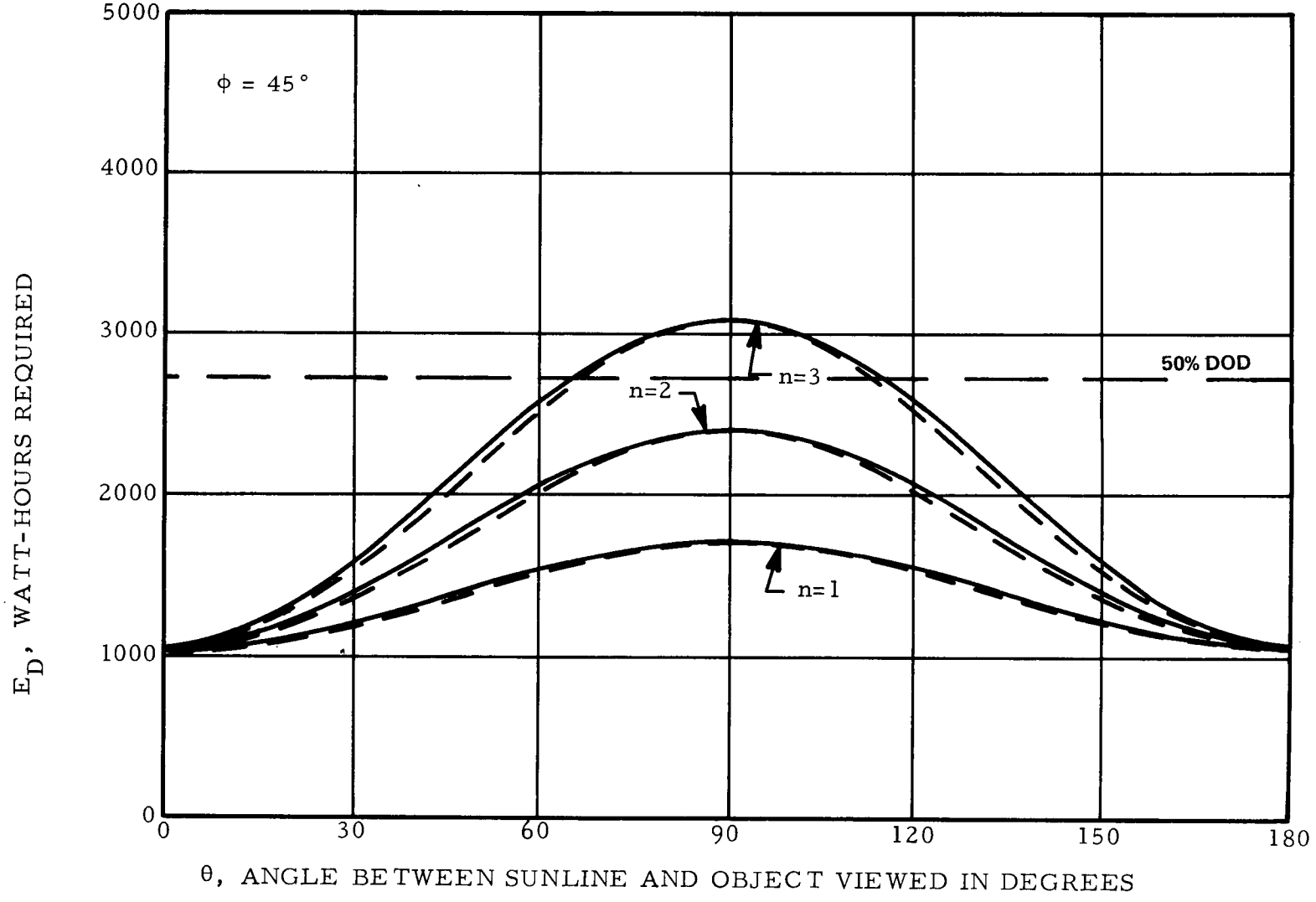

Figure IV-30. Energy required with ϕ = 45 degrees and end of life solar array.

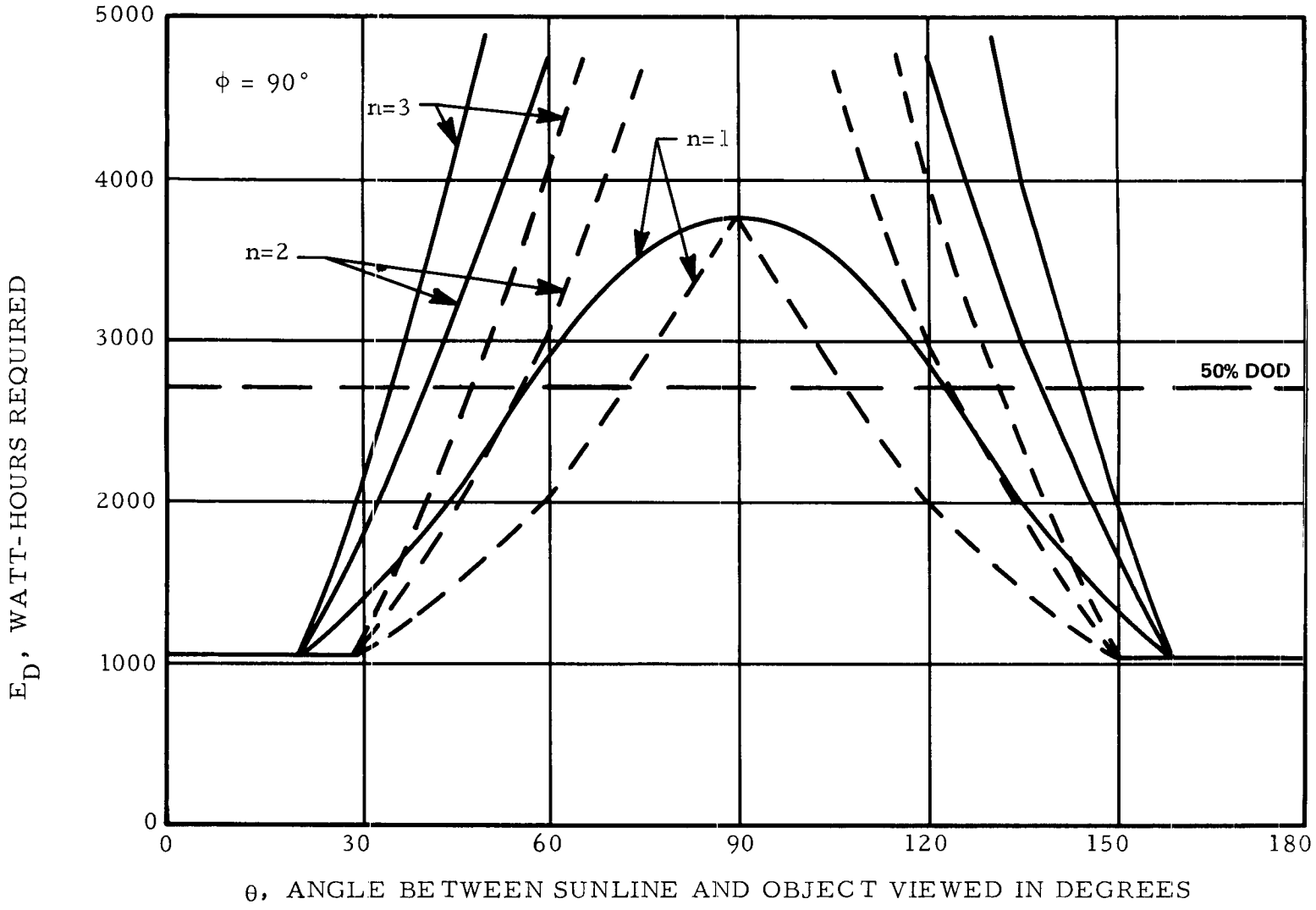

Figure IV-31. Energy required with ϕ = 90 degrees and beginning of life solar array.

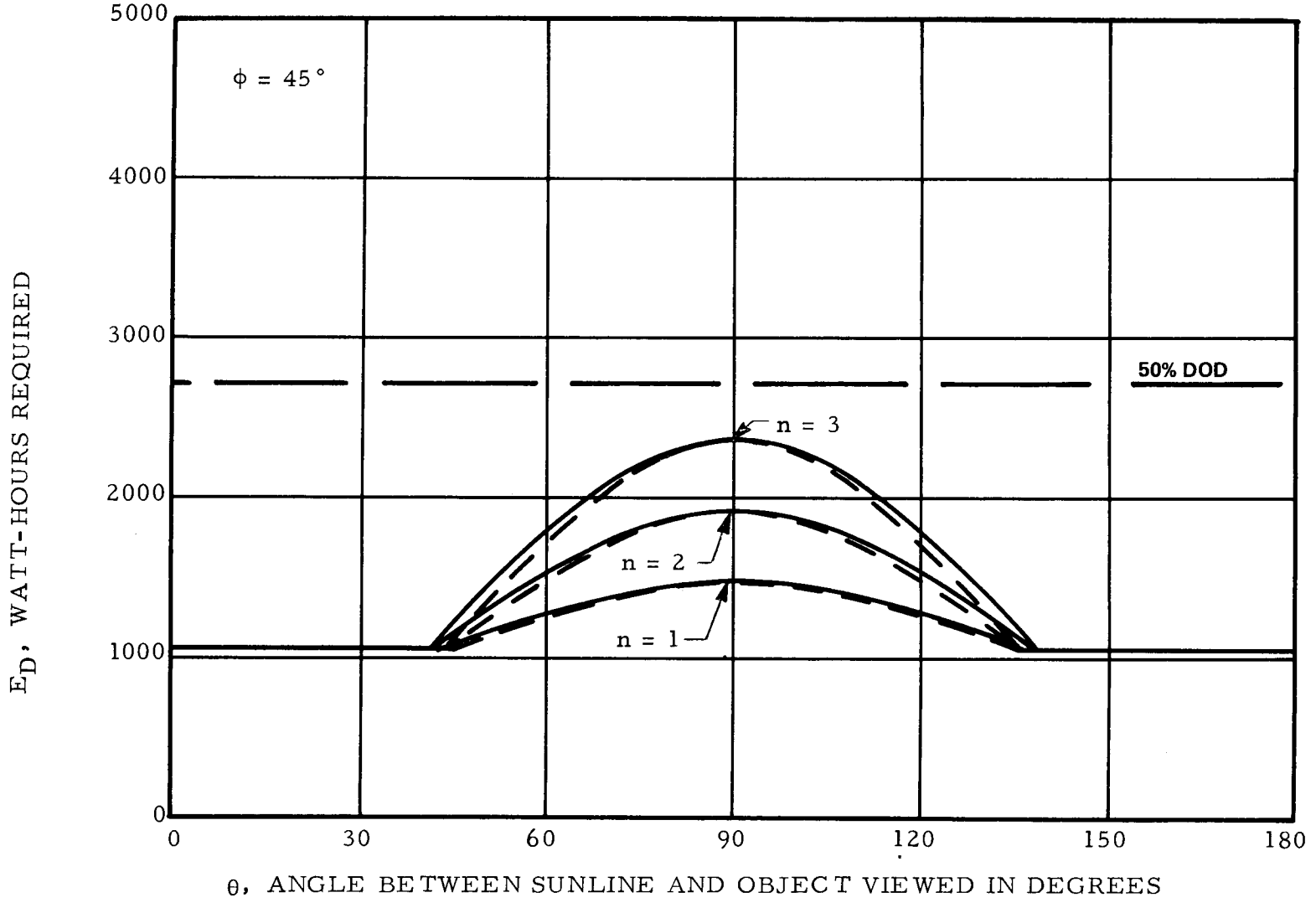

Figure IV-32. Energy required with ϕ = 45 degrees and beginning of life solar array.

For the reoriented array cases at BOL and EOM, θ and ϕ have been translated into percent of celestial sphere coverage. The information of Figures IV-29 through IV-32 can then be presented as the coverage offered as a function of off-sun orbits.

Assigning a unit radius to the celestial sphere, the total area is 4 π steradians. Neglecting the earth and moon obstructions (these exist for only a few days), the part of the celestial sphere that may be observed during any day is limited by the pointing restriction that does not permit the LST to look within 45 degrees of the sun. Considering the vehicle to be at the center of the celestial sphere and the 45 degrees to be a half cone angle, δ, the area, A_V, of the sphere that may be viewed is

$$A_V = 2\pi [1 - \cos(\pi - \delta)] \quad ,$$

$$A_V = 3.41\ \pi \text{ steradians} = 100\% \text{ pointing coverage by definition.}$$

Investigation of polarization and special orientation of a target requires a slit rotation about the vehicle X-axis. Since this rotation is accomplished by rolling the vehicle, it affects the power available from the solar array, as shown previously. Limited array power, in turn, imposes greater energy requirements on the batteries. The system capabilities have been assessed in terms of battery capacity required for a given number of orbits with off-sun pointing as a function of the X-axis orientation and the degree of roll required. If ϕ is restricted, coverage is also limited. To permit complete polarization freedom, ϕ must be 90 degrees, which is defined as 100 percent polarization coverage. Smaller ϕ angles are possible if long term scheduling is permitted. However, at any one given time, target polarization viewing would be constrained if ϕ is limited to less than 90 degrees. The freedom permitted in pointing, angle θ, directly affects the percent of the celestial sphere that may be viewed. Therefore, total target coverage is defined as the case where pointing is allowed to be

$$45 \text{ degrees} \leq \theta \leq 315 \text{ degrees}$$

and the roll is allowed to be

$$0 \text{ degrees} \leq \phi \leq 90 \text{ degrees} \quad .$$

When the EPS limits off-sun viewing determined by θ and ϕ, area of coverage is determined by

$$A_c = 2\pi (1 - \cos \theta) \quad .$$

and is expressed as a percent of the area, A_v.

From an array standpoint, the worst case exists when $\theta = \pm 90$ degrees and $\phi = 90$ degrees (designated as 100 percent coverage). Maintaining roll freedom of 90 degrees and restricting θ to ± 45 degrees reduces the battery size and weight penalty but also reduces the celestial sphere coverage to 60 percent. The number of consecutive orbits off the sun permitted is shown in Figure IV-33 as a function of the baseline battery limits and the percent of celestial sphere coverage. It can be seen that several orbits are allowed for the lower coverage cases up to about 60 percent. The baseline does not permit a full orbit for the extreme 100 percent coverage case.

An additional battery would be required for one orbit of full coverage. It may be noted that the additional power available from the array at BOL improves the low coverage cases but has no effect on the extreme 100 percent case.

D. Electrical Distribution

The SSM electrical distribution subsystem (EDS) accomplishes the distribution of power and electrical signals required to control and monitor the operations of the LST. It also accomplishes the electrical integration with the OTA/SIP, the Shuttle system, ground checkout facilities.

An elementary schematic of the SSM electrical system is shown in Figure IV-34. The diagram has been simplified for clarity — some of the redundancy and components of the subsystems have been omitted.

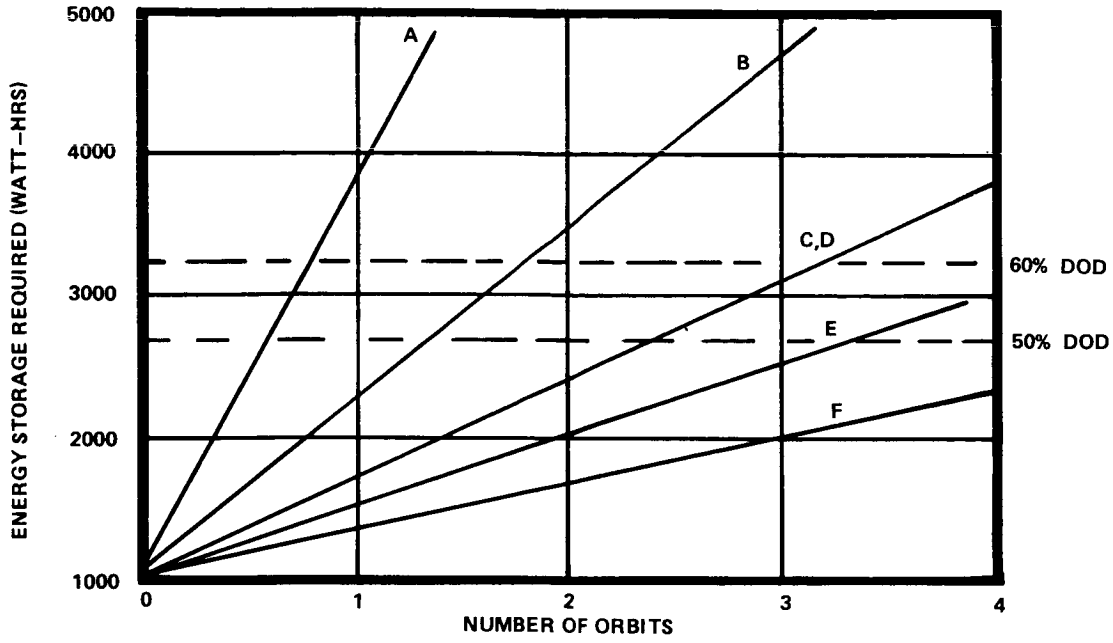

CASE. A. $\phi = 90^{\circ}$, $\theta = 90^{\circ}$, COVERAGE = 100%
B. $\phi = 90^{\circ}$, $\theta = 60^{\circ}$, COVERAGE = 72%
C. $\phi = 90^{\circ}$, $\theta = 45^{\circ}$, COVERAGE = 56%
D. $\phi = 45^{\circ}$, $\theta = 90^{\circ}$, COVERAGE = 100%
E. $\phi = 45^{\circ}$, $\theta = 60^{\circ}$, COVERAGE = 72%
F. $\phi = 45^{\circ}$, $\theta = 45^{\circ}$, COVERAGE = 56%
ϕ IS THE ROLL ANGLE
θ IS THE POINTING ANGLE

Figure IV-33. Reference EPS capabilities for polarimetry experiment.

In Volume II, the EDS was described in terms of functional networks designated as:

1. Data Networks.
2. Command Networks.
3. Power Networks.
4. Attitude Control Networks.
5. Test and Maintenance Support Networks.

The functions and major components of the data, command, and attitude control networks are adequately discussed in Chapters V and VI. Only the cabling and interfaces associated with these networks are addressed here. Power networks were divided into three sections — power transmission networks, main distribution networks, and secondary distribution network — for protection, control, and versatility.

1. Power Transmission Network

a. General. The power transmission network primarily services the electrical power subsystem. It provides cabling, junction assemblies, and interface devices for the transmission of power into the SSM from the solar arrays and for transmission of primary power between major power assemblies within the SSM. It also provides primary buses, power controls, detectors, and protective devices required for the primary networks. The two solar power distributors (SPDs) centralize and control the major part of the transmission network. Network concepts are described by the functional description of the SPDs.

b. Solar Power Distributors. Each of the two solar power distributors receives power from their respective wing panel. Each is designed to handle full spacecraft power; however, under normal operating conditions the load is shared between the two. Growth capacity is included in the design of the distributors. The following functions are performed by the solar power distributors:

1. Combine the outputs of the solar panel modules into common primary power buses.

2. Control routing of primary power to the battery chargers, ECAs, and the power regulators. (Also may be used to distribute unregulated power if required in the spacecraft.)

3. Perform detection and switching functions necessary to isolate array or load faults on the primary buses.

4. Provide redundant buses, switching, and outputs to bypass faults and to reroute power to EPS assemblies.

5. Provide redundant firing and safing circuitry for array pyrotechnic release devices.

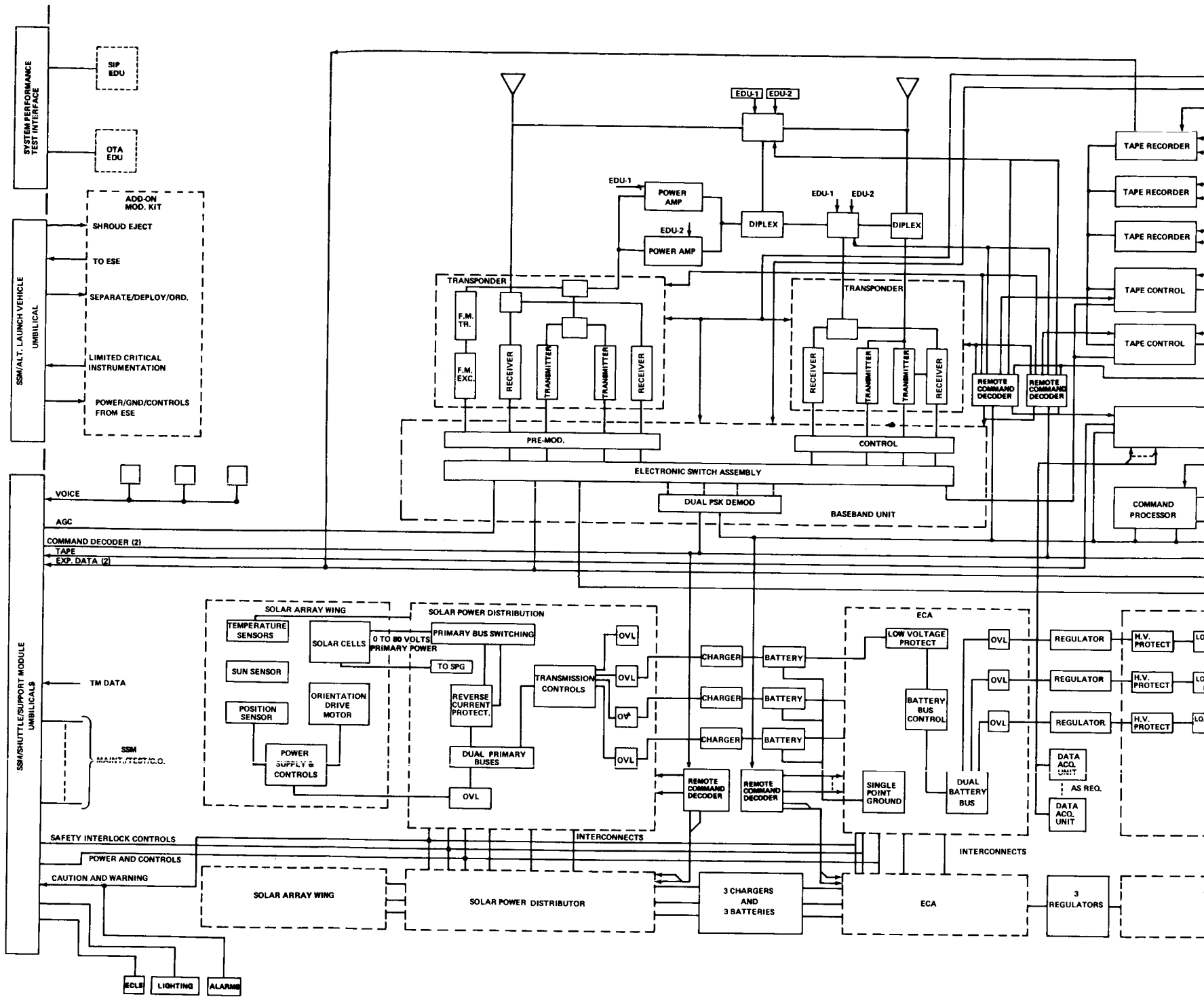
SYSTEM PERFORMANCE TEST INTERFACE
SIP EDU
OTA EDU
SSM/ALT. LAUNCH VEHICLE UMBILICAL
ADD-ON MOD. KIT
SHROUD EJECT
TO ESE
SEPARATE/DEPLOY/ORD.
LIMITED CRITICAL INSTRUMENTATION
POWER/GND/CONTROLS FROM ESE
EDU-1
EDU-2
POWER AMP
DIPLEX
TRANSPONDER
F.M. TR.
F.M. EXC.
RECEIVER
TRANSMITTER
REMOTE COMMAND DECODER
PRE-MOD.
CONTROL
ELECTRONIC SWITCH ASSEMBLY
DUAL PSK DEMOD
BASEBAND UNIT
TAPE RECORDER
TAPE CONTROL
COMMAND PROCESSOR
VOICE
AGC
COMMAND DECODER (2)
TAPE
EXP. DATA (2)
SSM/SHUTTLE/SUPPORT MODULE UMBILICALS
TM DATA
SSM
MAINT./TEST/C.O.
SOLAR ARRAY WING
TEMPERATURE SENSORS
SOLAR CELLS
SUN SENSOR
POSITION SENSOR
ORIENTATION DRIVE MOTOR
POWER SUPPLY & CONTROLS
SOLAR POWER DISTRIBUTION
0 TO 80 VOLTS PRIMARY POWER
PRIMARY BUS SWITCHING
TO SPG
REVERSE CURRENT PROTECT.
DUAL PRIMARY BUSES
TRANSMISSION CONTROLS
OVL
CHARGER
BATTERY
ECA
LOW VOLTAGE PROTECT
BATTERY BUS CONTROL
DUAL BATTERY BUS
SINGLE POINT GROUND
REGULATOR
H.V. PROTECT
DATA ACQ. UNIT
AS REQ.
SAFETY INTERLOCK CONTROLS
POWER AND CONTROLS
CAUTION AND WARNING
INTERCONNECTS
SOLAR ARRAY WING
SOLAR POWER DISTRIBUTOR
3 CHARGERS AND 3 BATTERIES
ECA
3 REGULATORS
ECLS
LIGHTING
ALARMS

Part #1

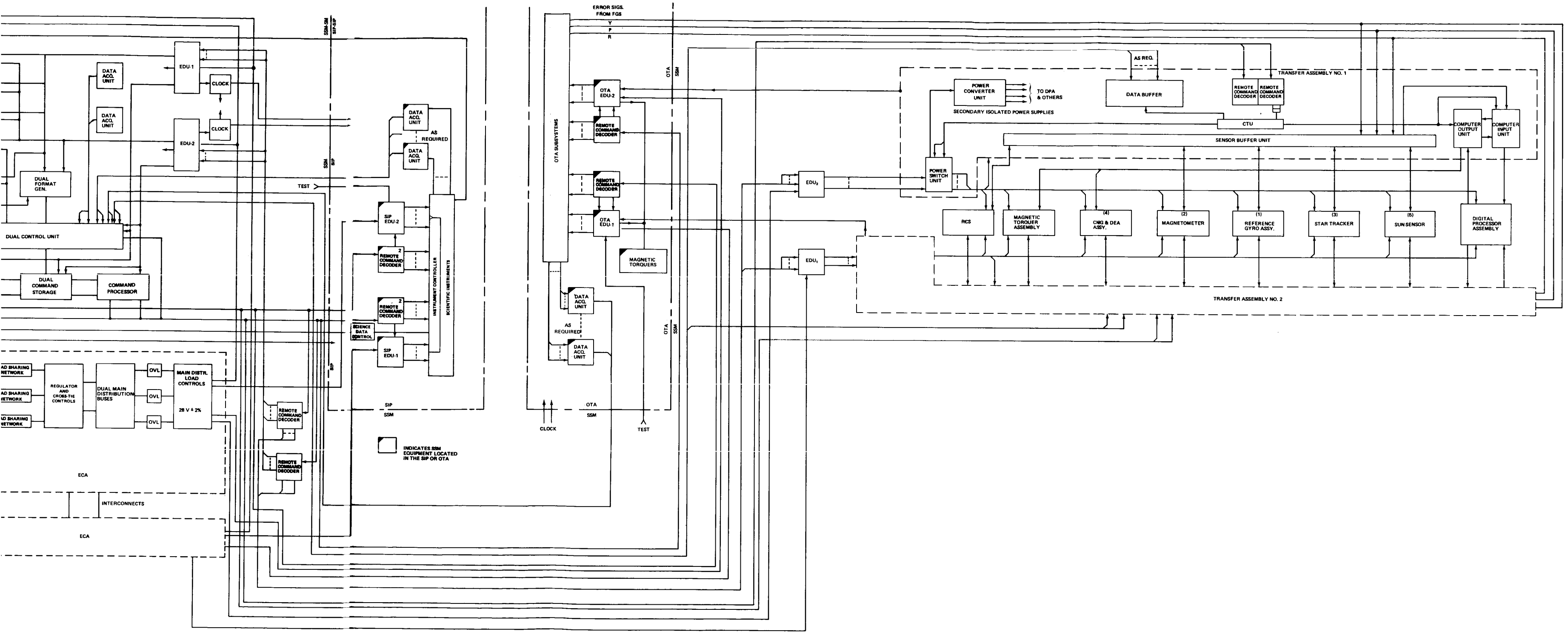

Part #2

Figure IV-34. Electrical system diagram — system support module (simplified).

6. Distribute power and signals to orientation drive control assemblies.

7. Provide a means of monitoring solar array voltages and currents for telemetery and fault detection. House peak power tracking circuitry for recharge control.

8. Receive, via external interfaces, power and control signals from electrical support equipment and implement the required functions for ground and in-space checkout operations. Also, return status information.

9. Provide a convenient access point for test and checkout of the solar array modules.

Although the solar arrays are not redundant, their size allows for degradation. Each wing is modularized for fabrication and protection reasons. The output of each module is transmitted to the SPDs over redundant lines. The SPDs receive the power from each module and can direct it to either of the redundant primary buses. The SPDs have provisions for optional blocking diode, plug-in modules if needed. The diodes are not presently used because of the protection devices provided, the normally-oriented array, and the absence of shadowing. The 0.8 volt drop across the diodes would add a power loss of about 50 watts to the system.

Power switches and relays are, in general, the magnetic latching type to conserve control power. Bifilar wound types were selected to minimize system switching transients. All relays are qualified and conform to MSFC-Spec-40M37496.

Switches, permitting the selection of the primary bus to which a given panel input is applied, allow half of the system to operate from two isolated buses or from one bus with the other in standby. These switches also serve as backup fault protection for the sources and lower the current to be cleared in the event of a fault. The inputs are segmented to assure that the contacts operate at a conservative current, compared to the rating. All contacts will be redundant.

A bus tie is provided, permitting half the system to operate in a single-bus mode for flexible power management. This switch controls power channeled to the second solar power distributor via the alternate primary bus should the loads be unbalanced or in the event that a source failure occurs.

Should the situation be reversed, a crosstie contractor is closed to take power from the other distributor. Normally, the switches will be open and the redundant primary bus will serve as a backup or transfer bus.

The primary output channels to ECAs and to the chargers have automatic overload protection. Signals derived from command inputs are required to switch buses and operational modes. Commands may also override protective switching for diagnostics and protection against sensor failure. Sufficient protection and redundancy is provided throughout the system to assure primary bus integrity. Overload protection of the redundant outputs to the prime loads is not provided to essential loads should the external system or subsystem degrade to abnormal emergency conditions. This alternate channel also assures that a protective device malfunction does not permanently interrupt service. Similarly, alternate channels to the ECAs are not overload protected. Protection within the ECAs is adequate to protect the alternate primary sources.

Input control cables are separate from power cables. Each solar distributor may receive control signals from either of the electrical control assemblies. Automatic and commanded signals originated in the ECAs perform fault isolation, operating mode selection, and power management functions. The SPDs have provisions for the incorporation of remote command decoders (RCDs) but requirements were not large enough to justify additional allocation of RCDs for electrical distribution functions. The units allocated to the EDS are located in the ECAs. Thus, command signals to the SPDs are derived from the ECAs. Instrumentation outputs, also, are separately routed to the ECAs.

Solid state logic, differential amplifiers, and driver circuits located in the SPDs sequence and control the switching that operates the deployment and retraction mechanisms upon command. Signals from the limit switches terminate the operation. Commandable switches may also deenergize the motors and are provided for backup to the limit switches. The SPDs also distribute power and signals to the assemblies that control the array orientation drive mechanisms.

The signals from all the sensors located on the array wings (e.g., temperature, wide angle sun sensors, limit switches) are routed through the SPDs. Array current and voltage monitors are located within the assembly. The circuitry which tracks the peak power of the array buses is also housed in the SPDs. Signals from these trackers are sent to the chargers to permit full use of array power or to limit battery charging should array power become limited.

An isolated section of the SPD contains redundant, controlled switches for firing pyrotechnic devices. Remotely controlled and manual safing provisions are made for these functions.

Electrical support equipment (ESE) and test connectors are provided for system testing, control and checkout, and in-orbit maintenance. External power which simulates the solar array is furnished to operate the EPS or to charge batteries while on the ground or during Shuttle operations. This connector accommodates hardwire control signals to operate the power bus switches and the critical power control sensors required for power management.

The test connector, in conjunction with switches, provide the capability for testing the solar array integrity and performance while the spacecraft is on the ground or in the launch vehicle. The Dark I-V Method is used to perform such tests. ESE power supplies, having characteristics similar to the solar array, may be connected to the terminals of each solar cell assembly on the solar panels in sequence. This permits recording of the reverse current characteristics of each solar cell assembly on each panel. Switches must be operated to isolate all system loads from the solar panel during these tests. Otherwise, erroneous data would be obtained due to load drain.

ATM and Skylab equipment represents some of the latest designs of distribution equipment developed and qualified. These assemblies have been modularized into function subassemblies for adaptability. These modules have the type of components, configuration features, characteristics, and ratings applicable to the LST. They are assembled and electrically interconnected to satisfy the specific LST requirements. These elements will be applied so that their rating is conservative compared to the requirement of the function. All components are manufactured in accordance with established specifications and fabrication processes. The designs are also well documented.

2. Main Distribution Network

a. General. The main distribution network receives and centralizes power from the EPS power assemblies and controls main power feeders. It distributes regulated power to decentralized secondary distribution units, sectionalized on a subsystem basis, or directly to some critical loads. It provides detection and fault isolation to protect the subsystems, the EPS, and the primary sources. Primary EDS interfaces with command and data

networks to permit remote electrical management of the system are located in this network. The centralized concept simplifies the design and offers better control of power for management and protection purposes. It maintains an independency between loads and the primary system and provides a convenient means of controlling redundancy. Distribution is divided into controllable, convenient sections. Incorporation of secondary distribution assemblies at the receiving end of these sections is a highly versatile distribution scheme, similar to that used by utility companies.

Specific functions of the main distribution network are explained by the functional description of the electrical control assemblies.

b. Electrical Control Assemblies. The main distribution network centers about the two electrical control assemblies (ECAs) that house redundant buses, crossties, switchgear, controls, and protective devices needed to assure reliable distribution and control of the network. Redundant cabling assures access to power for each subsystem. Input switching provides several channels to redundant EPS power sources in the event an EPS assembly becomes faulty. Protection is provided for EPS equipment and the loads. These assemblies represent the primary interfaces with the command and data systems for remote control and monitoring of electrical system functions.

The ECAs are modularized assemblies consisting of the same type of modules used for the SPDs. Because of the functional differences required, additional modules are needed and the electrical configuration is different. The size selected allows for six output cables from each assembly to secondary distribution units and for two outputs to major critical loads that may not be serviced through the secondary units. Each assembly provides three redundant outputs and inputs for the regulator assemblies. Redundant inputs are received from three batteries via the chargers. Inputs from the SPDs are also redundant. Separate control and instrumentation connectors are provided for the battery chargers, regulators, and the SPD serviced by the ECA. The crossties between the buses of the two ECAs provide a redundant output distribution network with multiple redundancy for access to power.

Each ECA controls inputs from each of three batteries and switches them to one of two buses as selected. Crossties to the other ECA permits one, two, or three of the other batteries to feed power to buses of the first ECA. Thus the batteries may be used individually or in parallel combinations up to six. Three dual limit detectors for overload and low voltage control the input switching to protect each of the batteries.

The redundant inputs from the SPD may also be controlled in the event of a primary system malfunction. Crosstie switches provide access to primary power from the second SPD via the second ECA.

Dual switching is provided for power to each of the regulators. Each regulator may be energized from either of the redundant buses. Any regulator has access to power from any battery when input crossties are operated. Therefore, the regulators may be operated in parallel combinations similar to the batteries.

Redundant buses and switching are provided by each ECA to receive power from three regulators. These distribution buses provide 28 Vdc, regulated to ±2 percent, to the units supplying the system loads. The networks supported by either ECA is assured access to regulated power by crosstie switching of the regulated buses between the ECAs. Voltage sensors for these buses are located in the ECA to provide feedback to the regulators for load sharing when they are operated in parallel.

The characteristics of the regulators provide inherent overload protection to the primary power sources; however, to prevent a load fault from causing low voltage on other sections that may be in parallel, delayed limit detectors are provided. These may bring a standby regulator on the line if this mode exists. If excessive load persists, the faulty section will be isolated. Over-voltage protection is also provided for each of the regulated buses to protect the loads from a possible short in a regulator. This could expose the loads to the high array voltage. Should the output of a regulator rise beyond 32 volts it will be isolated from the bus.

The decoders and data units in the ECAs provide the major command and data interfaces for the EPS and distribution networks, thus permitting remote operational control. Such provisions also enahnce the protection afforded to assure a reliable life. System integrity is monitored in sections for the various possible faults. Should a fault be indicated, the network responds to isolate the faulty section immediately. Depending on the loads involved and system conditions, subsequent corrective action occurs. For loads considered critical to the survival or recovery of the spacecraft, the network establishes redundant channels and/or sources to sustain the load or its alternate, as the case dictates. For less critical loads, isolation occurs and is indicated by telemetry to ground, awaiting corrective action by remote command. In both cases independent telemetry signals are provided to indicate conditions and corrective action taken. Also, provisions are made to override

isolation switching by command. This enables diagnosis of system conditions and assures that a fault in a protection device does not cause premature termination of operations.

The ECAs will have access to external interfaces for control and test during checkout and maintenance operations.

Protection against RF and conducted interference is provided in all networks to assure trouble-free operation. The ECAs incorporate transient suppression devices, accommodate the shielding requirements of distribution cabling, and provide for insertion of additional network filtering as needed. Consistent with reliable grounding schemes, the ECAs provide the single point ground for the entire system.

3. Secondary Distribution Network

a. General. The secondary distribution network consists of cabling, interface devices, protective devices, and controls for interfacing sections of the main distribution network with load to be controlled remotely. The electrical distribution units (EDUs) provide decentralized highly adaptive distribution service for the various subsystem loads and requirements. This is particularly attractive for separable elements for the LST, such as the optical telescope assembly (OTA). This concept provides versatility and growth without need for main network modification. It permits power network simplification consistent with the concept established for data and command networks.

b. Electrical Distribution Units. Eight EDUs are provided for the electrical system. These provide redundant distribution service to the SSM subsystems and to the OTA and SIP.

The subsystem power and hardware test interfaces with the EDS are primarily accommodated by the EDUs. The eight units defined are consistent with the system redundancy and subsystem requirements determined to date. However, system concepts allow the versatility of adding or subtracting EDU modules as the system design matures, depending on the specific detailed requirements to be established. For instance, several EDU submodules may be added to expand distribution service. On the other hand, a later subsystem configuration and location assessment may indicate that the ECAs can satisfy some of the requirements directly without sacrificing the reliability and versatility of the system.

The EDU consists of an input module and one or more output modules as required. The inputs are to be standardized for common interfaces with the electrical distribution subsystem. Electrical inputs from ECAs, remote command decoders (RCDs), and test cable are provided. Output modules consist of a family of adaptable subassemblies selected to satisfy specific requirements of each subsystem. The modular construction of the EDUs is consistent with that of the RCDs and DAUs so that these may be grouped together as one functional assembly when needed.

To complete the system protection scheme, the EDUs provide fault, over-voltage, and EMI protection for the major individual loads in the subsystem that interface with the power networks. Output power items to be operated by command are energized by the EDUs. Such commands received via the RCDs activate the proper power switching controls. Power semiconductors and relay matrices available in the EDU output modules can be used to produce parallel or subcontrolled stimuli from the serial commands.

The EDUs were sized for the largest block of secondary power initially anticipated. The unit size given in Table IV-8 was for a basic, three channel, 500 watt maximum unit and did not include add-on modules for specific output functions to be established. The latest load information indicates that a larger size is needed. Electrical rating adjustments have been made but time did not permit coordinating a new physical size.

The OTA represents the largest block of power to be supported by EDUs. As indicated in Volume IV, a 500 watt average rating may be low. Also, high peak requirements may be expected because of the mechanical drives in the system. The OTA concepts divided distribution into five parts with the thermal control subsystem having the highest potential average. For these reasons the basic EDUs are rerated to conservatively cover potential load growth.

The basic unit will have input connections for five separate inputs, redundantly wired, and five ground returns. Provisions for shielding, as required, will be made. The basic EDU input module will use four inputs and have protective isolation switching for four sections of outputs. Each of these controlled sections will be rated an average of 5 A at 28 to 30 volts, giving the basic input module a nominal rating of 600 watts. Redundant switch contacts shall be provided and these shall permit peaks of at least 7.5 A. Smaller switching modules may be used if loads are lower. An additional module will be added to the OTA units for the thermal load. Since this load may be 452 watts (16 A at 28 volts), 25 A master switches were selected for

this module. Thus, the EDU for the OTA would have a rating of 1200 watts. Input module protection is linked with the ECA and master switches are controlled via the ECAs.

Submodule selection for output modules permits subdivision of input modules into any number of outputs, depending on the ratings and number of modules used. Sixteen circuits at 1 A, or 8 at 2 A are convenient configuration ratings for a module. Two would be required for more outputs of these ratings. Larger numbers are available for individual outputs rated less than 500 mA, where semiconductor switches may be used. All output switching is to be controlled by remote command decoders. EDU output modules incorporate solid state circuitry and drive amplifiers for the size switching selected.

Electrical access to external connectors for test and checkout was requested but the specific number of functions and lines was not determined. Therefore a 39-pin connector was allocated on each EDU for this purpose. Since two EDUs are allocated for the OTA, for instance, the capability for 78 test lines exists, if needed. Test lines are not to be made redundant.

4. Test and Maintenance Support Networks. The test and maintenance support networks are activated only through external LST connections when electrical support equipment is available for the various test and maintenance operations. The test network will be common for, and made compatible with, both ground electrical support equipment (GESE) and in-space electrical support equipment (IESE). The maintenance networks are needed only for in-space maintenance with the Shuttle. These provide for illumination, local communications, life support sensors and accommodations, and warning alerts necessary for manned maintenance operations.

Based on historical safety concepts and procedures, approximately 39 kg of electrical equipment are installed in the LST to satisfy estimated interface, test, and maintenance requirements. These accommodations will be dependent on the mechanization and equipment provisions of the orbiter. The operational procedures and constraints and safety requirements have not yet been fully defined for the Shuttle.

Eight 30-watt fluorescent light fixtures are located in the vicinity of the OTA, SIP, and SSM equipment for visibility during maintenance. These units, which may be individually controlled, are powered from the IESE. The power needed will be supplied from the orbiter power source to the IESE.

A caution and warning assembly is installed to provide visual and audible alarms to a crew member working in the LST. He will be alerted of potential hazardous conditions that may occur in either the LST or the Shuttle. An isolated cable exchanges safety signals between the LST and Shuttle so that the same alerts are displayed at the payload work station, with some transferred to the cockpit.

Separate test cables are provided for the OTA, SIP, EPS, ACS, and C&DHS for easier integration and troubleshooting. This avoids complex harnesses and is consistent with modularization and maintenance concepts. It is expected that most of these will be small. They provide special hardwire access for checking redundancy or critical components, and permit checkout and fault location in the event of failures such as nonoperative command or data equipment. Should the number of external connectors be constrained by the docking adapter or the Shuttle system, a junction box will be added to the SSM to channel the internal test cabling to the interface connectors.

Coax cables provide data and command channels to the IESE for the normal checkout and maintenance. Normally, the onboard LST data and command equipment will be used for maintenance and checkout. The IESE serves as a command station and accumulates data during maintenance.

Three plug-in receptacles, cabling, and an interface connector provide a voice communication link to the Shuttle. This link is to be adapted to either suited or unsuited operations within the LST.

The LST has provisions to accept power from the Shuttle via the IESE. Control of power distribution and major EPS assemblies may be effected from the IESE.

5. System Hardware and Standards. The electrical system defined for the LST was based on the use of the latest applicable specifications and existing hardware qualified for similar space applications. The equipment shall be designed for reliable service, maintainability, and environmental conditions established for the missions. Conservative component ratings and established processes are to be used to avoid excessive testing. The need to impose flammability requirements of MSFC-Spec-101 was not established. Typical distribution hardware considered applicable and cost-effective was defined from that specified for HEAO.

a. Connectors. Zero-g connectors were considered for in-space replacement reasons. These offer handling and disconnection advantages for

suited man operations and are applicable to unpressurized payloads. Since the LST is pressured, such connectors are not required. They incur a 3 to 1 mass penalty and require more volume for cabling. Therefore, the standard circular connectors used for LST conform to MSFC-Spec-40M39569 and -40M38277.

b. Wire. To assure mechanical strnegth, wire shall be no smaller than AWG 24 and shall comply with MSFC-Spec-40M39513 as modified. Silver-plated, Kapton-insulated wire is recommended for LST because of its dielectric characteristics and weight. It offers a 2 to 1 reduction in harness weight compared to Teflon of the same voltage rating. In general, wire should be rated for 600 volts. This recommendation is contingent upon the results of outgassing tests being conducted.

c. Cabling. For general distribution cabling, the smallest gage wire allowable for external harnessing (box to box) shall be 24 gage. Shielded cable shall comply with MSFC-Spec-40M39526/5; unshielded cable will meet MSFC-Spec-40M39513/5.

Dielectric tests on cables shall be performed to meet MSFC specifications. The pin-to-pin resistance measurements will be made at 1500 volts.

Coaxial cables are recommended for digital data transmission to assure signal quality and avoidance of interference problems. Coaxial cables shall conform to MSFC-Spec-40M38286. Triaxial cables (shielded twisted pairs) were considered for this application and may later be proven to be adequate. This may offer some cost and connection advantages.

6. Electromagnetic Control. Rigid controls will be imposed on the design and implementation of the LST system to assure trouble-free operation, accuracy of controls, and high quality data. Applicable concepts and standards are given with the following paragraphs.

a. System Design Requirements

(1) Electrical Bonding. The structure will be electrically bonded to provide a low impedance electrical ground reference plane and an electrostatic discharge path between spacecraft, scientific instruments, and the boost vehicle.

(2) Electrical Grounding. A single-point electrical ground concept with design implementation will be specified in the electromagnetic control (EMC) plan.

b. System Compatibility Requirement. The spacecraft equipment and scientific instruments will be designed such that an electromagnetic compatibility margin exists at the integrated spacecraft level with respect to the self-generated interference environment in accordance with MIL-E-6051D.

c. System EMC Verification. EMC compatibility tests shall be accomplished to verify that the EMC plan has been satisfied. Tests shall be conducted on LST Integration Simulator and LST Integrated Vehicle.

d. Unit or Subsystem Requirements

(1) Electrical Bonding. A dc resistance of 2.5 mΩ or less per joint (MIL-B-5087B, Class R) and an impedance of 0.5 ohm or less at a frequency of 1.0 MHz are design goals.

(2) Electrostatic Grounding. A dc resistance of 1.0 ohm or less per joint (MIL-B-5087B, Class S) is planned.

(3) Electrical Grounding (implementation per Figure IV-35). Primary dc power employs single-point ground (SPG) located near ECAs. Secondary dc power employs dedicated transformer windings with internal vehicle ground point (VGP) for each applicable equipment load. Signal circuits employ the structure as a signal return path; the current limit is to be determined.

(4) Electrical dc Insolation. Primary dc power leads to unit case shall have a minimum dc resistance of 1.0 MΩ at 5.0 Vdc prior to electrical connection. Primary to secondary dc circuitry insolation shall be greater than 1.0 MΩ dc resistance prior to electrical connection.

(5) Interference Control Requirements. MIL-STD-461A requirements tailored specifically for the LST system will be integrated with the MSFC power quality requirements.

E. Electrical Interfaces

A significant amount of interface information was determined; however, the design status and depth of information available during this Phase A study did not permit or warrant detail interface descriptions. Full investigation and description of interfaces will be feasible only when the Shuttle systems capabilities and interfaces (under development) become firm and are detailed.

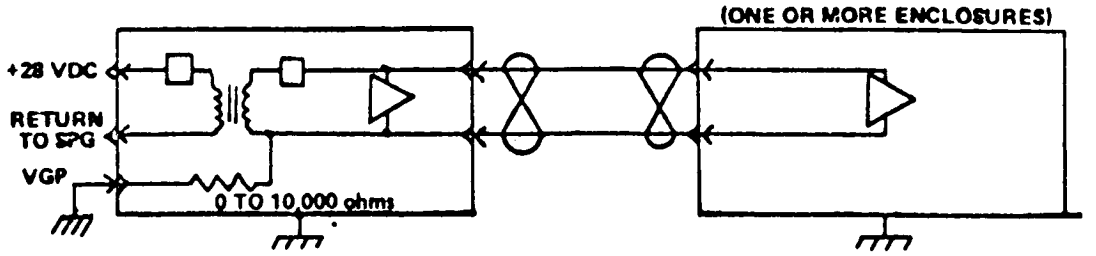

VGP FOR LOAD WITH SECONDARY POWER SUPPLY AND REMOTE LOAD

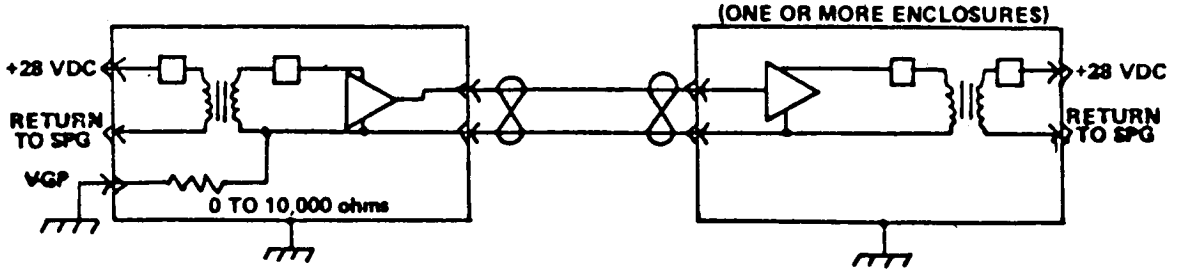

VGP FOR COUPLING LOADS WITH SECONDARY POWER SUPPLY

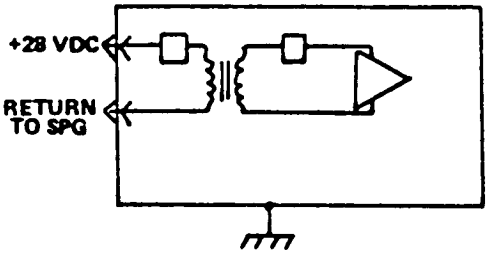

SECONDARY POWER SUPPLY AND CIRCUIT IN SINGLE ENCLOSURE

Figure IV-35. Electrical grounding schemes.

1. OTA/SIP Electrical Interface. No electrical interface exists between the OTA and SIP. The SSM will satisfy the interface requirements of both elements.

2. SSM/OTA/SIP Electrical Interfaces. The electrical functional requirements derived for power, data, commands, and attitude control are described in Chapters IV, V, and VI of this volume. The allocations and implementation are briefly described here.

Although functional requirements differ, it was intended to define standard interfaces for both the OTA and SIP and to maintain constant requirements at the separable, electrical interface plane to be defined by the SSM. This is accomplished by standardized, remote units located within these elements but furnished and controlled by the SSM. The separable interfaces are to be established at the input connectors to these remote units. The interfaces at the SIP differ only slightly from those for the OTA because additional data and command units were allocated for the SIP and several control signals are exchanged between the OTA and SSM. The simplified diagram shown in Figure IV-36 illustrates interface concept and units involved.

a. SSM/OTA Interface Allocations. Redundant remote distribution units are provided to permit a high degree of adaptability and versatility without significant influence on the inputs or separable interfaces. The interface allocations, including redundancy, are given in the following paragraphs.

(1) Remote Command Decoders. Two RCDs are allocated for redundancy. Each unit provides the capability to receive 256 digital commands.

(2) Data Aquisition Units. DAUs are allocated including redundancy. Each unit has the capacity to distribute 64 discretes or 8 digital words to the SSM data management subsystem. Data delivered to storage will be limited to a rate of 1.6 kbs. The sampling rate is 200 times per second for real-time data and 4 times per second for stored data. The OTA will condition signals, as necessary, to 5 volts before they are supplied to the DAU.

(3) Electrical Distribution Units. Two EDUs provide redundant access to power to be regulated at 28 ±2 percent Vdc. The number and characteristics of outputs are selectable and commandable by RCDs. Five separate inputs and ground returns are provided. The total rating of each unit is 1200 watts. The EDUs provide EMI protection and local fault isolation for over-voltage and overloads.

(4) Power. An average of 500 watts was allocated to the OTA for this study.

(5) Control Signals. Three line pairs are allocated for feedback signals from the OTA fine pointing subsystem to the SSM transfer assemblies. If these are amplified, high level analog signals, the same separable connectors designated for EDUs, should be used. Coaxial cable is recommended if these are high rate digital signals. Several lines are required for the SSM-supplied, magnetic torquers to be located on the OTA.

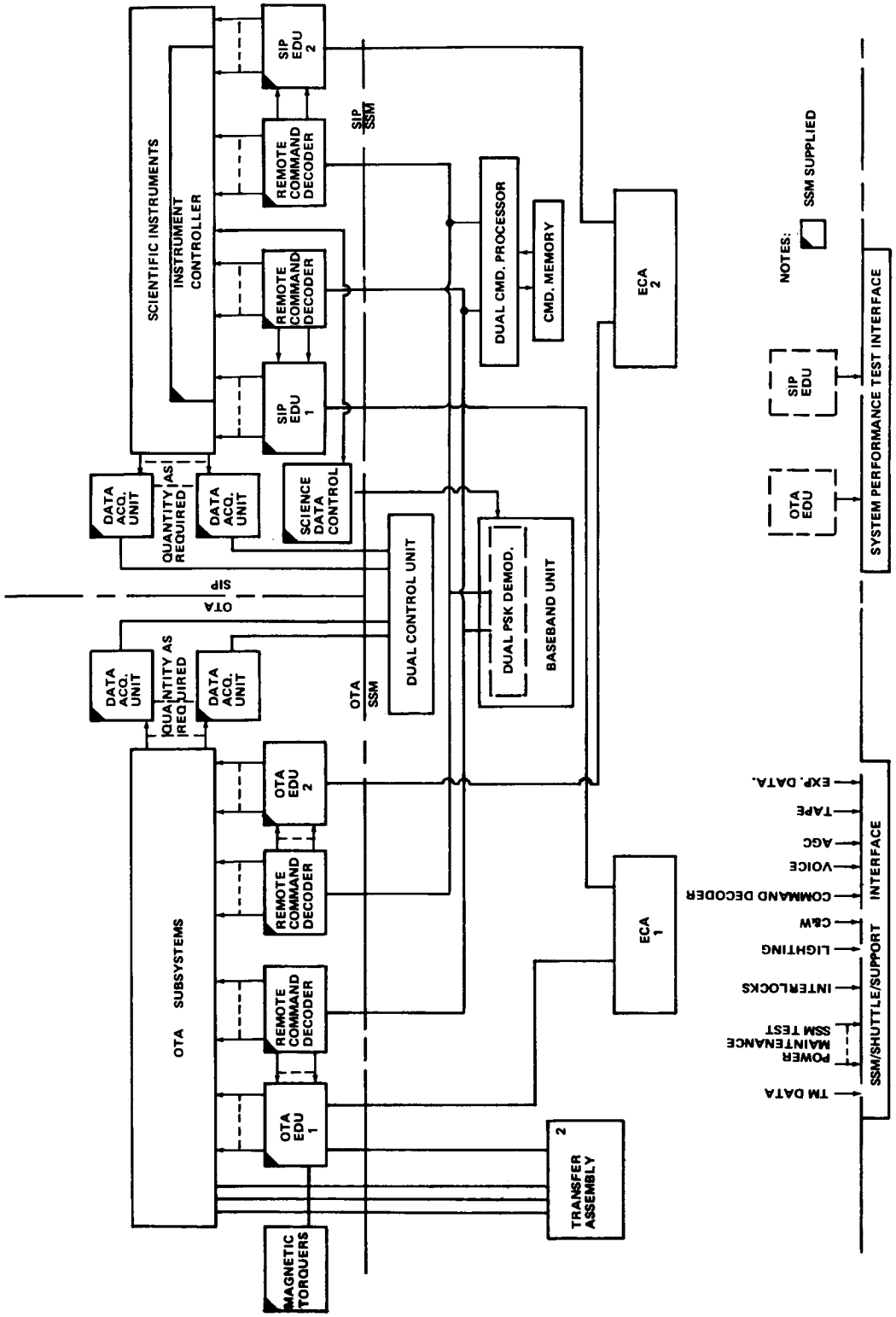

Figure IV-36. SSM electrical interfaces.

(6) Separable Connectors. Connectors allocated for the electrical separation plane between SSM and OTA will be attached to SSM cabling. These cables will be routed near the RCD, DAU, and EDUs on the OTA and will have sufficient free length for mating with these units after the OTA and SSM are assembled. Connectors allocated were:

1. Two standard circular connector for EDUs.

2. Two connectors for controls via EDUs.

3. One test and checkout connector, 39 pins to one EDU. (Connector on alternate EDU for expansion — not cabled)

4. Coaxial connectors for cabling to two RCDs, six DAUs, and two clocks.

5. Connectors for fine pointing feedback to be determined.

b. SSM/SIP Interfaces. These interfaces are implemented in the same manner as those for the OTA (refer to Figure IV-36).

(1) Four redundant RCDs as described for OTA, are provided.

(2) Twelve DAUs provide redundant data channels. These units have the same description as OTA units.

(3) Two EDUs are provided for redundant access to power. The units are equivalent to those for the OTA, except the additional input module was not provided and the unit rating was 600 watts.

(4) An average power of 500 watts was allocated to the SIP during this study.

(5) Separable Connectors. The separable connectors, for the electrical separation plane between the SSM and SIP, will be attached to SSM cabling. This cabling will be routed near the RCDs, DAUs, and EDUs where interface mating occurs. Cables will have sufficient free length to permit connection and tiedown after the SIP is installed on the SSM.

3. SSM/Shuttle Electrical Interfaces. Umbilical and external connections located on the LST are to be made compatible with launch vehicle provisions and with orbiter provisions for checkout and maintenance. Manual disconnects should satisfy the majority of the electrical interface requirements for the reference LST. The LST external connectors will be located around the docking port of the SSM for each access but will avoid interference with passageways and will not pass through doors for safety reasons. All cabling will be routed and/or protected to guard against possible damage during manned access operations. Cabling and hardware dedicated to test and checkout will not be redundant. The system design should provide access and installation features that will make replacement easy to accomplish if necessary; for instance, complex harnessing or installation strapping should be avoided.

Cabling and provisions for test and maintenance should be separated and electrically isolated, to the extent possible, from the active LST system to assure reliable, trouble-free operations.

The erection mechanism includes a docking adapter and airlock or tunnel for access to the SSM. The cabling on the Shuttle side can be routed into the pressurizable adapter using feedthrough connectors. These, then, are routed to the docking plane and are manually connected to the SSM connectors by either an unsuited or a suited man, as desired. Automatic flyaway connections do not appear to be necessary since the LST can be made self-sustaining by transferring power and control to the LST in advance of disconnection and the subsequent physical release and separation. Cabling to initiate release and separation of the spacecraft will be from connector panels in the cargo bay to the erection/docking mechanisms and need not interface with the SSM.

In general, cabling from the LST interface will be routed to in-space electrical support equipment to be located at a payload checkout station. Special routing requirements may develop for sending caution and warning information and special controls to the commander's station and to the mission specialist's station in the orbiter. At present, it appears practical and safe to accommodate such requirements by interfaces made at the IESE with these other stations.

a. SSM Interface Connector Allocation. The following connectors are consistent with preliminary orbiter interface documents and were allocated for typical functions as indicated:

1. Power and distribution control (1).

   a. 40 to 80 volts to primary buses.

   b. 28 to 30 volts to main distribution.

   c. Distribution switch controls.

   d. Voltage, current, switch status signals.

   e. Special battery conditioning and temperature.

   f. Load bank lines for array and battery checks.

   g. Transfer switch control.

   h. Lighting control.

2. Audio communication link (1).

   a. Voice link between LST and orbiter stations.

   b. Audible alarms.

3. Narrow band data coax (2).

   a. Data handling redundancy checks.

   b. Real time data.

4. Wide band data coax (2).

   a. Computer checks.

   b. Recorder playbacks.

5. Command coax (2).

   a. Inputs to LST command networks.

   b. Redundancy tests.

6. Caution and warning (1).

   See Table IV-18 for potential functions.

7. G, N, and C (1).

   a. Special test points for attitude control subsystem.

   b. Comparison with Shuttle system.

   c. Transfer assembly checks.

8. Data handling and communication test (1).

   a. Automatic gain control.

   b. Clocks.

   c. Control and baseband unit test points.

   d. Transponder checks.

9. OTA/SIP (1).

   a. Special test points for instruments.

   b. Distribution redundancy tests.

   c. Sensor calibration checks.

b. Electrical Support Equipment. The in-space electrical support equipment (IESE) which locates at the payload checkout station in the Shuttle will provide manual controls, visual indicators and instuments, CRTs and keyboard, power convertors, electronic buffers or adaptive circuitry as required, signal supplies, patch distributors, and interface connections required to operate and check out the various LST functions.

This equipment will have connections to interface with the cables routed to the SSM external connectors although the Shuttle requirement may impose special routing for caution and warning and audio cables. Ground electrical support equipment used for predelivery and prelaunch test will have interfaces made identical to those of the IESE in addition to other provisions.

TABLE IV-18. CAUTION AND WARNING PRELIMINARY INTERFACE

	No.	Phase Interface Applicable			Alert Location[a]
		Launch	Return	Maintenance	
LST Functions					
Cable/Umbilical Connected	4	X	X	X	C/W/L
LST Pressure	3			X	C/W/L
LST Temperature	2			X	W/L
CO_2 Level	2			X	W/L
O_2 Partial Pressure	2			X	W/L
External Command Interlock	2	X	X	X	C/W/L
Ordnance Networks Armed	2	X	X	X	C/W/L
Emergencies Suit Connection Ready	3			X	W/L
Battery Temperature/Pressure High	6	X	X	X	C/W/L
RCS Tank Pressure	2	X		X	C/W/L
RCS Tank Temperature	2	X		X	C/W/L
Distributor Buses Activated	3			X	L
Contamination Control	?	X	X	X	W
Shuttle Side Functions					
LST Overload/Reverse Current	3	X	X	X	C/W/L
EPS/Fuel Cells/Buses	5			X	C/W/L
Cryogenic Pressure/Temperature	6			X	C/W/L
ECLS Status	4			X	C/W/L
Stability and Control Status	1			X	C/W/L

a. C — Shuttle commander station, W — Shuttle work station, L — LST/SSM.

The IESE will serve as an interface adapter between the LST and the orbiter subsystems that will provide power, data, and communications services during launch and in-orbit checkout or maintenance operations. It will also have connections to ground utilities and services provided by carry-on cabling for installation checkout prior to the orbiter being staged or made ready.

c. Electrical Support Operations. Once the orbiter is made ready at the launch pad, it supplies services to the IESE for payload operation and checkout. The payload is then under local control of the crew from the payload checkout station or in some cases from the other orbiter stations. From this point on, RF command up-link or data down-link to the LST will be via the orbiter system. During launch and orbital checkout, the payload command system will be interlocked so that only hardwire commands via the IESE can operate LST equipment. Normal checkout and exercising of the LST subsystems will be accomplished from the payload checkout station using the coaxial cables provided for command and data retrieval. The IESE interfaces with the orbiter data and communications subsystem provide means of receiving commands and sending data to the ground over Shuttle channels. The orbiter can also provide computer and recorder services as needed.

The IESE receives power at 30 Vdc from the orbiter power subsystem during launch, orbital checkout, and maintenance operations. Manual controls, instrumentation, and converters in the IESE energize the LST buses and control distribution. Converters step up and control the voltage delivered to the primary (solar) buses. The IESE has special provisions for conditioning batteries and for load checks on batteries and arrays during maintenance. Controls and instrumentation are also provided for energizing contamination control equipment and for internal lighting.

The test connectors provide access to special test points within the SSM/OTA/SIP subsystems for calibrating sensors, troubleshooting faults, and evaluating the status and redundancy of various critical assemblies and instruments.

The voice communication link is provided for possible maintenance and replacement operations within the LST. The crew member in the LST is in constant communication with the Shuttle crew. This enhances the safety of such operations.

To assure safety to crew and equipment during the various operational periods with Shuttle support, caution and warning (C&W) signals are exchanged between the LST and orbiter. The rationale pertaining to selection of caution and warning provisions are:

1. C&W provides protection for crew and overall system.

2. One-way interface during launch and return (LST to Shuttle).

3. Two-way interface during maintenance.

   a. Alerts Shuttle crew and man in LST.

4. Exact requirement will depend on Shuttle C&W, number in crew, maintenance procedures, and work stations.

5. C&W system normally has:

   a. Redundant sensors, supplies, signal transmission.

   b. Voting logic in critical cases.

   c. Manual test and verification features.

6. LST provisions for C&W:

   a. Interface connectors-cables-sensors-alert lights/alarm box.

   b. Are isolated from LST functional system.

   c. Are energized from Shuttle side only when attached.

7. Spare C&W components will be carried on all LST visits.

Potential caution and warning functions were listed in Table IV-18 with an indication for the mission phase during which these functions will probably be monitored.

Revised interface documents indicate that the Shuttle can supply 1500 watts average and 3000 watts peak for payloads during ascent and descent. In orbital coast, 3000 watts average and 6000 watts peak can be sustained.

Such provisions are considered adequate to support the LST during launch and orbital checkout. It was estimated that 2700 watts would be the maximum requirement for the payload for worst-case maintenance conditions where the array was not operating and battery charging was needed. During such revisit operations, the power may be constrained if the 874 watts needed for contamination control is required for extended periods.

It appears that the 50 kW-h limit on energy is not sufficient to support an extended orbital checkout or a maintenance operation for the LST. It will require over 100 kW-h. The interface document, however, does permit the supply of additional reactants for the fuel cell power system from the payload or from tanks to be installed in the cargo bay. Selecting the add-on tank approach, the cost of tanks and plumbing hardware is defrayed by the Shuttle system. The only penalties to the payload are the installation charge and the weight. For nominal fuel cell performance the mass penalty should be about 0.45 kg/kW-h for reactants. The additional installation, therefore, would be in the order of 30 to 45 kg.

F. Trade Studies

1. EPS Configuration Tradeoff Analyses. Four EPS configurations were analyzed in the selection of the reference design. Each of the candidates has been used previously and is based on existing design and hardware technology. The four configurations were evaluated against LST basic requirements and probable ranges of operating conditions to determine whether or not significant performance, functional, or programmatic advantages were offered.

The first-order effects of EPS configurations on solar array power and energy storage requirements were determined as a function of the dark-to-daylight load ratio variation possible to evaluate whether or not the performance of the candidates depended on the load regime. In one case, the ratio of unregulated-to-regulated load was considered.

Subsequent consideration was given to reliability for expected ranges of environment, operational loading, and maintenance provisions. Inherent protection features, voltage, and current stress levels incurred on components, potential sensitivity to power management controls and adaptability to redundancy, modularization, and requirement changes were some of the qualities considered. EPS design and hardware costs can be related to solar array power and energy storage capacity; however, application and programmatic requirements, the design status of the rest of the system, and integration

can be significant cost drivers. In all cases, to be cost-effective, a high confidence in the system reliability must be established because the mission and vehicle survival is critically dependent on the EPS.

Cost avoidance is considered a prime requirement on configuration selection. Thus, the final selection should not occur until the system design has matured to the point where basic requirement ranges are well established, unless the design is highly modularized and versatile for adaptation to large changes in requirements. Equipment should be designed for low stress levels and should be conservatively rated for the range of design conditions expected. Components and modules should be selected to avoid costly, extensive development testing and qualification. The system should be resistant to abuse and abnormal load conditions, such as transients or EMI, and it should provide good protection and corrective features. To avoid extensive waiting time for requirements and to avoid difficult integration or costly changes after system assembly, the configuration should provide design isolation and features that desensitize EPS equipment to external system conditions and changes.

Analyses were based on a fixed 1500 watt orbital average load and on a 96.9 min orbit with maximum occultation of 35.5 min. The sensitivity of the candidate systems to load and time of occurrence is shown by the performance dependence on the dark-to-daylight load ratio variations considered.

Two of the configurations, designated as Type 1 and Type 2 in Figure IV-37, have the capability of tracking the peak power point on the solar array V-I curve. The Type 1 system is representative of the reference selected. The Orbital Workshop (OWS) part of the Skylab uses the Type 2 concept. The efficiencies and design parameters used in the analyses are identified in Table IV-19.

The Type 1 system contains a stepdown charger and a stepup-stepdown regulator. The regulator is designed for an input voltage to vary from the minimum battery voltage to the maximum solar array voltage. In the Type 2 system there is a stepdown preregulator and a stepdown load regulator.

The performance equations that determine the energy storage and solar array requirements for the Type 1 (reference design) configuration are given in Section C.2. Figures IV-5 through IV-8 show the energy required and the performance factor (ratio of solar array power to load power) as a function of dark-to-daylight load ratio.

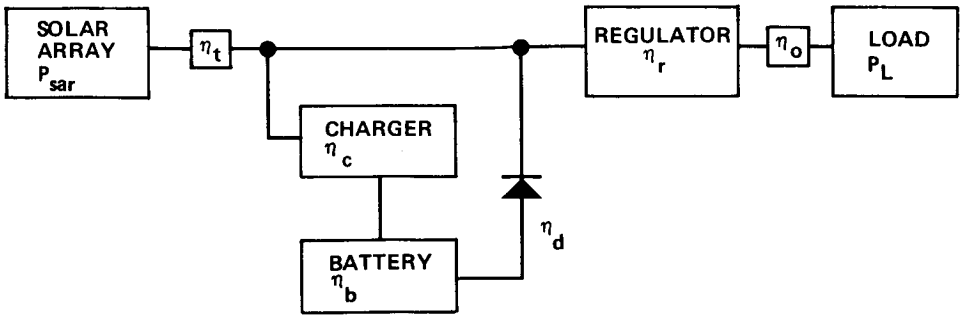

CONFIGURATION TYPE I

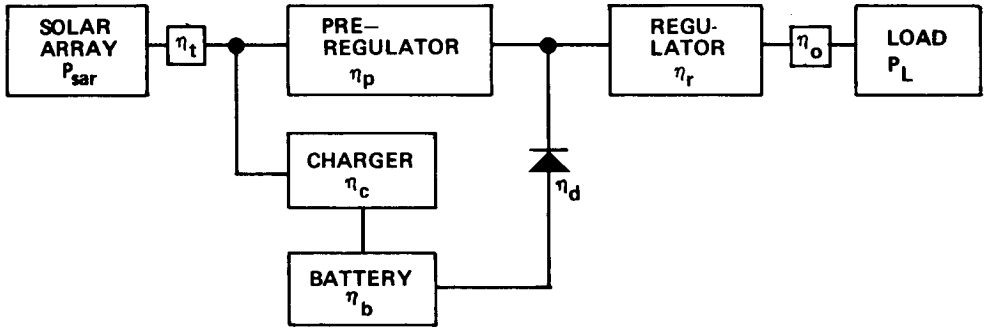

CONFIGURATION TYPE 2

Figure IV-37. Electrical power subsystem configurations Type 1 and Type 2.

Using the values denoted in Table IV-19, equations for Type 1 [equations (1), (2), (3), (5), and (8) (Section 3.2)] are applicable to the Type 2 configuration. Because of the series preregulator the equations for required solar array power is slightly different from equations (6) or (7) for the reference Type 1. The required solar array power for the Type 2 system may be determined from the following equation:

$$P_{sar} = \frac{P_{LS}}{\eta_o \eta_r \eta_p \eta_t} + \frac{E_D}{\eta_b \eta_c \eta_t t_s} \quad . \qquad (26)$$

TABLE IV-19. PARAMETERS AND VALUES FOR TYPE 1 AND TYPE 2 SYSTEMS

PARAMETER	SYMBOL	VALUES USED	
		TYPE 1	TYPE 2
SOLAR ARRAY TRANSMISSION EFFICIENCY	η_t	0.98	0.98
CHARGER EFFICIENCY	η_c	0.95	0.95
BATTERY EFFICIENCY (ENERGY OUT / ENERGY IN)	η_b	0.80	0.80
BATTERY TO REGULATOR EFFICIENCY	η_d	0.98	0.98
REGULATOR EFFICIENCY	η_r	0.91	0.95
DISTRIBUTIONS EFFICIENCY	η_r	—	0.95
PRE–REGULATOR EFFICIENCY	η_p	—	0.98
ORBITAL AVERAGE LOAD POWER – WATTS	P_L	1500	1500
DARK LOAD POWER – WATTS	P_{Ld}	–	–
LIGHT LOAD POWER – WATTS	P_{Ls}	–	–
DARK TIME – MINUTES	t_d	35.5	35.5
LIGHT TIME – MINUTES	t_s	61.4	61.4
DARK TO DAYLIGHT LOAD RATIO	J	–	–
SOLAR ARRAY POWER – WATTS	P_{sar}	–	–
BATTERY ENERGY STORAGE REQUIRED FOR t_d	E_D	–	–

Type 2 system performance is also given as a function of dark-to-daylight load ratio. Figures IV-38 and IV-39 illustrate the energy requirement and performance factor variation for the Type 2 system, respectively, as a function of the load ratio.

The energy requirements for Type 1 were slightly higher than for Type 2 but the performance factor was somewhat better. The preregulator efficiency penalizes the Type 2 configuration. Other variations considered where the preregulator handles both the charger and output loads gave much poorer performance. The Type 2 approach has additional disadvantages not obvious from the block diagram shown. To gain efficiency in power conditioning, nonisolated, stepdown converters are used in the regulator, preregulator, and charger. This incurs higher array voltages, higher stress on input components, and lower isolation protection. For an output equivalent to Type 1, the battery reliability and charge control is penalized by the requirement for a greater number of series cells per battery.

Two shunt-regulator schemes, designated as Type 3 and Type 4 systems, were also analyzed. These are shown in Figure IV-40. The design parameters assigned to the Types 3 and 4 systems are given in Table IV-20.

For the shunt-regulated systems, the performance is very dependent on the degree of regulation, the energy storage subsystem configuration, and the environmental and operational ranges expected. For the same design conditions used for Types 1 and 2, equivalent energy storage and input power requirements were determined for the Types 3 and 4 appraoches. Solar power requirements in these cases are those from the combined array and shunt. Additional considerations were given to shunt power dissipation and to parameters that affect the array size. Since the shunt concept is sensitive to regulation specifications, the effect of varying the unregulated-to-regulated load ratio was evaluated for the Type 3 configuration. Type 3 was used for this analysis because it seems that it would benefit most from broader regulation tolerances.

To the extent possible, the same relationships and symbols used previously were maintained, but equations differ because of the connection differences. As may be noted from Table IV-20, additional parameters are needed to distinguish between regulated and unregulated loads and the factor Z, representing the ratio of unregulated load to regulated load, is introduced as a variable for evaluating how regulation requirements affect the system. To avoid over complicating the analysis, Z is assumed to be the same for daylight and dark periods as given in equation (27):

$$Z = \frac{P_{UD}}{P_{RD}} = \frac{P_{US}}{P_{RS}} \quad . \qquad (27)$$

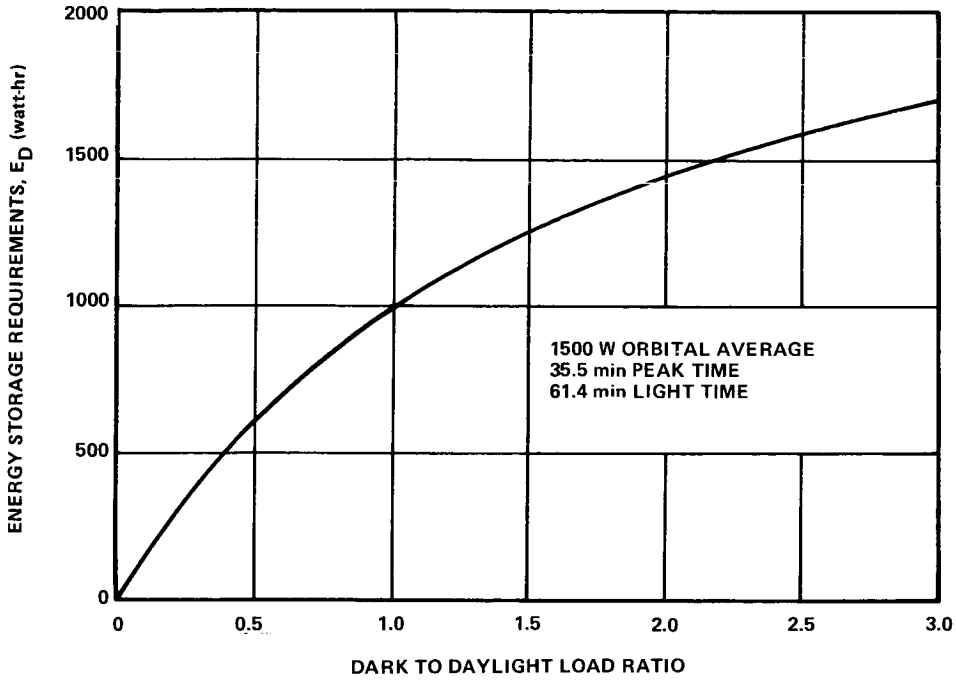

Figure IV-38. Energy storage versus dark-to-daylight load ratio for Type 2 system.

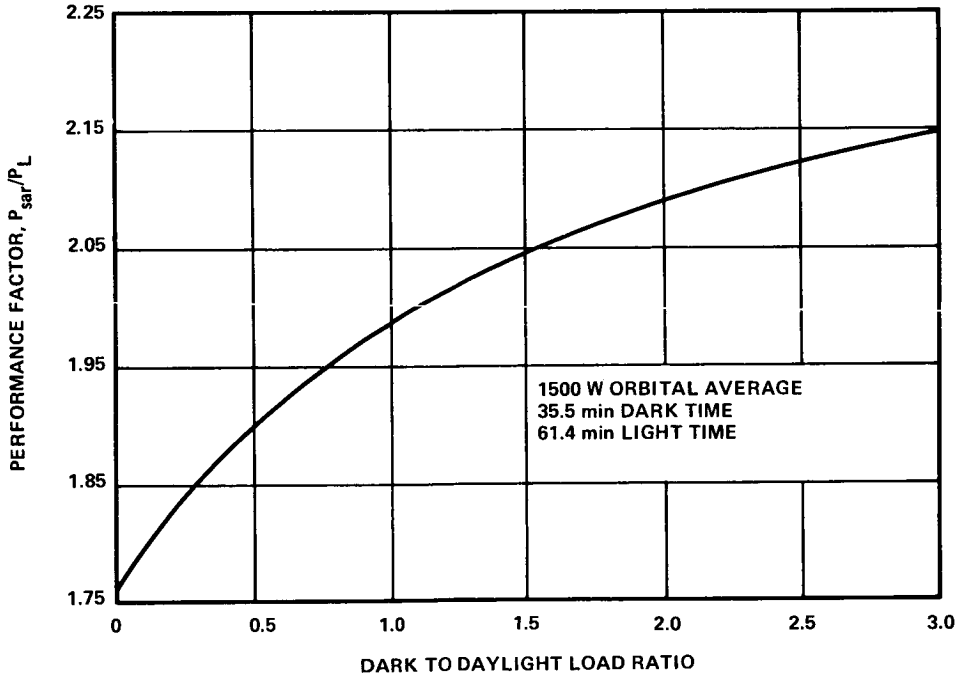

Figure IV-39. Performance factor versus dark-to-daylight load ratio for Type 2 system.

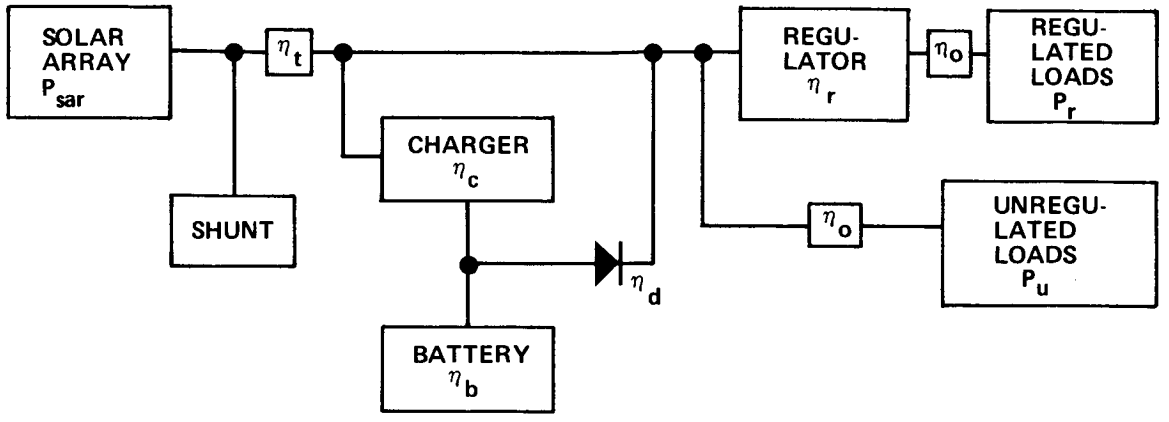

EPS TYPE 3

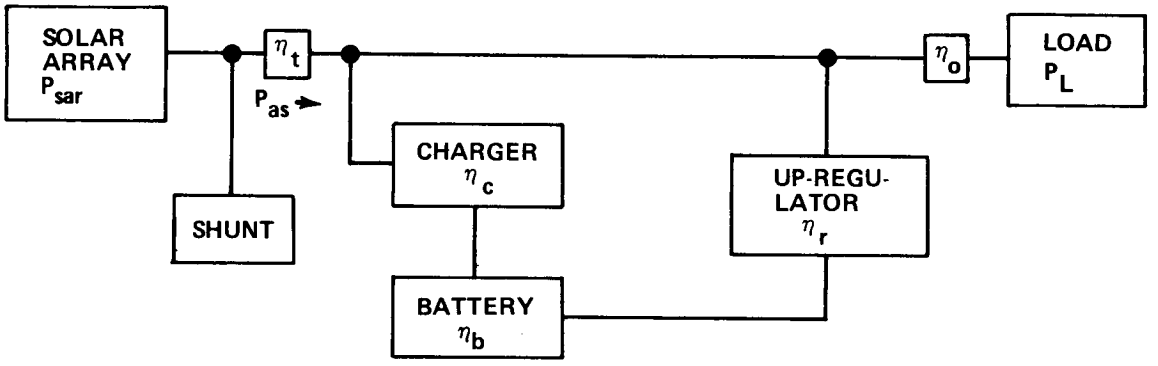

EPS TYPE 4

Figure IV-40. Type 3 and Type 4 configurations for electrical power subsystem.

The dark-to-light load ratio has the same significance as before but appears different for Type 3, as shown in equation (28):

$$J = \frac{P_{RD} + P_{UD}}{P_{RS} + P_{US}} \quad . \tag{28}$$

TABLE IV-20. PARAMETERS AND VALUES FOR TYPE 3 AND TYPE 4 SYSTEMS

PARAMETER	SYMBOL	TYPE 3	TYPE 4
SOLAR ARRAY EFFICIENCY	η_t	0.98	0.98
CHARGER EFFICIENCY	η_c	0.95	0.95
BATTERY EFFICIENCY	η_b	0.80	0.80
BATTERY TO REGULATOR EFFICIENCY	η_d	0.97	–
REGULATOR EFFICIENCY	η_r	0.92	0.93
DISTRIBUTION EFFICIENCY	η_o	0.98	0.98
DARK TIME – MINUTES	t_d	35.5	35.5
LIGHT TIME – MINUTES	t_s	61.4	61.4
DARK TO DAYLIGHT LOAD RATIO	J	–	–
UNREGULATED TO REGULATED LOAD RATIO	z	–	–
POWER REQUIRED FROM SOLAR ARRAY AFTER SHUNT	P_{as}	–	–
ORBITAL AVERAGE LOAD – WATTS	P_L	1500	1500
REGULATED DARK LOAD – WATTS	P_{rd}	–	–
UNREGULATED DARK LOAD – WATTS	P_{ud}	–	–
REGULATED LIGHT LOAD – WATTS	P_{rs}	–	–
UNREGULATED LIGHT LOAD – WATTS	P_{us}	–	–
BATTERY ENERGY STORAGE REQUIRED FOR t_d	E_a	–	–
DARK LOAD POWER	P_{Ld}	–	–
LIGHT LOAD POWER	P_{Ls}	–	–
ARRAY POWER TEMPERATURE COEFFICIENT	k_p	0.005	0.005
REFERENCE TEMPERATURE	t_i	28°C	28°C
POWER AT REFERENCE TEMPERATURE	P_i	–	–
AVERAGE ARRAY DAYTIME TEMPERATURE	T_a	–	–
MAXIMUM TEMPERATURE	T_m	–	–
CONSTANT OF PROPORTIONALITY	K	–	–
SIZE OF ARRAY	A	–	–
SIZE OF ARRAY FOR PEAK POWER TRACKING SYSTEM	A_p	–	–
SIZE OF ARRAY FOR A SHUNT REGULATED SYSTEM	A_s	–	–

The energy required during occultation is determined by either of the following equations:

$$E_D = \frac{t_d P_{UD}}{\eta_o \eta_d} \left(\frac{1}{Z \eta_R} + 1 \right) = \frac{t_d P_{RD}}{\eta_o \eta_d} \left(\frac{1}{\eta_R} + Z \right) \quad . \qquad (29)$$

$$E_D = \frac{J P_L t_d}{\eta_o \eta_d} \left[\frac{t_s + t_d}{(1 + Z) t_s + J (1 + Z) t_d} \right] \left[\frac{1}{\eta_R} + Z \right] \quad . \qquad (30)$$

The power required from the solar array-shunt combination is obtainable from several equations, one of which is

$$P_{AS} = \frac{P_L \left(1 + \eta_R Z \right)}{\eta_o \eta_R \eta_t} \left[\frac{t_s + t_d}{(1 + Z) t_s + J (1 + Z) t_d} \right]$$

$$+ \frac{E_D}{\eta_t \eta_b \eta_c \eta_s} \quad . \qquad (31)$$

The relative array sizes for a shunt-regulated and peak tracing system need to be determined in order to evaluate performance factors.

The maximum solar array power output change with temperature can be closely approximated by a linear function as follows:

$$P_{AS} = P_i \left[1 - k_p \left(T - T_i \right) \right] \quad . \qquad (32)$$

Systems with peak power tracking can use maximum solar array power at all times. From equation (32) it can be shown that the maximum average power available in the daytime is simply the solar array power at the average daytime temperature. The array is sized for end-of-life conditions and the combination of daylight time and corresponding average temperature that gives the largest array. On the LST, as with most systems, this is the maximum dark-time condition. The peak power tracking systems can deliver

power in excess of their worst case, end-of-life rating. Excess power would be available early in the mission when the array is not degraded and whenever the average daytime temperature is lower than the design value.

For most shunt-regulated systems, the array is designed to supply the required power at maximum temperature during the worst-case orbit. This requires the array voltage at maximum power and maximum temperature to be at least the minimum required by the load. The shunt operates so that the shunt current plus the current drawn by the charger and the loads will keep the array at an essentially constant voltage. Under light load conditions, the shunt must dissipate a power equal to the array output voltage times the array current less that drawn by any loads. Since the LST is to be highly controllable from the ground, the large load swings expected will result in high shunt dissipations which detract from the system reliability.

Using the power temperature relationship from equation (32) for a fixed power input, the ratio of the array size for a shunt system to the array size for a peak power tracking system can be determined.

The size of an array is proportional to the power output at temperature T. Let K be the constant of proportionality so that

$$A = K P_i \quad . \tag{33}$$

For the peak power tracking systems solving equation (32) for P_i with $T = T_a$, and substituting in equation (33), the size (A_p) of the peak power tracking system array is

$$A_p = K \frac{P_i}{\left[1 - k_p \left(T_a - T_i\right)\right]} \quad . \tag{34}$$

The size, A_s, of the shunt-regulated power system array is obtained by setting $T = T_m$. Therefore,

$$A_s = K \frac{P_i}{\left[1 - k_p \left(T_m - T_i\right)\right]} \quad . \tag{35}$$

For the same P and K, the ratio of the array sizes are

$$\frac{A_s}{A_p} = \frac{1 - k_p\left(T_a - T_i\right)}{1 - k_p\left(T_m - T_i\right)} \quad . \tag{36}$$

This size ratio only assures that both arrays can supply the same load power at the end-of-life, worst-case condition. The peak power tracking systems can supply substantially more power early in life or when the temperature is low. The shunt-regulated system cannot do this because of the fixed array voltage. It can supply a limited amount of additional power in early life due to the higher current available at the fixed array voltage.

The equations for the Type 4 configurations are similar to the foregoing equations except that the factor Z was not used. Curves illustrating the performance of the Types 3 and 4 systems are plotted on the same scale as used for Types 1 and 2, for comparison purposes. The energy storage requirement determined by equation (30) is shown for Type 3 as a function of the dark-to-daylight load ratio in Figure IV-41 for the two extreme values of Z. As indicated, the unregulated-to-regulated load ratio has a minor effect on energy storage. Comparing this figure with Figure IV-6 shows that energy requirements for Types 3 and 1 are equivalent for $Z = 0$. The Type 3 improvement with $Z = \infty$ is almost negligible.

The input power factor (ratio P_{as}/P_L) for the Type 3 configuration is plotted in Figure IV-42 for three values of Z. Here the advantages of high unregulated loads are noticeable but still small. The 1 percent difference between Type 3 at $Z = 0$ and Type 1 could easily be taken by the shunt, and regulation is sacrificed. Even with $Z = \infty$, the difference is less than 3 percent. This difference needs to be near 10 percent for Type 3 to be a good competitor, since voltage is clamped, and utilizing the array's peak power when cold is not possible. The array design is much more sensitive to the accuracy of thermal predictions.

Similar energy requirements and input power factor curves are given for the Type 4 system in Figures IV-43 and IV-44. Although energy reduction compared to Figure IV-6 is small, the solar power reduction of approximately 8 percent comparing Figures IV-44 and IV-8, is significant. Therefore, Type 4 should be a candidate for further study and evaluation.

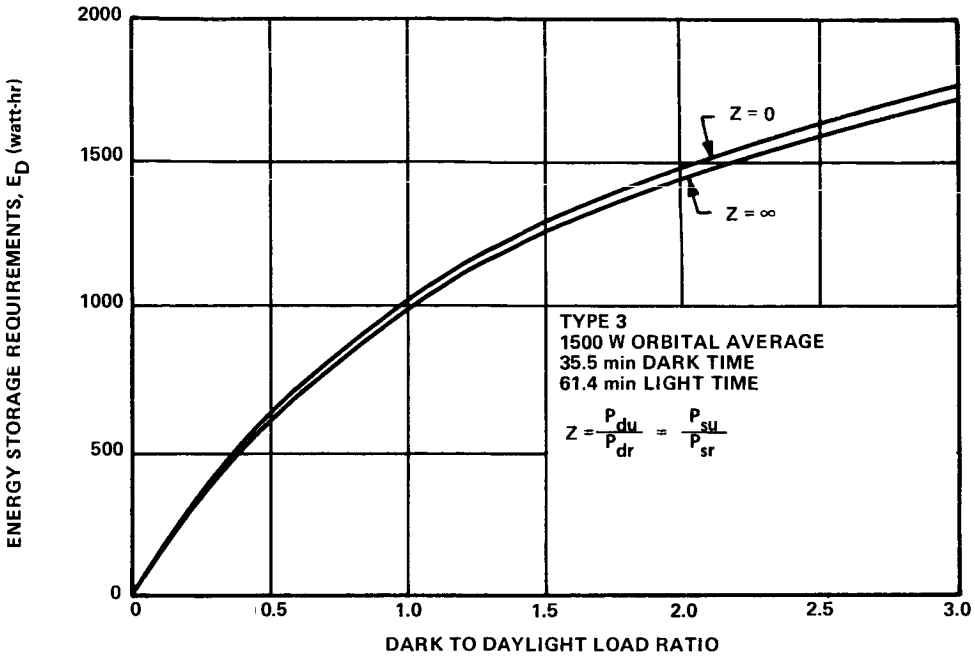

Figure IV-41. Energy storage versus dark-to-daylight load ratio for Type 3 system.

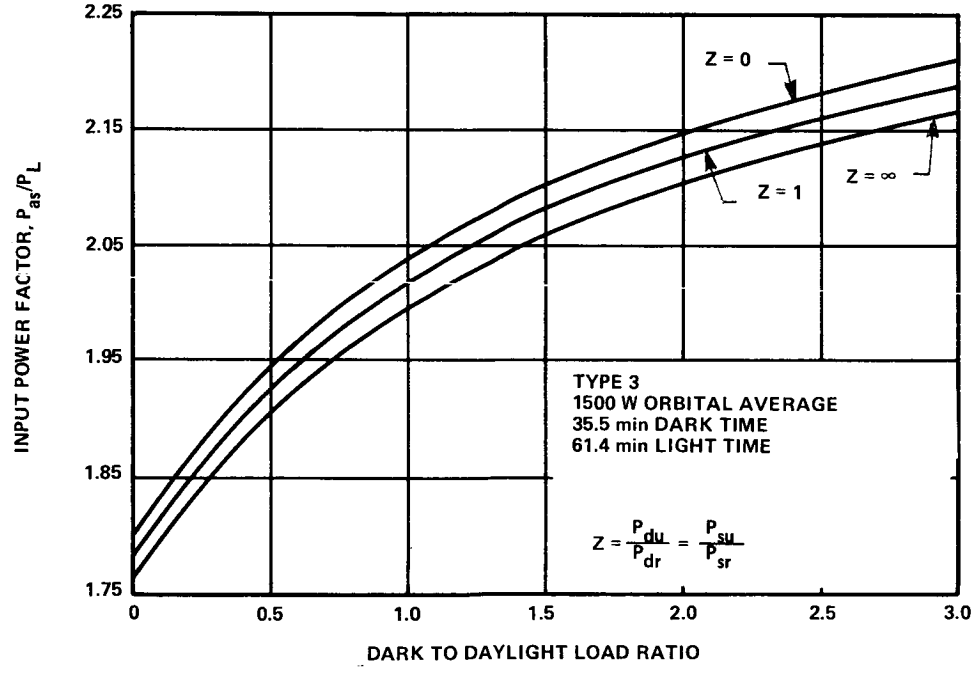

Figure IV-42. Input power factor versus dark-to-daylight load ratio for a Type 3 system.

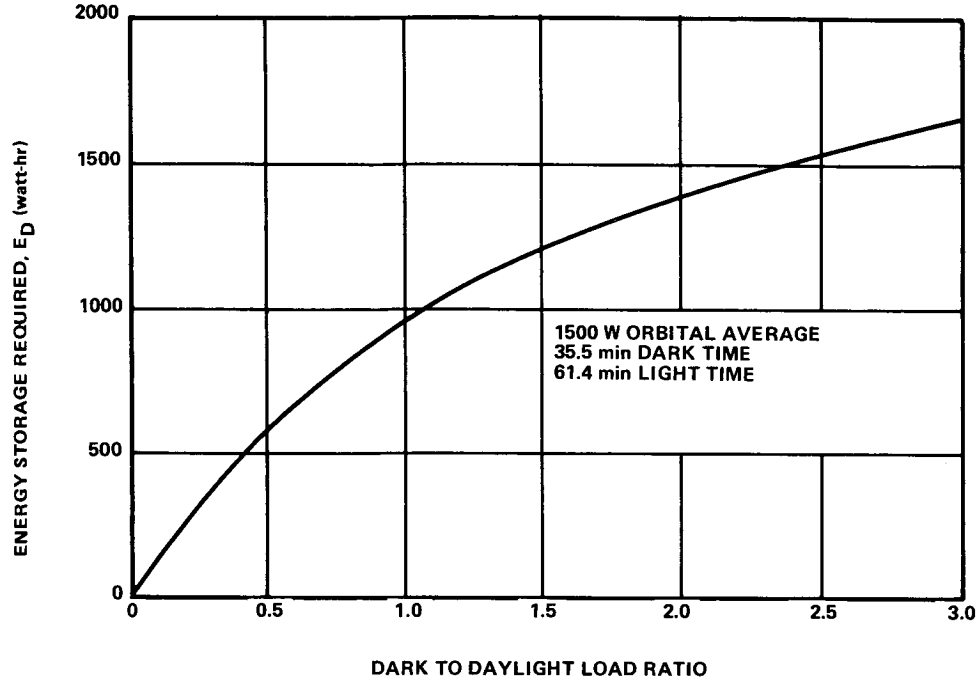

Figure IV-43. Energy storage required versus dark-to-daylight load ratio for Type 4 system.

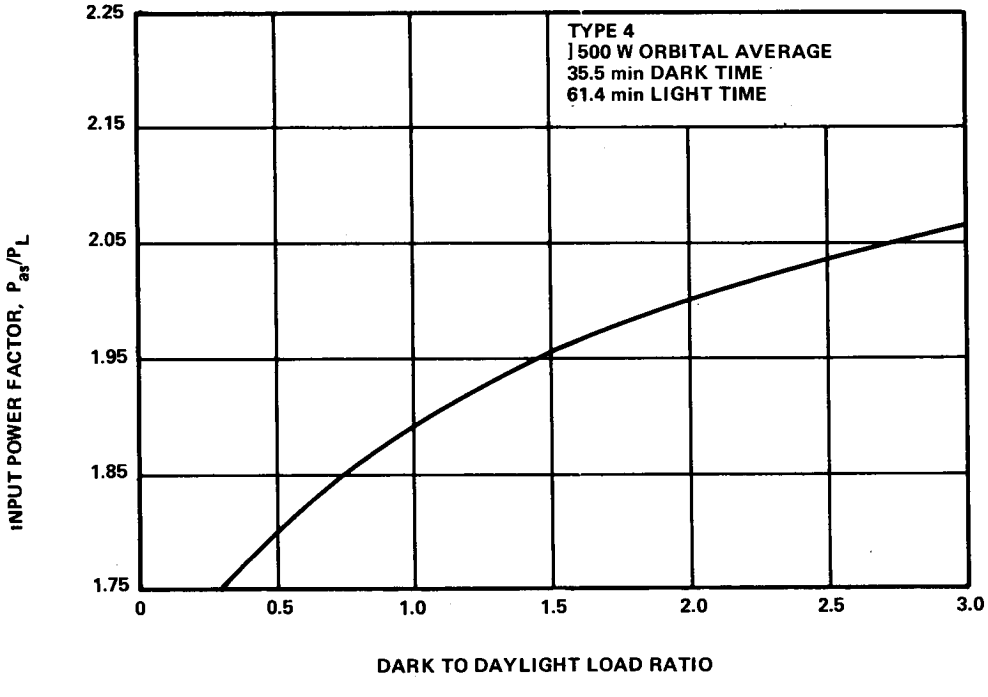

Figure IV-44. Input power factor versus dark-to-daylight load ratio for Type 4 system.

Although it has some of the disadvantages noted for Type 3, Type 4 is capable of maintaining close regulation. The shunt and the up-regulator from the battery together can be made to control the bus voltage throughout the orbit. Also the battery design and number of series cells are less constrained than by Type 3.

From equation (36), since the average temperature is always less than the maximum temperature ($T_a < T_m$), the size of a shunt-regulated array (A_s) is always larger than the size of peak power tracking system array (A_p) for the same power requirement. This must be taken into account in comparing performance factors. The unregulated array power is given by

$$P_{sar} = P_{as} \frac{A_s}{A_p} \quad . \tag{37}$$

Thus the performance factor, unregulated array power divided by available load power, is

$$M = \frac{P_{as}}{P_L} = \frac{P_{sar}}{P_L} \cdot \frac{A_s}{A_p} \quad . \tag{38}$$

This equation allows comparison of these two types of systems on an equal basis. Multiplying the input power factors given in Figures IV-42 and IV-44 by the ratio A_s/A_p results in a performance factor equivalent to those plotted in Figures IV-8 and IV-39.

On the basis of the above cursory analyses the Type 1 system appears to be the best candidate for LST when protection, design isolation, array utilization and other factors are considered. However, the Type 4 system performance indicated makes it worthy of further investigation.

2. Alternate Solar Arrays. The reference solar array configuration was selected early and had the benefit of more indepth analysis (e.g., structural, thermal, and dynamic) than the alternates studied. There were several reasons for considering alternate arrays: (1) The configuration and alternate launch vehicle constraints caused the reference design to be complex and massive, (2) retraction was required, and (3) the reference array is not a good candidate for in-space maintenance and replacement.

Several solar array designs developed under previous R&D contracts were evaluated for adaptation to the LST. There were several rollout, flexible panel types to consider. These had the same basic concept but differed in mechanization and detail. Semirigid, folding arrays were considered.

Designs for other programs using large arrays, e.g., Skylab, HEAO, ATM, OAO, SCS (Air Force), were also considered. These, however, were more conventional and similar to the reference design.

Of their own volition, several companies supplied design concepts derived from their recent studies related to LST. Some estimates based on previous programs were also offered.

A general appraisal of the various types of solar arrays is given in Table IV-21. The advantages and disadvantages compared reflect the rationale used to select the reference array design for the study.

In general, the same cell and coverslide characteristics were used for evaluation of alternates because these were considered good selections for the mission. Alternates not using these were adjusted for equivalent performance. Some consideration was given to thermal differences but these were not thoroughly analyzed. Time did not permit reconfiguration studies of the SSM to adapt alternates to dimensional and structural constraints.

a. Alternate No. 1 Solar Array. Aside from the conventional rigid arrays, the first alternate considered was the flexible, rollup solar array (FRUSA) developed for the Air Force. This is the only one of the flexible types that has been flight tested. Several variations of this design were suggested by others. The design goals for the FRUSA development were to deliver 1500 watts of raw power with a mass-to-power ratio of 15.88 kg/kW.

The flight tested FRUSA used 0.015 cm coverslides and $2 \times 2 \times 0.020$ cm N/P solar cells left over from another project. The cells were mounted on a substrate composed of 0.0025 cm Kapton film and 0.0025 cm fiberglass. The panel dimensions were 487.7×167.6 cm, giving 16.35 m^2 area for the two panels.

In general, the test results were good. Many deployment-retraction operations were performed. Mechanical and dynamic characteristics measured indicated good correlation with design predictions. The orientation system malfunction and minor instrument deficiencies noted did not affect usefulness of array tests for this flight. Although the electrical performance

TABLE IV-21. GENERAL APPRAISAL OF SOLAR ARRAY TYPES

Array Type	Advantages	Disadvantages
A. Rigid Foldout Panels	• Proven Technology • Proven Fabrication Methods • Presently, Lowest Cost • Conservative for Phase A Evaluation of LST • High Natural Frequency (0.6 to 1.0 Hz)	• High Weight • Constrained to Wraparound Stowage • Complex Retraction Restricts External Maintenance Concepts • Very Difficult to Replace In-Space at any Level
B. Type A with Phase Change Material (PCM)	• Reduces Thermal Cycle Stresses • Improves Reliability of Interconnects/Terminals • Can Increase Output up to 6%	• Heaviest Array • Unproven Fabrication Techniques • Compatibility with Adhesives not Verified • Maintenance Diminishes Attractiveness
C. Flexible Rollout Types	• Lowest Weight • Compact Stowage (Smallest Volume) • One Successful Flight • Easier Retraction • Better Adapted to In-Space Maintenance Concept	• Presently 15/20% Higher Cost (Could Change Before Phase C) • Most Complex Design • Low Natural Frequency (0.04 to 0.1 Hz) • Must be Retracted for Docking • Compatibility with Shroud Envelope not Verified
D. Semirigid Types (Rigid Module Frames with Flexible Substrate)	• Lower Weight than Type A but not Type C • Efficiency Increase Possible	• Has Most of the Disadvantages of Type A • Complex Fabrication

of the array was considered adequate, its power appeared low and the degradation rate of 18 percent for the first year was quite high for the given orbit. Such rates were near predictions in the report and the manufacturer attributes this mostly to the narrow coverslides used.

The FRUSA configuration is shown in Figure IV-45. The two flexible panels, on which cells are mounted, rollup on a single drum. A soft, cushion panel rolls between the cells and panels to protect the cells (and coverslides) from breakage or snagging. When the panels are deployed, the cushion panel rolls up on the cushion takeup roller that is gear synchronized with the drum. The extendible booms are of the "Bistem" type. When retracted, they are stored in two small cylindrical housings.

The spreader bars and boom compensators keep tension on the panels to maintain alignment during roll in/out and to keep the natural frequency from being excessively low.

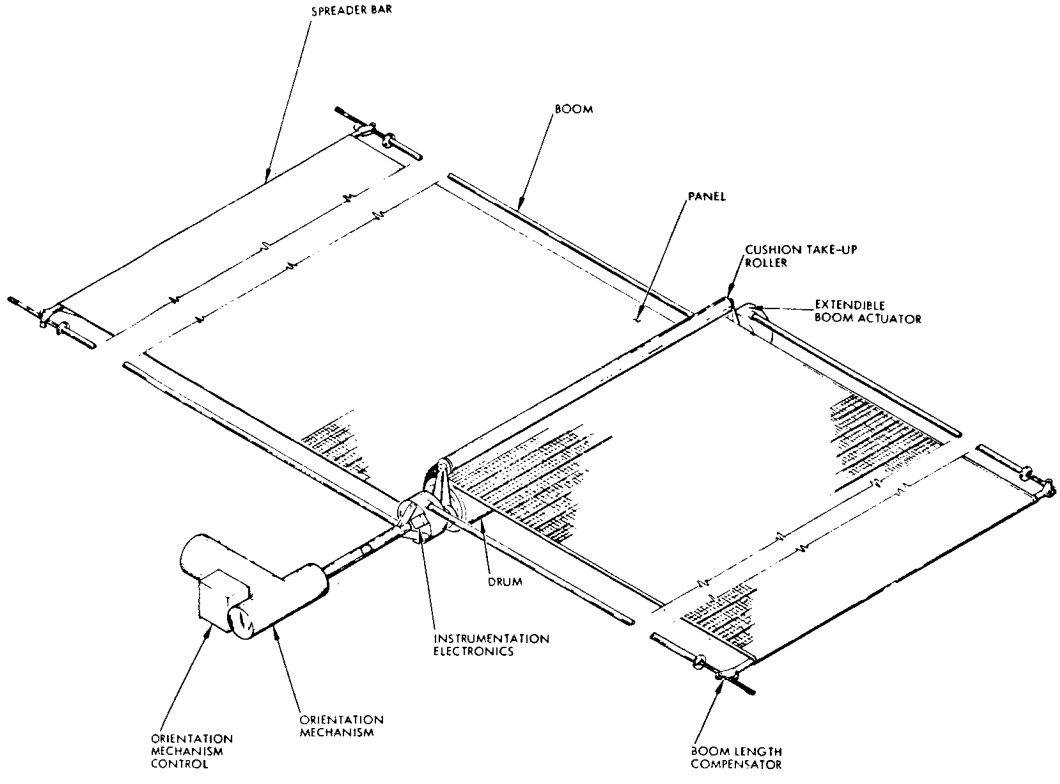

Figure IV-45. Solar array alternate no. 1.

The drum/actuator/panel assembly is mounted on a rigid, cylindrical boom as shown. The orientation mechanism and controls rotate the rigid boom for array orientation. The orientation mechanism was designed to drive two array assemblies, although only one assembly was used in the FRUSA flight test. This mechanism was specifically adapted to the flight test vehicle constraints for mounting on the forward end of the spacecraft.

Automated processes were developed to interconnect and assemble the solar cell coverslide modules. The cell assemblies are attached to the panels with adhesives. Flat conductors collect and deliver power to slip ring assemblies which transfer power across the rotary joints for transmission into the spacecraft.

Using the existing design dimensions and mounting provisions, this array would not fit within the shroud envelope on the reference SSM. Figure IV-46 shows the rollup drum assembly, mechanisms, and an end view of the stowed array. The 34.3 cm height of this assembly violated the shroud envelope. Changes were made to mountings, etc., to reduce the height, but these were not enough without modification to the basic array mechanisms. Information from the manufacturer indicated that variations were possible, but concepts adapted to the LST were not furnished. The fit was close enough, however, to consider it a feasible candidate worthy of further study. Study of shroud details, SSM modification, or modification to the array could make stowage practical for the LST.

Additional investigations considered modifications needed to make the electrical performance equivalent to the reference array design. Two assemblies with approximately 25 percent more area would be needed for LST. Since changes in width were considered most significant and expensive, the length of the booms and panels were extended to 588.6 cm. The manufacturer indicated that a maximum of 700 cm could be accommodated. Use of thicker cells and covers, considered necessary for the 5 year mission and economy, imposed thicker panels and an increase in drum diameter; neither is desirable. Analysis indicated that the panels should be about 0.025 cm thick and that larger boom diameters would be needed for the increased mass and length. The manufacturer did not agree that larger booms were meeded but indicated that larger booms and drive mechanisms were being designed.

Panel coatings or fiberglass panels were considered possible means of improving thermal characteristics for better cell efficiency and lower thermal cycle stresses.

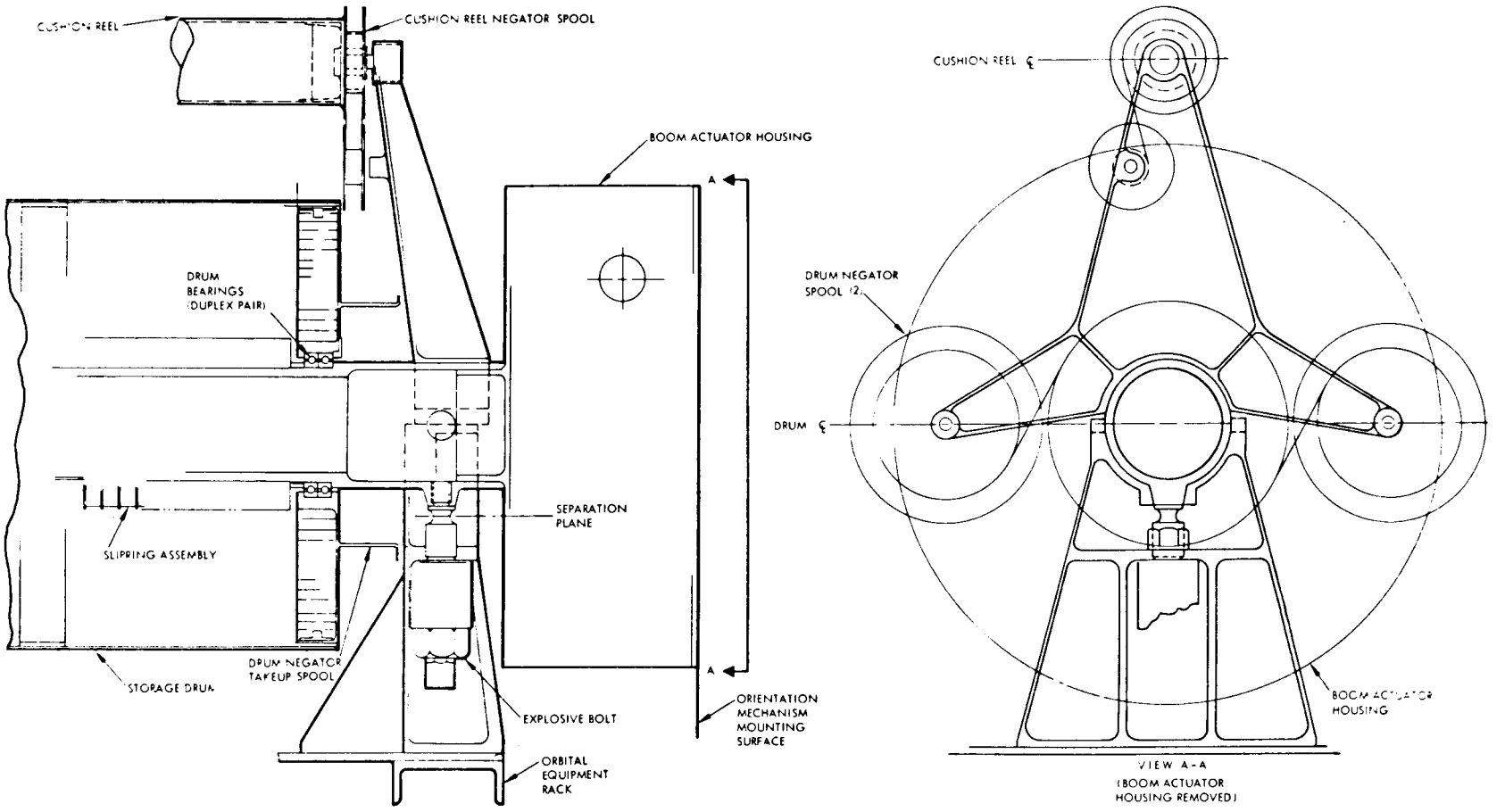

Figure IV-46. Mounting for alternate no. 1 array.

The characteristics of the "modified" FRUSA designated as Alternate No. 1 Solar Array, derived on a preliminary design basis, are shown in Table IV-22.

TABLE IV-22. ALTERNATE NO. 1 SOLAR ARRAY CHARACTERISTICS

Stored Dimensions:	
Height	34.3 cm
Length	45.7 cm
Width	194.9 cm
Unrolled Length	1223.0 cm
Panel Size	165.0 × 588.6 cm ($9.77\ m^2$)
Total Array Area	$39.02\ m^2$
Total Mass of Array and Orientation Mechanism	158.8 kg

b. Alternate No. 2 Solar Array. Figure IV-47 shows one wing on the second alternate, also a flexible, rollup type array mounted on the SSM. This alternate uses a central "Bi-stem" boom for extending and retracting two panels. The boom diameter is 3.5 cm, larger and thicker than the FRUSA, and is commensurate with the length and panel mass. This design simplifies the boom and actuator complexity since only one boom instead of four are used. Two drums instead of one is the penalty for the boom simplification.

The array storage drums, the interleaf storage drums, and extension actuator are mounted on a cradle which can rotate when released. The orientation mechanism located inside the SSM provides rotational drive to control the orientation of the solar cell panels.

Another advantage of this concept is that it does not require deployment of an additional rigid boom to permit panel extension and wing orientation. Also, it does not have to depend on the shroud mounting ring for bearing support. These aspects simplify deployment, retraction, and maintenance of the array.

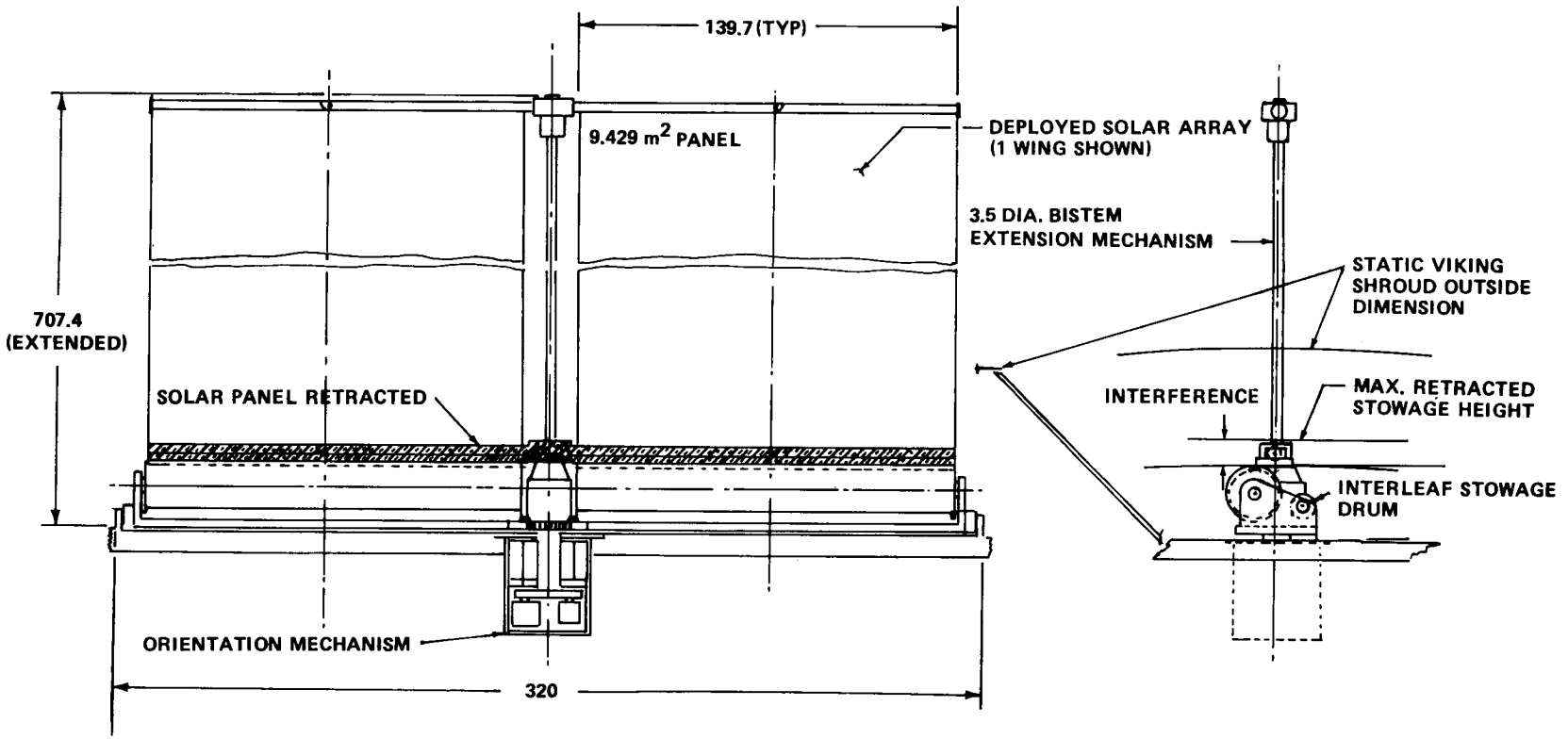

Figure IV-47. Solar array alternate no. 2.

Like alternate no. 1, however, its stowage height was too large to stay within the shroud envelope. The interfence was 7.1 cm; this is also close enough to consider feasible and worthy of further study.

As shown, alternate no. 2 would provide an area of 37.72 m^2 and its power performance would be equivalent to the reference array. Table IV-23 gives a mass summary for the second alternate.

TABLE IV-23. ALTERNATE NO. 2 SOLAR ARRAY MASS

Component	System Mass (kg)
Flexible Blanket (2)	80.76
Extension Mechanism (2)	7.26
Extension Boom (2)	7.26
Tiedown/Containment (2)	39.02
Solar Array Drive (2)	11.79
Drive Electronics (1)	1.81
Total Mass	147.90

c. Alternate No. 3 Solar Array. The third alternate may be considered a semirigid-type array because the solar cells are mounted on a flexible substrate and are attached to a rigid frame. As a wing assembly, this alternate is quite rigid.

Alternate array no. 3 utilizes a solar reflector/solar cell array to reduce the active array cell area. The reflector is integrated with the large triangular backbone structure that provides primary support for the solar cell panels. Figure IV-48 shows an outline drawing of this concept. Each wing consists of six segments. The innermost is a transition section from the drive mechanisms to the triangular backbone which runs down the other five solar cell modules. The solar cell modules are made of solar cells mounted onto a flexible substrate which, in turn, is mounted onto a low-mass

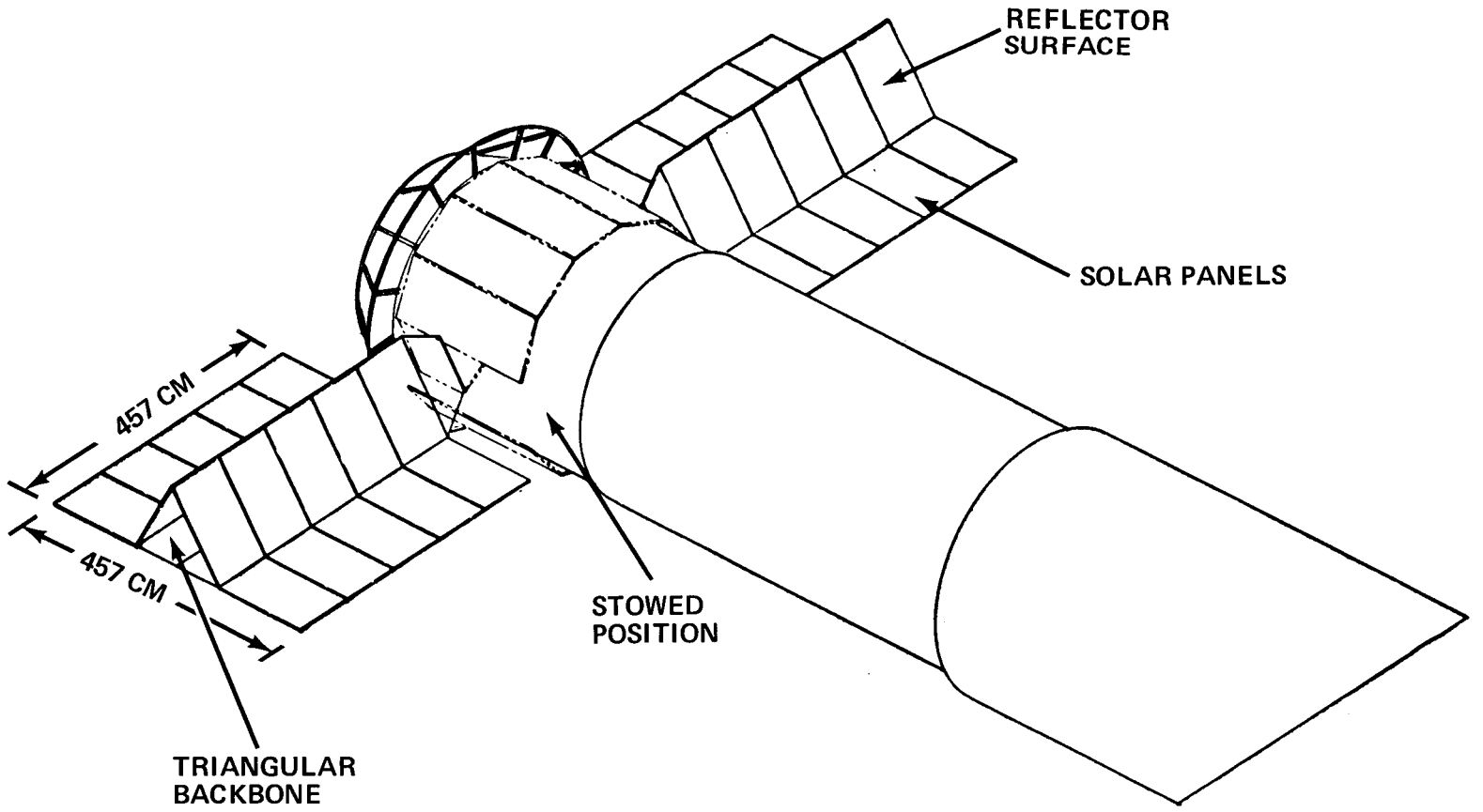

Figure IV-48. Solar array alternate no. 3.

isogrid rigid structure (a hollow structure like the floors of Skylab). The reflector/concentrators reportedly reduce the solar cell area required by about 33 percent, thereby reducing the solar panel costs. The reflector/concentrator costs and the lightweight structure costs would reportedly be as low as for the conventional honeycomb material. Resulting solar cell temperature increases have been considered in estimating the projected solar cell area reduction. R&D results have projected that the electroformed isogrid structures could be made at a low cost with the proper tooling.

It may be noted that stowage, deployment, and retraction concepts are similar to those of the reference array. When deployed, it is a more rigid structure. Also, this alternate meets the Titan shroud clearance constraints. The array area of 42.74 m^2 allowed for more degradation than used for the reference and also more area was needed to keep the cell temperature down because of the increased (reflected) illumination.

A mass estimate for alternate no. 3 array is given in Table IV-24.

TABLE IV-24. ALTERNATE NO. 3 SOLAR ARRAY MASS ESTIMATE

Component	Mass (kg)
Solar Cells, Coverslides, and Adhesives	40
Insogrid Substrates	410
Nylon Reflector	5
Hardware, Hinges	130
Total Mass	585

d. Alternate No. 4 Array. The variation of the reference design array using substrate loaded with a phase change material was considered as alternate no. 4. It is discussed in Section C.

e. Assessment of Alternates. Other alternates are under consideration but have not been evaluated. All of those shown offer advantages over the reference design and are worthy of more consideration. However, the better retraction and deployment design, the replaceability features, and the weight of the flexible, rollout types make them most attractive for the LST mission. An extensive investigation of cost is required to accurately determine whether or not any of the alternates offer a cost advantage to the program.

3. Battery Trades. Numerous battery tradeoffs were considered during the study in an attempt to optimize performance and to select optimum cell size and battery assembly configurations for the LST mission. Data on typical assemblies for other projects and on cell models available from four manufactures were used in these trade studies. The same LST load and environmental conditions used for the reference battery were used for the alternates considered.

Rectangular and cylindrical cells were considered. Most of the cylindrical cells produced are for small commercial applications such as radios, razors, flashlights, toys, etc. Preliminary designs were made to optimize assemblies for the application and for the variations in cell ratings and configurations considered. Energy, voltage, mass, and thermal characteristics of the assemblies were evaluated. In turn, these characteristics were also traded for their effects on system complexity, redundancy, controls needed, and subsystem mass. It was found that assembly characteristics are only slightly affected by variations in cell dimensions or manufacturers once the rating, style or type of cell construction, and the number of cells have been selected. A few examples of battery assembly characteristics are given in Table IV-25. These are typical of assemblies of the given cell rating, depending on passive thermal control. It may be noted that for the rectangular cells, the energy to mass ratio increased very slightly with rating size. The high performance of the cylindrical cell assembly results from the high pressure, low mass construction of the cells.

Three of the above battery assemblies are compared on a subsystem basis in Table IV-26. For the LST load and orbit requirements, the practical limits on cells per assembly, number of assemblies, and depth-of-discharge are shown. The mass of the battery assemblies, chargers, and total subsystem are compared at a DOD of 17.5 percent for the three configurations.

TABLE IV-25. TYPICAL BATTERY CHARACTERISTICS

Cell Configuration	Cell Rating (A-h)	No. of Cells	Assembly Rating (W-h)	Assembly Dimensions (cm)			Assembly Mass (kg)	W-h Per kg	W-h Per cm^2
				Length	Width	Height			
Rectangular	15	22	413	32.23	13.00	19.38	18.6	22.2	0.0508
Rectangular	20	22	559	33.27	16.94	18.80	23.6	23.7	0.0528
Rectangular	30	21	802	42.95	17.60	18.21	32.7	24.7	0.0586
Rectangular	31	24	922	50.47	17.60	18.21	37.2	24.8	0.0570
Cylindrical (Reference)	30	24	900	40.53	27.05	17.60	22.4	40.1	0.0466

TABLE IV-26. SUBSYSTEM COMPARISONS OF BATTERY ASSEMBLIES

Characteristic for Subsystem Range	Assembly Configuration[a]		
	20-A-h Cells Rectangular	31-A-h Cells Rectangular	30-A-h Cells Cylindrical
Cell Type	NiCd	NiCd	NiCd
Best Passive Control Temperature	10 ± 5°C	10 ± 5°C	10 ± 5°C
Feasible Cells/Assembly	24 to 28	21 to 28	21 to 28
Feasible No. of Assemblies	8 to 7	8 to 5	8 to 5
DOD Range	17.5 to 21%	12 to 21%	12 to 21%
Assembly Specific Energy	23.7 W-h/kg	24.8 W-h/kg	40.1 W-h/kg
Charger Penalty	6.8 kg/assembly	6.8 kg/assembly	6.8 kg/assembly
Subsystem Battery Requirement	8 Assemblies — 233.5 kg	6 Assemblies — 223.0 kg	6 Assemblies — 134.4 kg
Subsystem Charger Requirement	8 Chargers — 54.4 kg	6 Chargers — 40.8 kg	6 Chargers — 40.8 kg
Total Subsystem Mass	287.9 kg	263.8 kg	175.2 kg

a. All assemblies compared at 17.5% DOD.

Battery characteristics were evaluated for optimum operating conditions and for optimum use of the battery mass for long term mission intervals. The cycle life rating, DOD temperature, specific mass of the battery assemblies, and LST energy requirements determined the characteristics compared. Curves for cycle life as a function of temperature and DOD, as discussed in Section C and in Chapter VIII, served as a basis for determining performance as a function of DOD. Figure IV-49 is an example of the performance curves obtained for the 31-A-h rectangular cell assembly shown in foregoing comparisons.

For the design temperature, the cycle life limit and DOD were related to the total energy that an assembly would deliver. The energy required per orbit determined the battery mass as a function of DOD.

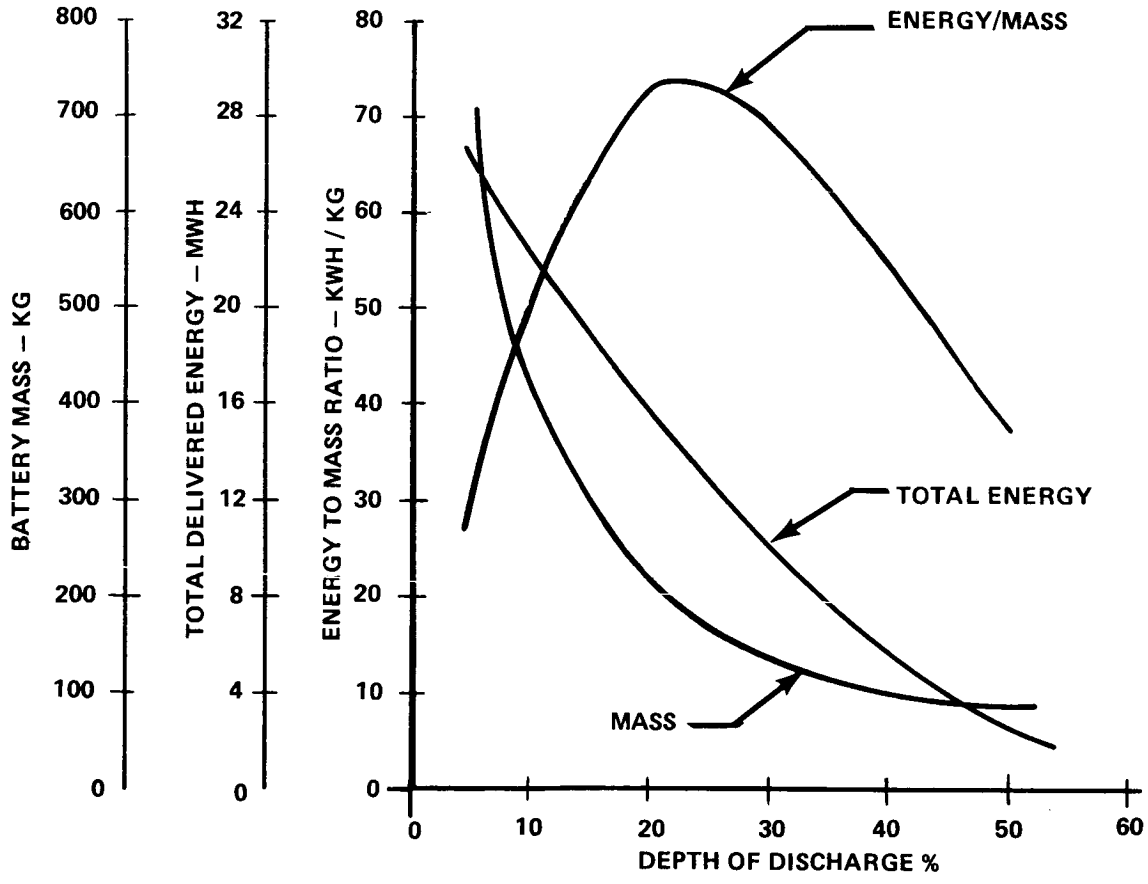

Figure IV-49. Battery performance comparisons, rectangular cell assemblies.

The total energy the battery would deliver during its life and the battery mass may be related for each DOD selected. Thus, the curve for total energy-to-mass ratio is determined. As indicated in Figure IV-49, the DOD should be about 21 percent for optimum use of the example battery. Optimistic cycle life curves were used for this example. On this basis, the optimum battery design should be for about a 2.5 year life.

CHAPTER V. COMMUNICATIONS AND DATA HANDLING

TABLE OF CONTENTS

TABLE OF CONTENTS (Concluded)

LIST OF ILLUSTRATIONS

LIST OF ILLUSTRATIONS (Continued)

LIST OF ILLUSTRATIONS (Concluded)

LIST OF TABLES

CHAPTER V. COMMUNICATIONS AND DATA HANDLING

The communications and data handling (C& DH) system design guidelines were derived from the collective data and command requirements of the optical telescope assembly (OTA), the scientific instrument package (SIP), and the support systems module (SSM). The philosophy used in configuring the reference design for early missions was to obtain the maximum worthwhile scientific data within the constraints of existing technology and ground facilities with no further investment in additional special data reduction equipment and/or ground facility modification. The growth potential to take advantage of possible increases in ground station capability and the availability of the Tracking and Data Relay Satellite System (TDRSS) for later Shuttle-launched LST missions was considered.

A. Requirements and Assumptions

In addition to the general requirements specified for the overall LST mission, the following specific requirements and assumptions were imposed on the Communications and Data Management function.

1. Communications Facilities

a. Ground Network. The ground network chosen for the LST reference design is the Spacecraft Tracking and Data Network (STDN). These stations include the Canary Islands (CYI), Ascension Island (ACN), Orroral Valley (ORRX) as a proposed site change for Carnarvon (CRO), Guam (GWM), Hawaii (HAW), and Goldstone (GDSX). For a 611 km (330 n. mi.) circular orbit with an inclination of 28.5 degrees, this network can achieve an average contact time of 26 minutes per revolution. The average contact time per revolution per station is 11.09 minutes. The calculations were based on existing STDN capabilities operating at 2200 to 2300 MHz.

Downlink capabilities at each station will permit a scientific data rate of 1 megabit/sec. The LST status, diagnostic, and command verification data will be transmitted down at a rate of 51.2 kbs. These rates have proved adequate to meet mission requirements.

b. Tracking and Data Relay Satellite Systems. Data relay satellites would not be available for early launches but might be considered later. VHF and Ku-band data relays may become available. The Ku-band relay is

projected as a 14.4 to 15.35 GHz system using a 2.4 m (8 ft) parabolic antenna on the LST. A system noise temperature of 1200°K, a video bandwidth suitable for color television, and an RF bandwidth of 200 MHz are projected.

2. Data Quality. The bit error rate (BER) for data and commands transmitted to the equipment onboard the LST must be less than one part in 10^9 (the probability of a bit error, P_e^b, is less than 10^{-9}). For data transmitted to the ground, the probability of a bit error will be less than 10^{-5} for differentially coherent phase shift keyed (PSK) operation.

3. Command Capability. A capacity for 5 hours of operations without contact for receiving commands will be provided. Command storage for 4000 28-bit words is provided. Command messages are received at a rate of 200 bits/sec.

4. Experimental Data. Experimental data will be sent directly from the SIP to ground through the communication system at a maximum rate of 1 megabit/sec. A camera tube resolution of 20 to 30 cycles/mm[1] and a 50 by 50 mm target is assumed as the design reference because this is thought to be likely from projections of the state of tube development at the time of flight of the LST. However, a resolution of 60 cycles/mm and a 50 by 50 mm target was used to size the C&DH system to provide for growth for possible increased image tube capabilities. The number of bits required for the high resolution picture frame is 576 megabits with 8 bits/sample coding and 4 samples/cycle sampling rate. At least one frame per orbit is required from the SIP. With a maximum downlink data rate of 1 megabit/sec a 576 megabit frame requires about 10 minutes of contact time to transmit to ground. Comparable numbers for a tube resolution of 20 cycles/mm would be 64 megabits/frame and would take 64 seconds of contact time to dump at a 1 megabit/sec rate.

B. Ground Station Network and Facilities

The primary guidelines used in this overall study were those that would satisfy the basic requirement of good scientific data being transmitted from the spacecraft to the ground. The ground network in existence during the LST mission flight time is probably one of the more important constraints.

1. The designation cycles/mm is used throughout this volume and is equivalent to the designation of a line pair/mm [V-1].

The network that will be used as design reference is STDN which is composed of the stations of the Manned Space Flight Network (MSFN) and the old Space Tracking and Data Acquisition Network (STADAN) system. However, only stations with unified S-band (USB) capability were selected for this mission. The locations of the stations comprising the STDN are indicated in Figure V-1. There is a possibility that this network will be limited to only 15 stations. The stations that are scheduled (or are being contemplated) for retirement are shown by the triangles on the map. The six stations were selected to provide support in the tracking of the spacecraft, commanding the spacecraft, and for retrieving data from the spacecraft in near-real and real time. Stored data may also be transmitted to these stations for forwarding to the control center.

Two criteria were used in selecting the stations. The first was that the station had to be visible to the spacecraft during its pass around the earth, and the second ground station selection parameter was the equipment available at the station.

1. Mission Coverage Analysis. Generally, the mission coverage requirement means that the only stations with coverage within a band less than 28.5 degrees of latitude north and south can be used. In Table V-1 the entire 15 STDN stations are shown with their corresponding latitudes. In some instances the spacecraft may be visible from stations at slightly more than 28.5 degrees of latitude north or south, but the time over those stations is greatly reduced. To confirm the coverage obtained from available ground stations with the LST launch data programmed for 1979 from the Merritt Island launch area, a coverage analysis was based on a circular orbit at an altitude of 611 km (330 n. mi.) and an inclination of 28.5 degrees (see Volume II, Mission Analysis).

To maintain the intensive communications and control links between earth and LST experiments, the STDN provides six ground tracking stations equipped with a 9.144 m (30 ft) diam antenna. The selected ground sites were originally CYI, ACN, CRO, GWM, HAW, and GDSX. Current NASA studies have dictated a requirement that the tracking facilities at CRO be phased out of the STDN in 1974. Since the LST is scheduled to operate initially in 1979, a subsequent simulation analysis has assumed a possible participation of ORRX instead of CRO.

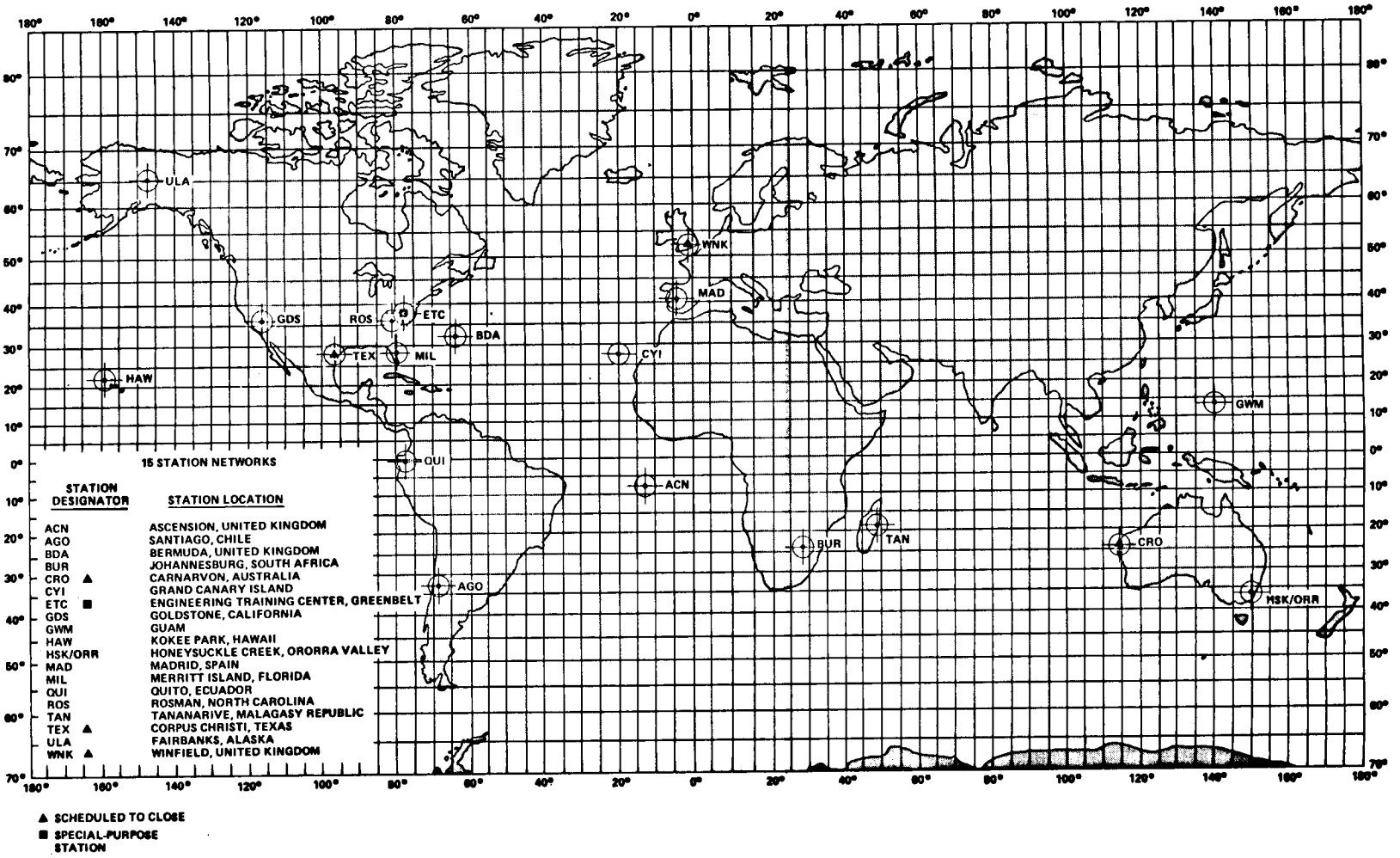

Figure V-1. STDN station map.

TABLE V-1. STDN GROUND STATION LOCATION

Station[a]	System	Latitude[b]	Longitude (E)	Height (Above Ellipsoid) (m)
Ascension Island	9.144 m (30 ft) USB	- 7° 57' 17.26"	345° 40' 22.59"	527
Santiago, Chile	S-band Goddard Range and Range Rate (GRARR) VHF GRARR Interferometer	-33° 09' 02.73" -33° 09' 05.21" -33° 08' 57.24"	289° 20' 03.25" 289° 20' 03.25" 289° 19' 56.40"	732 732 720
Bermuda	9.144 m (30 ft) USB FPQ-6 Radar FPS-16 Radar	32° 21' 04.50" 32° 20' 52.54" 32° 20' 53.04"	295° 20' 31.93" 295° 20' 47.91" 295° 20' 47.70"	-43 -45 -46
Johannesburg, Republic of South Africa	Interferometer	-25° 52' 58.86"	27° 42' 27.93"	Not Available
Grand Canary Island	9.144 m (30 ft) USB	27° 45' 52.33"	344° 21' 57.90"	179
Goldstone, Calif.	25.91 m (85 ft) USB 9.144 m (30 ft) USB Earth Resources Technology Satellite (ERTS)	35° 20' 26.74" 35° 20' 29.63"	243° 07' 35.05" 243° 07' 40.46"	921 946
Guam	9.144 m (30 ft) USB	13° 18' 38.07"	144° 44' 12.54"	114
Hawaii	9.144 m (30 ft) USB FPS-16 Radar	22° 07' 34.71" 22° 07' 24.61"	200° 20' 05.42" 200° 20' 04.00"	1143 1147
Honeysuckle Creek/ Ororral, Australia	25.91 m (85 ft) USB 9.144 m (30 ft) USB[c]	-35° 35' 00.58" -35° 37' 37.50"	148° 58' 40.12" 148° 57' 10.70"	1143 941
Madrid, Spain	25.91 m (85 ft) USB	40° 27' 17.97"	355° 49' 53.57"	763
Merritt Island, Fla.	9.144 m (30 ft) USB No. 1 9.144 m (30 ft) USB No. 2	28° 30' 29.78" 28° 30' 26.34"	279° 18' 23.51" 279° 18' 22.93"	-54 19
Quito, Ecuador	Interferometer	-00° 37' 20.62"	281° 25' 17.94"	3593
Rosman, N. C.	S-band GRARR VHF GRARR	35° 11' 45.05" 35° 11' 41.10"	277° 07' 26.23" 277° 07' 26.23"	880 880
Tananarive, Malagasy	S-band GRARR VHF GRARR Interferometer FPS-16 Radar	-19° 01' 09.33" -19° 01' 11.80" -19° 00' 27.10" -19° 00' 06.49"	47° 18' 12.56" 47° 18' 12.56" 47° 18' 00.46" 47° 18' 53.03"	Not Available Not Available Not Available Not Available
Fairbanks, Alaska	S-band GRARR VHF GRARR Interferometer	64° 58' 20.89" 64° 58' 19.19" 64° 58' 38.60"	212° 29' 22.41" 212° 29' 28.12" 212° 28' 40.90"	349 349 292

a. System locations are subject to minor changes as refinements in positional accuracies are made.
b. A minus sign (-) indicates south latitude.
c. Equipment to be moved from Carnarvon.

A Tracking and Data Relay Satellite (TDRS) concept using two tracking and data relay satellites placed in geostationary orbit to simulate tracking of the LST spacecraft over long arcs in the circular orbit was also analyzed. The primary aim of this hypothetical concept is to increase orbital and geographical coverage and to improve tracking accuracy. With its unique capability for the continuous reception of data in real time, the TDRS commands, tracks, and relays data from the LST to fewer ground stations. Although it would provide complete tracking coverage for the LST, the TDRS may have the problem of accessibility since the scientific data generated on the LST orbital mission would not require continuous real-time data dumping or real-time ground control of experiment and subsystem operations.

The STDN configuration was evaluated to satisfy one contact per orbit with a 5-minute minimal contact and to satisfy the minimum data hours that may be specified in the data handling requirements. An evaluation of ground coverage statistics for the reference design network is illustrated in Table V-2. Contact conditions are shown for a length of computer simulation of 70 orbital revolutions, which are adequate to assure reasonably stable statistics. In this table, the conditions computed are externally constrained by a minimum 5-minute contact time and elimination of the ground station with shorter contact time in the event of station multicoverage. This configuration could acquire an average contact time of 26 minutes per revolution. An average contact time of 11 minutes per revolution is established for each STDN station whenever a contact is made.

Table V-3 shows a summary of cumulative contact time per 24 hours for each STDN station, using the antenna horizon coverage limits as a constraining factor. Minimum zero-minute contact time is considered. The elimination requirement is not imposed on an overlapped station with a shorter contact time. A comparison of the individual station coverages in terms of minutes and seconds indicates that, when the overlapping elimination constraint applies, the ability to meet the one contact per orbit requirement decreases. Replacement of CRO by ORRX did produce a substantial reduction in the total station cumulative contact time per 24 hours.

The mission analysis using the TDRS shows that each communications satellite tracked the LST constantly for about an hour during each revolution. Thus, a 611-km orbit gives an average TDRS network coverage of about 95 percent compared with 26 percent coverage for the STDN Configuration.

The coverage statistics generated in the mission analysis indicate that the STDN Configuration which includes ORRX instead of to-be-phased-out

TABLE V-2. STDN COVERAGE SUMMARY FOR THE LST [a,b,c]

[orbital count = 70 revolutions, altitude = 611 km (330 n. mi.), inclination = 28.5 degrees]

Contact Conditions	STDN Configuration (611 km altitude)
Total contact time in 70 revolutions (min)	1796.97
Number of contacts in 70 revolutions	165
Percentage of contact time in 70 revolutions	24.65
Average contact time per revolution in 70 revolutions (min)	25.67
Average contact time per station per revolution with contact (min)	11.09
Minimum time of combined contacts during any revolution (min)	13.28
Minimum station contact time achieved (min)	5.03
Maximum time of combined contacts during any revolution (min)	47.07
Maximum station contact time achieved (min)	13.43
Average number of contacts per day	32
Minimum number of contacts per revolution	1
Number of revolutions without contact	0
Maximum gap duration achieved in 70 revolutions (min)	89.73
Average gap duration in 70 revolutions (min)	33.39
Percentage of coverage gap less than 1 hr long	92.07

a. Minimum 5-min contact time.
b. Elimination of overlapped station with shorter contact time.
c. Bias time for acquisition of signal (AOS) and loss of signal not deducted from contact time.

TABLE V-3. SUMMARY OF STATION CUMULATIVE CONTACT TIME PER 24 HOURS[a, b]

	STDN Network Configuration Tracking Station					
	CYI	ACN	ORRX	GWM	HAW	GDSX
Duration	Cumulative Contact Time (min:sec)					
First 24 hours	82:38	74:47	32:34	93:21	87:18	49:49
Second 24 hours	79:32	75:52	29:45	92:10	87:02	42:21
Third 24 hours	83:32	83:47	29:57	93:52	77:05	49:11
Fourth 24 hours	79:23	84:56	29:03	92:44	85:51	49:24
Fifth 24 hours	77:54	81:25	28:43	90:43	84:41	52:15

a. Minimum zero-minute contact time.

b. Elimination constraint not imposed upon overlapped station with shorter contact time.

CRO may be adequate for the LST coverage requirements. The TDRS concept, when developed and deployed, should be designed to track a spacecraft such as the LST. (See Chapter III, Mission Analysis in Volume II of this report for a more detailed discussion of station contact statistics.)

2. Ground Station Equipment. It was decided that only USB would be used in the overall mission operations. This assures compatibility with existing designs and enhances commonality between the LST and the High Energy Astronomy Observatory (HEAO). Table V-4 shows all the 15 stations and some of the stations that are planned for retirement and the equipment that is presently available or planned by the time LST would require it. As can be seen the stations with 9.144 m (30 ft) antennas are ACN, Bermuda, CRO, CYI, the Engineering Center at Goddard, GDSX, GWM, HAW, Merritt Island, Corpus Christi, and the Vanguard Ship. These have USB equipment. Several of these stations can be eliminated because they are keyed for other missions. In particular, this would eliminate Bermuda and Merritt Island. It is not planned to use the Vanguard Ship because of the long duration of the mission.

a. USB Stations. The receivers in the LST reference design operate at 2200 to 2300 MHz. It can be seen from Table V-4 that certain stations have reception capability at 2200 to 2300 MHz (or plan to have) but one finds that the command capability, the tracking, and the telemetry in these bands are not necessarily in agreement with the planned mission operation. For instance, only the MSFN stations have the capability of demodulating subcarriers which will be necessary for near real time and real time transmission of spacecraft data. It is also planned to use the USB command system for LST operation. The stations with the 9.144 m (30 ft) antennas have the USB capability. The tracking function is also planned to be performed on the USB for all known requirements. As indicated on the figure, Santiago has neither the 9.144 m (30 ft) antenna, the S-band command capability, or the S-band telemetry capability. Therefore, it was not considered in this overall mission even though it has been considered in the past as a possible site for HEAO missions. The six stations that were primarily considered as useful for this mission were ACN, CRO, CYI, GDSX, GWM, and HAW. Stations such as Madrid, Honeysuckle, etc., were not considered as primary candidates because they have 25.91 m (85 ft) antennas, which is an overkill of the problem in this case. The other stations which were not considered were Corpus Christi, since it is anticipated that it would be retired and that the equipment from GWM that has been moved to GDSX could be used in that location with similar latitude and longitude of the present site; Merritt Island, and Bermuda, which are primarily keyed for launch operations and are available only on a noninterfering basis with launch operations.

TABLE V-4. GROUND STATION CHARACTERISTICS

Station	9.144-m (30-ft) Antenna	Dual Command	Dual Downlinks	Display Engineering Data	Wide-Band Digital	Wide-Band Analog	Near Real-Time Engineering	Command	Remarks
Ascension Island	X	X	X	X	X	X	X	X	
Bermuda	X	X	X	X	X	X	X	X	Launch support only
Canary Island	X	X	X	X	X	X	X	X	
Fairbanks			X		X		X		Cannot see 28 degree orbit
Goldstone	X	X	X	X	X	X	X	X	Also has 25.91 m (85 ft) antenna
Guam	X	X	X	X	X	X	X	X	
Hawaii	X	X	X	X	X	X	X	X	
Honeysuckle/ Ororral	X	X	X	X	X	X	X	X	Transferred to Deep Space Instrumentation Facility (DSIF). 9.144 m (30 ft) antenna moved from Carnarvon.
Johannesburg			X		X		X		
Madrid		X	X	X	X	X	X	X	25.91 m (85 ft) antenna
Merritt Island	X	X	X	X	X	X	X	X	Launch support
Quito			X		X	X	X	X	
Rosman, N. C.			X		X	X	X	X	
Santiago			X		X		X		
Tananarive			X		X		X		

b. Ground Station USB Receivers. A block diagram of a ground station receiver is shown in Figure V-2 to give a better understanding of the constraints imposed upon the spacecraft by the ground stations. It should be noted that although much of the equipment was custom designed for the Apollo operation and can be adapted for the LST operation, it is certainly not optimum for that purpose. However, for the sake of standardization and reduced cost, it is anticipated that the LST can be designed to use it without any significant modifications other than in the software. Not shown in the diagram are the digital synchronizers and word synchronizers which are downstream from the overall receiver operation. The demodulations shown in the design are primarily for those 1.024 and 1.25 MHz subcarriers commonly used in Apollo. It is anticipated that these will be quite useful in the overall operation of the LST for voice, if necessary, and in some cases where real time data is transmitted to the ground simultaneously with voice and ranging.

The ranging portion of the circuit is not shown on the block diagram but can be visualized as a replacement for the base-band of the FM modulation. The ranging circuit uses PM-type modulation and determines the range and the range rate to the spacecraft on occasions when it is necessary to know the vehicle's position in order to update orbital predictions.

The basic design of the USB receiver is a phase locked loop operating at 10 MHz. In the FM mode, the frequency is taken from the IF amplifier, further amplified in a second IF stage at 50 MHz, and fed into a 50 MHz FM modulator that uses a closed loop. The bandwidth of the IF amplifier is about 11 MHz, which is further reduced to 7.5 MHz in the predetection filter preceding the FM detector in the upper right hand portion of the diagram. The 5 MHz is plus/minus 1 dB while in the PM mode it can be operated to -3 dB with 4 ±0.5 MHz of bandwidth. In the lower right hand side of Figure V-2 is shown a subcarrier demodulator as it demodulates the PM biphase modulation that contains the 1.25 MHz voice channel and the 1.024 MHz subcarrier for real time telemetry. It is quite evident that this design dictates the overall design of the spacecraft communication system and must be considered if the LST is to be compatible with the ground station. Each point in the overall design of the LST to ground station interface has been carefully taken into account in the spacecraft communication system reference design concept.

The USB system includes four main receivers and is capable of receiving four downlink frequencies simultaneously, provided the transmitting sources are within the USB antenna beamwidth. Two of these receivers have been modified so that they can be tuned across the 2200 to 2300 MHz frequency band, with open-loop mode IF bandwidths to 30 MHz

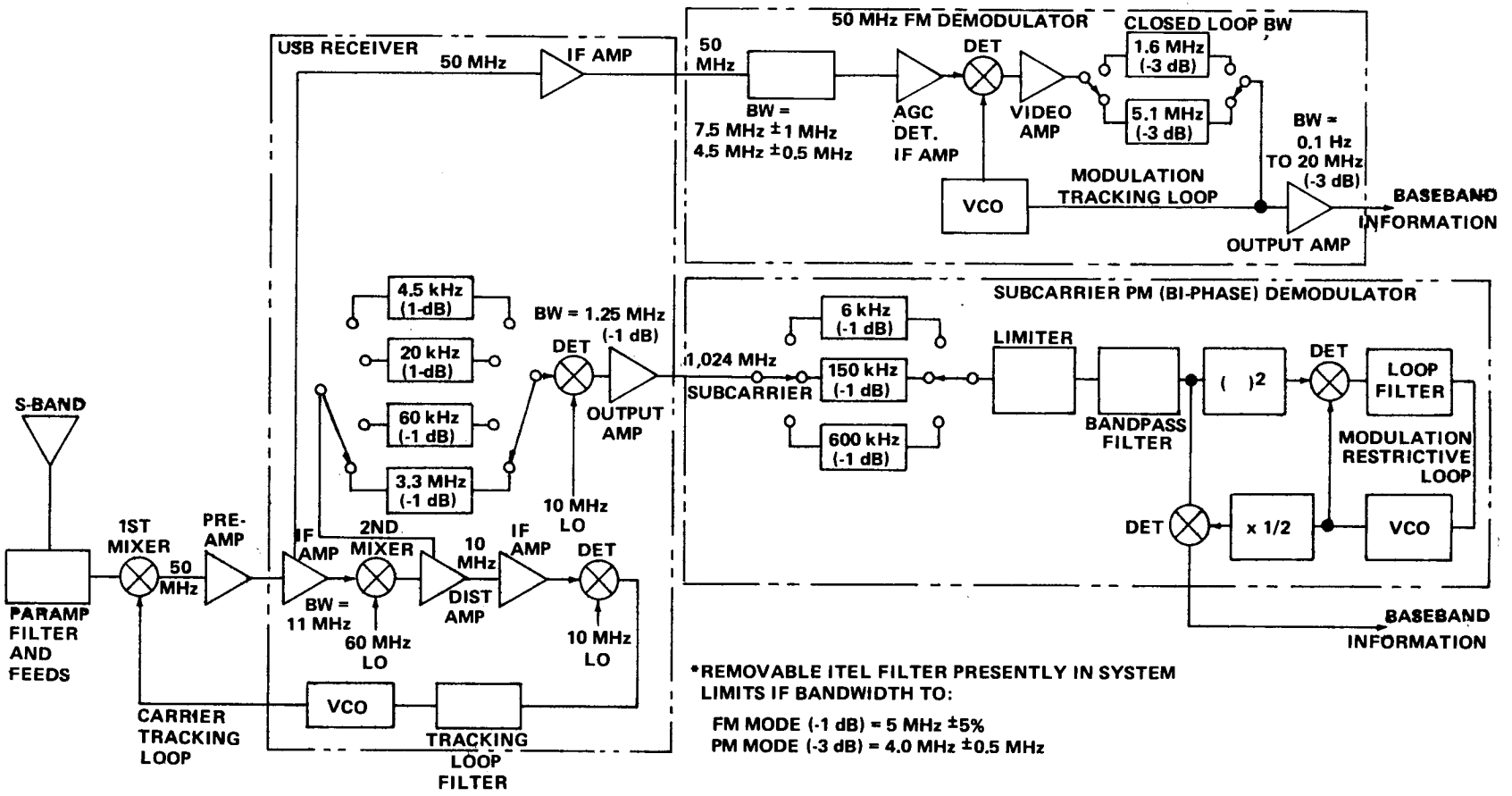

Figure V-2. USB single receiver and demodulator.

permissible. The remaining two are limited to 5 MHz open loop IF bandwidth frequency reception at Apollo frequencies in the range of 2270 to 2300 MHz. All four receivers have closed-loop (PM) IF bandwidths to about 3.3 MHz. Normally the downlink carrier will be modulated with a composite signal consisting of ranging data and modulated subcarriers, but as with the uplink, data may be modulated on the carrier. The receivers can be operated in either an open-loop or closed-loop configuration with carrier tracking loop bandwidths ranging from 12 to 700 MHz.

c. Command Transmission. The USB configuration has a capability of transmitting commands both in the UHF and the VHF frequency band. VHF command capability is possible in the 225 to 399.9 MHz region at most of the MSFN stations using equipment normally configured for VHF air-to-ground voice communications. In the latter case, tone encoders and decoders of the UHF command systems are used. However, only the lower frequency tones may be employed because of the transmitter bandwidth limitation. Also, amplitude modulation is employed instead of frequency modulation which makes it susceptible to noise.

The USB system is capable of transmitting commands on uplink frequencies of 2090 and 2120 MHz with the command data modulated directly on the carrier frequency or on a subcarrier prior to modulation on the main carrier. An update buffer is used to interface between the USB transmitting system and the command data processor. The command data processor is a Univac 642V computer. The buffer receives digital command data in parallel form from the processor and converts them to a 1 kbs serial data stream. The data, in turn, PSK modulates a 2 kHz sinewave and is linearly added with a phase coherent 1 kHz sinewave. This composite signal is then modulated onto the 70 kHz subcarrier or main carrier as desired.

The 1 kbs serial stream represents an intelligence rate of about 200 bits/sec because 5 to 1 sub-bit encoding is employed for security and for rejection of nonvalid commands. A variety of command word structures is available and the commands may be transmitted from the station or a command/control center through the station. Command verification is employed by sampling and demodulating the power amplifier output and performing a bit for bit comparison with a command computer. It can also be verified from the spacecraft through the telemetry downlink.

The power amplifier and USB antenna characteristics have been discussed earlier and are pointed out in Table V-5. The 9.144 m (30 ft) systems contain only one power amplifier capable of operating at 20 kW.

TABLE V-5. USB ANTENNA CHARACTERISTICS

Antenna	Station	Gain (dB)	Beamwidth (3 dB) (deg)	Polarization	Mount Orientation	Acquisition System	Acquisition Gain (dB)	Acquisition Beamwidth (deg)
9.144 m (30 ft)	MIL, BDA, ACN, CYI, ORO, GWM, HAW, TEX,	Rx — 44 Tx — 43	1.0	Right Circular Polarized (RCP)/Left Circular Polarized (LCP)[a]	+X East +Y North	Apex Mounted 107 m (42 in.)	22.0	10
25.91 m (85 ft)	MAD, GDS, HSK	Rx — 53.5 Tx — 51	0.3	RCP/LCP[a]	+X South +Y East	Apex Mounted 1.88 m (6 ft, 2 1/2 in.)	25.5	5

a. Remote selectable polarization for receiving (Rx) and transmitting (Tx).

However, when two signals are transmitted simultaneously, the power must be reduced to prevent intermodulation products. In most cases the power is reduced to 2 kW per uplink.

d. The USB Tracking System. When tracking a phase modulated carrier in a closed-loop mode, the USB tracking system maintains a continuous update of the position of the spacecraft by measuring the antenna pointing angle and range and the range rate of the vehicle with respect to the station. Each USB system can determine the range and the range rate of two vehicles simultaneously, provided both are within the beamwidth of the antenna, but, of course, it can only angle track on one vehicle.

(1) Ranging. A digital ranging technique is used to determine the range. In this system a pseudo-random binary code is phase modulated on the S-band uplink and transmitted to the spacecraft. A transponder system in the spacecraft extracts the ranging code and applies it to a coherent downlink carrier, which is transmitted back to the ground station. A ranging receiver accepts the ranging data from the main receiver at the 10 MHz IF. Here a correlation process occurs wherein the received code is compared with the time-shared code provided by the ranging system and thus turnaround time for the code is determined. From this information the spacecraft range is determined. It is possible to disable the full code modulation and use only the 2 bit clock code. This limits the spectral distribution due to ranging to a single spectral line at 496 kHz above and below the carrier frequency. The range to the spacecraft can be resolved to about 1 m and the maximum range tracking rate is about 12 000 m/sec. The other system and accuracy data are presented in Table V-6.

TABLE V-6. REPRESENTATIVE USB METRIC TRACKING ACCURACIES

Characteristic	Bias	Noise
Range	25	5
Range Rate (mm/sec)	500	5.5 (1/6 sec)
Angle (deg)	0.015	0.015

(2) Range Rate. Spacecraft range rate is determined by measuring the Doppler shift of the transponder carrier signal. The Doppler

counting system is designed to handle ± 180 kHz biased about a 1 MHz frequency. Doppler is counted in either of two operating modes, destruct or nondestruct. The first mode consists of simply determining the time required for a preset number of Doppler cycles to be counted. In the second mode, Doppler is counted continuously throughout the tracking period. The number of Doppler cycles in any given time period is then representative of the range rate of that period. The tracking data process formats the information for transmission to the central control center.

(3) Angle Tracking. All the USB stations have X-Y mounts. The X-Y mounts allow tracking through the zenith but have a gimbal restriction in two areas of about 6 degrees of elevation at the 9.144 m (30 ft) antenna stations. The stations are capable of tracking at an angular rate of 4 degrees/sec, with an angular acceleration of 5 degrees/sec^2. All the stations can be either auto-tracked or programmed. In the auto-tracked mode, the antenna monopulse tracking system, after the acquisition of the spacecraft, provides error signals to the USB servo system to keep the antenna pointed to the signal source. The angular direction to the spacecraft is measured by encoders mounted on the two antenna axes. In addition to the PM tracking, the system can provide angle track on suppressed carrier FM signals using separate cross correlation auto-track receivers.

(4) Acquisition. The programmed mode of using X and Y axis and time information can be supplied as acquisition data to position the antenna. The initial acquisition of the spacecraft signal is facilitated by a small acquisition parabolic antenna mounted in the center of the ground-based USB antenna. The wider bandwidth of the smaller antenna aids in the acquisition process. The gain of the antenna is approximately 44 dB for receiving and 43 dB for transmitting. The beamwidth is 1 degree and is capable of either right-hand circular polarization or left-hand circular polarization. This will become quite important in the overall design of the spacecraft since it will allow for frequency diversity and obtaining an omnidirectional pattern for the entire spacecraft. The acquisition antenna has only a 10 degree beamwidth and the acquisition gain is only 22 dB.

e. Noise Temperature. Low noise preamplifiers and multicouplers are connected between the antenna and the receiving equipment. The amplifiers are generally mounted on the antenna to minimize the system temperature. Multicouplers are used throughout the network to provide isolation between preamplifier and receiver and to permit the connection of several receivers to a single preamplifier.

USB antenna systems have several configurations resulting in a variety of noise temperatures. Many of the USB stations with the 9.144 m (30 ft) antennas have cryogenically cooled preamplifiers giving a system noise temperature of 95°K; the remaining stations with uncooled parametric amplifiers have noise temperatures of 170°K. The uncooled stations considered for the LST are CYI and Bermuda (BDA). To insure compatibility with all these stations, it will be necessary to use the 170°K figure for all link calculations even though many of the stations have the quieter front ends.

f. Telemetry. Pulse code modulation is the primary telemetry concept employed in the entire system to support space projects. The PCM decomutator systems are located throughout the network.

PCM systems are by several different manufacturers: Radiation, Dynatronics, EMR, and Magnavox are used in the network. All the equipment, including the necessary signal conditions and bit synchronizers, can operate under the control of stored programs or patchboards. In general, the units can handle PCM coded NRZ, RZ and split phase data with a data rate capability of 1 megabit/sec for NRZ format and 500 kbs for RZ and split phase. An exception is that of the Magnavox equipment, which can handle data rates of only 200 kbs. It is anticipated at the time of the LST mission that the equipment will be updated to a capability of 5.5 megabits/sec. The Dynatronics and Radiation stored program equipment utilizes magnetic core memories and can be programmed in any of three ways: by manual entry from the front panel, by paper tape reader, or by on-line computer. Output from the decomutators may be through the digital to analog (D/A) decomutator digital PCM suitable for future on-station processing or transmission to the central control. Displays vary with the different equipment but include recorders for D/A decomutation. They may be used to provide additional capability for support and to replace some of the patch panel program units. These decomutators will be capable of a data rate up to 5 megabits/sec.

g. Recording. Each of the stations contains a wideband magnetic tape recorder that has a response from 400 Hz to 1.5 MHz using direct recording techniques and from direct current to 500 kHz with FM recording at a tape speed of 120 in/sec. Tape speeds from 10 cm/sec (3 3/4 ips) to 300 cm/sec (120 ips) are available with proportional response in the frequency range. These recorders have 14 tracks with a capability of combining up to 7 tracks using FM recording and direct recording on the remaining tracks.

h. Computation and Data Processing. Each USB station has a significant computer capability, referred to as the remote site data processors (RSDP). Generally, each USB station has two identical Univac 642B

(modified) medium scale computers. Associated with these computers is an "expanded memory unit" which contains two memory systems, one associated with each computer.

Most of these USB stations have two smaller Univac 1218 computers. The RSDP computers are described briefly in the following paragraphs.

(1) Univac 642B Computers. The two 642B computer systems are capable of intercommunications via an intercomputer channel, allowing them to be operated as an integral unit. Normally one computer is designated as a command processor and the second as a telemetry processor, with the equipment configuration and software programming arranged so that if one computer fails, the other can be switched to perform the major mission functions of the failed computer. The expanded memory unit serves to double the memory capacity of each computer from 32 768 30-bit words and increases the number of input/output channels from 16 to 20. Other characteristics of the computer are a 2.0 μsec read-write cycle time, a magnetic core memory capable of being randomly accessed, and an overlap memory capability which can increase the execution speed of various programs. The following peripheral equipment, in addition to the expanded memory unit, is used with the Univac 642B computer.

(a) The Univac 1540 Magnetic Tape Units (MTUs). These contain four transports each and are accessible from either computer. The MTUs are capable of reading and writing with densities of 200, 556, or 800 bits/in. at a speed of 300 cm (120 ips) and will rewind at 600 cm/sec (240 ips).

(b) The Peripheral Communication System (PCS). This system contains data transmission units (DTUs) and a model 1000 interface system adapter (ISA). The DTUs are used by the computer to transmit and receive high-speed data. The ISA contains a Greenwich mean time (GMT) buffer, which transfers parallel GMT data from the station timing standard to the computers, and a computer address matrix (CAM) multiplexer, which provides a means of communication between the CAM keyboards and the computers.

(c) The 1299 Interconnection Panel. This panel is equipped with multipole, double-throw switches for connecting and disconnecting the peripheral equipment to and from the computers, thus providing system flexibility.

(d) The Univac 1232 Input/Output (I/O) Console. This console contains a paper tape reader, punch keyboard, and printer. It is used by the computer operator to load and control programs and to monitor computer operations.

(e) The Motorola TP-400 Printer. This printer interfaces with the printer systems adapter (1222), which serves as an interface between the computer and the high-speed printers located at the integrated operations control console (IOCC) and in the computer area.

(f) The Updata Buffer (UDB). This is the interface between the command computer and the RF transmission equipment and serves to transform digital command data to a form suitable for modulating the command transmitters.

(g) The 1259 Teletype Unit. This consists of a standard AN/UGC-13 teletypewriter (TTY) with an adapter to interface with the computer. It acts as an input/output device for the computer. The TTY is a Model 28 automatic send/receive (ASR) unit, which offers an automatic means of transmitting data between two points using either a land or radio link. The TTY may be operated with mechanical changes at speeds of 60, 75, 100, or 200 words per minute.

(2) Univac 1218 Computer. This computer has associated with it a 1232 I/O console and a 1259 teletype adapter with a modified ASR-28 TTY. The 1218 computer has a memory of 17 384 18-bit words (expandable to 32 768) and eight I/O channels. It electrically interfaces with the USB antenna position programmer (APP) so that it can process acquisition messages into pointing data for driving the USB antenna. The 1259 teletype antenna and the modified ASR-28 TTY interface the 1218 computer with off-station communications.

A second 1218 computer is being used to provide each USB station with a computer-controlled automated checkout system. This system, which will be used to perform tests and monitor-selected functions, is a recent implementation and is identified by the acronym ASTAM (automated system test and monitor).

(3) Remote Site Data Processing Capability. The remote site 642B computers are normally operated so that one performs command data processing and the other telemetry processing. Trajectory and tracking data processing is performed by the 1218 computer.

(a) Command Data Processing. The computer programs and equipment at the stations provide for receiving commands from a computer center. The commands are transmitted in a digital format together with a polynominal error checking code. The station computer program performs a check of the command and the error code and determines whether errors occurred during transmission. If an error is detected, the received command can be rejected and a retransmission request initiated. The software program performs five-to-one sub-bit encoding of the stored commands and sends this information to the UDB and transmitters for uplinking the information to a spacecraft. The computer also performs a command verification function in which data from the telemetry computer indicate that a command has been received by the spacecraft.

The use of the polynominal error checking code and sub-bit encoding is part of the secure updata transmission system which is designed to insure that the probability that a spacecraft will accept an invalid command is less than 1×10^{-9}. The computer can also be programmed to print out a command history which indicates each command transmitted, the commands accepted or rejected by the spacecraft as shown by telemetered data, the status of ground system equipment, the time of events, the output of the command verification receivers, equipment control and status information, and the timing system information which is provided to the computer. This command history information can also be formatted for transmission to the Operations Center.

(b) Telemetry Data Processing. In general, the reason for on-station telemetry data processing is to adapt or modify telemetered data rates to be compatible with the off-station communications line capability. The computational techniques for accomplishing this modification range from sophisticated data compression techniques to simple format filling. Some of these techniques are discussed briefly in the following paragraphs.

Format selection is a process whereby various formats are planned in advance of the mission, with each format containing only those parameters most pertinent to a particular phase of the mission. The desired format is then selected at the proper time in the mission sequence.

A similar process, parameter selection, involves selecting out of the telemetry data stream only those parameters desired to be transmitted in real time. The remaining data can be recorded and mailed back or alternatively transmitted in near real time postpass.

Rate reduction and truncation schemes may also be used; however, some loss of data results when using these techniques. Rate reduction involves transmission of a reduced number of samples (e.g., transmitting only every 10th sample of a particular word, thereby reducing the rate by a factor of 10) of a particular parameter and truncation and reduced number of bits (e.g., transmit the eight most significant bits of a 10-bit word). These techniques are applicable where the resultant deterioration in the parameter measurement would not be inconsistent with the planned use of the data. Again, the original bit stream can be recorded and transmitted postpass, for more detailed analysis.

Data compression programs are being readied for use with the Skylab program because studies and test have indicated that certain types of data can be "compressed" by significant ratios without data quality deterioration. For example, tests have shown that Apollo Command/Service Module data can be compressed by a ratio of 20 to 1. In addition, the Orbiting Astronomical Observatory (OAO) project has been using compression techniques at several stations where special computers have been installed for this purpose.

Data compression basically involves the removal of most of the redundancy in the data stream so that only a minimum number of bits are required to send the information over the data line. A compatible program must be used at the receiving center to interpret the compressed data.

i. National Aeronautics and Space Administration Communications Network (NASCOM). The NASCOM is a global system established and operated by NASA to provide long-line operational communications support for all NASA projects. The network provides for voice, data, and teletype communications between all ground stations and the appropriate operations and control centers. It also provides for television and other wideband transmissions from selected stations. The network includes land lines, submarine cables, microwave and satellite links, and necessary terminal and switching facilities. In general, geographically diverse routes have been established from each station where possible so that no total communications loss will occur if the primary route fails.

The NASCOM provides a system of full period leased voice circuits (nominal 3-kHz bandwidth) to virtually all station and terminal points in the NASCOM network. Essentially all voice/data circuits are routed either directly to the Goddard Space Flight Center (GSFC) switching, conferencing,

and monitoring arrangement (SCAMA) or through various overseas NASCOM switching centers where conferencing, monitoring, and test facilities are available. The voice links interface with air-to-ground voice equipment at manned flight support stations to support spacecraft voice communications in addition to the general mission support services.

In general, the voice/data circuits are conditioned and tariffed so that they may be switched easily to provide either voice or data communications.

High-speed data modem (called modem for modulator-demodulator) sets are provided at all STDN stations. Modems at STDN stations operate at 4800 bps or 7200 bps for transmission of telemetry data and at 2400 bps (different modems) for transmission of high-speed tracking data. By the third quarter of the calendar year 1972, the telemetry transmission rate was to be standardized at 7200 bps.

Analog data may also be transmitted over the 3-kHz voice/data lines either directly or using multiplex equipment described in the section on telemetry. TV channels for transmission of manned flight telecasts are leased as required.

C. Communications

With the ground station system now defined, the LST onboard communications system must be examined. This system receives all commands from ground and sends them to the data handling system for processing. In addition, all engineering and experimental data are routed to this system for transmission to ground.

1. Antenna Configuration Analysis. The operational requirement that the telescope be capable of pointing to any object in the heavens presents a major problem for the antenna subsystem. A near omnidirectional antenna coverage is required at a rather short wavelength, 6.35 cm (2-1/2 in.). The size of the vehicle and the solar array prevents a single antenna from radiating a spherical pattern. Several antennas located so that at least one would be in a favorable position with respect to the earth station is the only solution. However, there must be no multipath or other interference. To provide multiantenna coverage without interference some type of isolation (either phase, frequency, or space separation) must be used.

The shape and size of the spacecraft plays a major role in the location of the antennas. In this case the spacecraft is characterized as a cylinder with movable flat wings.

a. Antenna Configuration Tradeoff. Figure V-3 shows one possible antenna configuration for full 4π sr coverage. Four antennas would be located around the circumference of the cylinder midway from the end. Each of these four would be separated by 90 degrees. One antenna would be required at each end of the cylinder. Electromagnetic isolation must be used to prevent interferometer nulls. The two most commonly used techniques are frequency and polarization isolation. The ground station may be able to provide right- and left-hand circular polarization and transmit on two frequencies simultaneously. However, this still leaves two antennas that are not isolated.

Another possible antenna configuration places an antenna at either end of the cylinder (Fig. V-4). At least one antenna would be on a boom to insure overlapping coverage for the case when the axis of the cylinder is normal to the LOS to the tracking station. The advantage of this scheme is that either polarization diversity or frequency diversity could be used since only two antennas would be involved. If it were not for the solar array panels, this scheme would provide good coverage with a minimum number of antennas. However, the presence of the solar arrays could preclude overlap of the patterns and thus result in a serious null in the plane of the solar panels.

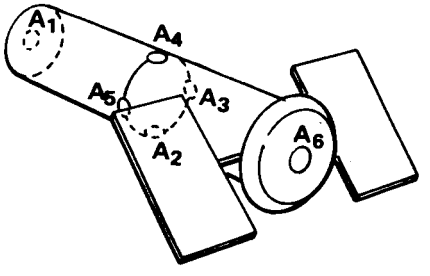

Figure V-3. Antenna configuration no. 1.

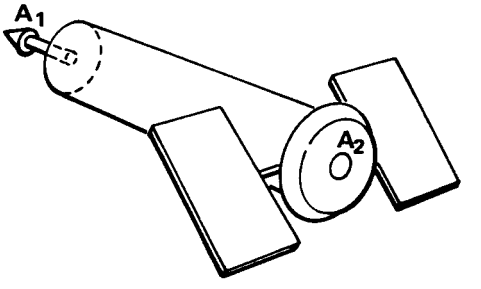

Figure V-4. Antenna configuration no. 2.

A third configuration would use two antennas 180 degrees apart on the cylinder body with one positioned on a boom and the other body mounted (Fig. V-5). Again, the solar panel could cause interference nulls in the

pattern coverage. The solar array apparently plays a larger role in the antenna location than any other factor. Therefore, it seems appropriate to try to find a location that minimizes this impact.

Figure V-6 shows a configuration that utilizes the solar arrays as antenna "booms." Here the antennas are positioned a considerable distance from the spacecraft. While both the telescope and solar arrays will no doubt have some impact on the resulting antenna pattern, this configuration provides a better coverage than either of the configurations shown in Figures V-3 or V-4.

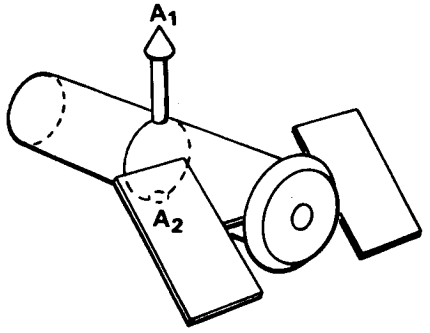

Figure V-5. Antenna configuration no. 3.

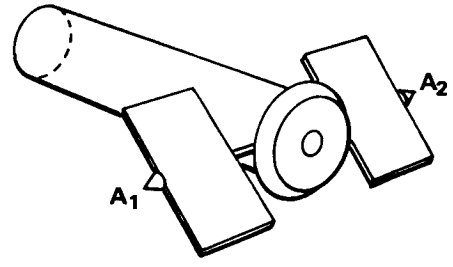

Figure V-6. Antenna configuration no. 4.

b. Antenna Pattern Tests. The uncertainty of the antenna performance in the presence of the solar array prompted the building and testing of a scale model. The conical spiral antenna was selected because the basic pattern is cardioidal in shape. A full-scale antenna was fabricated and tested at 2300 MHz to serve as a reference for the one-fifth scale model, which should have the same shape pattern except that it must radiate at 11 GHz. The one-fifth scale model antenna is shown in Figure V-7.

The test pattern for the full-scale antenna very nearly approached the theoretical cardioid shape. Extreme difficulty was experienced trying to duplicate this shape using the 11 GHz antenna. These two patterns are shown in Figures V-8 and V-9. The pattern shape of the smaller antenna was not symmetrical. Although this is a significant problem with very high frequency systems, its significance is reduced in the lower frequencies as evident in the 2300 MHz reference pattern.

Figure V-7. One-fifth scale model conical spiral antenna frequency — 11.0 GHz.

The test antenna was mounted on the tips of a scale model spacecraft and placed on the rotary table of an antenna range. The basic test setup is depicted by the artist's sketch in Figure V-10. Since the actual spacecraft would use two identical antennas, only a single antenna was used for the tests. In the case where the second antenna would be required, a composite pattern was devised using a mirror image of the single antenna pattern as the second antenna. The model can be rotated in azimuth by the

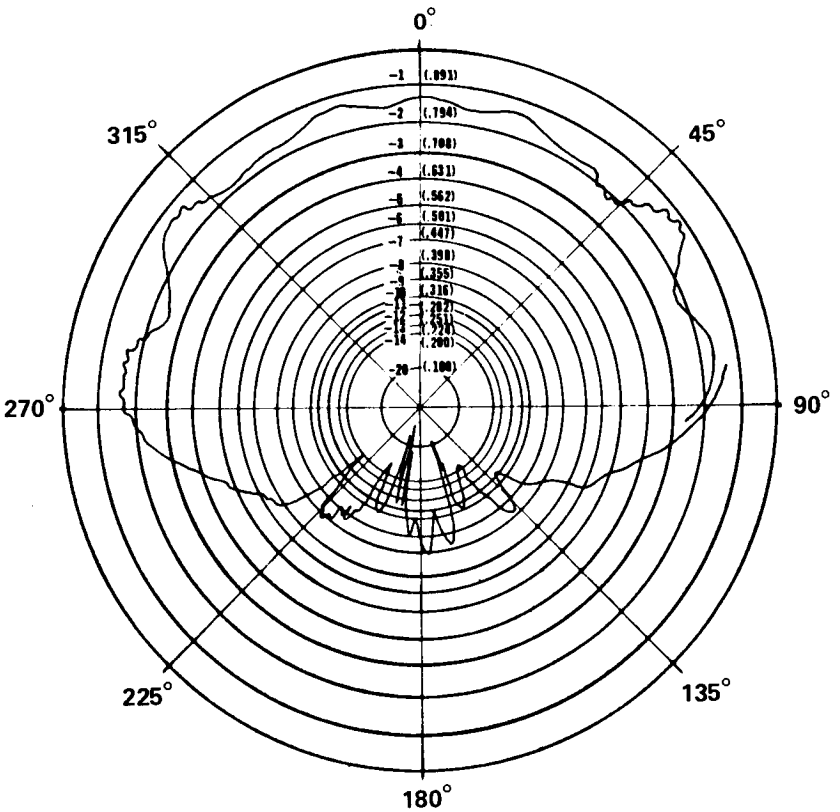

Figure V-8. Two-GHz antenna reference pattern.

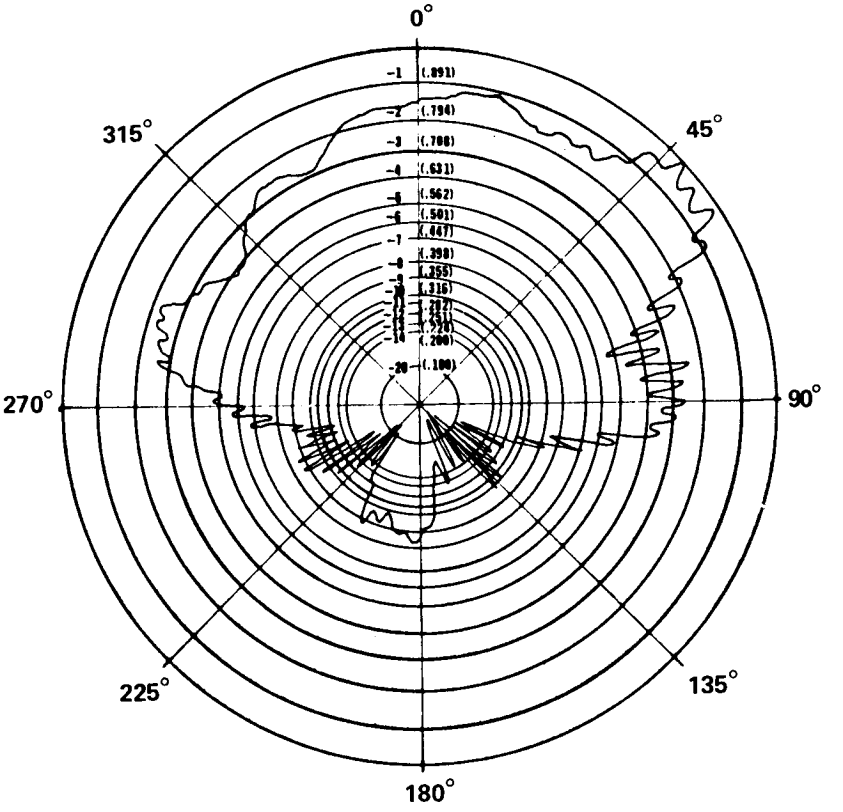

Figure V-9. One-fifth scale model reference pattern (11 GHz).

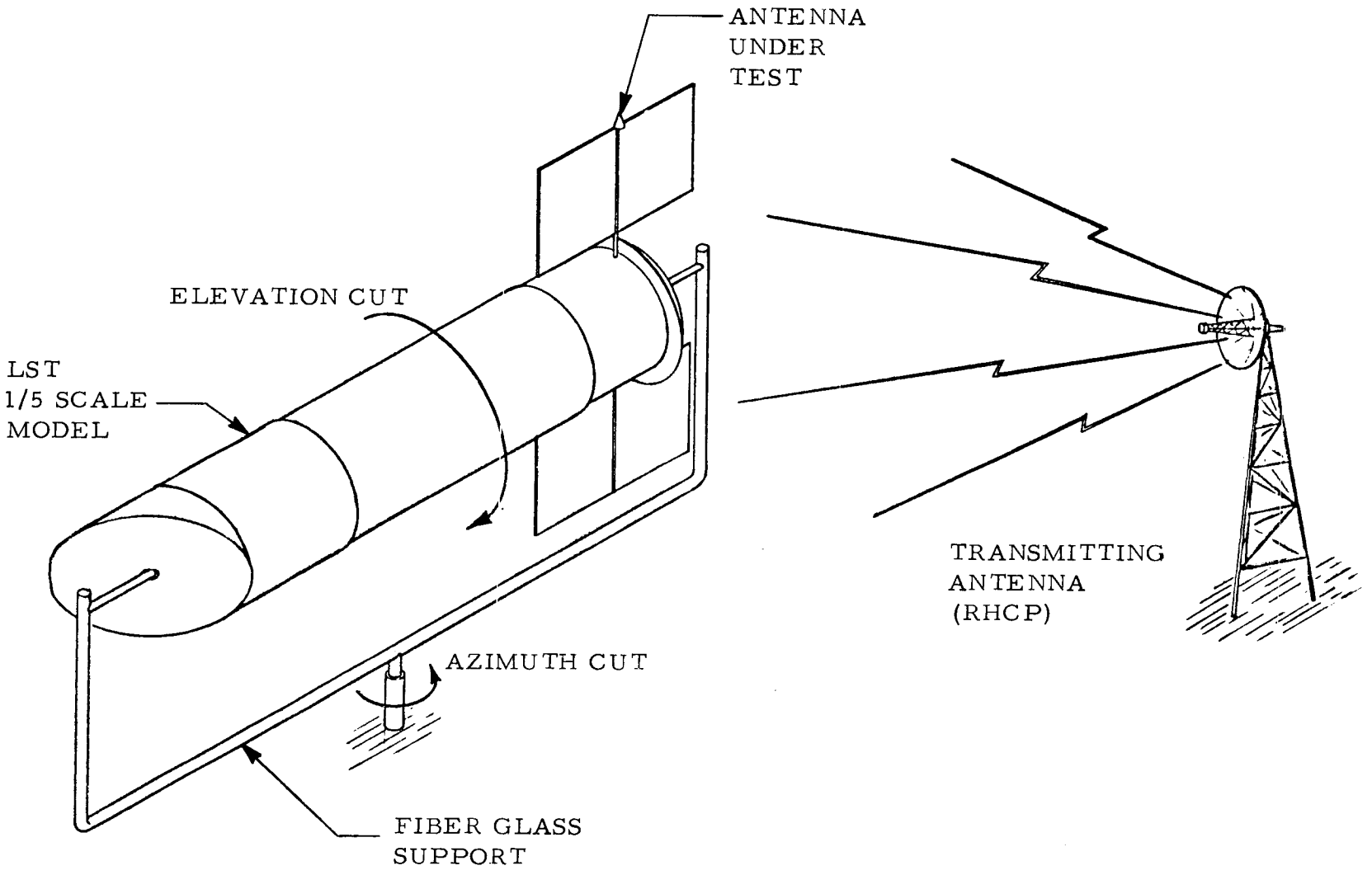

Figure V-10. Antenna pattern measuring arrangement.

turntable and can be rolled through 360 degrees in small increments and measurements made at each increment. The test antenna was used in a receive mode while the reference system transmitted at a known level. The entire operation was computer controlled. The solar array was placed in three positions (Fig. V-11). In the first position the plane of the solar array lies in a plane containing the long axis of the telescope. In the second position the plane of the array made an angle of 45 degrees with the plane passing through the axis. In the third position the solar array is 90 degrees to the long axis. Two patterns are shown in Figures V-12 and V-13. The influence of the solar array can be seen by examining two cases in the azimuth cut, with the panels parallel to the LST and at 45 degrees with the LST. The polar plots indicate a fairly uniform pattern. The area on the left side of the pattern is slightly diminished because of the characteristics of the test antenna and not the presence of the spacecraft. At about 40 degrees in a clockwise direction in the 45 degree solar array pattern (Fig. V-14), there is about a 5 dB null, which occurs again at 220 degrees. This appears to be due to solar array shadowing. With the solar panels parallel the elevation cut requires a composite pattern to analyze the basic design (Fig. V-15). Nulls of -8 dB appear at 5, 140, 220, and 355 degrees. These deep nulls are attributed to the characteristics of the test antenna and would not be present in the full-scale spacecraft configuration.

The data are plotted in a rectangular coordinate system (Fig. V-16) to show the ability of the antennas to provide 4π sr coverage. The areas have been coded to indicate pattern intensity. Again a composite was made to simulate two antennas, one on the end of each solar array. The codes cover a range from 0 to -6 dB. Below -6 dB is indicated by the clear. The area of the clear is extremely small (≈ 10 percent). The area covered becomes nearly 100 percent if the -8 dB level is considered. Two clean areas in the upper portion of the dark areas running from left to right appear to be due to fiberglass supports that hold the spacecraft model. The clear areas at the center that run vertically are due to improper overlap. The clear areas in the upper left and upper right are due to the poor shape of the test antenna. This would not be present in a full-size spacecraft.

The conical spiral antenna has proved to be a very good choice for boom mounting because its circularly polarized hemispheric coverage does not require a ground plane. With the solar panels retracted, the antenna centerlines are perpendicular to the spacecraft axis. This permits the establishment and maintenance of communications when the solar panels are not deployed. As the solar panels are deployed, the antennas will rotate to maintain the cone centerline normal to the spacecraft axis.

With only two antennas, both frequency and polarization diversity schemes can be considered. The hardware needed to implement each of these two schemes is given in Figures V-17 and V-18.

Frequency diversity seems to be much more complex because it requires two additional transmitters. However, the power should be comparable since the output of each of the transmitters in the polarization scheme must be double that for frequency diversity (each transmitter must drive two separate antennas). It may be that doubling the RF output power at these very low levels does not result in a doubling of the weight or primary power. This is not a serious consideration because of the small amount of weight in either case. Of prime importance is the capability of the ground station. Dual polarization transmission does not presently exist. Dual frequency operation is standard in the Apollo mission. A dual USB site is capable of receiving four frequencies or downlinks simultaneously. Therefore, to be sure of a feasible operation, some form of frequency diversity seems mandatory. If redundancy for each of the four transmitters in the frequency diversity case is required, the weight becomes a factor. However, this can be eliminated and ground operation simplified by reducing the number of links to two if a switch is added that connects both the transmitters to the antenna that has the strongest received signal (Fig. V-19). Thus, switched frequency diversity has been chosen for the design reference.

2. Reference Communications Configuration. The reference communications configuration shown in Figure V-20 consists of two unified S-band transponders, an Apollo Block II type called the engineering data transponder and a modified ERTS transponder (proposed for the HEAO-C) called the scientific data transponder. The engineering data (PM-FM) transponder and scientific transponder combination provides a flexible communications system. The PM receiver-transmit capability of the engineering transponder is required for tracking to match the ground station PRN ranging capability in the PM mode. The transponder also provides the PM data downlink for command verification, spacecraft housekeeping, and slow speed television data. The scientific transponder provides the high data rate (1 megabit/sec) downlink for the star field camera data.

The reference system uses four frequencies, two for the frequency diversified uplink and two for downlinks. Redundant information is sent from the ground to the LST on the two uplink frequencies. One of these frequencies is received through one of the antennas by the active receiver in the engineering transponder (the other receiver is in a standby condition) and sent to the PSK demodulator assembly in the data management equipment. The other uplink frequency is received through the other antenna by the active receiver in the

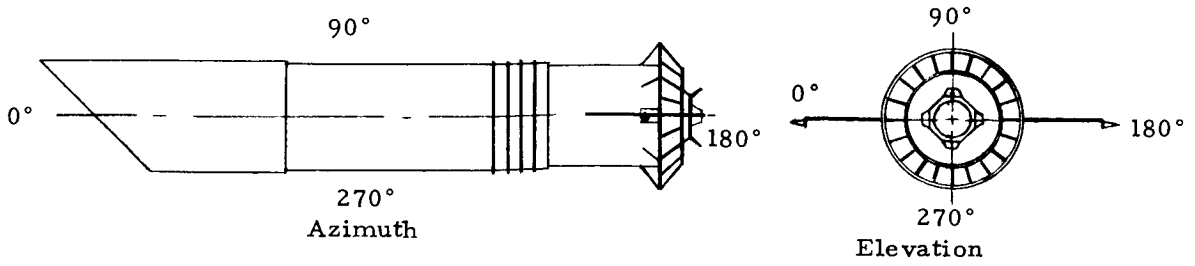

a. Case 1 (solar panels parallel to LST axis).

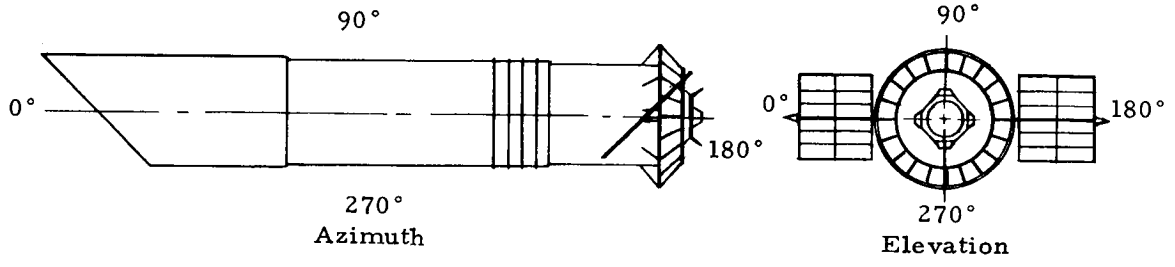

b. Case 2 (solar panels at 45 degrees with LST axis).

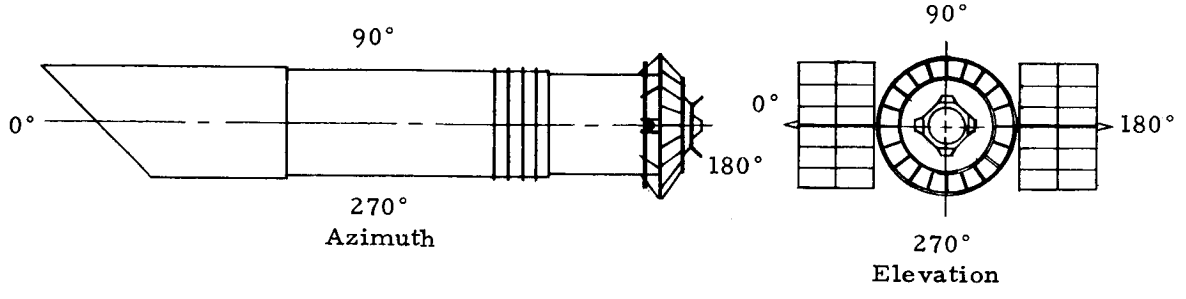

c. Case 3 (solar panels at 90 degrees with LST axis).

Figure V-11. Solar array positions.

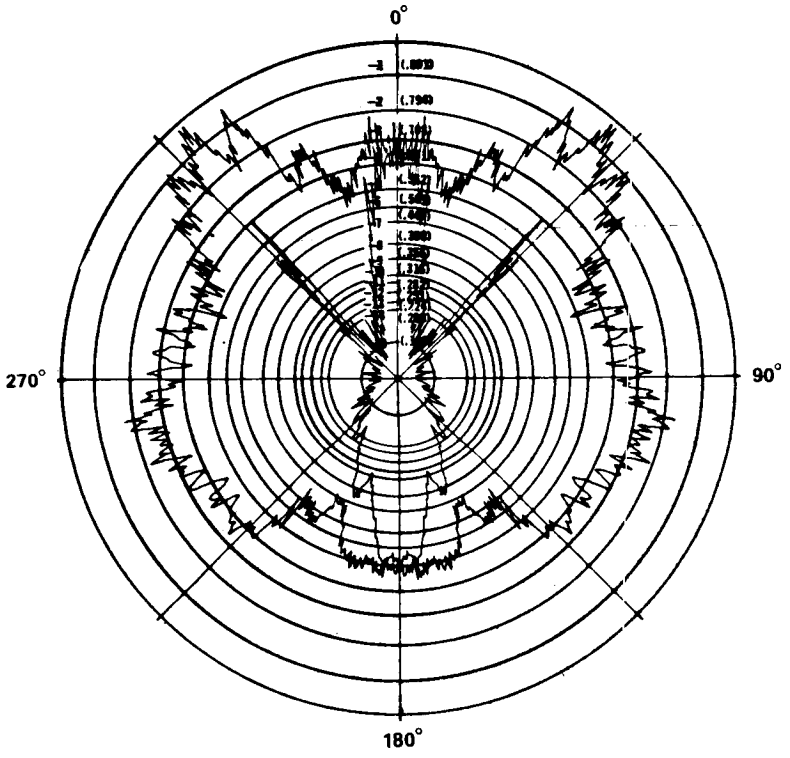

Figure V-12. Solar panels parallel elevation cut.

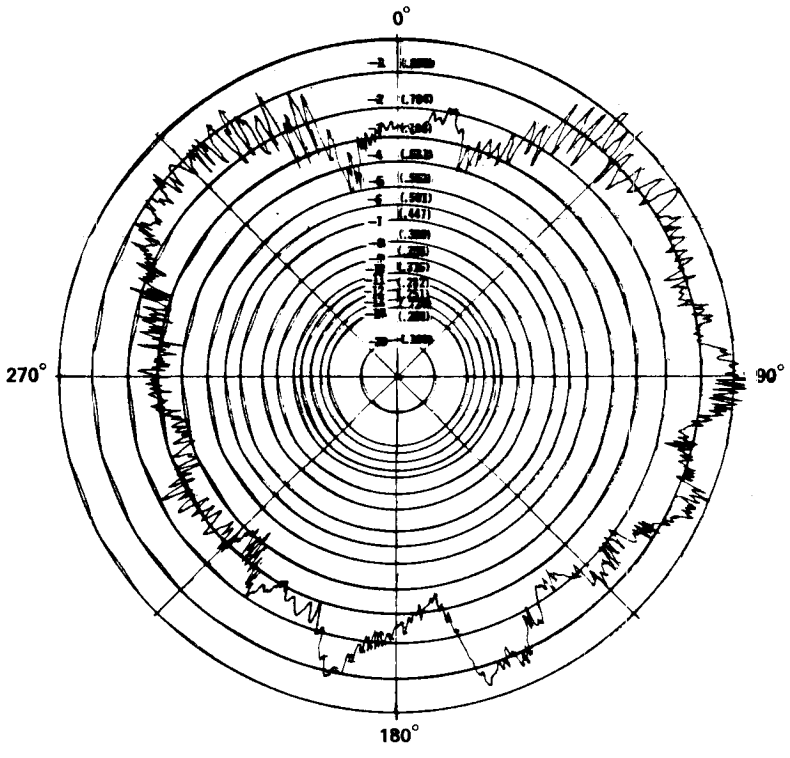

Figure V-13. Solar panels parallel antenna pointing up azimuth cut.

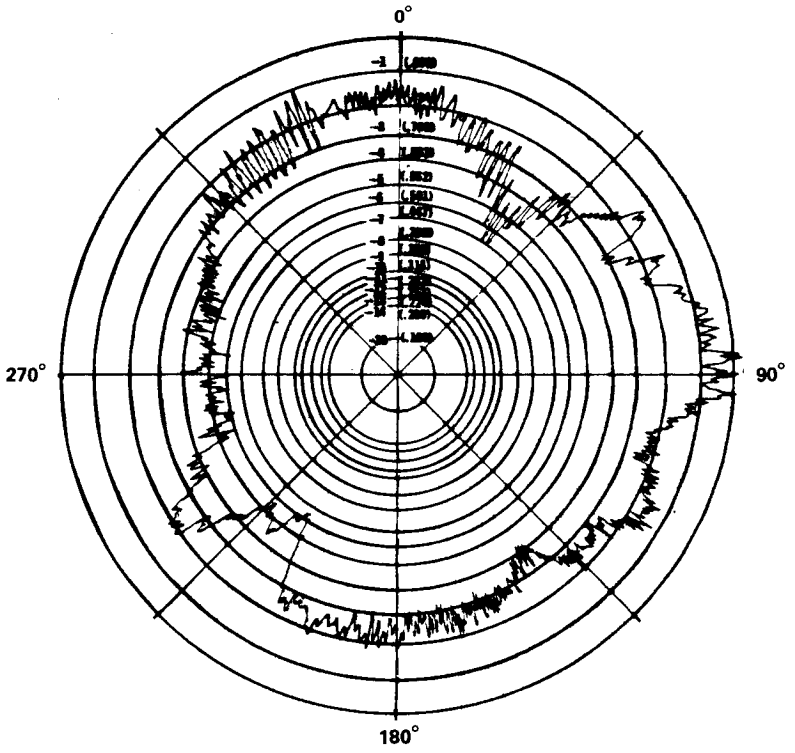

Figure V-14. Solar panels 45 degree antenna pointing up azimuth cut.

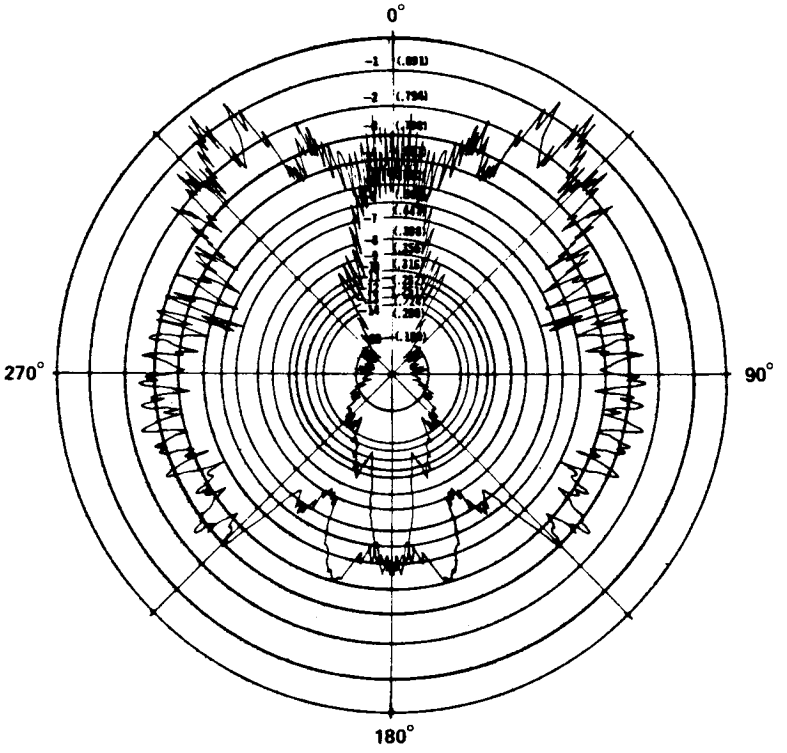

Figure V-15. Composite solar panels 45 degree elevation cut.

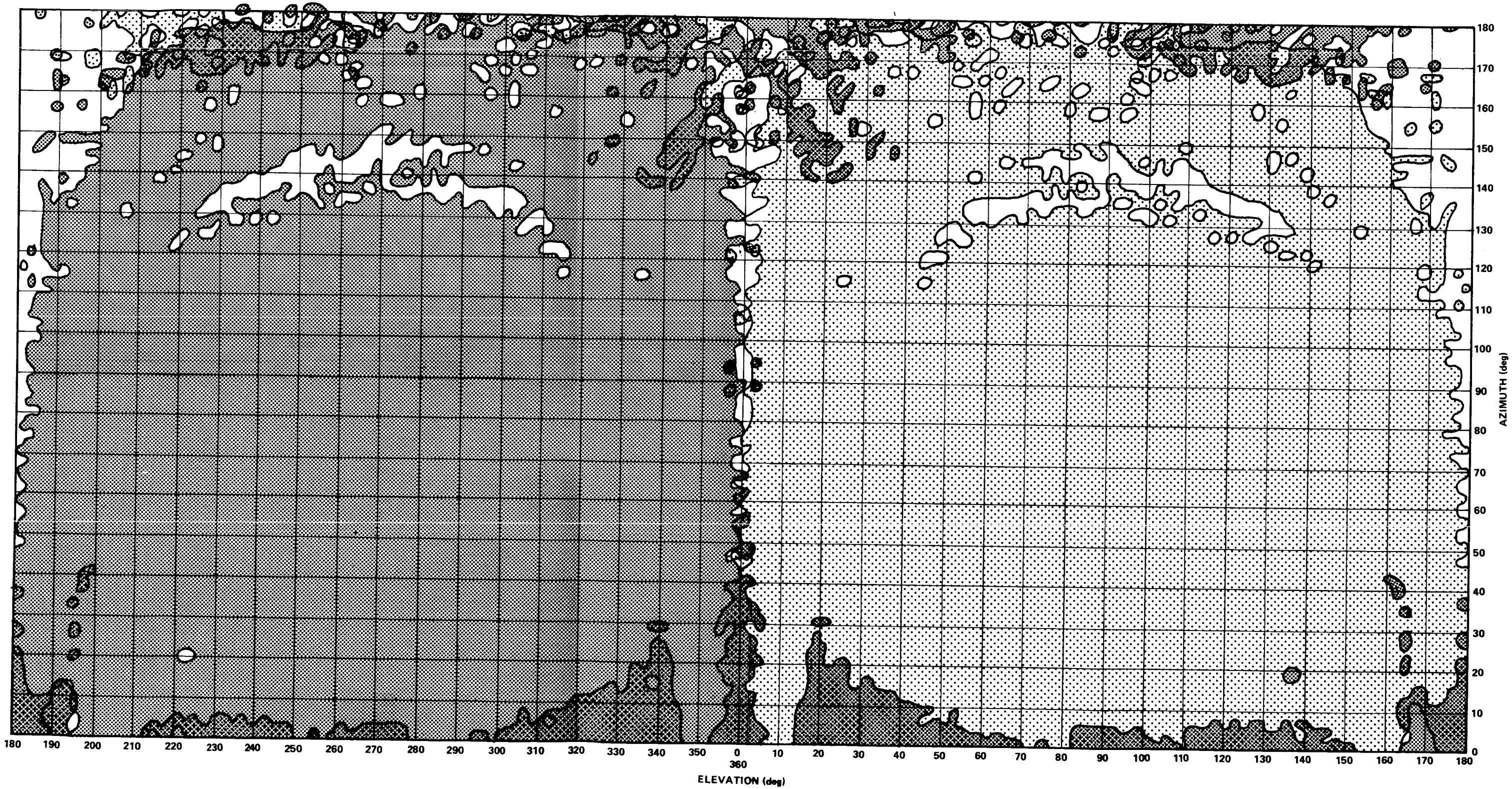

Figure V-16. Antenna coverage in rectangular form.

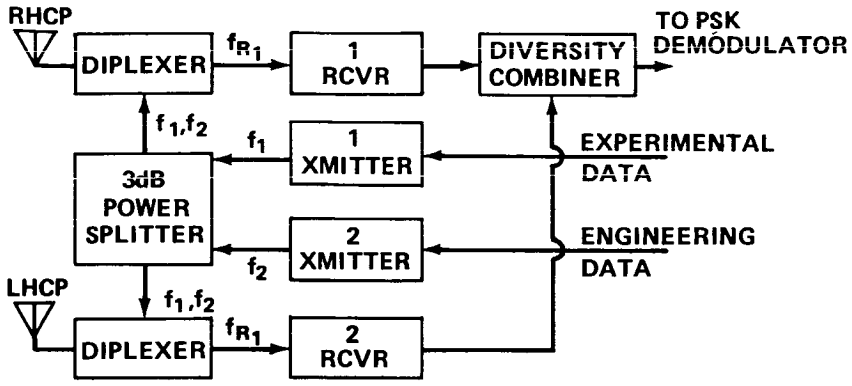

Figure V-17. Polarization diversity.

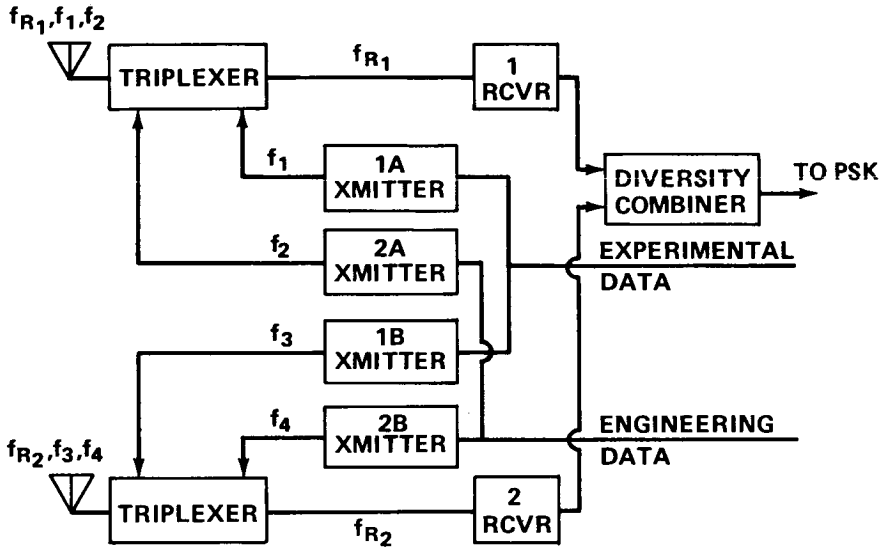

Figure V-18. Frequency diversity.

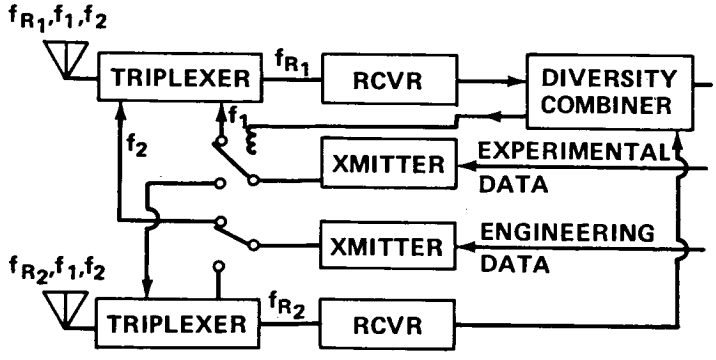

Figure V-19. "Switched" frequency diversity.

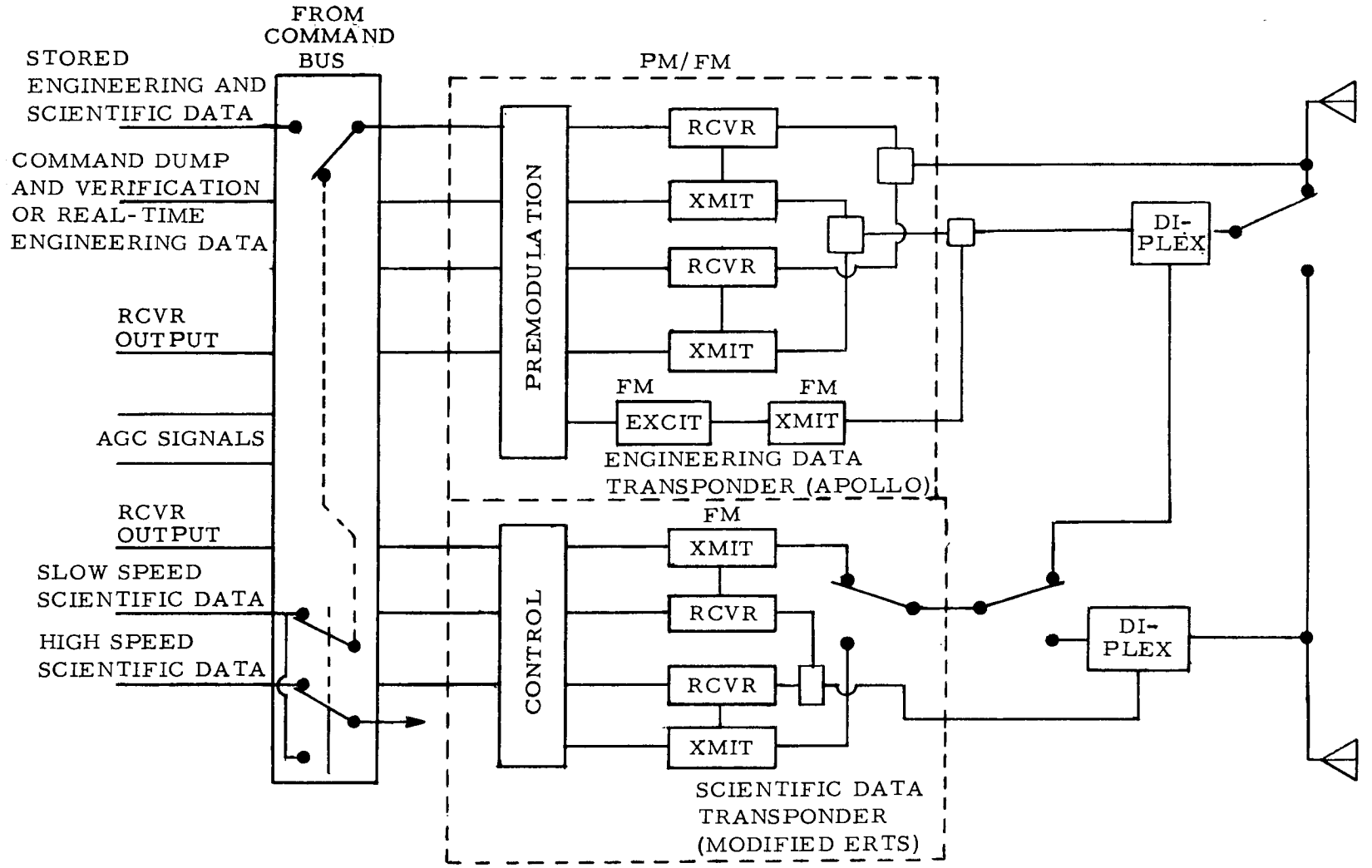

Figure V-20. The baseline communication system.

scientific transponder (one receiver is on standby) and also sent to the PSK demodulator assembly. This assembly uses the signal of highest strength and sends signals back to the communications equipment to switch both transmitter outputs to the antenna feeding the receiver with the highest automatic gain control (AGC) signal.

a. The Engineering Transponder Downlink. The engineering downlink consists of a baseband assembly, an active and a standby PM (phase modulated) transmitter, and an FM (frequency modulated) exciter and transmitter. Only one of the three transmitters can be used at any one time. The active transmitter feeds a diplexer that is switched to drive the proper antenna.

Real-time LST status, diagnostic, and command verification data are sent to the ground stations using a 1.025 MHz subcarrier transmitted on an active PM transmitter. The baseband of an active PM transmitter can be used for several purposes. In normal operations, the PM baseband is used to transmit stored LST spacecraft status and diagnostic data, a pseudo-random ranging signal, or a command storage dump. The PM baseband may also be used as a backup mode for the transmission of experiment data when it is not required for normal housekeeping operation.

When the engineering PM transmitters are not being used for transmission of spacecraft data, the FM transmitter can be used as a slow scan television data link from the slit jaw camera for ground station quick-look.

b. The Scientific Data Downlink. The scientific data downlink consists of two FM transmitters, one active and one on standby. The output of the active transmitter can be switched to one of two diplexers which feed the two spacecraft antennas. The modified ERTS transponder is dedicated to the transmission of scientific experiment pulse code modulated (PCM) data at a rate of up to 1 megabit/sec. This rate corresponds to the current single downlink capacity to ground stations for NRZ data streams. The ERTS transponder may also be used in a backup mode to transmit the FM video signal for slow-scan television coverage.

3. Operating Modes. There are several modes of operation of the communications equipment to provide normal mission operational requirements and backup should a primary mode of operation fail. The nominal modes are depicted in Figure V-21. The reference system has growth capacity for sending additional experiment data through the engineering link when desired.

	MODE	SPECTRAL DISTRIBUTION	DESCRIPTION
DOWNLINK	A1	PRN, 1.024 MHz, fc	PRN RANGING REAL TIME DATA 51.2 kbs/sec ON 1.024 MHz SUBCARRIER
	A2	fc, 1.024 MHz	STORED DATA ON BASEBAND REAL TIME ON 1.024 MHz SUBCARRIER
	B		1 MHz NRZ EXPERIMENTAL DATA ON BASEBAND
UPLINK	1		ACQUISITION
	2	70 kHz	COMMANDS ON 70 kHz SUBCARRIER
	3	PRN, 70 kHz	PRN RANGING COMMANDS ON 70 kHz SUBCARRIER

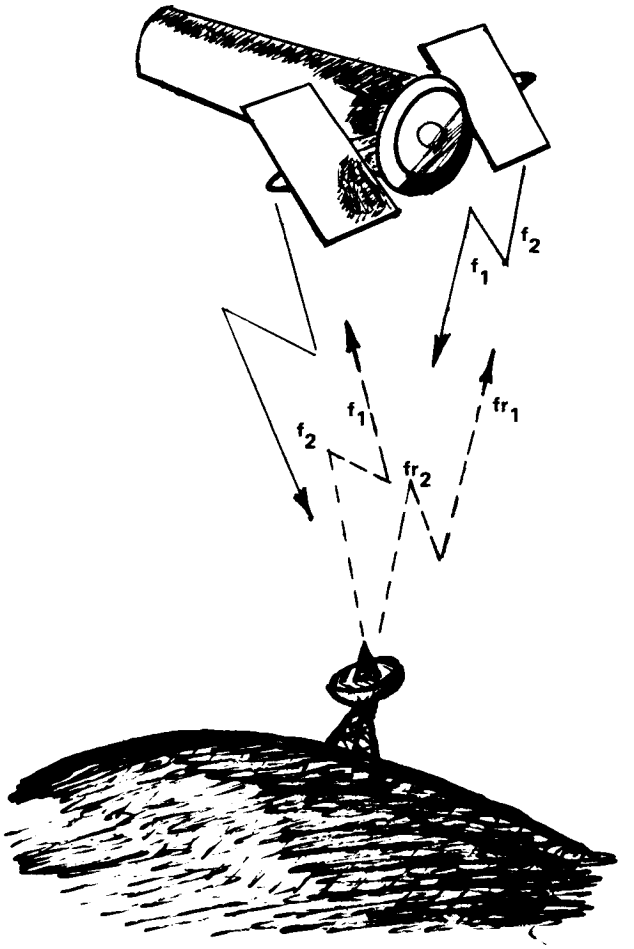

Figure V-21. Communications modes.

a. Uplinks Modes. Basically there are three uplink modes of operation (Fig. V-21). In the first mode (Mode 1) only the ground station carrier is transmitted to acquire tracking. The downlinks respond and the 0.9144 m (3 ft) antenna is used to locate the position of the spacecraft for ground station lockup of the antenna. Mode 2, the mode most often used, consists simply of commands transmitted on the 70 kHz subcarrier. In Mode 3, pseudorandom noise (PRN) ranging will be handled on the baseband in addition to the commands coming up over the 70 kHz subcarrier.

b. Downlinks Modes. The many downlink modes provide a very flexible and adaptive system which will be necessary for a long duration mission. In Mode A2 the PM transmitter sends stored LST spacecraft and diagnostic data on its baseband and real-time LST spacecraft and command verification data on a subcarrier. A command storage dump may also be executed over this PM transmitter. Scientific experiment PCM data are transmitted through the modified ERTS FM transmitter. Commands are received on the receiver with the higher AGC signal. This is the primary mode of operation. Mode A1, the tracking mode, is similar to Mode A2 except that the PRN ranging signal is transmitted on the PM baseband in place of stored spacecraft data. This is a required mode of operation during tracking. Mode B is the normal operational mode of the scientific link. It consists simply of PCM-FM modulation on the carrier. The data rate of 1 megabit/sec is well within the assigned bandwidth and should result in a very high-quality signal without intermodulation products from the subcarrier, etc.

c. Alternative or Contingency Modes. In addition to these primary modes there are alternative or contingency modes yielding increased system flexibility. The alternative mode is included for the transmission of tube data from the slit jaw camera. Here, slow-scan television replaces the stored spacecraft data transmission of the primary mode but uses the Apollo FM exciter and transmitter instead of the Apollo PM transmitter. There is also a contingency mode which provides for experiment PCM data normally transmitted by the ERTS FM transmitter to be sent through the PM transmitter on its baseband frequency. Real-time LST spacecraft data and command verification would use the subcarrier of the PM transmitter. Another contingency mode exists for use when the Apollo Block II type equipment is inoperative. The ERTS receiver can be used to receive commands to control the spacecraft or switch in standby Apollo transponder equipment.

D. Data Handling

The design reference data handling configuration shown in Figure V-22 contains all the equipment required to manage the flow of data to and from the LST, SIP, and SSM. This includes the receipt, processing, and execution of real-time and stored commands; the processing, formatting, storage, and forwarding for transmission of all diagnostic and status information from all LST systems and subsystems, and the routing of scientific data for transmission to ground stations.

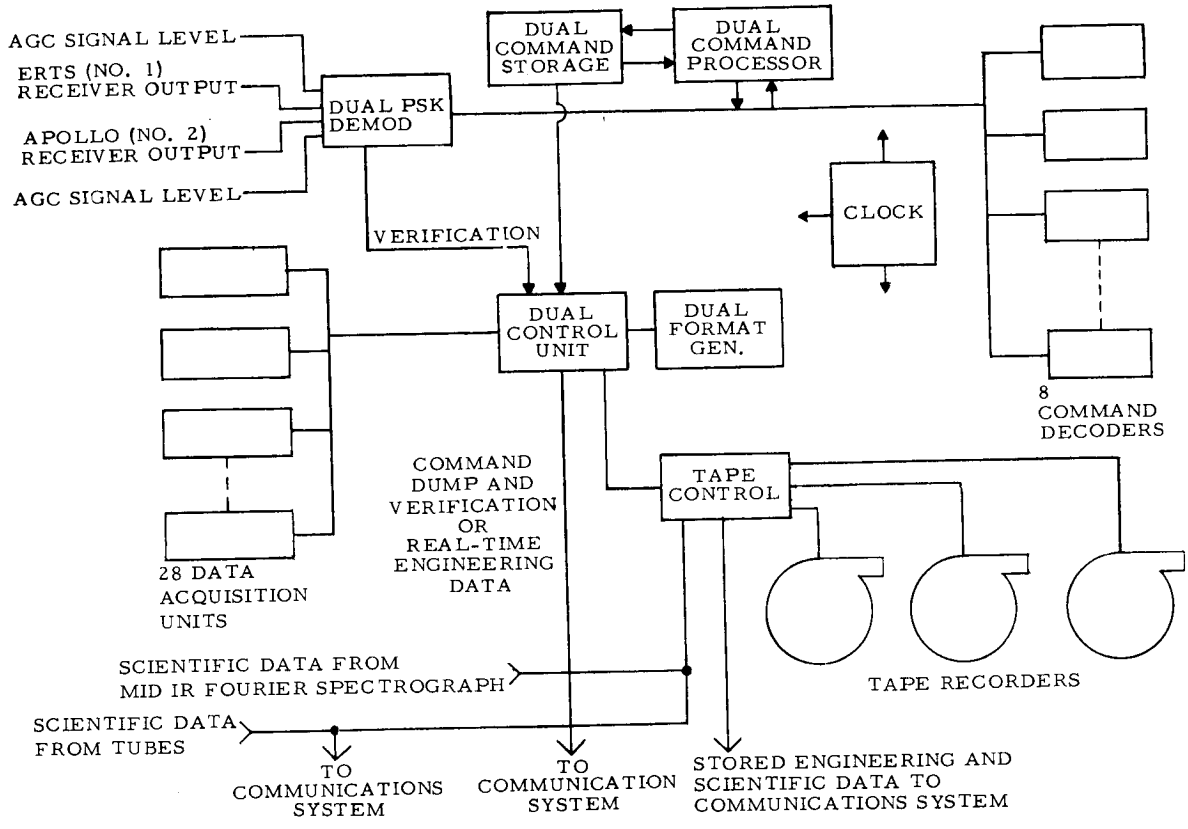

Figure V-22. Data handling system.

1. Command Distribution System. Command signals from the two active receivers (one engineering and one scientific transponder) enter the PSK demodulator assembly. This assembly selects the channel with the strongest AGC signal and sends a switching signal to the antenna switch so

that transmissions will be routed to the antenna receiving the strongest signal from the ground. The antenna switch can also be controlled by command from the ground stations. The commands are in the form of five sub-bits per information bit. Each command is checked for consistency with the command repertoire prior to verification to the ground through the control unit and communications equipment.

a. Word Format. The word format for LST commands is given in Figure V-23. A 2-bit vehicle address code is sent with each command. If the command has the proper code for the LST, a pulse is sent to the command processor and command decoders indicating that the following bits are either a real-time or stored command for the LST. Real-time commands contain 11 bits, a 3-bit address for the command decoders and an 8-bit command text. Stored commands contain 28 bits, which include a 17-bit time tag specifying at what time the command is to be executed. This time tag allows an accuracy of one part in 131 072 for command execution time, thus permitting a resolution of 1 second in a 36-hour period.

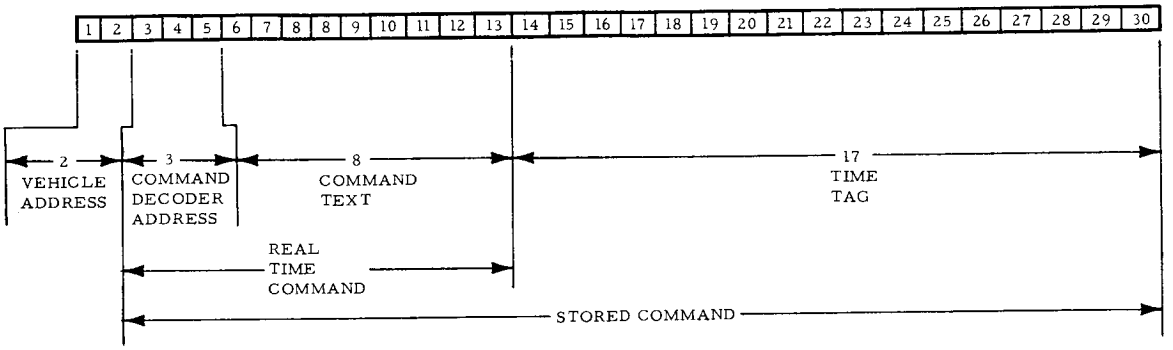

Figure V-23. LST command word.

b. Command Processor/Memory. All LST commands must be routed past a special-purpose unit located in the SSM called the command processor (Fig. V-24). The purpose of this unit is to inspect all commands and determine whether they are real-time or time-tagged commands. The 11-bit long real-time commands are not acted upon by the processor and are sent directly to the command decoders. Whenever a time-tagged command is recognized, the command processor stores the command in the next available write address of the plated wire command memory for later execution.

The command memory with a capacity for 4096 words of 28-bit length is continually read in cycles. As each word is read it is put into

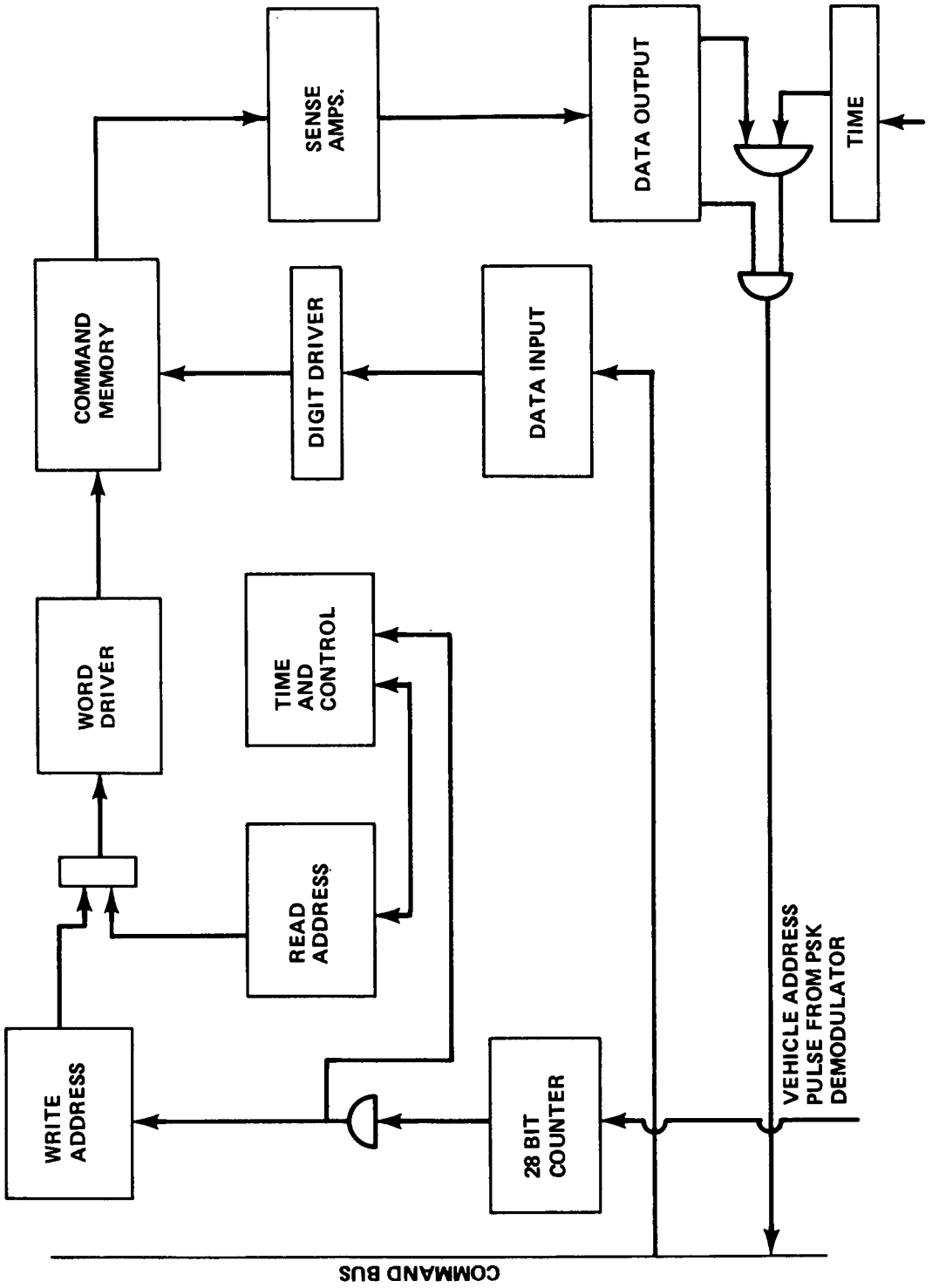

Figure V-24. Command processor.

an output buffer where its time tag is compared with the vehicle clock (Fig. V-24). If the time tag and clock agree, the 11-bit command is gated onto the command bus and acted upon as a real-time command.

c. Command Decoders. The 11 bits that are sent to the command decoders from the command processor are clocked serially into a register within each decoder. However, only the one decoder with the proper 3-bit address code can act upon the 8-bit command. What happens to this 8-bit command once it is accepted by the proper command decoder is a function of the location of the command decoder. In some cases the command may be left in digital form such as commands that are sent to the ASC computer. Other cases will require the 8 bits to be converted to an analog signal.

The 3 bits allotted for command decoder address allow eight decoders to be addressed. Eight redundant decoders are also included for increased reliability. The 8-bit command gives each decoder a repertoire of 256 different commands for its assigned equipment. The allocation of the decoders is given as follows:

Addressable Decoders	Total Including Redundancy	
2	(4)	ACS
1	(2)	Electrical Distribution
1	(2)	C & DH
1	(2)	Power
1	(2)	OTA/Fine Guidance
2	(4)	SIP
8	(16)	Total

Should it be determined that more than eight addressable decoders are needed, a bit will be removed from the time tag and added to the decoder address. With a 4-bit decoder address, 16 command decoders could be addressed. The price that must be paid for this increased number of addressable decoders is a loss in time resolution for command execution. A 16-bit time tag can resolve one part in 65 536 or approximately 1 second in 18-hours whereas the 17-bit time tag could resolve 1 second in a 36 hour period.

2. Data Acquisition System. The Data Acquisition System accepts both analog and digital data (status and diagnostic) from the OTA, SIP, and SSM equipment. These data can be handled in one of two modes. In the real-time mode the data are taken directly from the data acquisition units (DAUs), formatted, and sent to ground at a rate of 51.2 kbs. In the stored mode, data are stored on magnetic tape at a rate of 1.6 kbs until time for transmission to the ground stations at the 51.2 kbs rate.

a. Data Acquisition Units (DAU). The conceptual design of the DAUs needed to meet the LST format requirements is compatible with state-of-the-art technology in the field of remote multiplexing units. Each DAU is capable of addressing 64 lines, which may contain either analog or digital data. Digital data are received in parallel form by addressing eight lines containing discrete inputs. When a single line containing analog data is addressed, the analog sample is converted to an 8-bit digital word within the DAU. Analog inputs must be conditioned by the user to a 0 to 5 volt scale. It has been estimated that 28 of these DAUs would fulfill the LST requirements. These DAUs have been tentatively allocated as follows: SIP, 12; SSM, 10; OTA, 6. In the SIP it is desirable to have one DAU per instrument if possible to provide flexibility for future growth, and to facilitate instrument repair and replacement. However, both the number and location of the DAUs are certainly subject to change during the later phases of the LST study.

b. Control Unit/Format Generator. The control unit/format generator combination supervises the multiplexing of all engineering data. The control unit addresses lines within each DAU. Data from these lines are formatted by the format generator and either stored on tape or sent real-time to the ground. These two units are capable of handling several formats of data acquisition.

Each address initiated by the control unit results in a word of data for the format generator. In the stored mode 200 8-bit words constitute a frame of data that is stored on tape. Four of these 200 words (32 bits) are allocated for frame synchronization. The frame rate for this mode is 1 frame/sec, yielding a data rate of 1.6 kbs. This stored data can be played back 32 times faster than it is recorded, giving a 51.2 kbs transmission rate to ground. In the real-time mode the frame length is shortened to 128 words (still using 32 bits for synchronization) and the frame rate is increased to 50 frames/sec. This yields the 51.2 kbs transmission rate.

Each frame of data is composed of words or samples that are acquired or sampled at various rates. The three primary sampling rates are

1 sample/sec, 5 samples/sec, and 10 samples/sec. Table V-7 gives an approximate list of how many measurements are required within each LST subsystem and at what rate these measurements are sampled.

TABLE V-7. APPROXIMATE MEASUREMENT LIST.

LST Subsystem	Sample Interval (sample/sec)	No. of Measurements
Structure	5	30
Power	5	115
C & DH	5	100
Altitude Sensing and Control (AS & C)	5	142
	1	111
OTA	10	204
	1	62
SIP	10	20
	1	100

c. Tape Storage. Upon examining the tape system needed for storing data from the DAUs, one finds that several manufacturers have magnetic tape machines capable of recoding at the rate of 1.6 kbs. Past experience with unmanned spacecrafts indicate that they may go as many as three to four orbits in which a ground contact is not made because stations are out of operation for maintenance, other spacecraft are being launched, or because of a malfunction. A review of the stations selected for the mission simulation indicates that if certain stations should be out of operations, it might be two or three orbits before a tape recorder could be dumped to the ground. The orbital period is 96.9 minutes, resulting in about 291 minutes of data to be

played back during a single contact. Partial playbacks are not desirable. The average contact time is 11.00 minutes. Allowing time for spacecraft acquisition and tape recorder turn-on, the actual playback period is approximately 10 minutes. The ratio of record to playback would be about 30:1. A ratio of 32:1 results in a playback bit rate of 51.2 kbs, which is the standard bit rate for the ground station. The ratio 32:1 is very reasonable.

The reference design tape system used for storing data from the DAUs contain three tape units. For reliability only one track of data will be recorded per tape. The width of the tape is 0.636 cm (1/4 in.) and each unit will contain 7×10^2 m of tape. The recording tape speed will be 4.76 cm/sec (1.275 in./sec). Using this tape speed at a data rate of 1.6 kbs yields a bit packing density of approximately 336 bits/cm (850 bits/in.).

Figure V-25 shows the combined C & DH system for the LST.

3. Scientific Data Handling. Scientific experimental data will be gathered from the instruments contained within the SIP primarily by utilizing TV tubes as sensors. With TV sensors the electronic image from the sensor's target may be read sequentially, coded digitally, and transmitted to ground over the scientific transponder at a maximum rate of approximately 1 megabit/sec.

When considering the selection of an image tube for the LST, it should be noted that each instrument has its own requirements. The matching of the detector to the instrument for the best possible resolution, signal to noise (S/N) ratio, and high data collecting efficiency is the main objective. Desirable criteria for the tube are as follows:

1. Long Integration Time.
2. High Internal Gain.
3. Good Resolution at 50 percent Modulation Transfer Function (MTF).
4. Large Storage Capacity.
5. Large Format Size.
6. Low Internal Noise Background.
7. Space Qualified.

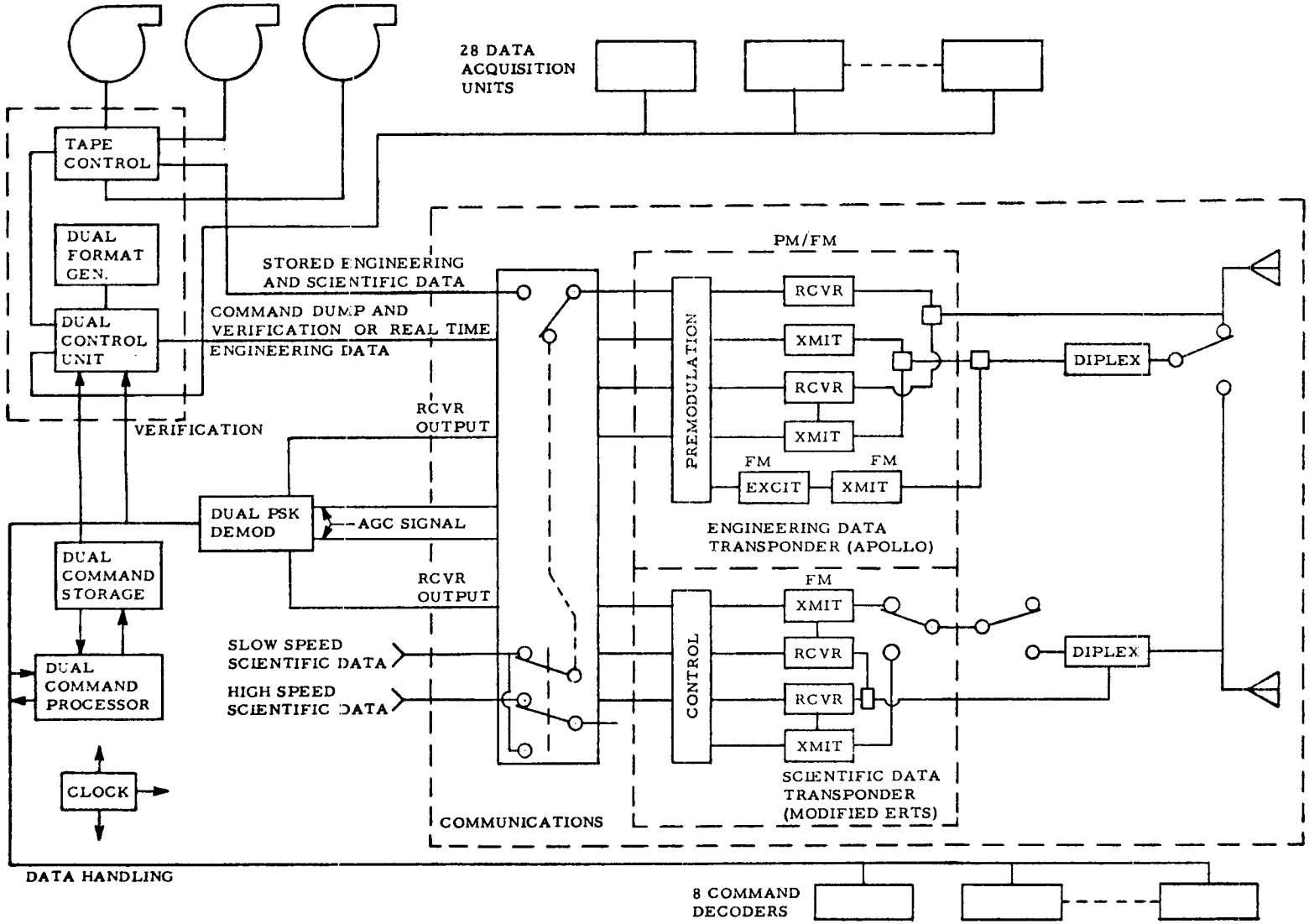

Figure V-25. LST communications and data handling system.

Preliminary specifications for the LST called for a TV tube having a 60 cycle/mm resolution at 50 percent MTF on a 50 by 50 mm target format. A survey of state-of-the-art tube technology revealed that the return beam vidicon (RBV) had the greatest promise of attaining this goal. However, the high conductivity of this tube's photoconductive target resulted in very limited integration time and target storage capability. To effectively utilize this tube in the LST project, a mass memory would be needed for storing tube images until ground contact was available. This memory would also be utilized with an averaging process required when using the RBV on high-magnitude stars for increasing S/N ratio.

a. Mass Memory Storage. Several considerations must be made to determine the size of a mass memory required for this case. The quantization noise and the inherent noise of the sensor will combine in an additive manner. To maintain an extremely high quality video signal means that the light signal collected (S) must be very large. If the S/N out of the camera is 45 dB and the degradation is to be limited to 1 dB, the value of S would have to be 256, which corresponds to 8 bits/word. It would take 10 bits/word for the quantization noise to be completely ignored. One final parameter — the sampling rate — must be established before the required storage can be determined. The Nyquist criterion states that $f_c \geqq 2f_m$ where $f \rightarrow$ sampling rate and $f_m \rightarrow$ highest signal frequency. The minimum sampling frequency must be twice the highest frequency in the signal. Stated another way, one sample must be made per half cycle. However, this results in low pass filtering of the signal with a response of 63 percent. To obtain a 90 percent response requires a sampling rate four times maximum or twice per half cycle. Now the required storage capability for onboard integration of images external to the camera tube can be determined. A tube target having a horizontal and vertical resolution of 60 cycles/mm on a 50 mm by 50 mm format will contain 3000 cycles per horizontal line or 6000 pixels. The four samples per cycles and 8 to 10 bits per sample would yield 9.6×10^4 bits for 8 bits and 1.2×10^5 for 10 bits to code a single line on the target. At the completion of each line the reading beam is returned to the left and lowered the equivalent of one pixel, then scanned across again. This continues until the beam reaches the bottom of the target, thus completing one frame of data. Since the vertical height of the target contains 600 pixels, a total frame of data would contain 5.76×10^8 bits for 8 bits of coding or 7.2×10^8 bits for 10-bit coding.

A memory large enough for a single frame of data presents a significant technology problem. Several techniques were investigated in hopes of finding a small, lightweight, low power, nonvolatile memory. Since the tube is read sequentially, the memory need not be random access.

The following memories were examined as candidates for the LST mass memory: ferrite core, tape recorders, magnetic bubble, plated wire, laminated ferrite, disc, drum, electron beam, charge coupled devices, metal nitride oxide silicon (MNOS), and complementary metal oxide semiconductor (CMOS). Estimates were made in each case for the following characteristics of a 300-megabit system: power, mass, volume, cost, data rate, and mean time between failures (MTBF). The results of this study are presented in Table V-8. The listed specifications were obtained from References V-2 through V-4 and a number of personal communications.[2]

A brief summary of the detailed results from portions of this study are included as follows.

(1) Tape Recorder. The main disadvantages of tape recorders stem from the fact that they are electromechanical devices built to very tight specifications. Wear of the tape, heads, and bearings limits the life of the tape system. The transfer of tape coating to the head and head material to the tape aggravates this problem.

Tape lives of over 10 000 passes have been attained, which would be inadequate for the highly used SIP mass memory. However, tape wear is being improved through the development of new surface lubricants which remain on the tape rather than shedding onto the head.

Head life is now somewhere between 4000 and 5000 hr, depending on the application. This figure is still being improved by the introduction of better alloy materials. Goddard Space Flight Center (GSFC) has let a contract to Applied Magnetics Corporation for a head that will have a 5-yr life.

---

2. Telephone conversation in spring of 1972 with Mr. Jim Dickson of SCI Systems, Inc., Huntsville, Ala., plated wire memory; with Mr. Bob Lindburg of General Instrument Corp., Systematics Magne-Head Div., Hawthorne, Calif., disc and drum memories; correspondence with Mr. John Kelly, Physical Electronics Group, Engineering Sciences Laboratory at Stanford Research Institute, Menlo Park, Calif., electron beam memory, and estimate on laminated ferrite memory specifications obtained from Mr. Harrison Garrett, Astrionics Laboratory, Marshall Space Flight Center.

TABLE V-8. PHYSICAL CHARACTERISTICS OF 300-MEGABIT CAPACITY MEMORY SYSTEMS

Memory Type	Power (W)	Weight [kg (lb)]	Volume [m^3 (ft^3)]	Cost (cents/bit)	Data Rate (bps)	MTBF (hr)
Ferrite Core	Several Hundred	135 to 550 (300 to 1200)	0.3 to 0.55 (9 to 17)	0.5	10^6	8000
Tape	8 to 10	9 to 14 (20 to 30)	0.02 (0.5)	(a)	(b)	(c)
Magnetic Bubble	25	27 (60)	0.02 (0.5)	0.003 to 0.0006	0.5×10^6 per channel	5800
Plated Wire	50 to 100	270 (600)	3.3 (100)	2.0	0.5×10^6	300[d]
Laminated Ferrite	50 to 100	450 (1000)	0.8 to 1.0 (25 to 30)			

TABLE V-8. (Continued)

Memory Type	Power (W)	Weight [kg (lb)]	Volume [m^3 (ft^3)]	Cost (cents/bit)	Data Rate (bps)	MTBF (hr)
Disc	Start 2000 Run 400	320 to 450 (700 to 1000)	0.5 to 0.8 (15 to 25)	(e)	0.5 to 10×10^6	(f)
Drum	Start 2000 Run 400	350 (800)	0.5 (14)	(g)	6 to 10×10^6	1000
Electron Beam[h]	1[i]	14[i] (30)	0.01[i] (0.3)	0.01 to 0.001	80×10^6	(j)
CMOS[k]	50 to 100	110 (240)	0.08 (2.5)	0.6	5 mega-bits	58 823 hr per chip
CCD (Charge Couple Device)[l]	0.3 (standby) 1 pJ per bit		1 mil^2 per bit	0.1		

TABLE V-8. (Concluded)

Memory Type	Power (W)	Weight [kg (lb)]	Volume [m^3 (ft^3)]	Cost (cents/bit)	Data Rate (bps)	MTBF (hr)
MNOS[m]	0 (stand-by) 50 nW per bit		160 mil^2 per 4K bit	1.0		

a. Cost of a spaceborne tape recorder is approximately $50 000.
b. Depends upon bit density and tape speed. The 0.5-megabit/sec data rate needed for the MSFN net can be attained.
c. Life expectancy of individual components is discussed in text.
d. The small MTBF is due to the electronics involved with the plated wire.
e. Estimated between $750 000 and $1 000 000 for 300-megabit system.
f. Launch critical.
g. Estimated $1 000 000 for 300-megabit system.
h. These specifications are projections. At present no known read/write erasable systems are available.
i. These numbers are for the tube alone.
j. Life expectancy, 20 000 hr.
k. Volatile; RCA.
l. Expert on production 1973 (Fairchild semiconductor).
m. Nonvolatile. Expect on production 1975 (Fairchild semiconductor).

Considerable bearing wear is included by shocks and vibrations, causing errors in record and playback. Low vapor pressure lubricants are necessary to reduce this wear, which becomes intense if resonance occurs. Various new developments for seals and lubricants are yielding continuous progress in the reduction of bearing wear.

Motor life is another parameter to consider when examining the tape system. A life of 25 000 hr is attainable; however, part of this is expended in ground testing. Mission experience has shown that mechanical problems limit the lifetimes of the motors.

The weight, power, and volume requirements for a 300 million bit tape system would be no problem. Exact values for these parameters will depend upon the system design. Rough estimates of these values taken from the Arthur D. Little, Inc., study [V-2] yield: weight, 14 to 18 kg (30 to 40 lb) (includes tape, motors, motor control, reels, write and read heads, information buffers, and parity checking electronics); volume, 0.02 m^3 (0.5 ft^3); and power, 8 watts to record and 10 watts to reproduce.

(2) Magnetic Bubble. The magnetic bubble technology was recommended by Arthur D. Little, Inc., [V-2] under NASA Contract NAS5-21531, presented in August 1970, as the most suitable replacement for spaceborne tape recorders in the mid-1970s. The tradeoffs discussed in this report led to the conclusion that a serial access memory which is nonvolatile, has nondestructive readout capability, and can be arranged in blocks is the most attractive contender as a replacement for a spaceborne tape system. These attributes would also be desirable for the mass memory needed for the SIP calculations. The magnetic bubble shift registers have all these properties.

The most pressing problem is with the storage medium for the bubbles. None of the materials which demonstrate bubble domains have been produced in large quantities of good quality. The two types of materials that seem to be best suited for bubble domain storage are the orthoferrites and the garnets. The garnets have some definite advantages over the orthoferrites, notably a smaller stable domain size, combined with a reasonable mobility, and a better response to cutting and polishing. It seems unlikely that one material will sweep the market as silicon did with the integrated circuit industry. Some materials will have the advantage on data rates and others may be able to attain a higher bit density. Surely there will still be other materials with varying degrees of these parameters. It is possible that certain materials will be better suited for a particular application than others.

The second problem associated with the bubble technology is the temperature sensitivity of the systems. The operation of this type of memory is highly dependent upon a predetermined and fixed ratio between the diameter of the bubble domain and the spacing of the bit storage cells.

In summary, the conceptual design of the magnetic bubble memory is attractive in many respects but there are several developmental problems still to be negotiated. The most important features of the further development of the bubble memory as far as NASA is concerned seem to be the improvement in the quality of the storage materials, the introduction of epitaxial growth techniques capable of producing materials with a low coercive force, the announcement of a material with a good temperature range, and continuing developments in photolithography.

(3) Electron Beam. Mass data storage using electron beam techniques is currently a developmental item. At present no known read/write erasable systems are available. However, a number of organizations are attempting to develop such systems.

It appears that the first prototype systems could be available during 1973, although their capacity is likely to be limited to 10^7 bits. Systems of 10^8 bits should appear about 12 months later. These systems should be in production in the period 1974 to 1976.

Larger memories of up to 10^{10} bits appear possible but there is still a large amount of R&D to be done. Big memories are likely to be compounded from a number of smaller channels or modules, enabling parallel access to read and write information. This subdivision will be controlled by the economics of tube fabrication and required system performance.

(4) Memory Summary. The majority of the mass memory systems surveyed had undesirable physical characteristics. The magnetic bubble and electron beam memory systems would seem to be the two best candidates from the standpoint of power, mass, volume, cost, and reliability. However, both of these memory schemes are still in the developmental stages. Thus no suitable mass memory system was found for the SIP. The question of system efficiency with no mass memory is treated in Appendix B.

b. Secondary Electron Conduction (SEC) Vidicon. With the mass memory scheme now considered a doubtful candidate for use in the LST data handling system, the constraining criterion in tube selection must be target storage capability, i.e., a tube must be found which has the ability to store a

single frame of data on its target until ground contact is made and yet attain suitable resolution, target size, etc. Upon this basis the SEC vidicon was chosen as the reference design tube for the LST.

The distinguishing characteristic of an SEC vidicon is its capability to store collected photons for several hours. This quality enables the SEC vidicon to integrate for hours on high-magnitude (dim) stars. On the other hand, if a low-magnitude (bright) star is viewed, causing a short integration time, the SEC vidicon can store the frame of data until a ground station is contacted. The contents of the tube can then be read out directly to ground.

The low conductance target of the SEC vidicon allows it to attain this long storage capability. This target, shown in Figure V-26, is constructed of KCl with an Al substrate. The price paid for this storage capability is low capacity and low resolution. The low capacity implies that it takes fewer photons per unit area to saturate the SEC vidicon target than it takes for the return beam vidicon (RBV). The present resolution of the SEC vidicon is approximately 20 cycles/mm at 50 percent MTF. The physical size of the SEC vidicon target is also small (25 mm by 25 mm) because of the strength limitations of the target material. However, a 50 mm by 50 mm target is presently being tested. Figure V-27 gives a basic operational schematic of the SEC vidicon and a list of tube characteristics.

The optimum readout time of the SEC vidicon is a function of the preamplifier because it is the dominant noise source of the tube. The first impression would be that only the bandwidth, input impedance, and the gain would be important. This would be true for high illumination; however, where the system is used for photon counting or low-light-level slow scan, the preamplifier, bias resistor, and shunt capacitance of the leads from the SEC vidicon to the amplifier become very important. The field effect transistor amplifier with its high imput impedance, low noise, and wide bandwidth makes it ideal for this application. Its low voltage gain, however, requires additional stages of amplification.

Calculations show that the preamplifier will operate with minimum noise contribution at approximately 30 kHz (see Appendix C). Utilizing this result with the sampling rates and encoding levels developed earlier, optimum readout rates can be determined. For 8-bit coding the readout rate = (4 samples/cycle) (8 bits/sample) (30 kHz) = 960×10^3 bits/sec. A 25 mm by 25 mm target with 20 cycles/mm at 50 percent MTF sampled and coded using the above specifications would contain 1.6×10^7 bits. Using the above readout

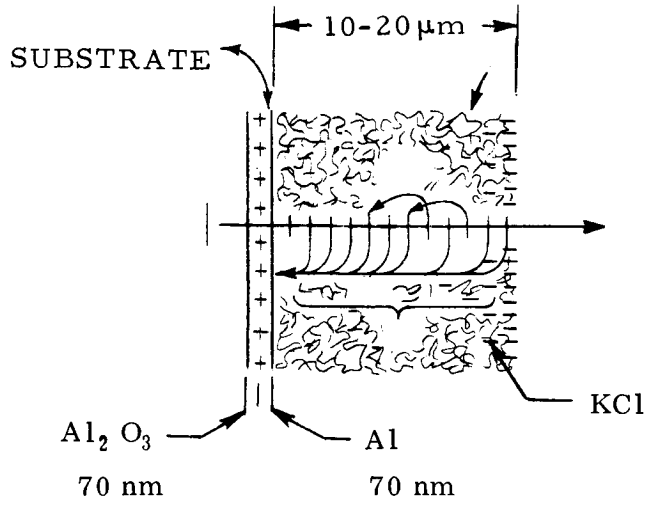

- MEDIUM TARGET GAIN (~100) OBTAINED BY SECONDARY ELECTRON CONDUCTION
- LOW CONDUCTANCE TARGET ALLOWS LONG INTEGRATION AND STORAGE TIMES
- SIGNAL IS PREAMPLIFIER NOISE LIMITED
- LOW CAPACITY TARGET

Figure V-26. SEC vidicon target cross section.

rate it would take less than 17 seconds to read out a frame of data. However, should the SEC vidicon reach the desired 50 mm by 50 mm format with 60 cycles/mm at 50 percent MTF, it would take 10 minutes to read out a single frame.

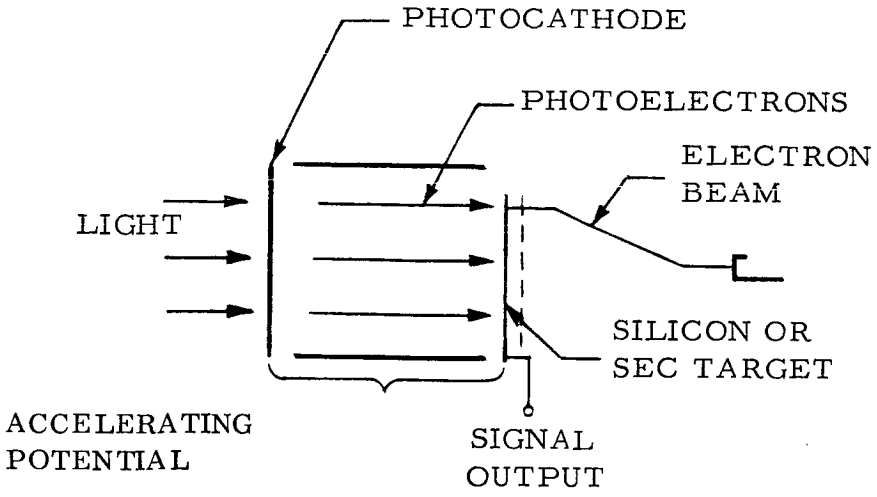

- PHOTOCATHODE AND STORAGE TARGETS SEPARATE
- TARGET GAIN AVAILABLE (50 - 100)
- OUTPUT SIGNAL FROM TARGET FED DIRECTLY TO PREAMPLIFIER
- PHOTOELECTRONS PRODUCE SPATIAL VARIATION OF CHARGE ON THE TARGET
- ELECTRON BEAM DESTROYS THIS SPATIAL CHARGE VARIATION, CREATING A SIGNAL CURRENT PROPORTIONAL TO THE SPATIAL CHARGE VARIATIONS
- SIGNAL CURRENT IS TIME CORRELATED WITH THE ELECTRON BEAM POSITION
- LOW CONDUCTANCE TARGET ALLOWS LONG INTEGRATION AND STORAGE TIME
- SIGNAL IS PREAMPLIFIER NOISE LIMITED
- LOW CAPACITY TARGET

Figure V-27. SEC vidicon.

Typical exposure times for the LST high resolution imagery experiments will be several hours and storage after exposure up to 1 hour. The usefulness of a television sensor for long exposures is directly related to the internal background within the television tube and the environment in which it must operate. This background consists of dark emission from the photocathode, field emission from the electrodes in the image section, and the phosphorescence of the materials that make up the image section of the tube. In a low earth orbit there will be a background caused by energetic particles striking the window, the walls, and the target of the television tube. Operation of the television system has demonstrated that the internal background is less than 100 background photoelectrons/cm^2/sec from the photocathode when the tube is cooled to 15° C.

There is little data on the background caused by energetic particle radiation of this type of sensor. Theoretical calculations are encouraging but hardly adequate because of the uncertainty of the model. To determine the feasibility of operating the camera as the basic device for storage, two tubes typical of the design that would be used in the LST were tested at Princeton University in proton and gamma ray environments. One tube had an MgF_2 window and the other a 7056 glass window. The TV tubes were operated during and after the irradiation period to measure the background caused by the radiation. The results of these tests have been plotted on a curve of background noise in Figure V-28 to indicate the magnitude of this form of background to that inherent in the tube and preamplifier. There are several possible explanations for the difference in the results on the glass and MgF_2 faceplates but they are not important to this discussion.

During these tests there was a gamma ray flux in the area caused by the main beam dissipating its energy in the dump located nearby. This added an undetermined background to the proton-induced background.

A 100 Curie source of Cobalt-60 was positioned 25 mm in front of the television tube window, resulting in a gamma ray flux of approximately 43 000 per cm^2. The C_O60-rays have energies of 1.17 and 1.33 MeV. The 3-mm thick MgF_2 window had a projected mass of 0.9 g/cm^2. With about 5 percent of the gamma rays undergoing Compton scattering in this distance, it is estimated that 2000 energetic electrons are produced per squared centimeter per second. The computed mean energy of the secondary electrons is 0.6 MeV. The 7056 glass window is 2.3 mm thick and has a projected mass of 0.6 g/cm^2. The energetic electron density in this case is approximately 1300 /cm^2 / sec.

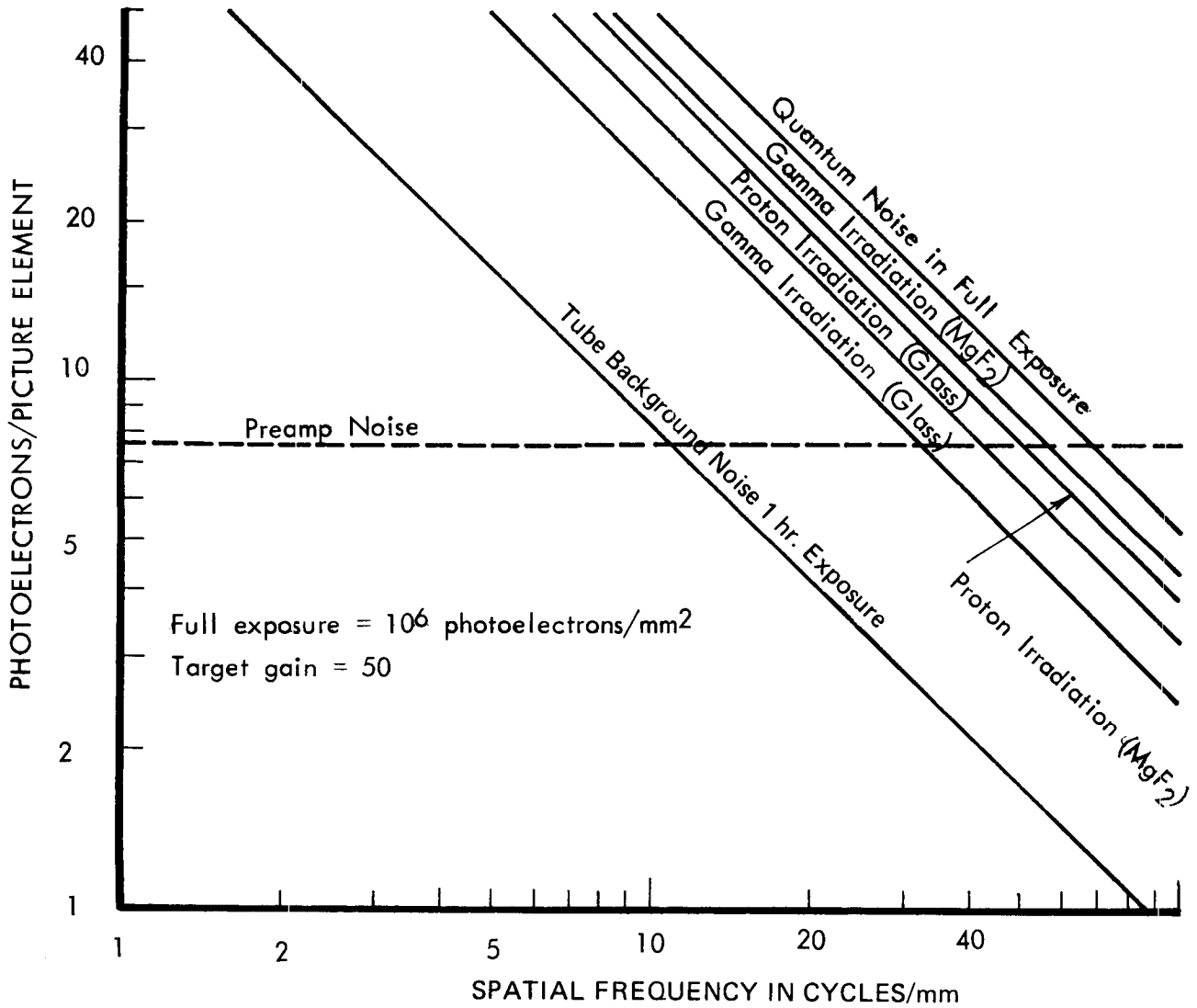

Figure V-28. Interim results of Princeton irradiation tests.

Each tube was irradiated for 40 minutes with the following results. The photocathode voltage of 8000 volts and the focus field of 0.008 T (80 G) were on during the irradiation. The results are again plotted to show a comparison with other parameters. This indicates a slightly higher level for gamma radiation than protons, which is not of particular concern since gamma radiation is easier to shield against.

The effect of these results on the LST mission can be extrapolated to show feasibility. The radiation environment inside the instrument compartment of the LST will be highly directional because of the relatively thick mirror and mirror cell in one direction and the support spacecraft in the other direction. The magnetic focus coils assembly for the television camera itself will be relatively thick and provide considerable attenuation. The proton dose rate averaged over several orbits is 2×10^6 protons/cm^2 per day, presuming an aluminum skin thickness of 3.5 mm and an orbit altitude of 6.1×10^5 m (330 n.mi.), 28.5 degree inclination. This is comparable to the dose received by the MgF_2 windowed tube when one considers that all of the photons were at the relatively high energy of 42 MeV. The glass window tube is more sensitive and it is probably more accurate to say that the tube sensitive to longer wavelength photons is more vulnerable. Even in this case the test dose is comparable to 2 to 3 hours in orbit. If the photocathode is turned off during the South Atlantic anomaly portion of the orbit, a substantial reduction in the background can be achieved. The absence of an afterglow following the irradiation period indicates that there should be no problem with storing an image during the pass through the anomaly.

In the SEC vidicon the target thickness is the determining factor of its resolution. It can be made thin but eventually reaches a point where mechanical considerations dominate. The thickness of the SEC vidicon is not directly measurable; however, the effective thickness can be calculated from the measured apparent capacitance. In a recent SEC vidicon tube the measurements indicated a target thickness of about 7 μm. Some data indicate a target thickness as thin as 3.56 μm. In Figure V-29 the MTF of image section, the electron beam, and the target have been plotted to indicate the influence of each.

The product of the individual parameter provides us with the expected system performance. These curves indicate that the SEC vidicon is a factor of three off the desired resolution (60 cycle/mm). While it is not the purpose of this section to discuss the scientific instruments, it can be shown that for a 50 percent response, the limiting resolution of a 3-m telescope at 500 nm (5000 Å) with f/96 focal length is only 22.5 cycle/mm.

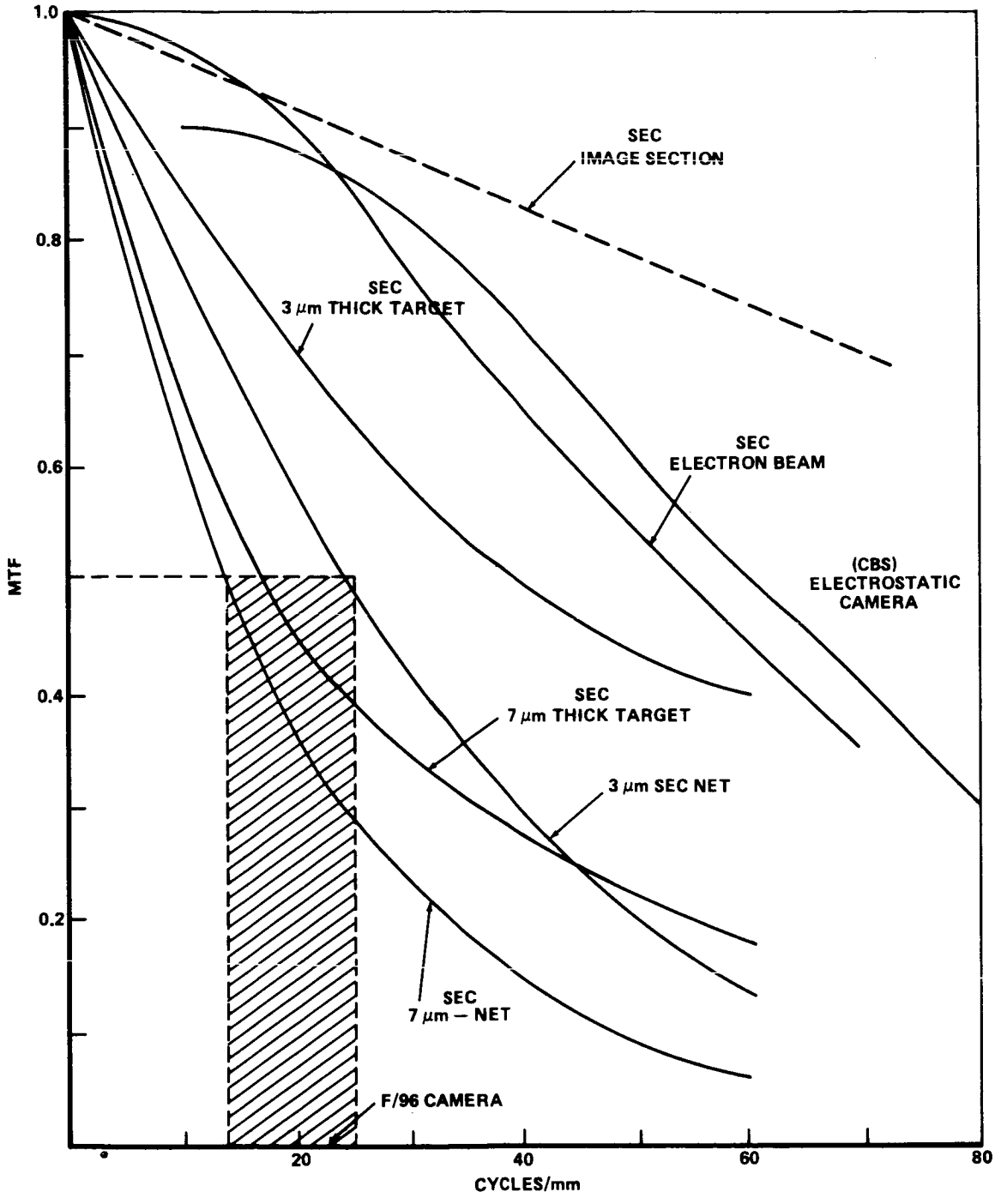

Figure V-29. SEC camera tube MTF.

A curve labeled electrostatic camera is also included that has a 60 cycle/mm resolution at the 50 percent response. This camera was under development by Columbia Broadcasting System for the outerplanet missions. The development has been discontinued because of budgetary restrictions. The design is quite unique in concept (Fig. V-30). The imaging section uses electrostatic focus and target material is SO_2. The SO_2 is deposited onto a drum that rotates in front of the photocathode for exposure and later through 180 degrees to the read-beam. The higher resolution is achieved with a thinner target than KCl. The drum is capable of storing 10 frames. Its mass and power compare favorably with the SEC vidicon, 60 watts readout and mass 23 kg (50 lb) for a 70 mm format. The prestorage target gain is quoted by the contractor to be 100 to 200. Magnetic focus in the image section could possibly improve the resolution to as high as 100 cycles/mm for 30 percent response.

E. Scientific Instrument Control

1. Introduction. The purpose of this section is to provide a reference design for the control of a typical set of instruments located in the SIP. Although the details of this set of instruments may change as the LST project progresses, they are assumed to be adequate for this reference design. They are

1. Mid-IR Fourier Spectrograph, 1.0 to 5.0 μm.
2. Faint Object Spectrograph, 0.66 to 1.0 μm.
3. Faint Object Spectrograph, 0.22 to 0.66 μm.
4. Faint Object Spectrograph, 0.110 to 0.22 μm.
5. Echelle Spectrograph, 0.18 to 0.35 μm.
6. Echelle Spectrograph, 0.11 to 0.18 μm.
7. Slit Jaw Camera Assembly.
8. One F-12 Camera.
9. Three F-96 Cameras; 0.115 to 0.3 μm, 0.16 to 0.6 μm, 0.5 to 1.1 μm.

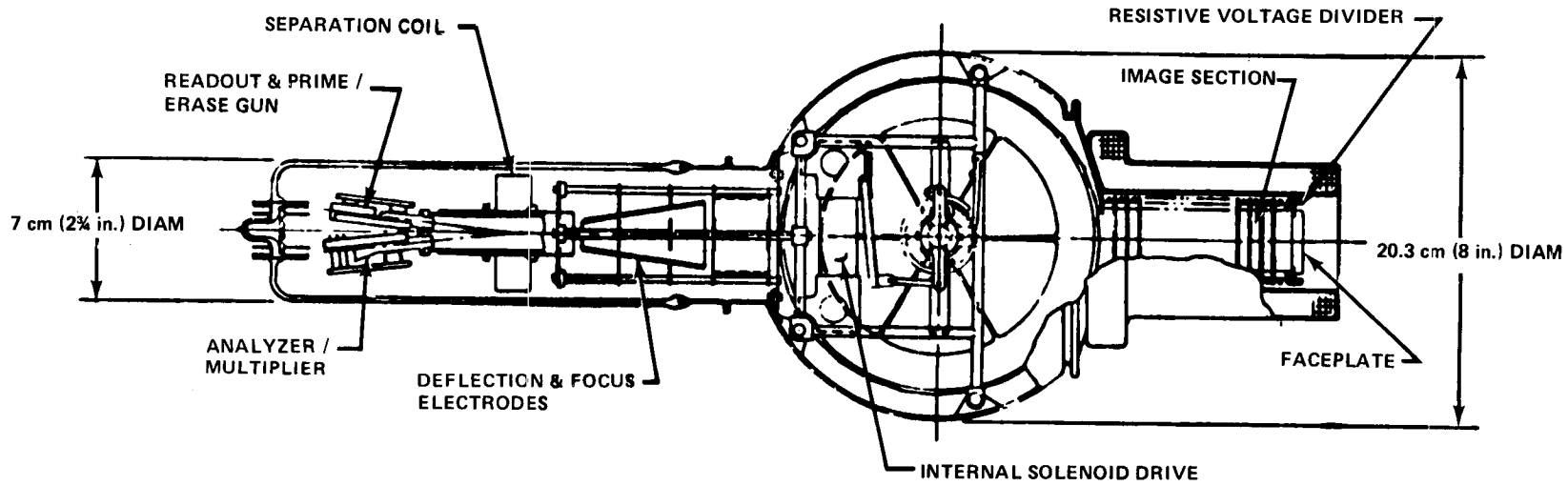

Figure V-30. Electrostatic camera tube — 10 storage frames.

The possibility that the control of these instruments as well as the control of other systems within the LST may require computer support raises the question of computer configuration and dedication, i.e., how many computers will be utilized and what will they control. Three primary LST functions were identified initially as candidates for onboard computer support.

1. ACS System and Solar Array Pointing.

2. Spacecraft Data Handling and the SIP and OTA Housekeeping (engineering data).

3. OTA and SIP Control and Computations.

Three computer configurations were considered to support these functions:

1. Alternative I — three separate computers, one for each function.

2. Alternative II — a single computer for all functions.

3. Alternative III — two separate computers.

a. Alternative I. The attitude control system (ACS) in the SSM requires a digital computer. The functions requiring the computer are control moment gyros (CMGs), strapdown inertial measurement unit, star trackers, sun sensors, and fine guidance sensor signals from the OTA.

SSM data handling requirements and the SIP and OTA engineering data requirements are not sufficient to justify a separate computer. The SSM data handling will be accomplished with special-purpose hardware. Engineering data from the SIP and OTA will be telemetered to the ground for processing. Onboard checkout will be minimum.

Part of the OTA and SIP control and computation function involves the figure sensors of the OTA which require digital computations to calculate the reference force input to the force actuators. However, these computations are only required once per week early after launching and one per month later in the mission. Data from the figure sensor can be transmitted to the ground, the computations performed, and the results transmitted up the command link to the force actuators. The OTA utilizes closed-loop servos for control and receives commands from the ground. Since the scientific data

taken from the SIP will not be processed onboard, there are no projected computation requirements for this unit. However, the control of the instruments within the SIP will require either a computer or special-purpose hardware for command sequencing and, possibly, data formatting.

Therefore, at most two computers or processors are required: the ACS definitely needs computer support; the SIP controlling system may need computer support. The question of a special-purpose controller versus general-purpose computer for SIP control will be discussed later.

b. Alternative II. Existing technology can readily provide a single digital computer that can perform both the required functions discussed above: ACS control in the SSM and SIP control. The single computer configuration will show an advantage in mass, power, and volume. However, the single computer configuration is a disadvantage for LST operational requirements. These requirements are

1. The LST must remain operational over a long period of time. The ACS is responsible for telescope pointing, solar array pointing, and the general safety and integrity of the spacecraft. The ACS is generally under control of the digital computer. The flight program of the computer and subsequent changes must be highly tested and verified before it is qualified to operate the spacecraft.

2. The utilization of the SIP must be flexible. Experimental procedures will change frequently. Probably many changes will be made within a few hours as the experimenter gets a quick look at the data. This type of operational procedure does not lend itself to extended testing and verification of flight programs for the computer.

Thus, these two requirements are not compatible and the single computer configuration is not recommended as the reference design.

c. Alternative III. This configuration consists of a digital computer for the ACS and a digital computer or a digital processor for SIP control. The details of the requirements for a digital computer or a simpler digital processor are discussed in the following sections.

2. Functional Analysis of SIP Instruments. In addressing the question of how best to control the instruments in the SIP, one must begin by isolating the controllable variables within each instrument. Once this is accomplished a control sequence or control flow chart can be established for each instrument and the conceptual design of a control system for the SIP can be discussed.

Figure V-31 shows the present complement of instruments contained in the SIP.[3] With the exception of the fine guidance sensors, whose operations are controlled by the pointing control system of the OTA, and the folding mirrors and f/96 optics, which are fixed in position, all other blocks shown in this figure contain elements that must be commanded to obtain the desired instrument operation. In the following paragraphs the makeup of each of these controllable blocks will be examined to determine what items have to be controlled and in what sequence they must be commanded. This will be followed by a discussion of the tradeoffs in controlling the SIP operation.

a. f/96 Camera Assembly. The f/96 camera assembly contains three image tube assemblies or cameras. Each tube is preceded by a filter selector. Only one of the three filter selector/tube assembly combinations can be utilized at any one time. The position of the mirror select and drive assembly determines which of the three combinations is used. The f/96 shutter positioned before the mirror select and drive assembly will be operated to either admit light or totally block the entrance of light. As mentioned above, the f/96 optics located in front of the shutter are fixed in position and thus require no control. By examining each of these components in further detail, one can determine what variables must be controlled.

(1) f/96 Shutter and Drive Assembly. Figure V-32 includes a concept of the operation of the f/96 shutter and drive assembly. The control logic shown in this figure will contain a position register which can be commanded to place the shutter in one of its two possible positions, open or closed.

(2) Mirror Select and Drive Assembly. A functional diagram of the mirror select and drive assembly is included in Figure V-32. The purpose of this mechanism is to direct the incoming light into one of the three filter selector/tube assembly combinations of the f/96 camera. This assembly can be controlled by commanding its position register. Two digital bits would be the minimum requirement for positioning the mirror to its three positions. If for some reason a finer mirror control were desired, more control bits would have to be allocated.

---

3. It should be noted here that this complement is subject to change. However, the discussion of command and control for the present group of instruments should provide a sound basis for deciding upon a general command and control mechanism for any instrument complement.

(3) Filter Assembly. The filter assembly is envisioned as a wheel containing several filters and perhaps one open hole. The desired filter could be positioned in front of the image tube by rotating the wheel. If no filter is desired, the wheel could be rotated until the open hole was in front of the tube.

The three filter assemblies used with the f/96 cameras can be controlled in a manner similar to that used for control of the mirror select and drive assembly. This is depicted in Figure V-32. Each of the filter assemblies would have its own position register for control of its filter wheel. The number of bits needed to command the position registers would depend upon the number of filters contained within the filter wheels and whether fine control over the wheel position is required.

(4) Image Tube Assemblies. Behind each filter assembly will be a tube assembly containing as SEC vidicon with associated electronics. Each tube contains different combinations of window and photocathode materials corresponding to the different spectral ranges to be imaged; however, all are controlled in a like fashion.

Two tube variables may be controlled: integration time and target scan rate. Setting an integration time for the tube could be accomplished by commanding the start and/or stop positions of a digital counter that would signal when to start and stop tube integration. By controlling the number of counts made by this counter, one could control the integration time. The target scan rate or readout rate is determined by the rate of the video clock shown in Figure V-33. This video clock rate may be controlled by a number of methods; the particular method used will depend upon the final scan control requirements. Regardless of the particular method of control, a digital command will select the appropriate clock rate. It is assumed that these clock rates will be chosen to yield tube data rates that are compatible with the receiving capabilities of existing ground stations. If it should be determined that multiple clock rates are required, provisions will have to be made for formatting tube data.

Once these variables are set, a tube command sequence can be initiated. This command sequence consists of the four mode commands shown in Figure V-34. Each mode command will start a specific hardware sequence, which will control all the operations within a tube mode. A possible hardware sequence is given for each mode in this figure.

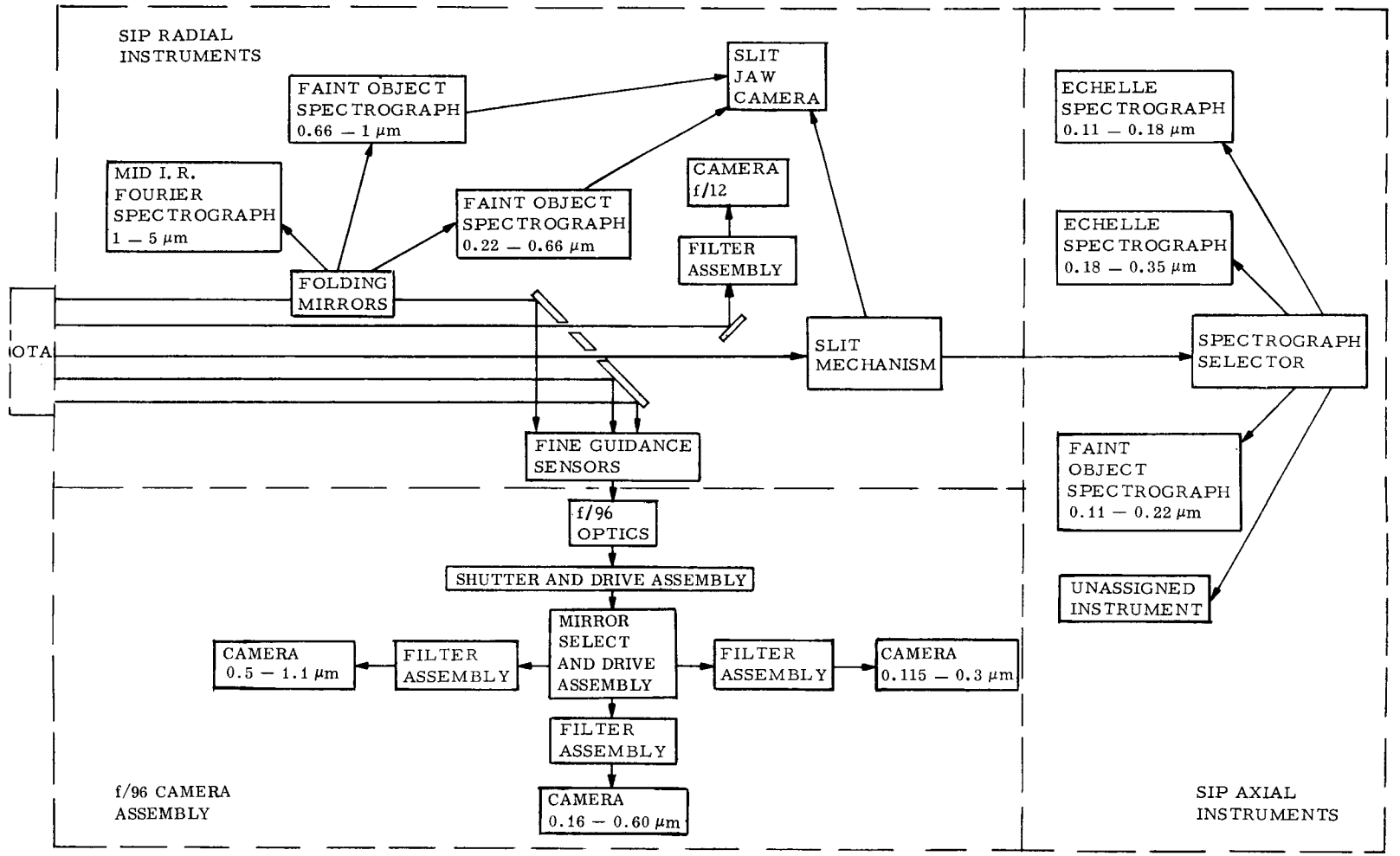

Figure V-31. Scientific instrument package.

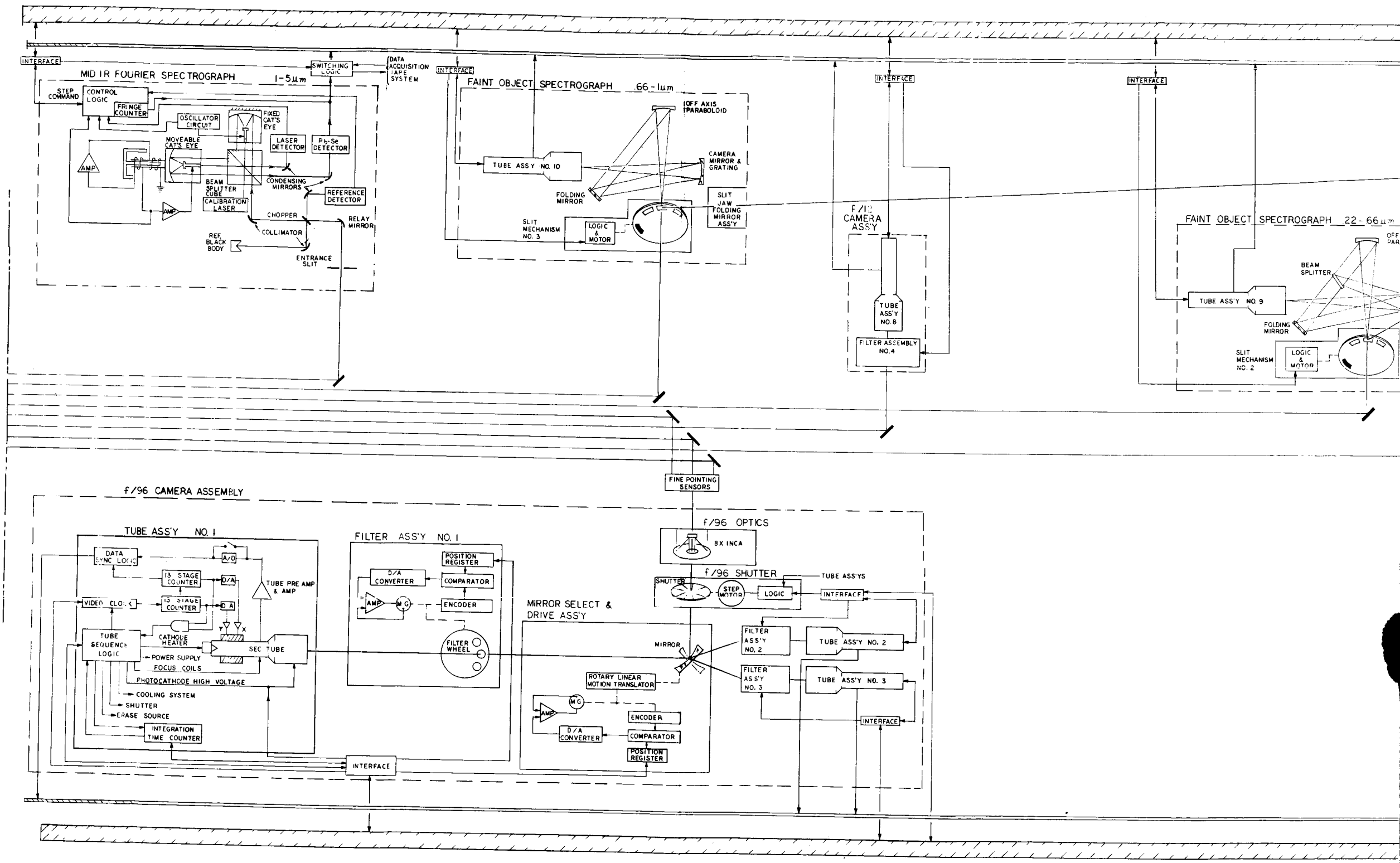
INTERFACE
MID IR FOURIER SPECTROGRAPH 1-5μm
STEP COMMAND
CONTROL LOGIC
FRINGE COUNTER
OSCILLATOR CIRCUIT
FIXED CAT'S EYE
MOVEABLE CAT'S EYE
LASER DETECTOR
Pb-Se DETECTOR
AMP
BEAM SPLITTER CUBE
CONDENSING MIRRORS
REFERENCE DETECTOR
CALIBRATION LASER
CHOPPER
RELAY MIRROR
COLLIMATOR
REF. BLACK BODY
ENTRANCE SLIT
SWITCHING LOGIC
DATA ACQUISITION TAPE SYSTEM
FAINT OBJECT SPECTROGRAPH .66-1μm
OFF AXIS PARABOLOID
TUBE ASSY NO. 10
CAMERA MIRROR & GRATING
FOLDING MIRROR
SLIT JAW FOLDING MIRROR ASS'Y
SLIT MECHANISM NO. 3
LOGIC & MOTOR
F/12 CAMERA ASS'Y
TUBE ASS'Y NO. 8
FILTER ASSEMBLY NO. 4
FAINT OBJECT SPECTROGRAPH .22-.66μm
BEAM SPLITTER
TUBE ASS'Y NO. 9
FOLDING MIRROR
SLIT MECHANISM NO. 2
LOGIC & MOTOR
OTA
FINE POINTING SENSORS
f/96 CAMERA ASSEMBLY
TUBE ASS'Y NO. 1
DATA SYNC LOGIC
A/D
13 STAGE COUNTER
D/A
TUBE PRE AMP & AMP
VIDEO CLOCK
TUBE SEQUENCE LOGIC
CATHODE HEATER
SEC TUBE
POWER SUPPLY
FOCUS COILS
PHOTOCATHODE HIGH VOLTAGE
COOLING SYSTEM
SHUTTER
ERASE SOURCE
INTEGRATION TIME COUNTER
FILTER ASS'Y NO. 1
POSITION REGISTER
D/A CONVERTER
COMPARATOR
ENCODER
AMP
MG
FILTER WHEEL
MIRROR SELECT & DRIVE ASS'Y
ROTARY LINEAR MOTION TRANSLATOR
f/96 OPTICS
8X INCA
f/96 SHUTTER
SHUTTER
STEP MOTOR
LOGIC
TUBE ASS'YS
FILTER ASS'Y NO. 2
TUBE ASS'Y NO. 2
FILTER ASS'Y NO. 3
TUBE ASS'Y NO. 3

Part # 1

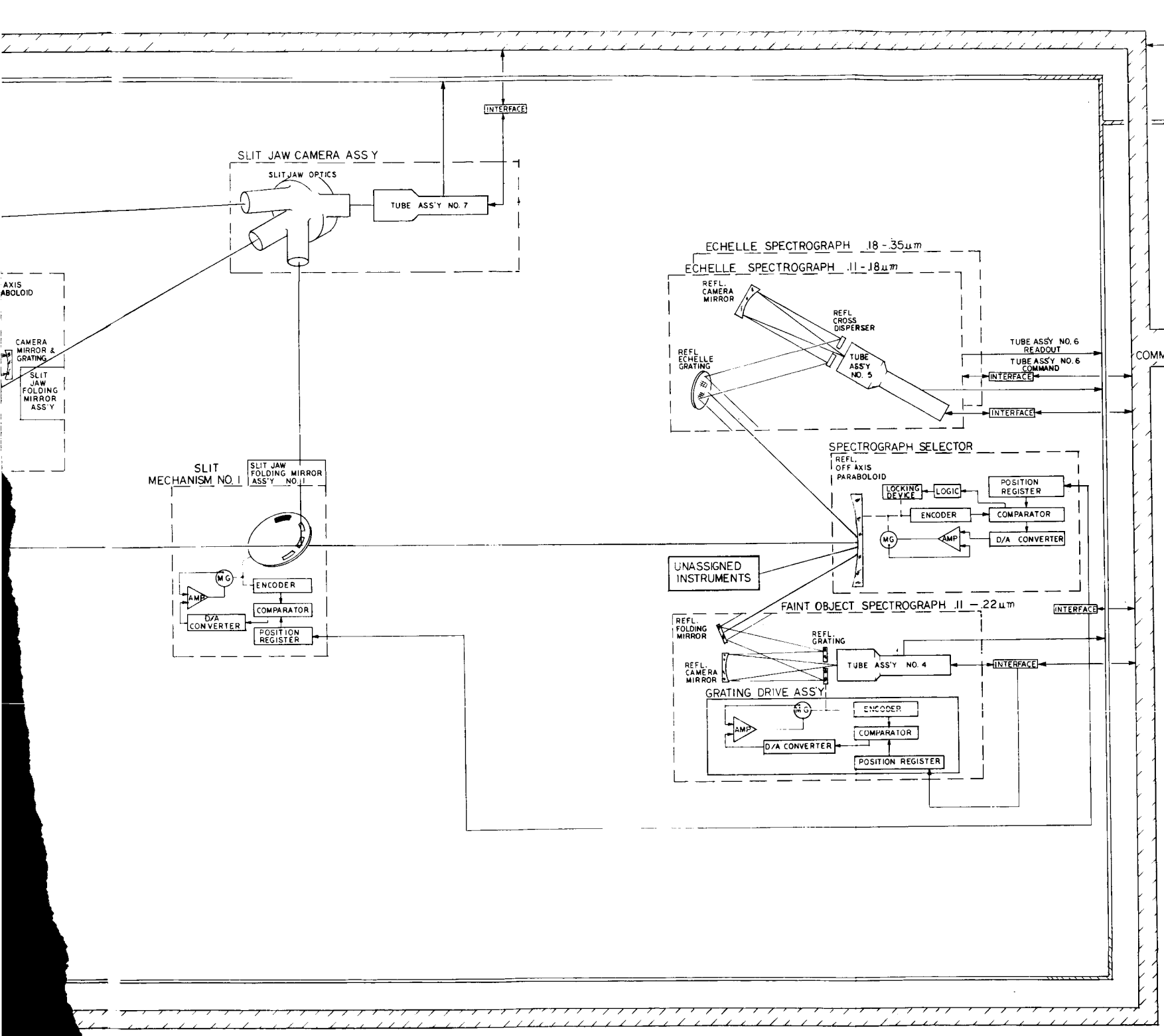

MEMORY SUBROUTINES

INSTRUMENT	ITEMS TO CONTROL
f/96 CAMERAS (3)	f/96 SHUTTER MIRROR SELECTOR & DRIVE ASS'Y FILTER ASS'Y NO. 1, 2 & 3 TUBE ASS'Y NO. 1, 2 & 3
ECHELLE SPECTROGRAPHS (2)	SLIT MECHANISM NO. 1 SPECTROGRAPH SELECTOR TUBE ASS'Y NO. 5 & 6
FAINT OBJECT SPECTROGRAPHS (3) AXIAL POSITION (1)	SLIT MECHANISM NO. 1 SPECTROGRAPH SELECTOR GRATING DRIVE ASS'Y TUBE ASS'Y NO. 4
RADIAL POSITION (2)	SLIT MECHANISM NO. 2 & 3 TUBE ASS'Y NO. 9 & 10
f/12 CAMERA	FILTER ASS'Y NO. 4 TUBE ASS'Y NO. 8
SLIT JAW CAMERA	SLIT MECHANISM NO. 1, 2 & 3 (OR 3 SHUTTER ASS'Y NOT SHOWN) TUBE ASS'Y NO. 7
MID I.R. FOURIER SPECTROGRAPH	SWITCHING LOGIC STEP COMMAND FOR REFERENCE COUNTER READ OUT DETECTOR AND FRINGE COUNTER
UNASSIGNED INSTRUMENT	SLIT MECHANISM NO. 1 SPECTROGRAPH SELECTOR

PHYSICALLY LOCATED WITH SIP

Figure V-32. SIP reference design.

Part #2

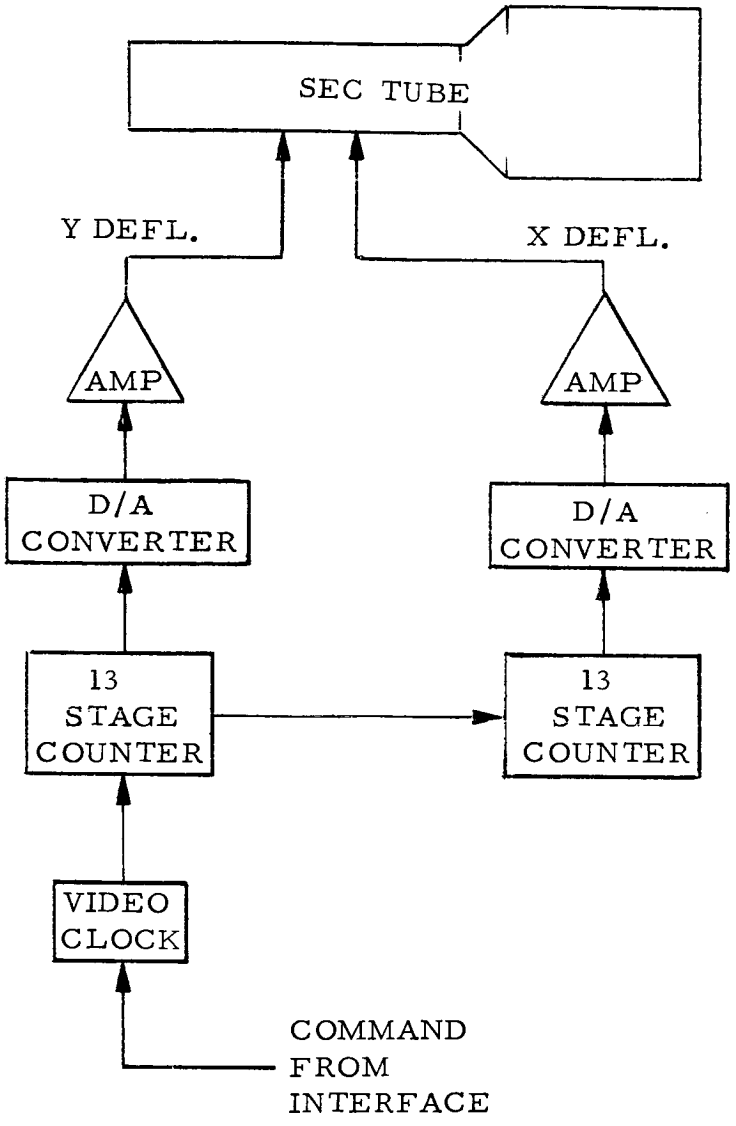

Figure V-33. Functional block diagram of digital scan control system.

Note that in the exposure mode the operation of the shutter has been listed as optional. The reasoning behind this follows. Two methods have been proposed for starting and stopping tube integration. In one method a mechanical shutter is operated to either pass or block light. This method is exemplified by the f/96 shutter. The alternative method relies upon the on/off switching of the high voltage (~8000 volts) between the photocathode and target of the SEC vidicon. When the high voltage is off, the photoelectrons from the photocathode are not accelerated to the tube target. Thus, the optical image on the photocathode is not projected to the target.

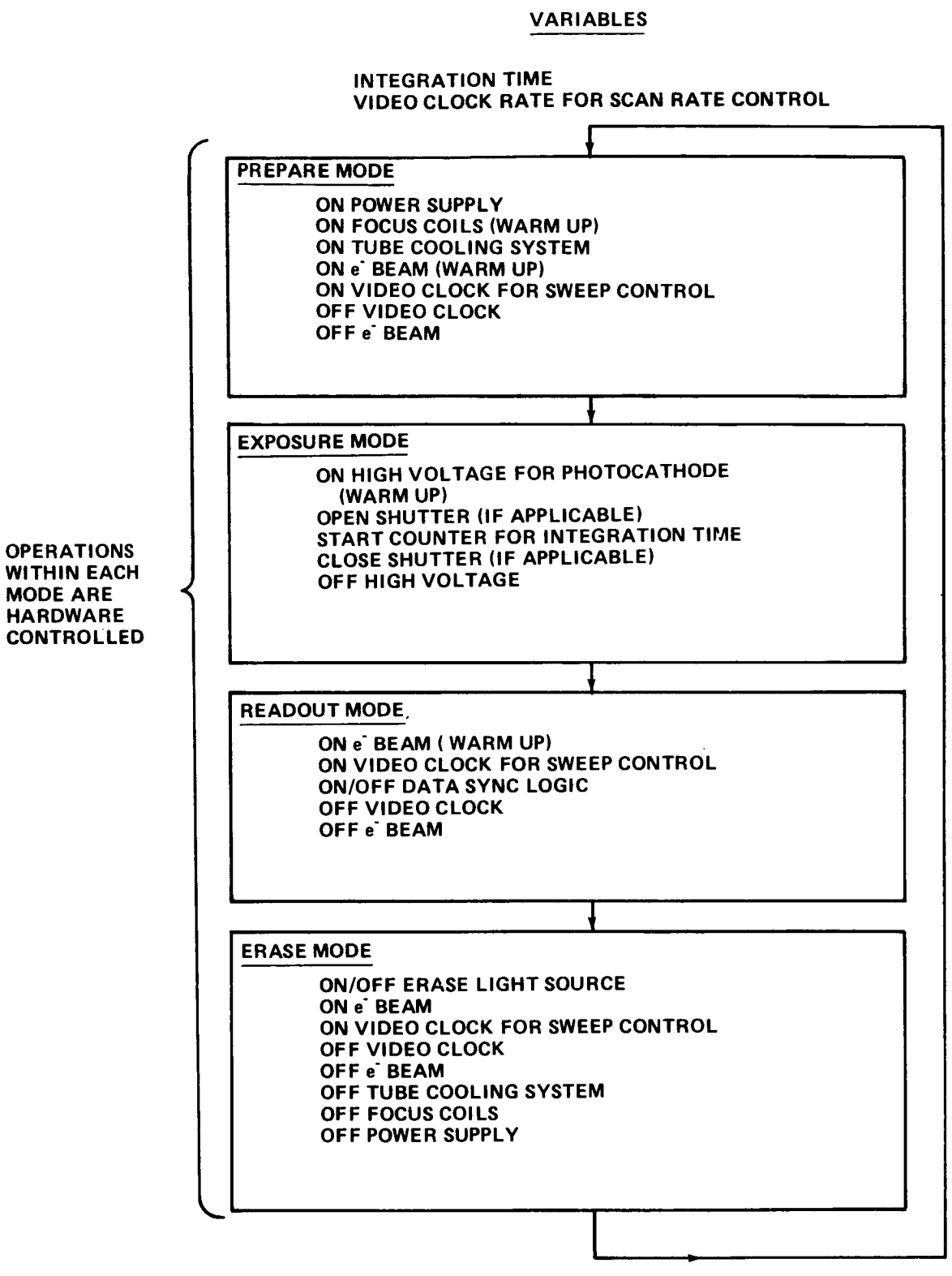

Figure V-34. Tube command sequence.

Regardless of which method is decided upon, the tube will be commanded by the same mode commands. The only impact upon these commands will be in the hardware sequence of operations in the Exposure Mode. For the mechanical shutter concept the hardware would command the shutter to either open or close. If the high-voltage method were used, the hardware would simply command it either on or off.

One exception to this concept of hardware-controlled sequences occurs during long integration times (hours) when it becomes necessary to start and stop tube integration due to occulted sources. When occultation occurs, it will be necessary to block the incoming signal to the tube target, using either one of the two aforementioned methods, and to halt the integration time counter. Once the source is reacquired, integration may be resumed. Thus, access will be required to both the integration time counter and either the instrument's shutter or the high voltage of the tube.

A functional block diagram of the SEC tube assembly is shown in Figure V-32. The f/96 camera structure will have three of these tube assemblies. This block diagram shows that the following components may be controlled: the tube sequence logic for giving mode commands, the integration time counter for setting the integration time and accounting for occultation, the video clock for setting scan rates, and, finally, either the photocathode high voltage or the instrument shutter (not shown) for stop/start integration control during occultation. The other items shown are under the hardware control of the tube sequence logic.

It has been proposed that for some instruments in the SIP only a portion of the SEC tube's target would be transmitted to ground. This can be accomplished by additional hardware within the tube assembly. By setting an additional variable register or registers (not shown in Fig. V-32), the hardware sequence can be switched to the desired sweep mode. No change in the tube mode command sequence need be implemented.

(5) Self Checking Capability. It should be pointed out at this time that a number of points within both the f/96 camera structure and those systems yet to be discussed will be monitored through the data acquisition system. Data from these points will be taken through DAUs and either transmitted real-time to ground or stored on tape recorders for later transmission. On the ground these data will be analyzed to insure that the instruments are in proper operating order. In addition to this checking capability, each instrument will have its own self-check procedure implemented through individual hardware packages called self-check logic. Upon command these

individual hardware units will distribute test voltages to numerous points within the instrument's control system. Some of the results of these test voltages will be hardware inspected to determine go/no go operation. The remainder of the results will be monitored through the data acquisition system.

(6) Control Sequence. Now that the discussion of controllable variables within each component of the f/96 camera assembly is completed, a control sequence for this structure may be formulated. The following sequence of commands would provide operational control:

1. Command instrument power on.

2. Initiate self-check logic for hardware test routine.

3. Read out engineering data to tape or ground.

4. Command position register of the mirror select and drive assembly.

5. Command position register of appropriate filter assembly.

6. Command the appropriate registers to set tube variables.

a. Integration time set by commanding start/stop position of integration time counter.

b. Scan rate set by commanding register for control of video clock rate.

7. Submit mode commands to tube sequence logic.

a. Prepare mode.

b. Exposure mode (command integration time counter and either shutter or photocathode high voltage during occultation).

c. Read out mode.

d. Erase mode.

b. SIP Axial Instruments. The SIP axial instrument group consists of two Echelle spectrographs for the wavelength ranges 0.11 to 0.18 μm and 0.18 to 0.35 μm, a faint object spectrograph for the wavelength range 0.11 to 0.22 μm, and an unassigned instrument. All these instruments share the same collimating mirror and entrance slit mechanism. If it is determined that shutters will be used, possibly one would be positioned in the vicinity of the entrance slit mechanism and shared by all the axial instruments.

(1) Spectrograph Selector. The collimating mirror for these instruments is contained in the spectrograph selector. It can be positioned to one of four positions to determine which of the four axial instruments is to be used. A conceptual block diagram of the spectrography selector is included in Figure V-32. This control mechanism is very similar to the one discussed previously, with the exception of the presence of a locking device to fix the mirror in place once it has been properly positioned. This locking device is under the hardware control of the digital comparator. Thus, the position register is still the only item to be commanded. Here again the number of command bits needed will be dictated by the final requirement on position control.

(2) Slit Mechanism. The slit mechanism, which is located at the telescope f/12 focal plane, contains the slits through which light passes before being directed to the appropriate instrument by the selector. Figure V-31 indicates the path of light to each of the axial instruments.

The slits within the slit mechanism will be located on a wheel. By controlling the position of this slit wheel, one may select a desired entrance slit. The proposed mechanism for controlling the position of the slit wheel is the same as the control mechanism for the filter wheel. The only requirement for control is the commanding of a position register. The number of bits needed for the command will be a function of the number of slits on the wheel and the possible requirement for fine control of the wheel position.

(3) Slit Jaw Camera. It has been proposed that a slit jaw camera be used in conjunction with all slit mechanisms. The purpose of this instrument is to provide a device through which the stellar field around an entrance slit may be examined to insure that the object of interest is positioned within the slit. If it is determined by examining the picture transmitted to ground by this camera that the object of interest is not positioned within the slit, then appropriate commands will have to be submitted to the spacecraft sensing and control system to reposition the telescope line of slight. The slit jaw camera provides a possible way of accomplishing this objective but it is not the only way. Other methods are presently being proposed and analyzed in an effort to optimize the SIP performance.

Figure V-35 presents a possible implementation of the slit jaw concept. The present complement of instruments in the SIP contains three slit mechanisms: one for the four axial instruments and one each for the two radial faint object spectrographs. The slit wheel within each mechanism can be controlled by commanding individual position registers as discussed earlier. Once a slit wheel has properly positioned a slit before the optics of an instrument, the image on the mirrored area surrounding this slit is projected through a slit jaw folding mirror assembly to one of the three optical paths of the slit jaw optics.

All three optical paths of the slit jaw optics are focused onto the slit jaw SEC tube's target. Various methods for selecting which of the three optical paths will be integrated on the tube's target at any one time are presently being analyzed. The method presented in Figure V-35 utilizes "nonreflective surfaces" on the slit wheels. By properly positioning the nonreflective portion of two slit wheels before two of the three optical paths, the third optical path may be integrated without interference and transmitted to ground for examination. This concept requires no movable parts within either the slit jaw fold mirror assemblies or the slit jaw optics. However, if it is determined that shutters will be used, the nonreflective surfaces would not be needed.

Based upon the concept of the slit jaw camera shown in Figure V-35, the following control sequence may be utilized.

1. Command instrument power on.

2. Initiate self check logic for hardware test routine.

3. Readout engineering data to tape or ground.

4. Command the position register of the two slit mechanisms not being used to properly position the nonreflective surfaces, or command shutters to close on two instruments.

5. Command the position register of the slit mechanism being utilized to position the proper slit (if not already done).

6. Command the appropriate registers to set tube variables.

7. Submit mode commands to tube sequence logic.

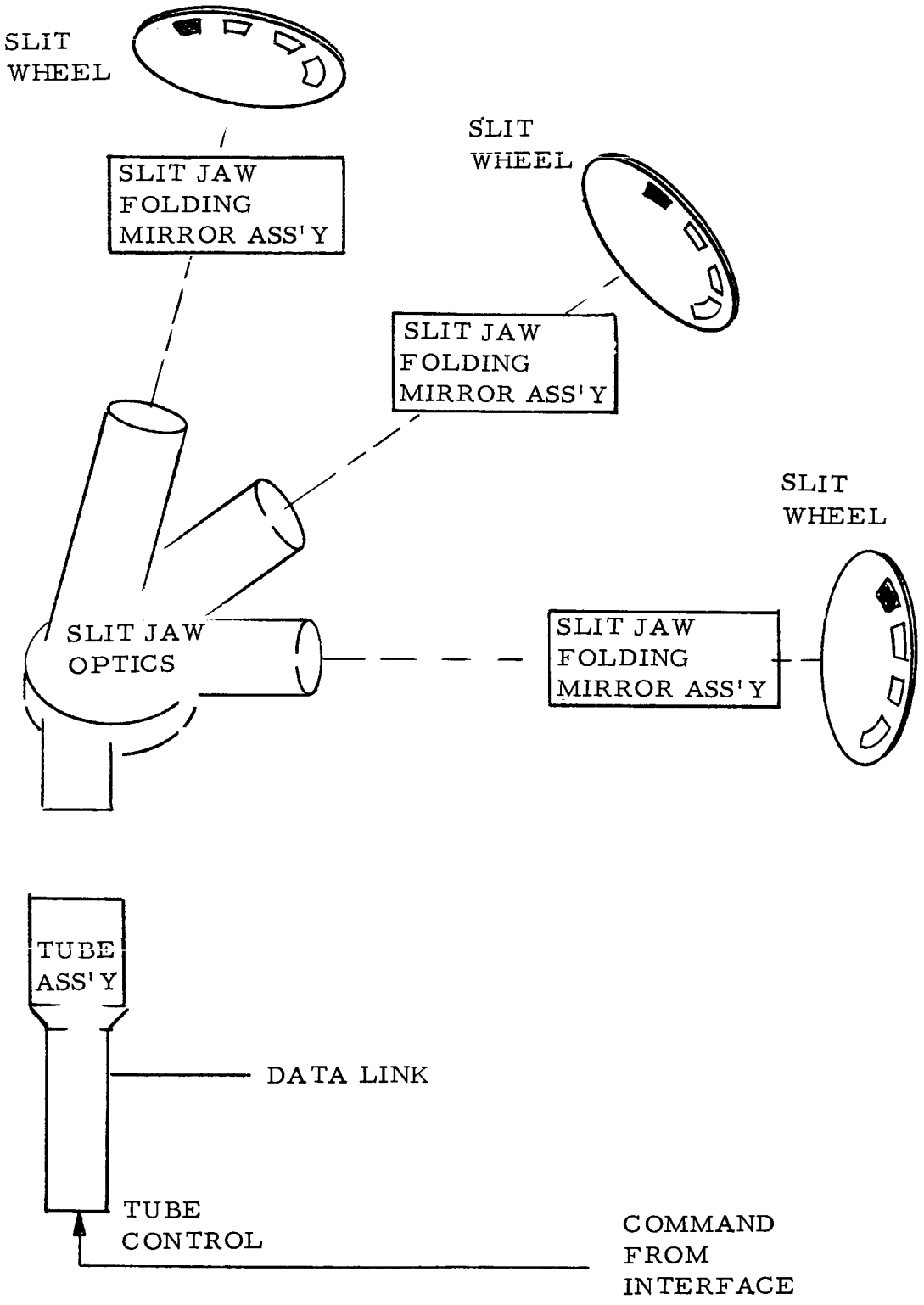

Figure V-35. Functional block diagram of slit jaw camera assembly.

It should be noted here that the silicon intensified target (SIT) vidicon is a strong candidate for replacement of the SEC vidicon in the slit jaw camera. Should this replacement occur, it is assumed that the SIT vidicon will be controllable through mode commands similar to the SEC control.

(4) Echelle Spectrographs. Two Echelle spectrographs are included in the axial instrument compartment. Both instruments contain a section of fixed optics followed by a tube assembly, as shown in Figure V-32. The differences between the two instruments are the rulings of the reflection gratings and cross dispersers and differences in the window and photocathode materials in the two tube assemblies.

The following control sequence was formulated for the Echelle spectrographs:

1. Command instrument power on.

2. Initiate self-check logic for hardware test routines.

3. Read out engineering data to tape or ground.

4. Command position register of slit mechanism.

5. Command position register of spectrograph selector.

6. Utilize slit jaw camera routine to check relative position of desired stellar object and slit.

7. Command the appropriate registers to set tube variables.

8. Submit mode commands to tube sequence logic.

(5) Faint Object Spectrograph. This spectrograph operates over the spectral range of 0.11 to 0.22 μm. A functional block diagram of this instrument is included in Figure V-32. Since this instrument contains two reflecting gratings, a grating drive assembly had to be included. This mechanism, similar to those previously discussed, operates through a position register. The control sequence for this instrument is as follows:

1. Command instrument power on.

2. Initiate self-check logic for hardware test routines.

3. Readout engineering data to tape or ground.

4. Command position register of slit mechanism.

5. Command position register of spectrograph selector.

6. Utilize slit jaw camera routine to check relative position of desired stellar object and slit.

7. Command position register of grating drive assembly.

8. Command appropriate registers to set tube variables.

9. Submit mode commands to tube sequence logic.

(6) Unassigned Instrument. The last instrument in the axial group is unassigned at this time. However, since it is positioned with the other axial instruments its operational control sequence would have to include control of the slit mechanism and the spectrograph selector. Further speculation on its control cannot be made at this time.

c. SIP Radial Instruments. The instruments in this group receive their light signals from the field select mirrors which divert the light from the optical axis of the telescope into the instrument's line of sight. These instruments include a mid-IR Fourier spectrograph covering the spectral range from 1 to 5 μm, an f/12 camera assembly, and two faint object spectrographs covering the spectral ranges from 0.22 to 0.66 μm and from 0.66 to 1 μm.

(1) Mid-IR Fourier Spectrograph. The basic operation of the mid-IR Fourier spectrograph is outlined in Figure V-36. After light has passed through an aperture, it is split by a beamsplitter into two directions. In one direction the light is reflected from a fixed mirror and in the other direction it is reflected by a movable mirror. Both reflected beams return to the beamsplitter, where a portion of each is passed to an intensity detector. Two items of information must be extracted from this instrument. First, the position of the movable mirror must be known, and second, the intensity reading of the detector for that particular position of the movable mirror must be monitored.

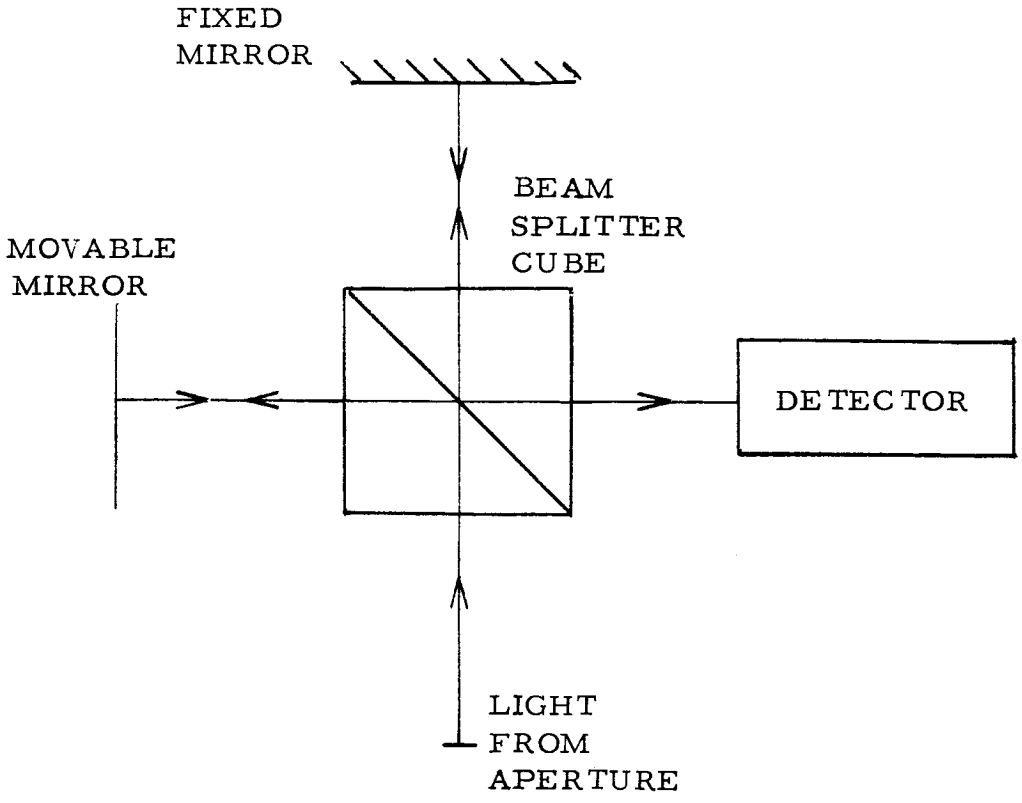

Figure V-36. Block diagram of mid-IR Fourier spectrograph.

A detailed functional block diagram of this instrument is presented in Figure V-32. Although the diagram included in the figure is more detailed than Figure V-36, the basic operation is the same. A step command from the command interface initiates a reference counter in the control logic which steps the movable cat's eye through a finite series of positions. This is analogous to the movable mirror of Figure V-36. A reading is taken from the Pb-Se detector at every position. This reading, along with periodic information about the position of the movable cat's eye taken from the fringe counter, is sent either directly to ground over the scientific data link or stored on the tape system within the data acquisition system for later transmission to ground. The quantity of data produced by this instrument (~2 megabits/interferogram) will not tax the tape system's capacity. Also, the movable cat's eye within this instrument may be moved at a slow enough rate to make the instrument's data rate compatible with the recording rate of the tapes.

By using this information, a possible control sequence for this instrument may be formulated as follows:

1. Command instrument power on.

2. Initiate self-check logic for hardware test routine.

3. Readout engineering data to tape or ground.

4. Command switching logic to route data either real-time to ground or to the data acquisition tape system for storage.

5. Submit step command to reference counter.

6. Read out fringe counter and Pb-Se detector.

(2) f/12 Camera Assembly. The f/12 camera assembly consists of two components, a filter assembly and a tube assembly (as mentioned before a shutter assembly may possibly be included with each instrument). The control mechanism for the filter selector will be similar to the ones used in the f/96 camera assembly and the tube assembly will have the same functional block diagram as the one shown in the f/96 assembly of Figure V-32.

The control sequence for the f/12 camera would proceed as follows:

1. Command instrument power on.

2. Initiate self-check logic for hardware test routine.

3. Readout engineering data to tape or ground.

4. Command position register of f/12 filter assembly.

5. Command appropriate registers to set tube variables.

6. Submit mode commands to tube sequence logic.

(3) Faint Object Spectrographs. The radial faint object spectrograph covering the spectral range from 0.22 to 0.66 μm is illustrated in Figure V-32. The only items to control in this instrument are the position

of the slit wheel and the operation of the tube assembly. Every other item is fixed in position. The proposed mechanism for controlling the position of the slit wheel is the same as the one shown for the slit mechanism used with the axial instruments. Thus, the position of the slit wheel is controlled by commanding a position register. Once again the size of the command will depend upon the tolerance to which the wheel position must be controlled.

The control sequence for this instrument is as follows:

1. Command instrument power on.

2. Initiate self check logic for hardware test routine.

3. Readout engineering data to tape or ground.

4. Command position register of slit mechanism.

5. Utilize slit jaw camera routine to check relative position of desired stellar object and slit.

6. Command appropriate registers to set tube variables.

7. Submit mode commands to tube sequence logic.

This control sequence may also be applied to the other radial faint object spectrograph covering the spectral range from 0.66 to 1 μm. The only difference in these two spectrographs lies in their fixed position optics and their image tubes.

3. Discussion of SIP Control. With control sequences for each instrument now defined, attention can be focused upon the choice of a controlling scheme for the whole SIP. In the following paragraphs two methods of SIP control will be examined: special-purpose hardware control and general-purpose computer control.

Commands that are addressed to the SIP's command decoder(s) will pass from the decoder(s) to a unit called the scientific instrument controller, as shown in Figure V-37. This controller, which will either be special-purpose hardware or a small computer, will supervise the distribution of command sequences to the instruments of the SIP. It will have the capability of storing instructions in its memory and recalling them upon command. Each instrument in the SIP has its own control sequence. These sequences are lists

of commands to be submitted to control points within the SIP at particular times. No calculations are required in the command sequences. The only variables associated with these sequences are the variable commands given to position registers (positions no. 1, no. 2, etc.) and possibly the time of execution of certain commands within the sequence. Once these variables are set within the control sequence, the control of the instrument is also set.

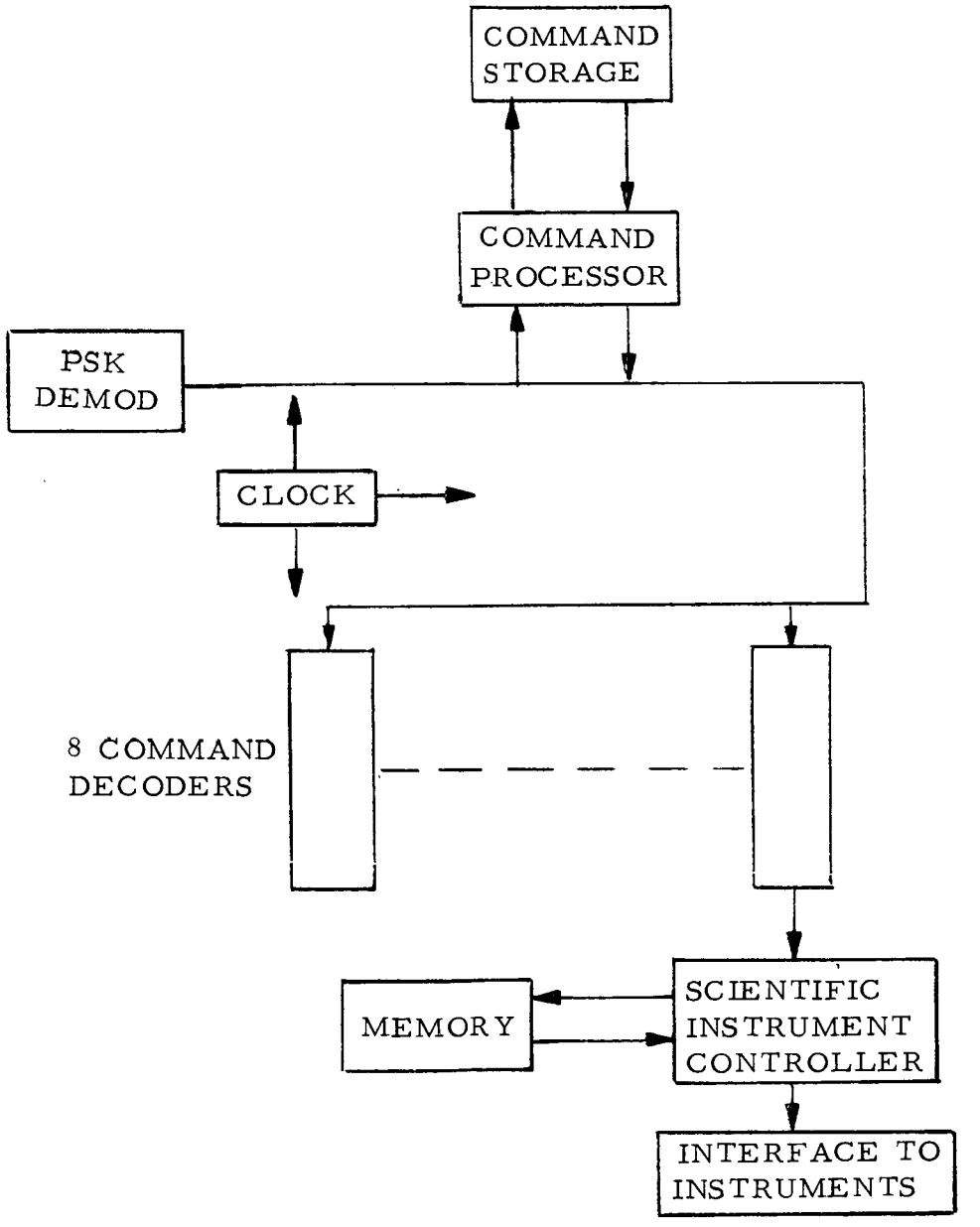

Figure V-37. Control of SIP by scientific instrument controller.

The scientific instrument controller memory will be loaded with the control sequences for all the instruments. Whenever an instrument is to be used, commands coming either real-time from ground or time tagged from the command processor will load any new variable instructions that are needed in the instruments control sequence and then call the sequence into operation.

a. Special-Purpose Controller. Since the control sequences for the proposed complement of instruments require no arithmetic computation to accomplish their control, a special-purpose controller will be sufficient for commanding the present SIP. A conceptual design of such a controller is shown in Figure V-38.

The control unit within this special-purpose controller will process interrupt requests coming either from the command processor through the command decoder(s) or from the instruments. It will provide signals to control the input/output (IO) operations of the memory and handle all output sync pulses on the controller to instrument control lines. It will also handle the input sync pulses for transferring information in from the command decoder(s) and handle any interrupt priority system that may be deemed necessary. The program counter will hold the address of the word currently being referenced in memory. The memory data register holds the word that is either written into or read out of memory. The select and timing section contains all the circuitry required for accessing a word in memory and supplies regulated word currents for either reading or writing. It will also contain timing circuitry for strobing the sense amplifier and providing digit current timing. The working registers will be multiple registers that may be needed to route information into and through the controller. The instrument selection register will contain the code of the instrument being commanded by the controller and the instrument command register would contain the command for the selected instrument. In essence, this design represents a small computer without an arithmetic capability.

Commands will be distributed to the appropriate control points in the SIP through an interface similar to the one shown in Figure V-39. Each instrument will have its own separate interface to facilitate the addition or substitution of instruments. The individual instrument interfaces will route commands from the command lines to the appropriate control points within the instrument. The instrument selection lines will be used to select the instrument to be commanded. The control lines to the instrument will synchronize all transfers of commands on the command lines and control any interrupt priority system. Signals on the instrument-to-controller control lines will permit the instrument to request a program interrupt, indicating that it is ready for a data transfer.

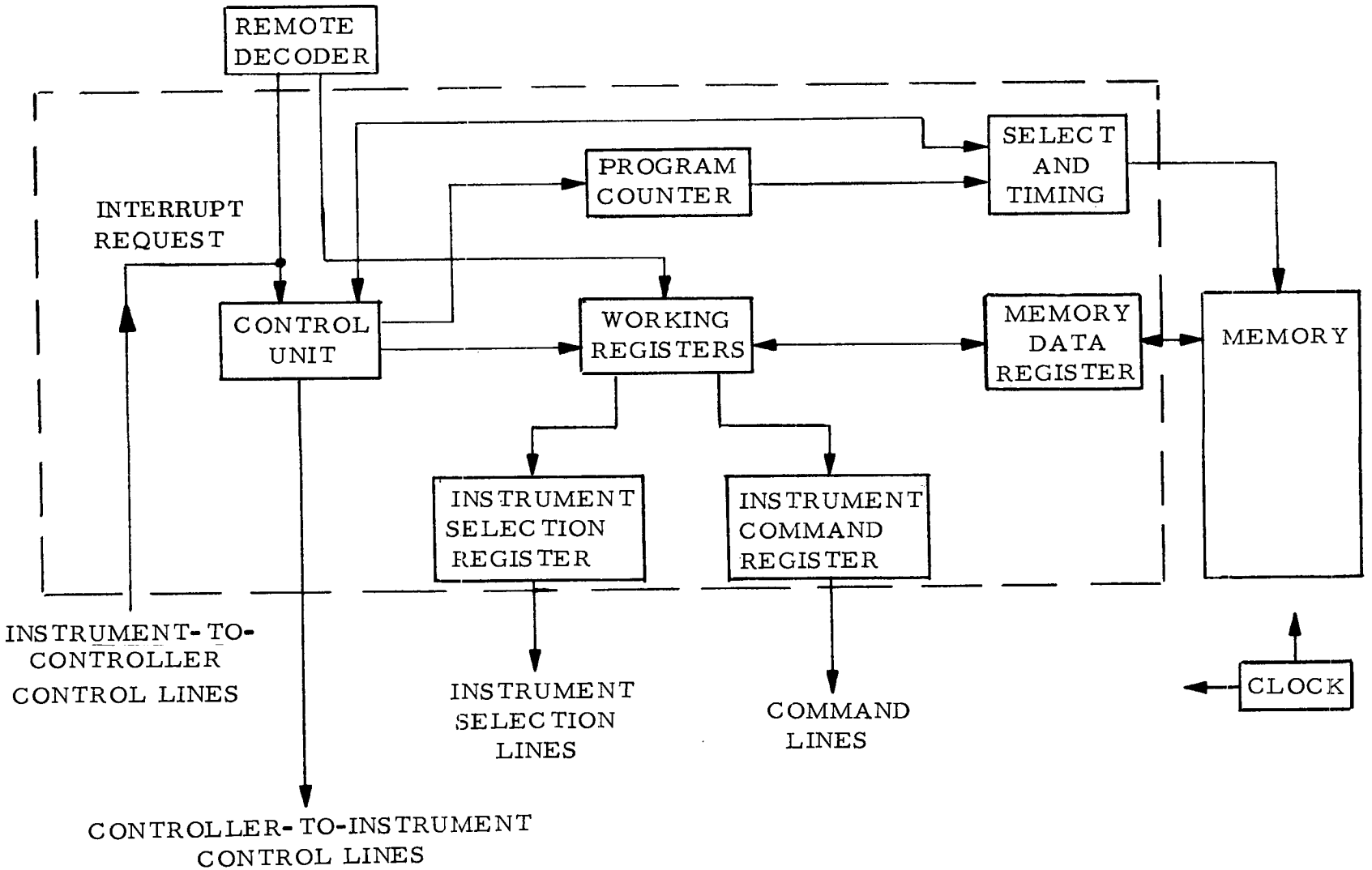

Figure V-38. Special-purpose design configuration for scientific instrument controller.

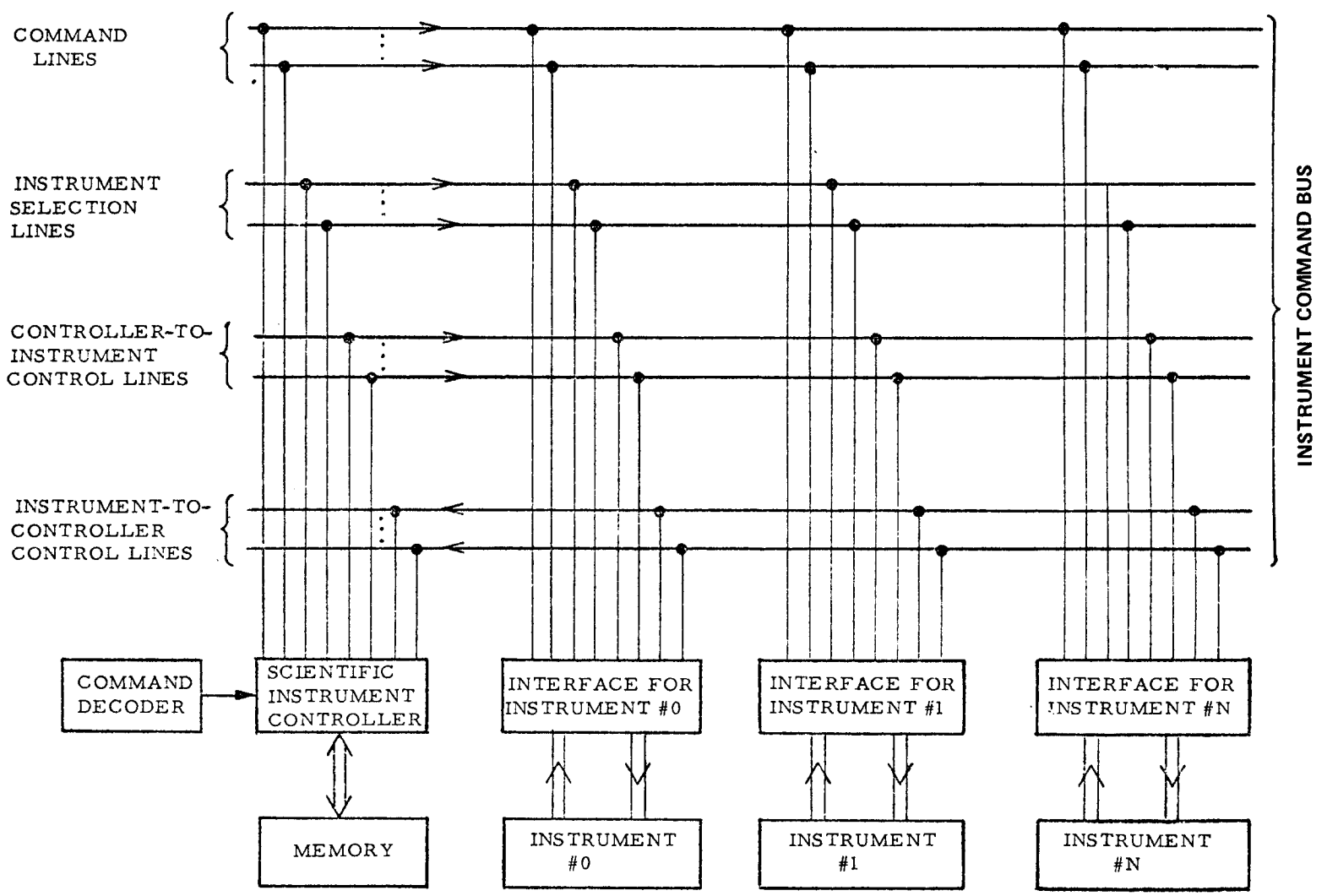

Figure V-39. Command interface between scientific instrument controller and SIP instruments.

b. General-Purpose Controller. If it should be determined at a later date that an arithmetic capability in the SIP would be desirable for onboard status checks of the instruments, computation requirements of a new instrument, etc., the special-purpose controller would be inadequate. In this case a small computer would be more desirable. The computer would have the same data handling capability of the special-purpose controller plus an arithmetic capability. A likely candidate for this role is Control Data's 469 computer, which has already been recommended for the ACS of the LST and other NASA projects.

A block diagram of the central processor of the 469 computer is presented in Figure V-40. This diagram is functionally the same as the special-purpose hardware conceptual design in Figure V-38 with the addition of an arithmetic unit.

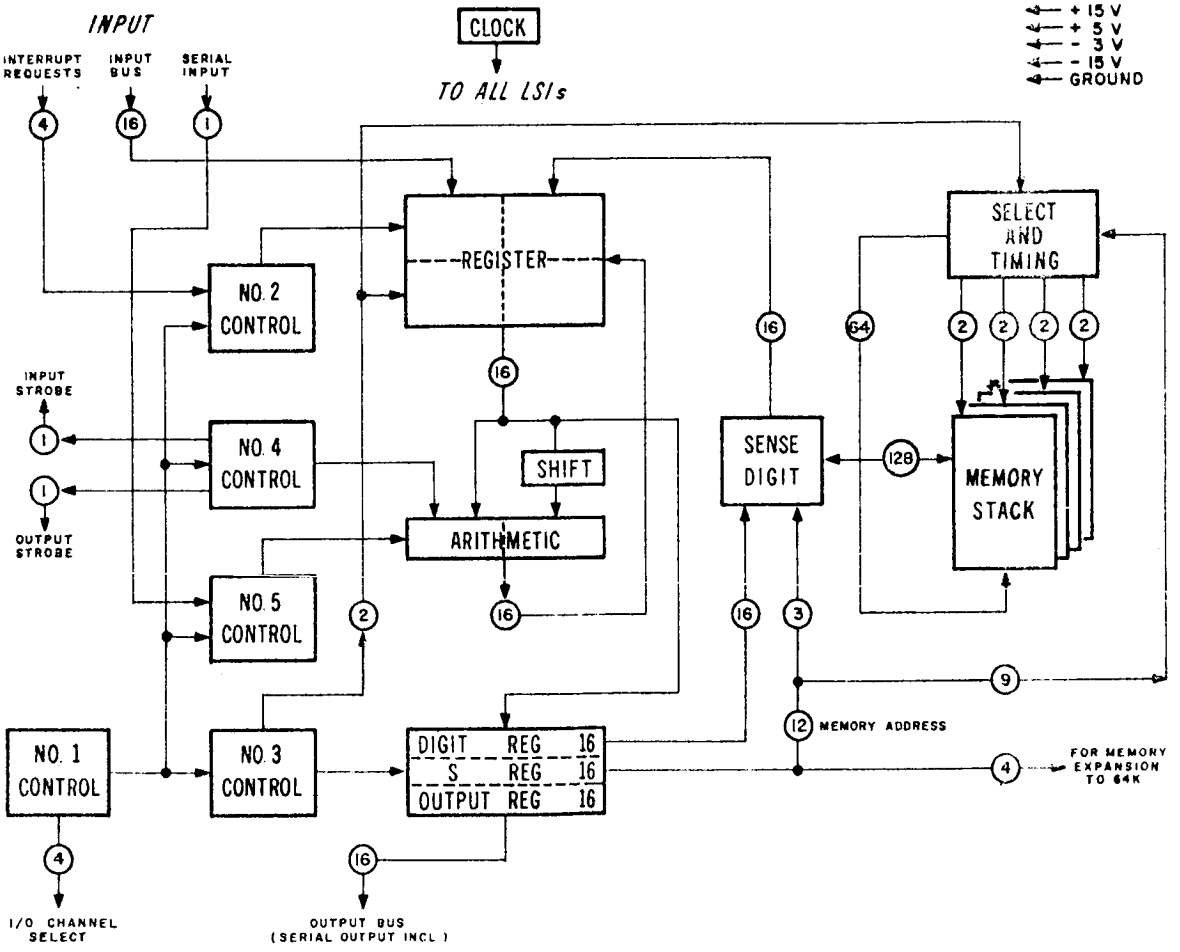

Figure V-40. 469 computer functional block diagram.

The arithmetic section consists of two identical metal oxide semiconductor/large-scale integrated circuits (MOS/LSI) devices, each being a fully self-contained 8-bit adder. The device has two holding registers which are inputs to the adding network. The adder also has the ability to perform a 1-bit right shift or masking operation.

An extra LSI register file is implemented in the central processor to perform the fast fractional multiply. It is shown as the box labeled SHIFT above the arithmetic LSIs in Figure V-40.

The control section of the 469 computer consists of five MOS/LSI devices. Control No. 1 provides signals to the remaining control devices and provides the four bits of channel information for IO operation. Control No. 2 processes interrupt requests and the associated selection of registers related to interrupt operation. Control No. 3 provides signals to operate the memory in conjunction with the central processor. Control No. 4 provides some commands to the arithmetic section as well as the input and output strobe signals for I/O operations. Control No. 5 handles the serial input and provides additional commands to the arithmetic unit.

The output register group consists of two MOS/LSI devices, each containing three general-purpose 8-bit holding registers. One register is used to hold data from the most recent parallel output instruction. These data will remain in the register until a new parallel output instruction is executed and will then go to the command lines of the output bus in a fashion similar to the transfer of data from the instrument command register in Figure V-38. The second register (digit) holds the data which are to be written into the memory. This register, in conjunction with the sense digit section, which contains all the necessary circuitry required for sensing signals from memory, provides a function similar to the memory data register of Figure V-38. The third register (S) is used to hold the address of the word being referenced in memory (program counter, Fig. V-38). The select and timing section provides the same function as the one in Figure V-38.

The register file for the 469 computer consists of 16 words of 16 bits each. The file is made up of four MOS/LSI devices, each consisting of eight words by 8 bits. The speed of the standard 469 computer is 2.5 MHz.

The memory used in this digital processor is constructed with plated wire elements. This type of memory allows random access and is word organized. It does not require rewriting after a read cycle and, therefore,

provides for faster operation through its inherent nonvolatile or nondestructive readout (NDRO) characteristics. The basic word length is 16 bits with a read cycle time of 1.6 μsec, a write cycle time of 2.4 μsec, and an access time of 500 nsec.

The size requirements placed upon this memory by the SIP instrument control sequences are expected to be minimal. Two K of this 16-bit memory should be more than sufficient for this purpose. Utilizing this size memory for the scientific instrument controller would yield a flexible unit with excellent expansion capabilities.

The physical characteristics of a 469 general-purpose computer with a 2K plated wire memory are as follows:

1. Weight: < 1 kg.

2. Volume: < 900 cm^3.

3. Power: < 15 watts.

With the discussion of both special-purpose hardware control and general-purpose computer control completed, the following observations can be made:

1. The only outstanding hardware difference in the two control schemes is the presence of an arithmetic unit in the general-purpose computer.

2. The special-purpose hardware would require a developmental cost, whereas the computer is readily available.

3. The arithmetic capability of the computer would provide more flexibility and a greater expansion capability than special-purpose hardware.

4. Should it be determined that data formatting of tube data is necessary, the computer could handle this development whereas the special-purpose hardware would possibly require additional hardware to accomplish it.

5. The main advantages to a special-purpose hardware controller would lie in its physical characteristics: smaller size and weight, smaller power requirement, and greater speed.

6. The question of reliability is more a function of system configuration (redundancy) than either special-purpose hardware or general-purpose computer per se.

On the basis of these observations, it is recommended that a general-purpose computer be utilized as the scientific instrument controller. Since the Control Data 469 computer has already been recommended for other related NASA applications, it would be logical to consider this unit for use here.

4. Reference Design of SIP Control System. On the basis of the functional analysis of the SIP instruments and the discussion of SIP control, Figure V-32 was developed as a reference design of the SIP control system. This figure shows the data paths from the SIP's remote decoder(s) to the control points within each instrument, the optical interface with the OTA, and also lists the points that must be commanded for proper operation of each instrument. To reduce repetition in Figure V-32 only one detailed portrayal was made of a tube assembly, filter selector, and slit mechanism. The detailed drawing of each was assigned the number one and subsequent repetitions were numbered accordingly.

F. Tracking and Data Relay Satellite System (TDRSS) to LST Data Link

1. Introduction. The design reference communication subsystem for transmitting scientific data to earth does not allow a continuous look at high data rate experiments because of the relatively narrow information bandwidth of the STDN ground intercommunication system and the intermittent contact time of satellites in low to medium earth orbits. Use of the synchronous altitude TDRSS with its wide information bandwidth and nearly continuous contact time will allow a real-time look at high data rate experiments. The following discussion contains tradeoffs in an alternative TDRSS terminal data link for the LST.

a. Design Approach. Wideband communication (greater than 10 MHz) from low to medium altitudes to earth via TDRSS requires a high gain antenna and moderate transmitter power. Fifty megabits of data require 2.4 m (8 ft) antenna dish and 40 watts of RF power, as will be shown later. One major design obstacle was the storage and deployment of two 2.4 m (8 ft) diameter dishes. Two antennas are required to minimize contact time outages.

Figure V-41 shows the LST in the payload bay of the orbiter. As can be seen, there are two areas where an angenna may be stowed. The volume between the sunshield end of the LST and the end of the cargo bay has more than adequate space for antenna stowage, as the figure shows. Since the antenna must gimbal to track the Tracking and Data Relay Satellite (TDRS), the antenna dish must be mounted on a boom. The boom could be attached to the sunshield or to the bottom of the OTA. Attaching the boom to the sunshield is not attractive because the sunshield deploys. This would make it necessary to have deployable signal and power leads to the antenna. Attaching the boom to the bottom of the OTA requires approximately a 7.6 m (300 in.) boom. In addition, the boom must have a joint at the end of the sunshield to allow the antenna to clear the cargo bay walls when stored. The other area in which to stow the antenna is between the SSM and the cargo bay wall. The dimension between the SSM and the bay walls is approximately 35 cm. In this case, a deployable dish would be required.

The choice of the type of transmitter is limited because 40 watts of power is required at Ku bank (13.5 to 15.3 GHz). Efficient solid-state generation of power at this frequency is not presently available. The most efficient and reliable source of power at the Ku band is the traveling wave tube (TWT) amplifier.

b. Typical Antenna Tracking Requirements. The angle tracking requirement of the antenna was assessed while the LST was fixed on several stars. Figures V-42 and V-43 are typical examples of the antenna requirements. As can be seen, the angle traced per orbit is approximately 1.4 rad (80 degrees) maximum and 0.15 rad (10 degrees) minimum.

Typical LST antenna rates for tracking a TDRS are shown in Figure V-44. This figure gives the tracking rates about two antenna axes for a single orbital period.

c. Tracking Methods. Three methods were considered in the selection of a tracking technique for the antenna system: programmed tracking, step tracking, and monopulse tracking.

(1) Programmed Tracking. This requires that the LST and TDRS positions be accurately known. In addition, computer support is required to generate the antenna look angles versus time for the particular orbit. These are not severe requirements, which makes programmed tracking a candidate tracking technique. Pointing errors due to the LST and TDRSS known position inaccuracies and their transformation into antenna look angles are within the pointing error budget. Other error sources to be considered are those caused by boom alignment, antenna bore sight, and boom deflection.

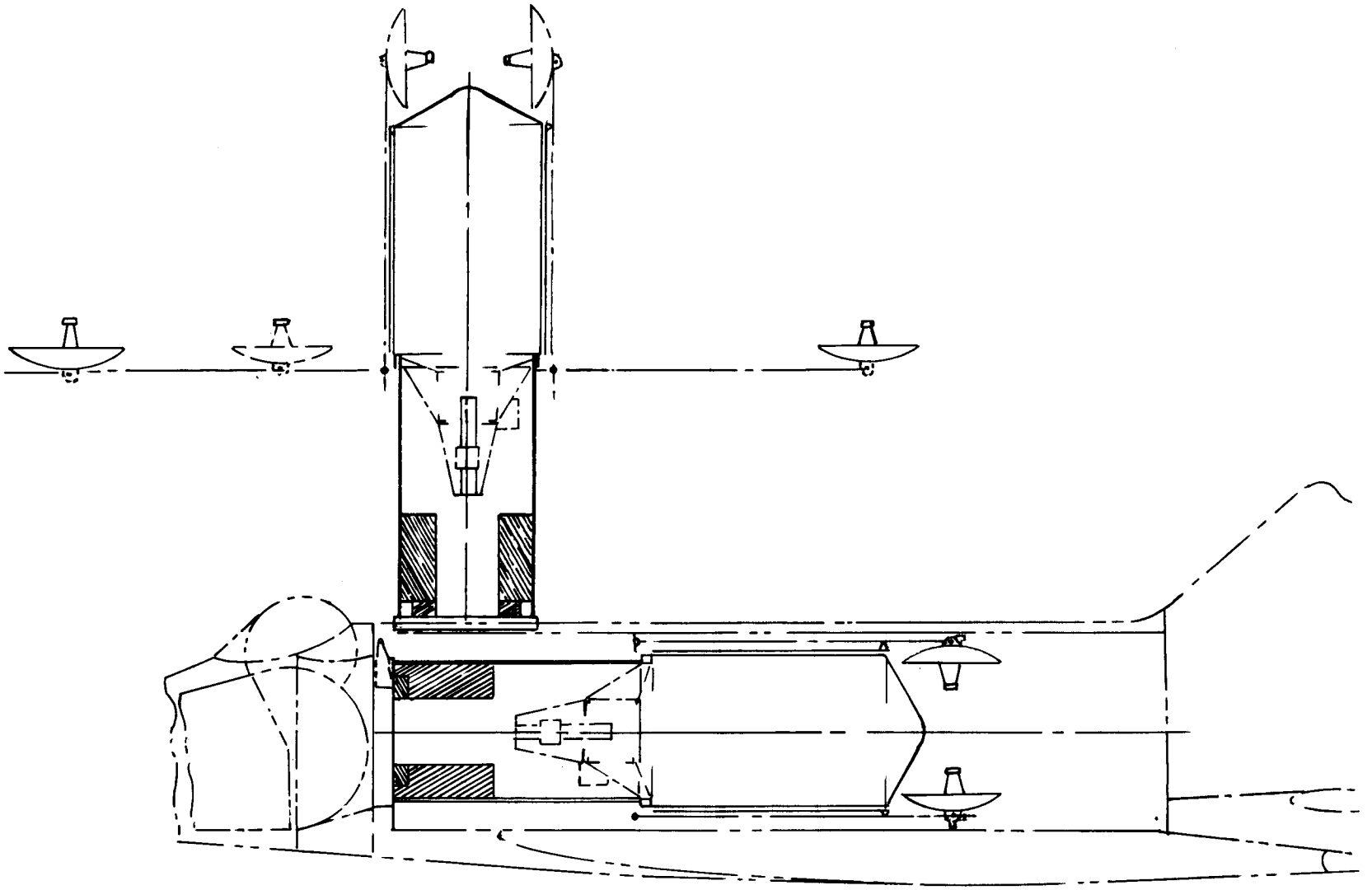

Figure V-41. The 2.4 m (8 ft) diam antenna stowed in aft payload bay and compatible with rollup or foldout solar panels.

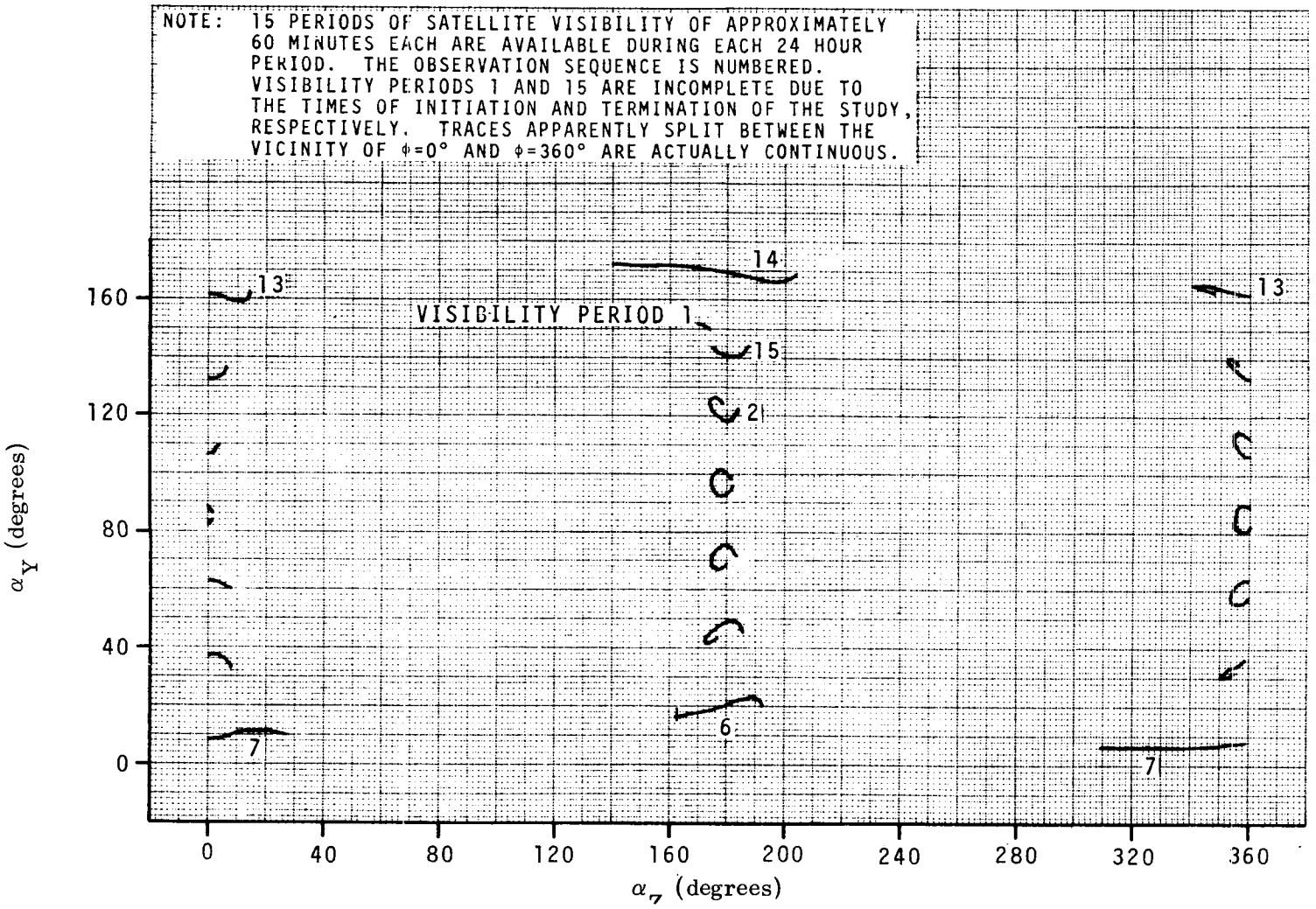

Figure V-42. Look angles from LST to TDRS — star declination = 0 degree, sun declination = -23.4 degrees (sun right ascension is 180 degrees greater than that of star).

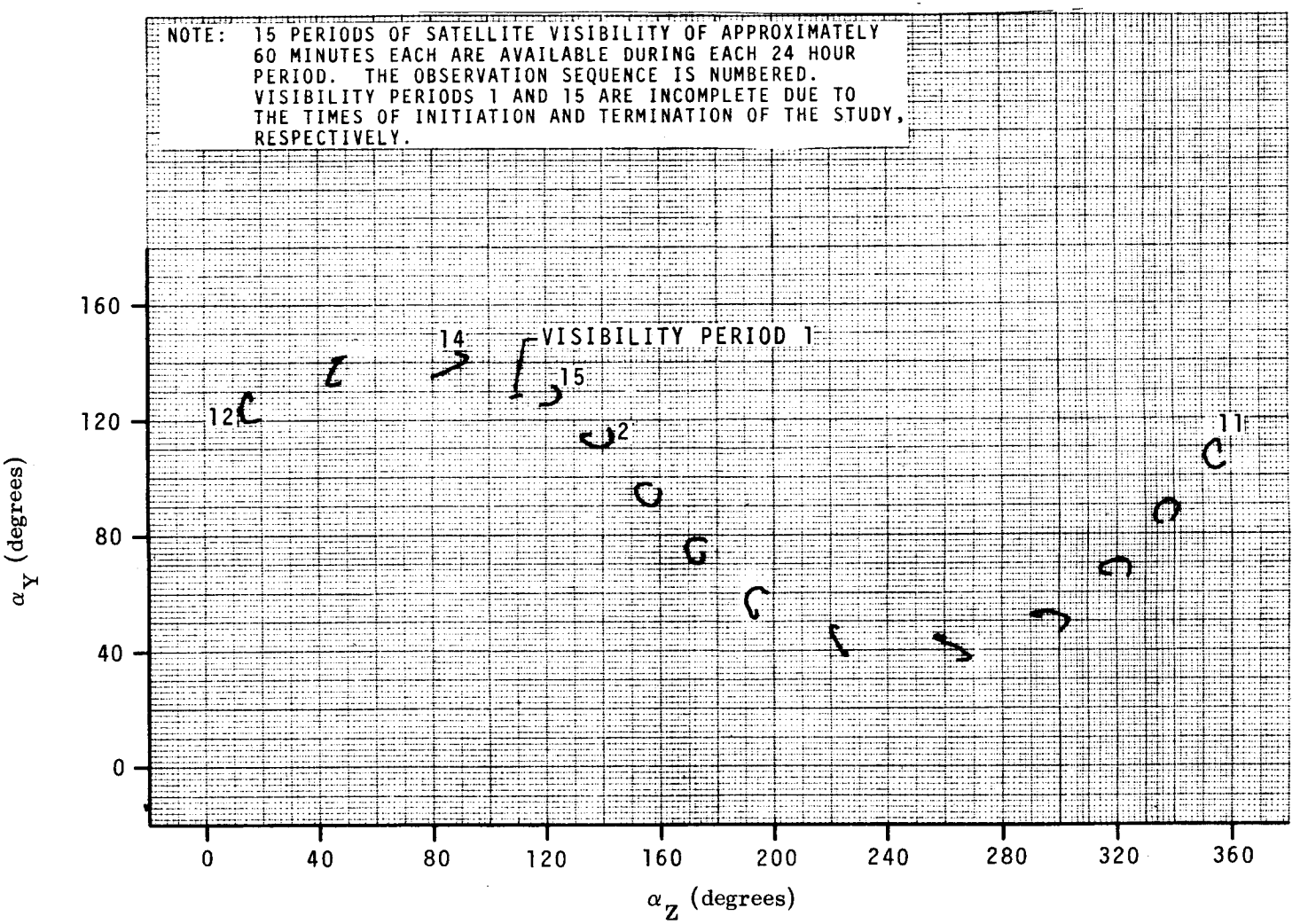

Figure V-43. Look angles from LST to TDRS — star declination = +40 degrees, sun declination = +23.4 degrees (sun right ascension is 90 degrees greater than that of star).

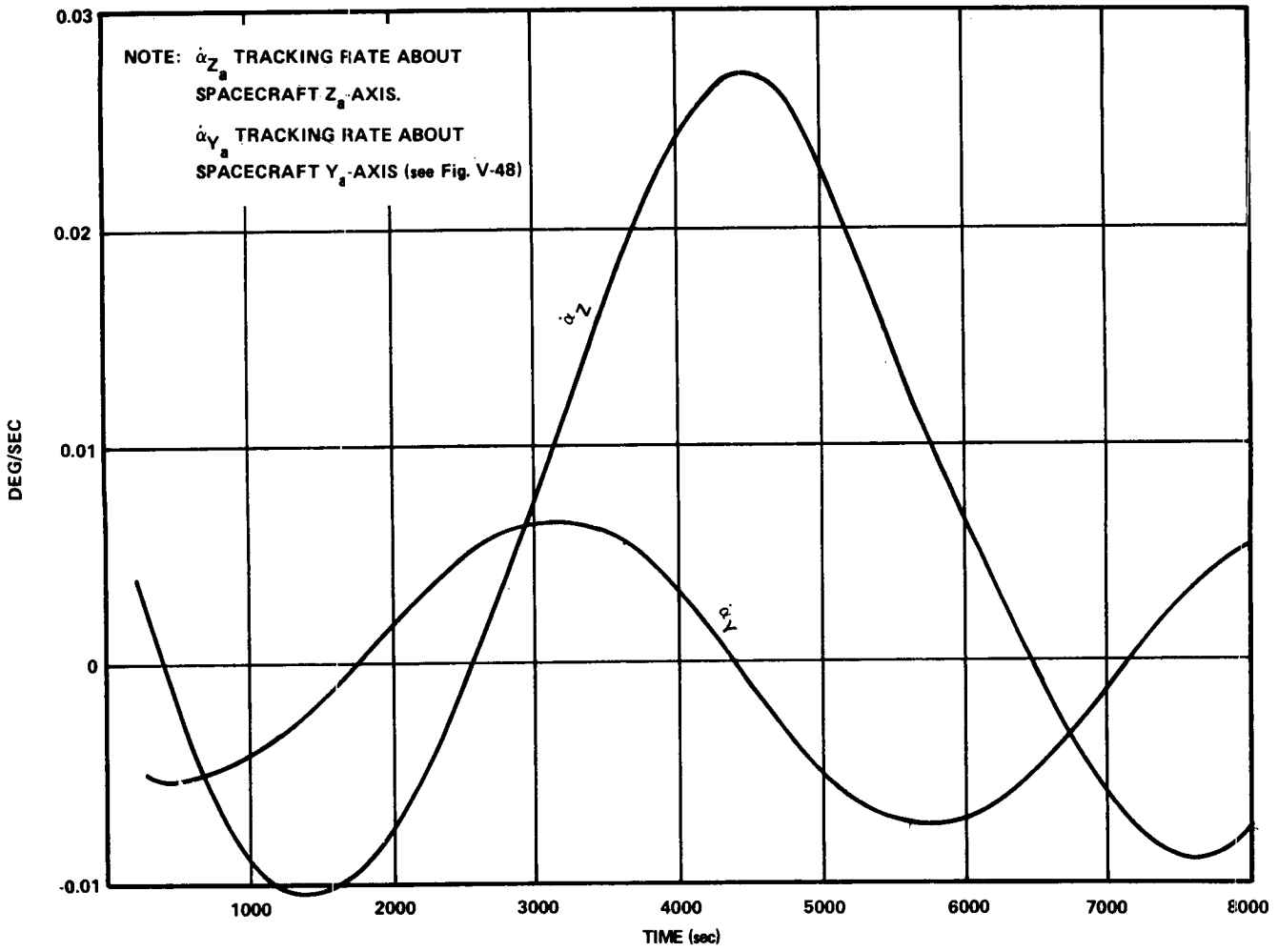

Figure V-44. LST antenna rotation rates required to track the TDRS.

(2) Step Tracking. The basic concept in step tracking is to sense variations in the strength of the received signal caused by perturbing the antenna position. The antenna is then moved to a position which maximizes the signal strength. Typically the antenna is randomly offset from neutral and the signal amplitude integrated for a given period. The antenna is then offset in the opposite direction and the signal amplitude is integrated again. The comparison of the two offset amplitudes with the neutral amplitude will then determine the direction in which to move the antenna. Step tracking has the advantage of requiring only a single channel receiver for operation. The primary disadvantage is its slow tracking capability because of the required signal integration time.

(3) Monopulse Tracking. In monopulse tracking, the direction in which to move the antenna for the maximum signal is determined by phase comparing the outputs from offset feeds with the sum of the feeds. Each feed determines a different beam offset according to the feed arrangement and accordingly can be used for angle determination. The primary disadvantage of monopulse tracking is the complexity because three receiver channels are required. The receiver requirement may be reduced through multiplexing techniques. The advantages of monopulse tracking are that it does not need computation support (except in acquisition) and a smooth continuous drive is imparted to the antenna, which results in minimum perturbations to the LST pointing stability. Because of these advantages, monopulse tracking was selected for the design reference concept.

2. Reference Design Description. The reference design configuration of the LST TDRSS terminal consists of two 2.4 m (8 ft) Ku band rigid dishes with subreflectors and a two-axis gimbal, a monopulse tracking system, a 40 watt TWT transmitter, and a data receiver.

Figure V-45 is a block diagram of the reference design. The 2.4 m antennas have a two-gimbal mounting and are located on the end of a 9.15 m (30 ft) boom. The boom is deployable and once deployed is locked in place. A servo system provides drive to the antenna. The servo drive signals are provided by a conventional monopulse tracking receiver and by the guidance computer in the SSM. The guidance computer calculates antenna look angles to the TDRS relative to the local body references using the known TDRS ephemeris and the ephemeris and attitude of the LST. The angle data provided to the servo should be accurate enough to place the TDRS in the 3 dB beam width of the antenna. In this case the monopulse receiver will detect acquisition, and automatic tracking will begin using error signals derived from the antenna feed. Should the TDRS not fall within the antenna beam width, a local scan routine would be initiated until acquisition is detected.

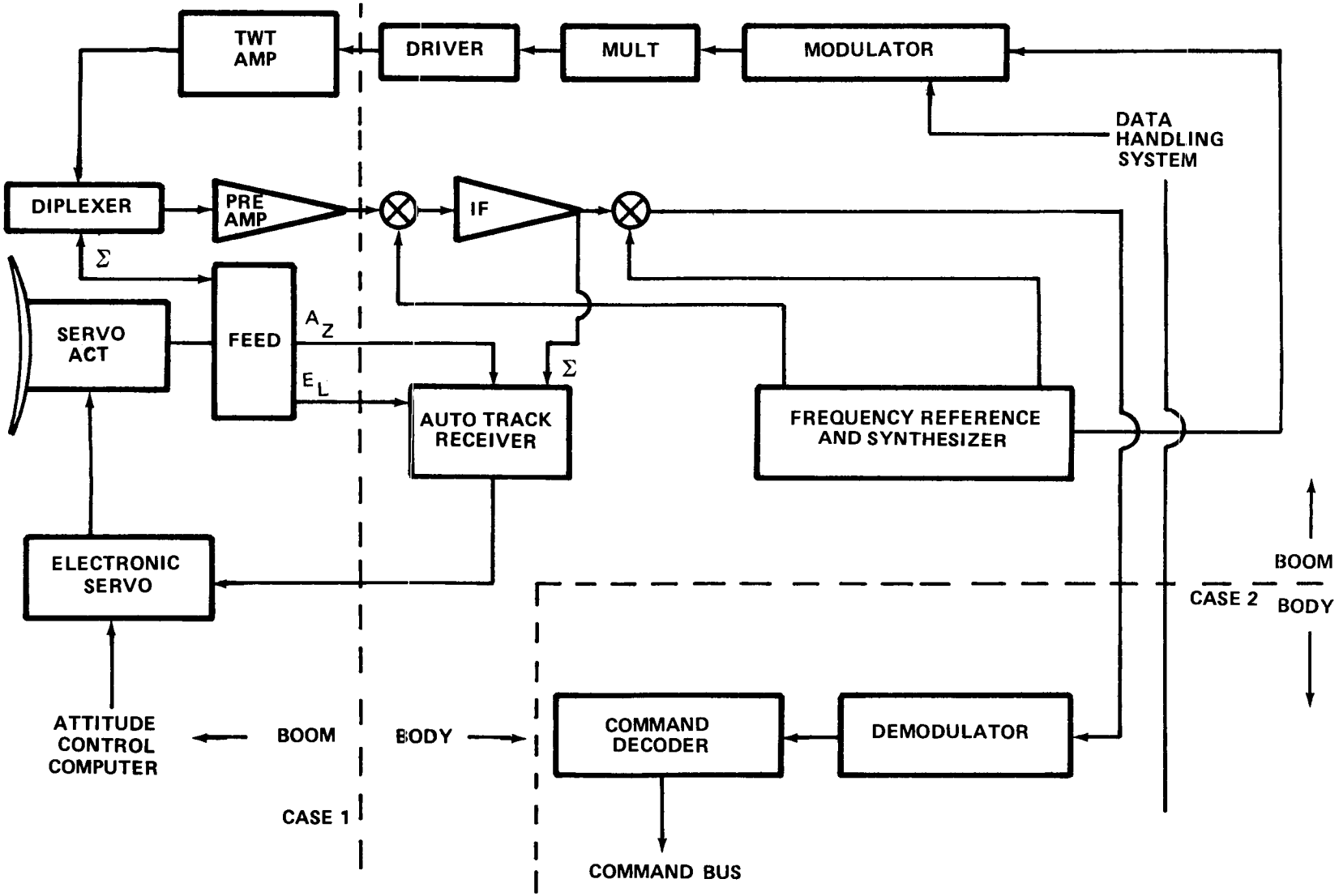

Figure V-45. LST Ku band terminal.

Since the antenna has two degrees of freedom, RF signals to the antenna must pass through rotary or flexible joints. Two means of hardware division were considered for the terminal. In Case 1, the transmitters, antenna feed, and preamplifiers are located on the antenna boom with the remaining hardware in the spacecraft. In Case 2, all hardware except the data receiver is located on the boom on the antenna side of the gimbal joint. The primary differences between the two cases are the equipment weight on the boom and the frequency of the signals that must pass through the rotary joints. In Case 1, the boom-mounted components are lighter than in Case 2; however, the RF signals would be at Ku band versus approximately 100 MHz for Case 2 and flexible cables could be used instead of a rotary joint transmission line.

A preliminary analysis of the pointing error produced by Case 2 indicates that the error is within the correction capability of the LST stabilization system. Because Case 2 is feasible and does not require the development of a two degree of freedom Ku band rotary joint, it is the recommended configuration.

The receiver is a double conversion type of standard design with crystal controlled local oscillators. The demodulator receives the second intermediate frequency and demodulates the command subcarrier to baseband. It then detects the command date to video. The detected video or digital code is then presented to the command decoder and processed identical to commands sent via the S-band link.

Information received from the data handling system is phase modulated on a reference frequency. This phase modulated frequency is then multiplied to Ku band. The driver and TWT amplifier then raise the power level to 40 watts prior to deplexing to the antenna.

Figure V-46 shows the antenna attached to the LST in the deployed position. The two gimbal axes will allow 360 degree movement around the boom and approximately 340 degree movement in the plane formed by the booms and the LST. The booms extend beyond the solar panels and thus the antennas are not blocked by the panels as they track the sun. Tables V-9 and V-10 show the estimated mass and power requirements of the TDRSS terminal. The mass and power estimations are in two parts, boom-mounted and spacecraft-mounted equipment. The boom-mounted components listed are for Case 2, in which the entire terminal minus the modulator and command decoder is located in an instrument container behind the antenna dish. Estimated battery, solar panel, and power conditioning weights are also included in the spacecraft-mounted portion of the terminal.

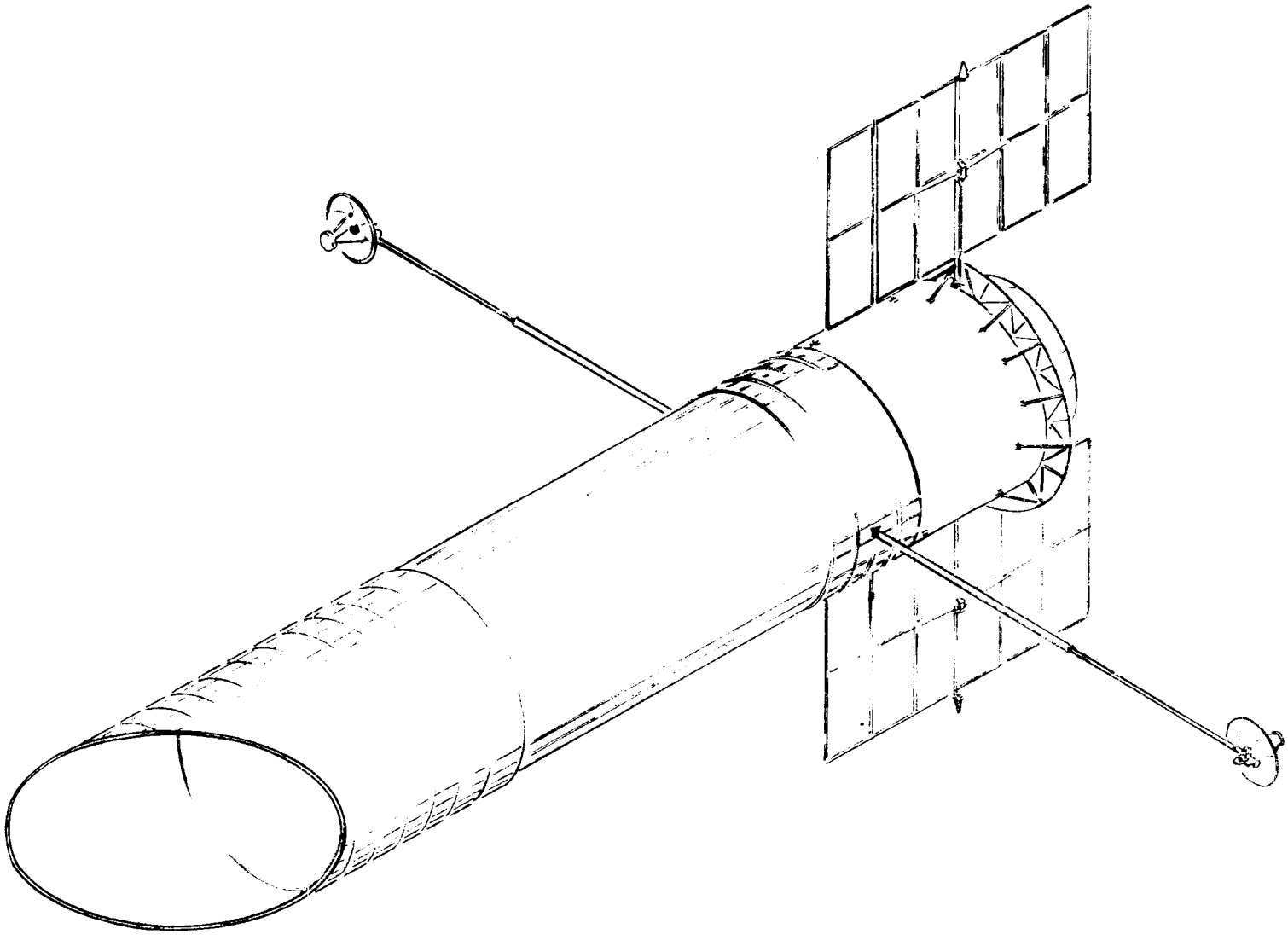

Figure V-46. LST TDRS terminal.

TABLE V-9. ESTIMATED MASS AND POWER REQUIREMENTS OF THE TDRSS TERMINAL — BOOM-MOUNTED EQUIPMENT

	Power (W)	Mass (kg)
Antenna Dish	-	5.4
Antenna Feed and Supports	-	2.3
Servo Motor, Signal Couplers Servo System	5	4.5
Preamplifiers	3	2.7
Auto-Track Receiver	10	2.3
Transmitter	210	10.5
Modulator/Driver	5	0.5
Total (Boom)	233	28.2

TABLE V-10. ESTIMATED MASS AND POWER REQUIREMENTS OF THE TDRSS TERMINAL — SPACECRAFT-MOUNTED EQUIPMENT

	Power (W)	Mass (kg)
Data Receiver	8	1.4
Energy Storage	-	11.6
Solar Array	-	8.1
Total (Spacecraft)	8	21.1
Total (Spacecraft and Boom)	241	49.4

3. Functional Analysis

a. Antenna and Amplifier Selection. The requirement for a 40 watt transmitter and a 2.4 m (8 ft) antenna was determined by considering the link margin calculation for 50 megabits of data via the TDRSS:

$$P/KT = P_t + G_t + L_s + L_m + G_r/T - K - M$$

where

P/KT = ratio of average signal power to noise power/dB-Hz

P_t = power transmitted,

G_t = transmitter antenna gain,

L_s = free space loss,

L_m = miscellaneous losses (atmospheric, pointing, etc.),

G_r/T = receiver antenna gain/system noise temperature = 13.63 dB/°K,

K = Boltzmann's constant,

and

M = link margin.

The assumptions and restraints are as follows:

Frequency	15.3 GHz
Distance	42 200 km
G_r/T	13.63 dB/°K
L_m	-5 dB
P/KT	10.8 dB-Hz

Thus,

$$10.8 = P_t + G_t - 208.67 - 5 + 13.63 + 228.6 - 6 \quad ,$$

$$P_t = 65.24 - G_t \quad ,$$

and

$$P_t = 34.15 - 20 \log D$$

A survey of Ku band power amplifier availability indicated that a 40 watt TWT amplifier would be the largest available in the allowed time frame with a reasonable risk factor. Figure V-47 is a plot of the link equation in terms of LST transmitted power versus antenna size and indicates that a 2.4 m (8 ft) antenna would be required. The following list shows the proposed TDRSS characteristics used in the analysis:

1. Receive Frequency — 14.4 to 15.35 GHz
2. System Noise Temp. — 1200°K
3. Antenna 1.5 m (5 ft) Dish — 44.43 dB
4. Beam Width — 0.8 deg
5. Antenna Gain to System Noise Temperature (G/T) — 13.63 dB/°K
6. Linear Frequency Translation
7. Limiting Amplifier

   Angle Modulation Only
8. Transmission Frequency — 13.4 to 14.2 GHz
9. Effective Isotropic Radiated Power (EIRP) — 52 dBW

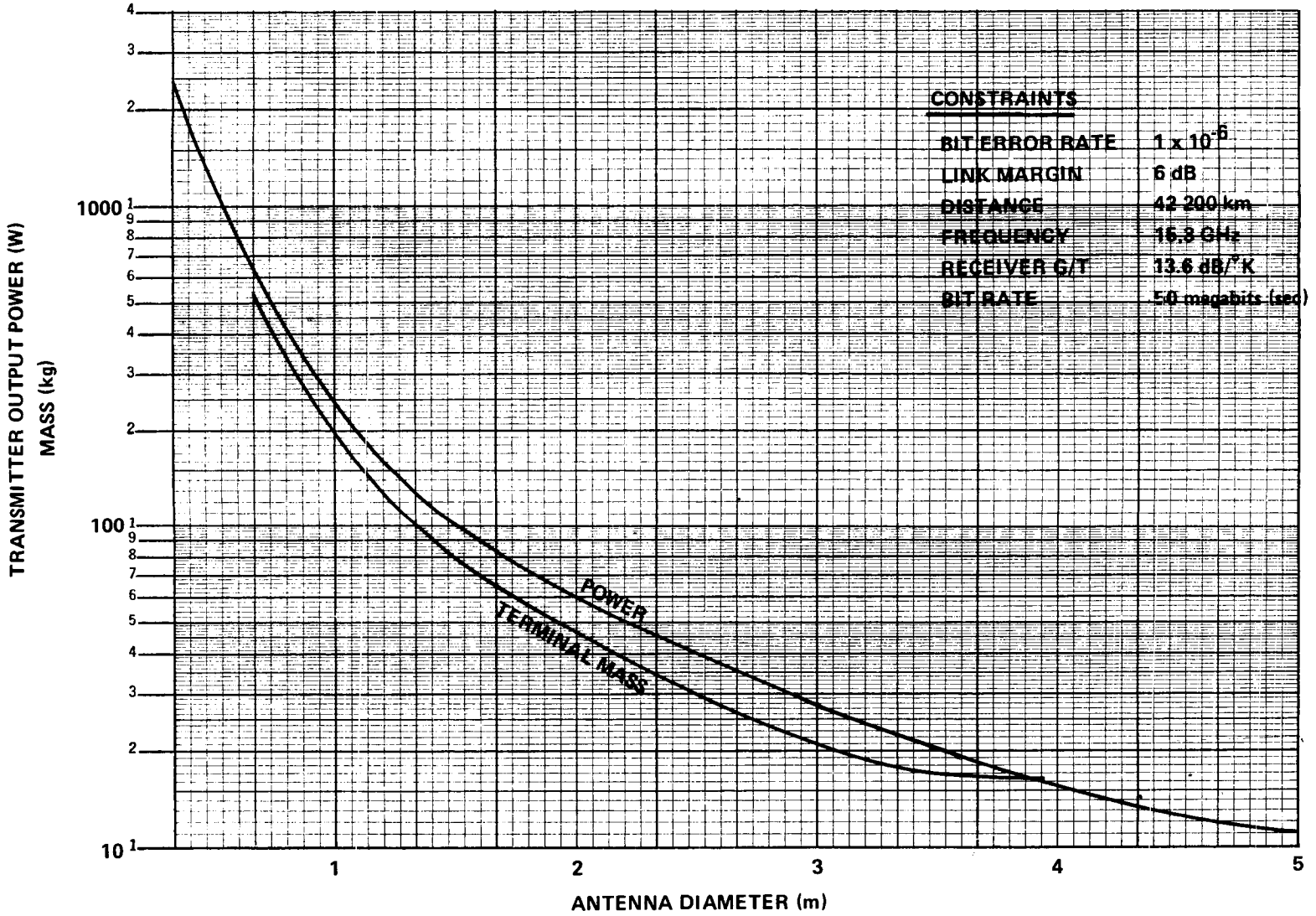

Figure V-47. TDRSS terminal weight/power versus antenna diameter.

Also shown in Figure V-47 is a plot of terminal mass versus antenna diameter. The antenna mass increases as diameter increases. However, this increase is more than offset by the reduction of transmitter, battery, solar cells, and power conditioning required as antenna diameter increases

b. Uplink Calculations. The capabilities of the TDRSS used as an uplink to the LST were also assessed. The results of a TDRS to LST link calculation shown in the following list allow an uplink information bandwidth of 1.66 MHz, which is more than adequate to meet the LST uplink requirements.

1. Effective Radiated Power (ERP) [1.2 m (4 ft) Dish, 10 W] — 52 dBW

2. Free Space Loss (42 000 km, 14.3 GHz) — -208 dB

3. G_r/T 2.4 m (8 ft) Dish, 2500°K — 14.6 dB/°K

4. Miscellaneous Losses (Pointing, Atmosphere, and Checkout) — -5 dB

5. Boltzmann's Constant — -228.6 dBW/°K-Hz

6. TDRSS Degradation — -1 dB

7. Link Margin — -6 dB

Total — 75.2 dB-Hz

Required Signal to Noise (S/N) — 13 dB

Excess S/N — 62.2 dB

Possible Bandwidth — $10^{6.22}$ = 1.66 MHz

c. Pointing Impact Assessment. An analysis was made to determine the effect that antenna tracking movements would have on the pointing accuracy of the LST. The nominal antenna movement rate (Fig. V-44) was taken to be 5.210^{-4} rad (0.03 degrees) per second while tracking the TDRSS and repositioning of 2.1 rad (120 degree) in 10 minutes while slewing to acquire the TDRSS. The antenna boom is 8.6 m (338 in.) long with a mass of 38.6 kg (85 lb) at the end. The polar mass moment of inertia is 13.44 kg-m^2

(10 slug-ft^2) and the mass moment of inertia about the Y_a and Z_a axis is 13.55 kg-m^2 (10 slug-ft^2). An antenna boom was designed for a fundamental natural frequency of about 1 Hz. The mass of one boom made of Lockalloy material is 43 kg (95 lbm). It has a circular section of 8.9 cm (3.5 in.) outside diameter and 0.95 cm (0.374 in.) thickness.

The roll error about the spacecraft X-axis caused by the movement of one antenna for tracking and another for repositioning is 4×10^{-4} arc sec for a boom natural frequency of 1 Hz. The roll error about the spacecraft Y-axis is about 8.5×10^{-5} arc sec for a boom natural frequency of 1 Hz. The roll error about the spacecraft Z-axis is less than that for the Y-axis. These roll errors in all three spacecraft axes are much less than the spacecraft pointing stability requirement of 0.005 arc sec. This shows that the movement of the antennas for simultaneous tracking and repositioning can be made without exceeding the pointing stability error tolerance of the spacecraft.

The error in the pointing axis of the antenna caused by the deflection of the boom is about 1.95×10^{-3} arc sec. This error is negligible in comparison with the allowable error limit in the antenna pointing axis of 4.4×10^{-3} rad (0.25 degree).

Figure V-48 shows the LST spacecraft with two deployed tracking antennas. The X, Y, Z coordinate system shown in this figure is centered at the center of gravity of the LST spacecraft with deployed solar panels and deployed antennas. The X_a, Y_a, Z_a coordinate system is centered at the tip of the antenna boom, as shown in Figure V-48 and rotates with the antenna relative to the X, Y, Z coordinate system.

The antennas have 2 degrees of freedom, a roll about the Y_a-axis and a roll about the Z_a-axis. The dimensions and the mass breakdown for the various parts of the antenna are shown in Figure V-48.

(1) Design of Antenna Boom. The antenna boom is 860 cm (~340 in.) long and supports an antenna mass of 38.5 kg (86 lbm) at its tip. The boom will be subjected to bending and torsion due to the application of torque for rotating the antenna. The smallest natural frequency in bending and torsion modes for the boom should be larger than the spacecraft control frequency. The boom is designed so that its smallest natural frequency in both the bending and torsion modes of vibration is about 1 Hz.

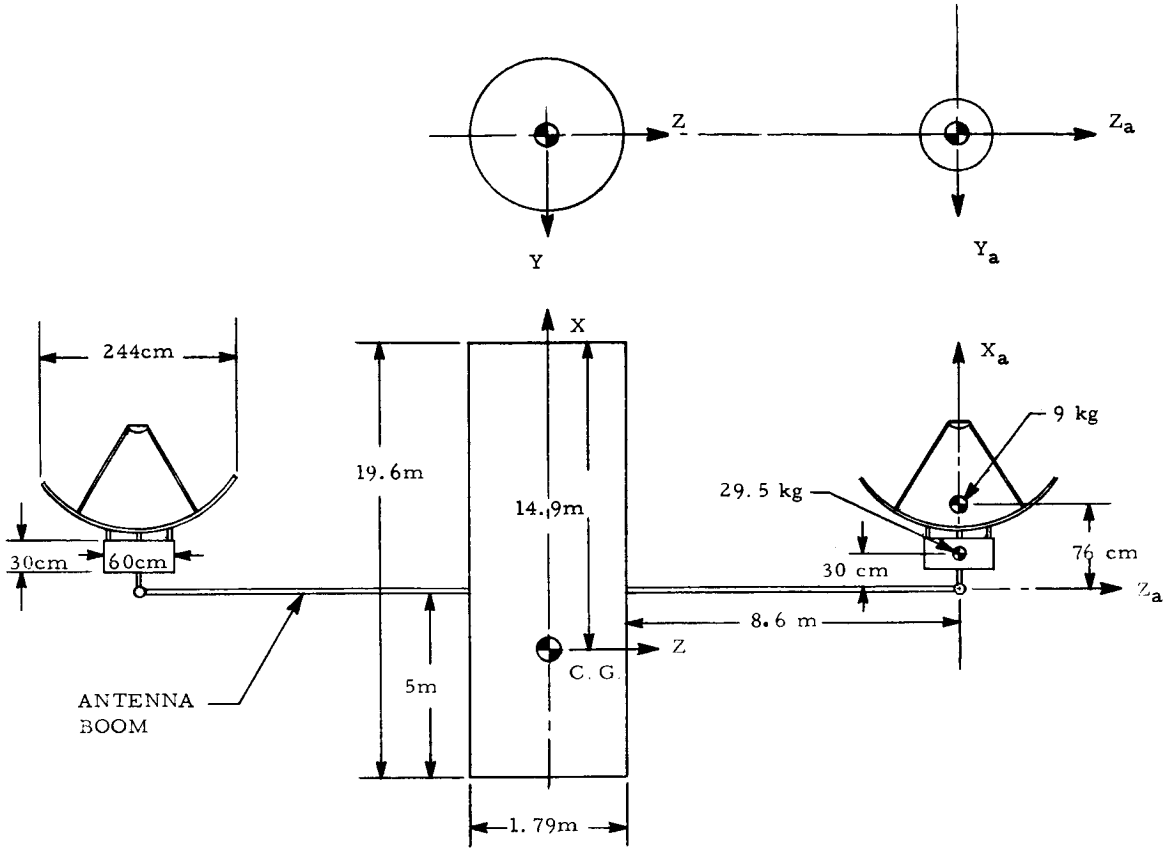

Figure V-48. Schematic of LST spacecraft with deployed antenna booms.

(a) Design in Bending. The fundamental natural frequency in bending for a cantilever beam fixed at the end attached to the spacecraft and supporting a tip mass at the other end is:

$$\omega_n = \left(\frac{K}{M + 0.23\ m} \right)^{1/2} \qquad (1)$$

where M is the tip mass at the end of the boom, m is the mass of the boom, and K is the spring constant in bending for the boom material. The value of the spring constant K for the cantilever boom is

$$K = \frac{3\,EI}{L^3} \qquad (2)$$

where E is Young's modulus of elasticity for the boom material, I is the area moment of inertia of the boom section, and L is the length of the boom.

Lockalloy (62 Be-38 Al) was selected for the boom material because it is light [material density = 2.1 gm/cm^3 (0.0756 lbm/in.^{3})] and has a high value of $E = 1.98 \times 10^{11}$ N/m^2 (28.7×10^6 lbf/in.^{2}). A Lockalloy hollow circular tube of 8.9 cm (3.5 in.) outside diameter and 0.95 cm (0.374 in.) thickness has a cross-sectional moment of inertia of 19 cm^4 (0.456 in.^{4}) and a mass of about 43 kg (95 lbm) for a 860 cm (340 in.) length. The fundamental natural frequency for the boom with the antenna at its end was computed as 6 rad/sec.

(b) Design in Torsion. The fundamental natural frequency in the torsion mode for the cantilever beam is

$$\omega_t = \left(\frac{K_t}{I + \frac{I_s}{3}} \right)^{1/2} \qquad (3)$$

where ω_t is the fundamental natural frequency in the torsion mode, K_t is the spring constant in torsion for the boom material, I is the polar mass moment of inertia for the tip mass, and I_s is the polar mass moment of inertia for the boom. The value of K_t for a cantilever beam is

$$K_t = \frac{GJ}{L} \qquad (4)$$

where G is the shear modulus for the boom [for Lockalloy, $G = 7.56 \times 10^{10}$ N/m^2 (11×10^6 lbf/in.^{2})], L is the length of the boom, and J is the polar area moment of inertia of the boom section.

The value of the polar mass moment of inertia, I, for the tip mass (one antenna) is 13.44 kg-m^2 (10 slug-ft^2).

For the same hollow circular section boom designed in bending, the fundamental natural frequency in torsion was computed as about 49 rad/sec. This shows that the designed boom is stiffer in torsion than in bending.

(2) Spacecraft Pointing Error Analysis. The mass moment of inertia of one antenna was calculated to be 13.55 kg-m^2 (10 slug-ft^2) about both the Y_a- and Z_a-axes. The momentum of an antenna moving at the maximum tracking speed of 5.2×10^{-4} rad/sec (0.03 degrees/sec) is 0.0071 N-m-sec (5.24×10^{-3} ft-lbf-sec). The momentum required for maneuvering the second antenna through 2.1 rad (120 degrees) in 10 minutes is 0.095 N-m-sec (0.07 ft-lbf-sec). This momentum is computed on the basis of accelerating the antenna for half the maneuver time and decelerating it for the remaining maneuver time. The total momentum required for the two antennas is maximum when the tracking momentum and maneuvering momentum are in phase; this value is 0.1021 N-m-sec (0.07524 fr-lbf-sec).

Driving mechanisms for moving individual antenna can be designed so that the vector sum of the driving mechanism momentum and the antenna momentum is zero. This will require a proper design of the torque motor and various gearing mechanism if used. When the vector sum momentum is zero at every instant of time, no reaction torque will act on the spacecraft. Under this condition the spacecraft pointing will not be disturbed. However, if the vector sum momentum is not zero at every instant of time, reaction torque will act on the spacecraft. If this reaction torque is not counteracted by the torque of the CMGs, spacecraft motion will result.

At the instant torques are applied for moving the antennas, the antenna booms will start vibrating because of their flexibility. The amplitude of the vibrations will depend upon the natural frequency and the damping of the booms. The amplitude of the vibrations also depends upon the type of torques applied. For example, if a ramp type of torque, a torque that increases linearly with time, is applied instead of a step-type torque, the amplitude of the boom vibrations can be decreased appreciably. In this study, however, the application of step-type torques for moving the antennas is assumed. It is also assumed that no cancellation of antenna momentum occurs by the driving mechanism momentum and that all the torque required for moving the antennas is transferred as a reaction torque to the spacecraft through the flexible booms.

(a) Roll Error About X-Axis. When torques are applied at both the antenna tips for tracking and repositioning of the antennas, the antenna booms deflect, as shown in Figure V-49. Using the Lagrangian formulation for the system dynamics, the value of the roll error, $\theta_x(t)$ about the spacecraft X-axis due to the application of step torques is .

$$\theta_x(t) = \frac{T\,t^2}{I_{sx}} - \frac{T\,K}{\omega_n^2}\left\{1 - \frac{1}{(1-\xi^2)^{1/2}} \exp\left(-\xi\omega_n t\right) \sin\left[\omega_n (1-\xi^2)^{1/2} t + \tan^{-1}\left(\frac{1-\xi^2)^{1/2}}{\xi}\right)\right]\right\} \quad (5)$$

where

$\theta_x(t)$ rotation of the spacecraft about the X-axis as shown in Figure V-49,

T step torque applied at both the antennas as shown in Figure V-49,

t time,

I_{sx} moment of inertia about the X-axis of the spacecraft with deployed solar panels and antenna booms,

M tip mass at the end of the boom (this includes the mass of the antenna disk and associated electronics and drive mechanisms),

m mass of the boom,

K constant defined by

$$K = 2\left(\frac{m_1 R_1 + 2MR_2}{I_{sx}}\right)\left\{\frac{I_{sx} \cdot (mR_1 + 2MR_2)\,L}{\left[\left(\frac{m}{2} + 2M\right)I_s + mMR^2\right]L}\right\},$$

R_1 distance of the center of mass of the boom from the X-axis of the spacecraft,

R_2 distance of the tip mass M from the X-axis of the spacecraft,

I_s spacecraft moment of inertia about the X-axis without antennas and antenna booms,

ω_n natural frequency of the antenna boom

R radius of the spacecraft as shown in Figure V-49,

and

ξ damping factor for the antenna boom.

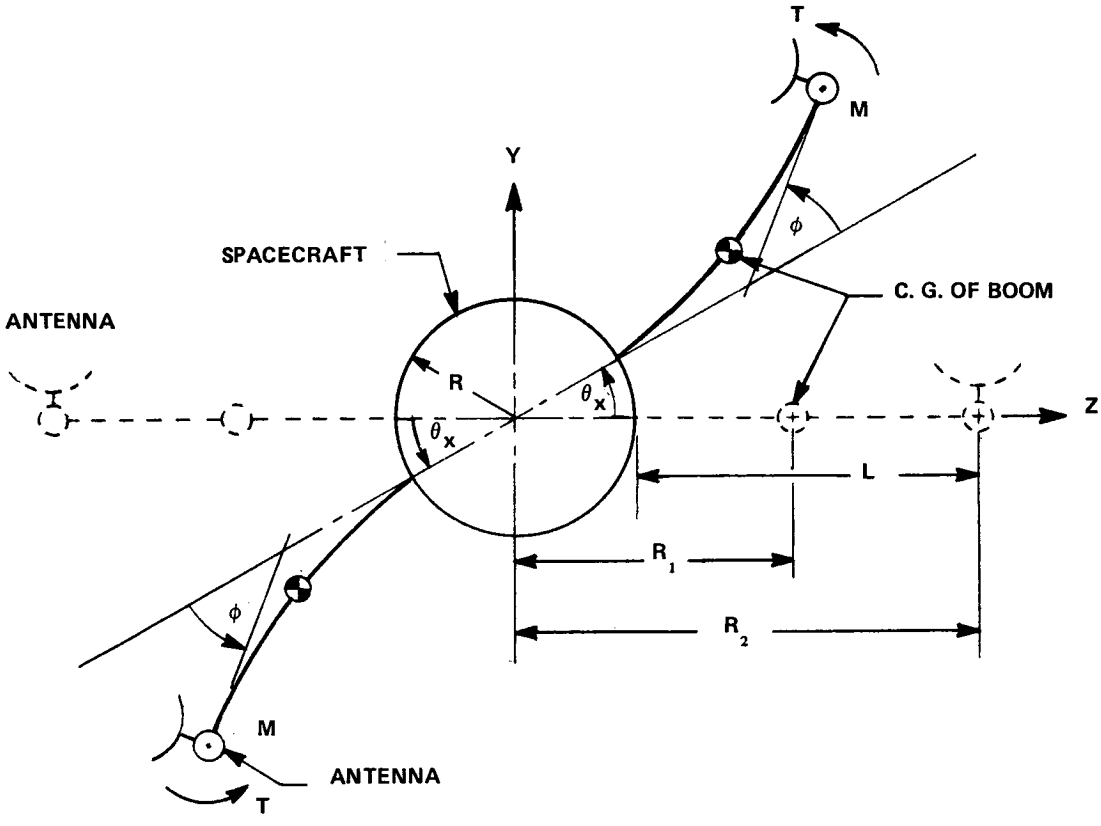

Figure V-49. Rotation of the spacecraft and deflection of the booms due to step torque T applied at the antennas.

Equation (5) has been derived by assuming that the LST main body is rigid and the antenna booms are elastic. Furthermore, it is assumed that the mass of the antenna is concentrated at the tip of the antenna boom and the mass of the boom is concentrated at the center of mass of the boom.

In equation (5), the first term represents the spacecraft motion considering the spacecraft and antenna booms as rigid and the second term represents the effect of the flexibility of the antenna booms on the spacecraft motion. It is noted from equation (5) that the first term is a direct current component and has no transients; however, the second term has exponentially decaying sinusoidal transients. The frequency of these transients is the same as the natural frequency of the antenna booms. The time constant τ, defined as the time taken for the transients to decay by 63 percent is approximately equal to

$$\tau = \frac{1}{\xi \omega_n} \quad . \tag{6}$$

The component of $\theta_x(t)$ given by the first term of equation (5) can be controlled by the use of CMGs because it is direct current, but the transient part of $\theta_x(t)$, given by the second term, cannot be controlled by CMGs because it contains high-frequency transients. The maximum value of the transient part, $(\Delta\theta_x)_{max}$, is given approximately by

$$\left(\Delta\theta_x\right)_{max} = \frac{2\,T\,K}{\omega_n^{\,2}} \quad . \tag{7}$$

The value of I_{sx} is 26 200 kg-m^2 (19 330 slug-ft^2) and the value of I_s is 14 650 kg-m^2 (10 810 slug-ft^2). These values produce a K value of 1.485×10^{-4}. Substituting this value of K into equation (7) gives

$$\left(\Delta\theta_x\right)_{max} = 2.97 \times 10^{-4} \left(\frac{T}{\omega_n^{\,2}}\right) \quad . \tag{8}$$

The amount of torque required for maneuvering one antenna is computed as about 3.25×10^{-4} N-m (2.4×10^{-4} ft-lbf). The above computation assumes that the antenna mass is accelerated half the time and decelerated the other half-time. The same amount of torque is more than sufficient for continuous tracking of the second antenna. Using this value of the torque in equation (8) gives

$$\left(\Delta\theta_x\right)_{max} = 7.13 \times 10^{-8}\left(\frac{1}{\omega_n^2}\right) \quad . \qquad (9)$$

(b) Roll Error About Y-Axis. Equation (9) gives the roll error about the spacecraft X-axis caused by the flexibility of the antenna boom. A similar equation is obtained for the roll error about the spacecraft Y-axis caused by the flexibility of the antenna boom. This equation is

$$\left(\Delta\theta_y\right)_{max} = 1.6 \times 10^{-8}\left(\frac{1}{\omega_n^2}\right) \quad . \qquad (10)$$

Equations (9) and (10) are plotted in Figure V-50. From this figure it is noted that the roll errors in both the spacecraft X- and Y-axes for $\omega_n = 6.28$ rad/sec (1 Hz) are much less than the spacecraft pointing stability requirement of 0.005 arc sec.

The effect of the antenna boom damping ξ (ξ lies in the range of 0.05 to 0.001) on the magnitude of the roll error $\theta_x(t)$ is very small, as noted from equation (5). However, the effect of ξ on the settling time t_s, which is approximately equal to $4/\xi\omega_n$, is more pronounced. The natural frequency of the antenna boom affects both the magnitude of the roll error and the settling time.

(c) Roll Error About Z-Axis. A torque applied about the Z_a-axis for moving the antenna will result in a roll error about the spacecraft Z-axis. The antenna boom will be in torsion because of this torque. Since the antenna boom is very stiff in torsion because of its high natural frequency in the torsion mode, the roll error about the spacecraft Z-axis will be less than that about the spacecraft Y-axis given in Figure V-50.

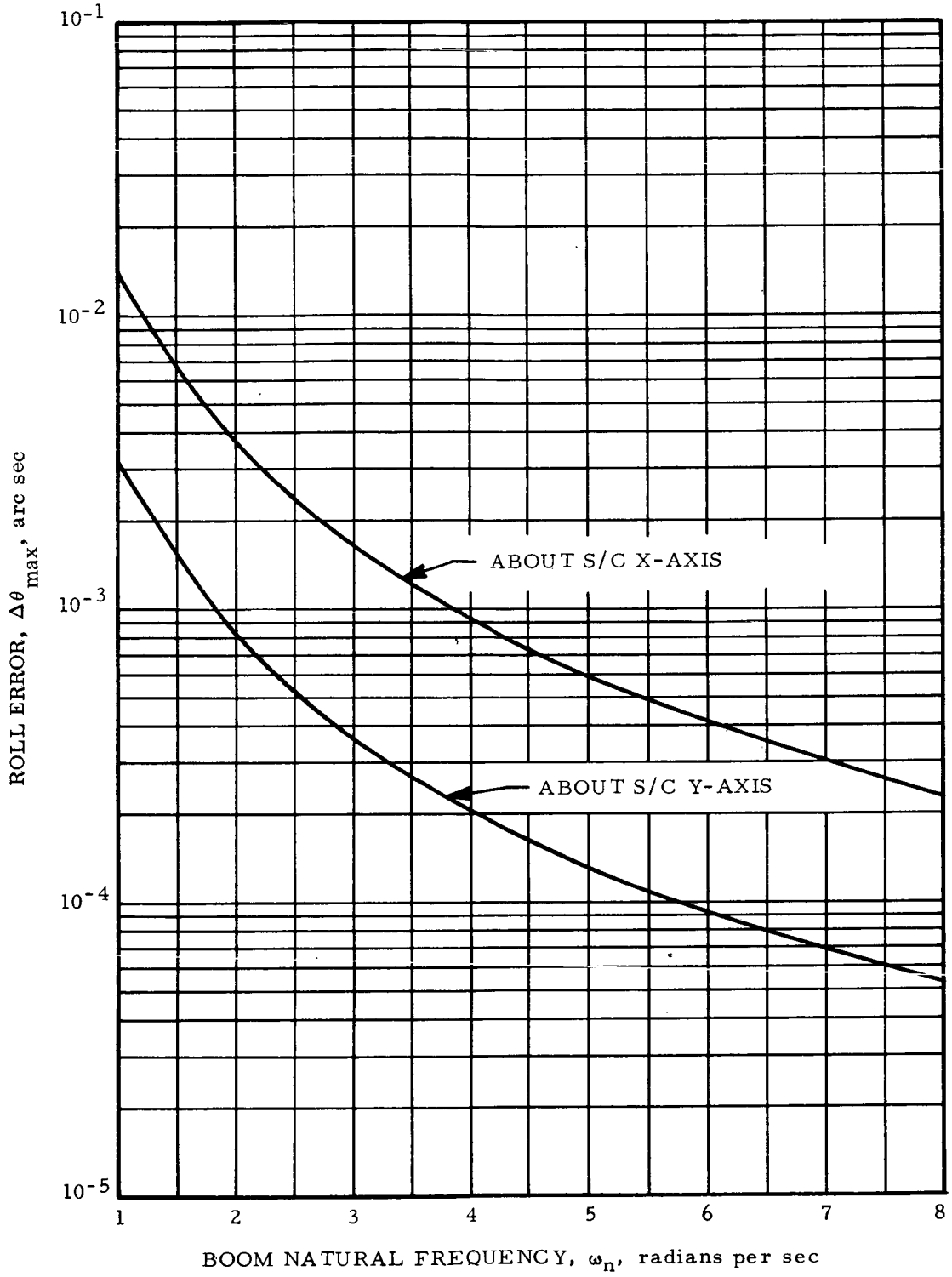

Figure V-50. Roll errors about spacecraft X- and Y-axes for various boom fundamental natural frequencies.

(3) Antenna Pointing Error. When torque is applied for moving the antenna, the antenna boom bends and with this the pointing axis of the antenna disk also bends, as shown in Figure V-49. The maximum angle through which the antenna axis rotates is

$$\phi = \left(\Delta\theta_x\right)_{max} + \phi_0 \qquad (11)$$

where ϕ is the antenna pointing axis rotation angle as shown in Figure V-49, $(\Delta\theta_x)_{max}$ is defined previously; its value is 4×10^{-4} arc sec for $\omega_n = 1$ Hz, and ϕ_0 is the steady-state deflection angle at the tip mass for a cantilever beam. The value of ϕ_0 is given by

$$\phi_0 = \frac{T\,L}{E\,I} \quad . \qquad (12)$$

Substituting the various values into equation (12), gives $\phi_0 = 1.55 \times 10^{-3}$ arc sec. Substituting this value in equation (11), gives $\phi = 4 \times 10^{-4} + 1.55 \times 10^{-3} = 1.95 \times 10^{-3}$ arc sec. This value of the antenna pointing error ϕ is within the allowable antenna pointing error of 4.4×10^{-3} rad (0.25 degree).

4. Conclusions. The following conclusions are made as a result of this preliminary study:

1. A TDRSS terminal is technically feasible for the LST.

2. Two steerable 42.4 m (8 ft) diameter Ku band antennas and a 40 watt transmitter will meet the requirement to relay the wideband data.

3. The antenna dishes must be mounted on booms to allow clearance to see around the solar panels in order to provide maximum coverage.

4. The pointing error imparted to the LST because of antenna motion is within the correction capability of the attitude sensing and control system (ASCS).

5. Recommendations. It is recommended that an in-depth analysis be made of the LST TDRSS terminal. The analysis should include but not be limited to the following areas:

1. Consider a rigid versus a rollup antenna reflector. A rollup reflector may alleviate the stowage problem. Cost and reliability should be included.

2. Examine the possible places to locate the antenna during storage and after deployment. Key issues are reliability, antenna blockage, or interference with other items such as solar arrays or star trackers.

3. Analyze the various antenna tracking techniques considering simplicity, accuracy, and the effect upon the LST pointing accuracy.

REFERENCES

V-1. Brown, Earle B.: Modern Optics. Reinhold Publishing Corp., New York, p. 491.

V-2. Mass Memory Applications Study. Contract NAS8-21531, Arthur D. Little, Inc., Cambridge, Mass., August 1970.

V-3. Matick, Richard E.: Review of Current Proposed Technologies for Mass Storage Systems. Proceedings of the IEEE, vol. 60, no. 3, March 1972.

V-4. Conceptual Design and Feasibility Evaluation Model of a 10^8 Bit Oligatomic Mass Memory. Contract NAS8-26670, Univac Division of Sperry Rand Corp.

CHAPTER VI. ATTITUDE CONTROL SYSTEM

TABLE OF CONTENTS

TABLE OF CONTENTS (Concluded)

LIST OF ILLUSTRATIONS

LIST OF ILLUSTRATIONS (Continued)

LIST OF ILLUSTRATIONS (Continued)

LIST OF ILLUSTRATIONS (Concluded)

LIST OF TABLES

DEFINITION OF SYMBOLS

Symbol	Definition
A	ampere
a_k	angle to momentum in face plane, k = 1, 2
$\overline{B}$	earth's magnetic field vector
b_k	angle of CMGs to momentum in face plane, k = 1, 2
C	cosine or CMG torque matrix
C^+	pseudo inverse of the matrix C
$\|CC^*\|$	determinant of the matrix CC*
D	diameter
f	momentum distribution function
GN_2	gaseous nitrogen
H	momentum or momentum per flywheel
h_i	momentum of i^{th} flywheel
I	vehicle inertia (subscript for axis identification)
i, j, k	unit vectors along X, Y, Z
k, K, L	constants (subscripts for identification)
kg	kilogram
L	length
$\overline{M}$	magnetic dipole moment vector
m	meter

DEFINITION OF SYMBOLS (Continued)

Symbol	Definition
N	newton
n. mi.	nautical mile
P	power
$\overline{R}$	unit local radius vector
S	sine
sec	second
T	tesla
$\overline{T}_c$	commanded torque vector
T_i	input torque
$\overline{T}_m$	magnetic torque vector
T_o	output torque
W	weight
X, Y, Z	right hand LST coordinate system
X_i, Y_i, Z_i	orthogonal coordinates for the ith CMG
X_s, Y_s, Z_s	right hand solar coordinate system
χ_{12}, χ_{34}	planar parameters defining f as function of h_i
α_i	gimbal angle for the ith CMG, i = 1, 2, 3, 4
β	skew angle of a CMG or RW
Δt	time stop or time interval

DEFINITION OF SYMBOLS (Concluded)

Symbol	Definition
δ_p	target pointing error
δ_s	solar offset angle
ϕ, ψ, θ	Euler angles (subscript c for commanded)
ω_o	orbital angular rate

Superscript	Definition
$^\circ$	dot for time derivative
—	bar for vector notation
~	tilde for a vector in matrix form
*	star for transpose of a matrix
-1	negative one for matrix inverse

CHAPTER VI. ATTITUDE CONTROL SYSTEM

A. Requirements

1. Guidelines and Constraints. An established guideline for commonality with the High Energy Astronomy Observatory (HEAO) subsystem was a strong driver in the selection of LST attitude control system (ACS) components. The basic reference for this selection was the TRW HEAO proposal [VI-1] in response to the HEAO RFP [VI-2]. However, it was recognized that the components defined in this document were preliminary and that the LST ACS should be updated as the HEAO design is finalized. Additionally, the decision was made late in the study to consider the Space Shuttle as the design reference launch and maintenance vehicle.

The following requirements have been specified for the LST mission:

1. Provide the capability for viewing any source on the celestial sphere at any time while satisfying sun, moon, and earth avoidance constraints. No observations will be made when the telescope line of sight (LOS) is within 45 degrees of the sun or within 15 degrees of the limb of the earth or moon.

2. Spacecraft coarse pointing accuracy.

   a. Two axes — ±30 arc sec, 3σ .

   b. About LOS — ±0.1 degree, 3σ .

3. Spacecraft fine pointing accuracy.

   a. Three axes — ±1 arc sec, 1σ , using the optical telescope assembly (OTA) fine guidance system (FGS).

4. Fine pointing accuracy (experiment LOS).

   a. Two axes — ±0.1 arc sec, 1σ (LOS relative to guide star locations).

5. Image motion stabilization.

a. Two axes — 0.005 arc sec, 1σ, using the OTA FGS.

b. About LOS — ±1 arc sec, 1σ.

6. Maneuvering.

a. 60 degrees in 40 min required.

b. 90 degrees in 5 min to be considered.

7. Provide momentum accumulation capability for a minimum of one orbit during experimentation without desaturation.

Additional requirements that are considered potential LST mission requirements are the following:

1. Boresight guiding (stars and planets).

2. Fine guidance adjustment capability — ±0.025 arc sec (2 axes).

3. Spectrometer slit scanning — 0.1 arc second steps over several arc seconds.

4. Provide the roll reference and maneuver requirements for spectrometer slit orientation.

These additional requirements were introduced late in the study and confirmation as real requirements necessitates a detailed study of the experiments, spacecraft, and ACS interfaces. In most cases, additional sensing capabilities will be required.

The following guidelines have been specified:

1. HEAO commonality.

2. Spacecraft and secondary mirror stabilization time of 5 min (includes OTA coarse/fine guidance handoff).

3. Antisolar hemisphere viewing is preferred.

4. Target selection will be made by ground command.

5. Use 1974 state-of-the-art for required hardware development.

6. Refurbish with Shuttle, as available, when indicated by ground diagnostics.

7. ACS assemblies including control moment gyros (CMGs) will be activated and partially checked out prior to release from the Space Shuttle.

8. The mass properties used for performance analysis and simulation are considered typical values and do not necessarily reflect the latest updating of the mass properties given in the master equipment list.

The primary requirement for a reaction control system (RCS) on the LST is to serve as an emergency backup control system to the LST primary ACS. Normally, during the entire LST mission, it is anticipated that there will be no disturbance torques of a magnitude that the CMGs cannot overcome. However, it is envisioned that during certain critical LST maneuver(s), abnormal control situations could occur and an RCS on the LST in a standby "go" condition would be highly desirable, e.g., during docking or misdock recovery of the LST and the Shuttle. Also, in the event of a complete or partial failure of the LST primary ACS, the RCS would provide the control torques necessary until the Shuttle can arrive to perform maintenance on the failed system.

The guidelines and assumptions considered for the RCS are as follows:

1. The primary launch vehicle for the LST is the Shuttle with the Titan IIIE as an alternate.

2. The CMGs are assumed to be spun-up prior to LST release from the Shuttle.

3. The LST is assumed to be released by the Shuttle in such an orientation that minimum maneuvering is necessary to acquire the sun.

4. The LST RCS must not be a contamination producing source.

5. Components of the LST RCS will have a shelf and operating minimum lifetime design goal of 2.5 years and, where possible, 5 years.

6. The LST RCS design will be based on meeting a man rating requirement.

7. The support systems module (SSM) will be pressurized so that man can perform orbital maintenance to the LST in a shirt sleeve environment. Limited extravehicular activity (EVA) will be allowed for maintenance.

8. The LST RCS design will be based on modularization such that RCS maintenance can be easily performed in orbit.

9. In designing the LST RCS, efficient use will be made of existing and proven components.

10. The LST RCS design will be based on maintaining a low total system weight, low cost, simplicity, and reliability.

11. The RCS will not be sized to be used as a backup to the magnetic torquers for CMG desaturation.

12. The RCS will be sized and used for abnormal control situations.

2. Reference Attitudes. Based on the guidelines and constraints, several reference attitudes must be defined to which the LST body-fixed axes are oriented during various operational modes. In Figure VI-1, the body principal axes and geometric axes are assumed to be identical and denoted by the (X, Y, Z) right-hand triad. The X-axis (minimum inertia) is along the LST line of sight and is referred to as the experiment or pointing axis. The Y-axis (intermediate inertia) is aligned with the solar wing gimbal axis of the LST. The Z-axis (maximum inertia) completes the triad and is perpendicular to the LST X-Y plane. It is directed outward from that side of the LST that is normally in the solar hemisphere. When the solar wings are initially deployed, they are rotated 90 degrees so that their active surface is normal to Z.

Since the LST depends upon solar energy to supply its power needs and the solar wings have only one degree of gimbal freedom, some restrictions must be placed upon the orientation of the LST. During normal operational modes, the LST's attitude is restricted so that the Z-axis is always in the solar hemisphere and contained in a plane defined by the sunline and the experiment source (target direction). With these restrictions, the LST can orient its experiment axis to any point on the celestial sphere and receive maximum solar energy by gimbaling its solar wings. Since one side of the

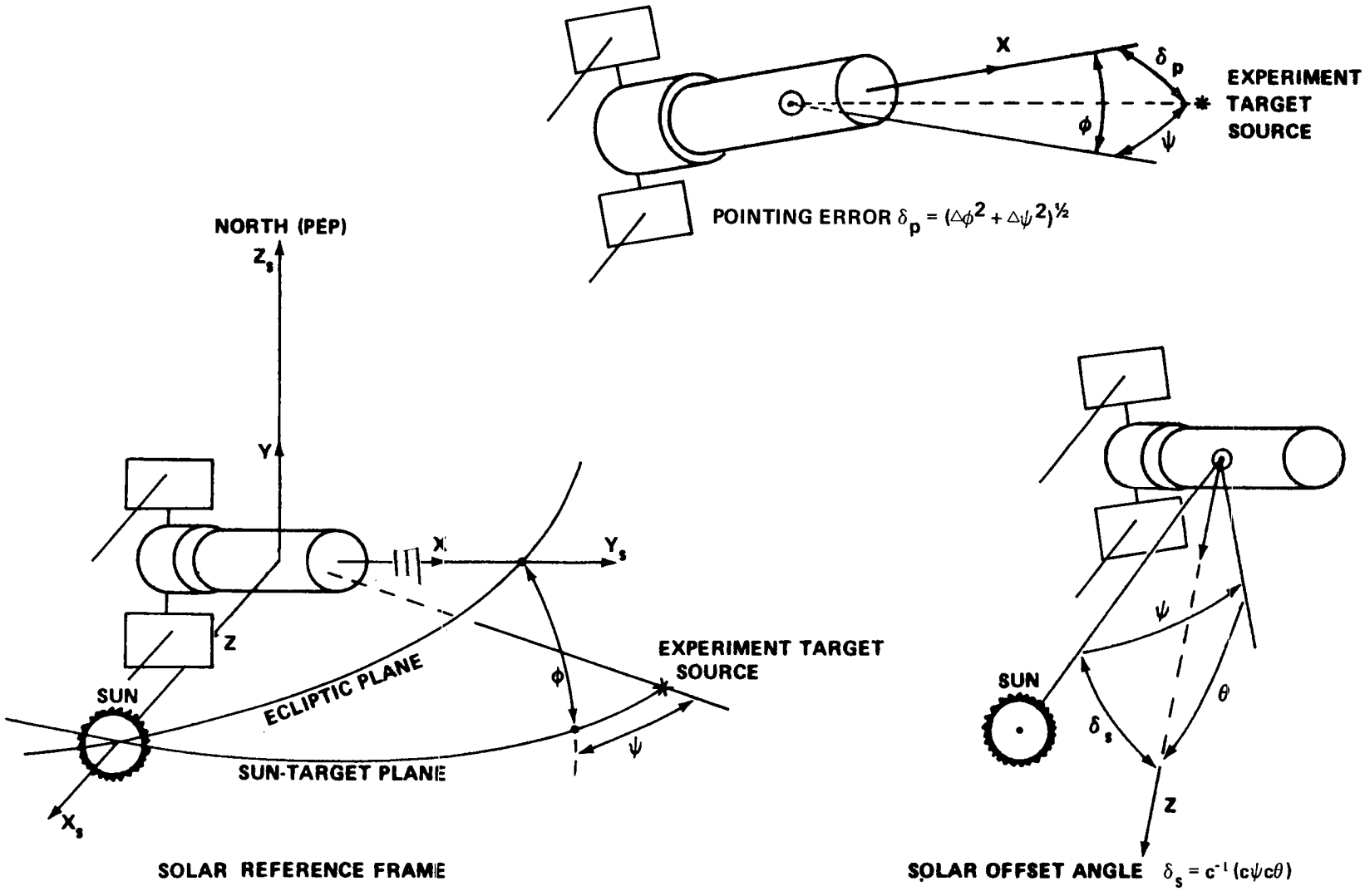

Figure VI-1. LST solar reference and Euler angles.

LST will normally be sunward, the thermal control system can be designed and subsystem mounting locations can be selected advantageously. As a reference, the solar wing gimbal position is measured relative to the vehicle X-Y plane. However, for short periods of time, the solar power and thermal constraints can be disregarded and the LST is permitted to acquire any inertial attitude (see Section A.3).

Since the solar wing normal usually points to the sun and the Z-axis must be in the solar hemisphere, solar ecliptic coordinates are defined and used to describe the attitude of the LST for simulation and analysis purposes. The solar ecliptic coordinate system is defined relative to the sun and ecliptic plane by the right-hand triad (X_s, Y_s, Z_s). The X_s-axis points to the sun, the Z_s-axis is perpendicular to the ecliptic plane (PEP), and the Y_s-axis completes the triad in the ecliptic plane. The attitude of the LST is specified by three Euler angles: ϕ, about the sunline; ψ, in the sun experiment target plane; and θ, about the experiment axis. To acquire a target during simulation runs, the vehicle is rolled about the sunline until the X-axis intersects the suntarget plane; it is then rotated about the Y-axis until the target is acquired. The third rotation, θ, is not used except to facilitate finding guide stars with star trackers centered about the negative Z-axis in the Y-Z plane. As illustrated in Figure VI-1, the pointing error is a function of $\Delta\phi$ and $\Delta\psi$. Normally, the solar gimbal angle is given by ψ and the Z-axis is offset from the sunline by the angle $\delta_s = C^{-1}[C\psi\, C\theta]$, where C represents the cosine function.

During the LST mission sequence, several ACS operational modes are utilized. In most cases, an attitude reference and body orientation can be defined for each mode. However, for some modes, the attitude is the same but the sensors used to obtain attitude error signals are different, thus defining a different ACS operation with the same general orientation. For example, coarse pointing and fine pointing modes have the same vehicle orientation requirements but differ in the sensors being used and the pointing accuracies obtained. Table VI-1 lists some possible reference attitudes that can be used to describe the LST's orientation during various ACS modes. After initial orbit attainment, the body rates are nulled and the sun is acquired. Then the LST is slowly rotated about the sunline until the star trackers on the negative Z-axis pick up selected guide stars. An initial reference is then established with the Z-axis pointing to the sun. Solar ecliptic coordinates can be used as a basis to describe the initial orientation of the LST and the guide star locations as illustrated in Figure VI-2. Once a target star has

TABLE VI-1. REFERENCE ATTITUDES

Reference Attitudes	Orientation	Use
Sun Acquisition	The Z-axis points toward the sun and all body rates are nulled.	Initial sun acquisition or reacquisition
Reference Alignment	The Z-axis points toward the sun and fixed star trackers (FSTs) about negative Z-axis are pointed toward guide stars.	Establish celestial orientation
Fine (Coarse) Pointing	The X-axis points to an experiment source, the Y-axis is perpendicular to the sunline, and the Z-axis is within the solar hemisphere.	Normal experiment operation
Special Pointing	The LST can assume any inertial attitude except those within sun avoidance cone. Solar power may not be received.	Unusual Experiment operation for short periods
Emergency Sun Acquisition	The Z-axis points toward the sun with roll about the sunline uncontrolled.	Failure modes
Solar Ecliptic	The Z-axis points to the sun, the Y-axis points north perpendicular to the ecliptic plane, and the X-axis completes a right-hand triad in the ecliptic plane.	Reference for description of vehicle attitude

been specified, new guide stars must be selected such that they are within the fields-of-view (FOV) of the active star sensors mounted in the -Z-Y plane when the X-axis is pointing toward the target source. The LST is then in a coarse celestial pointing mode (Fig. VI-3) and is ready to enter normal experiment operation. Whenever the OTA fine guidance sensor (FGS) star trackers have acquired other guide stars near the target star, the LST enters a fine pointing mode with the same inertial orientation. Data taking begins and continues until a new target source is selected.

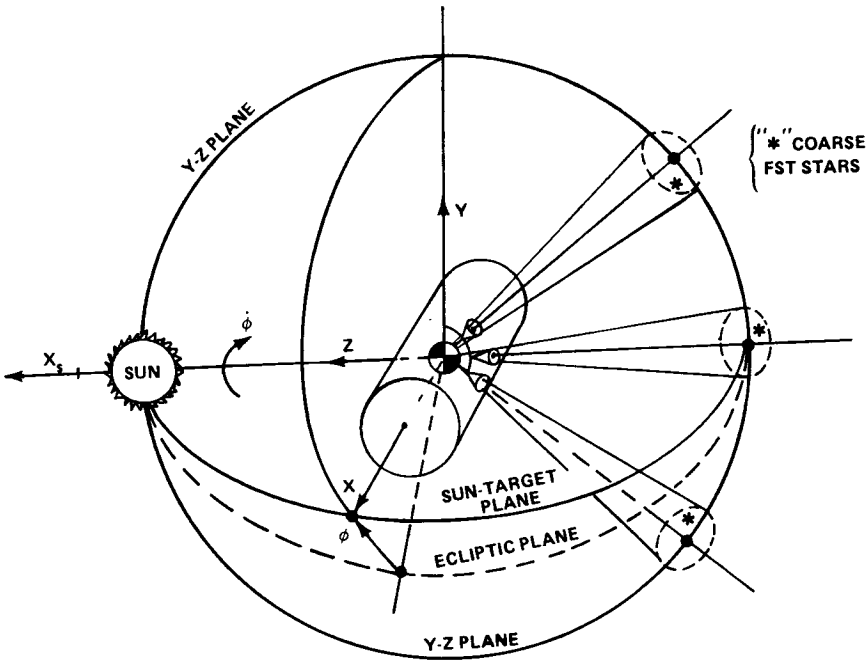

Figure VI-2. Roll about sunline to acquire inertial reference and to place the X-axis in the sun-target plane.

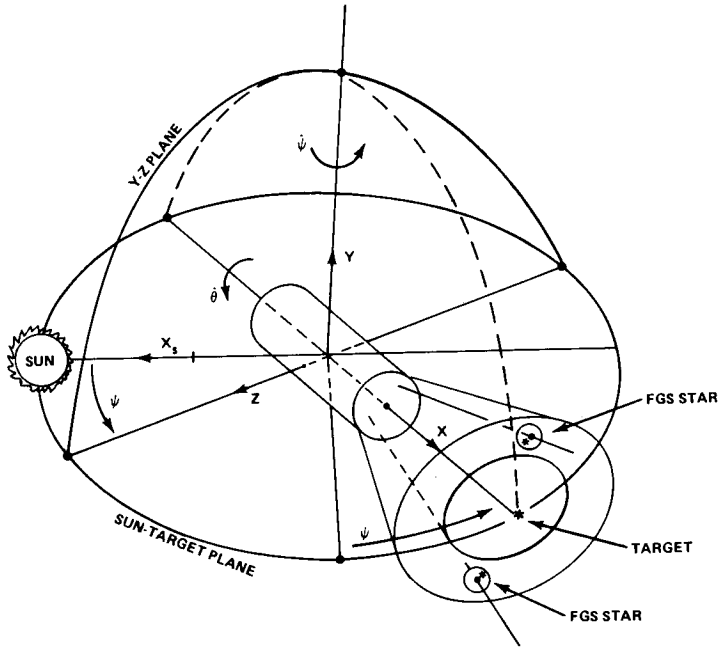

Figure VI-3. Roll about Y-axis to acquire target such that sun-X-Z are coplanar.

In the event of failures, emergencies, or loss of reference, the LST reacquires the sun and goes into a solar pointing attitude. The Z-axis points to the sun with roll about the sunline uncontrolled. Even though RCS has been selected for emergency backup, simulation and analysis have indicated that the magnetic torquer system (MTS) can hold the LST in such an orientation using only sun sensor attitude information. Such a control mode could be implemented so that its operation would not depend upon the onboard computer or CMGs.

Analysis has shown that the LST could enter a storage mode (with the solar wings folded against the vehicle) in which random tumbling is permitted and still receive enough solar power to keep the communications and thermal subsystems operating. There is no attitude reference for the storage mode. All the experiments and most subsystems must be turned off to conserve power as the LST awaits retrieval and/or repair by the Shuttle.

There may be unusual experiment operating modes or maneuvers for taking polarization data such that solar power might not be received. However, the allowable periods for such modes would be relatively short and depend upon the thermal and power (depth of battery discharge) restrictions. In a special pointing attitude, any inertial orientation can be attained. It is assumed that the experiment axis will either point to or point and rotate about a celestial target.

3. Mission Sequence. The principal operational control modes can be described under the following seven major headings:

1. Sun acquisition.
2. Reference alignment.
3. Maneuver.
4. Coarse pointing.
5. Fine pointing.
6. Special pointing.
7. Emergency sun acquisition.

Figure VI-4 is a flow chart showing the mode flow concept in changing from mode to mode. This concept is based on the assumption that the Space Shuttle provides the necessary support functions to place the LST into a correct orbit. The normal mode flow leading to data taking is indicated by the heavy arrows:

Sun acquisition.

Reference alignment.

Maneuver.

Coarse pointing.

Fine pointing.

The sun acquisition mode can be entered directly from any other mode without the aid of the RCS. This mode would be entered generally when all ACS components are functioning normally and a period of attitude hold with the sun vector normal to the solar wing surfaces is required.

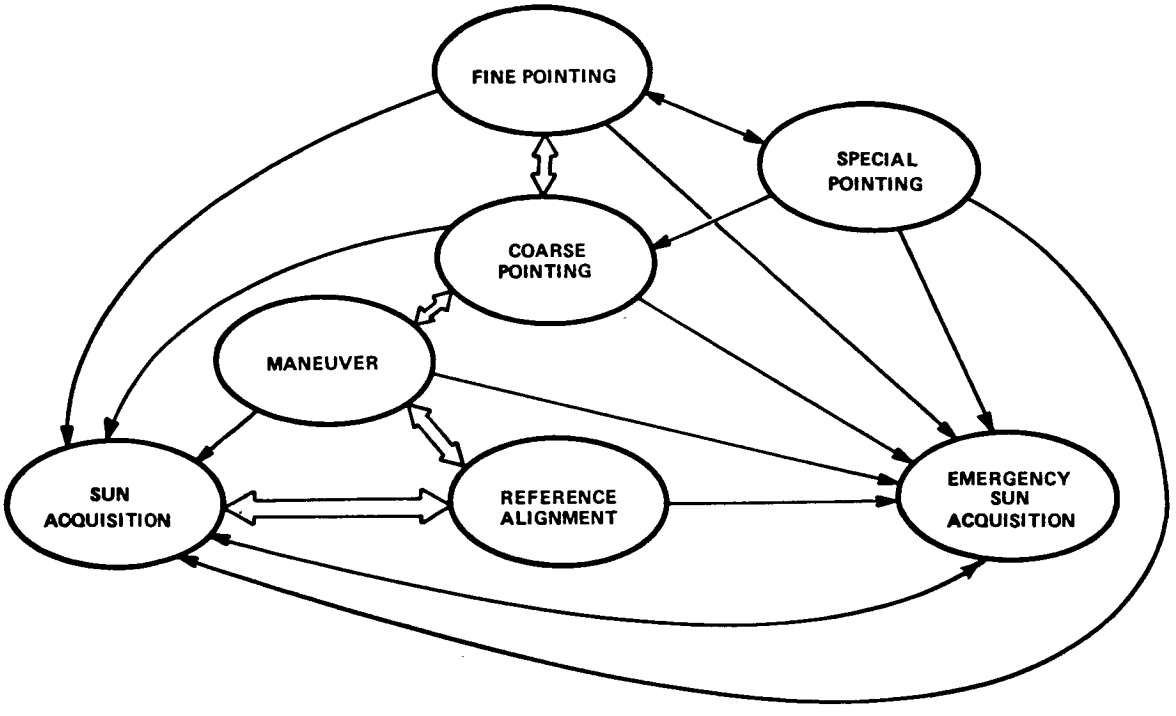

Figure VI-4. ACS control mode functions for LST.

The emergency sun acquisition mode can also be entered from any control mode. However, it is used after the occurrence of major system component failures. In this mode, the LST is placed in a stable two-axis sun hold mode for troubleshooting analysis.

The reference alignment mode serves to establish an initial analytic inertial reference frame for the onboard computation prior to the slew maneuver required to acquire the initial experiment orientation in the coarse pointing mode. During the experimentation phases of the mission, an inertial reference frame will be maintained in a continuously updated state in the digital processor assembly software. Therefore, it will not be necessary to return to the reference alignment mode before acquiring each new data source. Since celestial bodies are the primary reference sources for establishing an inertial reference frame, gyro drift compensations and computer software attitude solution parameters can be computed and updated in this mode.

The coarse pointing mode provides a means of transition from reference alignment to the fine pointing mode. The coarse mode uses the SSM sensors and actuators to align the LST in three axes to an accuracy suitable for the OTA fine guidance sensors to acquire the preselected guide stars in their coarse fields-of-view. Using the OTA FGS and the SSM actuators, the LST maintains the 1 arc sec spacecraft fine pointing accuracy.

The fine pointing mode is the primary experimentation mode. Using the OTA pointing control system for sensing and actuation, the experiment LOS is adjusted to point to the data source and to maintain pointing stability. A transfer from this mode to the special pointing mode is made when an experiment requires precise orientation of a spectrometer slit that cannot be obtained by normal fine pointing mode scheduling. The fine or coarse pointing modes can be reentered directly from the special pointing mode.

A maneuver mode has been selected to mechanize the maneuvers to the various data sources. This mode requires special sensor and actuator utilization to perform the maneuvers and acquire the coarse pointing attitude.

B. Design Reference System Description

The individual components of the LST/SSM ACS were selected largely to preserve commonality with the ACS components selected for the HEAO missions. Based on TRW information for HEAO Missions A and B and the

MSFC Phase A study report for the HEAO-C (NASA TM X-64652), hardware was selected to meet the LST ACS requirements. Final hardware selections will be made as a result of additional tradeoff studies and to maintain HEAO commonality as the HEAO designs are refined and updated.

Figure VI-5 provides a functional block diagram of the design reference ACS with a complete complement of sensors, actuators, and interface equipment to perform all phases of the LST mission. Also included in this block diagram are the key interfaces with the LST OTA/SIP system components. These interfaces are critical to establishing and maintaining LOS stability and will be discussed further in Section E. Table VI-2 provides a corresponding hardware summary for the SSM/ACS. The utilization of this hardware in various combinations to perform the required mission phases will be described in Section C and detailed component characteristics will be provided in Section G.

The three fixed star trackers (FSTs) are oriented in the Y-Z plane as shown in Figure VI-6. Normally, two are active with the third in a redundant standby status. When operated in this manner, approximately 99 percent coverage of the celestial sphere is attained with the capability of providing 3-axis attitude error signals. The accuracy of the trackers has been selected to adequately align the telescope LOS so that preselected guide stars will appear within the coarse FOV of the FGS star trackers located within the OTA.

Five coarse sun sensors (CSSs) are included. Three of these are body-mounted with two aligned to the +Z-axis (one redundant) and one aligned to the -Z-axis. Coverage of 4π steradians is provided for sun acquisition and emergency sun acquisition. The two remaining CSSs are located on the solar wings (one per wing) and provide monitoring of solar panel offset with respect to the sunline.

The reference gyro assembly (RGA) consists of six gyros arranged in a skewed dodecahedron configuration along with the necessary support electronics. In normal operation, four gyros are active and two are in a redundant standby mode. The four active gyros provide sufficient information for onboard fault detection, but not fault isolation, with respect to a particular gyro. The RGA and FSTs are to be physically located in the same area of the spacecraft and aligned to each other to provide an accurate operational interface.

A magnetometer sensing system (MSS) consisting of two 3-axis magnetometers (one redundant) is provided to sense the earth's magnetic

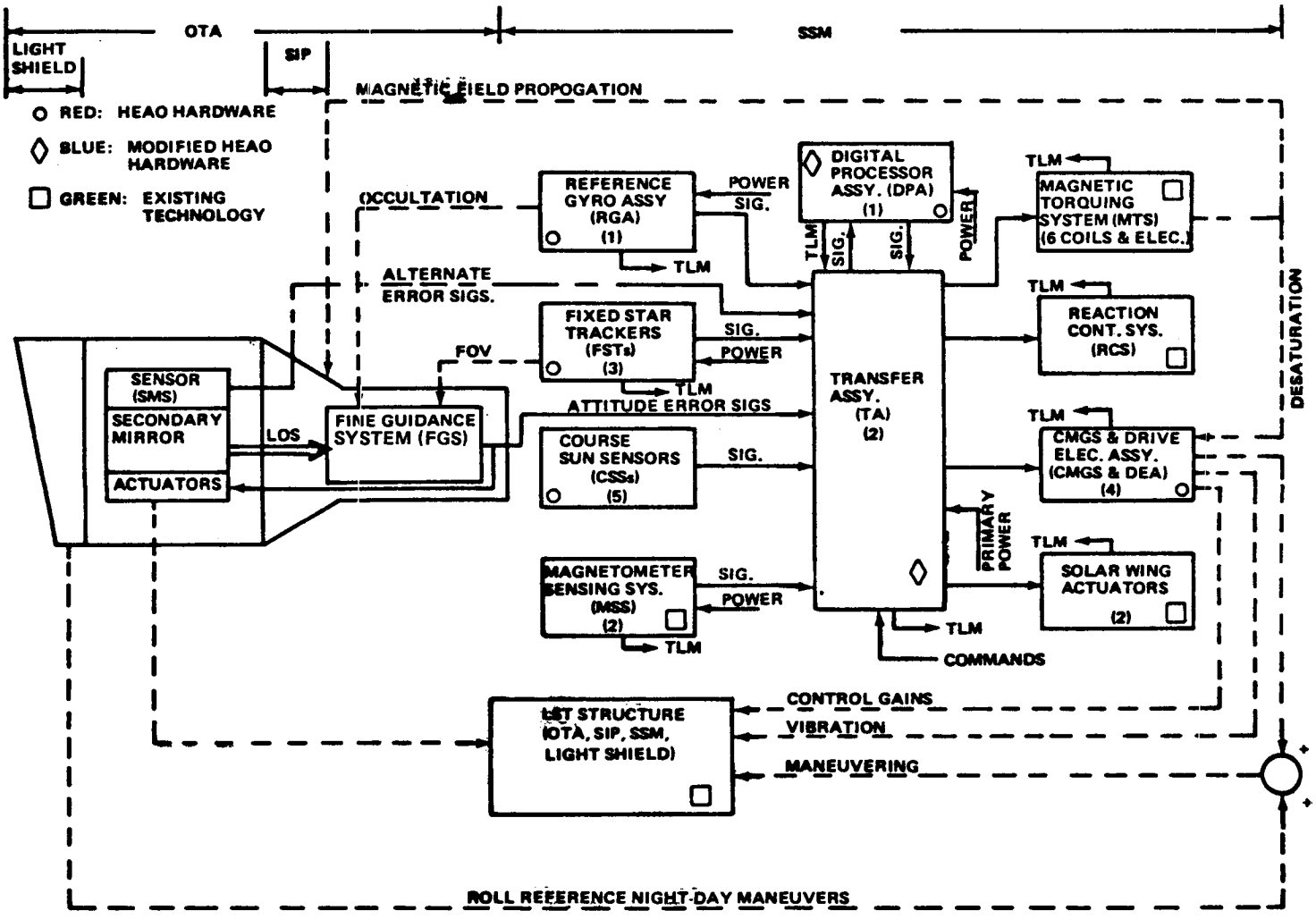

Figure VI-5. ACS block diagram and key interface for LST.

TABLE VI-2. SSM ACS HARDWARE SUMMARY FOR LST

Item	Number of Units	Unit Mass (kg)	Unit Average Power (W)	Unit Size (mm)	Total Mass (kg)	Total Average Power (W)
Coarse Sun Sensor (CSS)	5	0.1	0	47 D × 41	0.5	0
Fixed Star Tracker (FST)	3	5.5	5.0	114 × 114 × 406	16.5	10 (2 Active)
Star Tracker Shade	3	1.6	0	457× 305 Diag.	4.8	0
Reference Gyro Assembly (RGA)	1 (6 Gyros)	10.4	36 (9W/Gyro)	444 × 173 × 152	10.4	36 (4-Active)
Magnetometer (3-Axis)	2	3.0	2.0	127 × 127 × 254	6	2 (1 Active)
Control Moment Gyro and Drive Electronics Assembly (CMG & DEA)	4	80.9	17.0 Point 22.5 Slew	1019 × 775 × 584	323.6	68 90
Magnetic Torquer (MT)	6	23.5	5.0 Peak	1905 × 51 D	141	15 Average (30 Peak)
Magnetic Torquer Electronics (MTE)	1 (6-Channel)	2.3	5.0	203 × 102 × 102	2.3	5.0
Digital Processor Assembly (DPA) (Redundant)	1	6.2	16.0	107 × 130 × 366	6.2	16.0
Transfer Assembly (TA)	2	4.7	26.5	152 × 203 × 246	9.4	26.5 (1 Active)
RCS Electronics	2	7.3	11.0	229 × 356 × 178	14.6	0
GN_2 RCS					104	0
System Totals					639.3	178.5

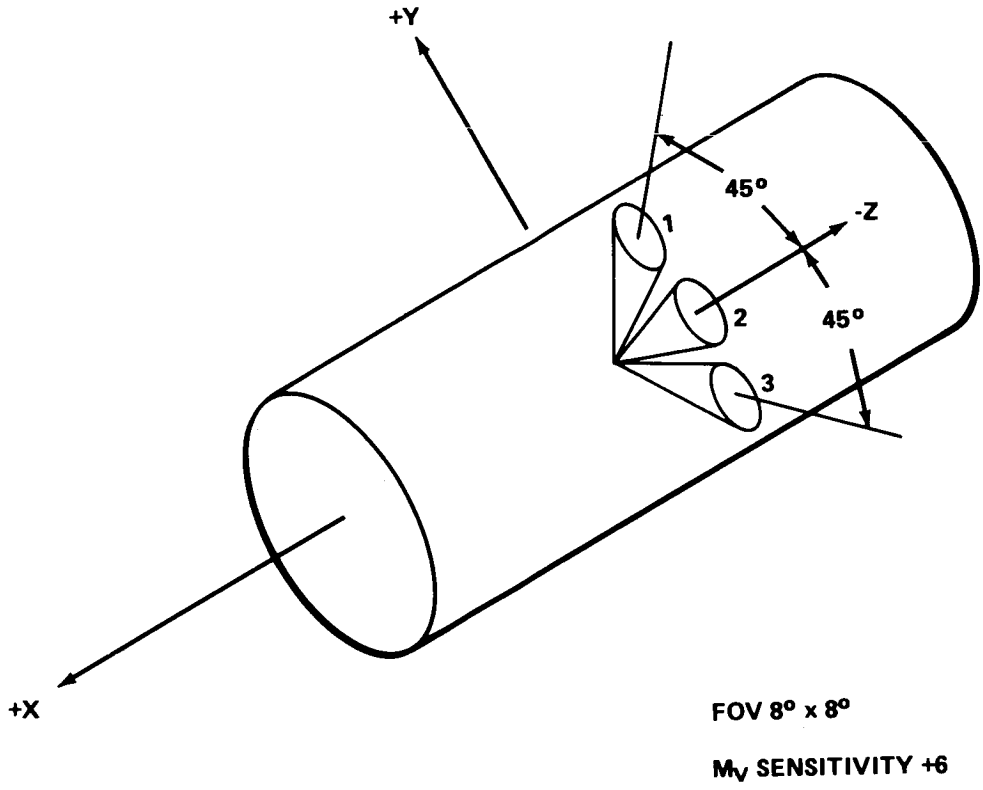

Figure VI-6. LST star tracker configuration.

field. Voltage outputs proportional to the field strength along each axis with the polarity of the signals indicating the field direction along each axis are used to calculate and generate torquing currents for the magnetic torquer coils.

The transfer assembly (TA) serves as an interface assembly for all ACS components. It has a sensor buffer unit that places the required sensors on line for the control mode in use and routes signals between the sensors and digital processor assembly (DPA) via the computer input/output section of the TA. The computer input/output section is the interface between the digital processor assembly (DPA), the sensors, and the actuators and includes provisions for multiplexing, D/A and A/D conversions, and signal conditioning. A power switching unit provides power to ACS components according to the control mode selection. A power converter unit converts

primary power to special voltage levels as required by ACS components and provides isolation of these special sources. The command and telemetry unit of the TA provides data buffer, and command storage and processing functions.

The DPA receives data inputs from the various sensors via the TA, processes the data, and provides the following outputs via the TA:

1. CMG gimbal commands.

2. Torque commands to the magnetic torquer system.

3. Gyro drift compensation obtained from onboard sensors or ground update commands.

4. Solar wing actuator commands.

Four single-gimbal CMG assemblies, each complete with redundant drive electronics assemblies (DEAs) are mounted in a skewed configuration so that each CMG can provide a portion of the momentum requirements for each control axis. The CMGs provide the momentum storage capability required to maintain the LST in an accurate inertial hold attitude and supply the control torques required to maneuver the LST. The magnetic torquers supply control torques for CMG momentum desaturation.

The cold gas reaction control system (RCS) provides the control torques to place and maintain the LST in the emergency sun acquisition mode attitude. An additional function of the RCS is to control the LST if large disturbances due to Space Shuttle misdock occur.

C. System Operation

The configurations of ACS sensors and actuators that are placed on line by the transfer assembly are given in Table VI-3 for the control mode functions of Figure VI-4. Included in Table VI-3 are OTA/SIP subsystems that are not listed as part of the ACS but are vital to data source acquisition and pointing stability through interfaces with the ACS.

All ACS components will be in an operating state at release into orbit and a partial checkout completed. The ACS will be in a sun acquisition mode configuration at release and no orbit adjust capability will be available.

TABLE VI-3. LST ACS CONTROL MODE CONFIGURATIONS

Subsystem	Sun Acquisition	Reference Alignment	Maneuver	Coarse Pointing	Fine Pointing	Special Pointing	Emergency Sun Acquisition
CSS	X						X
FST		X		X			
RGA	X	X	X	X	X	X	
Magnetometer	X	X		X	X	X	
DPA	X	X	X	X	X	X	
TA	X	X	X	X	X	X	X
Magnetic Torquer	X	X		X	X	X	
CMG	X	X	X	X	X	X	
RCS							X
Fine Guidance Sensor[a]					X	X	
Secondary Mirror Control[a]					X	X	
Special Sensors[a]						X	

a. OTA/SIP Subsystems — not part of ACS hardware.

The sun acquisition mode functions to align the +Z-axis to the sunline. It is a rate and position mode with the CSS supplying two-axis error information about the X- and Y-axis and the RGA providing three-axis rate signals. A rate stabilized attitude is maintained about the +Z-axis. A CSS aligned to the +Z-axis having a 2π steradian FOV and an identical CSS aligned to the -Z-axis provide 4π steradian sun sensing capability. A redundant CSS is provided for the +Z-axis. If the -Z-axis CSS senses the sun, bias commands are generated to torque the -Z-axis away from the sunline and bring the sun into the FOV of the +Z-axis CSS. Error signals from the CSS are then used in a null seeking mode by the vehicle control law to align the +Z-axis to the sunline in two axes to less than one degree. This attitude is maintained using the RGA for rate stabilization until orbit determination, final systems checkout, and preparations for entering the reference alignment mode have been completed. Control torques for sun acquisition and attitude hold are provided by the CMGs with the magnetic torquer coils providing momentum unloading for the CMGs.

The reference alignment mode (RAM) is entered from the sun acquisition mode and is used initially to establish a three-axis analytical inertial reference frame. This is used by the DPA in computing the maneuver to acquire the coarse attitude for the first data source. Later in the mission, it will be used at times when reference attitude has been lost or after the sun acquisition has been reentered for any reason.

The general steps to be followed in establishing the reference frame are:

1. Selection of reference stars by the control center.

2. Transmission of star data to the LST.

3. Roll about the sunline (if required) and acquire stars with the FSTs.

4. Perform three-axis hold on reference stars and adjust attitude if required.

5. Compute and store the reference frame in the DPA.

6. Compute and compensate RGA drift rates.

7. Compute and store attitude bias compensations.

8. Maintain attitude using the RGA during reference star occultations.

With two trackers operating, the FOV, sensitivity, and configuration of the FSTs provide the capability of acquiring one star per tracker for 3-axis control approximately 99 percent of the time for any attitude. This capability may eliminate the requirement for a roll about the sunline, and a star reference can be obtained by star identification by the method of comparing star magnitudes and separation angles with a stored star catalog. By their scan and acquisition routine, the FSTs will have selected the brightest stars in the FOV, thus simplifying the identification procedure.

The three-axis hold is accomplished under RGA control with updates from the star trackers. During this hold, gyro drift terms will be computed by a comparison of RGA and star tracker measurements, and drift bias compensations will be inserted into the individual gyro torquer loops. After compensations, the attitude bias terms to be used in the attitude error computations will be stored in the DPA.

During star occultations or when bright sources deactivate the star trackers, the attitude will be maintained using the RGA outputs. Attitude can be maintained to less than 30 arc sec during the occultation period.

A special maneuver mode is mechanized because the potential maneuver of 90 degrees in 5 min will require RGA system gains and quantizations to be modified. This is a direct result of the large rate difference between the highly stabilized pointing mode and the maneuver mode.

The following information is received from the control center prior to initiation of a maneuver:

1. Maneuver parameters.
2. Star data for stars acquired by the FSTs at maneuver completion.
3. Solar panel position commands.
4. Maneuver mode configuration command.
5. Maneuver initiation command.

To perform the maneuver, the RGA outputs are used in a strapdown calculation employing a four-parameter quaternion transformation. Maneuver parameters are used in onboard calculations to generate the maneuver commands for an eigenaxis maneuver to rotate the LST coordinate frame to the

desired attitude. To avoid damage and to facilitate operation of the FSTs, the eigenaxis and final reference stars should be selected so that, during the maneuver, the -Z-axis is directed to the antisolar hemisphere. The maneuver will be accomplished in three parts. These are an acceleration phase to reach a given rate about the eigenaxis, a coast phase to reach a specified angular rotation, and a deceleration phase at the end of which the rate will be reduced to zero at the desired angular rotation. Ramp torque commands with shaping filters will be used to reduce settling times and to minimize disturbances on the solar panels and LST structure.

The coarse pointing mode is designed to provide pointing of the LST to an accuracy of ±30 arc sec in 2 axes and 0.1 degree about the LOS. This accuracy is compatible with the coarse FOV of the OTA FGS sensors and permits the prepositioned fine guidance sensors to acquire the guide stars selected for a particular data source. The coarse pointing mode is entered at the conclusion of a maneuver when the FSTs have acquired their reference stars. At this time, control system parameters are reset for pointing and the RGA outputs are used by the DPA to compute CMG gimbal commands to maintain a stable three-axis hold. The FSTs provide attitude error information in three axes that is used to frequently update the RGA data in the DPA attitude error calculations. This stable three-axis hold is maintained until guide star acquisition by the fine guidance sensors is confirmed. At this time, the primary optical attitude error sensing functions are transferred to the fine guidance sensors. Gyro drift compensations and attitude error bias terms are updated while in the coarse pointing mode.

The fine pointing mode is entered upon guide star acquisition. The fine guidance system electronics, an OTA subsystem, processes the fine guidance sensor outputs and supplies three-axis attitude error signals via the TA to the DPA. Initially, this information is obtained from the FGS star trackers and is used to generate torque commands to point the spacecraft to ±1 arc sec and to bring the guide stars into the fine FOV of the sensors. After the fine pointing mode acquisition, the LOS is stabilized to 0.005 arc sec rms using secondary mirror position sensors. Roll errors are generated by an FGS star tracker.

In the fine pointing mode, sensor noise characteristics of the RGA and FGS will determine how signal mixing is mechanized to provide the control sensing functions. The RGA can be used as the primary sensor for the design reference ACS with the FGS three-axis error information used to provide frequent updates to attitude error calculations. This is desirable to provide smooth transition between control modes. Based on state-of-the-art gyro technology, this may also provide operational advantages from the standpoint

of sensor noise and structural disturbances. The alternate operating concept would be to use the three-axis FGS error signals as inputs to the DPA in generating control system actuator commands to directly control the LST LOS.

For this alternate scheme, the RGA outputs provide rate stabilization. When the guide stars become occulted or for any reason cannot be used in generating error signals, the RGA will assume the sensing function for control of the vehicle. During these periods, it is expected that the LOS will wander sufficiently to allow the guide stars to leave the fine guide field. This requires realignment of the LOS to bring guide stars back to the original position in the fine FOV. For very long viewing periods on one data source, this must be done numerous times and will take place automatically on reappearance of the guide stars.

The special pointing mode will be entered from the fine pointing mode because precise attitude positioning is required prior to small adjustments of a slit orientation. Special sensors may be supplied as a part of the individual spectrometers to detect the slit position with respect to the data source. A design reference option is to use the sensors in a very low frequency closed loop to reposition the secondary mirror or the FGS micrometer tilt plate through small angles and thus adjust the slit position with respect to the data source. This procedure avoids the ground loop and resulting time delays in precisely orienting the slit. However, ground confirmation probably will still be required. Alternates are to electronically reposition the slit on the detector of the scientific instrument or to perform the entire process through a control center to LST loop. Detailed definition of experiment hardware is required before a final decision can be made on the operating procedure.

Malfunctions of major ACS subsystems that would result in loss of LST attitude control will initiate the emergency sun acquisition mode either by onboard fault detection or ground control. The CSS provides attitude information which, combined with derived rate error signals, commands the RCS to torque the LST +Z-axis into two-axis alignment with the sunline. Rate from the CSS is obtained by differentiation of its output. Special networks are contained in the TA for implementing this mode without use of the DPA. This state will be maintained for troubleshooting analysis.

D. Trade Studies

1. Sensor Systems

a. Reference Gyro Assembly. The candidate gyro configurations, selection criteria, and design reference selection characteristics are

summarized in Table VI-4. The reliability and accuracy were considered to be the most critical selection criteria, but reliability eventually was the deciding factor. Further details on the reliability comparisons are given in Chapter VIII, Section B.2.

TABLE VI-4. REFERENCE GYRO-ASSEMBLY TRADES

Candidates:

- Dodecahedron — 6 Gyros — Skewed Configuration (3, 4, 5, and 6 Active Gyros)
- Tetrahedron — 4 Gyros — Skewed Configuration
- Five Pack
- Dual Orthogonal Triads

Selection Criteria:

- Reliability
- Accuracy
- HEAO Commonality
- Fault Detection

Design Reference Selection:

- Dodecahedron with 4 Active Gyros

Design Reference Selection Characteristics:

- Accuracy — Equivalent to 3-Axis Orthogonal Set
- Gyro and Electronics Modules Replaceable on an Individual Basis
- Replaceable to 4 arc sec Alignment with Mechanical References
- Fault Isolation — 4 Gyros Required to Detect Fault, 5 Gyros to Isolate Fault
- Accuracy Improvement by Running all 6 Gyros
- Alignment — Can be done as a Complete Package

The selection of the dodecahedron configuration led to a trade study concerning operational concepts with the goal of providing best reliability and acceptable accuracy. The four-active/two-standby concept proved to be most reliable and, in addition, provides easy implementation of fault detection. Fault isolation by onboard techniques can also be easily implemented by activating one standby gyro so that the minimum number of gyros for fault isolation are available. These techniques are factual and considerable hardware testing and system design have confirmed them.

There are actually 15 combinations of the 6 gyros taken in combinations of 4, but for the 2 LST axes requiring high precision, there are only 6 combinations acceptable from an accuracy standpoint. Thus, an acceptable combination of 4 gyros can be selected for initial operation, but, after 2 failures, there is the possibility that an acceptable combination from an accuracy standpoint might not be available. These considerations were factored into the reliability study and the design reference configuration was subsequently selected.

b. Fixed Star Tracker versus Gimbaled Star Trackers. Table VI-5 lists a number of tradeoff considerations used in selecting the fixed star tracker for the design reference system. The principal advantage of the gimbaled tracker is its large effective FOV that provides the capability to use bright stars for tracking and to center these brighter stars in the small instantaneous FOV. Good pointing resolution and low noise are a direct result. This large effective FOV, however, has the disadvantage of requiring a large viewing window which is a potential problem area for the LST.

The state-of-the-art on fixed star trackers is at a stage where tracking stars of +6 magnitude presents no great problem. Using this sensitivity for the LST trackers, with the accompanying reasonable FOV, provides excellent coverage of the celestial sphere. The selected configuration provides a measure of redundancy in that two of the three trackers operating gives a high probability of acquiring the one star per tracker required to obtain three-axis error information.

2. Momentum Exchange Systems. The basic objective of the LST attitude control system is to maintain a prescribed attitude (orientation) relative to inertial space as a function of time, irrespective of the orbital flight path. One of the most practical means for controlling the attitude are momentum-exchange devices. These can be reaction wheels (RWs), single gimbal control moment gyros (SGCMGs), or double gimble control moment gyros (DGCMGs).

TABLE VI-5. ACS STAR TRACKER TRADES

FIXED STAR TRACKER (FST) (DESIGN REFERENCE)	GIMBALED STAR TRACKER (GST)
Advantages HEAO Commonality Reliability Operational Simplicity Mounting Simplicity Cost, Weight, and Power	Advantages Large Effective FOV Small Instantaneous FOV Good Pointing Resolution Low Noise Equivalent Angle
Disadvantages Critical FOV versus Sensitivity Tradeoff Resolution is a Function of Star Location in FOV Requires Additional Trackers to Obtain Required Star Coverage More Sensitive Detector Required	Disadvantages Operational Complexity and Design Mounting Constraints Reliability Gimbal angle Encoder Gimbal Dynamics Cost, Weight, and Power

The candidate momentum-exchange systems considered for LST are shown in Figure VI-7 and in later sections by Figures VI-12 and VI-20. Figure VI-7 illustrates a three-DGCMG system and a four-RW system. (Two 4-SGCMG systems are shown in Figures VI-12 and VI-20.) A change in angular momentum of the momentum-exchange system will produce a torque on the LST and may be accomplished by varying the speed of a flywheel or by tilting the spin axis of a flywheel relative to the LST. For an RW, the flywheel axis of rotation is fixed relative to the LST and the speed is changed to produce a torque. For a CMG, the speed of the flywheel is constant with the spin axis direction relative to the LST changed to produce a torque. As depicted in Figure VI-7, each DGCMG has two gimbals by which the flywheel can be moved. Double gimbals permit the momentum vector of each CMG to be moved on a sphere of radius h, where h is the momentum per flywheel. Three DGCMGs provide a near-spherical momentum envelope of 3h radius and provide excellent utilization of the total system momentum capacity. Based on previous work during the Skylab program, steering laws and software for

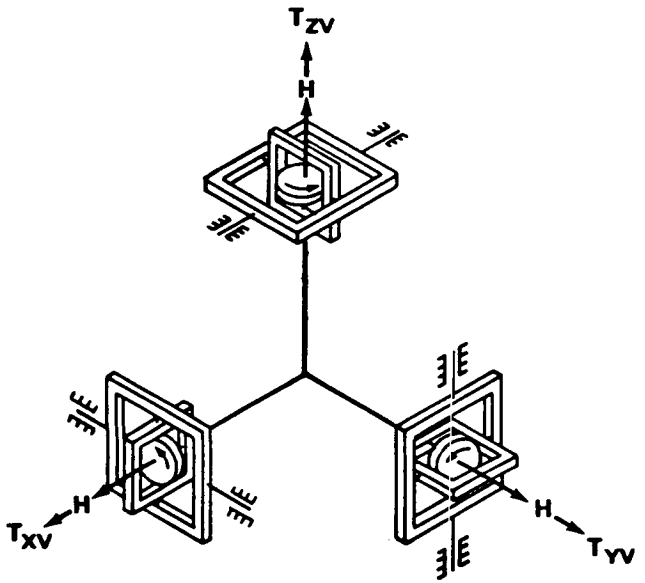

DOUBLE GIMBAL CMG CONFIGURATION

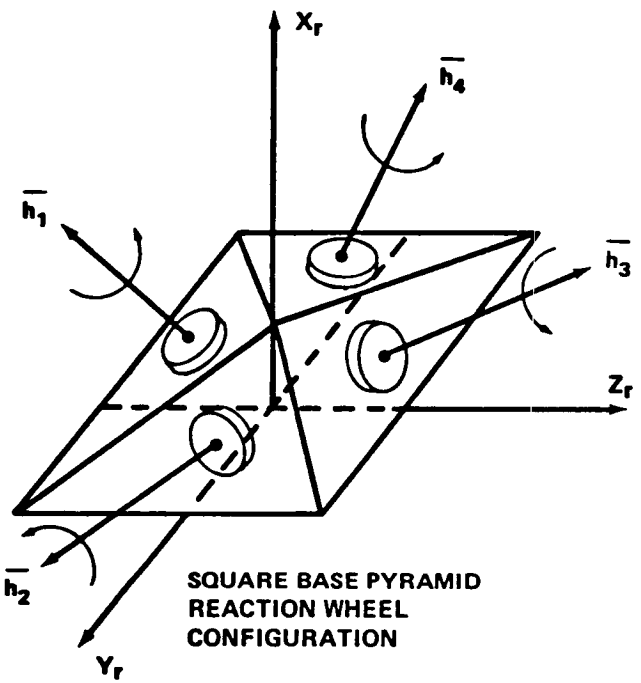

SQUARE BASE PYRAMID
REACTION WHEEL
CONFIGURATION

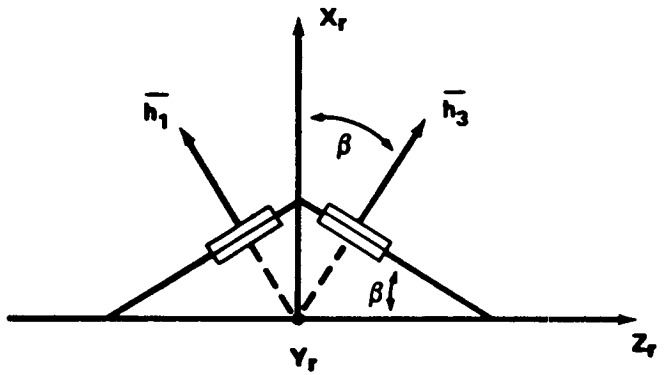

Figure VI-7. DGCMG and RW configurations considered for LST.

DGCMGs have been perfected and their operational characteristics determined with a high level of confidence. This past experience makes a system of three DGCMGs a possible candidate for LST.

The mounting arrangement of either RWs or SGCMGs can be selected to provide some desired value of momentum along each vehicle axis. As illustrated in Figure VI-7, the RWs are symmetrically arranged about the vehicle X-axis of minimum inertia. Each flywheel spin axis subtends an angle β with the X-axis. An RW can provide both torque and momentum only along its spin axis. In LST coordinates, the system momentum, $\bar{H}$, is the vector sum of the individual momentum vectors, $\bar{h}_i$. The normalized vector components of $\bar{H}$ are illustrated in Figure VI-8 as a function of the skew angle β for both the RW system and the four-skewed SGCMG system shown later in Figure VI-20. For the 4 RWs, a skew angle of 63.4 degrees results in equal momentum capacity per vehicle axis. Increasing β to 76 degrees results in the major LST axis having twice the momentum capacity of the minimum inertia X-axis. This type momentum distribution is desirable for the LST. By increasing β still further, very little additional momentum is gained in the Y-Z plane but much is lost on the X-axis. Therefore, an RW skew angle of 76 degrees is a reasonable selection for the LST. At most, note that only the momentum of two RWs can be obtained for either the Y- or Z-axis. Because of the momentum restriction in a single direction for each RW, a system of RWs has poor momentum utilization, resulting in a much higher system weight than an equivalent CMG system.

The solid lines in Figure VI-8 represent the normalized momentum components of the four-skewed SGCMG configuration in LST coordinates. A skew angle of 53.1 degrees produces equal momentum per axis. Decreasing β to 28.1 degrees produces twice the momentum capacity in the Y-Z plane (where it is needed for LST) than on the X-axis. About 3.8 h (h is the momentum per flywheel) is available in the Y-Z plane and 1.8 h out of plane on the X-axis. As illustrated, the 4-skewed CMG configuration can utilize the total system momentum of 4 h much better than RWs. Each SGCMG can provide momentum in a plane which is perpendicular to its gimbal axis, permitting good h_i utilization. The mounting arrangement of DGCMGs does not affect the momentum capacity per vehicle axis. Only 3 DGCMGs are required for LST and a 3 h capacity exists in every direction. DGCMGs provide the best possible h_i utilization.

Based on the LST impulse requirements, the fast maneuver of 90 degrees in 5 min (if imposed as a hard requirement) sets the momentum per vehicle axis that the momentum exchange system must provide. To attain

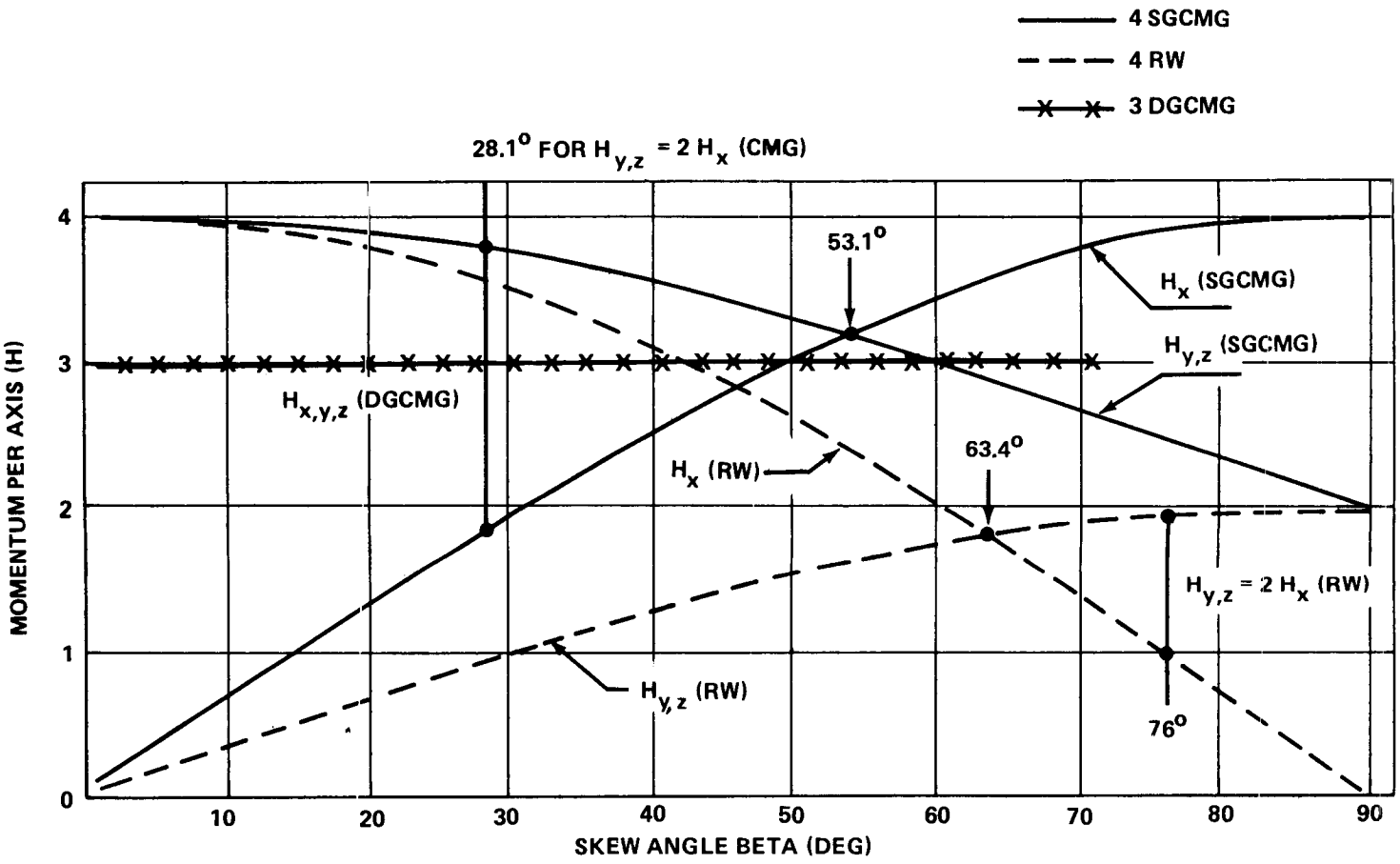

Figure VI-8. Normalized momentum per vehicle axis versus skew angle for four RWs or SGCMGs.

a maximum vehicle rate of 18 deg/min requires about 500 N-m-sec on the major inertia axis of the LST, as shown in Figure VI-9. However, when practical constraints are considered (such as gimbal rate limits, vehicle acceleration and deceleration values, and stabilization to the desired pointing direction after the maneuver), a momentum value of about 1000 N-m-sec is required for the LST to accomplish a 90 degree maneuver in 5 min. As indicated, the 4-skewed SGCMGs selected for LST have over 2500 N-m-sec on the major inertia axis, which is more than enough to meet the requirements for this maneuver.

Assuming that 1000 N-m-sec is required for the major inertia axis, Figure VI-10 indicates the flywheel momentum sizing required for a momentum-exchange system composed of either three DGCMGs, four-skewed SGCMGs, or four RWs. The DGCMG system requires 333 N-m-sec per flywheel with a total system momentum of 1000 N-m-sec. The SGCMG system requires about 265 N-m-sec per flywheel with a total system momentum of

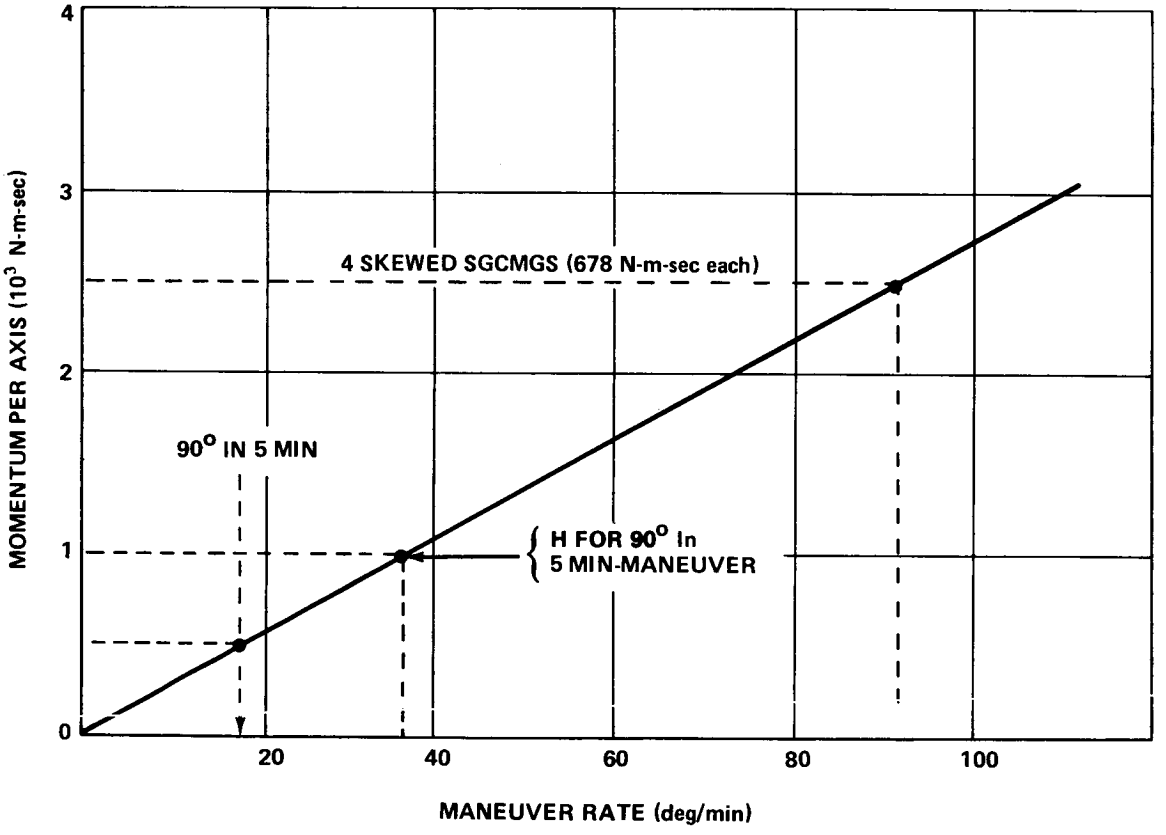

Figure VI-9. Momentum versus maneuver rate for $I = 95\ 041\ kg\text{-}m^2$.

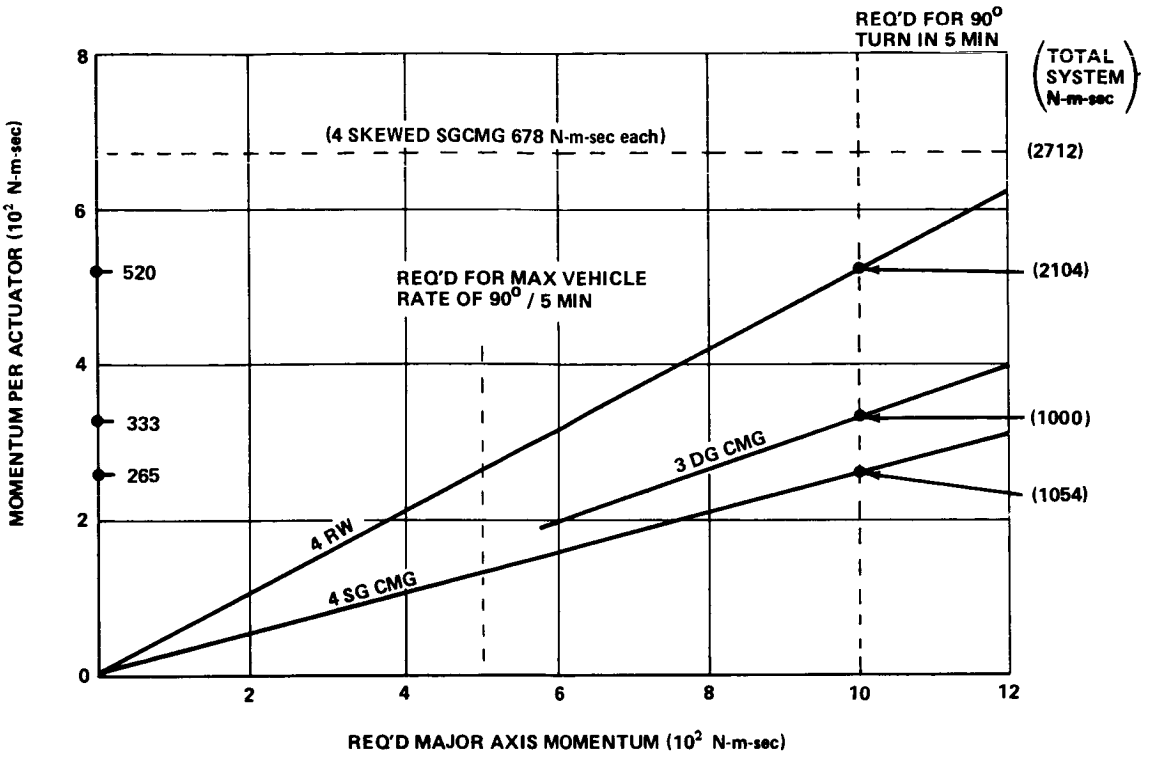

Figure VI-10. Actuator sizing as a function of the required momentum for maneuvering.

1054 N-m-sec. Although there are three DG and four SGCMGs, very little weight difference is expected between the two systems because each SG flywheel would be smaller than that of the DG. The RW system, however, requires 520 N-m-sec per flywheel for a total system momentum of 2100 N-m-sec, about twice that of the equivalent CMG system. As previously pointed out (Fig. VI-8), a system of RWs does not utilize its total momentum capacity very well. Given equal sizing criteria in terms of useable momentum per vehicle axis, an RW system would weigh about twice that of a CMG system.

When time optimal maneuvers are considered, the torque potential as well as available momentum becomes important. In a time optimal maneuver, all the torque available in the momentum-exchange system is used to initially accelerate the vehicle over the first half of the maneuver and, then, to decelerate over the last half of the maneuver interval. If the momentum-exchange system saturates before one-half the maneuver time, then a constant vehicle rate is maintained until the deceleration phase. Figure VI-11 illustrates some time optimal slewing considerations using momentum-exchange

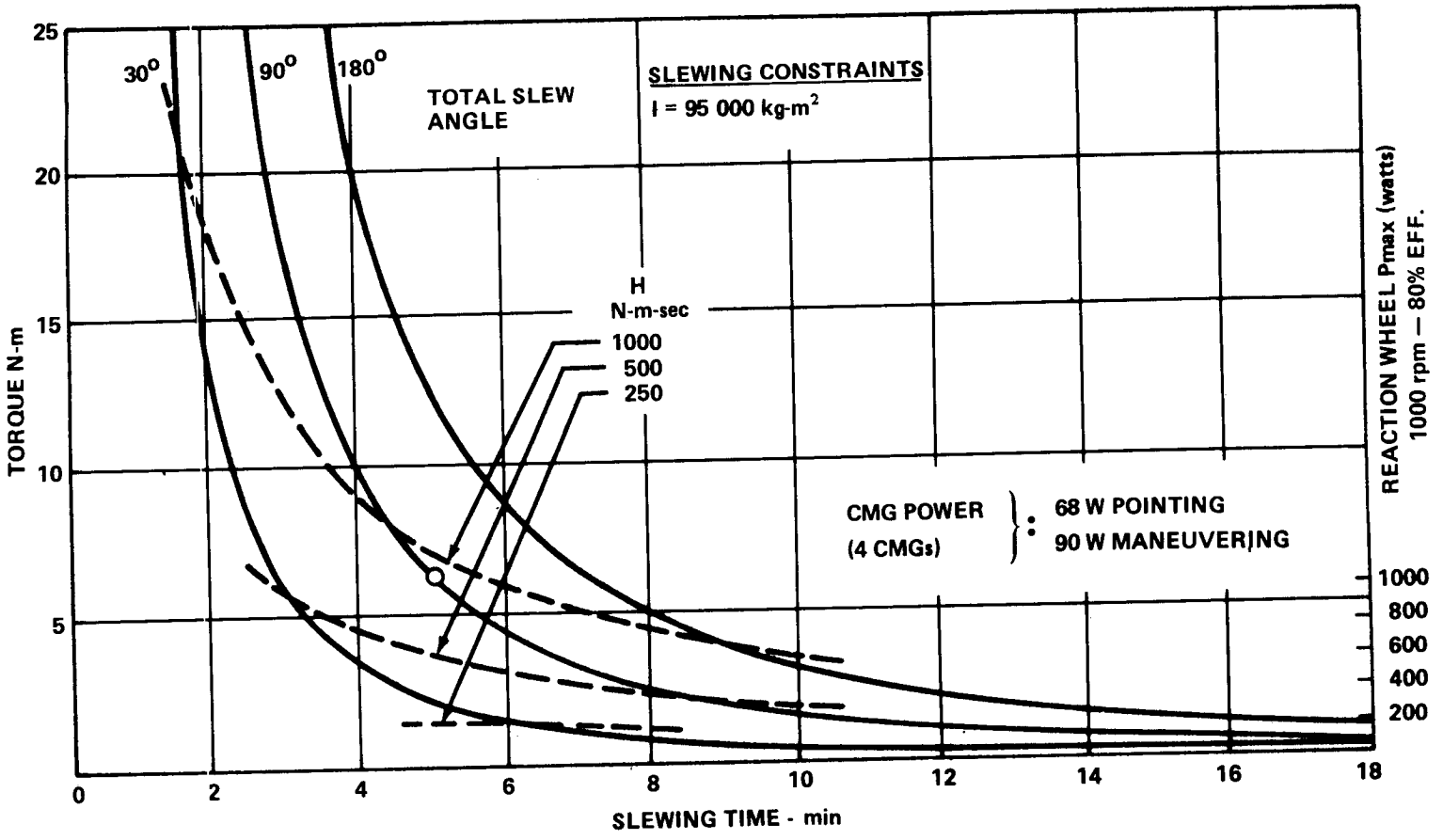

Figure VI-11. Time optimal slewing considerations.

systems as actuators. The solid lines represent the constant torque required as a function of maneuver time to accomplish either a time optimal 30, 90, or 180 degree maneuver. A 90 degree maneuver in 5 min requires a torque of about 7 N-m and an angular momentum of just under 1000 N-m-sec. The momentum accumulated while performing a maneuver is represented by the dashed lines. If the torque curve falls below a specific momentum curve, then the maneuver can be accomplished. For example, a 90 degree maneuver in 4 min cannot be performed using only 1000 N-m-sec momentum. As the maneuver time gets longer, less torque as well as peak momentum values are required.

Torque can be related to the power required to drive the actuators. RW system power is especially sensitive to torque output. RW power is the product of torque and flywheel speed or, equivalently, the momentum multiplied by the flywheel angular acceleration. Assuming the flywheel is operating at 1000 rpm with an efficiency of 80 percent, the ordinate on the right of Figure VI-11 gives the RW power to accomplish the maneuver. A 90 degree slew in 5 minutes requires an RW power input of over 1000 watts. In contrast, SGCMGs require very little additional power for slewing above that required to keep the flywheels spinning at a constant speed. The running power for four SGCMGs is about 68 watts and the maximum power used while slewing is only 90 watts. An equivalent DGCMG system can use about twice the power of a SGCMG system while maneuvering, because the outer gimbal must also hold against the inner gimbal while torquing. Either SG or DGCMGs can provide a high torque output with very little power penalty. However, the power requirements for RWs become excessive for the high torques required during a time optimal maneuver of the LST. If the 90 degree maneuver in 5 min is imposed, then the power required probably will eliminate RWs as a candidate momentum-exchange system for the LST.

Table VI-6 illustrates an actuator comparison for the candidate momentum-exchange systems for LST. The comparison factors are by no means complete and the ratings are somewhat subjective, based on opinion instead of deterministic analysis data in some cases. However, any of the candidate systems should be capable of holding the LST body pointing accuracy of 1 arc sec when used in conjunction with attitude error signals derived from the OTA FGS. Although RW power is excessive for fast slew rates, the RW power required for 60 degrees in 40 min (LST guideline) would be acceptable. Therefore, any of the candidate systems can also meet the LST maneuver requirements. Each actuator system is given a rating of 1, 2, or 3 for each comparison factor, with the higher numbers best. The individual factor ratings are summed to give the total rating for each actuator system. Surprisingly, there is very little difference between the candidate totals, even though there are big differences between ratings on specific comparison factors.

TABLE VI-6. ACTUATOR COMPARISON[a]

	Weight	Power	Reliability	H-Use	Gyro Hang-Up (ghu)	Complexity of steering Law	Failure Adaptation	H-Use After Failure	Expected Pointing Performance	Rapid Slewing	Total
3-DGCMG	2	2	1	3	2	2	2	3	1	2	20
4-SG SKEWED	3	3	2	2	1	2	3	2	2	3	23
4-SG 2-SPEED[b]	3	3	2	2	2	2	1	1	2	3	21
4 RW	1	1	3	1	3	3	2	1	3	1	19

a. High numbers are best — 1 = worst of group, 2 = average, 3 = best of group.

b. 2-SPEED — two scissored pair ensemble explicit distribution.

There is no weight or power difference between the four skewed or the two scissored pair ensemble explicit distribution (2-SPEED) SGCMG configurations. A system of three DGCMGs will weigh slightly more and require more power than a system of four SGCMGs because of the extra gimbals. An RW system (Figs. VI-8 and VI-10) will weigh about twice as much as a CMG system and will consume about twice as much power, especially when the vehicle is slewed (Fig. VI-11). The reliability of RWs should be greater than that of CMGs because the RWs have no gimbals. Because of the extra gimbals, the reliability of a system of three DGCMGs should be less than that for a system of four SGCMGs. As illustrated in Figure VI-8, DGCMGs can utilize all the system momentum in any direction. But RWs can utilize slightly less than half the system momentum for control purposes.

Gyro hang-up (ghu) is discussed for SGCMGs in Section F3.d. This is a gimbal angle combination that causes all the individual CMG torque vectors to lie in a common plane. The parallel and antiparallel constraints for DGCMGs are analogous to ghu. The momentum distribution steering law utilized for the Skylab program has solved the ghu problem for DGCMGs and the proposed 2-SPEED control (discussed in Section D.3) appears to solve the ghu problem for that particular SGCMG configuration. There is no known solution to ghu for the four-skewed SGCMG configurations. RWs do not have ghu or any analogous problem. The steering law for an RW system is constant gain which can easily be implemented in an analog fashion, but all CMG systems require an onboard digital computer to invert and multiply matrices and to handle the time varying calculations involved in the steering laws.

All actuator candidates have the ability to perform the LST control function with one flywheel unit deactivated. With the exception of the pseudo-inverse used for the four-skewed SGCMG configuration, all cases require reprogramming of the steering law or use of alternate algorithms. With the 2-SPEED steering law, the algorithm must be reprogrammed for an exact matrix inversion solution. With the four-skewed configuration, the pseudo-inverse reduces to an exact inverse without reprogramming or altering the algorithm used. The momentum use after a flywheel deactivation is proportional to that before the failure, except for the 2-SPEED which decreases.

The expected pointing performance is within the 1 arc sec range and does not include the impact of rotor imbalance, vibration propagation through the LST structure, and shock mounting each CMG or RW. Since the steering law for RWs is linear, composed of constants, and has only one variable (flywheel speed) per unit, RWs are expected to perform better than CMGs. The performance of DGCMGs are expected to be less than that of SGCMGs

because of the extra gimbals. The outer gimbal must provide a torque to counteract that of the inner gimbal as well as that required for control in its gimbal direction.

As previously pointed out, RWs cannot provide a high torque without imposing a severe power penalty. But SGCMGs are noted for their ability to provide high torque with a small power input. Due to the extra gimbals, DGCMGs do not have quite as much torque output as SGCMGs. As indicated by the overall totals for each candidate system, there is little if any difference between them. Although the four-skewed SGCMG configuration has the highest score, the comparative factors could be changed or reevaluated so that one of the other systems would appear more favorable. The general conclusion is that the momentum-exchange system for LST should be selected on the basis of available hardware or for commonality with other space programs. Since it is presently expected that the HEAO will utilize a configuration of four SGCMGs, the HEAO momentum-exchange system will be selected for the LST. Four SGCMGs with a skew angle of 30 degrees have been selected for LST (see section F.3) as a design reference for the Phase A study.

3. 2-SPEED SGCMG Configuration and Steering Law. Since the operation, mounting and steering laws for reaction wheels, 4-skewed SGCMGs, and DGCMGs are readily available in the literature, they will not be discussed in detail in this section. It is also well known that when a system of SGCMGs has its torque output axes all in a common plane, no torque can be produced perpendicular to that plane. Such a CMG system orientation has recently been defined as gyro hang-up (ghu). Although many attempts have been made to devise a method for detecting and avoiding ghu, none has been entirely successful and most have met with failure. Recently a new SGCMG configuration and steering law have been proposed as a solution to the ghu problem. The configuration, denoted as the 2-SPEED, was developed by Northrop [VI-3] and the Aero-Astrodynamics Laboratory of MSFC [VI-4].

The 2-SPEED acronym is somewhat misleading since the CMGs are not truly scissored pairs but can operate independently. This configuration consists of four SGCMGs that have been mounted such that their momentum vectors are restricted to two planes, as illustrated in Figure VI-12. The CMGs numbered 1 and 2 are restricted to face plane 1 with their gimbal axes perpendicular to this plane. A similar arrangement places CMGs numbered 3 and 4 in face plane 2. The two planes intersect along the Y-axis of the LST body coordinates illustrated in Figure VI-12, and each plane subtends an angle β (skew angle) with the Y-Z plane. For LST application, a 30 degree skew

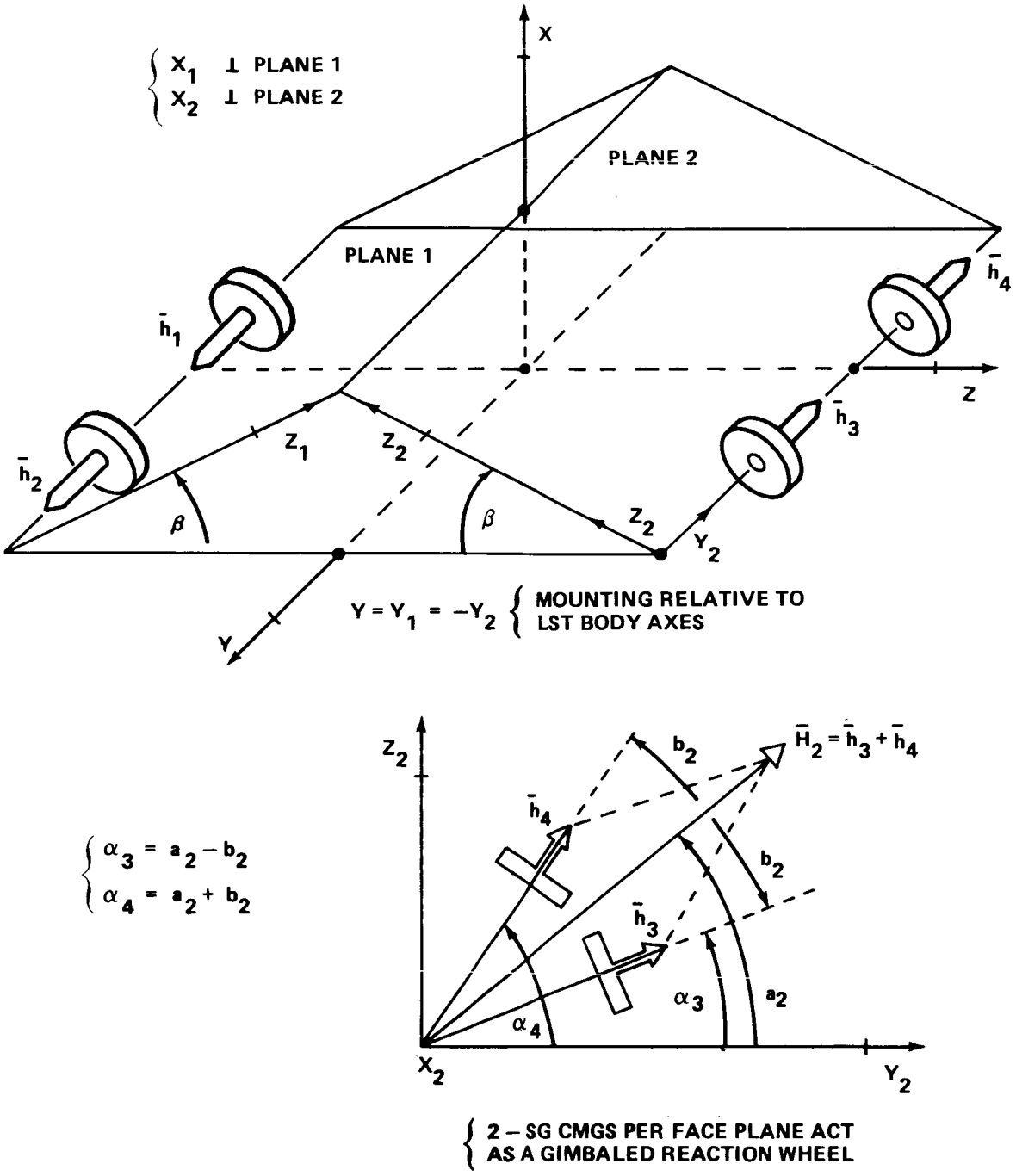

Figure VI-12. 2-SPEED mounting and face plane geometry.

angle has been selected to produce a momentum envelope somewhat proportional to the LST vehicle inertias. Each pair of CMGs produces momentum in its respective plane. By requiring that each CMG of a given pair contributes an equal amount of momentum to their planar momentum vector, the two CMGs

in a plane have the characteristics of a gimbaled reaction wheel. As shown in Figure VI-12, the planar position of the momentum vector, $\bar{H}_2$, in plane 2 is specified by the angle a_2 and its magnitude by b_2. Both the magnitude and direction of $\bar{H}_2$ can be varied. The total momentum acting on the LST is the vector sum of the momentum vectors in each face plane ($\bar{H} = \bar{H}_1 + \bar{H}_2$). By simplifying, the characteristic of the 2-SPEED is that the four SGCMGs are mathematically equivalent to two single gimbaled reaction wheels for which a steering law can be obtained without resorting to the pseudoinverse type solution.

Normally, the torque needed for vehicle control is known in the (X, Y, Z) vehicle coordinate system. This torque must be projected into the face plane coordinate systems to obtain components in the (Y_i, Z_i) $i = 1, 2$ directions. A 2×2 torque matrix for each plane is inverted to obtain the 2-SPEED steering law. To prevent program divergence when a singularity is approached, a constant is inserted as a replacement for the determinant in each 2×2 torque matrix. The known parameters at each solution time are the commanded torque in the two face planes (Y_1, Z_1, and Y_2, Z_2 components). The Z_1 and Z_2 components are unique, but since Y is the intersection between the two planes, Y_1 and Y_2 are not. The solution variables are $(\dot{a}_1, \dot{b}_1)$ and (a_2, b_2) for face planes numbers 1 and 2, respectively, which are directly related to CMG gimbal rates as shown in Figure VI-12. Momentum (or torque) can be arbitrarily distributed between the two planes in the Y direction as long as the sum equals that commanded. A momentum distribution function is used to prescribe how the Y-component is shared between planes while avoiding all or as many singularities as possible (see Section F3.d for singularity and ghu definitions). The distribution function selected [VI-4] is

$$f = 0.5 \left(\chi_{12} + 1\right)^2 + \left(\chi_{34} + 1\right)^2 - 4$$

where

$$\chi_{12} = h_{y_1} / \left(4 - h_{z_1}^2\right)^{1/2} ,$$

$$\chi_{34} = h_{y_2} / \left(4 - h_{z_2}^2\right)^{1/2} ,$$

and h is the momentum component in each face plane. By standard coordinate transformations, the values for h_{z_1} and h_{z_2} are uniquely determined as well

as their time derivatives (torques). The distribution function is utilized to obtain the torque components h_{y_1} and h_{y_2} in the Y direction by requiring that

$$\dot{f} = -kf$$

and using the relation $h_y = h_{y_1} - h_{y_2}$. The positive constant k depends on the solution time step used to update the steering law ($0 \leq k \leq 2/\Delta t$, where Δt is the time step) with $k = 2$ being a typical value. The partial derivatives of f are calculated and then the first order differential equation algebraically yields $\dot{h}_{y_1}$ and $\dot{h}_{y_2}$. Once the desired torque components are known in face plane coordinates, then the required CMG gimbal rate commands are obtained by inverting the two 2×2 face plane torque matrices. Using the 2-SPEED CMG configuration and steering law, CMG planar saturation occurs when either χ_{12} or $\chi_{34} = \pm 1$. The system is saturated when both of these conditions exist simultaneously. The CMG momentum is mapped into a square in the $\chi_{12} - \chi_{34}$ space. The distribution function is a circle in this space with center at (-1, -1) and radius 2. Once the program starts, the CMGs are forced to a momentum state that lies on a quarter arc of the circle between the points ($\chi_{12} = -1$, $\chi_{34} = 1$) and ($\chi_{12} = 1$, $\chi_{34} = -1$). As all the available momentum is used in the Y direction, saturation occurs on one of the points which are corners of the square. If $h_y = 0$, saturation in either the X or Z direction does not show up in the $\chi_{12} - \chi_{34}$ plane. Figure VI-13 illustrates the momentum square for the 2-SPEED distribution function with the $f = 0$ distribution solution. Only those points inside the square are obtainable. Singularities of the 2×2 planar torque matrices occur when a pair of CMGs in a plane are saturated (parallel) or antiparallel (self-cancelling), or equivalently when χ_{12} or χ_{34} equals 0 or ± 1. As long as only one $\chi_{ij} = 0$, the singularity will be passed. Obviously if both $\chi_{ij} = 0$, then the solution is not on the distribution curve. The sides of the square represent singularity of the two 2×2 face plane torque matrices, the $f = \pm 2$ corners represent antiparallel ghu, and the $f = 0$ corners represent true CMG system saturation.

Figure VI-14 shows the maximum momentum for the 2-SPEED configuration with a skew angle β of 30 degrees. The units are normalized in terms of momentum per CMG. As illustrated, 4 H is available in the Y direction, 3.5 H in the Z direction, and only 2 H on the minimum inertia axis.

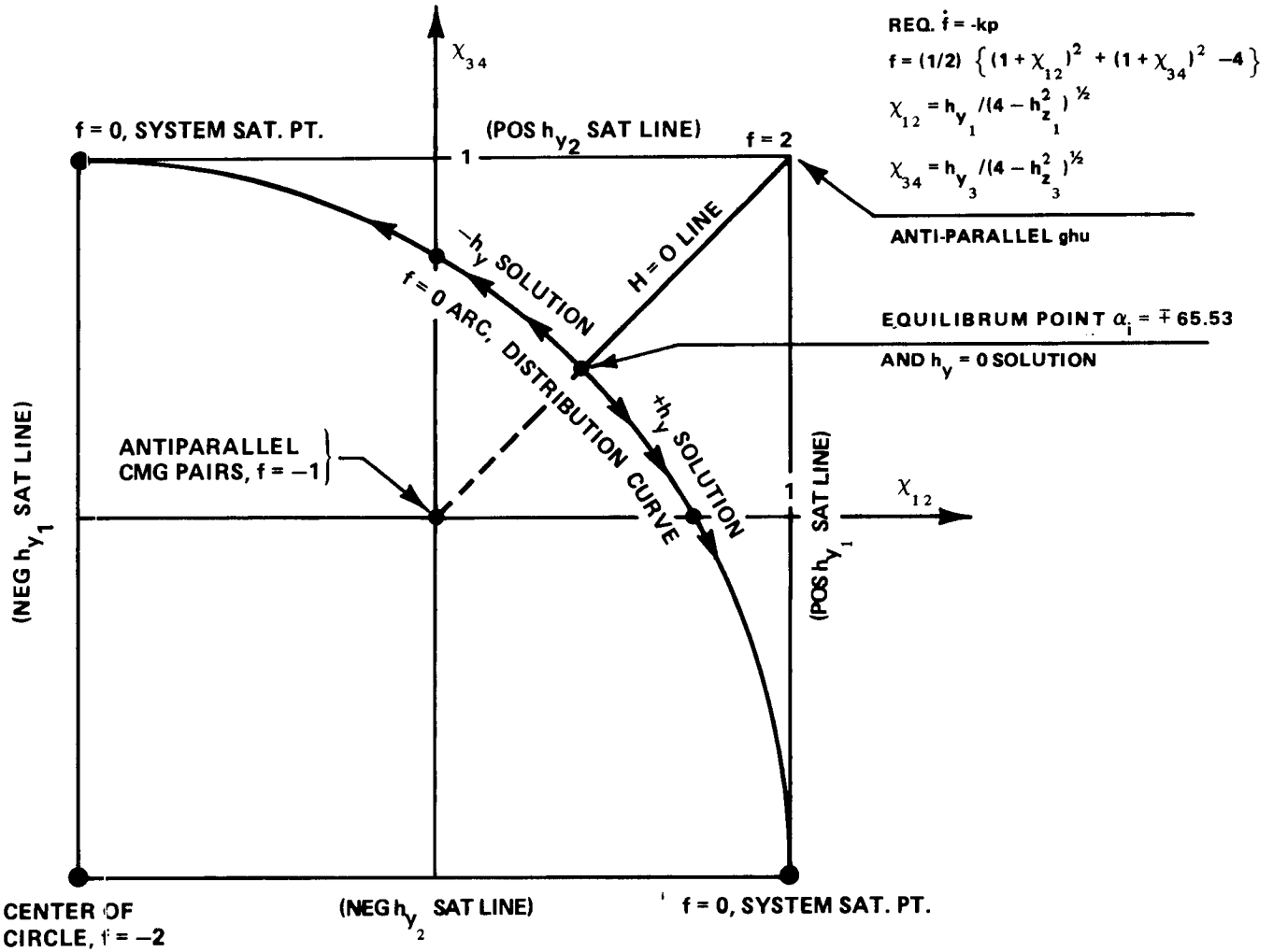

Figure VI-13. 2-SPEED momentum distribution function.

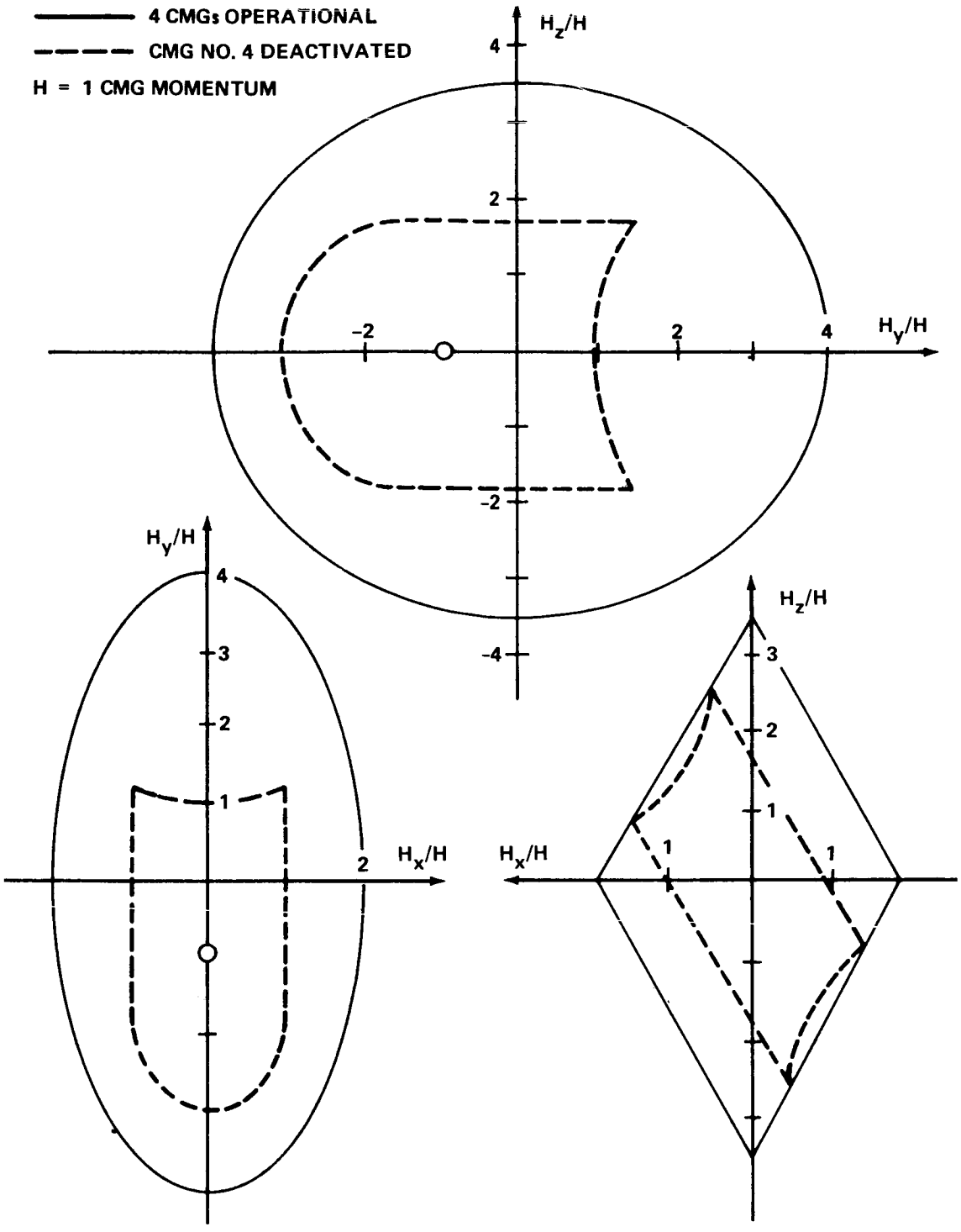

Figure VI-14. Momentum envelope for 2-SPEED.

This type CMG momentum distribution is well suited for the LST. When one CMG is deactivated, the momentum distribution is no longer symmetric, as indicated by the dashed lines for $h_4 = 0$, and the available H per axis is reduced by about 50 percent. Also, the steering law must be completely reprogrammed. With only three operational CMGs, a momentum distribution is not possible and an exact solution for the gimbal rates is obtained by inverting the 3×3 torque matrix (see Section F3.c).

In simulations, the 2-SPEED configuration and steering law was compared with the 2-SPEED configuration with the pseudoinverse steering law. In all cases, the standard 2-SPEED gave performance equaling that of the pseudoinverse. Constant torques were applied to force the pseudoinverse into ghu, at which point control was lost. Under similar conditions the 2-SPEED provided perfect control, even though gimbal angle combinations were encountered at which the torque matrix was singular. That is, the determinant of CC* can be zero while maintaining perfect vehicle control using the 2-SPEED. This ghu avoidance capability of the 2-SPEED makes it a prime candidate for the LST. The reasons it was not baselined instead of the four-skewed configurations with pseudoinverse steering are as follows: (1) It is still under development and additional tests could uncover faults, (2) the four-skewed with pseudoinverse adapts easier to a CMG failure, (3) for three-operational CMGs, the four-skewed momentum space is much larger than the 2-SPEED, and (4) ghu detection and avoidance is not needed for LST because the CMGs are oversized and the magnetic torquing system (MTS) continuously dumps momentum and can provide direct control if a ghu should be encountered. At first glance, the 2-SPEED appears simpler than the pseudoinverse. But when the distribution function and its derivatives are programmed, along with nonlinear logic, to prevent mathematical singularities, the 2-SPEED is more complicated than the pseudoinverse steering law. However, the 2-SPEED proves, beyond doubt, that a ghu avoidance steering law exists for a four SGCMG configuration without penalizing vehicle performance while permitting use of the entire CMG momentum envelope.

E. System Interfaces

1. Subsystems. Operationally, the major LST subsystems interfacing with the ACS are:

1. Electrical Distribution System (Chapter IV).
2. Communications and Data Handling System (Chapter V).
3. OTA Fine Guidance and Secondary Mirror Control Systems.

Refer to the referenced chapters for detailed description of the functions supplied by these systems.

Interfaces with the OTA fine guidance and secondary mirror control systems consist of:

1. Fields-of-View. The FSTs, their fields-of-view, and the absolute pointing capability of the ACS are designed to point the telescope with sufficient accuracy to acquire the guide stars in the FGS coarse fields-of-view.

2. Control for Fine Alignment. Using the three-axis attitude error signals generated by the FGS, the ACS actuator system provides pointing to the accuracy required by the FGS fine FOV.

3. Pointing Stability. Overall pointing stability to 0.005 arc sec in two axes is maintained by controlling the spacecraft to maintain the guide stars within the fine fields-of-view (< 1 arc sec) and by accomplishing final pointing stability with tip and tilt control of the secondary mirror.

4. Precision Slew. Precise positioning of spectrograph slits may become a firm requirement. This may lead to precise slewing of the spacecraft over very small angles using experiment sensors or a slit jaw camera to provide the intelligence for the slew.

Through the communications and data handling (C&DH) system uplink, commands and digital processor assembly (DPA) memory storage data will be provided. Generally, the commands will consist of operating instructions for the ACS, such as component configuration, operating modes, and execution details, all of which will be transferred to the transfer assembly (TA) through the remote decoder units. Memory data will be transferred directly to the DPA via the TA computer input/output unit. Typical types of stored data are star coordinates, gyro drift compensation updates, and maneuver instructions. Housekeeping data are provided via the TA command and telemetry unit to the C&DH downlink. Typically this data consists of component status monitor outputs and sensor outputs for use in ground computations of attitude.

Interfaces that occur due to interactions between systems and orbital conditions may be classified as:

1. Magnetic field propagation.

2. Occultation of guide stars.

3. Structural vibrations.

4. Momentum desaturation.

These subjects have been considered in the ACS and spacecraft design and operation. Details of the studies and results are contained in Section F.

2. LST/Shuttle Rendezvous and Docking. Primarily, rate stabilization of the LST must be supplied by the ACS during rendezvous and docking. A secondary requirement could be orientation of the LST to a specific attitude to aid in this operation. The ACS provides sufficient rate stabilization capability and, if no major component failure has occurred, the orientation capability exists. However, if major component failures have occurred, the rate stabilization capability may be all that is available.

The docking transponder subsystem has not been included as a part of the LST reference design due to lack of definition of the Shuttle rendezvous and docking system. Studies have been made of a corner reflector cube system used in conjunction with a laser radar system. Analysis has shown that a 0.1 m diameter cube used with a GaAs laser will have a range of about 43.5 km (27 mi) which is an adequate range for almost any low earth orbit rendezvous navigation and guidance scheme. The number and configuration of the cubes to provide adequate viewing will be dictated by the Shuttle needs. If a CW radar system is selected for the Shuttle, a compatible transponder system must be selected.

F. System Performance and Analysis

1. Disturbance Torque, Momentum Storage, and Impulse Requirements. For a vehicle in a 611 km (330 n. mi.) orbit, the dominant environmental disturbance is due to gravity gradient (g.g.). The other torques such as aerodynamic and solar radiation will be less than 10 percent of g.g. Normally, the magnetic torque can be neglected if the vehicle is magnetically clean. However, if materials such as invar, iron, or steel are used in the spacecraft structure, then the magnetic environment can produce torques almost equal in magnitude to the g.g. For preliminary design analysis purposes, it is assumed that the LST will be relatively magnetically clean and graphite epoxy instead of invar will be used for the optical bench. Internal movements of parts or rotating devices can also produce disturbance torques. These devices usually act over a short time interval and it has been assumed

during this phase of the study that all movements will take place prior to experimentation so that their effects will have decayed and can be neglected. For a long life mission such as LST, the g.g. disturbance torques and corresponding momentum accumulation along with the required maneuver rates will size the momentum exchange system.

It is required that, for a worst-case disturbance condition, the momentum exchange system be sized for at least one orbit's momentum accumulation during experimentation without desaturation. Then for average environmental torques, the ACS can maintain required stabilization for several orbits without desaturation. This type of criteria has been specified so that g.g. dump (desaturation using environmental g.g. field) can be utilized to reset the CMGs in the event the MTS has failed. However, during a programmed g.g. dump, the spacecraft's pointing requirements must be ignored and the vehicle must be maneuvered in a specific sequence such that the g.g. counteracts the accumulated momentum. Normally, the time required for g.g. dump is about the same as that required to saturate the CMGs under worst-case disturbances. Thus, under worst conditions, one-half of the experiment time would be lost and, under average conditions, about one-third of the time is required for momentum management using g.g dump as a failure mode.

The g.g. torque acting on the orbiting spacecraft is given by

$$T_{gi} = 3\omega_o^2 (I_j - I_k) \bar{R}_j \bar{R}_k$$

where ω_o is the orbital rate, $I_{j,k}$ are the principal inertias, $\bar{R}$ is the local vertical unit vector in principal body axes and (i, j, k) correspond to the (X, Y, Z) body axes. Depending on the subscripts, either the X, Y, or Z, gravity gradient torque component can be obtained. Since the maximum value of the product $R_j R_k$ is 0.5 [VI-5], the maximum g.g. torque is given by

$$T_{gi\ max} = (1.5)\ \omega_o^2 |I_j - I_k| \quad .$$

The maximum g.g. torque values for the design reference configuration are listed in Table VI-7. As indicated, the maximum always occurs about the axis of intermediate inertia, which for LST is about 0.14 N-m (0.1 ft-lb).

For an inertially orientated vehicle, the torque components are cyclic with a frequency of 2 or 4 times the orbital rate. However, at least one component will be offset from zero, resulting in a slow momentum buildup with time which can eventually saturate the momentum exchange system (CMGs) unless some type of desaturation device is utilized. This slow momentum buildup is denoted as secular momentum. The maximum secular momentum per orbit due to g.g. torque is also shown in Table VI-7 for each vehicle axis. The Y-axis can accumulate 410 N-m-sec (302 ft-lb-s) per orbit. Assuming four 678 N-m-sec (500 ft-lb-sec) CMGs skewed at 30 degrees for the design reference momentum exchange system, the CMGs can be saturated in 6.2 orbits without momentum desaturation or dump. If only 3 of the 4 CMGs are operational, then saturation can occur in 4.4 orbits. However, the basic ground rule is at least one orbit between dumps. Therefore, either 4 or 3 operational CMGs have adequate momentum capacity for over 400 percent increase in g.g. disturbance torque. Thus, the vehicle inertias can become larger and more unfavorable with respect to the design reference analyzed during this study without impacting the selected momentum exchange system.

The second factor that sizes the momentum exchange system is the maneuvering requirement. The guideline is 60 degrees in 40 min with a possible requirement of 90 degrees in 5 min for unusual cases. As shown in Table VI-8, the momentum required on the major axis of inertia is 498 N-m-sec (367 ft-lb-sec) to maneuver at a constant rate of 18 deg/min. Since some time is required to build up to the maximum rate and to stop once the maneuver is completed, the actual momentum required to accomplish the maneuver can be almost twice that required to attain 18 deg/min. Therefore, about 995 N-m-sec (734 ft-lb-sec) were assumed to be required for the maneuver. However, the 4-skewed CMG system has 2530 N-m-sec (1865 ft-lb-sec), over twice that required for the fast maneuver. The number of orbits required to saturate the 3 operational CMGs under worst-case g.g. torque disturbances, the momentum required to accomplish the 90 degree turn in 5 min, and the

TABLE VI-7. MAXIMUM GRAVITY TORQUE AND MOMENTUM

Axis	T (N-m)	H Cyclic (N-m-sec)	H Secular/ Orbit (N-m-sec)	No. of Orbits for CMG Saturation
X	0.0057	5.27	16.3	83.3
Y	0.1403	130.2	410	6.2
Z	0.1347	124.9	393	6.4

total CMG momentum available are shown in Table VI-9 for the case where CMG number 4 has been failed. On the major inertia axis, more than 1851 N-m-sec (1356 ft-lb-sec) are available. This is about twice that required for the fast maneuver. The experiment pointing axis (X) has over thirty times the momentum required for the minimum maneuver. Based on simulation results, there is no difference between the performance of four or three

TABLE VI-8. CMG MOMENTUM FOR MANEUVER[a]

Axis	H (18 deg/min) (N-m-sec)	H (Required) (N-m-sec)	H (Available) (N-m-sec)	Max Turn Rate (deg/min)
X	77	155	1356	318
Y	480	960	2529	95
Z	498	995	2520	91

a. 60 deg/40 min = 4.363×10^{-4} rad/sec $\Rightarrow$ $h_x = 4.7$ N-m-sec
$h_y = 29.5$ N-m-sec
$h_z = 30.6$ N-m-sec

TABLE VI-9. CMG MOMENTUM WITH NUMBER 4 CMG OUT[a]

Axis	No. of Orbits for g.g. Saturation	H Required to Maneuver (N-m-sec)	H Available (N-m-sec)	Max Turn Rate (deg/min)
X	62.5	155	1017	238
Y	4.4	960	1797	70
Z	4.7	995	1851	67

a. 60 deg/40 min = 4.363×10^{-4} rad/sec $\Rightarrow$ $h_x = 4.7$ N-m-sec
$h_y = 29.5$ N-m-sec
$h_z = 30.6$ N-m-sec

operational CMGs, and either case has a momentum envelope that is oversized for LST. Therefore, one CMG could be held in standby status and made operational only after a failure of one of the three operational CMGs, if reliability and operational simplicity so dictates. Based on g.g. disturbances with 10 percent added for other environmental disturbances, the required maximum torque for attitude hold is 0.006 N-m (0.0046 ft-lb), 0.155 N-m (0.114 ft-lb), and 0.148 N-m (0.109 ft-lb) on the X-, Y-, and Z-axis, respectively. The corresponding momentum for one orbit hold without dumping is 18 N-m-sec (13 ft-lb-sec), 450 N-m-sec (332 ft-lb-sec), and 433 N-m-sec (319 ft-lb-sec). If the 90-degree in 5-min maneuver is required, then the momentum for the maneuver is about twice that required for environmental disturbances and establishes the LST momentum requirement of about 995 N-m-sec (734 ft-lb-sec) on the major axis of inertia and 155 N-m-sec (114 ft-lb-sec) on the experiment pointing axis.

For long life missions such as LST, a considerable amount of fuel would be required to desaturate the secular momentum due to biased environmental forces if RCS dumping were utilized. Assuming a cold gas RCS with a specific impulse of 70 sec, about 1.1 kg (2.43 lb) per day or 402 kg (887 lb) per year is required to dump the average momentum accumulated. Over a long period, the average momentum is only about one-half of the maximum secular momentum per orbit as shown in Table VI-7. When one axis attains its maximum secular H per axis, the other two components are zero. In most inertial pointing orientations, the secular H will be distributed between the vehicle axes, but the total magnitude will always be less than the maximum on any individual axis. Since the fuel weight and/or possible contamination may be prohibitive, a magnetic torquer system (MTS) is proposed for LST. The MTS must be sized to dump the maximum secular momentum per orbit. The MST design for LST is contained in Section F.4. As proposed, the MTS will be used continuously to keep the CMGs near a small value of momentum. Hence, whenever a maneuver sequence is initiated, almost the full CMG momentum capacity will be available for the maneuver. The CMGs must be sized only to obtain the specified maneuver and not to attitude-hold for one orbit and then do the maneuver unless failures in the MTS are considered.

2. Sensing System. Sensor noise from the reference gyro assembly and fine guidance star trackers will be a critical factor in determining the pointing stability. Two simplified attitude control systems were analyzed on a single-axis basis to parametrically relate pointing stability errors to system bandwidth for the three major disturbance sources, gravity gradient torques, gyro noise, and star sensor noise. As shown in Figure VI-15, one

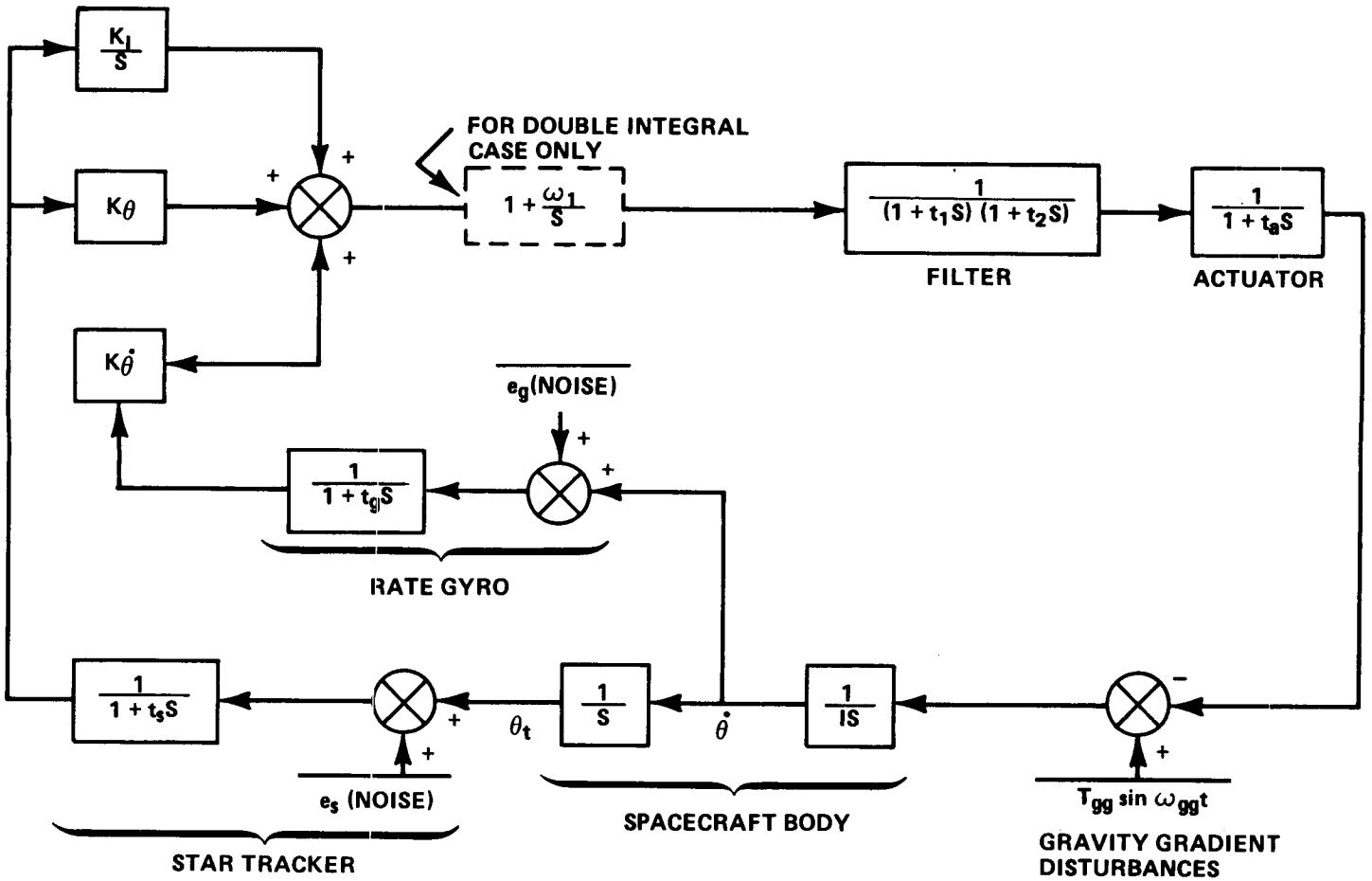

Figure VI-15. Basic system block diagram for proportional, derivative, and integral or double integral control.

system uses proportional, derivative, and single integral control to generate actuator commands while the other system uses proportional, derivative, and double integral control.

Based on the assumption that the errors due to the major error sources were uncorrelated, the RSS error was expressed as

$$\theta_t = \left[(\theta_{gg})^2 + (\theta_g)^2 + (\theta_s)^2\right]^{1/2} \text{ arc sec (RSS)} \quad .$$

The expressions for θ_{gg}, θ_g, and θ_s, the pointing errors due to gravity gradient torques, gyro noise, and sensor noise, respectively, were developed from the single integral system block diagram and are

$$\theta_{gg} = \left(\frac{\zeta_c \, \omega_{gg} \, T_{gg} \, g^2 \times 10^5}{2\sqrt{2}\,\pi^3 \, I}\right) \frac{1}{(BW)^3} \quad ,$$

$$\theta_g = \left[\frac{N_g \, g^2}{16\,\pi\,\zeta_c\,(g-1)}\right]^{1/2} \frac{1}{(BW)^{1/2}} \quad ,$$

$$\theta_s = \left[\frac{\pi\,(4\,\zeta_c^{\,2}+1)\,N_s}{4\,\zeta_c\,(g-1)}\right]^{1/2} (BW)^{1/2} \quad ,$$

where ζ_c is the damping factor, ω_{gg} is the frequency of gravity gradient torques (twice orbital frequency), T_{gg} is the gravity gradient torque magnitude, g is the gain margin, I is vehicle moment of inertia, BW is system bandwidth, N_g is the gyro noise spectral density — constant over BW, and N_s is the star sensor spectral density — constant over BW.

The three individual error magnitudes as a function of system bandwidth are plotted in Figure VI-16. The following system parameters were used:

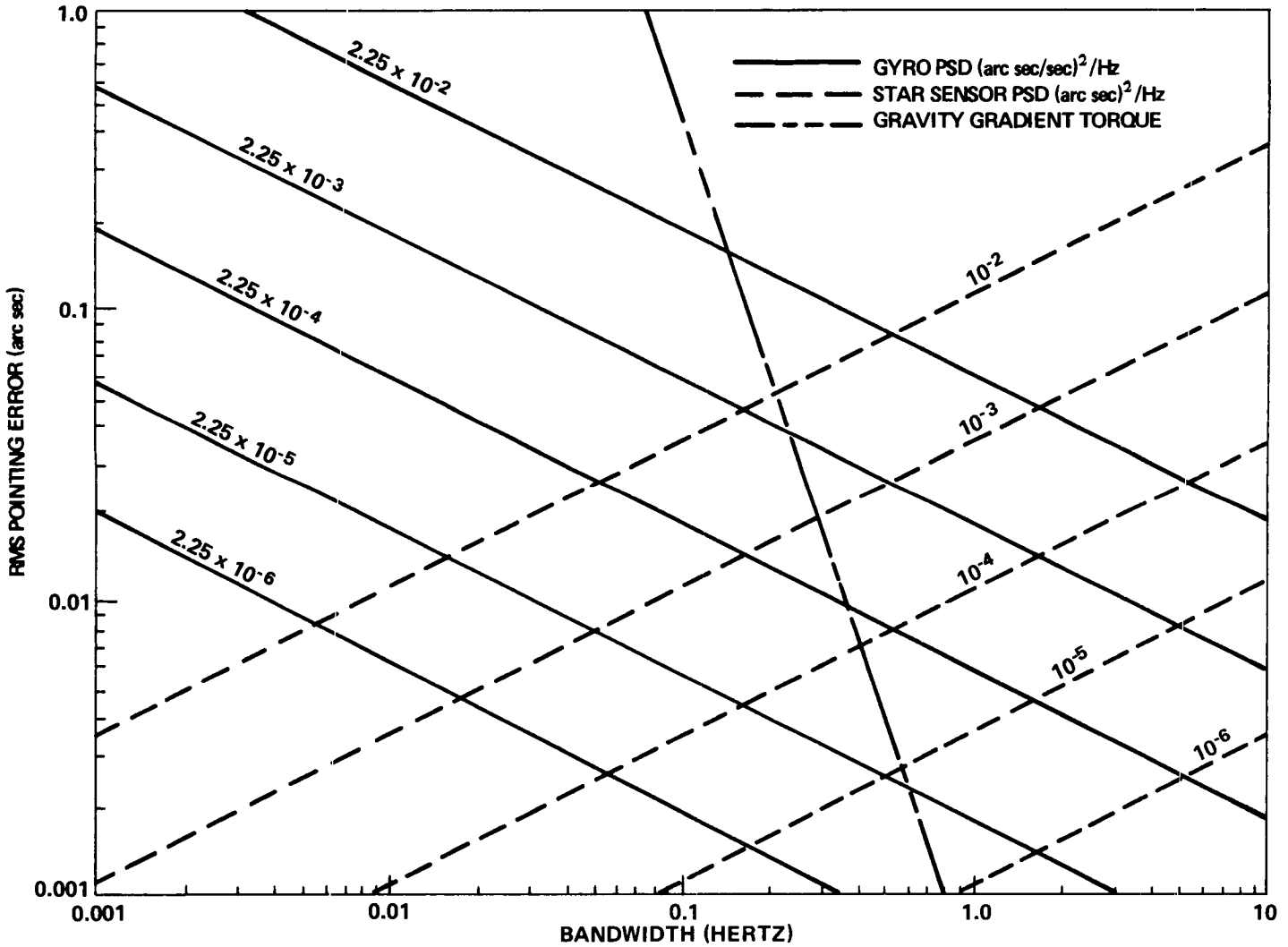

Figure VI-16. LST/ACS pointing errors due to sensor noise and gravity torque disturbance — proportional, derivative and integral control.

$$\omega_{gg} = 0.002 \text{ rad/sec} \quad ,$$

$$T_{gg} = 0.2 \text{ N-m } (0.15 \text{ ft-lb}) \text{ rms} \quad ,$$

$$I = 122\,400 \text{ kg-m}^2 \ (90\,000 \text{ slug-ft}^2) \quad ,$$

$$g = 4 \ (12 \text{ dB}) \quad ,$$

$$\zeta_c = 0.707 \quad .$$

To facilitate the selection of the gain constants, the following expressions are plotted as a function of bandwidth in Figure VI-17:

$$K_I = \left(\frac{4\,\pi^3\,I}{\zeta_c\,g^2}\right) (BW)^3 \quad ,$$

$$K_{\dot{\theta}} = \left(\frac{\pi\,I}{\zeta_c}\right) (BW) \quad ,$$

$$K_\theta = \left(\frac{4\,\pi^2\,I}{g}\right) (BW)^2 \quad .$$

If values of star sensor and gyro noise are known, the plotted data can be used to select a system bandwidth to minimize the total RSS error. Following the bandwidth selection, the control gains can be determined from the curves of Figure VI-17. Since pointing error due to gyro noise decreases with increasing bandwidth and pointing error due to star sensor noise increases with increasing bandwidth, a compromise bandwidth selection is required. The data may be used also to determine the limiting values of noise to obtain an acceptable total error because, in general, the bandwidth first selection would be based on a stable system with very low steady state error due to gravity gradient torques.

Based on a general look at expected gyro and star sensor noise data, the conclusion is that pointing stability cannot be maintained to the specified requirement by gyro control. However, star sensor control appears feasible. Computer studies using actual models of the sensors and actuators must be made to substantiate the analysis made using ideal sensors and actuators.

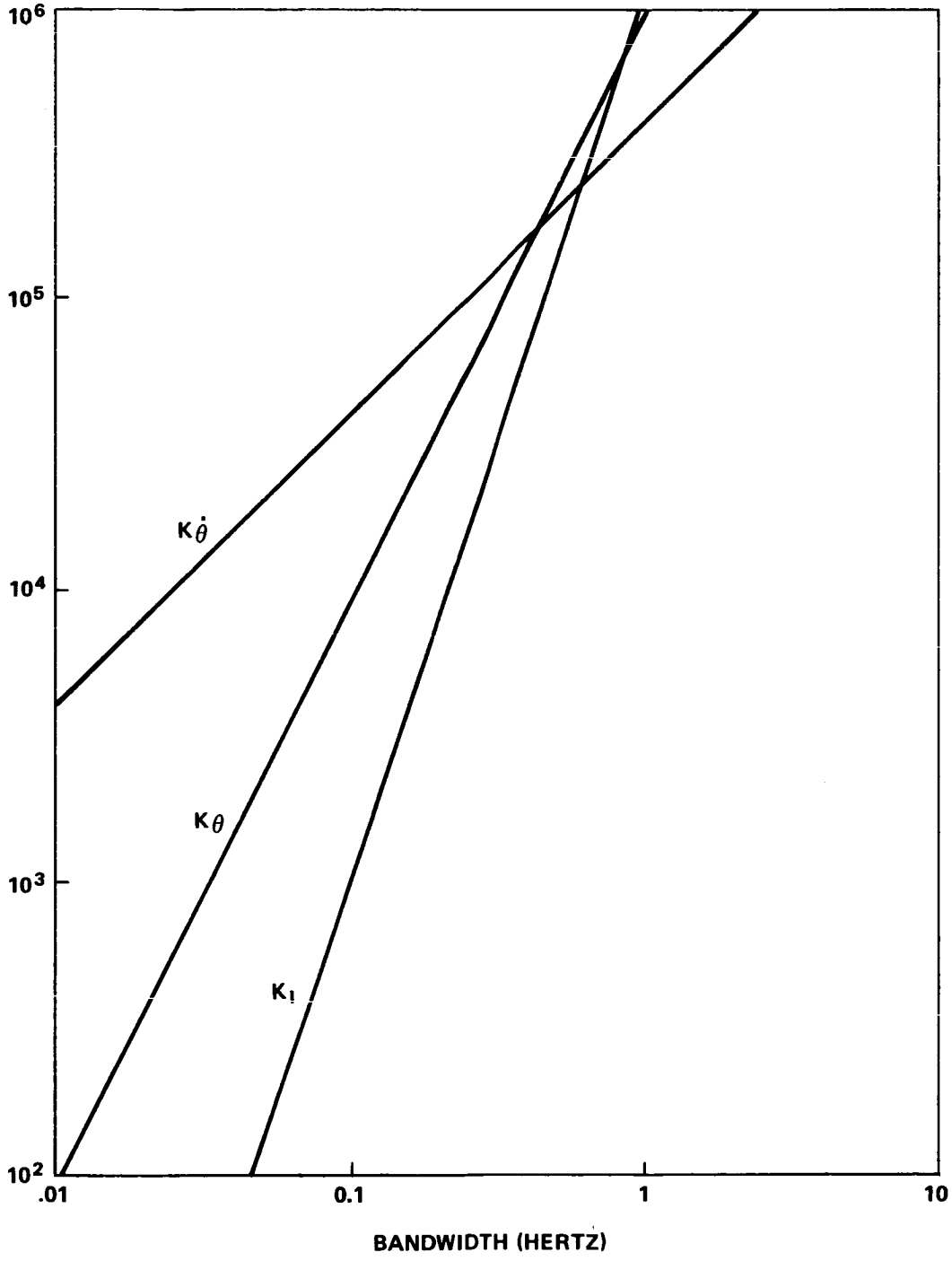

Figure VI-17. Gain constants for single integral case.

For the system using double integral control, the expressions developed for gravity gradient and sensor errors are

$$|\theta_{gg}| = \left| \frac{\sqrt{2}\, T_{gg}}{\omega_{gg}\, I\, S\left[\left(\frac{S}{Kg\,\omega_{gg}}\right)^2 - 2\zeta_c\left(\frac{S}{Kg\,\omega_{gg}}\right) + 1\right]\left(1 - \frac{S}{g\,\omega_{gg}}\right)} \right|$$

arc sec (rms) ,

$$\theta_g = \left(\frac{Kg\, N_g}{16\,\pi\,\zeta_c}\right)^{1/2} \frac{1}{(BW)^{1/2}} \quad \text{arc sec (rms)} \quad ,$$

$$\theta_s = \left[\frac{\pi\,(4\,\zeta_c^{\,2} + 1)\, N_s}{4\, g\, K\, \zeta_c}\right]^{1/2} (BW)^{1/2} \quad \text{arc sec (rms)} \quad ,$$

where

$$K = \frac{\omega_1}{\omega_c} = 10 \quad ,$$

$S = j\omega_s$ = system bandwidth,

$$\omega_s = g\, K \omega_c \quad .$$

The remaining constants are identical to those used for the single integral case. Figure VI-18 is a plot of the relations versus bandwidth.

The gain constants are plotted as a function of bandwidth in Figure VI-19 for the following expressions:

$$K_I = \frac{8\,\pi^3\, I}{\sqrt{2}\, g^2\, K^2} (BW)^3 \quad ,$$

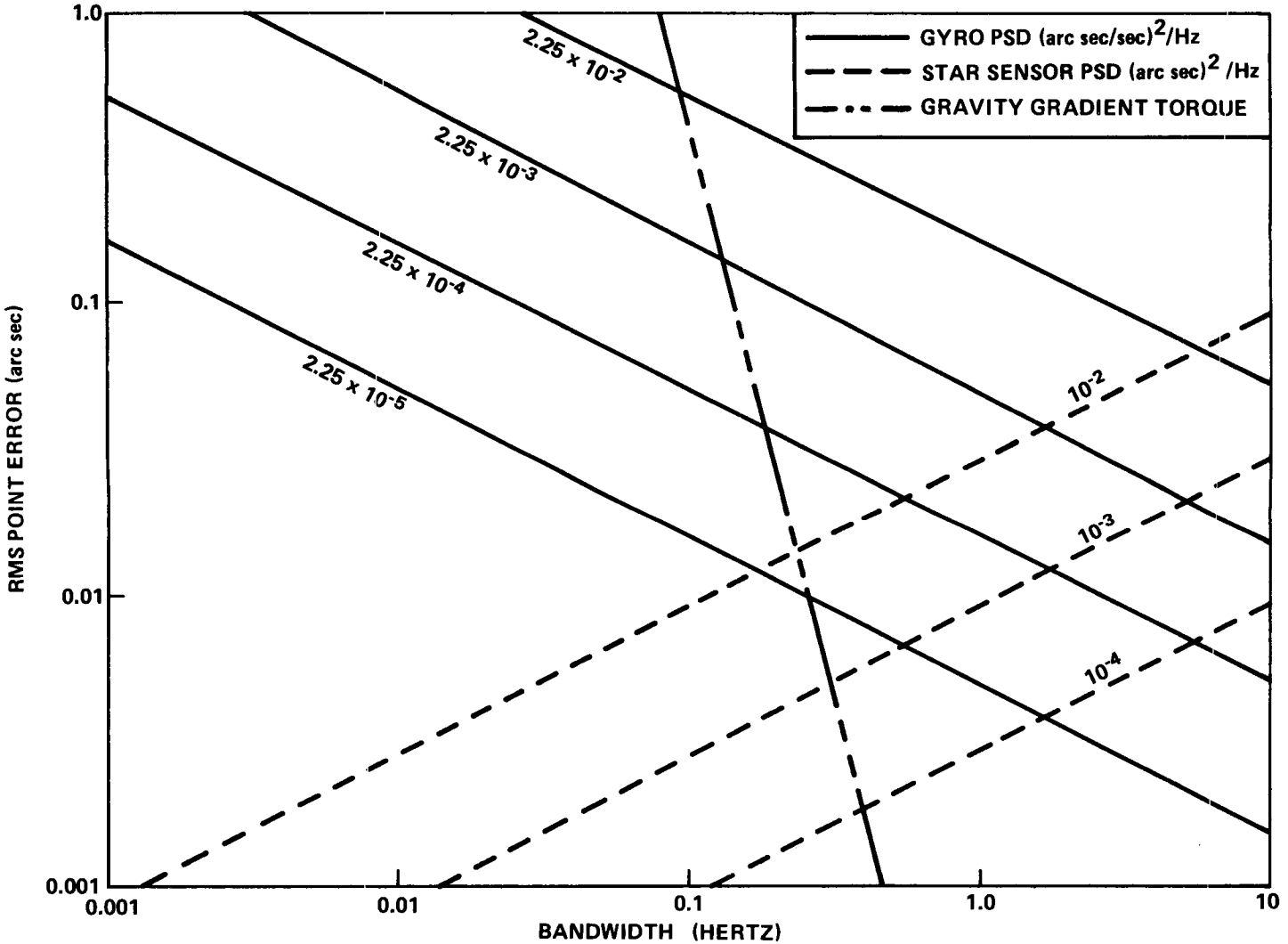

Figure VI-18. LST/ACS pointing errors due to sensor noise and gravity torque disturbance — proportional, derivative and double integral control.

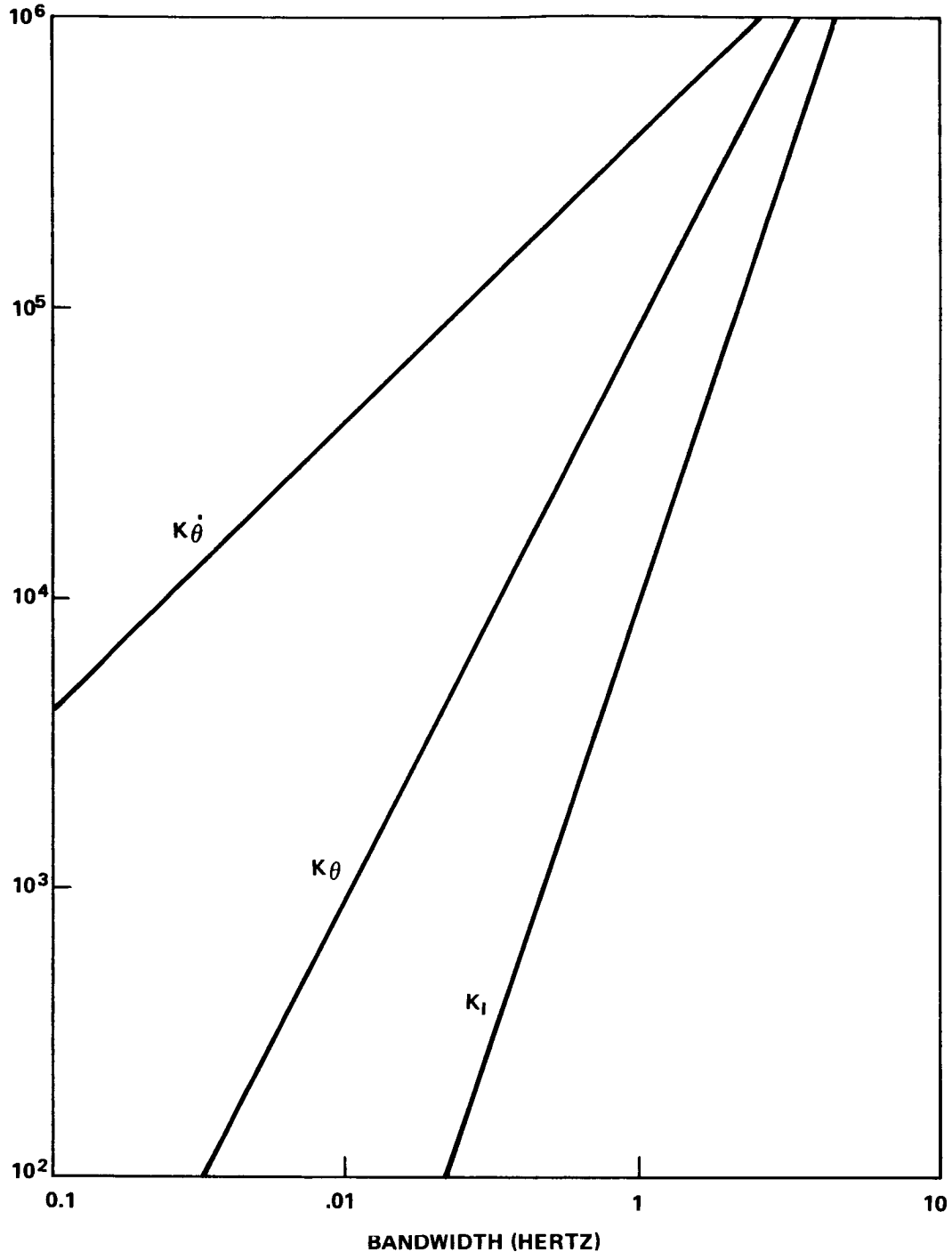

Figure VI-19. Gain constants for double integral case.

$$K_\theta = \frac{4\sqrt{2}\,\zeta_c\,\pi^2\,I}{g\,K}\,(BW)^2 \quad ,$$

$$K_{\dot{\theta}} = \pi\sqrt{2}\,I\,(BW) \quad .$$

As in the single integral case, the error due to gyro noise decreases with increasing bandwidth for the double integral case, but for a given spectral density the errors in the double integral case are larger. The error due to star sensor noise increases with increasing bandwidth; however, for a given spectral density, the errors are less for the double integral case. The total RSS error may not be appreciably different for the single and double integral cases and the final choice will be based on system stability and the method of primary control. Further computer studies are required in which realistic sensor and actuator models are incorporated into the analysis and a parameter sensitivity analysis accomplished.

A general conclusion is that gyro control alone is not a feasible approach to meeting the pointing stability requirement and if gyros are used as primary control, frequent updates from the star sensor system will be required. In fact, the updates must be so frequent that the system will act as if pointing stability is being maintained with star sensor information.

3. CMG System. Based on previous study results (see Section D.2), CMGs offer several advantages over reaction wheels, especially from a power and weight viewpoint. From a hardware availability standpoint, there are several single gimbal CMGs that are sized appropriately for the LST spacecraft with respect to both torque and momentum. Moreover, for maximum commonality with the HEAO, the same type SGCMGs could be used for the LST momentum exchange system. The CMG system is required to provide enough momentum accumulation capability to counteract all environmental disturbances for a minimum of one orbit during experimentation without desaturation. In addition, the CMGs must also provide enough torque and momentum to maneuver at least 60 degrees in 40 min, with a desirable goal for special maneuvers of 90 degrees in 5 min. Sufficient reliability and/or redundancy must be incorporated to attain satisfactory performance over the total mission duration.

The mounting of the CMGs relative to the vehicle reference axes will determine the shape of the maximum envelope within which the CMG system can provide momentum. In general, for an inertially oriented spacecraft that does not maneuver frequently, the momentum envelope should be

sized proportional to the vehicle inertia distribution. However, when the spacecraft is reoriented, stored CMG momentum is transferred from one axis to another. In cases for which many maneuvers are made or when the spacecraft spins, the CMGs should be mounted to produce a near-spherical momentum envelope. Although the LST maneuvers quite often, it has a magnetic torquing system (MTS) which continuously keeps the stored momentum contained about either a zero or selected bias value. For the LST, therefore, the CMGs should be mounted to produce momentum proportional to the spacecraft inertias.

a. Four Skewed Configuration. The SGCMG mounting arrangement relative to the LST is shown in Figure VI-20. Four SGCMGs are mounted symmetrically about the experiment pointing X-axis. Each CMG momentum (and torque) vector is restricted to a plane that is skewed relative to the vehicle Y-Z plane by the angle β. The four planes form a pyramid whose apex is aligned with the vehicle X-axis, and each CMG gimbal axis is perpendicular to its associated plane. As shown, the CMG system is at a zero momentum state. When the CMGs are gimbaled, both the torque and momentum vectors of each individual CMG change relative to the LST axes, but the gimbal axes remain fixed relative to the LST structure. As a result of the mounting arrangement, each CMG can contribute momentum along each axis of the LST. If any of the four CMGs fail and is powered down, the remaining three CMGs can provide three-axis attitude control and completely satisfy all the LST control requirements. With help from the MTS, two CMGs can be used to control the LST in a degraded operational mode.

b. Momentum Envelope. Both an analog and a digital program were developed to determine the maximum momentum surface that can be generated by a particular set of SGCMGs. Regardless of the CMG gimbal positions, there is always some total momentum vector which is the vector sum of the individual CMG momentum vectors. If the CMGs are caused to rotate in some random fashion, the locus of the tip of the total momentum vector will describe a solid in momentum space. The boundary of this solid is the maximum momentum surface, or momentum envelope. This envelope is a function of the number and mounting arrangement of the CMGs and is independent of the control law used to command the CMGs.

The projection of the momentum envelope onto both the Y-Z and X-Z planes for the four SGCMG configuration shown in Figure VI-20, is shown in Figure VI-21. Since the X-Y view is identical to the X-Z view, it is not shown. With a skew angle of 30 degrees, the momentum envelope approximates an oblate spheroid. The normalized units shown have been obtained by dividing the total momentum vector by the momentum, H, per

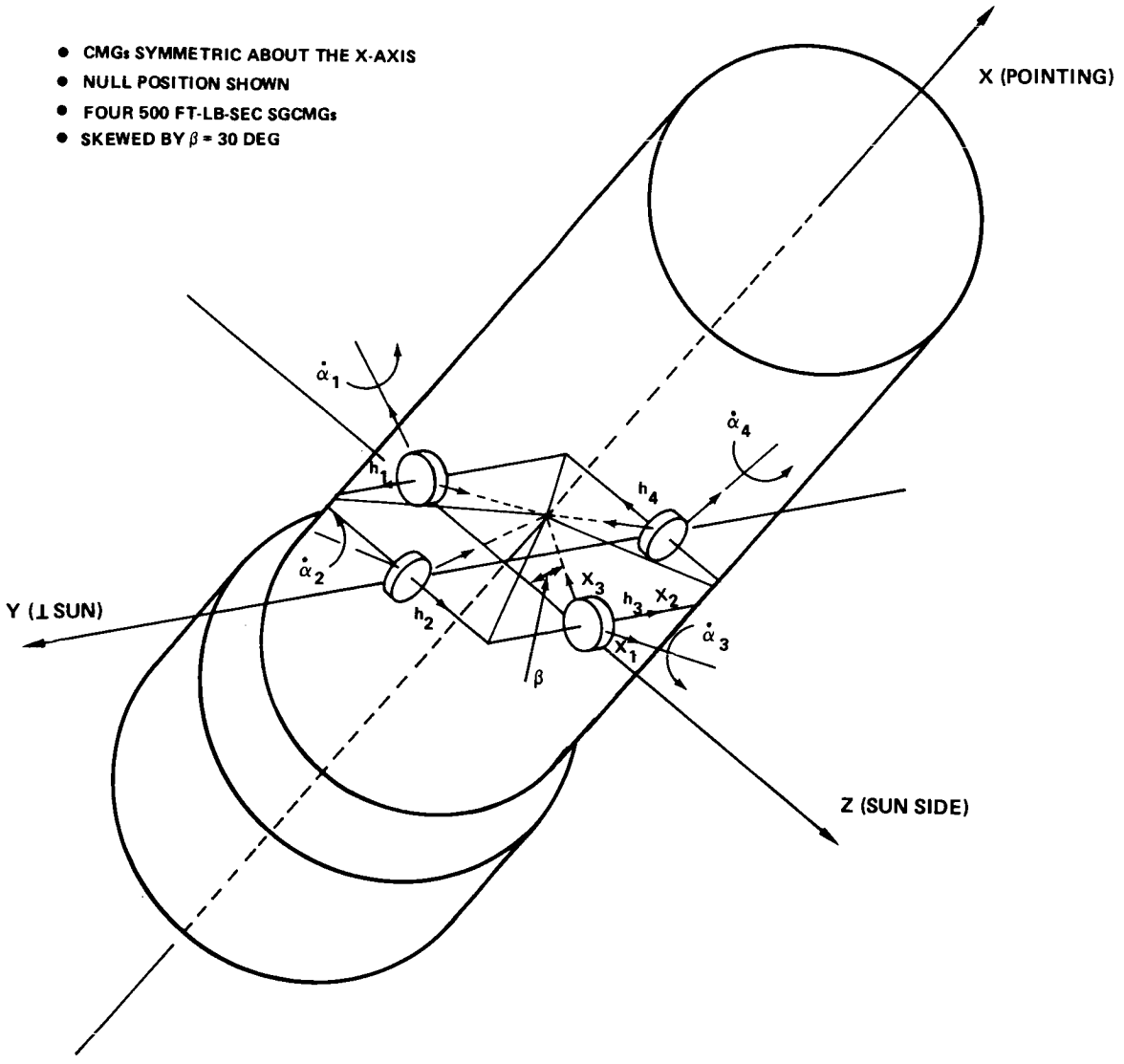

Figure VI-20. LST reference design CMG configuration.

individual CMG. In the Y and Z directions, the capability is 3.73 H per axis. In the minimum inertia axis, X, the capability is 2.0 H. By increasing the skew angle to 53.1 degrees, a near-spherical envelope with 3.2 H per axis is obtained. By decreasing the skew angle, the profile shown is reduced on the X-axis with some corresponding increase on the Y- and Z-axis. A skew angle of 30 degrees has been selected for the LST to produce momentum somewhat proportional to the vehicle inertias.

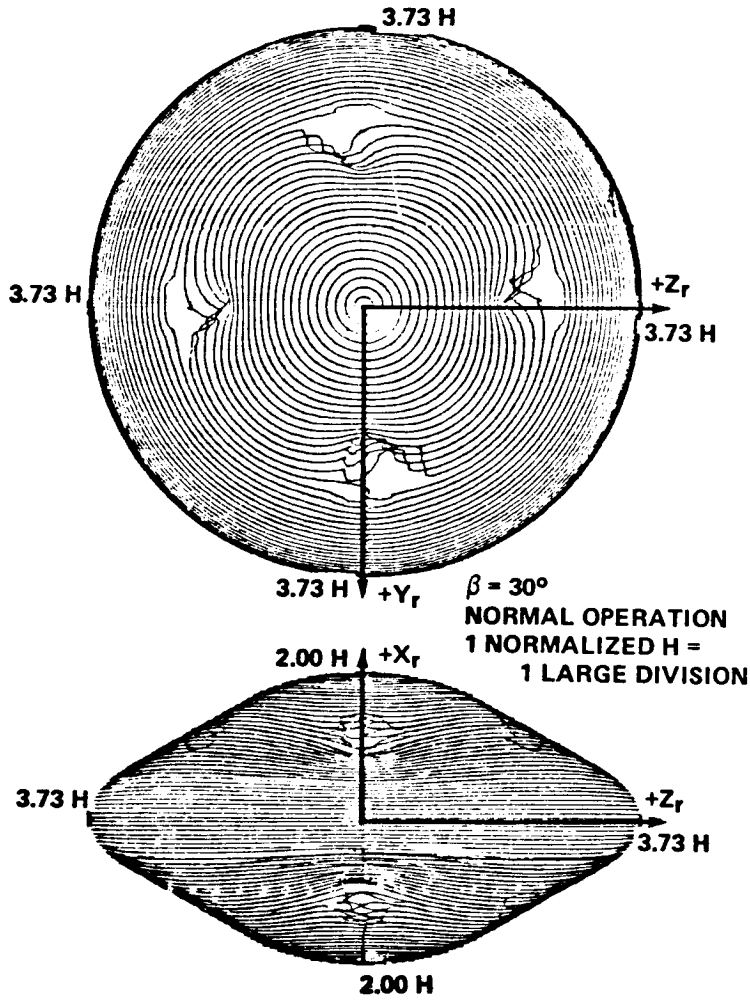

Figure VI-21. CMG momentum envelope.

When one CMG has been failed, the envelope is no longer symmetric and a bulge occurs along the gimbal axis of the failed CMG. Figure VI-22 illustrates the momentum envelope when CMG number 4 has been deactivated. Only the X-Z view is symmetric. The momentum attains a maximum value of 2.9 H along the gimbal axis of the deactivated CMG. Indentures or depressions of about 1.3 H occur along the gimbal axes of the other 3 CMGs. As previously shown in Tables VI-8 and VI-9, either the four or three operational CMG cases can meet all LST momentum requirements. Assuming 678 N-m-sec (500 ft-lb-sec) per CMG, the total momentum available with four CMGs operating is over six times the actual requirement and four times with three operational.

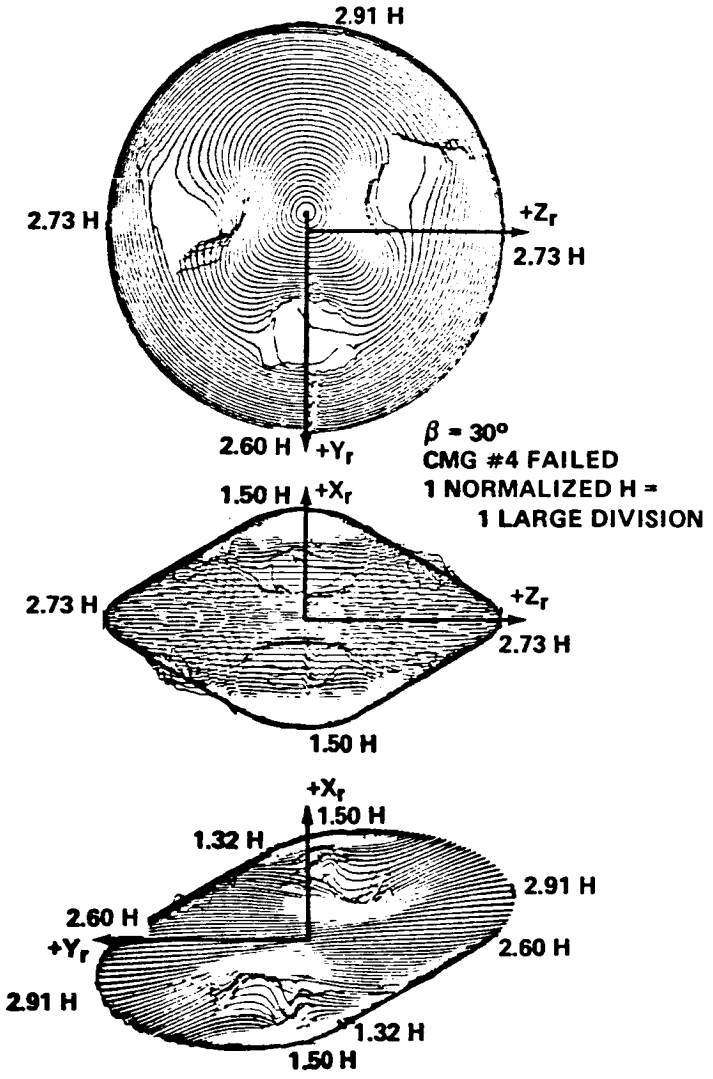

Figure VI-22. CMG momentum envelope with CMG no. 4 failed.

c. Steering Law. When the CMG gimbal angles are moved, a corresponding change occurs in the momentum relative to the body axes. By definition, torque is the inertial time rate of change of angular momentum. Therefore, torque stabilization of the LST requires a controlled rate of change of the CMG gimbal angles. One general problem area is to derive the gimbal rate commands so that the LST is torqued by the CMGs in some desirable manner. The general spacecraft control law (commanded torque) is usually derived as a linear combination of sensor outputs such as rate gyros, sun sensors, star trackers, etc., which have been weighted by a constant gain

on each output. The gains are selected to produce the desired vehicle response and stability characteristics. Ideal LST control would be obtained if the torque called for by the vehicle control law, $\bar{T}_c$, could be exactly produced by the CMGs. The CMG gimbal rate commands required to make the CMG torque an approximation of $\bar{T}_c$ are denoted as the CMG steering law.

The standard approach for obtaining the steering law is to equate the total rate of change in CMG angular momentum, $\dot{\bar{H}}$, to the commanded torque, $\bar{T}_c$. The CMG torque, $\dot{\bar{H}}$, is mathematically related to the gimbal rates through a torque matrix, C. If the number of SGCMGs is N, then C is a $3 \times N$ matrix with its columns being vectors aligned with each individual CMG torque vector. For the four-skewed CMG configuration, there are three equations (components of $\dot{\bar{H}}$) and four unknowns (CMG gimbal rates, $\dot{\alpha}$). To obtain an exact solution, a constraint equation or relation between the unknowns is needed. For each constraint or assumption that is made, a different solution (steering law) will be obtained for the gimbal rates. One type solution that has performed well in simulations of the LST is the Moore-Penrose pseudoinverse, which minimizes the norm of the gimbal rates. The steering law is obtained through the solution of

$$\tilde{T}_c = \dot{\tilde{H}} = C \dot{\tilde{\alpha}} \quad .$$

The pseudoinverse of C is given by

$$C^+ = C^* (CC^*)^{-1}$$

where the superscript asterisk represents the transpose of a matrix and minus one represents the usual inverse of a square matrix. To obtain the inverse, the determinant of CC^* must be calculated and when it is zero a solution does not exist. To prevent such a singularity from causing program divergence, software limits could be incorporated in the computer routine for calculating the inverse. Assuming $|CC^*|$ is not zero, the pseudoinverse steering law is given by

$$\dot{\tilde{\alpha}} = C^+ \tilde{T}_c$$

When a CMG fails, the failed CMG must be identified and the corresponding column of C set to zero. The pseudoinverse need not be reprogrammed. With one of four CMGs deactivated, C reduces to a 3×3 matrix that has an exact inverse, in which case the pseudoinverse also reduces to the exact inverse.

As noted previously, the columns of C are torque vectors for each CMG. When all the torque vectors are coplanar, the determinant of CC* is zero, producing a mathematical singularity in the steering law. For this condition, the CMG system cannot produce a torque perpendicular to the plane in which all CMG torque vectors lie. If $\bar{T}_c$ is then perpendicular to $\dot{\bar{H}}$, the CMGs cannot provide any of the desired control torque, consequently vehicle control will be lost. If $\bar{T}_c$ is not perpendicular to $\dot{\bar{H}}$ when (CC*) is zero, then the pseudoinverse solution will produce part of the desired control torque. Although the pointing error will increase as the singular condition is passed, vehicle control will not be lost. In digital simulations with cyclic environmental disturbances acting on the LST, the only singular conditions which prevented proper operation of the steering law were those which also corresponded to CMG saturation. In most cases for which an internal singularity was approached, a small pointing error was observed, but the CMG system would recover and operate satisfactorily until CMG saturation was reached. However, when constant torques were commanded (without the cyclic disturbance torques), internal singularities could always be encountered with subsequent loss of control. Only about 50 to 60 percent of the momentum envelope is usable if it is required to avoid all posible singularities. This singularity free momentum solid is large enough to meet all LST pointing control requirements without dumping any momentum for at least one orbital period. More research is needed to fully understand the singularities associated with SGCMGs and to develop possible avoidance schemes.

d. Gyro Hang-Up (ghu). When $|CC^*| = 0$, there is a direction in momentum space in which a torque cannot be produced. This direction is a line perpendicular to the plane in which the CMG torque vectors are coplanar, commonly referred to as the hang-up plane. If the commanded torque is perpendicular to the hang-up plane, then the CMGs cannot produce any part of this torque and vehicle pointing control is lost. Such a condition will be defined as gyro hang-up and is identified whenever the scalar product between the commanded torque and the CMG torque is zero ($\bar{T}_c \cdot \dot{\bar{H}} = 0$). Before ghu can occur, $|CC^*|$ must be zero and $\bar{T}_c$ must be perpendicular

to the hang-up plane. However, if $\bar{T}_c$ is in the hang-up plane, complete control authority is available even though $|CC^*| = 0$. In many simulation runs, $\bar{T}_c$ would subtend an angle less than 90 degrees with the hang-up plane. For this case, the CMGs would produce a part of the commanded torque, a pointing error would be observed, the CMGs would be driven out of the hang-up condition, and pointing control would be resumed. However, once the outer boundary of the momentum envelope is reached, the CMGs are saturated and in ghu.

Using the pseudoinverse steering law, these gimbal angle combinations which produce $|CC^*| = 0$ correspond to potential ghu conditions. But other steering laws were investigated in which mathematical singularities occurred that did not cause $|CC^*|$ to be zero, such as the Brown Engineering Company (BECO) H-distribution or the Bendix summation of three gimbal inverses. Still other steering laws such as the maximum contribution or the transpose with torque feedback had no mathematical singularities but certain gimbal angle combinations would prevent the commanded torque from being generated by the steering law. During the LST studies, several programs were developed to investigate the singularities and possible ghu conditions associated with SGCMGs. For a given CMG momentum state, it was determined that the corresponding gimbal angle set was not unique. But for a given CMG gimbal angle set, the momentum state is unique. Starting from a specific gimbal angle set, the momentum space was spanned in radial lines to produce distinct surfaces, lines and points at which $|CC^*| = 0$ and the potential for ghu existed. However, changing the gimbal set (with the same initial momentum state) and again spanning momentum space would result in an entirely new set of possible ghu surfaces. If all possible surfaces where $|CC^*| = 0$ are viewed in momentum space, control with SGCMGs appears almost impossible [VI-6]. However, only those surfaces associated with the initial gimbal set are meaningful.

With four CMGs operating, an infinite number of initial gimbal sets produce a zero momentum state. Moreover, at a zero H state the gimbal angles can be changed without torquing the vehicle. Hence, an initial gimbal set should be selected to give the largest momentum space without hang-up surfaces. Additionally, if the direction of the commanded torque is known over an extended time interval, the initial gimbal set can be selected so that the entire momentum solid in the desired direction can be used for control purposes.

Starting with the initial gimbal set $\alpha_i = 0$ $(i = 1, 2, 3, 4)$, the momentum state is zero. Those possible ghu surfaces associated with $\alpha_i = 0$

are shown in Figure VI-23 for the Y-Z and Z-X planes. In the Y-Z plane there is a square box composed of line ghu possibilities which appear as points ($H_z/H = 1.75$ H) in the Z-X plane. In either plane, the outer boundary is the maximum momentum envelope which is always a ghu surface. The LST momentum requirement for one orbit attitude hold under worst-case environmental torques is also shown by the dashed lines in the planes. The requirement for secular gravity gradient momentum storage is a flat disk of 1.2 H diameter in the Y-Z plane and a thickness of 0.048 H in the Z-X plane, if H = 678 N-m-sec (500 ft-lb-sec) per CMG. For this case, the momentum required to produce a vehicle angular rate of 18 deg/min is 0.73 H on the Y-Z axes and only 0.11 H on the X-axis. With four CMGs operating, there is more than enough singularity free momentum space to meet the LST requirements. Although there are other possible ghu surfaces out of the planes shown, a momentum sphere of at least 3.5 H diameter exists in momentum space that is completely free of any possible ghu surfaces.

By changing the initial gimbal set, different ghu surfaces are obtained. In Figure VI-24, the initial gimbal set is +60, -60, +60, and -60 degrees for α_i, respectively, with i = 1, 2, 3, 4. Notice that the previous ghu in the Y-Z plane has now become two points with the rest of the Y-Z plane completely free of singularities. In the X-Z plane, there are still two point singularities (on the X-axis) and a ghu line appears vertical to the X-axis at $H_x/H = 1.1$ H. If the sign on the initial gimbal set is reversed, then the point singularities in the Y-Z plane are rotated 90 degrees and the line singularity in the Z-X plane appears on the negative X-axis. In any case, there is enough singularity free momentum space to accomplish the LST mission without singularity (ghu) detection and avoidance schemes.

When one CMG is deactivated, the remaining three CMGs can also produce enough singularity free momentum to meet the LST requirements. With a skew angle of 30 degrees there is a sphere of at least 1.8 H diameter centered about a zero momentum state. As the skew angle is increased, the singularity free space in the Y-Z plane decreases slightly but increases in parallel Y-Z planes offset on the X-axis. By offsetting its center from zero, a 1.8 H diameter sphere of singularity free momentum space can be obtained with almost any skew angle. Once a CMG has failed, the gimbal angles will automatically be forced by the MTS to a state such that the momentum is near zero. Without the MTS, however, the initial gimbal angles with their corresponding momentum states must be specified for each CMG failure case. For each CMG that has been failed, there are eight possible gimbal sets for the remaining three CMGs that can produce a zero momentum state. Four correspond to positive values of the determinant of the 3×3 torque matrix and the

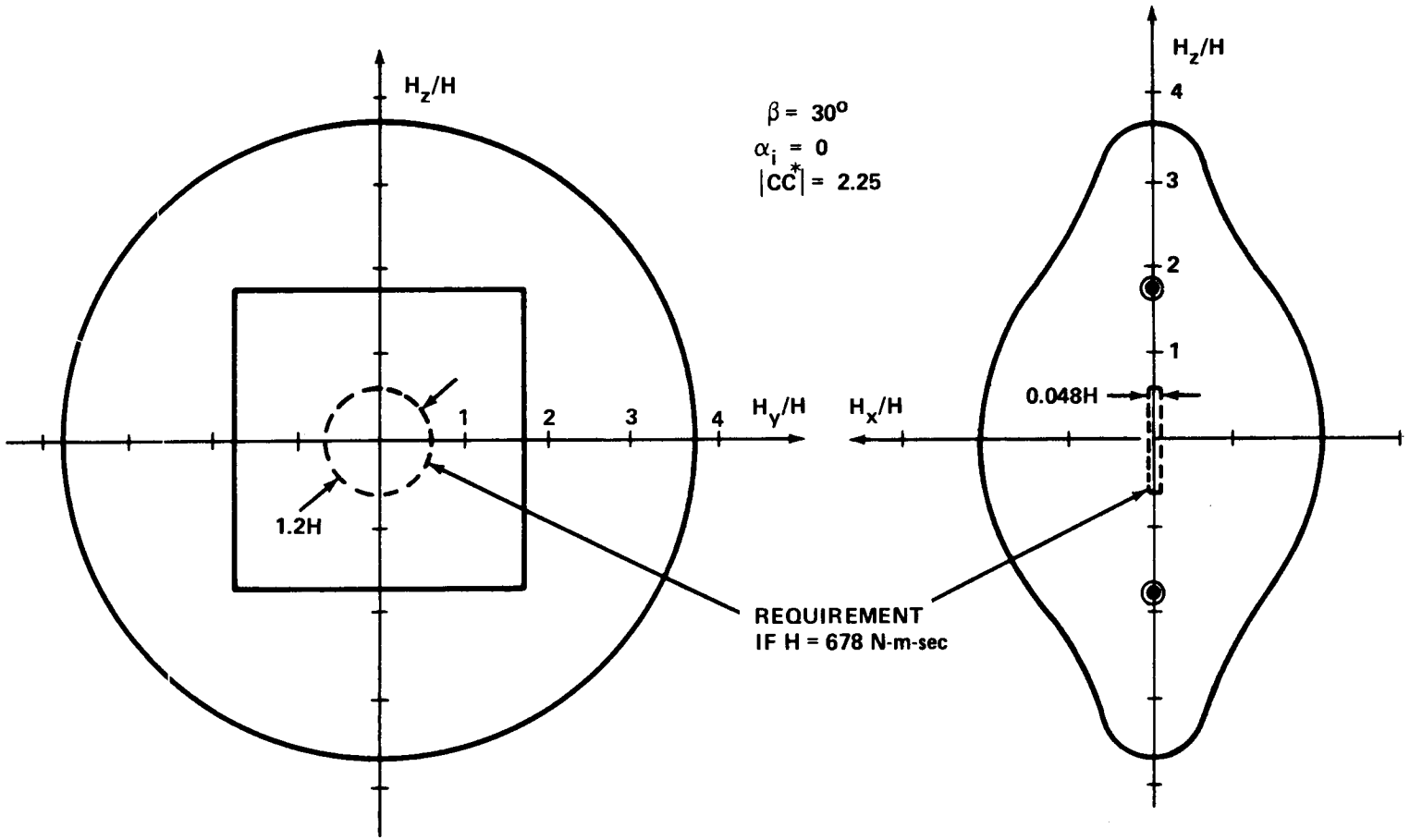

Figure VI-23. Four skewed CMG ghu surfaces in momentum space for the initial gimbal set (0, 0, 0, 0).

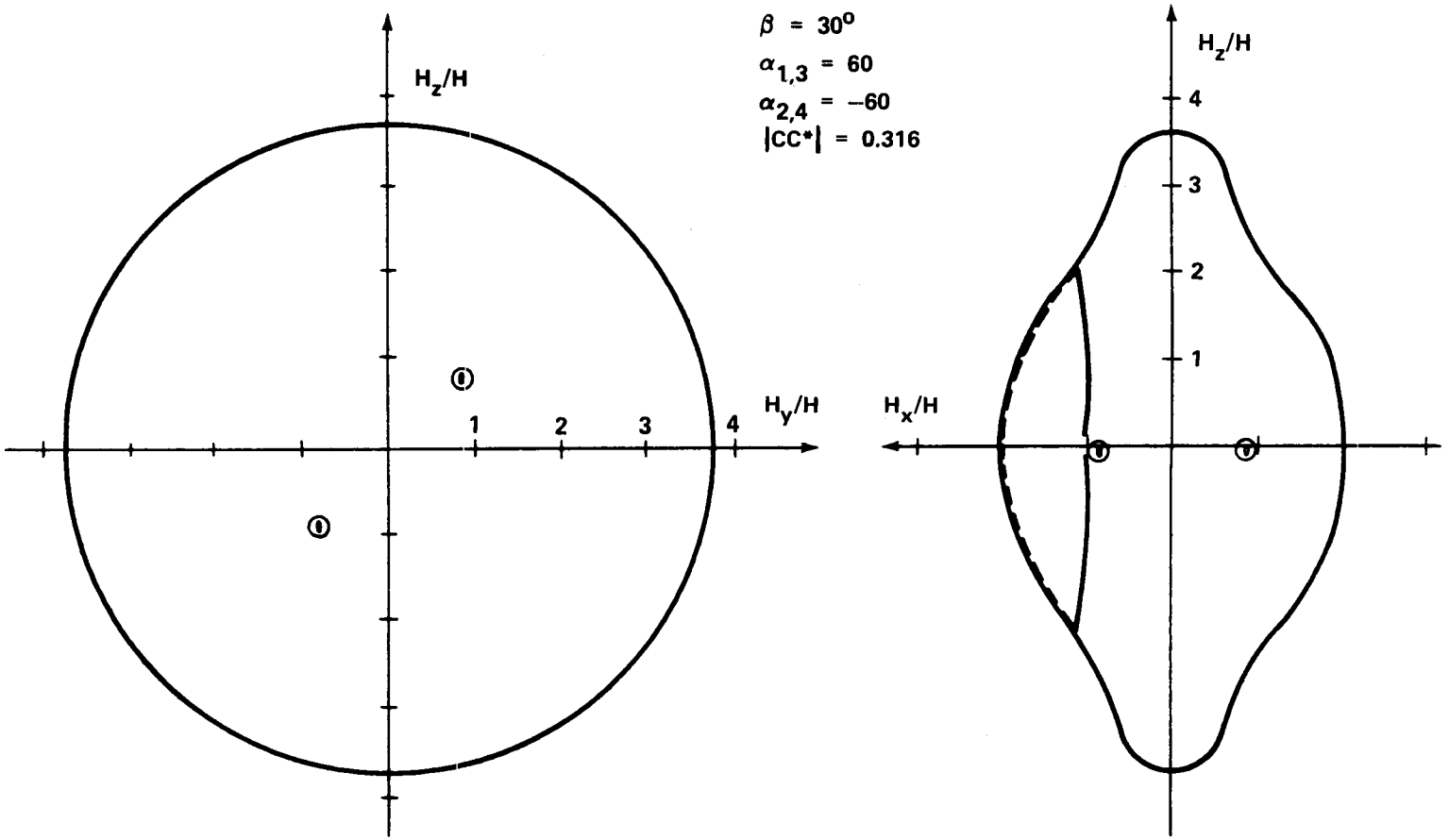

Figure VI-24. Four skewed CMG ghu surfaces in momentum space for the initial gimbal set (60, -60, 60, -60).

other four to negative values. The total momentum space can be spanned using only the four initial gimbal sets corresponding to a positive determinant. With one CMG deactivated, the steering law can be obtained as an exact solution of the equation $\tilde{T}_c = C\,\dot{\tilde{\alpha}}$; because C is a 3×3 matrix, the inverse of which exists if $|C| \neq 0$. If the initial gimbal set produces a positive determinant, obviously $|C|$ cannot go negative without penetrating a singularity surface. By selecting the proper initial gimbal set out of four possibilities, the CMG momentum state can vary from zero to saturation along any selected line without encountering a singularity. This initialization makes possible the use of the entire momentum solid for control purposes. As shown in Figure VI-25, however, enough singularity free momentum space exists about the origin to meet LST requirements without gimbal angle initialization. With CMG number 4 deenergized, the initial gimbal set $\alpha_1 = -35.27$ degrees, $\alpha_2 = 0$ degrees and $\alpha_3 = 35.27$ degrees has been selected to produce the zero momentum state. The disk shaped LST momentum requirement has been superimposed on Figure VI-25 assuming that H = 678 N-m-sec (500 ft-lb-sec) per CMG.

Since either three or four operational CMGs can meet all LST requirements, only three CMGs could be active with the fourth on standby in case of a failure, especially if it would increase overall reliability or lifetime of the CMG system. As long as the required singularity free momentum space is available, there is no difference in LST pointing performance using either three or four CMGs. As indicated by the momentum envelopes as compared with the actual LST requirement, using 678 N-m-sec (500 ft-lb-sec) CMGs produces a much oversized system. A CMG system with only half as much momentum per CMG would be more than adequate for LST.

e. SGCMG Shock Mount Dynamics Study. Torques and forces generated internally by control moment gyros as a result of rotor imbalance and bearing characteristics are transmitted to the LST structure and are a potential source of pointing error. Shock mounts to isolate the CMGs from the structure are considered to be a solution to the problem; however, the dynamics of a shock-mounted CMG can also create problems. A study was made to analyze the performance of shock-mounted CMGs in terms of pointing stability of the LST.

The dynamics analysis study was conducted in the following basic parts:

1. A model was developed for two-axis control using one shock-mounted SGCMG per axis.

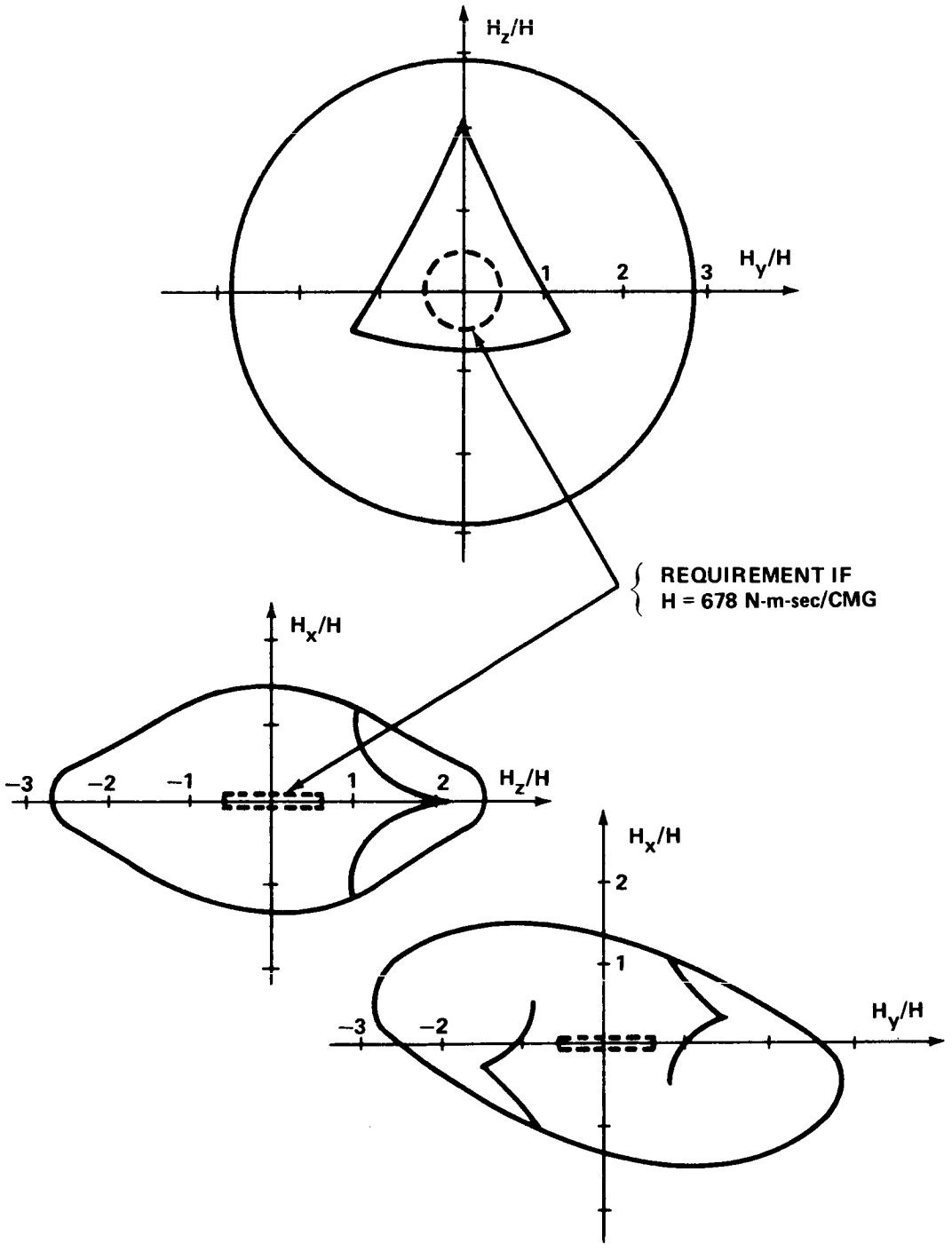

Figure VI-25. Three CMG ghu surfaces for the gimbal set (-35.27, 0, 37.27), CMG no. 4 out.

2. Transfer functions were developed for the model and frequency versus amplitude plots were constructed.

3. Torque disturbances were applied to the transfer functions and the outputs were applied to a simplified structural model to obtain pointing errors.

Figure VI-26 is the model used to develop the transfer functions. CMG A and CMG B are identical except the orientations are such that CMG A controls the Z-axis and CMG B controls the Y-axis. The spring-represented shock mounts for both rotational and translational isolation contain both spring constant and damping. $\Delta\dot{\theta}_1$, $\Delta\dot{\theta}_2$, and $\Delta\dot{\theta}_3$ represent input rates to the shock-mount system about the X-, Y-, and Z-axis, respectively.

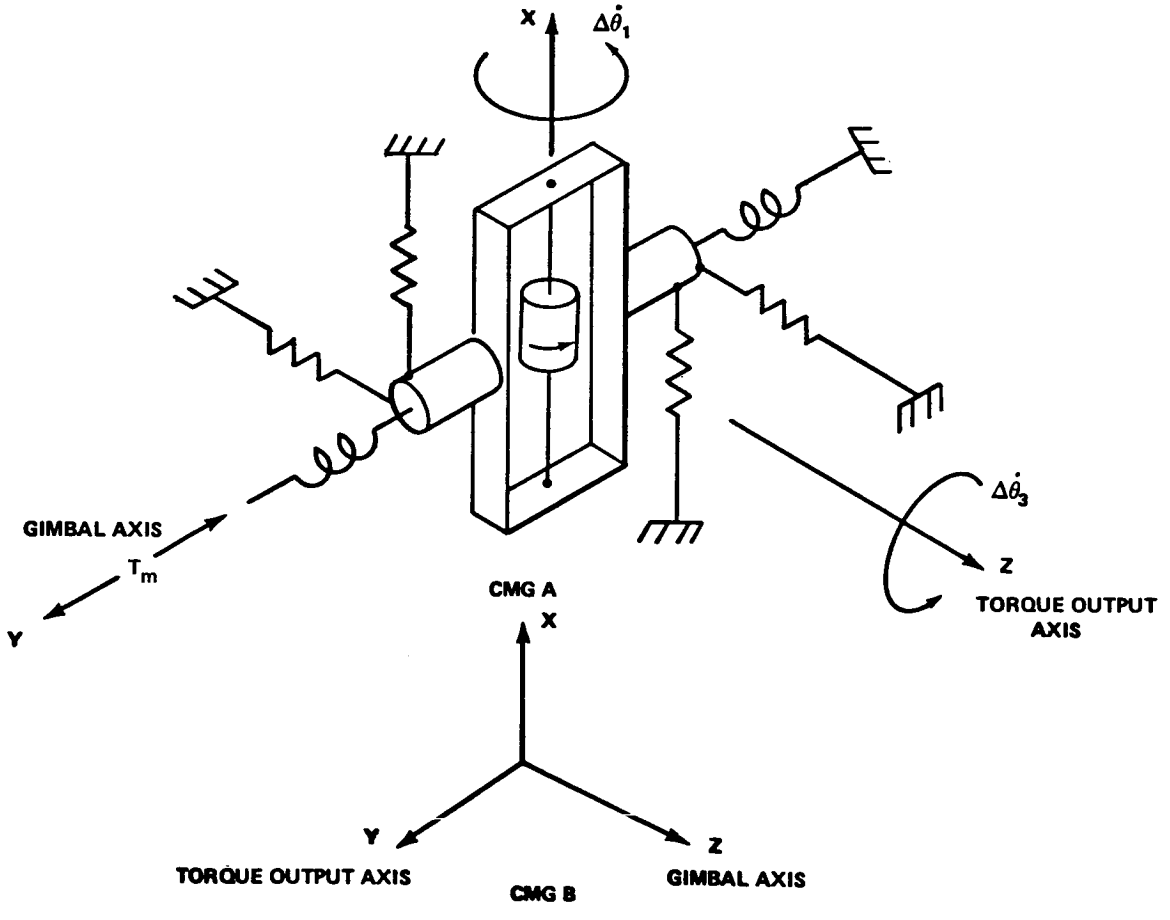

Figure VI-26. SGCMG shock mount, two-axis dynamics analysis study.

Figure VI-27 is the simplified two-axis block diagram obtained from the model. Cross coupling loops, as well as direct coupled torque loops, are included. The terms are defined as follows:

h	angular momentum for CMG A and CMG B.
$\dot{\theta}_{2b}$, $\dot{\theta}_{3b}$	shock mount rates for CMG B about Y- and Z-axis, respectively.
$\dot{\theta}_{2a}$, $\dot{\theta}_{3a}$	shock mount rates for CMG A about Y- and Z-axis, respectively.
T_{vya}, T_{vza}	vehicle torques about Y- and Z-axis due to CMG A.
T_{vyb}, T_{vzb}	vehicle torques about Y- and Z-axis due to CMG B.
T_{yb}, T_{zb}	disturbance torques to CMG B about Y- and Z-axis.
T_{ya}, T_{za}	disturbance torques to CMG A about Y- and Z-axis.
ω_y, ω_z	vehicle rates about Y- and Z-axis.
θ_y, θ_z	vehicle angular displacement about Y- and Z-axis.

Figure VI-28 provides frequency response plots of the various direct coupled transfer functions as a function of the CMGs angular momentum. The shock mounts are 20 hertz mounts with damping factor equal to 0.1 of critical. An ideal gimbal servoloop ($\dot{\alpha} = \dot{\alpha}_c$) was considered. The significant points of the direct coupled case are:

1. Shock mount characteristics are provided by the H = 0 curve.

2. H not equal to zero — Attenuation occurs at the shock mount frequency but high and low frequency peaks appear.

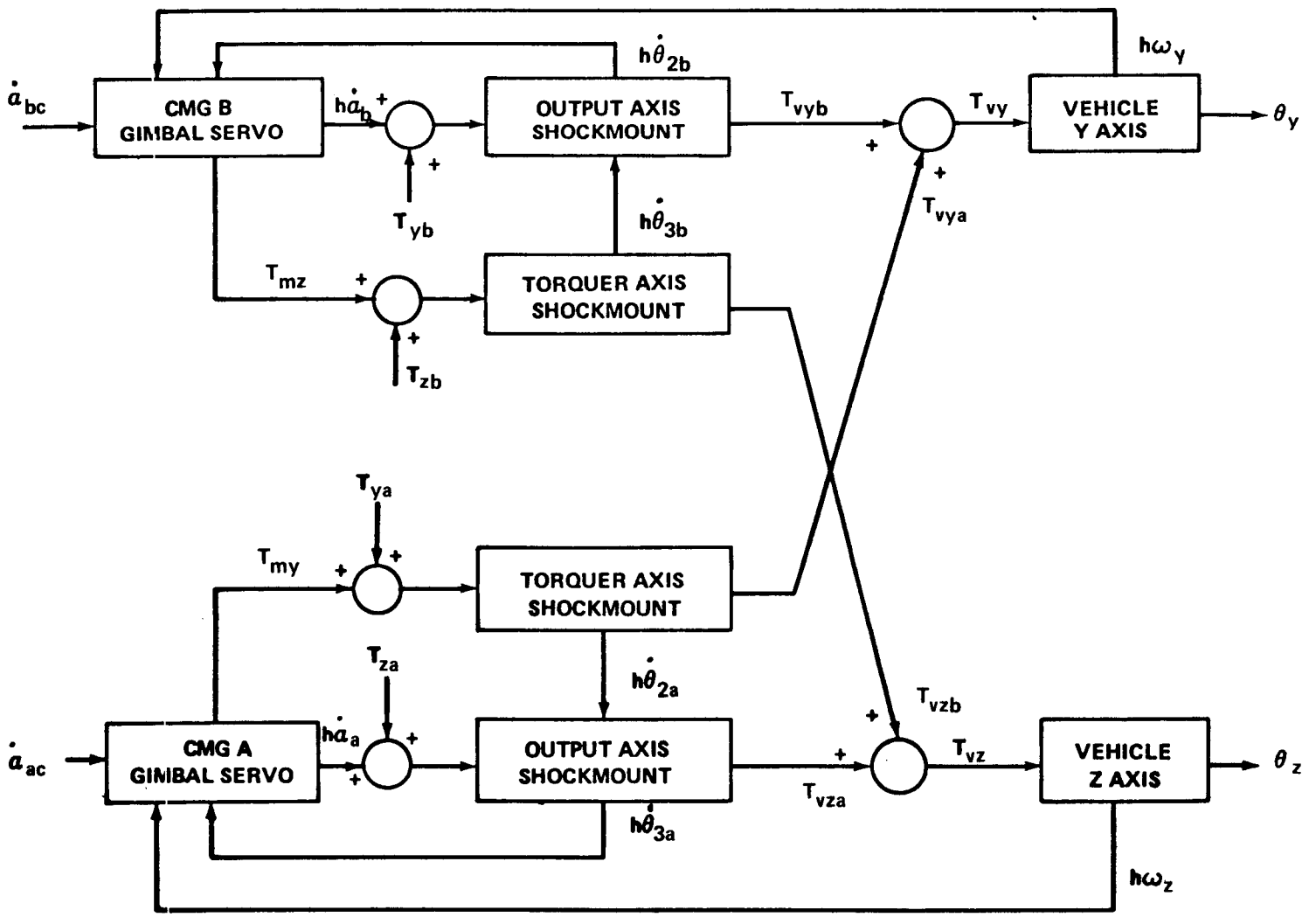

Figure VI-27. Two-axis block diagram for SGCMG shock mount dynamics study.

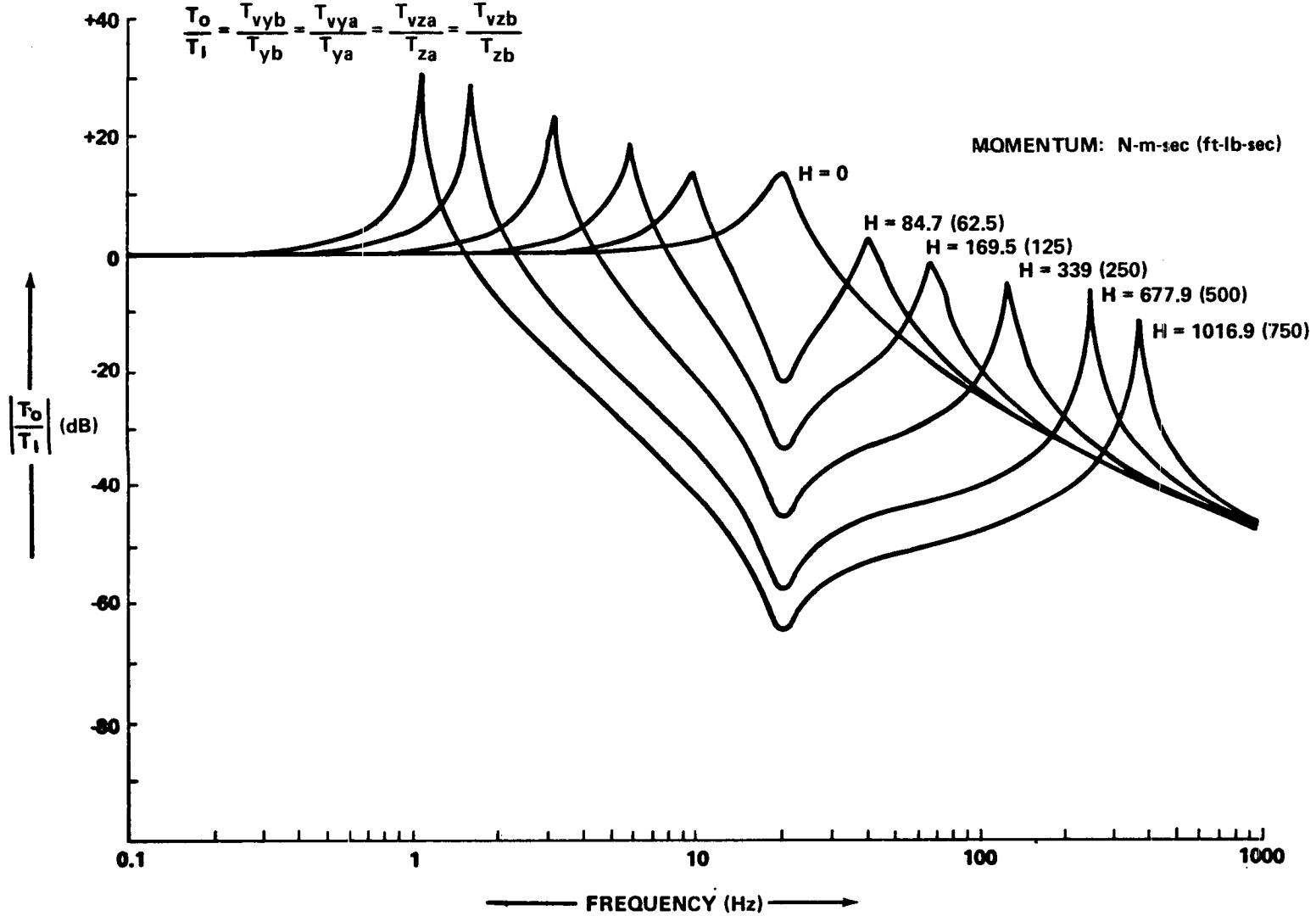

Figure VI-28. Shock mount frequency characteristics versus momentum (direct coupled case).

3. H increasing — The peaks become more pronounced and are spaced farther apart on the frequency scale.

4. Attentuation increases at the mount frequency with increasing H, but the peaks grow.

Figure VI-29 provides frequency response plots of the various cross coupled transfer functions as a function of angular momentum. The peaking attributed to the shock mount is noticeable at low H values and, as H increases to a practical operating point, the two peaks appear as in the direct coupled case. Very little attenuation occurs at the shock mount frequency.

The condition, in both cases, of high frequency peaks occurring approximately at the fundamental rotor frequency is undesirable since torques at these frequencies and their harmonics need isolation from the structure. The low frequency peaks are near the solar wing modes and it must be determined whether disturbances at these frequencies are generated by the CMG.

The final step in the study was to insert the CMG disturbances into the LST structure and determine the pointing errors resulting as seen by the optical system. The following steps were used to determine the error:

1. The structural frequency modes were determined using the structural model described in Chapter II of this volume.

2. The displacements at each structural node for torque or force inputs at the CMG node were obtained as a displacement per unit torque or force.

3. The pointing error sensitivities with respect to displacements were computed from the LST/OTA optical model.

4. The pointing error per unit torque or force input was obtained by combining the structural response data and the optical sensitivities.

5. An empirical CMG forcing function containing disturbances at the fundamental and four harmonic frequencies was selected and wheel speeds were selected to match disturbance frequencies to structural vibration frequencies.

6. The CMG forcing function was applied directly to the structure (no shock mounts) at the CMG location and the pointing error was determined for both force and moment inputs for the selected wheel speeds.

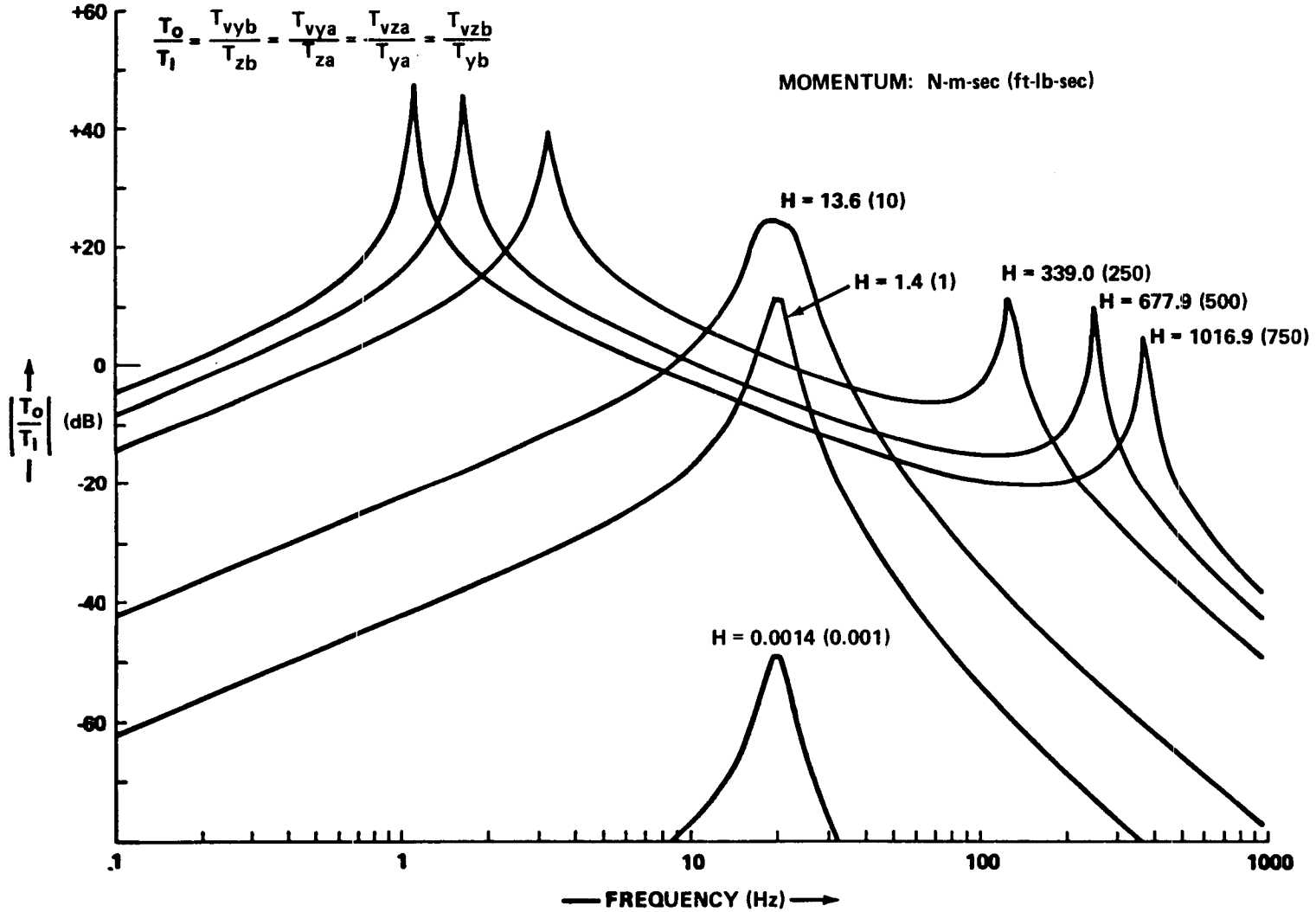

Figure VI-29. Shock mount frequency characteristics versus momentum (cross coupled case).

7. The total pointing error was determined as a root-sum-square value obtained from the resultant force and moment errors.

8. The shock mount transfer functions for the direct and cross coupled cases were separately inserted between the CMG forcing functions and the structure, and pointing errors obtained.

9. A total RSS pointing error for each wheel speed was determined by combining the errors for force and moment disturbances.

Figure VI-30 is a plot of the RSS errors obtained for force and moment disturbance as a function of rotor frequency or speed. Curves are given for both the no-shock-mount case and for the case using 20 Hz, 0.1 damping factor shock mounts. Table VI-10 summarizes the frequencies used and the resultant pointing errors.

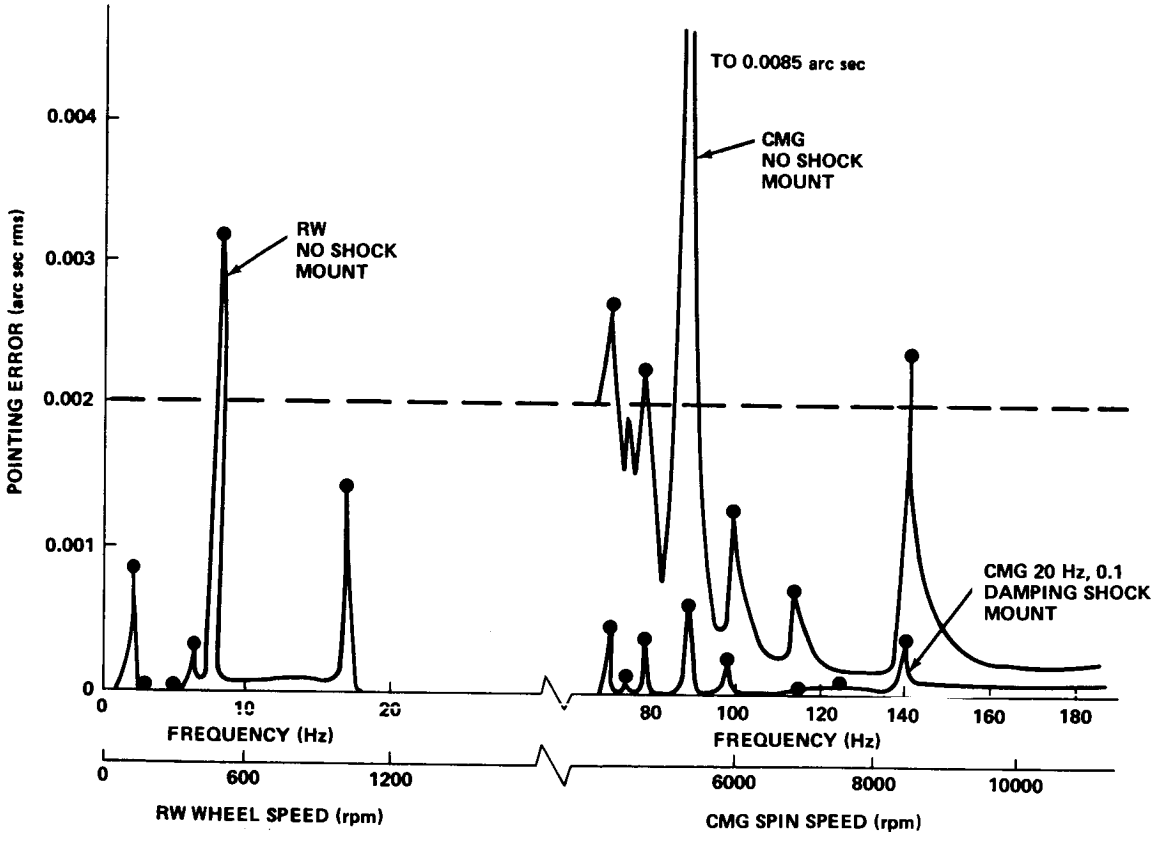

Figure VI-30. CMG and reaction wheel (RW) vibration effects.

TABLE VI-10. PEAK POINTING ERROR FOR APPLIED FORCE AND MOMENT CMG DISTURBANCE INPUTS

Wheel Speed (rpm)	RSS Error With Shock Mounts (arc sec)	RSS Error Without Shock Mounts (arc sec)
8460	4.1×10^{-4}	2.3×10^{-3}
6840	5.2×10^{-5}	7.1×10^{-4}
5850	5.3×10^{-4}	1.3×10^{-3}
5300	6.3×10^{-4}	8.5×10^{-3}
4740	3.9×10^{-4}	2.3×10^{-3}
4410	1.4×10^{-4}	1.9×10^{-3}
4270	4.7×10^{-4}	2.7×10^{-3}

The following conclusions may be obtained from the analysis with the simplified structure model:

1. CMGs without shock mounts are a major source of pointing error and, to be acceptable for LST, a speed must be carefully selected to avoid structural resonances.

2. Shock mounts reduce the pointing errors to nearly acceptable values at any wheel speed; however, selection of wheel speed can reduce errors to insignificant values.

3. Further analysis using more sophisticated structure models and CMG torque and force signatures is required.

4. Pointing errors for a non-shock-mounted RW are given in Figure VI-30. These errors can be reduced with shock mounts but, since the RW controls by varying rotor speed, the selection of speed cannot be used to further reduce pointing errors.

4. Magnetic Torquer System (MTS)

a. Magnetic Torque. Control moment gyros require periodic dumping of momentum to prevent saturation. If a torque source such as reaction jets are used for desaturation, a considerable amount of propellant

is required for long lifetime missions such as the LST. In addition, contaminants from some propellants can cause degradation of optical surfaces. For long lifetime missions, it seems only natural to consider the productive use of environmental forces such as the gravity gradient or earth's magnetic field. Previous studies for the Skylab program show that g.g. can be utilized to dump CMG momentum. However, during dump, the spacecraft's pointing requirements must be ignored and the vehicle maneuvered in a specific sequence such that g.g. counteracts the accumulated momentum. Under unfavorable conditions, g.g. dump could consume a considerable portion (half or more) of the available time. For the LST, experiment viewing time takes priority and precludes the use of g.g. dump, except as a backup measure.

Currently, the earth's magnetic field offers the greatest potential for utilizing the environment for LST control purposes, without sacrificing experiment viewing time by imposed maneuvers or orientation restrictions.

Basically, the advantage of using controlled interactions with ambient fields is that no propellant need be carried aboard the vehicle for CMG momentum dump, and lifetime is not limited by expendables. The use of the earth's magnetic field requires that electromagnets be installed on the spacecraft, along with a magnetometer to measure the strength and direction of the geomagnetic field, $\overline{B}$. From a prior knowledge of the physical characteristics of the electromagnets and the state of the CMG momentum, an appropriate amount of electric current is passed through the solenoid of each electromagnet to produce a dipole moment, $\overline{M}$. The magnetic moment generated by the electromagnets will then react with the geomagnetic field to produce a torque, $\overline{T}_m$, on the spacecraft. The CMGs then act to counteract this torque, resulting in momentum dump of the CMGs. The magnetic torque produced obeys the vector cross product

$$\overline{T}_m = \overline{M} \times \overline{B} \quad .$$

It is apparent that the torque produced is perpendicular to both the dipole moment and the earth's field. Although limited in magnitude by the electromagnet size, the direction of the dipole can be produced in any direction. At any instant of time, the magnitude and direction of the earth's field depends on the spacecraft's orbital position relative to the surface of the

earth. The vector components of $\overline{B}$ would be obtained by onboard magnetometers. The magnitude of $\overline{M}$ varies as a function of the currents being passed through the coils at any time. To maximize the torque produced by a given current, the dipole generated should be perpendicular to the earth's field. Moreover, it is apparent that a torque cannot be produced in the direction of $\overline{B}$.

At some instant of time, the desired torque may be aligned with $\overline{B}$, in which case it cannot be produced. However, these periods are relatively short because, as the orbital position of the LST changes, a corresponding change occurs in the direction of the earth's field. Over any time interval during an orbit, the CMGs produce the desired torque required for fine control, and the magnetic torque, if available, is used to dump the momentum accumulated in the CMGs. The magnetic system proposed for the LST provides a torque proportional to the stored momentum. As such, it is a secondary control torque and, if it cannot momentarily be produced, the vehicle performance is not degraded.

Typical values for the components of the earth's magnetic field are shown in Figure VI-31 as functions of the LST's longitude and latitude. The orbit starts at the morning terminator at the time of winter solstice with the north magnetic pole tilted toward the sun. The southward component is always negative since the field dipole is directed from south to north. As the earth rotates and the orbit regresses, the components change slowly with time and generally repeat themselves every 24 hours. The onboard magnetometer measures the field in LST body coordinates. Therefore, the measured values depend on the spacecraft's inertial orientation in space as well as the orbital parameters. The total magnitude varies from about 2.5×10^{-5} T (0.25 gauss) to 4×10^{-5} T (0.4 gauss), with an average of about 3×10^{-5} T (0.3 gauss). A spherical harmonic expansion was used to generate the field components shown in Figure VI-31 for the year 1980. Essentially, the $\overline{B}$ field generation with appropriate transformations to LST body coordinates performs the functions of the magnetometer for analysis and simulation of the LST.

b. Torquer Sizing. As a general sizing criterion, the electromagnets must produce enough torque to counteract the average g.g. plus an additional 10 percent to account for other disturbance torques such as aerodynamic and solar radiation. For the LST, the maximum g.g. torque is 0.141 N-m (0.104 ft-lb). The average g.g. torque plus 10 percent is about 0.0814 N-m (0.06 ft-lb). Using an average value of 3×10^{-5} T (0.3 gauss) for the geomagnetic field, the required magnetic dipole capacity per vehicle axis is

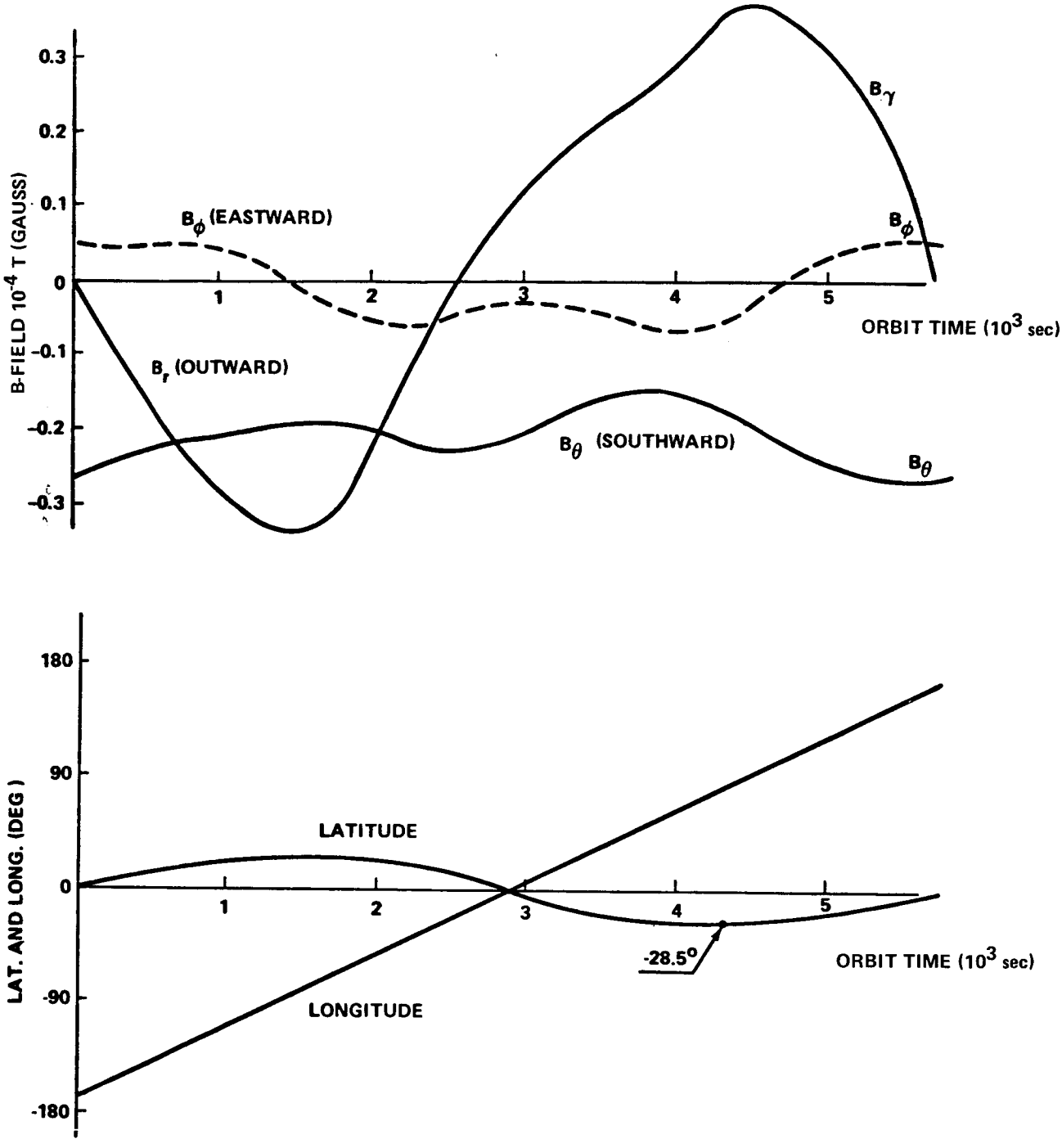

Figure VI-31. Components of the earth's magnetic field as functions of the LST longitude and latitude.

$$M = \frac{T\ (avg)}{B\ (avg)} = \frac{0.0814}{3 \times 10^{-5}} = 2712\ A - m^2 \left(0.2\ \frac{ft\text{-}lb}{gauss}\right).$$

For direct control, the MTS must produce a torque equal to or greater than that of g.g., in which case a dipole moment per axis of 4610 A-m^2 (0.34 ft-lb/gauss) is desirable. Because of the magnetic cross product law, torque on one axis is produced by the coils on the two transverse axes. For these reasons a value of 4000 A-m^2 (0.3 ft-lb/gauss) per vehicle axis was selected as a basis for designing the electromagnets for the LST. Digital simulations were used to verify the design value. With the field profile shown in Figure VI-31 projected in LST body axes, over 814 N-m-sec (600 ft-lb-sec) momentum can be dumped during one orbit's time using three orthogonally mounted electromagnets each limited to 4000 A-m^2. The maximum g.g. secular momentum for LST is only 410 N-m-sec (302 ft-lb-sec), hence the coils are oversized by a comfortable margin and permit an electromagnet failure without endangering the mission. In the event of CMG failures, the MTS can help provide direct control torque.

Instead of one electromagnet per vehicle axis, the design dipole value can be generated by two equivalent electromagnets per axis. The location of the MTS on the LST is shown in Figure VI-32. A total of six electromagnets, two per vehicle axis, are used on the LST spacecraft with the following advantages:

1. Each is physically smaller, making mounting easier.

2. Each can be driven by a separate electrical channel, providing greater redundancy.

3. The length to diameter ratio is greater which reduces the demagnetization factor, thus increasing efficiency.

As illustrated, there are two straight electromagnets aligned with the X-axis and four curved electromagnets. Two of the curved torquers are aligned such that their magnetic moment lies along the Y-axis, and the other two aligned for a Z-axis dipole. The curved electromagnets have the same curvature as the OTA and each is electrically equivalent to a straight electromagnet. Although alternate mounting locations were examined such as on the light shield or the SSM, each case posed problems. The light shield is not thick enough for the torquers to be embedded in the structure, and complicated rollout cabling is required when the light shield is extended. The

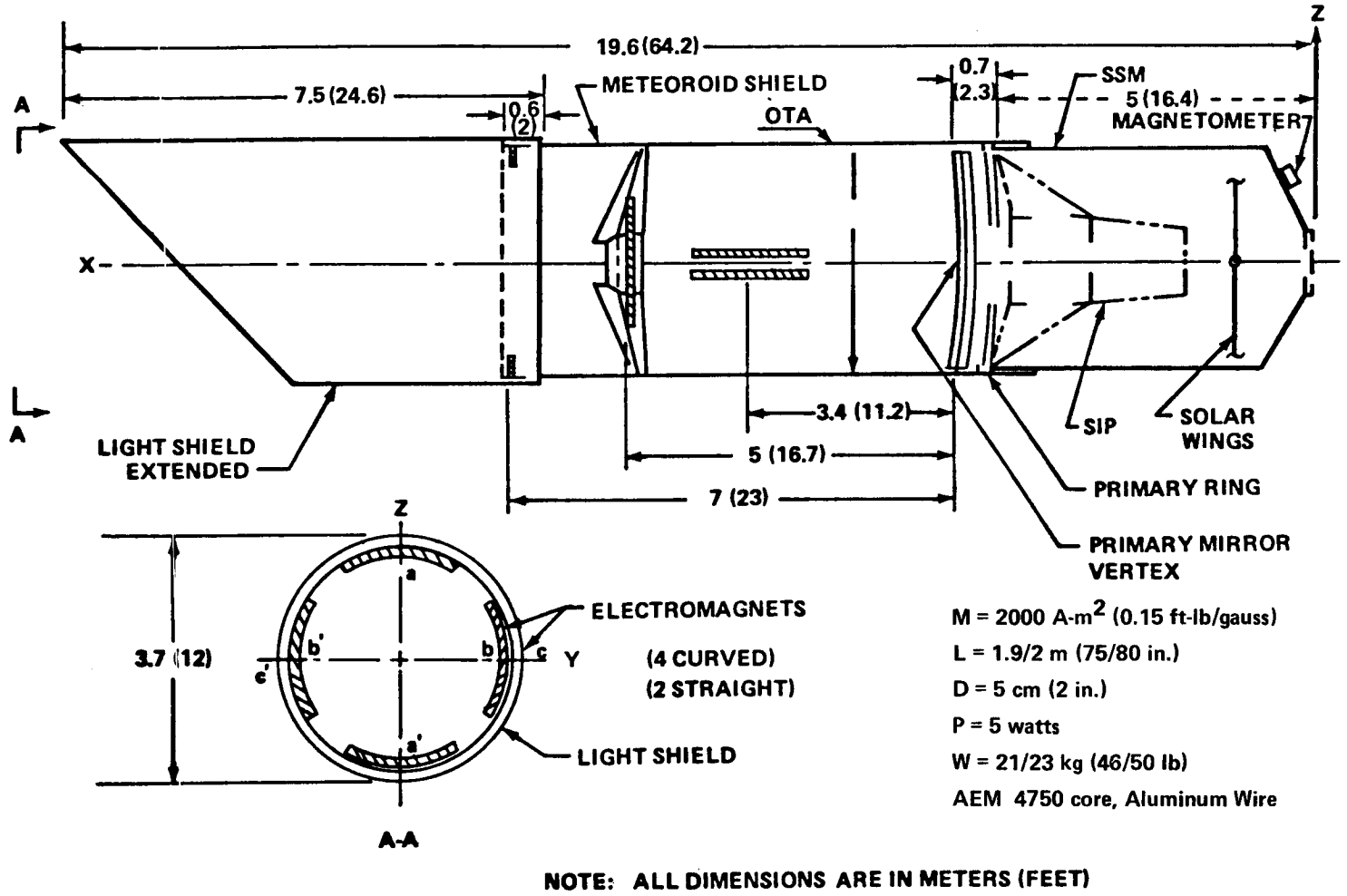

Figure VI-32. Design reference location and orientation of electromagnets for LST.

SSM mounted torquers produced a magnetic field about 10 times that of the earth's field in the SIP area where magnetically sensitive instruments are located. The OTA mounting arrangement is a compromise between the two alternates. The various design data for the electromagnets are listed in Table VI-11. To produce the same dipole as an equivalent straight electromagnet, a curved electromagnet is 13 cm (5 in.) longer and weighs 1.8 kg (4 lbm) more. Each electromagnet solenoid is made of aluminum wire and is designed for a maximum power of 5 watts. Thus, the total maximum power for the 6 electromagnets is 30 watts. However, the total average power usage is expected to be about 10 watts.

TABLE VI-11. ELECTROMAGNET DESIGN DATA
(ONE ELECTROMAGNET)

Maximum Magnetic Moment Required	2000 A-m^2 (0.15 ft-lb/gauss)
Curved Weight	22.7 kg (50 lb)
Straight Weight	20.9 kg (46 lb)
Curved Length	203 cm (80 in.)
Straight Length	191 cm (75 in.)
Radius of Curvature	183 cm (72 in.)
Diameter	4.19 cm (1.65 in.)
Core Diameter	3.73 cm (1.47 in.)
Maximum Power	5 W
Material of Core	AEM-4750
Material of Solenoid Wire	Aluminum
B-H Design Data Flux-Density	1.2 T (12 000 gauss)
Field Density	1592 A/m (20 oersted)
Total Weight[a]	141 kg (310 lb)
Total Max Power	30 W
Total Average Power[b]	10 W

a. The total weight includes 8 kg (18 lb) contingency for mounting hardware, etc.

b. The efficiency of power usage has not been determined. Note that 15 W is assumed in Table VI-2, page VI-14.

AEM-4750 core material was selected because of its low hysteresis and coercive force characteristics. Other materials, such as permendur, have a higher maximum flux density than AEM-4750 but due to large hysteresis it would be much harder to control the dipole moment. The solenoid through which current is passed is wound around the core material. As an alternate, solenoids, without core material (open coils) were considered, but a comparison of weight, power, dimensions, and mounting arrangement shows that open coils weigh more for the same amount of power than coils with cores. Moreover, open coils would have to be looped around the outer perimeter of the LST, thus, complicating the mounting and producing high magnetic fields inside the LST. Another alternate considered was variable permanent magnets (VPMs) instead of electromagnets. VPMs consist of a core of permanent magnetic material surrounded by a magnetizing coil which is activated only when the magnetic state of the core is to be changed. Once the desired magnetic moment is achieved, the current can be turned off without affecting the magnetic state of the VPM. Thus, the average power consumption for relatively long periods of steady-state operation would be negligible, but high power is required for short durations to change the magnetic state. Moreover, additional sensors must be installed on each VPM to determine its magnetic state. Although a VPM system weighs less than the electromagnets baselined for LST, its operation is more complex. Operation of the VPMs would be commanded from the ground based on predictions of the average expected g.g. torque and the earth's magnetic field. Since average instead of actual values are used there will be a significant residual momentum after every orbit. The CMGs will eventually saturate, requiring some sort of maneuvering for backup g.g. desaturation. Thus, VPMs are not recommended for LST.

c. Magnetometer. The type of magnetometer manufactured by Dalmo-Victor that was used on the OAO spacecraft can be used on the LST spacecraft. This magnetometer measures the goemagnetic field along each of the spacecraft axes and converts this to a dc voltage. The magnetometer weighs 3 kg (6.5 lbm) and requires a power of 2 watts.

The magnetometer should be located on the spacecraft where the geomagnetic field is practically undistorted due to the field of the electromagnets and induced magnetic moments. The farthest the magnetometer can be placed from the electromagnets is at the subsystem end of the spacecraft where the magnetic field due to the 6 electromagnets is about 1×10^{-6} T

(0.01 gauss). This field is about 3 percent of the average geomagnetic field of 3×10^{-5} T (0.3 gauss) and should cause no significant errors in the magnetometer measurements. However, if more accuracy is desired, the magnetometer could be operated in discrete time intervals. The geomagnetic field changes very slowly as the spacecraft orbits (two cycles per orbit) and, therefore, it can be treated essentially as constant over small intervals of time, say of the range of 1 min. Thus, the geomagnetic field can be accurately measured at discrete intervals by switching off the electromagnets for short durations of time (about 5 sec).

In the event the three-axis magnetometers used onboard the spacecraft fail, the following two schemes could be used to provide signals for changing the magnetic state of the electromagnets. In the first scheme, the magnetic moment for each electromagnet is changed whenever the geomagnetic field components in the spacecraft axes change directions. Ground computation can be made to determine the geomagnetic field components along the spacecraft axes from a known model of the geomagnetic field and the position and orientation of the spacecraft. From this information, the magnetic moment required for each electromagnet over a certain averaging period can be computed. The averaging period is equal to the time between the direction changes of the geomagnetic field components in the spacecraft axes. Generally this period is equal to about a quarter of an orbit. Necessary ground commands will be sent to the spacecraft such that in each quarter orbit the magnetic state of the electromagnets is changed. The frequency of these commands can be reduced from four times per orbit to once in two or three orbits depending upon the accuracy of the model used to represent the actual geomagnetic field. It is possible to compute and store in the onboard computer the changes required for the next two or three orbits.

In the second scheme, a known geomagnetic field model is programmed onboard the spacecraft. This geomagnetic field model is used in the event of a magnetometer failure. A fairly accurate and easily programmed model is a tilted dipole model for the geomagnetic field. This model would require frequent updating through ground commands. In addition, it would require information on spacecraft inertial orientation and spacecraft orbital parameters.

The advantages of the second scheme over the first is that it is continuous and all the computations are performed onboard the spacecraft. The disadvantage is that it will require computer storage area for the geomagnetic field model. The number of ground commands required for either scheme is expected to be nearly the same. The first scheme is preferred over the second because of its low storage capacity requirements.

d. Dipole Control Law. The mathematical logic and mixing of information required to compute the desirable dipole moment of each electromagnet is denoted as the dipole control law. The dipole moment is directly proportional to the current being passed through the solenoids at any time. Since the MTS must produce a torque proportional to the CMG momentum, $\bar{H}$, but opposite in direction for momentum dump and a torque in the same direction as the commanded torque, $\bar{T}_c$, for direct control, the magnetic torque equation, $\bar{T}_m$, is set equal to

$$\bar{T}_m = K_c \bar{T}_c - K_d \bar{H} = \bar{M} \times \bar{B}$$

where K_c and K_d are proportionality constants that must be selected for proper operation. Taking the vector cross product of $\bar{B}$ on the left with both sides and assuming $\bar{M} \cdot \bar{B} = 0$ produces the following dipole control law:

$$\bar{M} = [K_c (\bar{B} \times \bar{T}_c) - K_d (\bar{B} \times \bar{H})]/B^2 \quad .$$

The vector form can be expanded to obtain the dipole component per vehicle axis. Since each axis has two equal electromagnets, the dipole command per axis is prorated equally between two solenoids. The dipole moment commanded can be related to current and voltage that must be applied to the coils of each electromagnet.

The actual dipole moment generated is limited by the physical properties of the electromagnets such as the maximum available current, number of turns in the coils, and the shape and volume of the core material. For design purposes, a maximum of 10 watts per vehicle axis has been assumed which for the LST MTS corresponds to a limit of 4000 A-m^2 (0.3 ft-lb/gauss) per vehicle axis. During simulation of the LST MTS, the dipole moment of each axis was hard-limited to the electromagnet design value. Many runs were made varying the gains K_c and K_d to determine their proper values.

Total LST control system performance was relatively unchanged when K_c was varied, either with or without magnetic dump. Apparently, the response time of the CMGs is so fast relative to the magnetic control loop that the CMGs produce most of the commanded torque. During a

CMG failure, however, and during the momentum redistribution after a CMG has been deenergized, the direct magnetic control loop prevents excessive vehicle pointing errors and quickly helps drive the CMGs to a new operational null. Direct magnetic control also permits pointing control in the event two CMGs have failed. An appropriate value for K_c is unity.

In contrast, LST pointing performance changed drastically as the desaturation gain K_d was varied. The results also depend upon the commanded torque and the control system bandwidth as well as the value of K_d. For moderate pointing requirements such as 1 arc min, integral control is not required. In this case magnetic momentum dump of the CMGs improved both pointing performance and stability characteristics of the spacecraft. A linear analysis indicated that the MTS introduces the integral of the commanded torque through the CMG-magnetic control loop. As the pointing requirements approach that of LST (1 arc sec), the control system bandwidth must be increased. For this case, the MTS can introduce a disturbance that adds to the total pointing error. The LST pointing error as a function of the MTS desaturation gain K_d is shown in Figure VI-33. A value of $K_d = 0.1$ results in a possible pointing error of 0.8 arc sec or less and is an appropriate value to use for a body pointing requirement of 1 arc sec. However, if fine body pointing down to 0.0025 arc sec is required for the LST (either in lieu of, or as a backup to the secondary mirror control system), then integral control must be added to the commanded torque. To prevent the MTS from causing pointing errors, the value of K_d must be reduced to about 0.005. Since the maximum dipole moments are limited, lowering the value of K_d makes the electromagnets operate in a linear mode most of the time. As K_d is increased, the coils act in a bang-bang type mode each time the earth's field components change sign. Thus, for proper operation, K_d must be large enough to cause the CMG momentum to be dumped but small enough to prevent attitude pointing errors.

e. Magnetic Field Propagation. Figures VI-34 and VI-35 show the magnetic field strength distribution inside the LST caused by all six electromagnets. The X, Y, and Z parameters used in these plots are the Cartesian coordinates previously shown in Figure VI-32. In generating these plots, it is assumed that all 6 electromagnets are operating and generating their maximum magnetic moment of 2000 $A\text{-}m^2$. The direction of each electromagnet is parallel to the positive direction of the respective axes to which

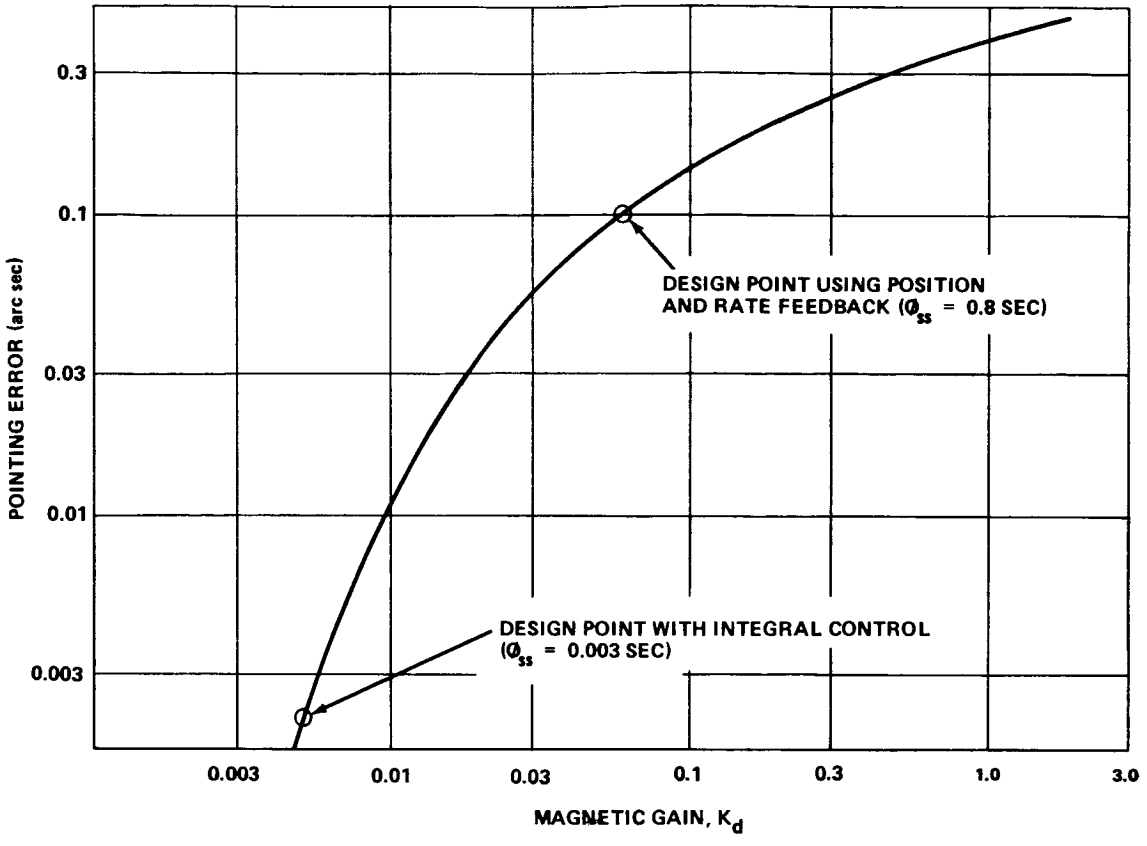

Figure VI-33. Errors due to magnetic dump of the CMGs.

they are aligned (Fig. VI-32). The curved electromagnets have been replaced by equivalent straight electromagnets in generating the field propagation data: 1.9 m (75 in.) in length with a dipole moment of 2000 A-m^2. At any specified point on the vehicle, the magnetic field is a vector whose components are composed of the vector addition of the propagated field vector of each electromagnet at that point. The field strength magnitude at each specified point is calculated using the normal vector magnitude.

Figure VI-34 shows the field strength along two lines parallel with the X-axis in the X-Y plane. The field strength is slightly higher in the X-Y plane in the SSM section than in the X-Z plane because of the presence of the two electromagnets aligned parallel to the X-axis in the X-Y plane. Although the field was calculated over the total LST volume at points located on the corners of a 15.2 cm (6 in.) square lattice, only the X-Y plane field is illustrated. The field is plotted along the lines [Y = 0, Z = 0 and Y = 1.22 m (4 ft), Z = 0] with distance along the X-axis as a variable. In the

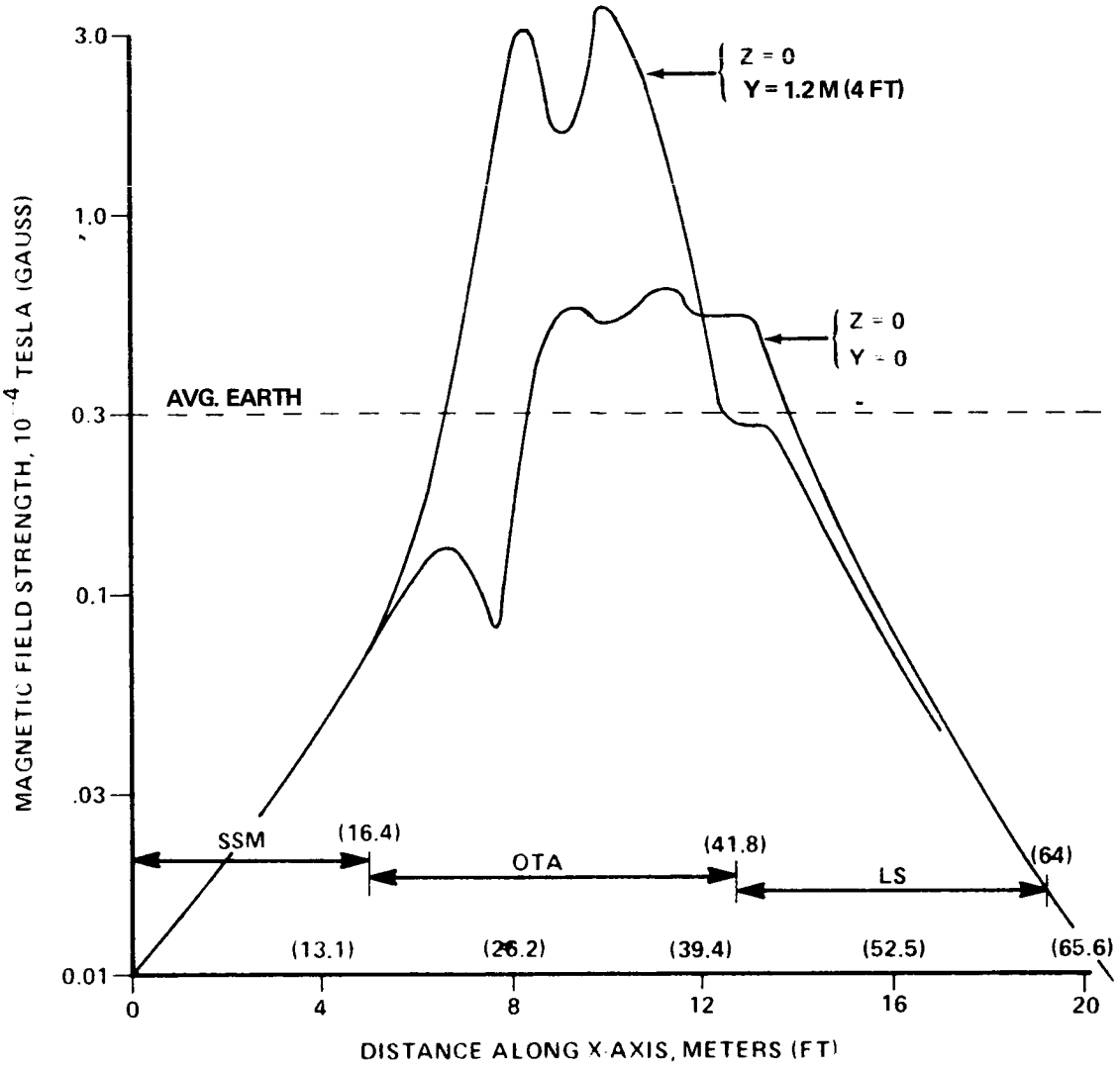

Figure VI-34. Magnetic field with 6 electromagnets on OTA, Z = 0.

SSM area, the field is less than 1×10^{-5} T (0.1 gauss) and at the aft end about 1×10^{-6} T (0.01 gauss), which is much less than the earth's average field of 3×10^{-5} T (0.3 gauss). In the center of the OTA near the electromagnets, the field is about equal to that of the geomagnetic field. As an electromagnet is approached, the field becomes much higher. Within 0.3 m of an electromagnet the field is about 4×10^{-4} T (4 gauss) and inside an electromagnet is is 1.2 T (12 000 gauss). Near the ends of an electromagnet the field is much higher than near the sides at the same distance.

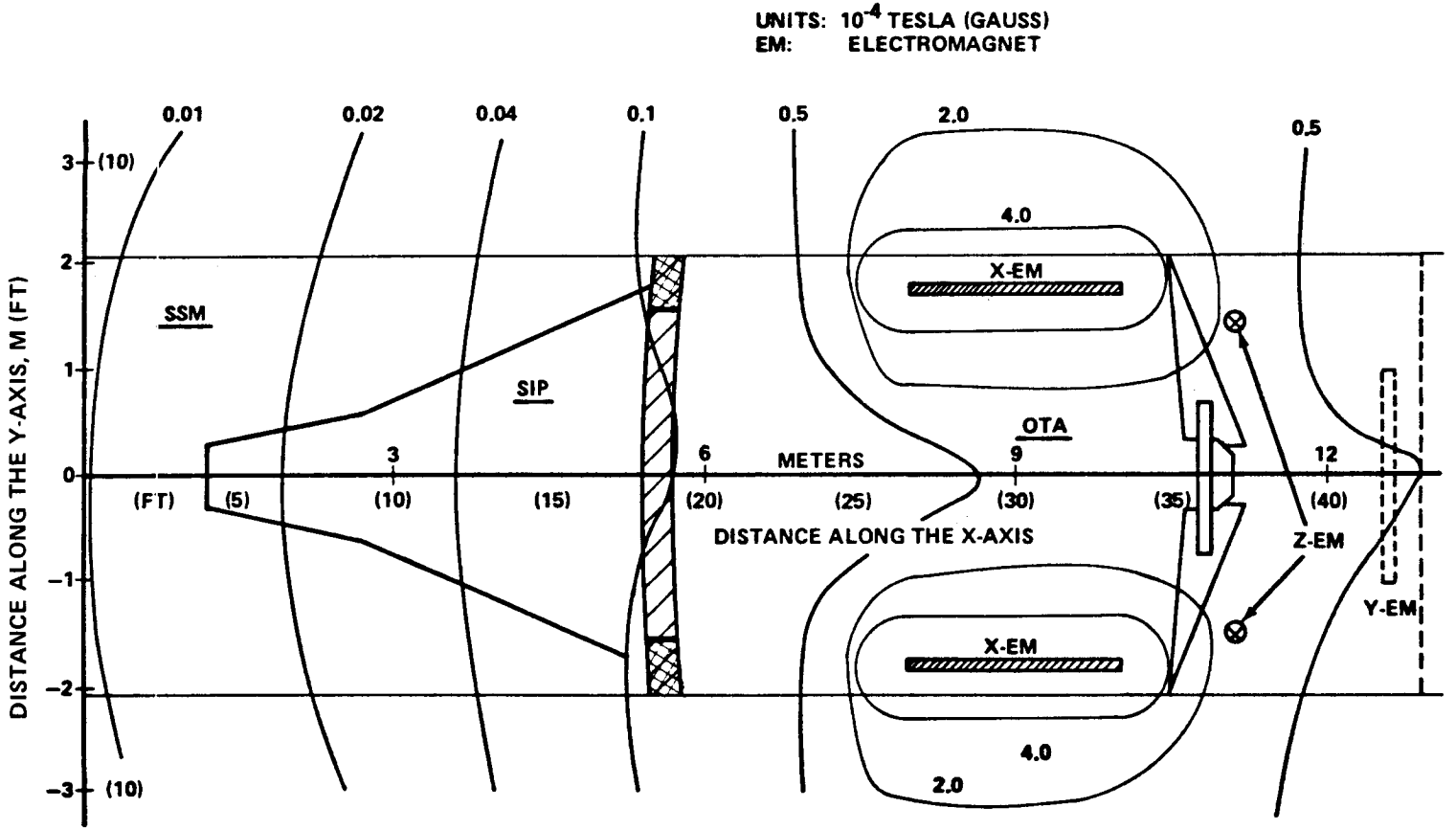

Figure VI-35. X-Y plane isomagnetic field distribution.

Figure VI-35 shows an isomagnetic plot of lines of equal field strength in the X-Y plane superimposed on a rough sketch of the LST. The electromagnet locations are illustrated relative to the SSM, SIP, and OTA. However, the Y electromagnet is not in the X-Y plane, consequently no isomagnetic lines surround it. Also the Z-electromagnet is perpendicular to the plane, thus, contributing very little in the plane. Since the field aft of the primary mirror is much less than the earth's ambient field, no additional shielding (other than that required for the geomagnetic field) will be required for magnetically sensitive components located in the SIP and SSM areas.

As previously stated, the magnetometer should be located as far from the electromagnets as possible so that a true measure of the earth's field can be obtained without errors. On the aft end of the SSM, the field is less than 1×10^{-6} T (0.01 gauss), or about 3 percent of the earth's field. This small value should cause no significant errors in the magnetometer readings and the MTS can be used continuously, without stopping to measure the geomagnetic field periodically.

If, as an alternate mounting arrangement, the electromagnets are located on the outer perimeter of the SSM, the field inside the SSM and SIP will be about 10 times that of the earth's ambient field. Additional shielding for magnetically sensitive components will impose a small weight penalty. For continuous MTS operation, the magnetometer should ideally be located on the light shade or the end of the OTA. But, if the magnetometer is also located on the SSM, then the MTS would be operated in the off-on type mode previously described: The electromagnets are turned off for a short period while the field is measured, then turned on for a longer period using the measured data as constants. The on-off period ratio can be about 100 sec on to 4 sec off.

Invar material has been proposed as an alternate to graphite epoxy material for use in the telescope truss structure and the SIP structure of the LST spacecraft. The Invar material used in the structure can be either hard drawn or annealed.

The weight of Invar proposed is approximately 400 kg (880 lbm) and the volume is approximately 4.9×10^{-3} m^3 (3000 $in.^3$). The presence of Invar in the telescope will have two effects. Magnetization of the Invar by both the Earth's magnetic field and the field produced by the electromagnets will result in the production of counter control torques and the alteration of the field distribution shown in Figure VI-35. Since the strength of the field produced by the electromagnets over the majority of the telescope length is less than the earth's magnetic field, the effects of the Invar from these sources will be very small and have been ignored. The effect of the earth's field can be significant, however, and is discussed below.

Figure VI-36 shows the B-H characteristic for annealed Invar. Data for this figure were obtained from the Alloy Digest, March 1964 issue. It is noted that annealed Invar is likely to be magnetized in the earth's magnetic field. The maximum value of the earth's magnetizing force at orbit altitude is about 32 A-m (0.4 oersted). Corresponding to this value of H, the value of magnetic induction, B, obtained from Figure VI-36 is about 9.5×10^{-2} T (950 gauss). The resulting magnetic moment induced in the Invar in the direction of B is 3740 A-m^2. This is more than the capacity of one electromagnet. This large magnetic moment induced in the Invar will result in a large magnetic field at the SIP and SSM, which is highly undesirable and may result in the requirement for shielding many spacecraft components.

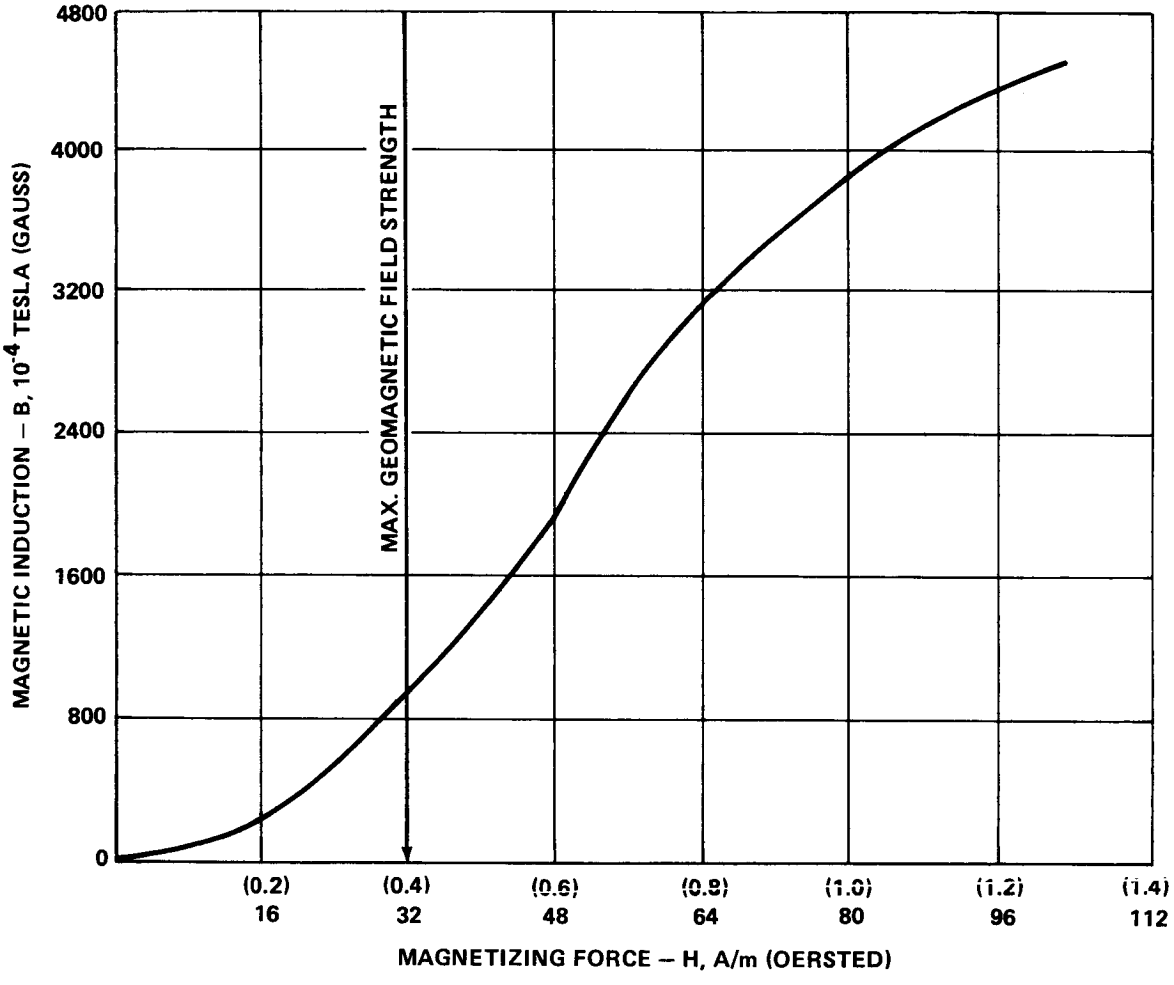

Figure VI-36. B-H characteristic for annealed Invar.

The magnetic moment induced in the Invar by the earth's field is parallel to the field and will produce no disturbing torque for the initial spacecraft orientation. When the spacecraft is reoriented with respect to this field, a new moment is induced; but there is also a moment due to the residual magnetism from the previous orientation. That component of the residual magnetic moment that is normal to the earth's field will produce a disturbance torque on the spacecraft. The magnitude of this component under worst conditions is equal to the moment produced by the total residual magnetism in the Invar. No experimental data on the residual magnetism (hysteresis properties) of Invar could be obtained; however, Itek personnel estimated it to be 10 to 30 percent. A value of 20 percent was used in the present analysis. This gives the residual magnetism normal to the earth's field as 748 $A\text{-}m^2$. The maximum disturbance torque produced on the spacecraft is then 0.03 N-m (0.022 ft-lbf). This is about 20 percent of the maximum gravity gradient torque. Because of the large induced magnetism in the Invar and the consequent large magnetic field and disturbance torque, the use of annealed Invar on the LST spacecraft should be kept to a minimum.

Since the amount of magnetism induced in the hard drawn Invar is lower than the annealed Invar, the hard drawn Invar is recommended for any use in the structure. However, Itek Corp. personnel have recently stated that the magnetic properties of hard drawn Invar change with time and its resistance to magnetization decreases. If this is true, the actual magnetic field distribution due to the geomagnetically induced magnetism in hard drawn may approach that computed for the annealed Invar. Based on this observation, only the results of magnetic field distribution from geomagnetically induced magnetism in annealed Invar are given to characterize the torque produced and the propagated field.

The magnetic field propagation due to the magnetism in the annealed Invar structure induced by the geomagnetic field is shown in Figure VI-37. Various assumptions were made in computing this magnetic field distribution because of the complex structure of the LST. One of these assumptions is that the field distribution in an annealed Invar structure corresponds to the field distribution of an equivalent bar magnet. The length of the equivalent bar magnet is 8.4 m (330 in.), which is the length of the telescope truss plus the SIP structure, and it produces a dipole moment of 3740 $A\text{-}m^2$.

One end of the equivalent bar magnet is at the aft end of the SIP, within the LST SSM. The abscissa of Figure VI-37 represents the distance along the longitudinal axis of the LST spacecraft from the end of the Invar structure toward the base of the SSM. From this figure it is seen that

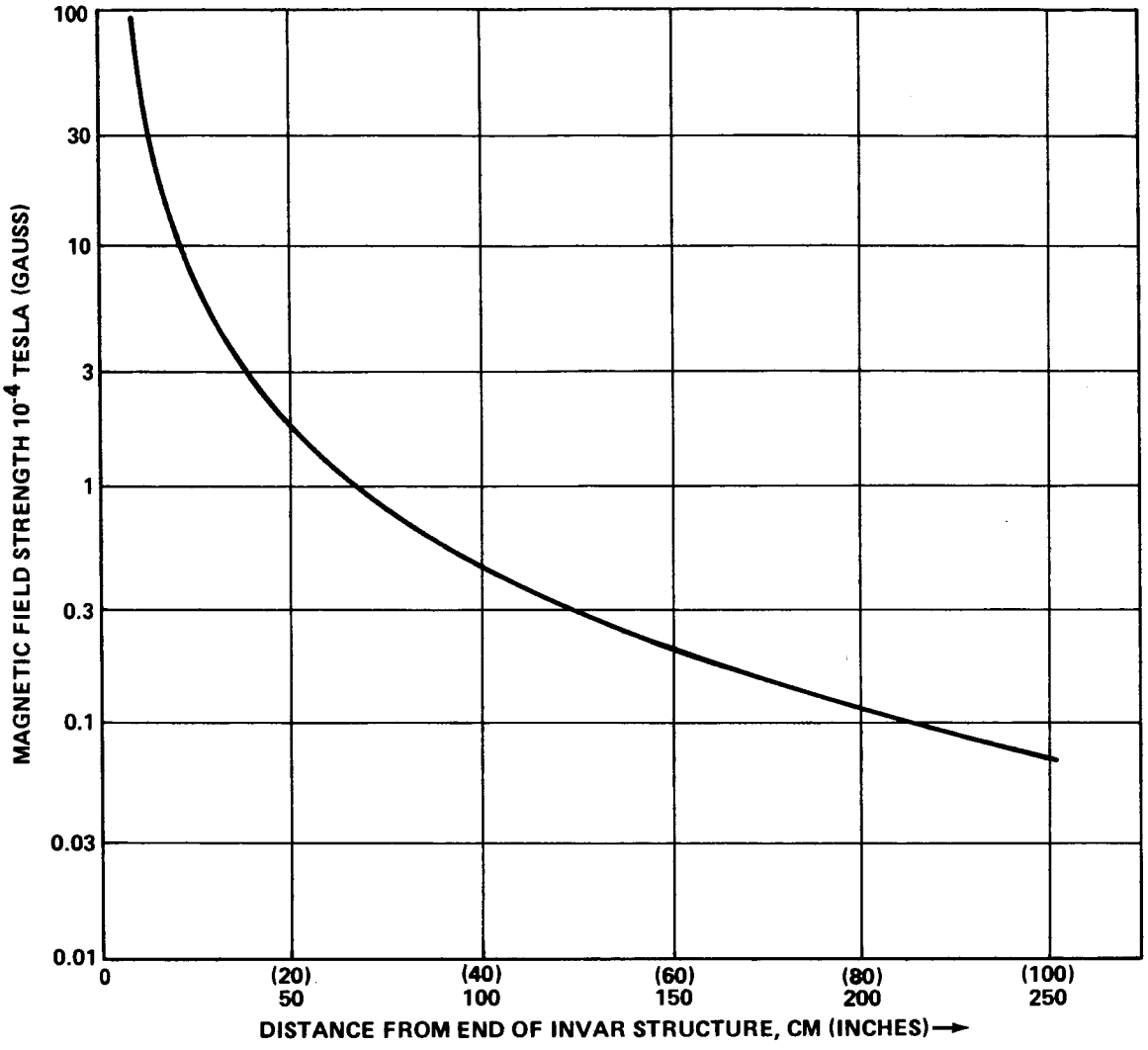

Figure VI-37. Magnetic field distribution — Invar structure in the geomagnetic field.

the field near the end of the Invar is high but that it drops very rapidly outside the Invar. Because of the high field strength, some magnetic sensitive components in the SIP and SSM will require magnetic shielding if Invar is used.

It is expected that the instruments located within the SIP will be adversely affected by a magnetic field strength over a few gauss. All points on the plot shown in Figure VI-37 lie outside the SIP structure; therefore, the field strength within the SIP at points near annealed Invar members

can be greater than 100 gauss. Magnetic shielding can reduce this field at the instrument if this does not interfere with light paths into the detectors. Magnetic sensitive components should not be placed adjacent to the Invar structure. Depending upon the field sensitivity of the particular component, it should be mounted some small distance away (especially from the ends) from the Invar structure. The high induced fields expected in annealed Invar seem to make this material unsuitable for use in the SIP structure. A graphite-epoxy material would be much more suitable from a magnetic interference standpoint.

5. Reaction Control System

a. Guidelines. The selected LST configuration has an RCS in addition to the primary control system. The design guidelines for the RCS have been outlined in Section A.1 from which the following guidelines for RCS analysis were obtained. The RCS may be used for:

1. Emergency control during a failure of ACS major subsystems.

2. Backup control while in the vicinity of the Shuttle.

3. Larger control authority in case of misdock.

b. RCS Performance. A preliminary timeline of possible LST RCS use was devised to obtain propellant requirements using the dual thrust level reaction jets described in the system implementation section. Assuming a Shuttle launch with utilization of Shuttle control during CMG spin-up, the RCS may first be used after release of the LST from the Shuttle. As a worst-case, the release transient will be assumed to be equal to docking transients. A simple analysis was made of two rigid bodies in collision with the total momentum converted to an LST angular rate. The result was

$$\dot{\phi} = 11.74\, \nu_0 \quad ,$$

where ν_0 is in m/sec and $\dot{\phi}$ will be deg/sec. In addition to this angular rate, the Shuttle limit cycle rate will be added, to give

$$\dot{\phi} = 11.74\, \nu_0 + 0.1 \quad .$$

Using a closure velocity 0.0348 m/sec (0.1 ft/sec), an angular rate of 0.46 deg/sec is obtained for the LST. It was felt that a reasonable approximation to an actual collision is to distribute this in an RSS sense giving 0.26 deg/sec on each axis. To remove these rates 222.4 N-sec (50 lb-sec) of impulse will be required. Three misdocks were assumed to be budgeted giving three times the above figure or 667.2 N-sec (150 lb-sec). Figure VI-38 shows the comparison between RCS control and CMG control during a low velocity collision. The attitude overshoot and recovery times allowed by the CMGs are somewhat larger than those allowed by the RCS. For the case shown, the CMGs may suffice but, for larger closure velocities, the RCS would be much more desirable.

Next, consideration was given to an emergency hold mode. Assuming no pointing requirements and three-axis stabilization to 0.5 deg, the X-POP mode (X-axis perpendicular to the orbit plane) was studied. If this mode were maintained for 29 days, 10 230 N-sec (2300 lb-sec) impulse would be required (assuming a regulated GN_2 RCS). As the attitude hold accuracy is decreased (greater than 0.5 degree), the impulse requirements increase due to larger gravity gradient torques.

If the LST has a pointing requirement during the emergency mode (i.e., the solar wings normal to the sunline), the worst-case gravity gradient conditions could be encountered, requiring a much larger than desirable propellant loading. Using the coarse sun sensor as a pointing reference allowing tumble about the sunline and considering average gravity gradient torques on the 2 controlled axes, the LST can be stabilized to ±10 degrees about 2 axes for 16 days using 10 230 N-sec (2300 lb-sec) impulse. With the worst-case gravity gradient torques and 2-axis stabilization, the 10 230 N-sec (2300 lb-sec) impulse will permit control to ±10-degree accuracy for 7 days.

The final RCS control function budgeted is the docking requirement. A simple percentage (10 percent) of the misdock budget was allocated for docking, giving 67 N-sec (15 lb-sec) impulse. The complete impulse budget is given in Table VI-12.

A brief comparison was made between a blowdown RCS similar to the one used on Skylab and the regulated RCS selected for the LST. Table VI-13 shows the propellant consumption comparison between the regulated and blowdown systems. Obviously, the blowdown system is quite wasteful with respect to limit cycle propellant consumption due to the relatively large blowdown minimum impulse bits (MIBs). The MIB, in effect, gives the

ANGULAR RATE IMPARTED TO LST DUE TO MISDOCK WITH MANIPULATOR ARM* (V_o in m/s)

$\dot{\phi}_1 = 11.74\ V_e$ deg/sec

$= 11.74 \times 0.0348$ deg/sec

$= 0.36$ deg/sec

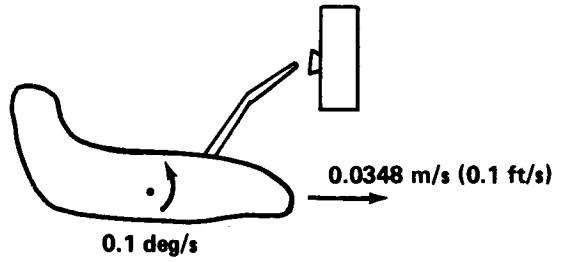

ANGULAR RATE IMPARTED TO LST DUE TO LIMIT CYCLING OF THE SHUTTLE ACS

$\dot{\phi}_2 = 0.1$ deg/sec

ASSUMED CMG SYSTEM TORQUE = 13.55 N-m (10 ft-lbf)

MAX. MAGNETIC CONTROL TORQUE = 0.27 N-m (0.2 ft-lb)

RECOVERY TIME AND OVERSHOOT

RCS	MAGNETIC + CMG's
t = 11 sec	t = 54 sec
ψ = 2.5 deg	ψ = 12.2 deg

MAGNETICS ONLY

t = 1 to 2 ORBITS

LST CAN TUMBLE

MAXIMUM LST ANGULAR RATE

$\dot{\phi} = 0.46$ deg/sec

* ALL MOMENTUM IS TRANSFORMED INTO ANGULAR RATE ABOUT ONE AXIS

Figure VI-38. RCS control versus CMG control during collision.

TABLE VI-12. RCS IMPULSE BUDGET FOR LST

		Impulse	
		N-sec	lb-sec
Compensate LST/Shuttle Separation Transients (0.26 deg/sec, 3 axes)		222.4	50
Emergency Control Mode	1. X-POP, 3-Axis Control, 29 Days 2. 2-Axis Control Solar Pointing with 2-Axis Estimated Secular Momentum as Disturbance: 16 Days 3. 2-Axis Control Solar Pointing with Worst-Case Gravity Gradient, 7 Days	10 230.9	2300
Misdock (3 budgeted)		667.2	150
Docking		66.7	15
Total		11 187.2	2515

TABLE VI-13. PROPELLANT REQUIREMENTS FOR VARIOUS FLIGHT MODES OF THE LST AS A FUNCTION OF THE MINIMUM IMPULSE BIT AND THE CONTROL DEAD BAND

KILOGRAMS (POUNDS) OF PROPELLANT PER DAY @I_{SP} = 65 SEC

X-POP

MIB / d.b.	REG-ULATED	BLOWDOWN			
	.0222 (.005)	2.22 (.5)	8.89 (2)	17.79 (4)	22.24 (5)
.5	.558 (1.23)	4.76 (10.5)	107.5 (237)	267.6 (590)	428.2 (944)
5	.558 (1.23)	.86 (1.9)	6.85 (15.1)	27.2 (60)	39.5 (87)
10	.558 (1.23)	.72 (1.6)	3.62 (8)	12.9 (28.5)	19.8 (43.7)

X-IOP

MIB / d.b.	REG-ULATED	BLOWDOWN			
	.0222 (.005)	2.22 (.5)	8.89 (2)	17.79 (4)	22.24 (5)
.5	2.72 (6)	6.94 (15.3)	109.7 (242)	269.9 (595)	430.5 (949)
5	2.72 (6)	3.08 (6.8)	9.07 (20)	29.5 (65)	41.7 (92)
10	2.72 (6)	2.90 (6.4)	5.76 (12.7)	15.06 (33.2)	22.0 (48.6)

WORST CASE GRAVITY GRADIENT

MIB / d.b.	REG-ULATED	BLOWDOWN			
	.0222 (.005)	2.22 (.5)	8.89 (2)	17.79 (4)	22.24 (5)
.5	5.9 (13.1)	10.1 (22.2)	112.9 (249)	273.0 (602)	433.6 (956)
5	5.9 (13.1)	6.17 (13.6)	12.2 (27)	32.6 (72)	44.7 (98.6)
10	5.9 (13.1)	6.12 (13.5)	9.02 (19.9)	18.3 (40.3)	25.2 (55.5)

AVERAGE GRAVITY GRADIENT

MIB / d.b.	REG-ULATED	BLOWDOWN			
	.0222 (.005)	2.22 (.5)	8.89 (2)	17.79 (4)	22.24 (5)
.5	1.6 (3.5)	5.8 (12.9)	108.8 (240)	268.5 (592)	429.1 (946)
5	1.6 (3.5)	1.9 (4.3)	8.1 (17.8)	28.4 (62.6)	40.5 (89.3)
10	1.6 (3.5)	1.7 (3.8)	4.6 (10.2)	13.9 (30.7)	20.9 (46.1)

MIB- MINIMUM IMPULSE BIT IN NS (lb_f-S)

d.b.- DEAD BAND (DEGREES)

smallest possible angular rate achievable with the RCS; so, as the MIB goes down, excessive limit cycle operation is also reduced. The smallest MIB in each new heading of the figure is that of the regulated system. The MIBs to the right of the regulated system represent variations in the blowdown system as a function of propellant used. Propellant weights are found as a function of the MIB and the deadband by tracing rows and columns to their intersection. Even at the end of the mission, the blowdown system does not compare favorably with the regulated system. From a stabilization and control viewpoint, a regulated system is definitely preferred since the control torques for the blowdown system are much too large for efficient limit cycle operation. Only if a modified blowdown system with a much lower MIB were built would it become a viable candidate.

c. Recommendations. It is recommended that two-axis control be used during the emergency sun acquisition mode with the coarse sun sensor providing attitude information. The 2 controlled axes can be stabilized to an accuracy of 10 degrees by this method, allowing the solar wings to operate near peak power. Attitude rate can be obtained by differentiating the outputs of the sun sensors. For three-axis control, logic must be supplied in the TA to obtain attitude and rate from the RGA. This is desirable during Shuttle docking (with a failed LST central processor) to allow the LST to be three-axis stabilized.

It should be reiterated that the RCS is desirable as a backup control system during those times when the Shuttle is in the close vicinity of the LST. Much more control authority is available during docking (with the possibility of collision outside expected tolerances) than is available from the primary control system.

6. System Simulation

a. Description. A digital computer program was utilized to simulate the dynamic behavior of the LST in a circular earth orbit. The program is basically designed to simulate the LST over a several-orbit time period and is utilized to determine the overall compatibility of the subsystems making up the total attitude control system and to verify the gain selections to meet overall performance requirements. This simulation does not take into account the hardware nonlinearities such as CMG dead zones and friction or sensor noise. In a real system, permissible gains are limited by noise levels, mechanical resonances, CMG vibration, and angular rates acceptable to the fine pointing system. Even at maximum permissible gain, actual system performance is limited by hardware constraints such as the dead zone

of the CMG gimbal tachometer and the static and running friction of the gimbal bearings. Only rigid body dynamics are incorporated in the digital simulation. Therefore, the gains can be arbitrarily increased to attain whatever pointing accuracy is specified without the usual restrictions of body flexibility effects.

The equations which were programmed were Euler's equations for rotational motion about the principal LST body axes, a 1, 2, 3 Euler angle sequence to relate the body axes to the solar reference coordinates, transformational matrices to relate the environmental forces to the LST body axes, control logic which relates the LST attitude errors through appropriate feedback gains to the commanded torque, a CMG steering law which converts the commanded torque to an applied torque through the CMG dynamics, a spherical harmonic expansion to generate the earth's magnetic field, and magnetic control logic for CMG momentum management. For added realism, the program included all natural movements which could affect the orbital motion of the LST, such as the earth's rotation, regression of the ascending line of nodes, and the earth's revolution about the sun. Since the dominant environmental torque is that caused by g.g. and the LST uses a magnetic torquing system for CMG momentum exchange, the only environmental torques simulated were those due to g.g. and magnetic effects.

A simplified block diagram (Fig. VI-39) illustrates the LST overall system simulation. Those blocks below the dashed line represent environmental torque generators for the g.g. and magnetic torques which act on the LST as functions of the time-varying orbital parameters. The blocks above the dashed line represent the LST and control system components. Several limits were incorporated into the program, such as magnetic dipole and CMG gimbal angle rate limits. Since the CMGs are oversized for the LST and since a pointing mode is being simulated, hard limits on the CMG gimbal positions and on the control law outputs have no effect on overall system performance and were deleted from the program after having been initially included. The CMG gimbal angles have unlimited angular freedom. The LST is represented by Euler's equations. Kinematic relations represent sensors which provide attitude rate and position information, and the generator for the earth's magnetic field represents an onboard magnetometer. The control law, CMG steering law, and coil dipole commands represent equations which are normally solved by the onboard computer. The CMG angle rate limit, the CMGs, and the limit dipoles blocks represent the corresponding hardware components. As discussed in Sections F.3 and F.4, the CMG steering law is the Moore-Penrose pseudoinverse of the CMG torque matrix which converts the commanded torque into CMG gimbal rate commands. The coil dipole commands are generated by the vector cross product of the earth's field and

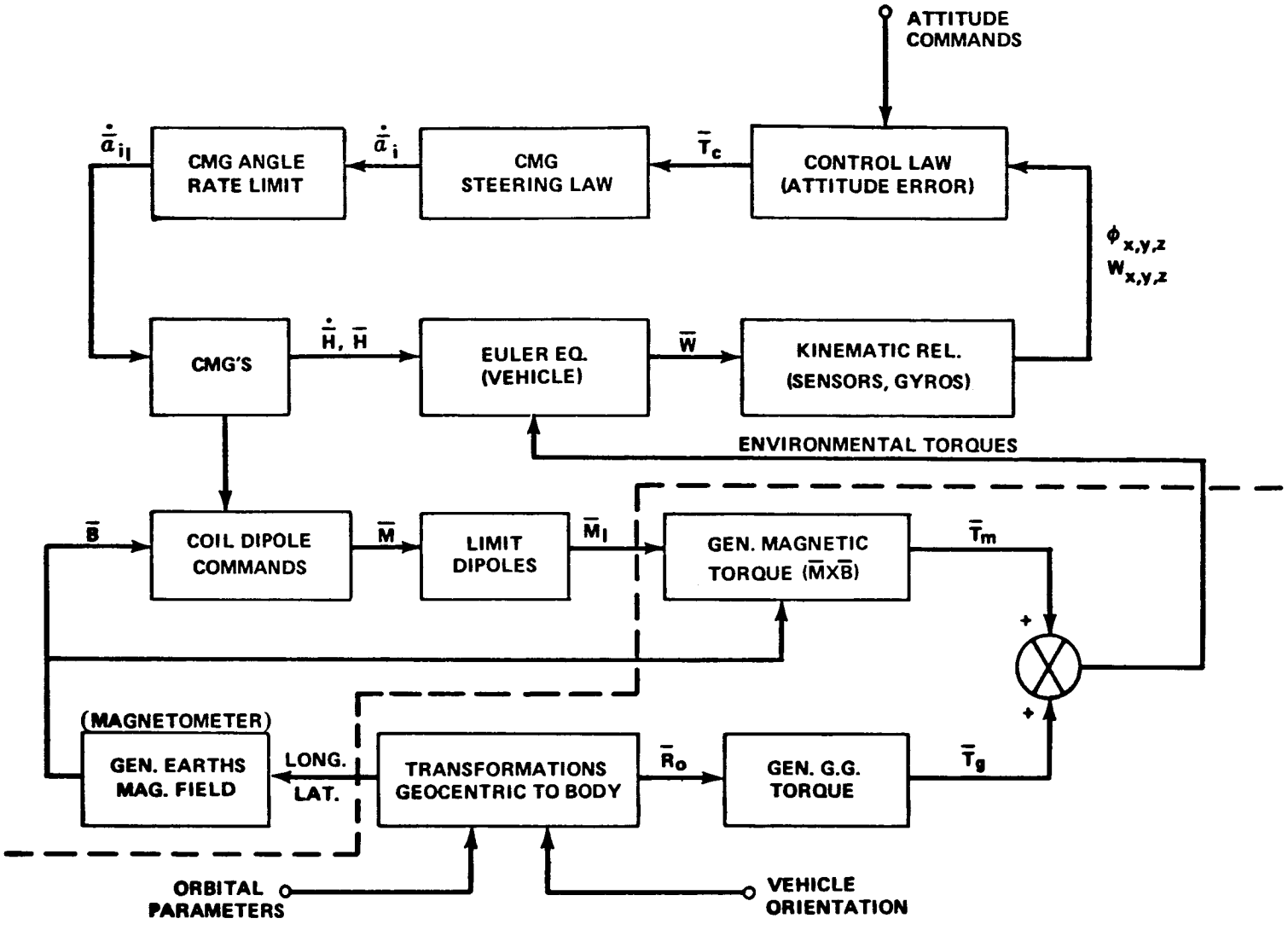

Figure VI-39. Block diagram of the LST digital simulation.

desired magnetic torque vectors. The desired magnetic torque is composed of two factors. These are the CMG momentum state weighted by K_d to dump CMG momentum and the commanded torque weighted by K_c to provide direct control in the event of CMG failures. The connection between $\bar{T}_c$ and $\bar{M}$ is not illustrated in Figure VI-39.

The control law is composed of attitude position, rate, and integral of position components, each weighted by a feedback gain which has been selected to give the desirable LST pointing performance and stability

characteristics as shown in Figure VI-40. Without integral feedback, a control system bandwidth of 0.1 Hz must be selected to attain a steady state pointing error of 1 arc sec or less under the maximum g.g. torque acting on LST. At that design bandwidth and assuming a control system damping of 0.7, the corresponding position gain on the major inertia axis is about 37 500 N-m/rad (27 642 ft-lb/rad). By adding integral of position feedback while holding the rate and position gains constant, the steady state pointing error can be reduced to about 0.001 arc sec. As shown in Figure VI-41, the steady state pointing error decreases as the integral gain is increased. But eventually, as the integral gain approaches the position gain value, instability occurs. To reduce the pointing error further, the bandwidth must be increased, resulting in higher values for both the position and rate gains. A practical upper limit on bandwidth is about 0.4 Hz to attain LST fine body pointing.

b. Parameters. Many cases were simulated for various LST configurations, orbital conditions, and control gains. However, the simulation results to be shown are all for only one LST configuration and one type orbit so that data can be compared under the same environmental conditions. Table VI-14 shows the vehicle and simulation parameters. The LST inertias for the graphite-epoxy OTA are more favorable than earlier pre-Phase A inertia values. The position and rate gains were selected to give a natural frequency of 0.628 rad/sec based on an assumed damping ratio of 0.7. The corresponding time period is 10 sec. The integral of position feedback gains and the MTS gains, K_d and K_c, were empirically derived from simulation data. Based on the electromagnet sizing and CMG selection, the values for the dipole limit, momentum per CMG, and CMG skew angle represent hardware limitations. At each half-second of orbital time, the equations in the simulation were solved and the results printed out on each 50 sec interval.

Table VI-15 illustrates the standard orbital parameters for LST. At a circular orbit of 611 km (330 n.mi.), the orbital rate is 1.08×10^{-3} rad/sec with a period of 5824 sec. All the simulation data have been plotted as a function of orbital time scaled in 1000 sec increments. The orbit starts at the time of winter solstice with the ascending line of nodes on the morning terminator. The earth is positioned under the orbit such that the north magnetic pole is tilted toward the sun. The spacecraft is inertially oriented with its long axis (X) pointing to the sun, major inertia axis (Z) northward perpendicular to the ecliptic plane, and its solar panel gimbal axis (Y) perpendicular to the sunline in the ecliptic plane. Although the orbital inclination should be 28.5 degrees, a value of 21.55 degrees was used in the simulation runs to produce a 45 degree angle between the X-axis and the local vertical. This type orbit and vehicle orientation will produce a g.g. torque that will cause the CMGs to saturate more rapidly than any other and represent a worst case for attitude hold.

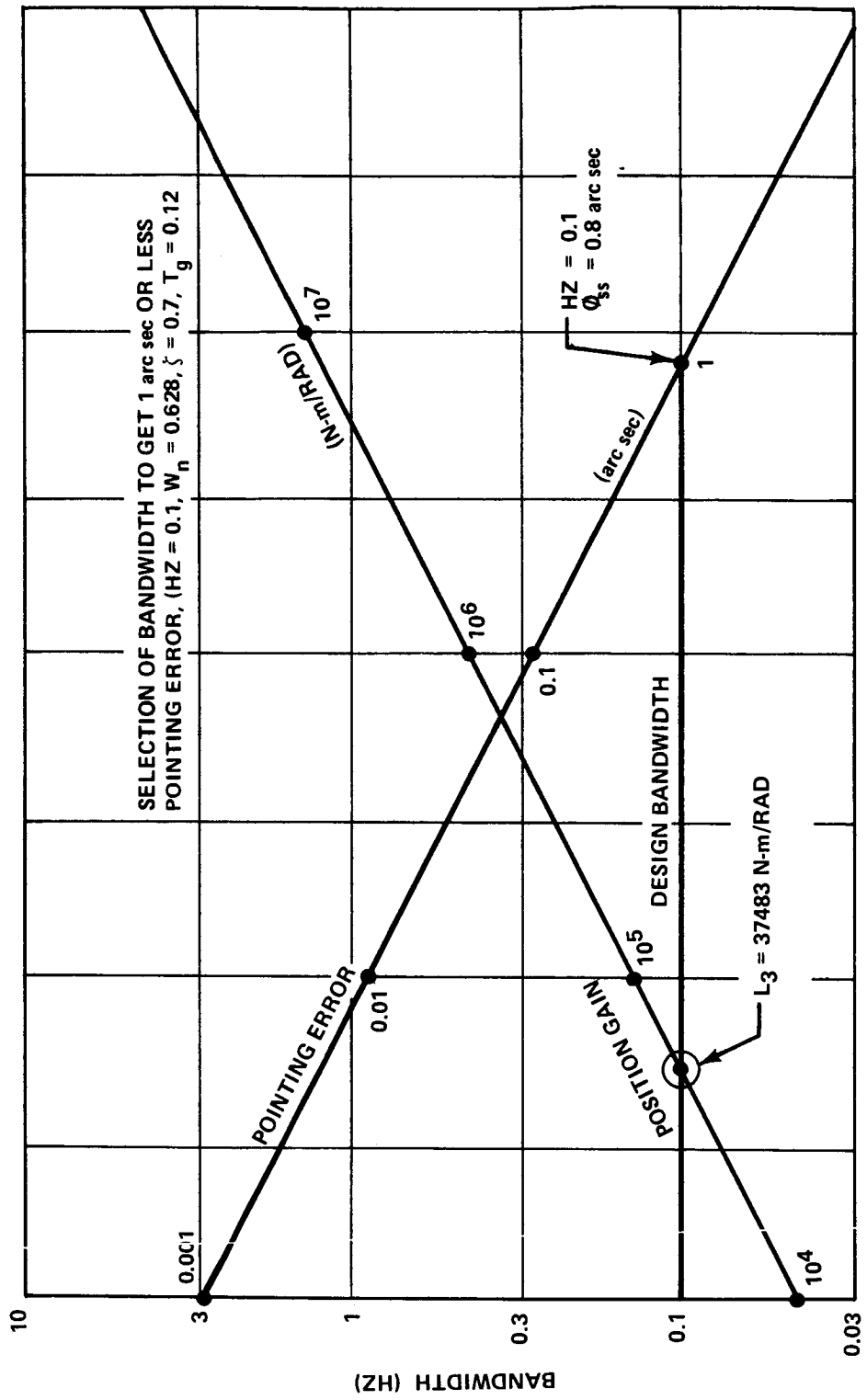

Figure VI-40. Selection of bandwidth for 1 arc sec pointing.

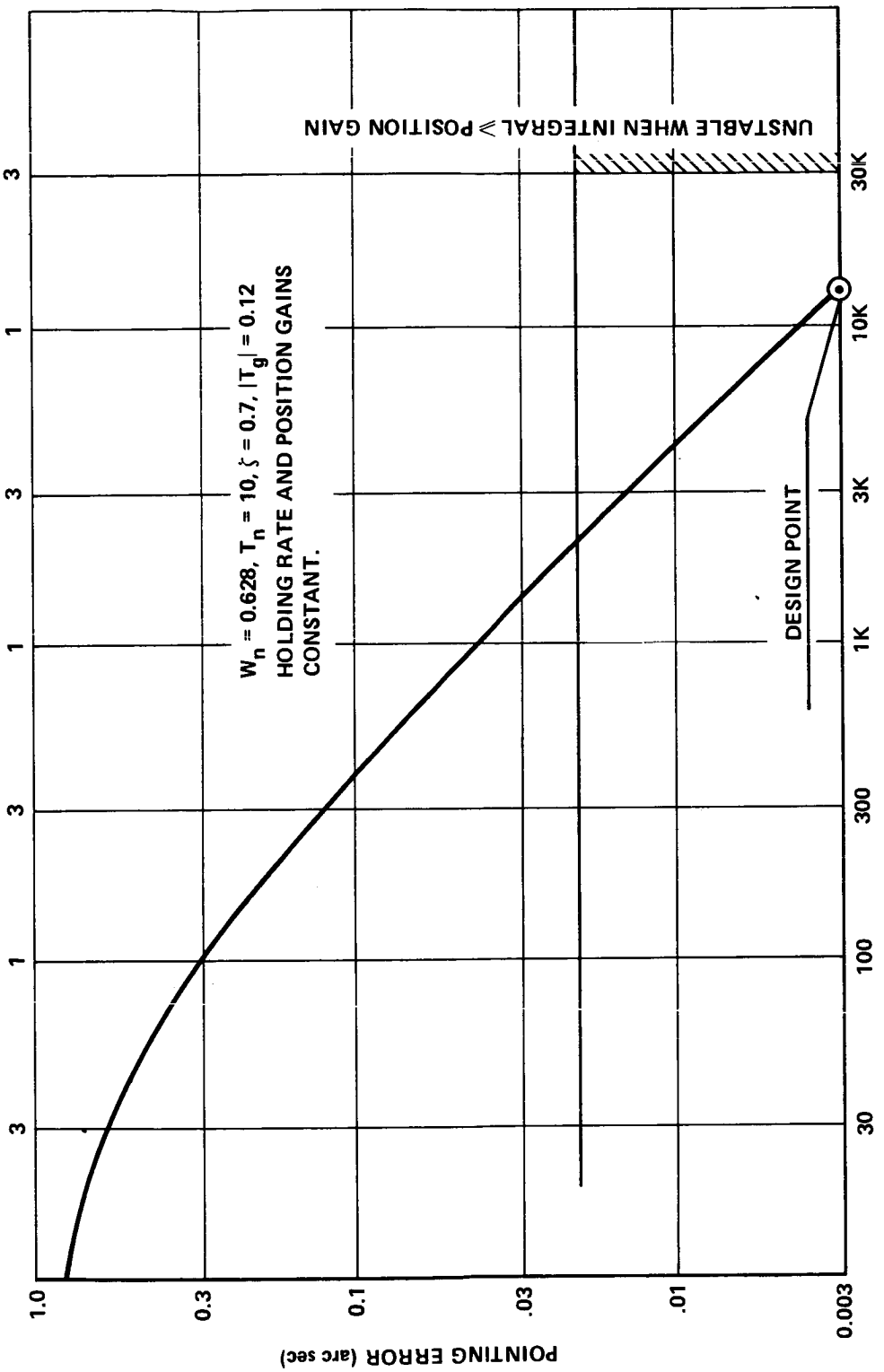

Figure VI-41. Selection of integral feedback to reduce pointing error.

TABLE VI-14. VEHICLE AND SIMULATION PARAMETERS[a]

Symbol	Value	Parameter
IX	14 658 kg-m^2 (10 810 slug-ft^2)	Pointing Axis Inertia
IY	91 785 kg-m^2 (67 688 slug-ft^2)	Intermediate Axis Inertia
IZ	95 041 kg-m^2 (70 089 slug-ft^2)	Sunward Axis Inertia
WT	7846 kg (17 283 lbm)	Vehicle Weight
L_1	-5781 N-m/rad (-4263 ft-lb/rad)	X Position Gain
L_2	-36 200 N-m/rad (-26 696 ft-lb/rad)	Y Position Gain
L_3	-37 483 N-m/rad (-27 642 ft-lb/rad)	Z Position Gain
K_1	-12 887 N-m-sec/rad (-9504 ft-lb-sec/rad)	X Rate Gain
K_2	-80 697 N-m-sec/rad (-59 511 ft-lb-sec/rad)	Y Rate Gain
K_3	-83 559 N-m-sec/rad (-61 622 ft-lb-sec/rad)	Z Rate Gain
L_x	-1356 N-m-sec (-1000 ft-lb-sec)	X Integral of Position Gain
L_y	-13 560 N-m-sec (10 000 ft-lb-sec)	Y Integral of Position Gain
L_z	-13 560 N-m-sec (10 000 ft-lb-sec)	Z Integral of Position Gain
K_d	+0.005	Dipole Gain for CMG Momentum Dumping
K_c	1.0	Dipole Gain for Direct Magnetic Torque
M_1	4000 A-m^2 (0.3 ft-lb/gauss)	Dipole Limit per Axis
H	678 N-m-sec (500 ft-lb-sec)	Momentum per CMG

TABLE VI-14. (Concluded)

Symbol	Value	Parameter
β	30 deg	CMG Skew Angle
$\dot{\alpha}_1$	1 deg/sec	CMG Gimbal Rate Limit
W_n	0.1 Hz	Control Bandwidth with $L_{xyz} = 0$
ζ	0.7	Damping
T_n	10 sec	Control Period
DT	0.5 sec	Simulation Solution Time Step
TP	50 sec	Solution Printout Interval

a. The mass properties are those existing at the time of the simulation and should be considered as typical values. They do not necessarily reflect the latest updating of the mass properties given in the master equipment list.

TABLE VI-15. ORBITAL PARAMETERS

Symbol	Value	Parameter
AA	611 km (330 n.mi.)	Orbital Altitude
I	28.5 deg	Orbital Inclination
λ	270 deg	Solar Position for Winter Solstice
Ω	deg	Morning Terminator Orbital Line of Nodes
$\dot{\Omega}$	-7.3 deg/day	Orbital Regression
Ω_e	345 deg	Greenwich Meridian to Tilt Magnetic Pole Sunward
T_o	5814 sec	Orbital Period
ω_o	0.001, 078, 78 rad/sec	Orbital Rate
e	23.45 deg	Angle Between Ecliptic and Equatorial Planes
$\overline{B}$		Earth's Magnetic Field Generated by Spherical Harmonic Coefficients

c. Results. Figure VI-42 illustrates the g.g. torque vector components and magnitude relative to the LST body axes. The Y component is biased negatively and attains its maximum possible value of 0.14 N-m (0.104 ft-lb). Other orbital conditions, however, can cause the biased torque to appear on either the X- or Z-axis or to be prorated between all axes simultaneously. The maximum permissible g.g. torque always occurs on the intermediate axis of inertia, the Y-axis for LST. The corresponding g.g. momentum components and magnitude are shown in Figure VI-43. The biased Y-axis torque produces a secular momentum of 410 n-m-sec (302 ft-lb-sec) in one orbital period. As long as the same vehicle orientation is maintained, the momentum buildup continues. To prevent CMG saturation, the MTS for the LST must be able to compensate or dump this secular momentum. Both the X and Z momentum components are cyclic. But due to LST body symmetry about the X-axis, both the torque and momentum values are near zero. With the MTS turned off, the CMG torque and momentum components are the same as those shown for g.g.

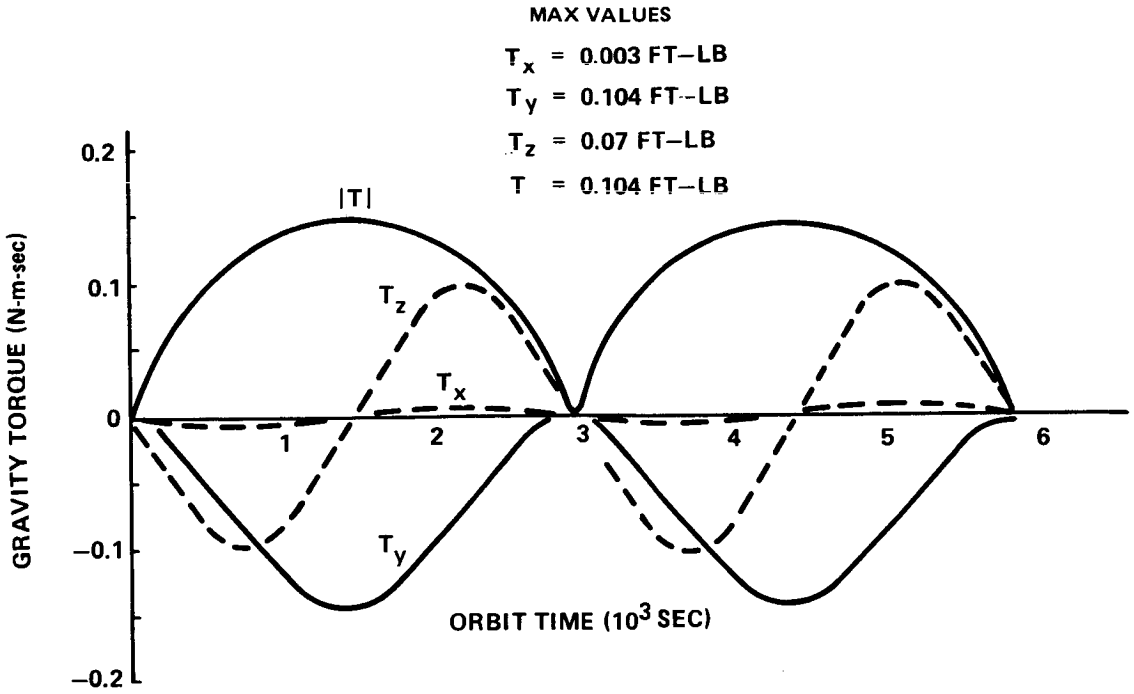

Figure VI-42. Gravity disturbance torque.

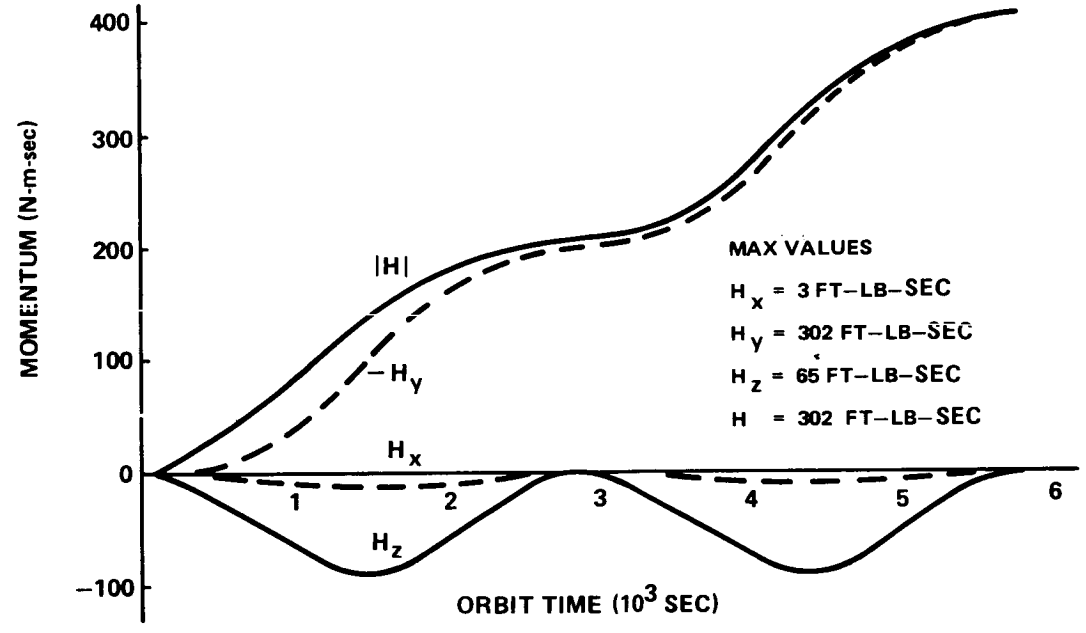

Figure VI-43. Gravity momentum components.

The accumulated CMG momentum is shown in Figure VI-44 with and without the MTS dumping momentum. The difference between the two curves represents the momentum dumped by the MTS. During the one orbit period, all the secular and a large part of the cyclic g.g. momentum has been dumped.

Using only position and rate feedback signals, a control system that performs well will produce an attitude error signal proportional to the disturbance torque. Such a pointing error can be observed in Figure VI-45. Without the MTS, the peak error is 0.8 arc sec and occurs at the same orbit time as the peak g.g. torque. But with the MTS operational, the magnetic torque required for magnetic momentum dump acts as a second disturbance torque and the peak values do not correspond to g.g. With magnetics, the peak pointing error (0.6 arc sec) occurs about midway in the one orbital period.

When integral of position feedback is included in the control law, the pointing error is no longer shaped like the disturbance torque. As shown in Figure VI-46, integral control reduces the pointing error (by about a factor of 100) to about 0.003 arc sec without the MTS active and about 0.005 arc sec with the MTS active. Using integral control, the magnetic dump gain, K_d, has been reduced from 0.1 to 0.005. As the pointing requirement gets

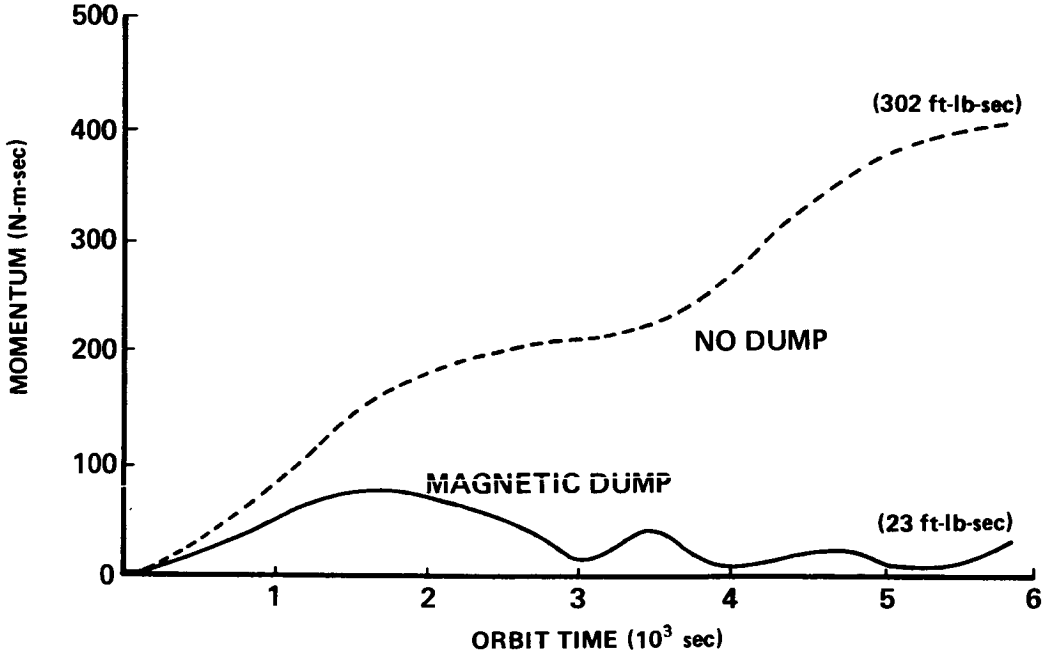

Figure VI-44. Accumulated CMG momentum.

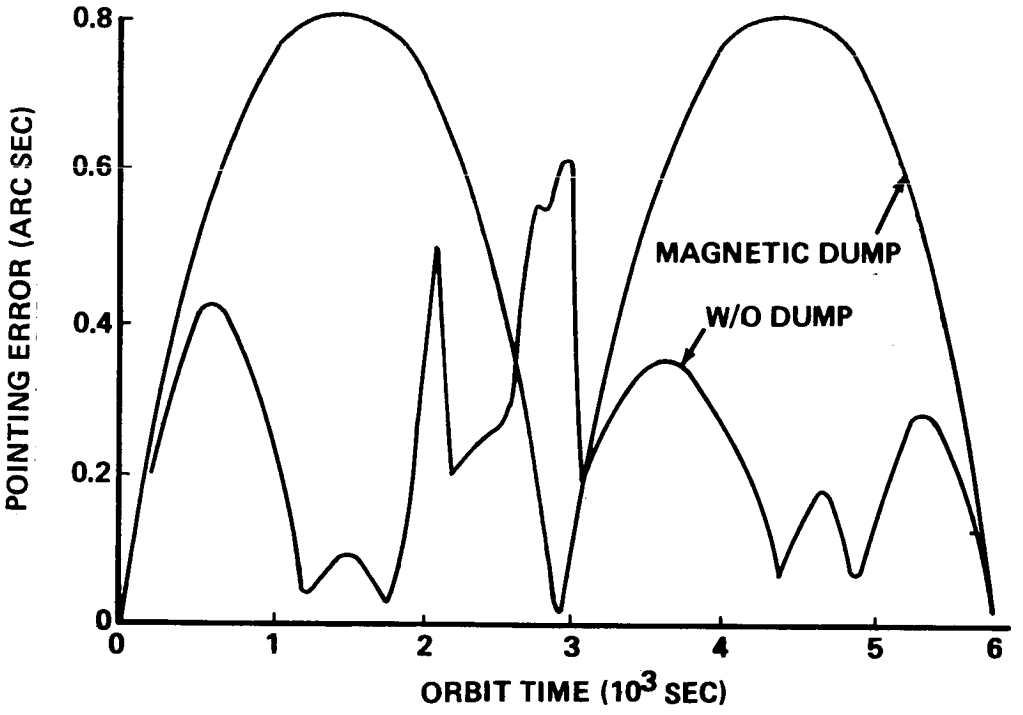

Figure VI-45. Attitude pointing error using position and rate feedback.

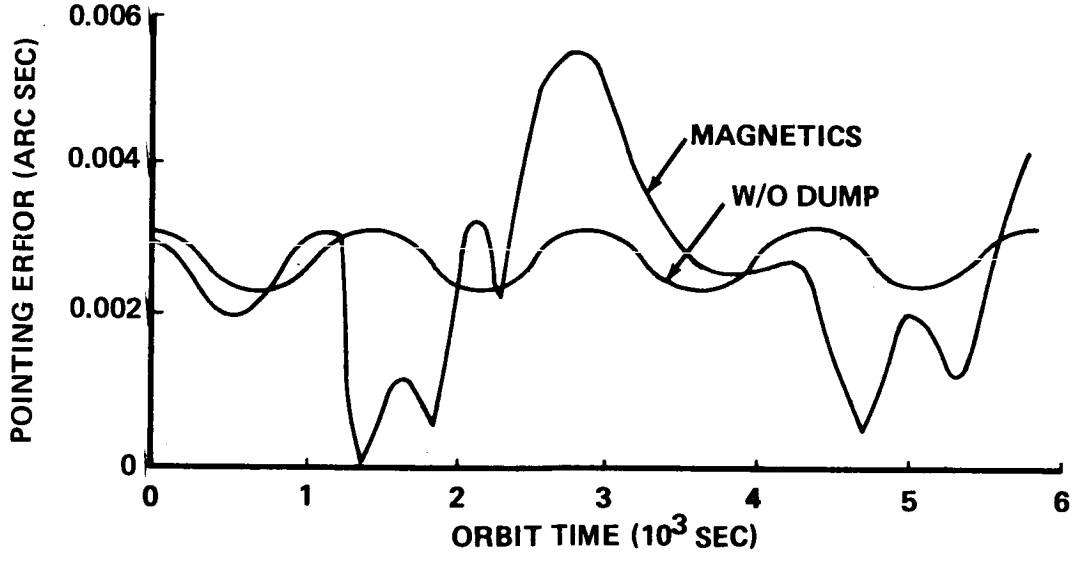

Figure VI-46. Attitude error using integral feedback with and without magnetics.

smaller, the MTS gains must be reduced to make the electromagnet dipole operate in a near-linear mode to prevent excessive pointing errors. As previously shown in Figure VI-44, very little momentum is accumulated in the CMGs with the MTS operating. Consequently, the gimbal angles stay small compared with those obtained without using the MTS. The CMG gimbal angles using position and rate feedback control without the MTS active are shown in Figure VI-47. Gimbal angles numbers 2 and 4 attain a maximum of about 20 degrees near the end of one orbit. If continued, a possible gyro hang-up condition would have occurred when gimbals 2 and 4 reached ±90 degrees, respectively, with gimbals 1 and 3 near zero. In this particular situation, the hang-up plane is the X-Z vehicle plane and the hang-up direction is the Y-axis about which the secular momentum is building up. The gimbal angles with the MTS operating are shown in Figure VI-48. The maximum value attained by any CMG gimbal angle is only about 4 degrees. Very little difference can be observed in the gimbal angles when integral feedback is added. So the gimbal angles are not shown for those cases.

Components of the earth's magnetic field in geocentric coordinates have been shown previously in Figure VI-20. These components are operated on by appropriate transformations to obtain the field components in LST body coordinates as illustrated in Figure VI-49. The onboard magnetometer would measure these components. For the particular orbit analyzed, the LST is in a solar pointing mode. Thus, B_x is the sunward, B_y is the

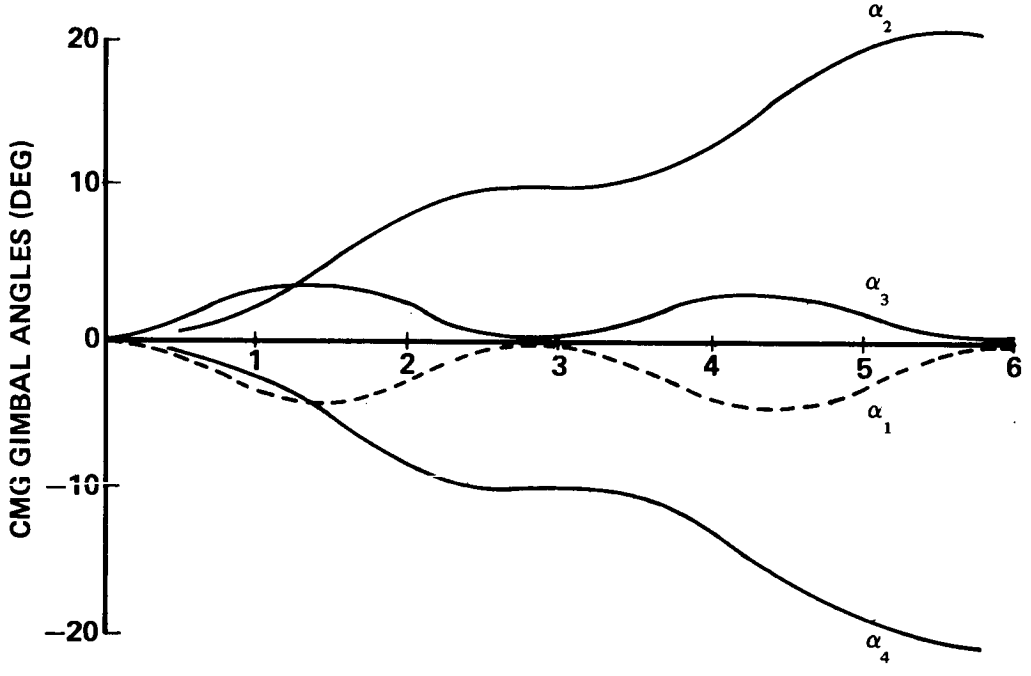

Figure VI-47. CMG gimbal angles without magnetic dump.

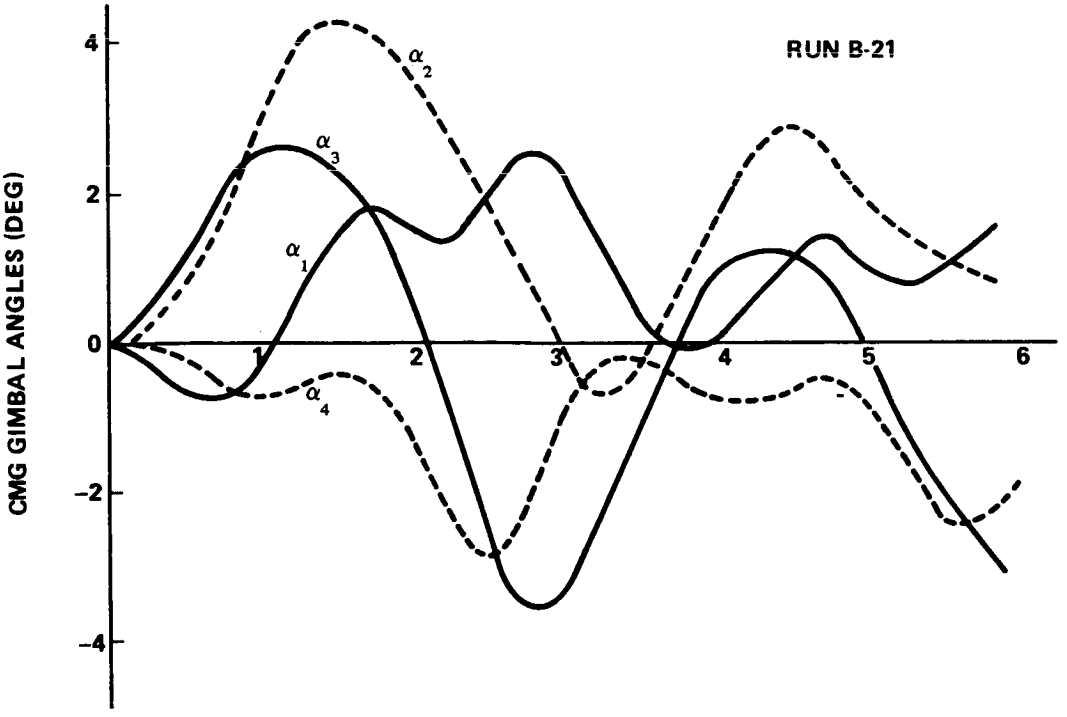

Figure VI-48. CMG gimbal angles with magnetic dump.

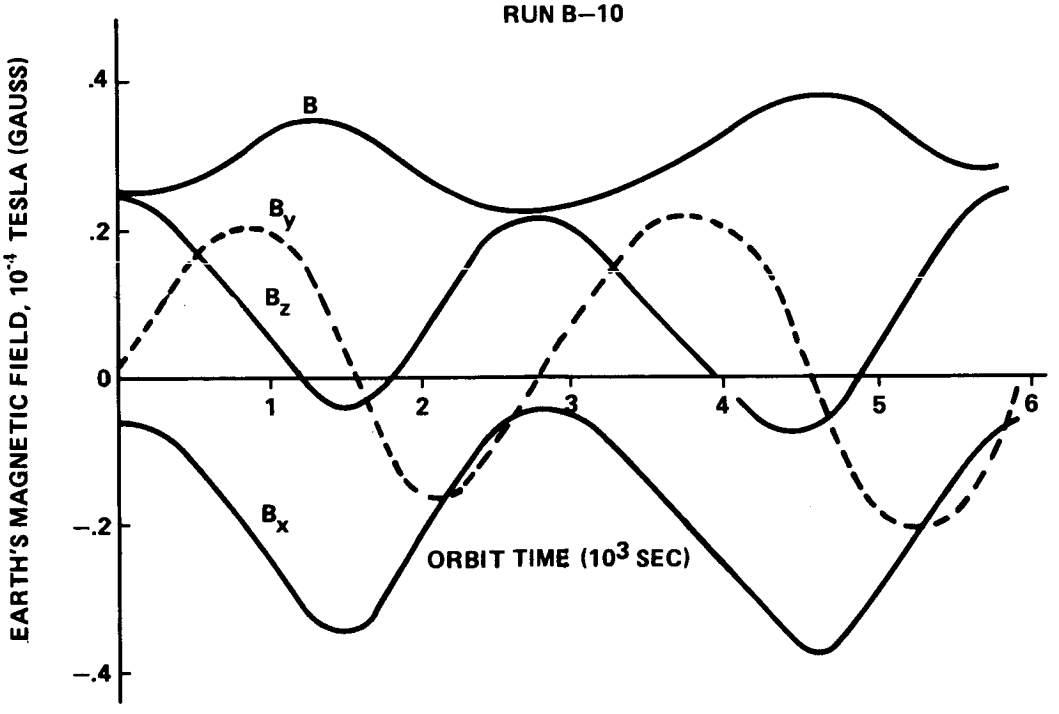

Figure VI-49. Earth field components in body coordinates.

perpendicular to the sun in the ecliptic plane, and B_z is the perpendicular to the ecliptic component. The total magnitude is given by B. Since the secular g.g. momentum is on the Y-axis, the M_x, M_z, B_x, and B_z components through the cross product dipole law will dominately be used to form a Y-axis torque TM_y which is dumping the secular momentum. As shown in Figure VI-50, both M_x and M_z reach their maximum permissible values of 4000 A-m^2 (0.3 ft-lb/gauss) and are saturated during parts of the orbit. Once the magnetic dipole vector has been generated, it reacts with the ambient earth's geomagnetic field to produce the torque components shown in Figure VI-51. The maximum value attained is about the same as the maximum g.g. torque, 0.14 N-m (0.1 ft-lb).

For comparison purposes, the total magnitudes of the g.g., magnetic, and CMG torques are plotted in Figure VI-52. Without the MTS, the CMG and g.g. torques are identical (not shown); but with the MTS, the magnetic torque approximates that of g.g. The CMG torque is generally less than either the magnetic or g.g. torque, indicating that the use of the MTS results in lower CMG gimbal rates as well as small deviations in gimbal angles from their null or reference starting positions.

CMG Number 4 was deleted from the simulation by setting its momentum to zero along with its corresponding columns in the CMG torque matrix. No change was made in the pseudoinverse routine and the three

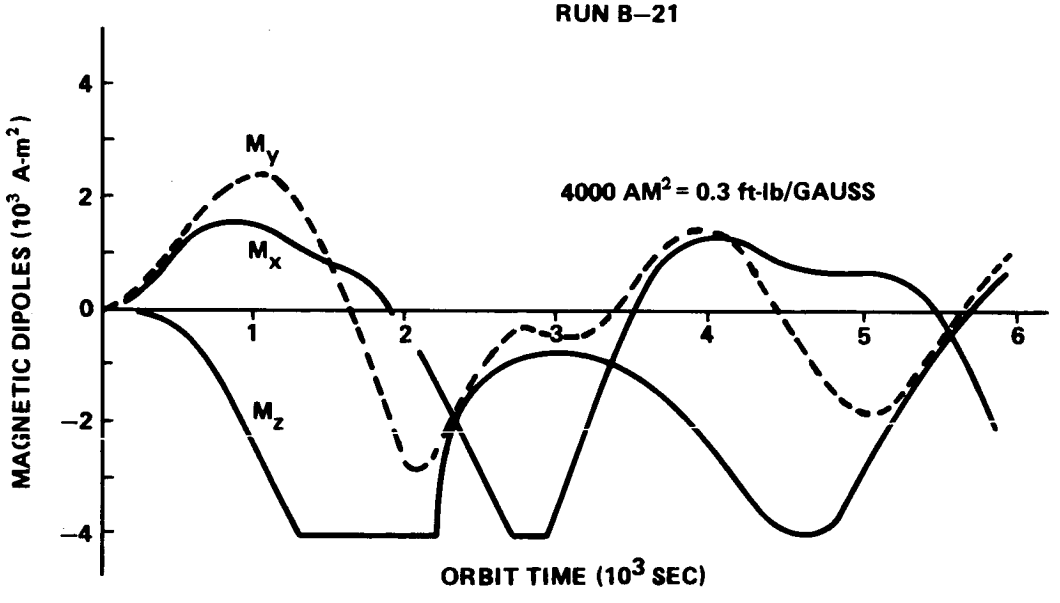

Figure VI-50. Magnetic torquer dipoles to continuously reset the CMGs.

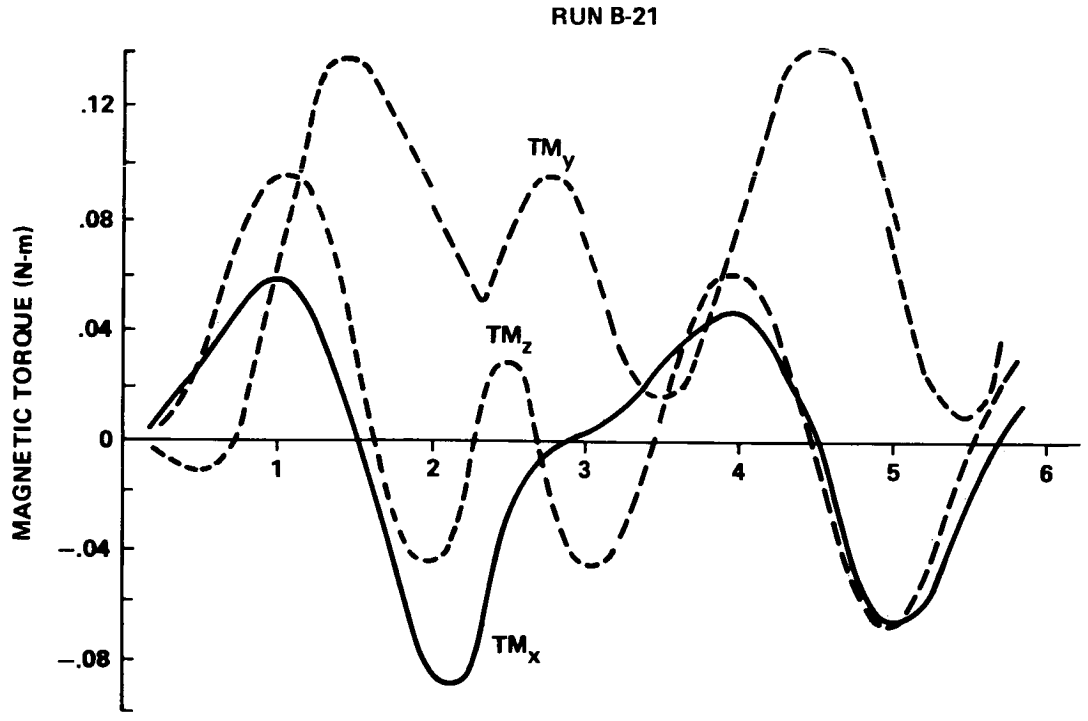

Figure VI-51. Magnetic torque to reset the CMGs.

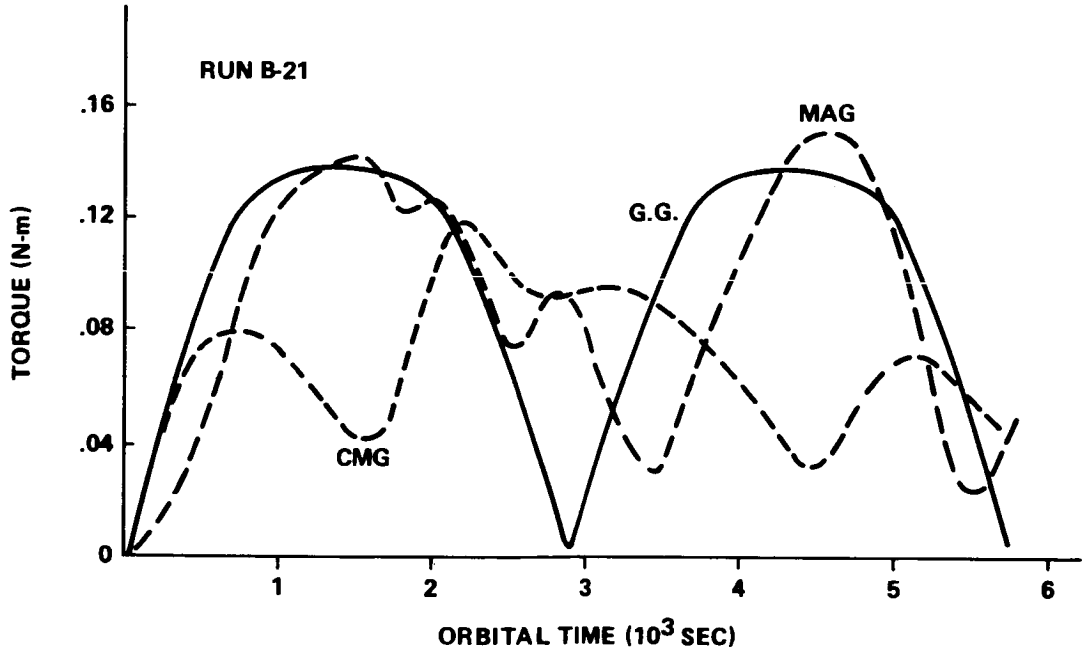

Figure VI-52. Absolute gravity (G.G.), magnetic (MAG) and CMG torque.

operational CMGs were not initialized to a new zero momentum state. At the start of the run, there was a biased momentum of 678 N-m-sec (500 ft-lb-sec) on the positive Z-axis with the gimbal angles at zero. At the initial orbital position, the MTS started forcing the CMGs to a new reference position at which the momentum is zero. After about three-fourths of an orbit, a new CMG null position was established with $\alpha_1 = -35$, $\alpha_2 = 0$, and $\alpha_3 = 35$ degrees and the CMG momentum near zero. During this reinitialization period, the pointing error was less than 0.006 arc sec. During the next orbit, after the new CMG null was established, the performance was the same as with all four CMGs operating (see Figure VI-46). In addition, the CMG gimbal angles deviated less than 4 degrees from their new reference position. Other CMGs were failed with similar results, although in each case, the CMG null reference position would be different.

Since the Z-axis electromagnet is utilized more than others, the dipole limit on the Z-axis as well as CMG Number 4 were set to zero. This situation corresponds to failures of the two electromagnets whose dipoles are aligned with the Z-axis of the LST as well as a CMG failure. The pointing performance was slightly degraded by the other dipoles reacting in more of a nonlinear manner and all the secular g.g. momentum was not dumped. At the half-orbit time point, the pointing error peaked at 0.009 arc sec (as compared with 0.005). By the end of one orbit, only about half the secular g.g. momentum had been dumped. Under worst-case conditions, the three operational CMGs could have been saturated in about 10 orbits. However, it is quite likely that a new vehicle orientation (experiment pointing target) would have been selected during this time interval, thus alleviating the problem. If not, the LST would have to be maneuvered in a g.g. momentum dump sequence. During 10 orbits, however, the earth would have rotated about 243 degrees, with very little change in the orbit relative to solar coordinates and the local vertical, thus drastically changing the geomagnetic field in LST coordinates. Therefore, CMG saturation in 10 orbits may or may not occur. In a subsequent run, the earth was rotated 180 degrees under the orbit so that the north magnetic pole was initially tilted away from the sun. By the end of an orbit, the peak accumulated momentum was about one-fourth that of the maximum g.g. secular momentum. There was no observed increase in pointing errors in this subsequent run. The tentative conclusion is that the three operational CMGs would not be saturated by worst-case g.g. torques even with the electromagnets on one vehicle axis inoperative.

Additional runs were made with and without the MTS in which the momentum per CMG was varied. Without the MTS, the H per CMG could be reduced to 136 N-m-sec (100 ft-lb-sec) and still meet the basic LST

objectives. With this low H value, a singularity of the torque matrix was always approached at about one-half orbit and saturation occurred at about 1.3 orbits. When a singularity internal to the momentum envelope was approached, a pointing error peak of about 10 arc sec was observed over a 100-sec interval, after which, normal pointing performance was maintained until saturation. However, by selecting a different initial gimbal angle set (see Section F.3.d and Figure VI-24), the singularity conditions changed such that none were approached until CMG saturation. In this case, the performance was not degraded by using small CMGs. With the MTS, the pointing performance was the same as that obtained with the baseline momentum value per CMG. The baseline momentum of 678 N-m-sec per CMG could be reduced significantly without affecting the LST performance and still meet all mission objectives.

G. System Implementation

1. Sensors

a. Reference gyro assembly (RGA). The RGA contains six single-degree-of-freedom, Northrop GI-K7G gas-bearing spin axis gyros with their input axes oriented normal to the surfaces of a dodecahedron. Any three gyros can provide three-axis attitude measurement capability.

The gyro pickoffs are maintained at null by pulse width modulated capture loops. During experimentation, each pulse output of the pulse torque loop represents an input axis angular increment of 0.02 arc sec. The output pulses are accumulated in the pulse accumulator of the transfer assembly and sent to the digital processor assembly for further processing and attitude and rate computations.

To provide system accuracy equivalent to a three-axis orthogonal set of gyros as well as onboard fault detection capability, four gyros will be active and their outputs used simultaneously in attitude computations.

The dodecahedron RGA will be implemented in an all-orthogonal structure by the use of three gyro twin-pack assemblies. Each twin-pack will have the two gyros mounted on a plate with their output axes parallel. The input axes of the two gyros will be skewed by 31 degrees 43 arc min 2.9 sec to form a two-plane configuration. When mounted mutually perpendicular, the three plates configure the dodecahedron arrangement.

The electronic subassemblies will be packaged into potted functional modules, each designed to interface with a gyro twin-pack. Each electronic channel consists of a dc power supply, a gyro rotor excitation supply, torque to rebalance electronics, readout and countdown logic, and a gyro temperature controller.

Figure VI-53 defines the RGA configuration and summarizes the performance characteristics.

b. Fixed Star Tracker (FST). The FST characteristics are summarized in Table VI-16 and a simplified sketch of the FST and the electronics block diagram are shown in Figure VI-54. The FST is a conventional image dissector type star tracker that provides two-axis information from the outputs of the two-axis electromagnetic deflection coil currents. An internal threshold can be set by command so that the FST will respond to the brightest star in its FOV having a magnitude of greater than +3.0, +4.0, or +6.0. For magnitudes of +6.0 or higher, additional filtering will be provided to obtain the required accuracy. The noise equivalent angle (NEA) versus star magnitude relations are depicted in Figure VI-54 and show how a reduction in bandwidth through additional filtering can improve accuracy.

The sunshade for the FST is of typical design and will require modifications to fit the mounting location. An attentuation of 10^8 in sunlight or earth shine is provided when the boresight is within 48 degrees of these energy sources.

The following three basic functions are supplied by the power supply:

1. A constant current for the focus coil to maintain gain and linearity.

2. Voltages for the dissector photodiode and dynode chain.

3. Secondary electronics power.

An additional feature may be required by the LST FST to avoid arcing when high voltage is applied at the same time critical pressure exists in the FST. This high voltage arcing can be avoided by pressurizing the tracker for early operation and later venting to the space vacuum. A period of 8 to 10 hours may be required to vent below critical pressure. If early operation is not mandatory, then initial pressurization will not be required, but the venting period is still necessary. This pressurization-depressurization feature is not considered to be a high cost item.

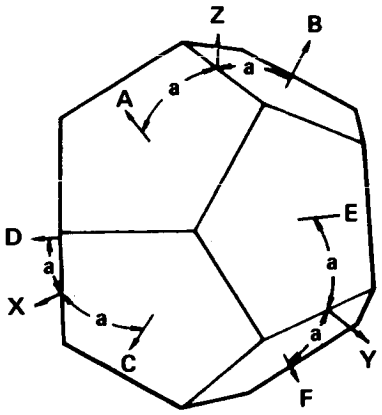

a = 31° 43′ 2.9″
INPUT AXES ORIENTATION WITH RESPECT TO THE REFERENCE TRIAD AND DODECAHEDRON

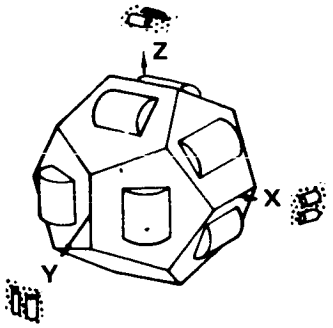

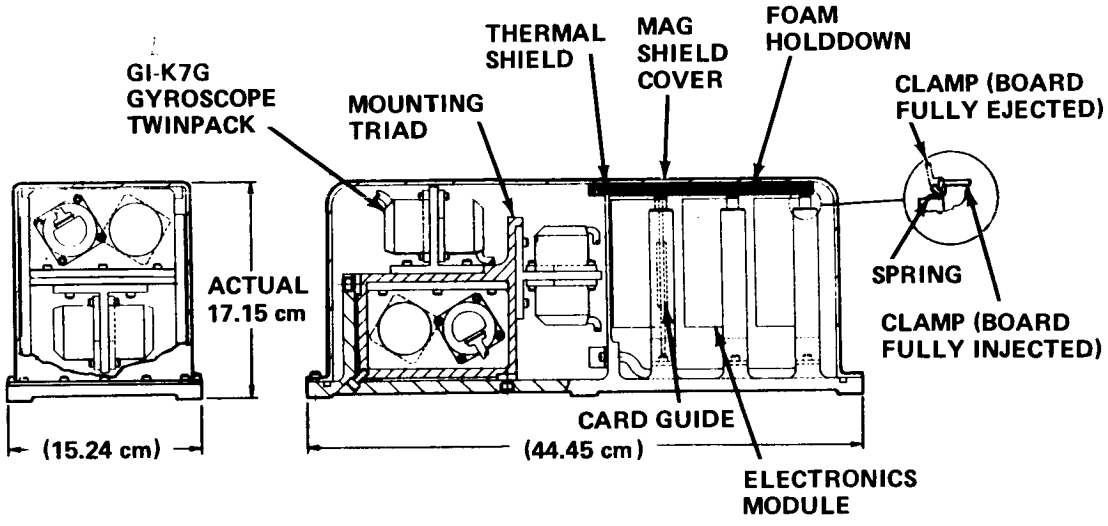

RGA PERFORMANCE CHARACTERISTICS (PER CHANNEL)

QUANTIZATION (FINE POINTING MODE)	0.02 arc sec/pulse
MAXIMUM INPUT RATE PER AXIS	3.0 deg/sec
SCALE FACTOR	
NON-LINEARITY (TO 0.0175 radian/sec)	400 ppm
15 min STABILITY	10 ppm (1σ)
1-yr STABILITY (10°C TO 32°C)	1300 ppm
G-INSENSITIVE DRIFT	0.005 deg/hr (1σ)
DYNAMIC DRIFT (RECTIFICATION)	0.003 deg/hr
INPUT AXES ALIGNMENT	
15 min STABILITY	6 arc sec
30 day STABILITY	30 arc sec
MAGNETIC FIELD SENSITIVITY	4.85 nrad/sec/T

Figure VI-53. RGA configuration and performance characteristics.

TABLE VI-16. FST CHARACTERISTICS SUMMARY

Field of View (FOV) Acquisition Instantaneous FOV	 8 deg × 8 deg 11 arc min diameter
Lens	Super Farron 75 mm f/0.87
Image Tube	F4012 Image Dissector
Sensitivity	6th Mag AO Stars
Accuracy (1 Hz Bandwidth) Noise Equivalent Angle Bias and Drifts Linearity (Calibrated)	 10 arc sec (measured) 6 arc sec 0.1 percent
Position Address Gradient	1 V/deg
Output Signals	X Position Y Position Signal Strength Mode
Input Signals	Command Search On/Off Command Threshold
Power	5 watts (measured)
Input Voltage	+15 Vdc and +5 Vdc
Size	11.4 cm × 11.4 cm × 40.6 cm
Weight	5.4 kg (12 lb)
Design Features Integral Bright Object Sensor and Shutter High Reliability Image Dissector Signal Strength Output Tracks Brightest Star Above Threshold Commandable Thresholds Sunshade to Provide Minimum of 10^8 Sunlight Attenuation	

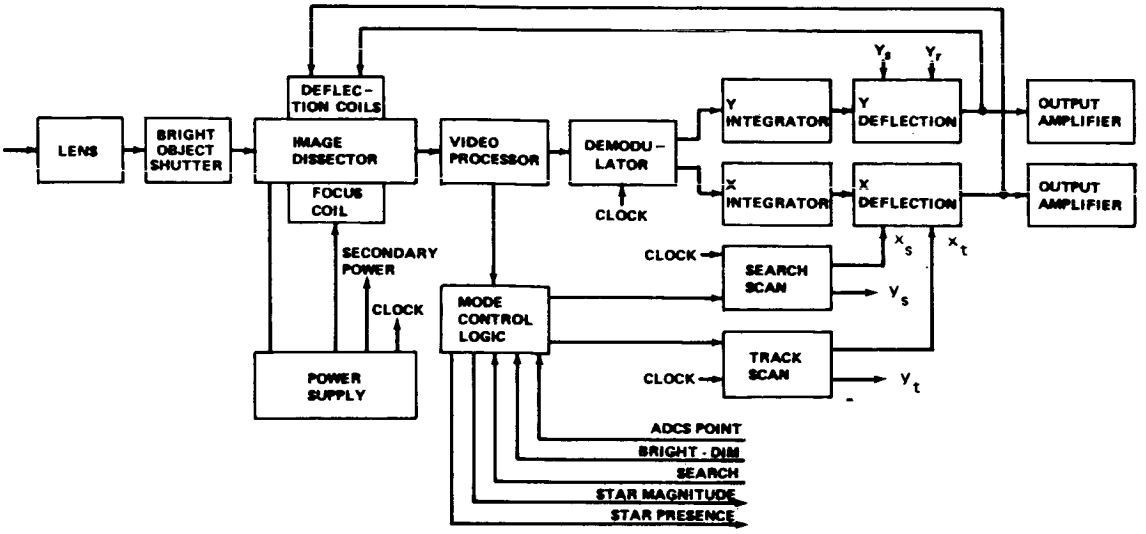

CUTAWAY OF F4012 IMAGE SECTION

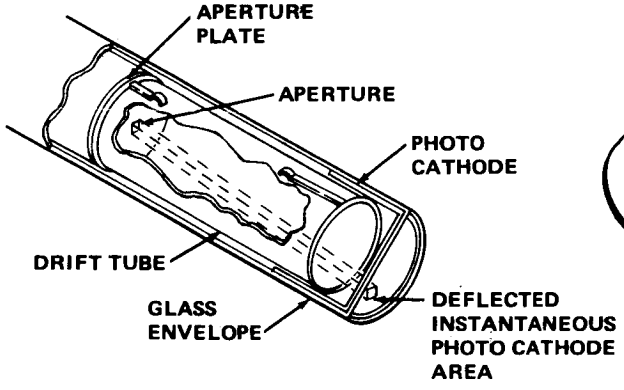

STAR TRACKER ASSEMBLY

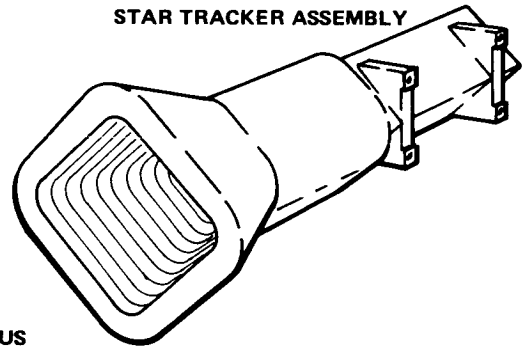

NOISE EQUIVALENT ANGLE VS STAR MAGNITUDE

NOISE EQUIVALENT ANGLE (NEA) OR RMS TRACKING ERROR HAS BEEN MEASURED FOR SEVERAL BANDWIDTHS. IN THE POINTING MODE, THE BANDWIDTH OF THE SENSOR CAN BE LOWERED FOR 1 Hz AND THE NEA REDUCED CONSIDERABLY.

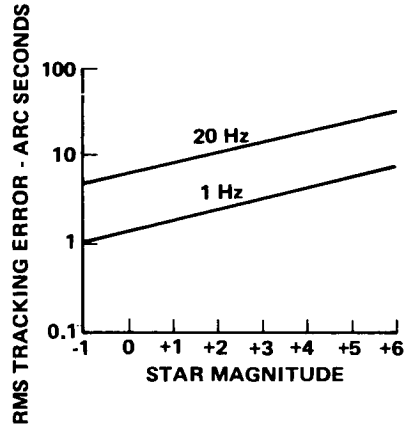

Figure VI-54. FST and electronics.

c. Coarse Sun Sensor (CSS). Each of the five identical CSSs is a two-axis, dual mode, (2π steradian FOV with a ±10 degree linear range) analog sun sensor manufactured by Bendix Corporation. It is similar to the model 1771858 unit except the glass dome is to be replaced by a quartz cylindrical dome.

Each unit consists of 12 solar cells (Fig. VI-55) with four of the cells mounted in a quad cell arrangement in a plane normal to the CSS optical axis. Light reaching these cells passes through a square aperture placed in front of the quad cell. Symmetric error signals are obtained by electrically differencing output currents from diametrically opposed cells in the TA. The quad cell provides the ±10 degree linear output which decreases for offset angles larger than 10 degrees. The remaining eight cells are placed around the periphery of the quad cell in an octagonal arrangement. These cells are placed at right angles to the plane of the quad cell and are biased off mechanically in the central 20-degree cone about null by a shadowing boss extending into the FOV of the peripheral cells. The peripheral cells provide sunline polarity information over the remainder of the hemisphere not covered by the quad cell by electronically differencing diametrically opposed pairs of cells in the TA.

The following is a summary of the physical and functional characteristics of the CSS:

Mass	0.1 kg (0.20 lb)
Size	4.8 cm × 4.1 cm Baseplate — 6.4 cm diameter
Power	None, a passive device
Detector Type	Silicon solar cells (12 cells)
Output	0 to 5 mA
Null Sensitivity	0.20 mA/deg
Linear Range	±10 degrees, both axes
Linearity	2 percent
Null Accuracy	6 arc min

d. Magnetometer. The magnetometers manufactured by Dalmo-Victor and used on the OAO spacecraft are suitable for the LST. This fluxgate type magnetometer measures the geomagnetic field along each of the vehicle axes and converts this to a dc voltage. The following are principal characteristics:

1.	Range	±60 microtesla
2.	Sensitivity	4.167×10^{-2} Vdc/microtesla

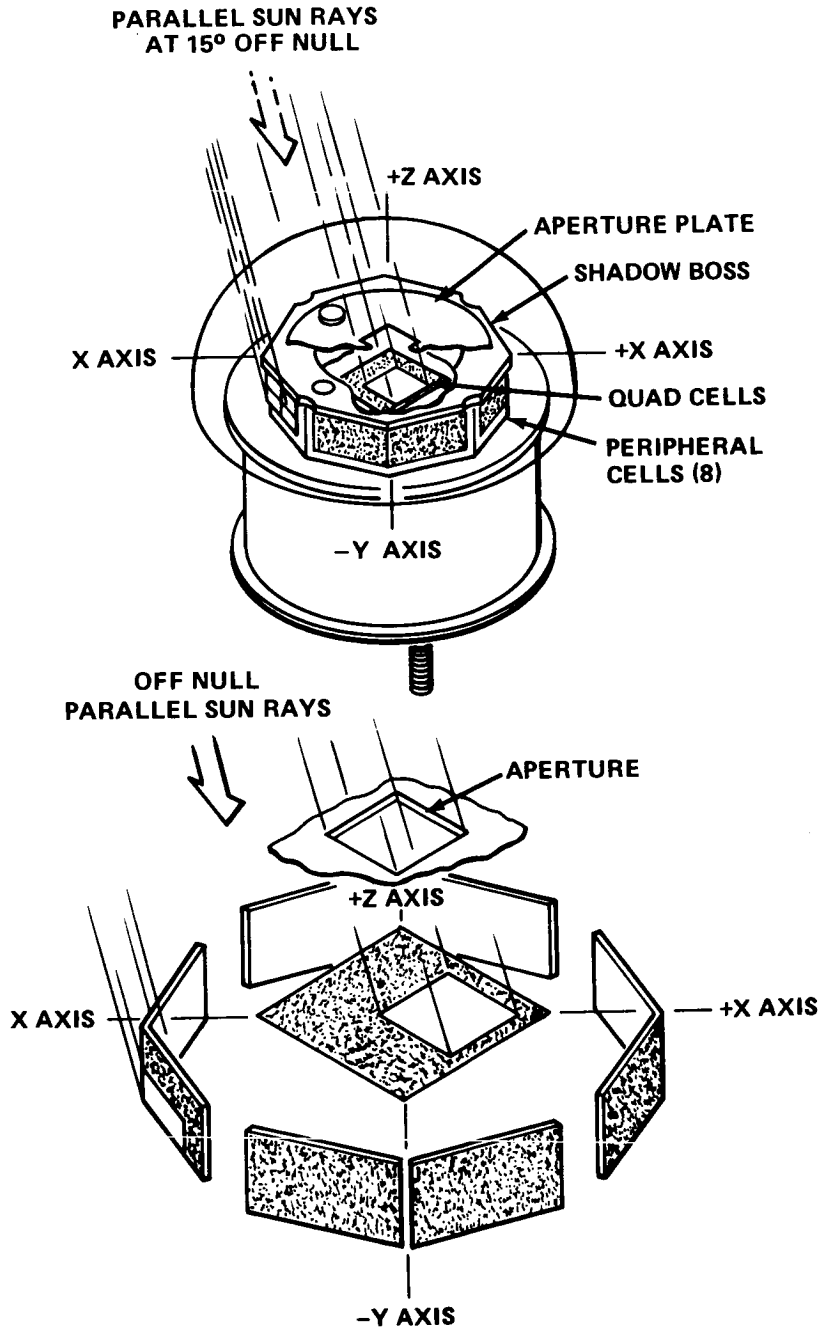

Figure VI-55. Coarse sun sensor operation diagram.

3.	Dimensions	26.7 cm × 12 cm × 12 cm
4.	Frequency Response	280 Hz
5.	Mass	3 kg (6.5 lb)
6.	Power	2 watts

To avoid distortion of the measured geomagnetic field, the magnetometer will be located on the spacecraft with as much separation as possible from the magnetic torquer coils. Other extraneous magnetic fields must also be considered. However, the magnetic torquer coils are considered to be the major source of interference to the magnetometer measurements. If the physical locations of the components do not solve the magnetic interference problem, an alternate scheme of sampling the magnetometer outputs can easily be implemented. In this scheme, the outputs of the magnetometer can be sampled at intervals of roughly 1 min while the torquing currents to the coils are turned off. This procedure should be satisfactory because of the slow geomagnetic field changes (two cycles per orbit) that occur as the LST orbits the earth.

2. Actuators

a. Control Moment Gyros. The design reference CMG system requires four SGCMGs arranged in the configuration described in Section F.3 and shown in Figure VI-20. Each CMG assembly is complete with an active and redundant drive electronics assembly (DEA) and requires only primary power input for operation.

The CMG selection for LST is based on the report cited in Reference VI-1. As the HEAO CMG design and specifications become finalized, the CMG selection for LST will be updated to preserve commonality.

Figure VI-56 is an outline drawing of the CMG assembly. Basic functional and physical characteristics are:

1.	Momentum	610 N-m-sec, nominal Speed Control 1.0 percent 407 to 814 N-m-sec
2.	Runup and Rundown Time	4 hr, nominal
3.	Steady State Gimbal Torque	8.4 N-m, minimum

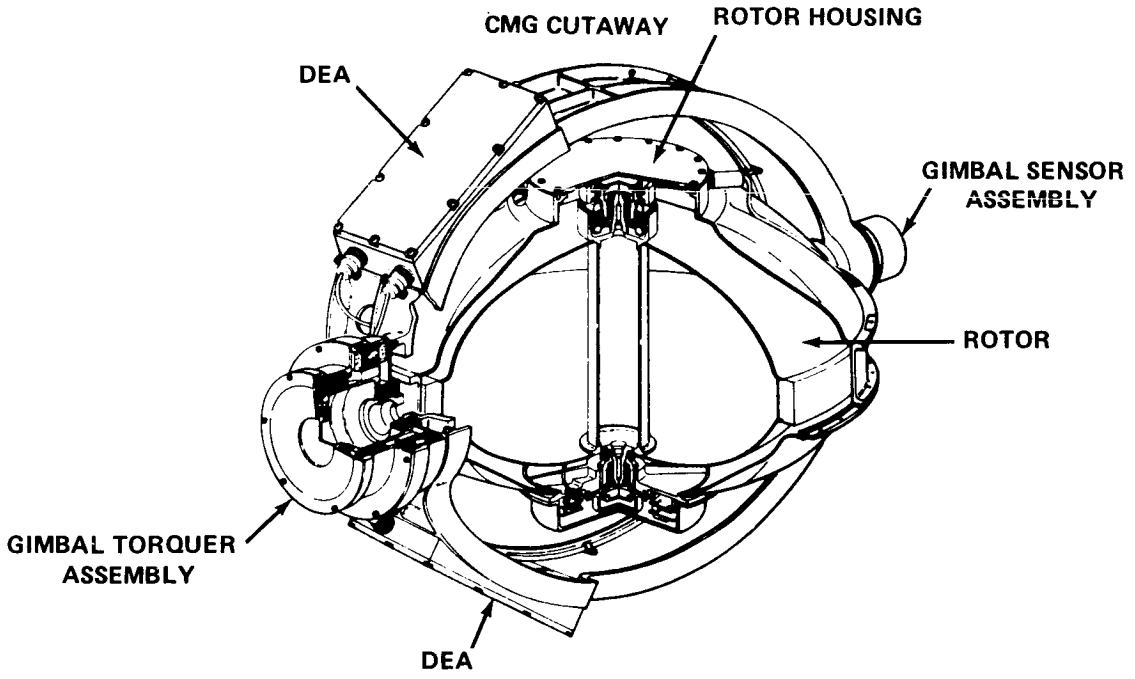

Figure VI-56. CMG cutaway drawing.

4.	Peak Gimbal Torque	13.6 N-m, minimum
5.	Minimum Commandable Rate	0.005 deg/sec to 0.05 deg/sec
6.	Steady State Spin Motor Power	14 W nominal, 33 W max
7.	Spin Motor Runup Power	90W, max
8.	Torque Motor Power (At Steady State Torque)	14 W, max
9.	Static Balance	3.5×10^{-4} N-m
10.	Dynamic Balance	3.5×10^{-3} N-m^2
11.	Monitoring Signals	
	a. Gimbal Rate: Range, Accuracy	±10 deg/sec, ±1.0 percent
	b. Wheel Speed Accuracy	±1.0 percent

c.	Spin Motor Current Accuracy	±3.0 percent
d.	Spin Bearing Temperature Accuracy	±5.0 percent
e.	Torque Motor Current Accuracy	±3.0 percent

Two major departures from the HEAO CMG assembly design are required to meet LST pointing requirements. First, the gimbal control electronics must include proportional plus integral control to reduce the effects of the CMG gimbal nonlinearities. In conjunction with this change, the outer control loop that includes the sensors, CMGs, and vehicle dynamics must have compensation to conform with the CMG gimbal design and integral networks to provide the high gain at low frequency necessary for very small angle errors in the presence of disturbance torques. Second, shock mounts to isolate CMG force and torque disturbances from the LST structure will be required to maintain the LOS optical stability. Both of these subjects were discussed in Section F, the system performance and analysis section of this document.

b. Magnetic Torquer System (MTS). The complete design details, operation descriptions, and performance analysis are contained in Section F.4.

c. Reaction Control System (RCS).

(1) Configuration Summary

(a) General. A functional schematic of the RCS selected for the LST is shown in Figure VI-57. The RCS is a pressure regulated, gaseous nitrogen, propulsion system modularized into three basic elements — a propellant tank, a black box, and two major thruster modules. Auxiliary items, most of which are contained in the black box, are latching solenoid isolation valves, filters, pressure regulators, check valves, pressure and temperature transducers, pressure gages, manual shutoff valves, pneumatic disconnects, propellant fill and drain valve, wire harness, and interconnecting plumbing. The RCS elements are assembled in the SSM as shown in Figure VI-58. A mass statement for the RCS is shown in Table VI-17.

The significant RCS features are as follows:

1. Twelve thrusters are used; six are active and six are standby.

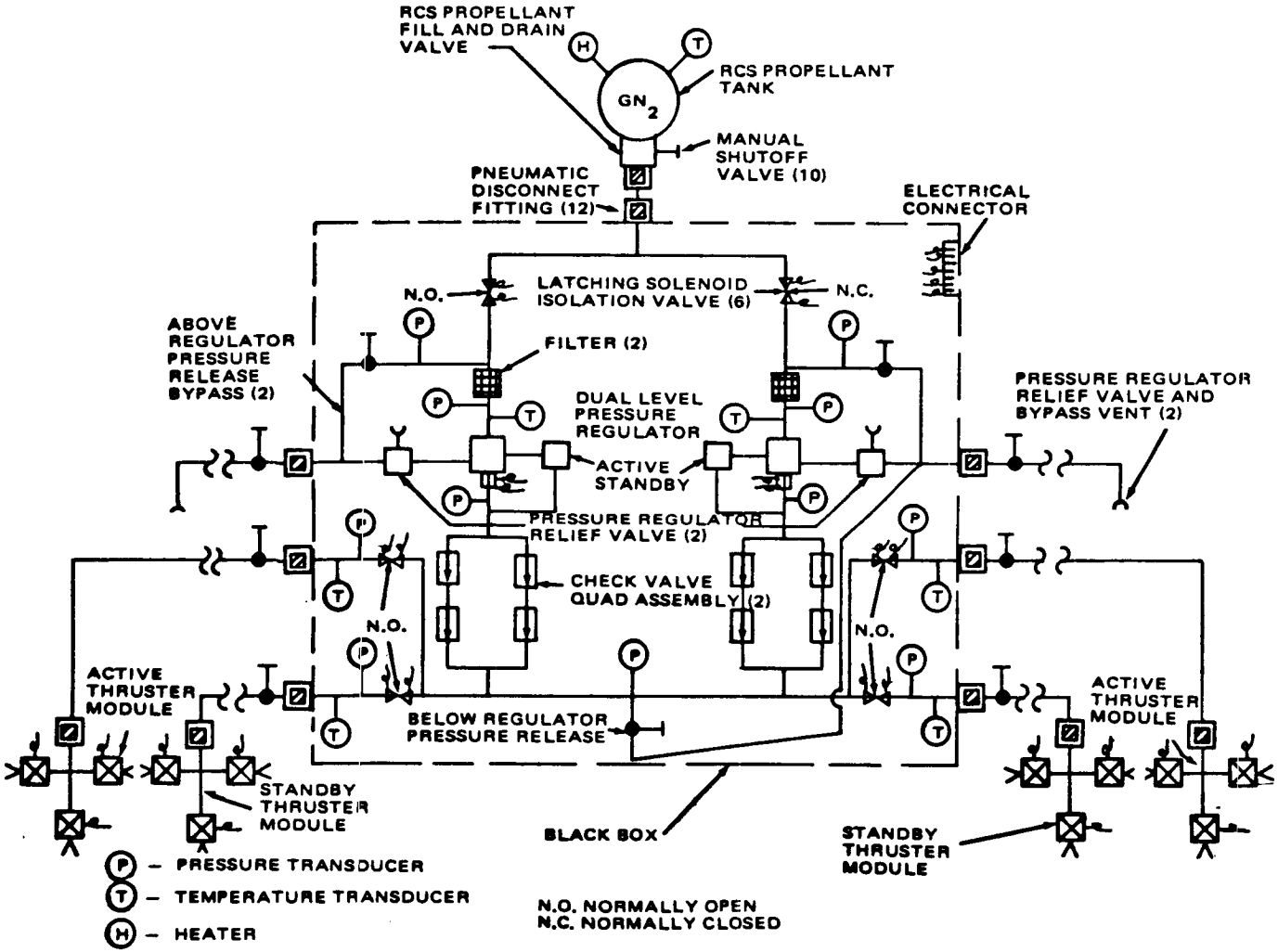

Figure VI-57. LST reaction control system schematic.

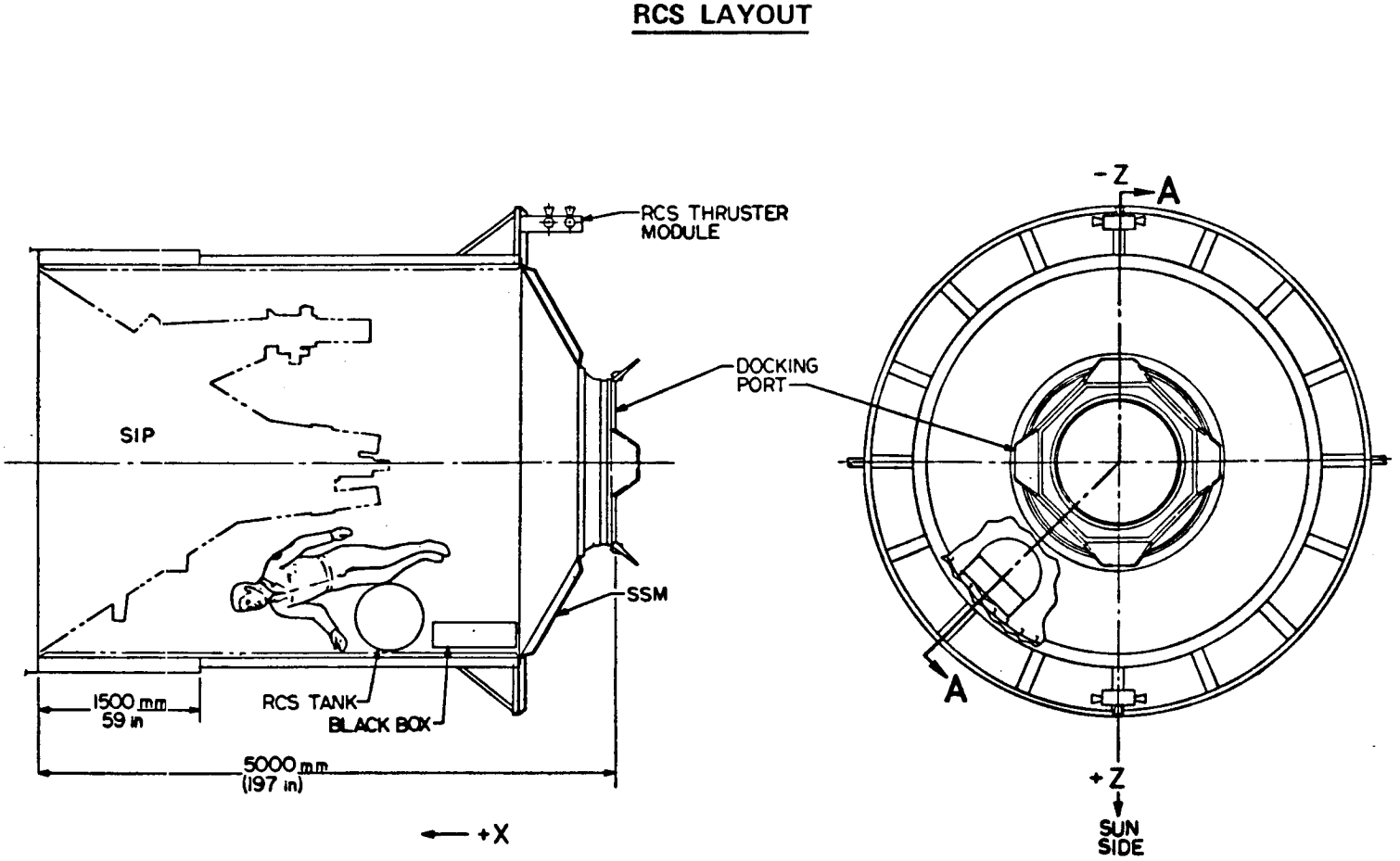

Figure VI-58. Layout of the LST Reaction Control System major component locations.

TABLE VI-17. REACTION CONTROL SYSTEM MASS SUMMARY

Item	Mass (kg)	Mass (lbm)
Tank, Including Thermostats and Heaters	25.54	56.30
Manual Shutoff Valve (10)	4.54	10.00
Solenoid Isolation/Shutoff Valve (6)	10.89	24.00
Pressure Regulator, Including Relief Valves and Filter (2)	7.26	16.00
Check Valve, Quadratic Assembly (2)	0.73	1.60
Pressure Transducer, Other than Regulator (6)	0.76	1.68
Pressure Gage (3)	0.54	1.20
Temperature Transducer, Other than Tank (6)	0.41	0.90
Thruster Module, Major (2)	9.07	20.00
Plumbing and Fittings	9.07	20.00
Black Box Structure	9.07	20.00
Tank Retention and Other Structure	6.80	15.00
Systems Dry Mass	84.68	186.68
Propellant GN_2 [a]	19.50	43.00
Total System Mass	104.18	229.68

a. Redundant Propellant ≈ 1.36 kg (3.00 lbm).

2. One tank is utilized to store the GN_2 propellant.

3. A dual-level pressure regulator is used. With the regulator operating in the high mode, the thrust level is 44.48 N (10 lbf). With the regulator operating in the low mode, the thrust level is 2.22 N (0.5 lbf).

4. With the exception of the tank, RCS component redundancy is available.

5. Modularization of the RCS provides for ease in maintenance.

6. Most components are off-the-shelf items.

(b) Propellant Tank. In determining the amount of propellant needed to satisfy the allocated impulse budget (see Section F.5) for the LST, it was assumed that the RCS will provide an average theoretical specific impulse of 65 seconds, resulting in a GN_2 requirement of 17.69 kg (39 lbm).

An investigation to determine the availability of existing GN_2 storage tanks revealed two that could be considered for application to the LST RCS. One is a GN_2 tank used in the Skylab thrust attitude control system (TACS) and the other is a cold gas storage tank used in the backup RCS for the Lockheed Satellite Control Section.

The Skylab tank shell is made of 6Al-4V titanium alloy. The tank is spherical with a diameter of approximately 0.61 m (2 ft), weighs 53.07 kg (117 lbm) empty, and is man-rated. In a fully-loaded operating condition, the tank contains 28.58 kg (63 lbm) of GN_2 at an operating pressure of approximately 2.14×10^7 N/m^2 (3100 psi). The McDonnell Douglas Corporation provides the tank for the Skylab TACS.

The Lockheed Satellite Control Section backup RCS tank selected is also made of 6Al-4V titanium alloy. The tank (manufactured by Pressure Systems, Inc. for Lockheed) is spherical with a diameter of approximately 0.57 m (22.25 in.), weighs 25.54 kg (56.3 lbm) empty, and has a safety factor of 2.0 (burst pressure/operating pressure). In a fully loaded operating condition, the tank contains approximately 19.50 kg (43 lbm) of GN_2 at an operating pressure of 2.07×10^7 N/m^2 gage (3000 psig). The Lockheed tank was selected because its capacity approximates that needed for

the LST emergency modes. The tank consists of two forged hemispheres which are tungsten-inert-gas welded to a transition joint to form a sphere. The tank assembly has a thermal management system which includes a flight heating system and a ground heating system, each containing two heaters, a thermostat, and an electromagnetic interference (EMI) suppressor. Associated with the thermal management system are two electrical connectors and a temperature sensor. The tank is covered with multilayer insulation, such as aluminized mylar. When the tank is applied to the LST RCS, the ground thermal management system will be deleted.

The Lockheed tank has been qualified to perform to the Satellite Control Section requirements during exposure to orbital conditions for a period of 6 months. How much longer the tank can perform beyond this time period is unknown. There is no known reason why the tank cannot perform under orbital conditions for 2.5 years or beyond; however, testing to prove this would be required.

Since the tank has only a single port, an integral manual shutoff/fill and drain valve associated with this port will be required. Associated with this valve will be a pneumatic disconnect fitting to provide an attachment for the propellant supply line which leads to the black box. This same fitting will also be used for filling the tank. The addition of the valve/pneumatic fitting to the tank will be a necessary tank modification.

Since a bump or scratch on the surface of the tank when fully loaded could cause the tank to explode, a protective cover around the tank will also be required. Other necessary modifications to the tank and to what extent the tank should be requalified for application to the LST RCS should be determined in the LST Phase B study effort.

(c) Black Box. The black box houses the numerous auxiliary RCS components (valves, regulators, etc.) as well as a few primary RCS components which cannot easily be replaced on orbit on an individual basis. Should a component in the black box fail and cause the successful operation of the RCS to be in jeopardy, the black box can simply be replaced during an LST maintenance period. Because of the large number and type of components in the black box, and hence the greater probability of a failure, complete redundancy in black box components was provided.

Even though the components in the black box are existing items, the black box does not exist. As a proposed concept, the black box is to consist of two primary structural members — a baseplate and

a protective cover. The baseplate will be designed as the load-carrying structure for the internal and external components. Mounting structure will be provided on the baseplate for attaching the individual components and for retaining the plumbing, pneumatic disconnects, and wire harnesses. The baseplate will also have the necessary structure for attaching the box to the SSM. A protective cover will fit over and attach to the baseplate. The cover can be made of fiberglass or some lightweight sheet metal.

The black box will be designed and configured for minimum weight and volume, and for ease in handling; however, for purposes of this study, the box is envisioned as being rectangular and measuring 0.18 m × 0.51 m × 0.71 m (7 in. × 20 in. × 28 in.).

(d) Thruster/Thruster Module. Since the RCS is an LST backup control system, the thrust level and minimum impulse bit (MIB) requirements could vary over a broad spectrum. RCS control requirements for very small LST disturbances as well as for very large LST disturbances could be necessary; therefore, rather than optimize a thrust level, an MIB, and a thruster system for the LST, an existing system was selected that is thought to most nearly satisfy the expected LST thruster requirements.

The Agena RCS thrust valve cluster is selected as the basic thruster module for the LST RCS. The solenoid-operated thrust valve cluster consists of three identical thrust valve cartridges mounted on a single manifold containing a pressure port and electrical receptacle common to the three valves. As shown in Figure VI-57, four of these modules are utilized by the LST RCS. Two of the modules are active and two are standby. An active module and a standby module are clustered into a single major module for mounting to the LST (Fig. VI-58). The two major modules are mounted 180 degrees apart, and each module is located 90 degrees from the solar panel support structure. This arrangement minimizes the thruster plume impingement on the solar panels. The thruster modules are mounted to the LST as far aft as possible and as far radially as possible to take advantage of the maximum lever arm distance which in turn minimizes the propellant weight required. The structural makeup of the major module and its design for attaching to the LST should be determined in the Phase B study. However, the method selected for attaching the modules to the LST must be simple enough for man to be able to replace them by means of an extravehicular activity (EVA).

(2) LST RCS Maintenance Procedure. Reference is made to Figure VI-57 in conjunction with the following description of the LST RCS maintenance procedure. Assume that, during one of the LST maintenance

visits, the RCS propellant is found to be almost depleted, a major component failure has occurred in the black box, and one of the major thruster modules has been switched to its standby system because of a valve failure in the active system. During this maintenance visit, the GN_2 tank would need to be refilled or replaced with a full tank, the black box would need to be replaced, and one or both of the thruster modules would need to be replaced.

Maintenance of the RCS is initiated by bleeding down the pressure inside the RCS to equal the pressure inside the SSM. With the pressure inside the RCS equivalent to that in the SSM, the manual shutoff valve on the tank and in each line leading to the exterior of the spacecraft is closed. A pneumatic fitting at the tank, which connects the tank to the line leading to the black box, is disconnected. After an electrical connection to the tank has been disconnected, the tank is removed from its support rack structure and placed in the Shuttle supply/spares area.

Next, the black box is removed from the SSM. Removal of the black box consists of disconnecting seven pneumatic fittings — one fitting for each line which leads to the exterior of the spacecraft and the fitting for the line which leads from the tank — the black box electrical connector, and removal of the black box from its support structure. A new black box is placed in proper position in the SSM and is connected following the reverse of the procedure used to remove the old black box.

If GN_2 resupply facilities are on board the Shuttle, the tank will be refilled and reconnected to the LST RCS; otherwise, the Shuttle will have to bring a fully-loaded replacement tank from the ground, and the old tank will be flown back to the ground for resupply and later use. Regardless of the resupply method, the tank is placed in its support rack structure and is connected following the reverse of the procedure for its removal, except that the tank manual shutoff valve will not be opened until the RCS is together and ready to operate. In the interest of safety during a maintenance visit, it is suggested that the fully loaded RCS tank be one of the last items to be placed in position prior to the astronaut's leaving the SSM.

The major thruster module will have to be replaced by means of an EVA. The two feed lines leading to the module are easily disconnected by means of a pneumatic disconnect similar to that used on the black box. The two electrical connections to the module are disconnected and, by some simple means, the entire module is separated from the LST. The reverse of this procedure is followed in mounting the new module. The expected life remaining in the other module determines whether or not it should also be replaced during this maintenance visit.

A worst-case RCS maintenance procedure was just described. Of course, any one major element can be replaced without having to replace the others. The described RCS checkout procedure is only suggestive and is subject to variation.

(3) Conclusions and Recommendations. The RCS described herein is a simple, regulated GN_2 system modularized into three basic elements to provide ease in manned orbital maintenance. Most of the components are existing and are used in operational space systems. However, some of the components may need to be modified and quality-tested for application to the LST. The use of these existing components will result in a low-cost RCS for the LST spacecraft.

Modularization of the RCS also provides for growth potential. Should the RCS propellant budget increase substantially, the black box can be modified for the connection of additional tanks, or a single common manifold can be provided for the tanks which, in turn, connects to the black box. Modification of the black box would not be necessary with the common manifold approach. Volume is also available in the SSM for additional propellant tanks.

During the LST Phase B study, considerable attention should be devoted to determining the exact requirements for an RCS on the LST. Should the desirability for an RCS on the LST continue to exist, an effort should be made to keep the impulse budget low enough for the RCS to remain a simple GN_2 system. From the standpoint of reliability, lifetime capability, system cost, and contamination effects, it is desirable that a GN_2 RCS be retained for the LST instead of a hydrazine or hot gas system.

Should a GN_2 RCS be selected for the LST during the Phase B study effort, a detailed study should be performed to determine whether the RCS should be a simple blowdown or regulated system. The reliability needed in RCS components as well as the extent of redundancy in these components should be determined. The feasibility of the RCS maintenance method should also be investigated. Also, since dry nitrogen gas will be used by the LST onboard contamination control system (CCS), an analysis should be performed to determine the feasibility of using a common GN_2 supply source for the RCS and the CCS.

A complete description of the RCS selected for the LST will be published in a NASA TM X.

3. Signal Processing

a. Transfer Assembly (TA). The TA combines in one assembly all circuits and processing functions that are required to interconnect and operate the various ACS assemblies and to provide their interface with other LST subsystems as required. The TA is a modified HEAO design based on LST ACS and overall systems requirements. It consists of the following subassemblies:

1. Sensor buffer unit (SBU).

2. Computer input/output unit.

3. Command and telemetry unit (CTU).

4. Power converter unit (PCU).

5. Power switch unit (PSU).

The SBU contains all the circuitry for buffering and processing the gyro and coarse sun sensor signals. By ground command, four gyros of the RGA are selected using the SBU gyro select logic, and the gyro outputs are processed by a set of four pulse accumulators. The accumulators are strobed and reset on command by the DPA. The circuitry for the emergency sun acquisition mode that uses the CSS data to command the RCS is provided by the SBU. Selection logic for the FSTs and magnetometers also exists in the SBU.

The computer input and output units provide the buffering interface between the DPA and the ACS and other subassemblies. The input buffering has three functional circuits: Bilevels; analog to digital; and serial digital. The bilevels serve as a power enable signal for each DPA module and determine the DPA operating configuration. The analog signals originate at the sensors and actuators and each input is selectively multiplexed and applied to the A/D converter.

The CTU provides the interface buffering for most of the ACS and permits ACS data to be handled by software routines within the DPA. This concept simplifies the wiring and interfaces and provides the maximum flexibility for data handling without affecting the hardware interface. A telemetry buffer provides for a temporary storage of 16-bit words from the DPA. The arrangement allows the DPA to output telemetry data in large batches at less frequent intervals, thus reducing a critical timing burden on the DPA. Command processing is provided by an input register, control logic, and TA

command storage designed to interface with the remote command decoders of the C&DH system. TA command data such as power enables, mode selection, etc., are identified, received, and placed in the TA command storage register. All other command data are directed to the computer input unit for inputting to the DPA. Cross strapping allows inputs to be used with either redundant TA.

A power converter unit derives secondary power from primary power and supplies this to ACS subsystems, primarily the DPA and TA, as required. It also provides electrical isolation to selected TA and ACS circuitry.

By application of power, the power switching unit provides the relays and circuits for switching and selecting all assemblies within the ACS. Each redundant TA can independently select any combination of assemblies within the ACS. The redundant TAs are provided with the input and output cross strapped signals.

b. Digital Processor Assembly (DPA). The design reference DPA selected is a modular internally redundant version of the Control Data Corporation (CDC) 469 computer that was also selected for HEAO. Modifications to the DPA software to conform to the LST ACS mission requirements will be made, but the hardware will be essentially identical to that used in the HEAO.

A general block diagram of the DPA is shown in Figure VI-59 complete with the cross strapping to interconnect the DPA central processors with either redundant TA. An input/output block diagram of a basic single central processor unit is shown in Figure VI-60.

Characteristics of the DPA are:

1. Dual redundant CPU.
2. Six 2000-word, self-contained memory modules.
3. Modules interconnected via dual redundant buses.
4. Secondary power obtained from the TA.
5. P-MOS/LSI technology.
6. 16-bit instruction and data words.

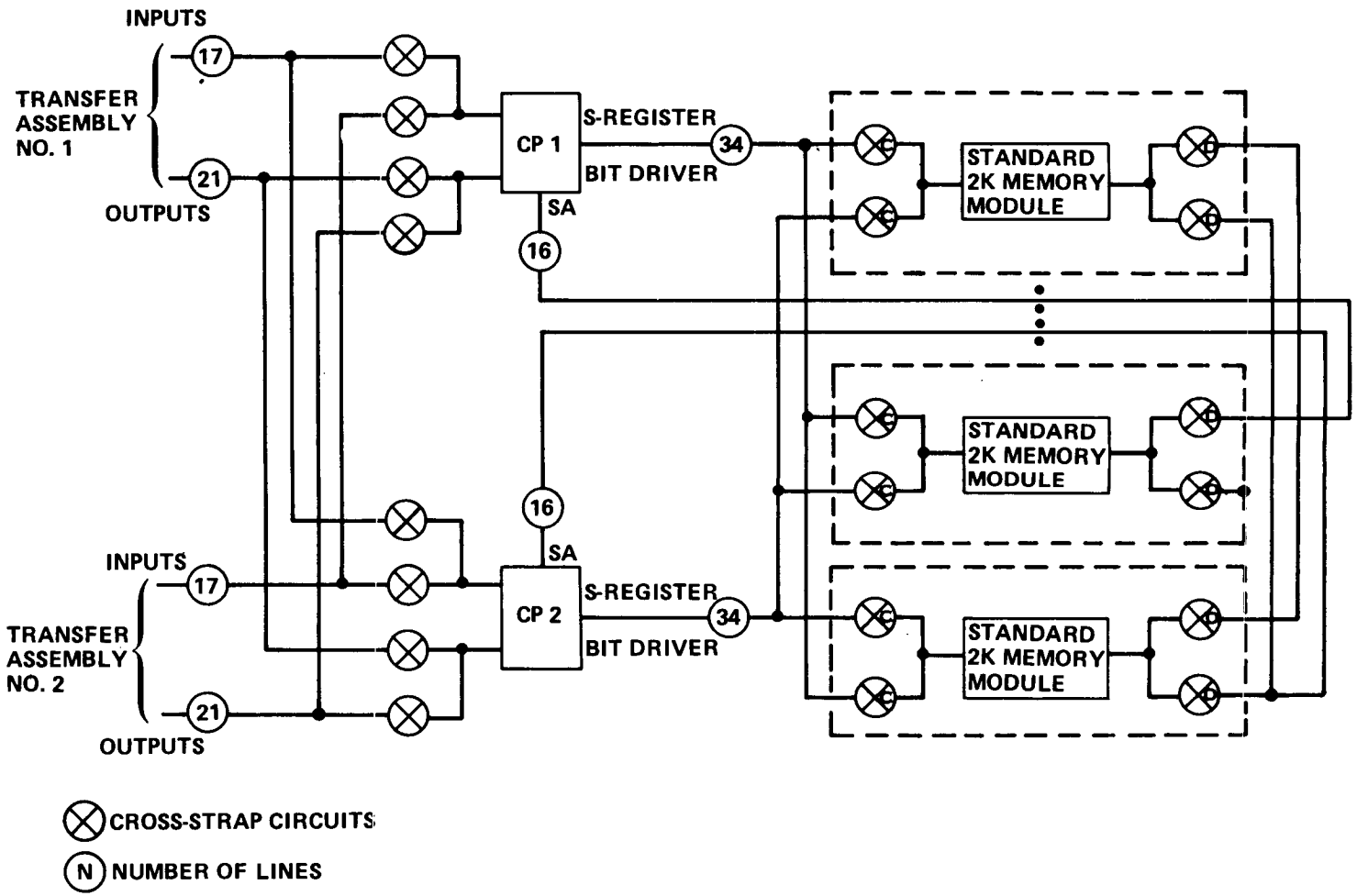

Figure VI-59. LST ACS DPA functional block diagram.

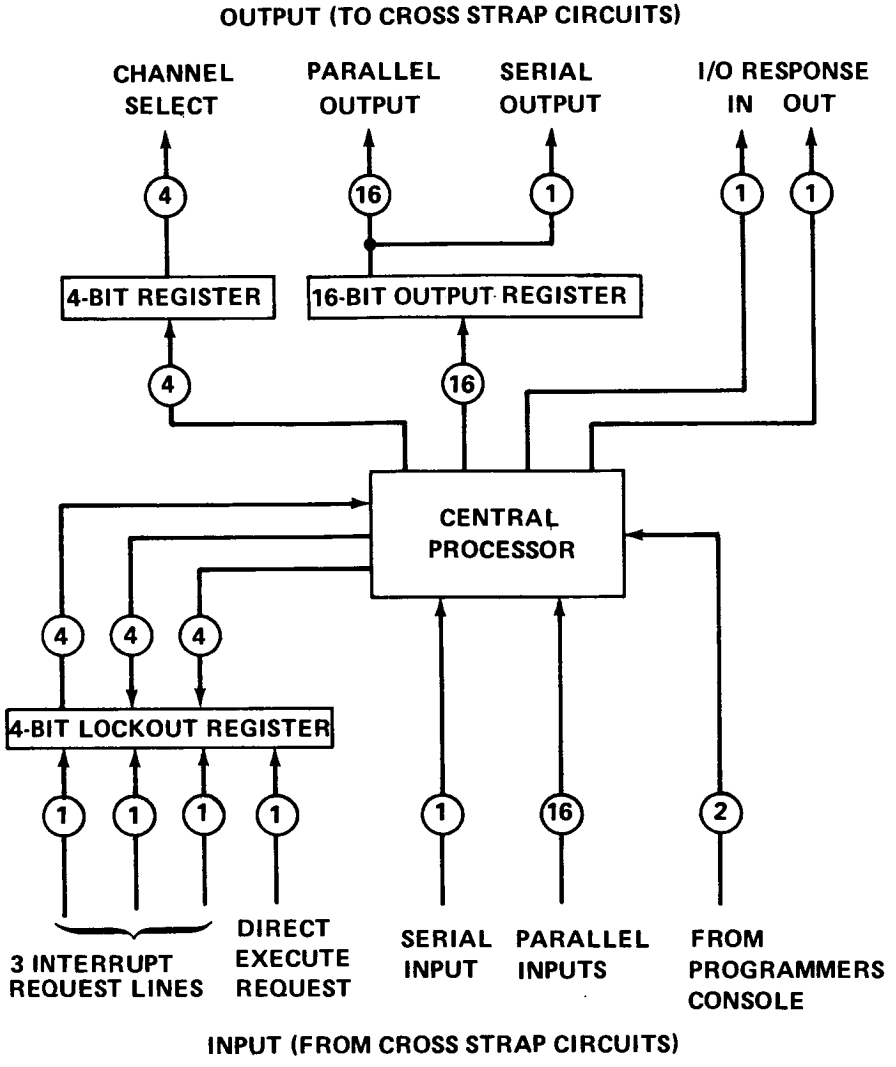

Figure VI-60. Basic single central processor unit input/output block diagram.

7. Fixed point fractional two's complement arithmetic.

8. 5-mil, NDRO plated wire memory.

9. 42 instructions.

10. 4 index registers.

11. 3 interrupt levels.

12. Memory expandable to 64 000 words in 2000-word increments.

The operating configuration of the DPA is controlled and selected by the online TA. Each module of the DPA receives a separate bilevel power enable signal from the TA that places it either in an operating or standby mode. The DPA is then reset and initialized by a control signal sent to the operating CPU. This causes the program counter to be initialized to a known starting location from which the first program instruction is fetched.

As part of the normal executive program function, the CPU transmits a discrete signal to the TA each time the program completes a major program cycle. This signal causes the fault timer in the TA to be zeroed. In the event that either the selected CPU or memory module have failed to the point at which the operating configuration cannot proceed through a normal program cycle, the TA fault timer will overflow, indicating an inoperative system. At this point, the DPA is shut down until commanded into a new configuration by the ground station.

A provision is incorporated to bootstrap a new program into the memory units via the uplink command system. This is accomplished by loading a few selected memory locations with a "bootstrap loader" routine via the externally forced direct execute instruction. The processor is then initialized by the TA and proceeds to software bootstrap the remaining program into memory.

H. Conclusions and Recommendations

The design reference ACS used in conjunction with the OTA fine guidance system (FGS) will satisfy the LST pointing requirements. The dodecahedron RGA using four active gyros, with frequent updating by the OTA FGS error signals, will provide sufficient accuracy to meet the 1 arc sec, 3-axis, pointing requirements during experimentation. Two-axis control of the LOS to maintain a 0.005 arc sec pointing stability requires tip and tilt positioning of the secondary mirror in response to FGS star tracker outputs. During occultation of the FGS guide stars the RGA can provide the sensing function to maintain the LOS excursions within the limits of the FGS coarse fields-of-view.

Sensor noise (RGA and FGS) is critical to obtaining the required 0.005 arc sec pointing stability and will be one of the primary factors limiting the body pointing capability of the ACS and the pointing stability. A thorough investigation of sensor noise must be continued. Estimates of the FGS noise indicate that the expected levels are acceptable. However, these estimates in general have been based on photon noise studies and more detailed investigations are required to determine the FGS total system noise. Gyros in the RGA are marginal from a noise standpoint and realistic noise factors must be established, followed by development of techniques to minimize the effects of gyro noise.

The system signal processing concept and the interface operation of the RGA, FST, and FGS requires further analysis. Digital versus analog or hybrid techniques should be analyzed and recommended designs generated. The designs should be confirmed by prototype system tests.

The nonlinear properties of the CMG gimbal components are a source of pointing instability. These properties include friction, tachometer noise and threshold, electronics dead zones, torque motor threshold, and angle resolver threshold. Investigations in this area must be continued to obtain realistic nonlinear models and to obtain CMG system designs that minimize the effects of nonlinearities.

Internally generated CMG forces and torques when transmitted by the LST structure to the critical optical components generate pointing errors. This vibration propagation and its effects must be thoroughly investigated. Detailed dynamic models of CMGs should be generated and realistic force and torque signature data accumulated. Properly designed shock mounts can reduce the pointing errors, and rotor speed selection to avoid structural reasonances can further reduce the errors to a level consistent with the overall pointing requirements. These factors should be included in any CMG studies.

A digital processor dedicated to the attitude control system is recommended. Assigning control functions to a central processor introduces problems in system test and calibration, software design and updating, and system interfaces.

The impact of additional requirements that dictate precision slewing should be assessed. Precision slewing for planet surveys with a narrow spectrometer slit, comet tracking, and precision positioning of spectrometer slits are typical examples. Additionally, an assessment must be made of the hardware and operational techniques required to meet requirements of this nature.

The actuator systems recommended for LST are a cold gas RCS for emergency or failure mode operation over a short interval or where high torques may be required; an SGCMG system for normal operational modes such as stabilizing, pointing, or maneuvering modes; and an MTS for momentum management of the CMGs. Although the LST requirements with a Shuttle launch do not dictate an RCS, a low impulse, cold gas RCS has been placed on the reference LST, because it raises the confidence level for mission success. The RCS will be in a standby operational status during orbital insertion by the Shuttle or when docking is attempted. The RCS will also be used during abnormal situations. For example, if the computer should fail, the CMGs and MTS could not be used. While the failure is being analyzed and corrective actions taken, the RCS through simple analog programming, which bypasses the computer, would bring and hold the LST in a solar pointing orientation. Additional studies should be done to define the sensor logic and algorithms required to implement the RCS for emergency operations.

The four-skewed SGCMG configuration has been selected for LST. A skew angle of 30 degrees provides a momentum envelope somewhat proportional to the LST inertial values. Even with one CMG deactivated, the momentum envelope is still shaped properly for LST control purposes. A momentum value of 678 N-m-sec (500 ft-lb-sec) per CMG unit has been used for study purposes. However, such a value produces a grossly oversized momentum exchange system for LST, even when a CMG is deactivated. Simulations indicate no difference between the performance obtained using either four or three CMGs. Although all four CMGs would normally be used, consideration should be given to using only three, with the fourth deactivated until needed after a failure, especially if reliability or lifetime of the total system could be enhanced. The CMG system momentum capacity permits continuous experiment data gathering without desaturation for 6.2 orbits (4.4 orbits with three-CMG operation) under worst-case environmental disturbances. A maximum turning rate of 91 deg/min (67 deg/min with three CMGs) can be obtained about the major inertial axis. Although the four-skewed CMG system exceeds LST requirements, there are several obvious advantages to an oversized system:

1. Growth potential — The vehicle inertias can become much larger and more unfavorable without impacting the momentum-exchange system.

2. Commonality — Use available CMGs from other programs, such as HEAO.

3. Failure — One CMG can be failed and normal operations continued using only three CMGs.

4. Permits the use of g.g. dump modes in the event of MTS failure.

5. Ghu — Singularity detection and avoidance schemes are not required. (Inside the maximum momentum envelope there is a ghu free envelope that meets all LST requirements.)

6. Gimbal angles remain small permitting a constant gain steering law to be analog programmed for possible failure modes.

7. Permits the MTS to be turned off for several orbits while experiments extremely sensitive to magnetic fields are conducted.

The CMG steering law recommended is the Moore-Penrose pseudo-inverse. This type steering law is relatively easy to implement and gives excellent performance. In the event of a CMG failure, the steering law need not be reprogrammed or any changes made in the computational algorithms. The failed CMG must, however, be identified and the corresponding column elements in the CMG torque matrix set to zero, in which case the pseudo-inverse reduces to the exact solution. Most other steering laws considered for LST would require major reprogramming to accommodate a CMG failure.

The MTS recommended for LST is used mainly for momentum management of the CMGs. The system of six electromagnets generate a dipole moment in any specified direction by passing current through the appropriate coils. Analysis has shown that the magnetic field produced by the MTS is more than 10 times less than the earth's ambient field in the SSM-SIP areas. Thus, there are no additional shielding requirements for magnetically sensitive instruments over that normally required for the earth's field. Moreover, location of the magnetometer on the aft end of the SSM permits the earth's geomagnetic field to be measured while using the MTS. Thus, continuous use of the MTS is recommended, in which case the CMG momentum variation remains small. As a secondary use, the MTS is programmed to produce direct vehicle control torques, permitting a greater depth of CMG failure and faster recovery during and after a failure mode. Since the MTS is sized for direct torque control, it is oversized for CMG momentum management. Any two of the electromagnets can be deactivated and the remaining units can meet the main objective of momentum dumping. Some of the advantages of the MTS proposed for the LST are listed below:

1. No RCS or fuel weight is required for normal operational modes.

2. Lifetime is not limited by expendables.

3. CMG saturation detection is not required for continuous desaturation.

4. Prevents CMG ghu.

5. One CMG fail operational capability.

6. Operation with only two CMGs is possible with some degradation.

7. Small size CMGs could be used.

8. Very small gimbal angles permit a constant gain CMG steering law, if desired.

9. Automatically forces CMGs to a null position, without programming.

10. All the CMG momentum is available for maneuvers, since the normal CMG momentum state stays near zero.

Most of the MTS analysis was done assuming a linear system. However, the materials used in constructing the electromagnet core may possess nonlinear characteristics, such as hysteresis, and the OTA structure could interfere with the dipole produced, changing its magnitude as well as direction. Electromagnets of the size proposed for LST should be manufactured and tested for magnetic operating characteristics such as current input to produce the dipoles, the ability to linearly control its magnetic state, and the fields propagated.

Since the CMGs are oversized and the MTS provides direct torque, ghu detection and avoidance are not required for LST. However, ghu is a general problem area that needs further investigation. To date, the 2-SPEED CMG configuration and steering law is the only candidate that has been developed that appears promising. In the event 2-SPEED is further developed and shown practical, it should also be considered for LST.

REFERENCES

VI-1. TRW, Inc.: HEAO, Technical Proposal for Phase C/D. Report No. 17622, August 27, 1971.

VI-2. NASA George C. Marshall Space Flight Center: HEAO RFP No. DCN-1-1-21-00109.

VI-3. Northrop Services, Inc.: Alternate SGCMG Control System for HEAO. Memo 9243C-72-43, June 8, 1972.

VI-4. A GCMSFC: Summary Description of the 2-SPEED Steering Law and Configuration for Single Gimbal CMGs. Report No. S&E-AERO-DO-33-72.

VI-5. Billy G. Davis: A Discussion of Orbital Workshop Orientation and Gravitational Effects. NASA TM X-53829, May 5, 1969.

VI-6. Bendix Corp.: High Accuracy Stabilization and Control Report No. MT-2383, Navigation and Control Div. Denver, Colorado, December 14, 1971.

CHAPTER VII. MAINTAINABILITY ANALYSES

TABLE OF CONTENTS

LIST OF ILLUSTRATIONS

LIST OF TABLES

CHAPTER VII. MAINTAINABILITY ANALYSES

A. Introduction

The mission goal of the LST is to provide 15 years of on-orbit observation time. Present plans call for the initial 5 years of observation to be performed by the precursor LST, with the remaining 10 years of on-orbit operation being accomplished by the advanced LST.

In order to maintain an acceptably high level of operational performance during the entire 15-year LST mission duration, the following three interrelated factors must be considered:

1. Provide for instrument update when warranted by changing interest or advance in technology.

2. Assure system performance for long-time observatory operation.

3. Minimize total LST program cost.

The following two options exist to sustain the LST performance at the desired level for the 15-year mission duration:

1. Expendable LST — in this option a new LST is placed on orbit when the operational LST malfunctions.

2. Maintainable LST — this option provides for repair of the malfunctioning LST to return it to the desired performance level.

Presented below is a comparison of the program costs for both the expendable and maintainable LST options with the maintainable LST serving as a reference and assigned a relative program cost of unity:

Configuration Option	Flight Articles Required	Total Relative Payload Cost
Expendable LST	8	1.8
Maintainable LST	2	1.0

In the above table, the number of LST vehicles required for the expendable program is based on a component design lifetime of 2 years over the 15-year program duration. The number of LST vehicles required for the maintainable option includes one precursor for the first 5 years and one advanced LST for the remaining 10 years.

Also, from the above table, the potential cost savings resulting from the maintainable LST option is approximately 44 percent of the expendable LST program costs — certainly greater than the uncertainties attendant with current cost estimating techniques. In view of the magnitude of this potential cost savings resulting from the maintainable LST option, the expendable LST option was removed from further consideration.

B. Maintenance Trade Study Approach

A preliminary maintainability analysis was conducted for the LST mission to determine and define a feasible maintenance concept. The four following maintenance modes were initially considered for the LST spacecraft:

1. On-orbit manned maintenance — pressurized.
2. On-orbit manned maintenance — unpressurized.
3. On-orbit manipulator maintenance.
4. Ground-based maintenance.

1. Definition of Maintenance Modes

a. On-Orbit Manned Maintenance — Pressurized. This maintenance mode provides the crewmen direct access to the replaceable subsystems elements and scientific equipment under shirtsleeve conditions and for this reason requires a smaller design impact to the replaceable elements than is required by other in-flight maintenance modes. The shirtsleeve environment and associated contamination control system for this maintenance mode are provided by the Shuttle orbiter and chargeable to its payload. Of the three on-orbit maintenance modes considered, the pressurized (shirtsleeve) mode enables the maintenance crew to perform more detailed and precise maintenance tasks and to accomplish them more easily, more quickly, and with less risk.

b. On-Orbit Manned Maintenance-Unpressurized. The general configuration and equipment arrangement selected for this maintenance mode is similar to the mode described in the preceding paragraph, except that no pressure vessel is provided and all maintenance operations are performed in pressure suits under intravehicular activity (IVA) conditions. (IVA is defined as "activity performed in space or on a celestial body by an astronant internal to the space vehicle, under vacuum conditions.") Life support of the pressure suits may be provided via backpacks or umbilicals. At the present time the umbilical mode appears to offer the advantages of smaller suit volume and a lower suit-induced contamination rate.

c. On-Orbit Manipulator Maintenance. This maintenance mode was developed by the Goddard Space Flight Center (GSFC) and was selected as its preferred maintenance concept for the LST servicing. In GSFC's "Large Space Telescope (LST) Preliminary Analysis and Design Report," the center's manipulator maintenance concept was described in the following manner.

The teleoperator system to be used to conduct in-orbit resupply and mission update operations consists of the following assemblies and functions:

1. A service module platform, which is attached to the Space Shuttle and contains the spare subsystem and instrument modules, designed to dock with the observatory.

2. A manipulator system, which is also located within the service module platform, to perform the physical activity of removing the malfunctioning subsystem and/or instrument modules and inserting new subsystem and/or instrument modules.

3. A system of pilot (astronaut) operated controls, located within the Shuttle command cabin, used to control subsystem box position and rate of travel and also subsystem to spacecraft lock/unlock functions.

4. A system of visual sensors and monitors to provide the pilot with a display of all external resupply activities.

d. Ground-Based Maintenance. This maintenance concept entails retrieval of a malfunctioning LST by the Shuttle orbiter for return to earth for maintenance and refurbishment. An immediately obvious disadvantage of this mode is the requirement for an extra Shuttle launch.

2. Maintenance Mode Comparison. The maximum design lifetime for life-limited subsystems and instruments has been assessed as being 2 1/2 years. Consequently, initial maintenance trade studies were conducted assuming that scheduled maintenance is performed every 2 1/2 years. Since the precursor LST is to have 5 years of service, one scheduled service mission was planned and costed for comparison.

The trade study was carried out in the following manner. Specialists in the various discipline areas assessed each maintenance mode with regard to the impact on the design of the LST configuration, design and operational flexibility, performance characteristics, complexity, and developmental and performance risks.

C. Maintenance Mode Study Results

Table VII-1 lists some 20 factors comparing and contrasting the four considered maintenance modes. At this time the comparison is qualitative, and as yet no attempt has been made to quantify or to arrive at "figures of merit" for the various comparison remarks. From a technical viewpoint, it can certainly be argued that all four maintenance options are feasible — each with certain attractive and detrimental features. Careful perusal of the table does, however, indicate that of the four maintenance options, the on-orbit manipulator mode is the least attractive because of its shortcomings in the areas of (1) ease of maintenance tasks, (2) quantity/complexity of separate operations required, (3) growth potential and flexibility for design changes, (4) interconnection quantity and complexity, (5) ease of maintenance tasks, (6) logistics weight and volume requirements, (7) mission sharing possibilities, (8) alignment and calibration capability, (9) special tool requirements.

Primarily because of pressing commitments on other aspects of the LST study, a complete technical assessment of the four maintenance modes was not possible during this phase of the study. Study plans called for establishing a reasonable baseline maintenance mode for design and costing purposes for this study phase and establishing a firm preferred maintenance method at a later date. As will be seen later, the selected maintenance concept for this study phase was chosen primarily on a cost basis.

1. Flight Sharing. Table VII-2 is a listing of the support system module (SSM) subsystems and scientific instrument package (SIP) and optical telescope assembly (OTA) scientific instruments which would be replaced

TABLE VII-1. MAINTENANCE MODE COMPARISONS

Factor	Pressurized On-Orbit	Unpressurized On-Orbit	On-Orbit Manipulator	Ground Serviced
Level of Maintenance	Black Box to Subsystem	Black Box to Subsystem	System	Any Desired Level
Quantity/Complexity of Separate Operations Required	Moderate quantity. Complexity not a problem in shirtsleeve environment.	Moderate quantity. Complexity slightly increased due to pressure-suited maintenance.	Greater quantity. Considerable complexity imposed on automated carousel. Large, bulky boxes weigh up to 900 kg and fairly intricate maneuvers required.	Minimum
Time Required for Maintenance	Short	Longer due to pressure-suited maintenance	Considerable (2 carousels required)	Minimum
Turnaround Time	2-5 days	2-5 days	2-5 days	30 days minimum
Growth Potential & Flexibility for Design Changes	Excellent due to packaging freedom	Excellent due to packaging freedom	Box structures restrict growth and flexibility, especially pie-shaped radial instrument compartment. Interface at focal plane, lack of room for instrument growth and for baffles.	Excellent due to packaging freedom
Interconnection Quantity & Complexity	Few per box. Shirtsleeve operation allows standard connections and uncomplicated operations.	Few per box. Standard connections, somewhat more complex operations due to pressure suit.	Moderate quantity. More complex due to automatic operations, major concern.	Few per box. Shirtsleeve operation allows standard connections and uncomplicated operations.
Accessibility to Replaceable Units	Excellent. Direct access to internally mounted components	Excellent. Direct access to internally mounted components.	Good for systems and radially mounted instruments. LST must be rotated on carousel. Poor for axially mounted instruments.	Excellent. Direct access to all components.

TABLE VII-1. (Continued)

Factor	Pressurized On-Orbit	Unpressurized On-Orbit	On-Orbit Manipulator	Ground Serviced
Ease of Maintenance Tasks	Good. Weightless Condition requires use of handholds, foot or body restraints.	Good. Less than pressurized due to pressure suit operation.	Most difficult. High skill requirements for manipulator operator.	Provides easiest accomplishment of maintenance tasks
Use of Man's Capabilities	Excellent	Good. Somewhat limited by restrictions of the pressure suit.	Uses man for manipulator operation only	Excellent
Complex Remote Handling Maintenance Devices	None	None	One or two automated carousels	None
Spares for Refurbishment and Repair	Small subsystems or component modules mounted on racks in Shuttle bay or crew compartment	Small subsystem or component modules mounted on racks in Shuttle bay or crew compartment	Large system or subsystem modules mounted on racks in Shuttle bay. Must be transferred to and from Shuttle bay by manipulators.	Maximum flexibility due to spares availability and ready access
Logistics Mass/ Volume to Orbit (total life limited item replacement plus total science update)	1687 kg (3720 lb) 6.3 m^3 (223 ft^3) Volume available in cargo bay, Sortie Lab, or crew compartment	1358 kg (2994 lb) 5.4 m^3 (190 ft^3) Volume available in cargo bay, Sortie Lab, or crew compartment	3652 kg (8050 lb) 127 m^3 (4487 ft^3) Note: The storage of system boxes and radial instruments apparently fills one carousel and a second one must be designed and used for the on-axis instruments.	Not applicable
Mission-Sharing Possibilities on Maintenance Flights	Excellent, especially with Tug flights, which predominate.	Excellent, especially with Tug flights, which predominate.	Poor. Volume required by two carousels plus full spares/ update complement is so great that LST could not be retrieved on same flight if ground service is required.	Poor

TABLE VII-1. (Continued)

Factor	Pressurized On-Orbit	Unpressurized On-Orbit	On-Orbit Manipulator	Ground Serviced
LST Hardware Lifetime Requirements	Minimizes lifetime requirements and associated costs. Since mission-sharing possibility is excellent, can have more frequent maintenance trips of shorter duration as failures dictate. (Unscheduled maintenance concept.)	Same as pressurized maintenance	Maximum lifetime required due to large weight and volume of spares, science update items, and automated carousels	Long life required due to penalties accruing from unshared Shuttle flights and more extensive and expensive ground operations
Science Downtime During Maintenance	2-5 days	2-5 days	2-10 days	1-6 months
Other Considerations	Possibly none. However, if "unscheduled maintenance" concept is used, traffic density, queueing, etc. must be considered. With a Shuttle launch rate of two per month, a reasonable worst case estimate is 1-2 months down time.	Same as pressurized maintenance	If two carousels are required for scheduled maintenance, two Shuttle launches are required. It is doubtful if one payload could schedule two consecutive Shuttle flights. For "unscheduled maintenance" flight-sharing of this configuration is difficult. With a Shuttle launch rate of two per month, a reasonable worst-case is 3-6 months for either case.	Possibly none (for scheduled ground return and relaunch). For "unscheduled maintenance" a longer time is required to schedule the mostly unshared return trip than the 1-2 months shown in Col. 1 for the shared up-trip. Two to four months is probably more reasonable. The mostly unshared relaunch scheduling effort could begin at the time of failure and if the wait is longer than 3-10 months from then, no additional wait would be required.

TABLE VII-1. (Concluded)

Factor	Pressurized On-Orbit	Unpressurized On-Orbit	On-Orbit Manipulator	Ground Serviced
Hazard to Crew Due to Direct Involvement in Maintenance Operations	Minimum. Safer than Apollo or Skylab EVA activities.	Slightly more hazardous than pressurized maintenance mode due to intravehicular activities (IVA)	None	None
Alignment and Calibration Capability	Excellent. Maximum accuracy possible due to man in shirtsleeve environment. Does not have to withstand relaunch.	Excellent but accuracy degraded slightly for suited operation. Does not have to withstand relaunch.	Probably feasible but with reduced accuracy. Does not have to withstand relaunch.	Excellent accuracy on ground but has to withstand relaunch.
Tool Requirements	Standard hand tools would be required. Module alignment and quick release mechanisms are presently available.	Same as pressurized	Special manipulator tools would have to be designed to provide alignment of modules and power attachment and release	Standard shop tools would be required
Contamination Protection During Maintenance	Active contamination control system required. Class 10 000/100 000 hybrid system recommended (see Appendix.)	Contamination potential less than pressurized mode. Effluents from pressure suit may be area of concern.	Spares and automated carousel in Shuttle cargo bay must be maintained moisture and contaminant free	Entire LST must be maintained clean to disassemble and clean on ground. This may be a major problem area.
Quantity of SSM Spares Inventory (cost must include purchase, storage, assembly into replaceable units, and testing)	16% (Only failed and life-limited items)	16% (Only failed and life-limited items)	100% except for arrays. There will be some life-limited and failed items in each box. Therefore, many non-life-limited and nonfailed items must be replaced.	16% (Only failed and life-limited items)

TABLE VII-2. TOTAL MAINTENANCE MISSION EQUIPMENT LOAD

Component	Quantity	Unit Mass (kg)	Total Mass (kg)	Unit Volume (m^3)	Total Volume (m^3)
• Life-Limited Components					
Tape Recorder	3	5.44	16.32	0.00793	0.02379
Battery	6	21.09	126.54	0.02011	0.12066
			142.86		0.14445
		+20% Contin.	28.57	+50% Contin.	0.07223
		Total =	171.43	Total =	0.21668
		=	(378 lb)	=	(7.65 ft^3)
• Typical Random Failure Items					
Reference Gyro Assembly (RGA)	1	10.45	10.45	0.01133	0.01133
Digital Processor Assembly (DPA)	1	6.20	6.20	0.00566	0.00566
Control Moment Gryo (CMG)	1	80.90	80.90	0.46162	0.46162
Regulator	1	3.50	3.50	0.00850	0.00850
Remote Decoder	1	0.45	0.45	0.00283	0.00283
Data Acquisition Unit (DAU)	1	0.10	0.10	0.00014	0.00014
			101.60		0.49008
		+20% Contin.	20.32	+50% Contin.	0.24504
		Total =	121.92	Total =	0.73512
		=	(269 lb)	=	(25.96 ft^3)

TABLE VII-2. (Continued)

Component	Quantity	Unit Mass (kg)	Total Mass (kg)	Unit Volume (m^3)	Total Volume (m^3)
• Total Science Update Items					
f/12 Camera & Filter Wheel	1	70.40	70.40	0.03228	0.03228
f/96 Camera & Filter Wheel	3	67.13	201.39	0.02266	0.06797
f/96 Camera Selector Assembly	1	21.32	21.32	0.02549	0.02549
f/96 Magnifier & Housing	1	15.42	15.42	0.05947	0.05947
Fine Guidance Assembly	1	116.48	116.48	0.09062	0.09062
Echelle Spectrograph	1	51.76	51.76	0.16142	0.16142
Echelle Spectrograph	1	51.76	51.76	0.14726	0.14726
Faint Object Spectrograph (UV)	1	55.79	55.79	0.09912	0.09912
Faint Object Spectrograph (IR)	1	45.36	45.36	0.18408	0.18408
Faint Object Spectrograph (IR)	1	44.45	44.45	0.07363	0.07363
Fourier Interferometer	1	18.14	18.14	0.09912	0.09912
Focus Sensor	1	12.66	12.66	0.00566	0.00566
Figure Sensor	1	17.36	17.36	0.00566	0.00566
Collimator Assembly (UV Spectrograph)	1	9.10	9.10	0.01982	0.1982

TABLE VII-2. (Concluded)

Component	Quantity	Unit Mass (kg)	Total Mass (kg)	Unit Volume (m^3)	Total Volume (m^3)
• Total Science Update Items (Concluded)					
Slit Assembly (Axial Spectrograph Mechanism etc.)	1	4.54	4.54	0.01982	0.01982
Slit Jaw Camera	1	42.18	42.18	0.27470	0.27470
			778.11		1.36612
		+20% Contin.	155.62	+50% Contin.	0.68306
		Total =	933.73	Total =	2.04918
		=	(2059 lb)	=	(72.37 ft^3)
Subtotal, Spares, & Instruments			1227.08 kg (2708 lb)		3.0098 m^3 (105.98 ft^3)
Support Equipment (Contamination Control + Miscellaneous)			459.94 kg		3.3134 m^3
Total for This Mission			1687.02 kg (3720 lb)		6.31442 m^3 (223 ft^3)

during a scheduled maintenance flight. The total mass and volumes including allowances for packaging were used in the maintenance mission analysis trades. Since the on-orbit maintenance mission does not utilize either the full weight nor volume payload capability of the orbiter, LST costs could be reduced if some other mission shared the flight with the LST maintenance mission. Employing this premise, the Space Shuttle Mission Model was surveyed to locate compatible payloads to share flights with the LST maintenance mission. A copy of the mission model used in this study appears in Table VII-3.

Currently, there are no ground rules as to how Shuttle flight costs are to be prorated for mission sharing. Costs could be prorated on payload mass ratio, payload volume ratio, on-orbit operations time ratio, etc., or a combination of some or all of the aforementioned factors. As a result of discussions with engineering cost personnel, it was decided to select payload mass as the basis for prorating mission sharing costs for this study.

The selection of payload mass ratio as the basis of cost proration means that LST costs can be minimized by selecting the heaviest payloads possible to share the LST maintenance mission flights; in this respect, Space Tug missions proved to be some of the best candidates for mission sharing. Table VII-4 presents the portion of the total number of payloads requiring the Tug. There are ample Tug missions to share LST maintenance mission costs.

Before investigating specific flight sharing cases, it should be noted that flight sharing does not apply to the earth return maintenance mode. Since this mode requires retrieving the LST, which uses most of the orbiter payload bay volume, few payloads can be identified to share such flights.

Servicing the LST at its orbit of 611 km (330 n.mi.) requires the orbiter to use an on-orbit maneuvering system (OMS) propellant tank which is located in the aft end of the payload bay. The full OMS tank weighs 5443 kg (12 000 lb) and is chargeable to the LST maintenance mission as part of the required LST payload weight.

2. Specific Flight Sharing Cases. Figure VII-1 presents the maximum payload length that can be accommodated for three specific flight sharing cases.

a. Unpressurized Spares in the Cargo Bay. In this case, the spares are packaged in the cargo bay for on-orbit manipulator maintenance. A total length of 3.66 m in the payload compartment is allocated for spares packaging, manipulator access, and airlock module. Allowance for the OMS

TABLE VII-3. NASA HEADQUARTERS MISSION MODEL
NASA PAYLOADS (LESS LUNAR)

NO	NASA-NO	TITLE	INC	APO	PERI	DIA	LEN	WT	VOL	VEL	79	80	81	82	83	84	85	86	87	88	89	90	TOTAL
1	NA2-1	EXPLORERS - LEO	28.50	297	297	2.6	6.2	373	33	683	1	1	1	1	1	1	1	1	1	1	1	1	12
2	NA2-2	EXPLORERS - SYNC	28.50	19323	19323	2.6	6.2	373	33	10928	0	1	0	0	0	1	0	0	0	1	0	1	4
3	NA2-3	HIGH ENERGY ASTRONOMY OB	28.50	250	250	8.8	43.0	18264	2615	526	1	0	0	0	1	1	0	0	0	0	1	0	4
4	NA2-4	HEAO - REVISITS	28.50	250	250	15.0	5.0	3500	885	526	0	1	1	1	0	1	2	2	2	1	0	1	12
5	NA2-5	LARGE SPACE TELESCOPE	28.50	330	330	12.4	41.7	18581	5036	793	1	0	0	0	1	0	0	0	0	1	0	0	3
6	NA2-6	LST - REVISITS	28.50	330	330	15.0	5.0	3500	885	793	0	1	1	1	0	1	1	1	1	0	1	1	9
7	NA2-7	LARGE SOLAR OBSERVATORY	55.00	270	270	14.0	54.0	32282	8300	593	0	0	0	0	0	0	0	0	1	0	0	0	1
8	NA2-8	LSO - REVISITS	55.00	270	270	15.0	5.0	3500	885	593	0	0	0	0	0	0	0	0	1	1	1	1	4
9	NA2-9	LARGE HI ENERGY TELESCOP	28.50	400	400	10.0	32.0	15781	2513	1019	0	0	0	0	0	0	0	0	0	0	1	0	1
10	NA2-10	LHET - REVISITS	28.50	400	400	15.0	5.0	3500	885	1019	0	0	0	0	0	0	0	0	0	0	0	1	1
11	NA2-11	RADIO ASTRONOMY OBSERVAT	28.50	38646	38646	10.0	25.0	2385	1963	13661	0	0	0	0	0	0	0	0	0	0	0	1	1
12	NA2-12	ASTRONOMY AND PHYSICS OB	55.00	270	270	14.0	42.0	23569	6465	593	1	1	1	1	2	2	2	2	2	2	2	20
13	NP2-13	EXPLORERS - UPPER ATMOSP	90.00	2000	100	4.0	8.0	1160	100	2781	1	0	1	0	1	0	1	0	1	0	1	0	6
14	NP2-14	EXPLORERS - MEDIUM ALTIT	90.00	20000	1000	5.0	8.0	570	157	11412	1	0	1	0	1	0	1	0	1	0	1	0	6
15	NP2-15	EXPLORERS - HIGH ALTITUD	.00	0	0	4.0	6.0	640	75	14419	0	1	0	1	0	1	0	1	0	1	0	1	6
16	NP2-16	GRAVITY AND REL SAT LEO	90.00	500	500	7.6	12.0	462	635	1333	1	0	0	1	0	0	0	0	0	0	0	0	2
17	NP2-17	GRAVITY AND REL SAT SOL	.00	0	0	8.5	6.8	770	385	22219	0	0	0	0	0	0	0	1	0	0	0	1	2
18	NP2-18	ENVIROMENTAL PERT SAT A	55.00	6900	6900	7.0	12.0	4350	462	12850	0	0	1	0	0	1	0	0	0	0	0	0	2
19	NP2-19	ENVIROMENTAL PERT SAT B	55.00	6900	6900	10.0	15.0	8700	1178	12850	0	0	0	0	0	0	0	0	1	0	0	1	2
20	NP2-20	HELIOCENTRIC AND INTERST	.00	0	0	10.0	10.0	616	785	28919	0	0	0	0	0	0	0	0	0	0	1	0	1
21	NP2-21	PHYSICS LAB	55.00	270	270	14.0	42.0	22811	6465	593	0	0	0	0	0	0	0	0	0	1	0	1	2
22	NU2-22	MARS VIKING	.00	0	0	12.0	16.0	7491	1810	12319	2	0	0	0	0	0	0	0	0	0	0	0	2
23	NU2-23	MARS ROVER	.00	0	0	12.0	16.0	5548	1810	12319	0	0	0	0	0	0	0	1	0	0	0	0	1
24	NU2-24	VENUS PIONEER	.00	0	0	10.0	15.0	878	1178	13019	0	1	0	0	0	0	0	0	0	0	0	0	1
25	NU2-25	VENUS RADAR MAPPER	.00	0	0	10.0	12.0	2081	942	13019	0	0	0	0	0	0	2	0	0	0	0	0	2
26	NU2-26	VENUS LARGE LANDER	.00	0	0	10.0	10.0	1169	785	13019	0	0	0	0	0	0	0	0	0	0	2	0	2
27	NU2-27	MERCURY ORBITER	.00	0	0	12.0	25.0	5166	2827	16719	0	0	0	0	0	0	0	0	0	2	0	0	2
28	NU2-28	PIONEER - JUPITER ORBITE	.00	0	0	10.0	20.0	1948	1571	23819	1	0	0	0	0	0	0	0	0	0	0	0	1
29	NU2-29	MARINER - JUP/URAN FLYBY	.00	0	0	10.0	15.0	1540	1178	25669	2	0	0	0	0	0	0	0	0	0	0	0	2
30	NU2-30	PIONEER - JUPT PROBE	.00	0	0	10.0	17.0	794	1335	24319	0	0	0	2	0	0	0	0	0	0	0	0	2
31	NU2-31	PIONEER - SAT PROBE	.00	0	0	10.0	17.0	850	1335	22719	0	0	0	0	0	0	2	0	0	0	0	0	2
32	NU2-32	MARINER - JUPT ORBITER	.00	0	0	12.0	16.0	2500	1810	23819	0	0	0	0	0	0	0	1	1	0	0	0	2
33	NU2-33	URANUS PROBE/NEPT FLYBY	.00	0	0	12.0	17.0	4990	1923	31819	0	0	0	0	0	0	0	0	2	0	0	0	2
34	NU2-34	MARINER - SATURN ORBITER	.00	0	0	12.0	17.0	2368	1923	25219	0	0	0	0	0	0	0	0	0	0	1	1	2
35	NU2-35	ENCKE SLOW FLYBY	.00	0	0	12.0	17.0	3159	1923	21919	1	0	0	0	0	0	0	0	0	0	0	0	1
36	NU2-36	ENCKE RENDEZVOUS	.00	0	0	10.0	20.0	3193	1570	21919	0	0	0	0	0	0	2	0	0	0	0	0	2
37	NU2-37	ASTEROID RENDEZVOUS	.00	0	0	10.0	20.0	3640	1570	10919	0	0	0	0	0	0	0	0	0	0	0	2	2
38	NE2-38	EARTH OBSERVATION SAT;	98.00	500	500	10.0	11.5	2400	903	1333	1	1	1	0	1	0	1	0	1	0	1	0	7
39	NE2-39	SYNC EARTH OBSERVATION S	.00	19323	19323	8.0	12.0	2500	603	14103	0	1	0	1	0	0	1	0	1	0	0	1	5
40	NE2-40	TIROS	103.00	906	906	8.0	12.0	1380	603	2487	0	0	1	0	0	0	0	0	0	0	0	0	1
41	NE2-41	SYNC METEROID SATELLITE	.00	19323	19323	6.0	6.0	535	170	14103	0	0	1	1	0	0	0	0	0	0	0	0	2
42	NE2-42	EARTH-RESOURCES SAT	98.00	500	500	10.0	11.5	1800	903	1333	2	2	0	0	0	1	1	0	0	0	0	0	6
43	NE2-43	SYNC EARTH OBSER SAT/PR	.00	19323	19323	10.0	12.0	2640	982	14104	0	0	0	0	0	0	0	0	0	0	0	1	1
44	NE2-44	EARTH OBSERVATION LAB	90.00	100	100	14.0	19.0	12462	2825	0	0	1	1	1	1	1	1	1	1	1	0	0	9
45	NE2-45	GEOPAUSE	90.00	270	270	5.0	9.0	710	177	903	1	1	0	0	0	0	0	0	0	0	0	0	3

TABLE VII-3. (Concluded)

NO	NASA-NO	TITLE	INC	APO	PERI	DIA	LEN	WT	VOL	VEL	79	80	81	82	83	84	85	86	87	88	89	90	TOTAL
46	NC2-46	APPLICATION TECH SAT	.00	19323	19323	9.0	25.0	3000	1590	14104	1	0	0	1	1	0	1	0	1	0	1	0	6
47	NC2-47	SMALL APP TECH SAT-SYNC	.00	19323	19323	3.0	7.0	300	49	14104	1	1	1	1	1	1	1	1	1	1	1	1	12
48	NC2-48	SMALL APP TECH SAT-POLAR	90.00	300	300	3.0	7.0	300	49	693	1	1	1	1	1	1	1	1	1	1	1	1	12
49	NC2-49	TRACKING AND DATA RELAY	.00	19323	19323	10.0	17.0	1760	1335	14104	0	0	0	0	3	0	0	0	0	0	3	0	6
50	NC2-50	DISASTER WARNING SAT	.00	19323	19323	10.0	17.0	1760	1335	14103	1	0	0	0	0	0	0	0	0	0	0	0	1
51	NC2-51	SYSTEM TEST SATELLITE	.00	19323	19323	12.0	15.0	2860	1696	14103	0	1	1	1	1	1	1	0	1	1	0	0	8
52	NC2-52	COMM/NAV EXPERIMENTS	28.00	200	200	14.0	55.0	17910	8467	354	1	1	0	0	1	1	0	0	1	0	0	1	6
53	NC2-53	COMM/NAV LABORATORY-SORT	28.00	200	200	14.0	41.0	17510	6311	354	0	0	1	1	0	0	1	0	0	0	1	0	4
54	NC2-54	COMM/NAV LABORATORY-RAM	55.00	270	270	14.0	45.0	36500	6927	593	0	0	0	0	0	0	0	1	0	1	0	0	2
55	NB2-55	BIO-RESEARCH MODULE	28.50	300	300	3.0	5.0	370	35	693	2	0	0	0	0	0	0	0	0	0	0	0	2
56	NB2-56	TELEOPERATOR	28.50	300	300	4.0	3.0	960	35	693	1	0	0	0	0	0	0	0	0	0	0	0	1
57	NB2-57	MINI 7 -DAY MODULE	.00	250	250	14.0	32.0	14041	4926	525	0	1	1	1	0	0	0	0	0	0	0	0	3
58	NB2-58	MINI 30-DAY MODULE -SORT	.00	250	250	14.0	32.0	18891	4926	525	0	0	0	0	1	1	0	0	0	0	0	0	2
59	NB2-59	MINI 30-DAY MODULE -RAM	55.00	270	270	14.0	32.0	26576	4926	593	0	0	0	0	0	0	1	1	0	0	0	0	2
60	NB2-60	STATION LAB EXP	55.00	270	270	14.0	32.0	28984	4926	593	0	0	0	0	0	0	0	0	1	0	0	0	1
61	NT2-61	METEROID EXPOSURE MOD	28.50	270	270	14.0	35.0	10000	5388	593	0	1	0	0	1	0	0	0	0	0	0	0	2
62	NT2-62	MATERIAL SCIENCE EXPER	.00	0	0	7.0	10.0	2720	385	0	1	1	1	1	1	2	0	0	0	0	0	0	7
63	NT2-63	ADVANCED TECH EXP	28.50	250	250	14.0	47.5	13781	7310	525	0	1	0	1	0	1	0	0	0	0	0	0	3
64	NT2-64	TECHNOLOGY AND NAT SC LA	55.00	270	270	14.0	32.0	19113	4926	593	0	0	0	0	0	0	1	0	0	0	0	0	1
65	NS2-65	CREW MODULE	55.00	270	270	14.0	45.0	20000	6927	593	0	0	0	0	0	1	0	0	0	0	0	1	2
66	NS2-66	POWER/SUBSYSTEMS	55.00	270	270	14.0	58.0	20000	8928	593	0	0	0	0	0	1	0	0	0	0	0	1	2
67	NS2-67	GENERAL PURPOSE LAB	55.00	270	270	14.0	45.0	20000	6927	593	0	0	0	0	0	1	0	0	0	0	0	0	1
68	NS2-68	CREW/OPERATIONAL LOGIST	55.00	270	270	14.0	28.0	20000	4310	593	0	0	0	0	0	0	5	6	6	6	6	6	35
										TOTAL	26	21	17	19	20	28	24	24	29	20	30	89	287

NON-NASA PAYLOADS

NO	NASA-NO	TITLE	INC	APO	PERI	DIA	LEN	WT	VOL	VEL	79	80	81	82	83	84	85	86	87	88	89	90	TOTAL
1	NCN-7	COMMUNICATION SATELLITE	.00	19323	19323	9.0	22.0	1490	1400	14132	2	1	1	0	2	1	1	0	0	2	1	0	11
2	NCN-8	U.S. DOMESTIC COMMUNIC.	.00	19323	19323	15.0	25.0	3545	4418	14132	1	2	1	1	2	2	2	2	2	2	2	2	21
3	NCN-9	FOREIGN DOMESTIC COM.	.00	19323	19323	4.0	12.0	1030	151	14132	0	2	6	2	2	0	0	4	5	2	1	2	25
4	NCN-10A	NAV/TRAFFIC CONTROL	29.00	30000	16000	5.0	8.0	725	157	13932	3	1	2	0	1	0	1	0	1	0	1	0	10
5	NCN-10B	NAV/TRAFFIC CONTROL	5.00	19300	19300	5.0	8.0	725	157	13882	0	1	1	0	1	0	1	0	1	0	1	0	5
6	NE0-7	TOS METEOROLOGICAL SATEL	100.00	700	700	5.0	6.0	1030	118	1932	1	1	1	1	1	1	1	1	1	1	1	1	12
7	NE0-15	SYNCHRONOUS METEOROLOGIC	.00	19323	19323	5.0	8.0	1035	157	14132	1	1	1	1	1	1	1	1	1	1	1	1	12
8	NE0-16	POLAR EARTH RESOURCES	100.00	500	500	6.0	12.0	2590	339	1382	4	0	4	0	4	0	4	0	0	0	6	0	22
9	NE0-11	SYNCHRONOUS EARTH RESOUR	.00	19323	19323	6.0	6.0	1030	170	14132	0	0	0	0	0	0	4	0	0	4	0	0	8
										TOTAL	12	9	17	5	14	5	15	8	11	12	14	6	128

TABLE VII-4. TOTAL NUMBER OF PAYLOADS REQUIRING THE TUG

- Total Number of Payloads (1979-1990): 415

Astronomy	Space Physics	Earth Orbital	Com/Nav[a]	Planetary	Non-NASA
72	29	101	57	28	128

- Tug required for approximately 224 payloads (54%)

5	25	5	33	28	128

a. Communication/Navigation.

tank and the Tug leaves 2.44 m of payload bay length for the Tug payload. An automated payload packaging technique was utilized to scan the mission model and select payloads which could share the LST maintenance mission, given these constraints. Table VII-5 presents the resulting list of compatible missions. Each row of the table lists a payload, its orbit characteristics, its physical dimensions, and the calendar year of flight. At the lower right of the table are annual totals of payloads available for LST maintenance mission sharing. The major point to be learned from this table is that ample candidates for flight sharing exist each year.

b. Spares in Pressurized Service Module. The second case presented in Figure VII-1 is for the on-orbit manned maintenance mode, utilizing a service module. The service module depicted in the sketch has the dimensions of a current short Sortie Lab. The LST would be docked to the service module with the latter being utilized as an operations base for maintenance activities and a storage area for spares. Since, as is shown in Figure VII-1, only 1.22 m of the payload bay remain for the Tug payload, the number of payload flight sharing candidates is substantially reduced, as shown in Table VII-6. In addition, in this case, the LST maintenance mission incurs the cost of carrying the 4536 kg (10 000 lb) service module to orbit.

c. Spares in the Crew Compartment. Preliminary investigation revealed approximately 8.5 m^3 (300 ft^3) of volume available in the crew compartment for packaging LST instruments and spares inventory and the necessary support equipment. In this case, maintenance would be performed by docking the orbiter to the LST and using the crew compartment as the

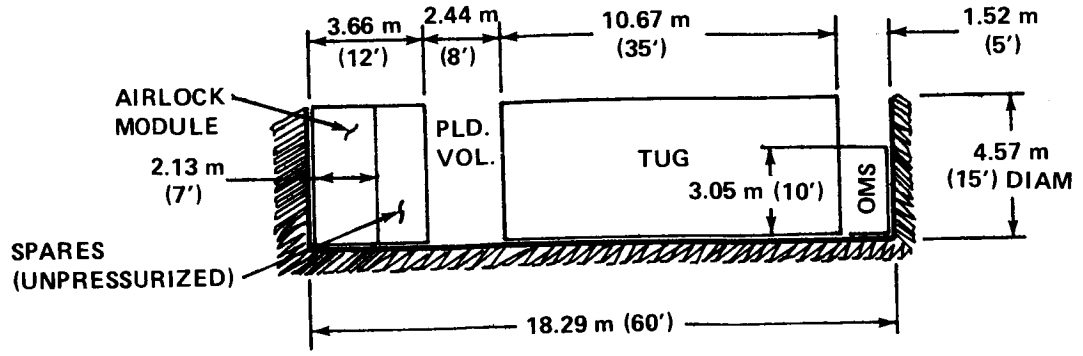

UNPRESSURIZED SPARES IN CARGO BAY

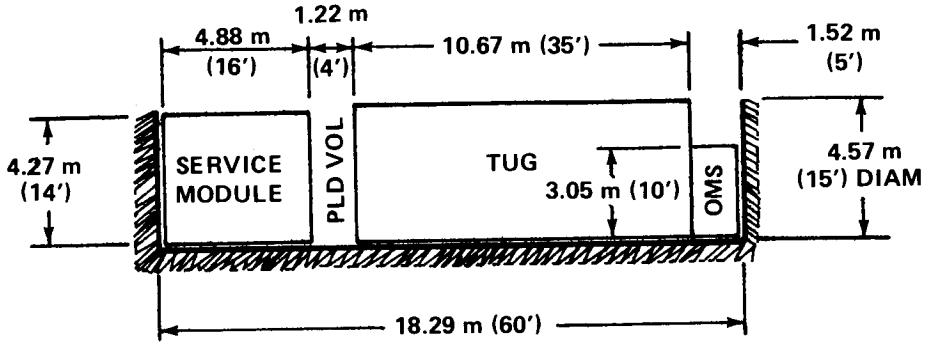

SPARES IN PRESSURIZED SERVICE MODULE

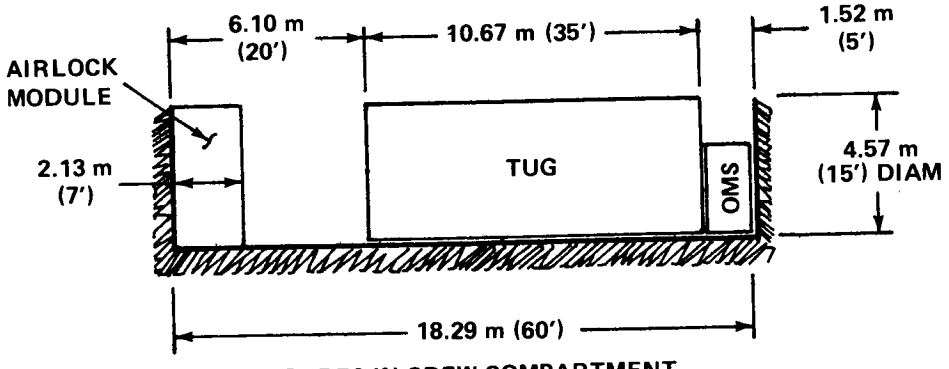

SPARES IN CREW COMPARTMENT

8.5 m^3 (300 ft^3) AVAILABLE IN CREW COMPARTMENT.

NOTE: PD BASELINE REUSABLE TUG USED IN CAPTURE ANALYSIS.

Figure VII-1. Maximum payload length for various spares locations.

TABLE VII-5. LST REFURBISHMENT COMPATIBILITY ANALYSIS — UNPRESSURIZED MODE

NO	NASA-NO	TITLE	INC	APO	PERI	DIA	LEN	WT	VOL	VEL	79	80	81	82	83	84	85	86	87	88	89	90	TOTAL
1	NA2-1	EXPLORERS - LEO	28.50	297	297	2.6	6.2	373	32	683	1	1	1	1	1	1	1	1	1	1	1	1	12
2	NA2-2	EXPLORERS - SYNC	28.50	19323	19323	2.6	6.2	373	32	12928	0	1	0	0	0	1	0	C	0	1	0	1	4
3	NA2-3	HIGH ENERGY ASTRONOMY OB	28.50	250	250	8.8	43.0	18264	2615	526	1	0	0	0	1	1	0	C	0	0	1	0	4
4	NA2-4	HEAO - REVISITS	28.50	250	250	15.0	5.0	3500	885	526	0	1	1	1	0	1	2	2	2	1	0	1	12
5	NA2-8	LST - REVISITS	55.00	270	270	15.0	5.0	3500	885	593	0	0	0	0	0	0	0	0	C	1	1	1	4
6	NA2-9	LARGE HI ENERGY TELESCOP	28.50	400	400	10.0	32.0	15781	2513	1019	0	0	0	0	0	0	0	0	0	0	1	0	1
7	NA2-10	LHET - REVISITS	28.50	400	400	15.0	5.0	3500	885	1019	0	0	0	0	0	0	0	0	0	0	0	1	1
8	NP2-13	EXPLORERS - UPPER ATMOSP	90.00	2000	100	4.0	8.0	1160	100	2781	1	0	1	0	1	0	1	C	1	0	1	0	6
9	NP2-14	EXPLORERS - MEDIUM ALTIT	90.00	20000	1000	5.0	8.0	570	157	11412	1	0	1	0	1	0	1	C	1	0	1	0	6
10	NP2-15	EXPLORERS - HIGH ALTITUD	.00	0	0	4.0	6.0	640	75	14419	0	1	0	1	0	1	0	1	0	1	0	1	6
11	NP2-16	GRAVITY AND REL SAT LEO	90.00	500	500	7.6	12.0	462	635	1333	1	0	0	1	0	0	0	0	0	0	0	0	2
12	NP2-17	GRAVITY AND REL SAT SOL	.00	0	0	8.5	6.8	770	385	22219	0	0	0	0	0	0	0	1	0	0	0	1	2
13	NP2-21	PHYSICS LAB	55.00	270	270	14.0	42.0	22811	6465	593	0	0	0	0	0	0	0	0	1	0	1	0	2
14	NE2-41	SYNC METEROID SATELLITE	.00	19323	19323	6.0	6.0	535	169	14103	0	0	1	1	0	0	0	0	0	0	0	0	2
15	NE2-42	EARTH-RESOURCES SAT	98.00	500	500	10.0	11.5	1800	903	1333	2	2	0	0	0	1	1	0	0	0	0	2	8
16	NE2-44	EARTH OBSERVATION LAB	90.00	100	100	14.0	19.0	13462	2924	0	0	1	1	1	1	1	1	1	1	1	1	1	11
17	NE2-45	GEOPAUSE	90.00	270	270	5.0	9.0	710	176	593	1	1	0	0	0	0	0	0	0	0	0	0	2
18	NC2-47	SMALL APP TECH SAT-SYNC	.00	19323	19323	3.0	7.0	300	49	14104	1	1	1	1	1	1	1	1	1	1	1	1	12
19	NC2-48	SMALL APP TECH SAT-POLAR	90.00	300	300	3.0	7.0	300	49	693	1	1	1	1	1	1	1	1	1	1	1	1	12
20	NC2-53	COMM/NAV LABORATORY-SORT	28.00	200	200	14.0	41.0	17510	6311	354	0	0	1	1	0	0	1	C	0	C	1	0	4
21	NB2-55	BIO-RESEARCH MODULE	28.50	300	300	3.0	5.0	370	35	693	2	0	0	0	0	0	0	C	0	C	0	0	2
22	NB2-56	TELEOPERATOR	28.50	300	300	4.0	3.0	960	35	693	1	0	0	0	0	0	0	C	0	C	0	0	1
23	NB2-57	MINI 7 -DAY MODULE	.00	250	250	14.0	32.0	14041	4926	525	0	1	1	1	0	C	0	C	0	C	0	0	3
24	NB2-58	MINI 30-DAY MODULE -SORT	.00	250	250	14.0	32.0	18891	4926	525	0	0	0	0	1	1	0	C	0	0	0	0	2
25	NB2-59	MINI 30-DAY MODULE -RAM	55.00	270	270	14.0	32.0	26576	4926	593	0	0	0	0	0	0	1	1	0	C	0	0	2
26	NB2-60	STATION LAB EXP	55.00	270	270	14.0	32.0	28984	4926	593	0	0	0	0	0	0	0	0	C	1	0	0	1
27	NT2-61	METEROID EXPOSURE MOD	28.50	270	270	14.0	35.0	10000	5387	593	0	1	0	0	1	0	0	0	0	0	0	0	2
28	NT2-62	MATERIAL SCIENCE EXPER	.00	0	0	7.0	10.0	2720	384	0	1	1	1	1	1	2	0	0	0	0	0	0	7
29	NT2-64	TECHNOLOGY AND NAT SC LA	55.00	270	270	14.0	32.0	19113	4926	593	0	0	0	0	0	0	1	0	0	0	0	0	1
30	NS2-68	CREW/OPERATIONAL LOGIST	55.00	270	270	14.0	28.0	20000	4310	593	0	0	0	0	0	0	5	6	6	6	6	6	35
31	NCN-10A	NAV/TRAFFIC CONTROL	29.00	30000	1600	5.0	8.0	725	157	13932	3	1	2	0	1	0	1	C	1	0	1	0	10
32	NCN-10B	NAV/TRAFFIC CONTROL	5.00	19300	1930	5.0	8.0	725	157	13882	0	1	1	0	1	0	1	C	1	0	1	0	6
33	NE0-7	TOS METEOROLOGICAL SATEL	100.00	700	700	5.0	6.0	1030	118	1932	1	1	1	1	1	1	1	1	1	1	1	1	12
34	NE0-15	SYNCHRONOUS METEOROLOGIC	.00	19323	19323	5.0	8.0	1035	157	14132	1	1	1	1	1	1	1	1	1	1	1	1	12
35	NE0-11	SYNCHRONOUS EARTH RESOUR	.00	19323	19323	6.0	6.0	1030	170	14132	0	0	0	0	0	0	4	0	0	4	0	0	8
											--	--	--	--	--	--	--	--	--	--	--	--	--
										TOTAL	19	17	16	13	14	14	25	17	21	20	21	20	217

TABLE VII-6. LST REFURBISHMENT COMPATIBILITY ANALYSIS — PRESSURIZED MODE

NO	NASA-NO	TITLE	INC	APO	PERI	DIA	LEN	WT	VOL	VEL	79	80	81	82	83	84	85	86	87	88	89	90	TOTAL
1	NA2-1	EXPLORERS - LEO	28.50	297	297	2.6	6.2	373	32	683	1	1	1	1	1	1	1	1	1	1	1	1	12
2	NA2-4	HEAO - REVISITS	28.50	250	250	15.0	5.0	3500	885	526	0	1	1	1	0	1	2	2	2	1	0	1	12
3	NA2-8	LSO - REVISITS	55.00	270	270	15.0	5.0	3500	885	593	0	0	0	0	0	0	0	0	1	1	1	1	4
4	NA2-9	LARGE HI ENERGY TELESCOP	28.50	400	400	10.0	32.0	15781	2513	1019	0	0	0	0	0	0	0	0	0	0	1	0	1
5	NA2-10	LHET - REVISITS	28.50	400	400	15.0	5.0	3500	885	1019	0	0	0	0	0	0	0	0	0	0	0	1	1
6	NE2-44	EARTH OBSERVATION LAB	90.00	100	100	14.0	19.0	13462	2924	0	0	1	1	1	1	1	1	1	1	1	1	1	11
7	NE2-45	GEOPAUSE	90.00	270	270	5.0	9.0	710	176	593	1	1	0	0	0	0	0	0	0	0	0	0	2
8	NC2-48	SMALL APP TECH SAT-POLAR	90.00	300	300	3.0	7.0	300	49	693	1	1	1	1	1	1	1	1	1	1	1	1	12
9	NB2-55	BIO-RESEARCH MODULE	28.50	300	300	3.0	5.0	370	35	693	2	0	0	0	0	0	0	0	0	0	0	0	2
10	NB2-56	TELEOPERATOR	28.50	300	300	4.0	3.0	960	35	693	1	0	0	0	0	0	0	0	0	0	0	0	1
11	NB2-57	MINI 7 -DAY MODULE	.00	250	250	14.0	32.0	14041	4926	525	0	1	1	1	0	0	0	0	0	0	0	0	3
12	NB2-58	MINI 30-DAY MODULE -SORT	.00	250	250	14.0	32.0	18891	4926	525	0	0	0	0	1	1	0	0	0	0	0	0	2
13	NB2-59	MINI 30-DAY MODULE -RAM	55.00	270	270	14.0	32.0	26576	4926	593	0	0	0	0	0	0	1	1	0	0	0	0	2
14	NB2-60	STATION LAB EXP	55.00	270	270	14.0	32.0	28984	4926	593	0	0	0	0	0	0	0	0	1	0	0	0	1
15	NT2-61	METEROID EXPOSURE MOD	28.50	270	270	14.0	35.0	10000	5387	593	0	1	0	0	1	0	0	0	0	0	0	0	2
16	NT2-62	MATERIAL SCIENCE EXPER	.00	0	0	7.0	10.0	2720	384	0	1	1	1	1	1	2	0	0	0	0	0	0	7
17	NT2-64	TECHNOLOGY AND NAT SC LA	55.00	270	270	14.0	32.0	19113	4926	593	0	0	0	0	0	0	1	0	0	0	0	0	1
18	NS2-68	CREW/OPERATIONAL LOGIST	55.00	270	270	14.0	28.0	20000	4310	593	0	0	0	0	0	0	5	6	6	6	6	6	35
										TOTAL	7	8	6	6	6	7	12	12	13	11	11	12	111

maintenance base of operations. As shown in Table VII-7, the flight sharing analysis for this case revealed that 77 percent of payloads in the mission model could share flights with the LST maintenance mission.

Because of these results, on-orbit manned maintenance using the service module was no longer considered a viable option.

3. Number of Shuttle Flights Required. Table VII-8 shows the number of Shuttle flights chargeable to each of the candidate maintenance options. As an example, to determine the number of Shuttle flights charged to on-orbit unpressurized (manipulator) maintenance, locate this maintenance mode in the far left column. The column to the immediate right describes the initial maintenance upflight. In this case, a Tug mission was selected to share the orbiter upflight costs. The current round-trip cost for a Shuttle flight is estimated at $10.5 million. One-way flight was considered to be half the round-trip cost or $5.25 million. Recalling that costs are prorated on payload mass ratio, the LST portion of the cost is determined as follows:

1. LST Maintenance Mission Mass

Spares Plus Support Equipment	3 652 kg
OMS	5 443 kg
Total	9 095 kg

2. Shared Payload (Tug Mission)

Tug Payload	467 kg
Tug	16 818 kg
Total	17 285 kg

3. Total Flight Payload Mass 26 380 kg

The LST portion of the flight is $5.25 M $\frac{9\,095}{26\,380}$ = $1.81 M

The next two columns, Retrieval of LST and Return LST to Orbit, do not apply to this maintenance option. The last column contains the orbit flight sharing for the earth return flight. The procedure for calculating prorated costs is the same as previously described. Note that the Tug mass

TABLE VII-7. LST SPARES COMPATIBILITY ANALYSIS — CREW COMPARTMENT MODE, AIRLOCK MODULE IN BAY

NO	NASA-NO	TITLE	INC	APO	PERI	DIA	LEN	WT	VOL	VEL	79	80	81	82	83	84	85	86	87	88	89	90	TOTAL
1	NA2-1	EXPLORERS - LEO	28.50	297	297	2.6	6.2	373	33	683	1	1	1	1	1	1	1	1	1	1	1	1	12
2	NA2-2	EXPLORERS - SYNC	28.50	19323	19323	2.6	6.2	373	33	12928	0	1	0	0	0	1	0	0	0	1	0	1	4
3	NA2-3	HIGH ENERGY ASTRONOMY OB	28.50	250	250	8.8	43.0	18264	2615	526	1	0	0	0	1	1	0	0	0	0	1	0	4
4	NA2-4	HEAO - REVISITS	28.50	250	250	15.0	5.0	3500	885	526	0	1	1	1	0	1	2	2	2	1	0	1	12
5	NA2-5	LARGE SPACE TELESCOPE	28.50	330	330	12.4	41.7	18581	5036	793	1	0	0	0	1	0	0	0	0	1	0	0	3
6	NA2-6	LST - REVISITS	28.50	330	330	15.0	5.0	3500	885	793	0	1	1	1	0	1	1	1	1	0	1	1	9
7	NA2-8	LSO - REVISITS	55.00	270	270	15.0	5.0	3500	885	593	0	0	0	0	0	0	0	0	1	1	1	1	5
8	NA2-9	LARGE HI ENERGY TELESCOP	28.50	400	400	10.0	32.0	15781	2513	1019	0	0	0	0	0	0	0	0	0	0	1	0	1
9	NA2-10	LHET - REVISITS	28.50	400	400	15.0	5.0	3500	885	1019	0	0	0	0	0	0	0	0	0	0	0	1	1
10	NA2-12	ASTRONOMY AND PHYSICS OB	55.00	270	270	14.0	42.0	23569	6465	593	1	1	1	1	2	2	2	2	2	2	2	2	20
11	NP2-13	EXPLORERS - UPPER ATMOSP	90.00	2000	100	4.0	8.0	1160	100	2781	1	0	1	0	1	0	1	0	1	0	1	0	6
12	NP2-14	EXPLORERS - MEDIUM ALTIT	90.00	20000	100	5.0	8.0	570	157	11412	1	0	1	0	1	0	1	0	1	0	1	0	6
13	NP2-15	EXPLORERS - HIGH ALTITUD	.00	0	0	4.0	6.0	640	75	14419	0	1	0	1	0	1	0	1	0	1	0	1	6
14	NP2-16	GRAVITY AND REL SAT LEO	90.00	500	500	7.8	12.0	462	635	1333	1	0	0	1	0	0	0	0	0	0	0	0	2
15	NP2-17	GRAVITY AND REL SAT SOL	.00	0	0	8.8	6.8	770	385	22219	0	0	0	0	0	0	0	1	0	0	0	1	2
16	NP2-18	ENVIROMENTAL PERT SAT A	55.00	6900	6900	7.0	12.0	4350	462	12850	0	0	1	0	0	1	0	0	0	0	0	0	2
17	NP2-20	HELIOCENTRIC AND INTERST	.00	0	0	10.0	10.0	616	785	28919	0	0	0	0	0	0	0	0	0	1	0	0	1
18	NP2-21	PHYSICS LAB	55.00	270	270	14.0	42.0	22811	6465	593	0	0	0	0	0	0	0	0	1	0	1	0	2
19	NU2-25	VENUS RADAR MAPPER	.00	0	0	10.0	12.0	2081	942	13019	0	0	0	0	0	2	0	0	0	0	0	0	2
20	NU2-26	VENUS LARGE LANDER	.00	0	0	10.0	10.0	1169	785	13019	0	0	0	0	0	0	0	0	0	0	2	0	2
21	NE2-38	EARTH OBSERVATION SAT.	98.00	500	500	10.0	11.5	2400	903	1333	1	1	1	0	1	0	1	0	1	0	1	0	7
22	NE2-39	SYNC EARTH OBSERVATION S	.00	19323	19323	8.0	12.0	2500	603	14103	0	1	0	1	0	0	1	0	1	0	0	1	5
23	NE2-40	TIROS	103.00	906	906	8.0	12.0	1380	603	2487	0	0	1	0	0	0	0	0	0	0	0	0	1
24	NE2-41	SYNC METEROID SATELLITE	.00	19323	19323	6.0	6.0	535	170	14103	0	0	1	1	0	0	0	0	0	0	0	0	2
25	NE2-42	EARTH-RESOURCES SAT	98.00	500	500	10.0	11.5	1800	903	1333	2	2	0	0	0	1	1	0	0	0	0	2	8
26	NE2-43	SYNC EARTH OBSER SAT/PR	.00	19323	19323	10.0	12.0	2640	942	14104	0	0	0	0	0	0	0	0	0	0	1	1	1
27	NE2-44	EARTH OBSERVATION LAB	90.00	100	100	14.0	19.0	13462	2925	0	0	1	1	1	1	1	1	1	1	1	1	1	11
28	NE2-45	GEOPAUSE	90.00	270	270	5.0	9.0	710	177	593	1	1	0	0	0	0	0	0	0	0	0	0	2
29	NC2-47	SMALL APP TECH SAT-SYNC	.00	19323	19323	3.0	7.0	300	49	14104	1	1	1	1	1	1	1	1	1	1	1	1	12
30	NC2-48	SMALL APP TECH SAT-POLAR	90.00	300	300	3.0	7.0	300	49	693	1	1	1	1	1	1	1	1	1	1	1	1	12
31	NC2-53	COMM/NAV LABORATORY-SORT	28.00	200	200	14.0	41.0	17510	6311	354	0	0	1	1	0	0	1	0	0	0	1	0	4
32	NB2-55	BIO-RESEARCH MODULE	28.50	300	300	3.0	5.0	370	35	693	2	0	0	0	0	0	0	0	0	0	0	0	2
33	NB2-56	TELEOPERATOR	28.50	300	300	4.0	3.0	960	35	693	1	0	0	0	0	0	0	0	0	0	0	0	1
34	NB2-57	MINI 7 -DAY MODULE	.00	250	250	14.0	32.0	14041	4926	525	0	1	1	1	0	0	0	0	0	0	0	0	2
35	NB2-58	MINI 30-DAY MODULE -SORT	.00	250	250	14.0	32.0	18891	4926	525	0	0	0	0	1	1	0	0	0	0	0	0	2
36	NB2-59	MINI 30-DAY MODULE -RAM	55.00	270	270	14.0	32.0	26576	4926	593	0	0	0	0	0	0	0	1	1	0	0	0	2
37	NB2-60	STATION LAB EXP	55.00	270	270	14.0	32.0	28984	4926	593	0	0	0	0	0	0	0	0	1	0	0	0	1
38	NT2-61	METEROID EXPOSURE MOD	28.50	270	270	14.0	35.0	10000	5388	593	0	1	0	0	1	0	0	0	0	0	0	0	2
39	NT2-62	MATERIAL SCIENCE EXPER	.00	0	0	7.0	10.0	2720	385	0	1	1	1	1	1	2	0	0	0	0	0	0	7
40	NT2-63	ADVANCED TECH EXP	28.50	250	250	14.0	47.5	13781	7310	525	0	1	0	1	0	1	0	0	0	0	0	0	3
41	NT2-64	TECHNOLOGY AND NAT SC LA	55.00	270	270	14.0	32.0	19113	4926	593	0	0	0	0	0	0	1	0	0	0	0	0	1
42	NS2-68	CREW/OPERATIONAL LOGIST	55.00	270	270	14.0	28.0	20000	4310	593	0	0	0	0	0	0	5	6	6	6	6	6	35
43	NCN-9	FOREIGN DOMESTIC COM.	.00	19323	19323	4.0	12.0	1030	151	14132	0	2	6	2	2	0	0	4	5	2	1	2	24
44	NCN-10A	NAV/TRAFFIC CONTROL	29.00	30000	16000	5.0	8.0	725	157	13932	3	1	2	0	1	0	1	0	1	0	1	0	10
45	NCN-10B	NAV/TRAFFIC CONTROL	5.00	19300	19300	5.0	8.0	725	157	13882	0	1	1	0	1	0	1	0	1	0	1	0	6
46	NE0-7	TOS METEOROLOGICAL SATEL	100.00	700	700	5.0	6.0	1030	118	1932	1	1	1	1	1	1	1	1	1	1	1	1	12
47	NE0-15	SYNCHRONOUS METEOROLOGIC	.00	19323	19323	5.0	8.0	1035	157	14132	1	1	1	1	1	1	1	1	1	1	1	1	12
48	NE0-16	POLAR EARTH RESOURCES	100.00	500	500	6.0	12.0	2590	339	1382	4	0	4	0	4	0	4	0	0	0	6	0	22
49	NE0-11	SYNCHRONOUS EARTH RESOUR	.00	19323	19323	6.0	6.0	1030	170	14132	0	0	0	0	0	0	4	0	0	4	0	0	8
										TOTAL	25	24	31	19	24	21	34	24	31	26	34	37	321

TABLE VII-8. SHUTTLE FLIGHTS REQUIRED FOR VARIOUS SCHEDULED MAINTENANCE METHODS

Maintenance Mode	Initial Maintenance Upflight	Retrieval of LST	Return LST to Orbit	Orbiter Return Flight
On-Orbit Manipulator	• LST Maintenance 3 652 kg (8 050 lb) Spares 5 443 kg (12 000 lb) OMS • Shared Payload 467 kg (1 030 lb) Satellite 16 818 kg (37 077 lb) Tug	Not Applicable	Not Applicable	LST Maintenance 3 652 kg Spares Plus Empty OMS Tank — 544 kg Shared Payload 2 659 kg (5 863 lb) Tug
On-Orbit Pressurized	• LST Maintenance 1 688 kg (3 722 lb) Spares 5 443 kg (12 000 lb) OMS • Shared Payload 467 kg (1 030 lb) Satellite 16 818 kg (37 077 lb) Tug	Not Applicable	Not Applicable	LST Maintenance 1 688 kg Spares Plus Empty OMS Tank — 544 kg Shared Payload 2 659 kg (5 863 lb) Tug
Earth Return	Any Shuttle Ascent Flight (No Charge to LST Program)	Retrieve LST (No Payload Sharing)	Return LST to Orbit (No Payload Sharing)	Orbiter Returns Empty; Few Payloads Are Available to Share Return Flight

shown reflects propellant consumption and satellite deployment. The final result is that the LST program is charged for a portion of the cost of one round-trip Shuttle flight for on-orbit manipulator maintenance.

The on-orbit pressurized (manned) maintenance flight sharing is similar to the previously discussed case. It, too, is charged for a portion of one round-trip flight on the orbiter. Detailed cost comparisons are discussed later.

Earth return maintenance is not charged for the initial Shuttle upflight. The LST will be retrieved on the down leg of a mission to deploy a payload. Studying Table VII-8 reveals that the LST program is charged for one and one-half round-trip Shuttle flights for the earth return maintenance option. As will be discussed later, orbiter flight costs are a major discriminator when comparing maintenance options.

4. Orbital Operations During Flight Sharing. Thus far the discussion on flight sharing has been devoted to the physical compatibility of payloads. The operational compatibility of shared payloads will now be considered. Figure VII-2 shows that it is operationally feasible to deploy a Tug at a 185 km (100 n.mi.) orbit, have the orbiter transfer to a 61 km (330 n.mi.) orbit, rendezvous with the LST, perform the LST maintenance mission, have the Tug rendezvous with the orbiter at the 611 km orbit, and have the orbiter return to earth with the empty Tug. The upper timeline in Figure VII-2 illustrates Tug events, whereas the lower timeline presents current LST maintenance activities. The 124 hours available for LST maintenance represents a minimum value due to a combination of worst case assumptions with respect to Tug phasing.

Detailed crew activity schedules of the maintenance operations show that the required maintenance can be performed by two crewmen in 2 working days. Therefore, flight sharing with Tug missions provides ample time to conduct the LST maintenance.

5. Scheduled Maintenance Cost Comparison. The results of the cost comparison study of the three candidate scheduled maintenance methods are given in Table VII-9. On-orbit pressurized maintenance was selected as the cost study reference design, and costs are presented as millions of dollars difference (Δ) from the reference design. The four cost columns give delta cost for (1) shuttle flights, (2) design, development, test, and engineering (DDT&E), (3) recurring cost, and (4) total cost.

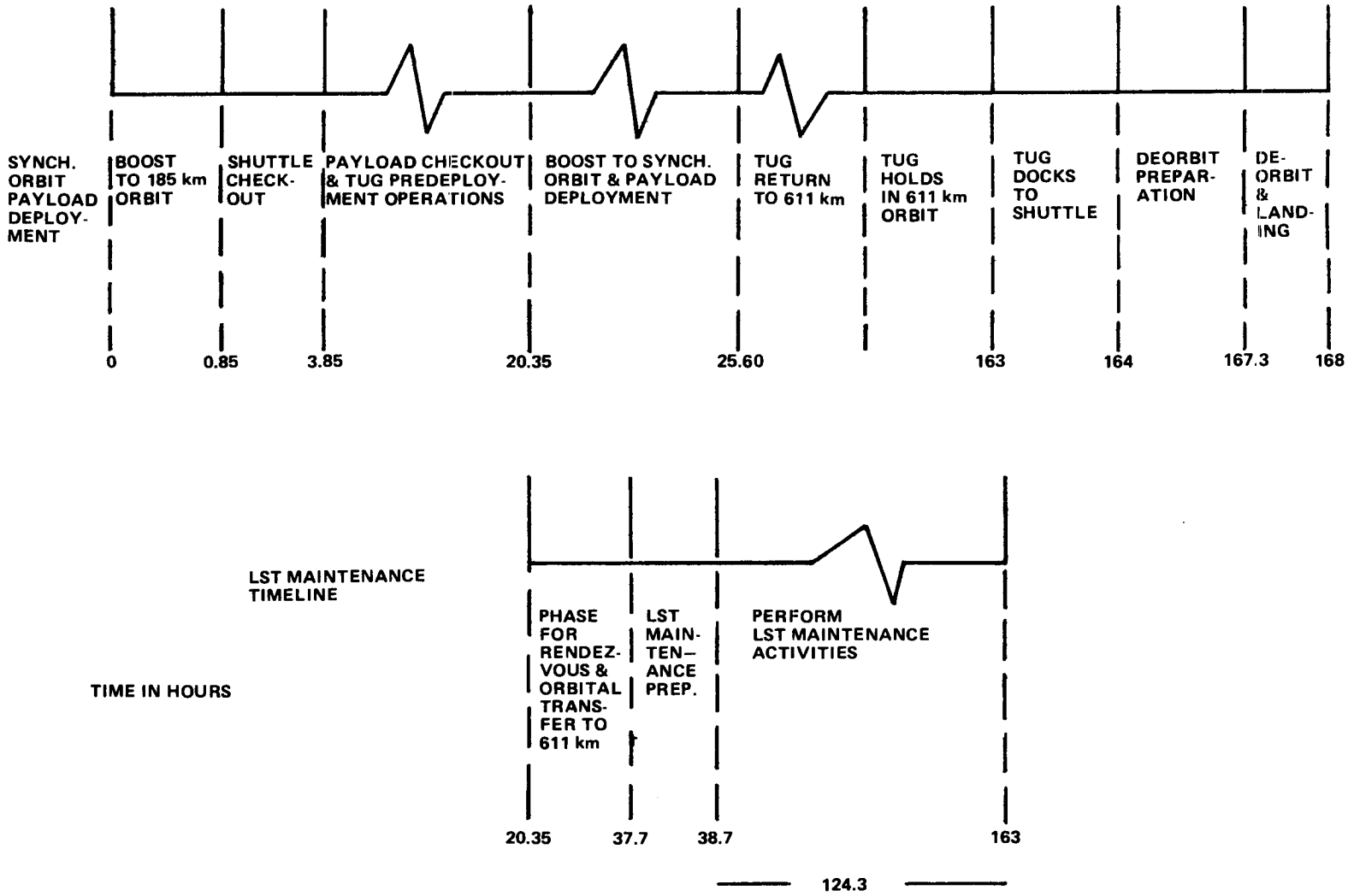

Figure VII-2. LST shared mission to synchronous orbit.

TABLE VII-9. LST SCHEDULED MAINTENANCE COST COMPARISON[a,b]

Maintenance Mode	Shuttle Cost	DDT&E	Recurring	Total
(Reference Design) Pressurized On-Orbit Maintenance	0	0	0	0
Unpressurized On-Orbit Maintenance Using Manipulators	1.09	31.93	1.93	34.95
Unpressurized On-Orbit Maintenance Using Manipulators (Increased Configuration & System Testing)	1.09	55.27	1.93	58.29
Earth Return Maintenance	11.82	-(11.97)	8.99	8.84

a. Reference design maintenance mode for cost study is on-orbit pressurized.
b. Cost numbers are in $ Millions (Δ) from baseline.

The Shuttle flight costs for the on-orbit pressurized maintenance and the on-orbit unpressurized maintenance using manipulators are nearly equal since both missions were shared with a Tug flight. The earth return case is based on the cost of one and one-half round trips above the design reference mission.

Two sets of cost numbers are presented for the on-orbit unpressurized maintenance method using manipulators. These two cases bracket a range of estimates (NASA and industry) which results from an uncertainty as to the type and amount of required testing. More details on this subject will be presented later. From Table VII-9, on-orbit unpressurized maintenance using manipulators is seen to be the least attractive option from a cost standpoint and was dropped from further consideration at this time.

Although earth return maintenance appears to be more costly than on-orbit pressurized maintenance, the $8.84 million is considered to be within the accuracy of the cost estimating techniques. Therefore, the earth return and on-orbit pressurized maintenance were considered equal competitors at this point.

The major items contributing to the high DDT&E cost of the on-orbit unpressurized maintenance using manipulators are:

1. Structure — $3.97M greater than design reference.
2. Electrical power — $5.60M greater than design reference.
3. Test hardware — $3.17M greater than design reference.
4. Special manipulator — $20.00M.

These high costs are the result of more complex and highly integrated modules, complex umbilicals, extensive testing, and special equipment. It is possible that these costs could show a substantial increase if configuration and subsystem test requirements increase. A conservative estimate of manipulator maintenance costs incorporating a maximum amount of testing is $57.2M above the reference design as shown in Table VII-9.

Again referring to Table VII-9, the Shuttle flight cost for the earth return maintenance option is $11.82 million greater than the design reference. With sharing effects included, the design reference maintenance mission Shuttle flight cost is $3.93M. Although scheduled maintenance may be planned, contingency or unplanned maintenance must be considered as a very realistic possibility. The cost impact if an additional maintenance visit is required during the 5-year precursor mission is presented in Table VII-10. Again the cost design reference is on-orbit manned maintenance with one maintenance mission. The costs shown are in millions of dollars difference from the design reference. It is clear that the earth return maintenance cost is highly sensitive to the number of maintenance missions required. As a result of these findings, the on-orbit manned maintenance concept was selected as the recommended maintenance mode for purposes of detailed study.

6. Recommended Reference Design Maintenance Method. The selection of on-orbit manned maintenance was made under the ground rule of one scheduled maintenance mission after 2 1/2 years of LST operation. Perturbation of the schedule was accomplished by assessing the impact of a contingency maintenance flight. Therefore, inherent in the scheduled maintenance

TABLE VII-10. LST MAINTENANCE COST IMPACT DUE TO ADDITIONAL SHUTTLE FLIGHTS[a,b]

Maintenance Mode	Δ Cost for One Maintenance Mission	Δ Cost for Two Maintenance Missions
On-Orbit Manned Maintenance	0 (Design Reference)	5.9[c]
Earth Return Maintenance	8.8	31.8[d]

a. Cost design reference is on-orbit manned maintenance with one mission.
b. Cost comparison is in $ millions Δ from baseline.
c. Design reference maintenance Shuttle costs resulting from flight sharing plus $2.0M for spares.
d. Includes $7.19M recurring costs and $15.75M for one and one-half additional Shuttle flights.

concept is the requirement for designing to accommodate unscheduled contingency maintenance. It follows that if the LST requires maintenance prior to the scheduled time, unscheduled maintenance will probably be performed. If the LST is performing at an acceptable level at the time for scheduled maintenance, maintenance will probably be postponed until required. Therefore, unscheduled maintenance better satisfies real-world requirements.

In summary, the selected maintenance concept is unscheduled, on-orbit manned maintenance without using a servicing module (Sortie Lab). Equipment will be replaced only when required because of failure or scientific update. Unscheduled maintenance will allow for reduction in design lifetime of equipment from 2 1/2 years to some shorter time. Future studies will determine the least-cost design lifetime/maintenance frequency combination.

To reduce costs the LST maintenance mission will share Shuttle flights with other payloads. The LST may be returned to earth for major maintenance when dictated by complexity of repair or when science desires a major upgrading of optical or instrument systems. Table VII-11 presents a listing of the items which would probably be replaced on an unscheduled or "typical" maintenance mission.

TABLE VII-11. "TYPICAL" UNSCHEDULED ON-ORBIT MAINTENANCE MISSION EQUIPMENT LOAD

Component	Qunatity	Unit Mass (kg)	Total Mass (kg)	Unit Volume (m^3)	Total Volume (m^3)
• Life-Limited Components					
Tape Recorder	3	5.44	16.32	0.00793	0.02379
Batteries	6	21.09	126.54	0.02011	0.12066
			142.86		0.14445
		20% Contin.	28.57	50% Contin.	0.07223
		Total =	171.43	Total =	0.21668
		=	(378 lb)	=	(7.65 ft^3)
• Typical Random-Failure Items					
Reference Gyro Assembly (RGA)	1	10.45	10.45	0.01133	0.01133
Digital Process Assembly (DPA)	1	6.20	6.20	0.00566	0.00566
Control Moment Gyro (CMG)	1	80.90	80.90	0.46162	0.46162
Regulator	1	3.50	3.50	0.00850	0.00850
Remote Decoder	1	0.45	0.45	0.00283	0.00283
Data Acquisition Unit (DAU)	1	0.10	0.10	0.00014	0.00014
			101.60		0.49008
		+20% Contin.	20.32	+50% Contin.	0.24504
		Total =	121.92	Total =	0.73512
		=	(269 lb)	=	(25.96 ft^3)

TABLE VII-11. (Concluded)

Component	Quantity	Unit Mass (kg)	Total Mass (kg)	Unit Volume (m^3)	Total Volume (m^3)
• Typical Science Update Items					
f/96 Camera & Filter Wheel	3	67.13	201.39	0.02266	0.06797
Echelle Spectrograph	1	51.76	51.76	0.16142	0.16142
Faint Object Spectrograph	1	55.79	55.79	0.09912	0.09912
			308.94		0.32851
		+20% Contin.	61.79	+50% Contin.	0.16426
		Total =	370.73	Total =	0.49277
		=	(817 lb)	=	($17.41\ ft^3$)
Subtotal Spares, & Instruments			664.08 kg (1465 lb)		$1.44457\ m^3$ ($51.01\ ft^3$)
Support Equipment (Contamination Control + Miscellaneous)			459.94 kg		$3.31344\ m^3$
Total for This Mission			1124.02 kg (2478 lb)		$4.75801\ m^3$ ($168\ ft^3$)

D. Crew Time for Typical Maintenance Mission

Table VII-12 lists the discrete crew maintenance tasks, the associated crew time to perform each task, and the overall crew time to replace various components. The replacement items selected for the preliminary analysis of crew maintenance time are those for a "typical" unscheduled maintenance mission and include those shown in the following list:

1. Life-Limited Items
   - a. Tape Recorder — 3
   - b. Battery — 6
2. Typical Random-Failure Items
   - a. Reference Gyro Assembly (RGA) — 1
   - b. Digital Processor Assembly (DPA) — 1
   - c. Control Moment Gyro (CMG) — 1
   - d. Regulator — 1
   - e. Remote Decoder — 1
   - f. Data Acquisition Unit (DAU) — 1
3. Typical Science Update Items
   - a. f/96 Camera & Filter Wheel — 3
   - b. Echelle Spectrograph — 1
   - c. Faint Object Spectrograph (UV) — 1

The following assumptions were used in the crew maintenance time analysis:

1. All replacement items are readily accessible in a resupply vehicle.
2. The resupply vehicle is docked directly to the SSM.

TABLE VII-12. PRELIMINARY ANALYSIS OF CREW MAINTENANCE TASK TIME[a]

Subsystem	Task Analysis	Estimated Crew Time (min)	Total Elapsed Time (min)
Tape Recorders (3)	● Insure tape recorders are electrically isolated	2	
	● Disconnect electrical connections	6	
	● Remove units from mounts	9	
	● Transfer used subsystems to resupply module	6	
	● Stow temporarily	2	
	● Remove new tape recorders from launch restraints & stow temporarily	4	
	● Transfer new units to LST	2	
	● Permanently stow used tape recorder in resupply module	5	
	● Mount new units in LST	10	
	● Reconnect electrical interface	5	
	● Test units	5	
	Estimated Crew Time Required	56	
	20% Contingency	11	
	Total	67 (1 hr, 7 min)	

a. Mode — on-orbit pressurized (shirtsleeve).

TABLE VII-12. (Continued)

Subsystem	Task Analysis	Estimated Crew Time (min)	Total Elapsed Time (min)
Batteries (6)	• Remove dummy plug & plug in test connector from Shuttle	10	
	• Discharge batteries		430
	• Disconnect test connector + operational connector	10	
	• Put a shorting plug on test + operational connectors	5	
	• Remove battery and stow	30	
	• Transfer new battery to LST + secure in place	30	
	• Plug in charger	10	
	• Plug in test connector	10	
	• Charge and test batteries		1190
	• Remove test connector	10	
	• Replace dummy plug in test connector	10	
	• Reconnect operational connector	5	
	Estimated Crew Time Required	130	1210
	20% Contingency	26	242
	Total	156 (2 hr, 36 min)	1452 (24 hr, 12 min)

TABLE VII-12. (Continued)

Subsystem	Task Analysis	Estimated Crew Time (min)	Total Elapsed Time (min)
Reference Gyro Assembly (RGA)	• Electrically isolate system	1	2
	• Run down system		
	• Disconnect electrical interface (3)	3	
	• Disconnect physical interface	5	
	• Remove and transfer to Shuttle	4	
	• Temporarily stow	2	
	• Remove new system	4	
	• Permanently stow used RGA in resupply module	3	
	• Transfer new system to LST	4	
	• Secure in place	5	
	• Reconnect electrical connections (3)	3	
	• Spin up all units		30
	• Test and check out subsystems	20	—
	Estimated Crew Time Required	54	50
	20% Contingency	11	10
	Total	65 (1 hr, 5 min)	60 (1 hr)

TABLE VII-12. (Continued)

Subsystem	Task Analysis	Estimated Crew Time (min)	Total Elapsed Time (min)
Control Moment Gyro (CMG)	• Turn off power to CMG	1	241
	• Run down CMG		
	• Unplug electrical connections (4) on gimbal control electronics units	4	
	• Remove constraint bolts on mounting brackets	10	
	• Remove CMG and transfer to Shuttle	5	
	• Temporarily stow	2	
	• Release new CMG from launch restraints	5	
	• Permanently stow used CMG unit in Shuttle	10	
	• Transfer new CMG to LST	5	
	• Secure with mounting brackets	10	
	• Connect gimbal control electronics units (4)	4	
	• Activate power to CMG	1	

TABLE VII-12. (Continued)

Subsystem	Task Analysis	Estimated Crew Time (min)	Total Elapsed Time (min)
Control Moment Gyro (CMG) (Concluded)	• Run up all CMG units		402
	• Check and test systems	15	—
	Estimated Crew Time Required	72	432
	20% Contingency	14	86
	Total	86 (1 hr, 26 min)	518 (8 hr, 38 min)
Digital Processor Assembly, Regulator, Remote Decoder, Digital Acquisition Unit (These are simple "blackbox" items)	• Insure subsystem is electrically isolated	2	
	• Disconnect electrical connections	2	
	• Disconnect physical interface	3	
	• Transfer used subsystem to Shuttle and stow temporarily	5	
	• Remove new subsystem and stow temporarily	3	
	• Stow used subsystem in Shuttle permanently for earth return	5	
	• Transfer new subsystem to LST	2	

TABLE VII-12. (Continued)

Subsystem	Task Analysis	Estimated Crew Time (min)	Total Elapsed Time (min)
Digital Processor Assembly, Regulator, Remote Decoder, Digital Acquisition Unit (These are simple "blackbox" items) (Concluded)	• Secure new subsystem in place in LST	4	
	• Reconnect electrical lines	2	
	Estimated Crew Time Required	28	
	20% Contingency	6	
	Total	34	
f/96 Camera[b]	• Disconnect electrical connections from cameras (3)	3	
	• Remove camera tubes from main body of instrument	20	
	• Transfer tubes to Shuttle and stow temporarily	15	
	• Disconnect fasteners from mounting brackets + flanges	15	
	• Transfer instrument to Shuttle and stow temporarily	5	
	• Remove new instrument and transfer to LST	6	
	• Mount new instrument to brackets	15	

b. Assumes LST is docked to Shuttle and pressurized. Cathode tube has attained thermal equilibrium with ambient.

TABLE VII-12. (Continued)

Subsystem	Task Analysis	Estimated Crew Time (min)	Total Elapsed Time (min)
f/96 Camera[b] (Concluded)	• Remove new tubes from Shuttle and mount to new instrument in LST	20	
	• Reconnect electrical connections (3)	6	
	• Stow old instrument permanently in Shuttle	10	
	• Stow old tubes permanently in Shuttle	3	
	Estimated Crew Time Required	118	
	20% Contingency	24	
	Total	142 (2 hr, 22 min)	

b. Assumes LST is docked to shuttle and pressurized. Cathode tube has attained thermal equilibrium with ambient.

TABLE VII-12. (Continued)

Subsystem	Task Analysis	Estimated Crew Time (min)	Total Elapsed Time (min)
Echelle Spectrograph	● Electrically isolate instrument	2	
	● Unplug electrical connection	2	
	● Remove constraint pins and bolts	8	
	● Remove instrument and transfer to Shuttle	5	
	● Stow temporarily in Shuttle	3	
	● Remove new instrument and stow temporarily	4	
	● Stow old instrument permanently in Shuttle	8	
	● Transfer new instrument to LST	2	
	● Mount new instrument	8	
	● Connect electrical plug	2	
	Estimated Crew Time Required	43	
	20% Contingency	9	
	Total	52	

TABLE VII-12. (Concluded)

Subsystem	Task Analysis	Estimated Crew Time (min)	Total Elapsed Time (min)
Faint Object Spectrograph, f/12 Camera	See the preceding Echelle Spectrograph Task Analysis	43	
	20% Contingency	9	
	Total (Each)	52	

3. All mechanical, electrical, and fluid connections are the "quick-disconnect" type.

4. Maintenance times are for one crewman working in a shirtsleeve environment; i.e., on-orbit pressurized maintenance mode.

The total crew maintenance time for the replacement of all components in the "typical" unscheduled maintenance mission is slightly greater than 12.5 hours. The total time required for the maintenance operations is about 41.5 hours.

E. Neutral Buoyancy Simulation Activities

Neutral buoyancy simulation activities are in process to further evaluate both the shirtsleeve and the IVA maintenance modes. The pressurized (shirtsleeve maintenance) configuration will be evaluated first using a full-scale mockup of the SSM and SIP in Marshall Space Flight Center's (MSFC's) Neutral Buoyancy Facility. Essentially the same mockup will then be utilized to evaluate IVA maintenance of the same SIP and SSM elements.

The LST mockup represents the flight vehicle design as it existed in late June 1972, with some minor modifications. The mockup has been designed in four major subassemblies to facilitate configuration changes and equipment updates. The major subassemblies comprising the mockup — the docking port, the 3.04 m cylindrical section, the SIP, and the SIP adjustment section — are depicted in Figure VII-3. Most "blackbox" items are mounted on the docking port section on a ring shelf immediately inside the crew entry port. Large components such as the CMGs, the reaction control system (RCS) module, the GN_2 sphere, and the batteries are mounted on removable pallets within the 3.04 m cylindrical section. The SIP mounts to the inside surface of the SIP adjustment section, which in turn mounts to the 3.04 m cylindrical section. This arrangement permits a fore-and-aft SIP adjustment capability of approximately 1.01 m. Planned neutral buoyancy simulation tests will serve to determine the minimum SIP/Docking Port clearance necessary for manned maintenance.

To permit an early initiation of simulation activities, the SIP mockup will be built in two stages. The first (preliminary) stage will include high-fidelity structure and a detailed f/96 camera mockup, while the remaining SIP equipment will be represented only by clearance envelopes, as shown in Figure VII-4. The second stage of the SIP mockup will be achieved by replacing

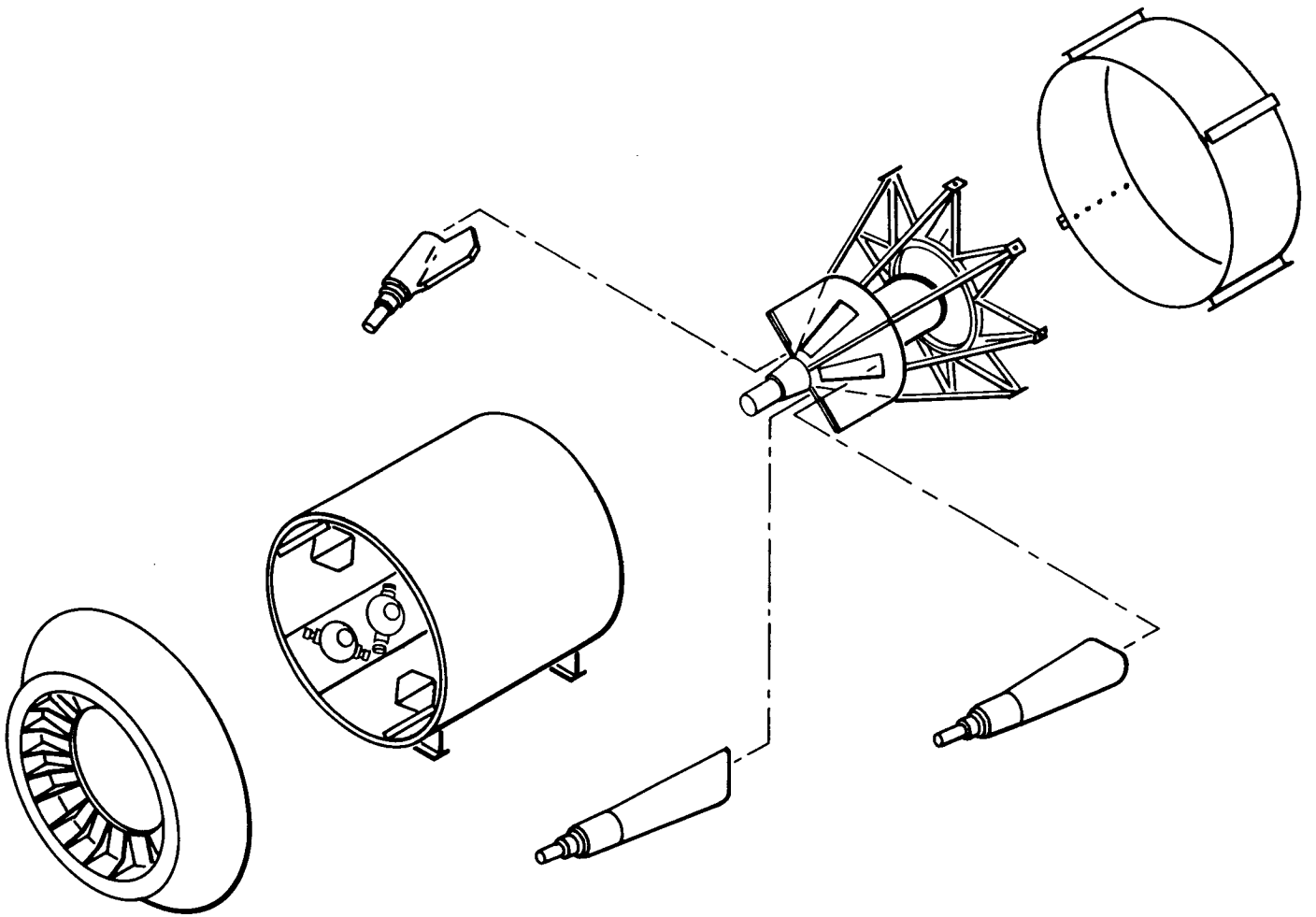

Figure VII-3. Subassemblies of the LST neutral buoyancy mockup.

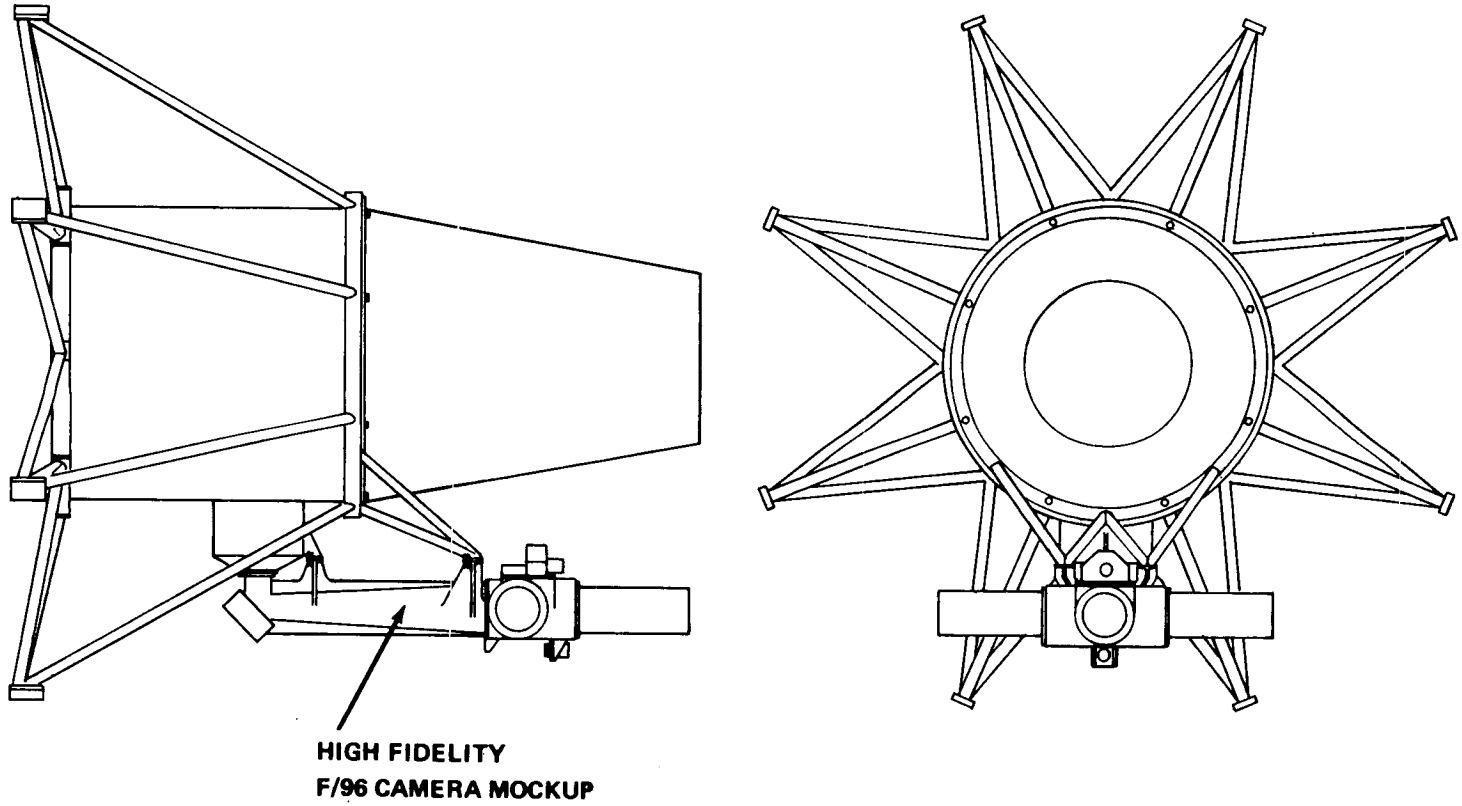

Figure VII-4. Preliminary SIP for the MSFC LST neutral buoyancy mockup.

the axial and radial bay clearance envelopes with detailed mockups of the remaining SIP equipment. The assembled mockup, including the preliminary SIP, is as shown in Figure VII-5. The mockup will be placed in the Neutral Buoyancy Facility in the horizontal position.

Planned simulations with the SSM and the preliminary SIP include the removal and replacement of the following items:

1. Selected components mounted on the ring shelf.
2. RCS module and GN_2 sphere.
3. CMGs.
4. Batteries.
5. Small pallet-mounted items.
6. f/96 camera.

Simulations will be conducted in both the shirtsleeve and pressure-suit modes and will be used to evaluate mobility aids, operational techniques, clearance envelopes, and crew time required to remove and replace each item. The SIP position will be varied during removal and replacement of large items, such as the CMGs, to determine the minimum SSM length required for manned maintenance.

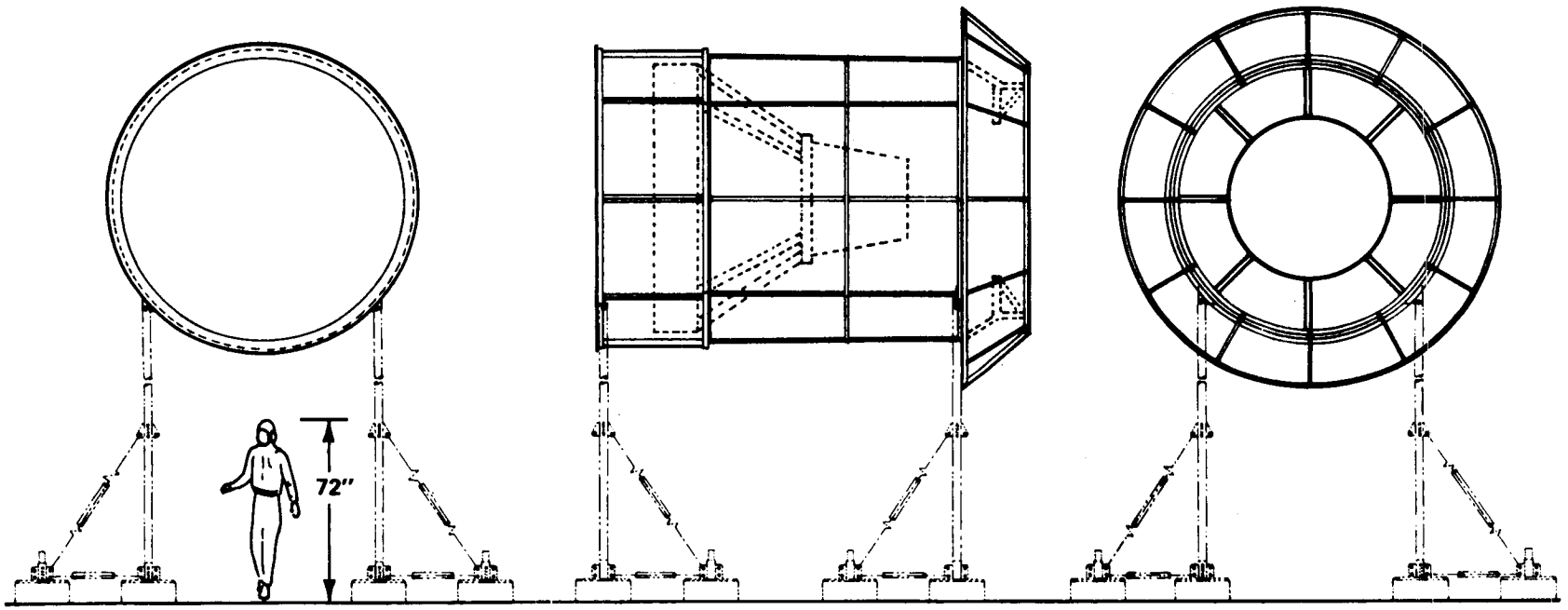

Figure VII-5. Neutral buoyancy mockup.

CHAPTER VIII. RELIABILITY ANALYSIS

TABLE OF CONTENTS

LIST OF ILLUSTRATIONS

LIST OF ILLUSTRATIONS (Concluded)

LIST OF TABLES

CHAPTER VIII. RELIABILITY ANALYSIS

A. Support Systems Module Reliability Point Estimate

1. Introduction and Support Systems Module Reliability Summary. The purpose of the reliability point estimate exercise described here is to provide assurance that no serious reliability flaws have been incorporated into the design reference. Tho this end, only that equipment essential to the LST mission objectives and/or survival of the LST is considered in this estimate. "Survival" refers to those configurations of failed and unfailed equipment that permit the Shuttle to dock with the LST for either return-to-ground (retrieval) or on-orbit maintenance. "Success" is defined to require only that the support systems module (SSM) equipment failure combinations allow the collection, storage, and transmission of undegraded scientific data and enable the SSM to receive and respond to ground commands. This success definition permits a number of degraded modes (reduction of LST efficiency, but not data quality) which are discussed in Section C of this chapter.

A 1-year SSM reliability goal of 0.95 was established for this exercise. This number was selected to ensure a credible assurance of no serious design flaws and to allow for SSM equipment commonality with the High Energy Astronomy Observatory (HEAO) program spacecraft. In general, such reliability goals are, or should be, established by a reliability allocation procedure — allocation being a dynamic programming term used to denote a reliability requirement determined to optimize some system parameter such as cost or performance subject to constraints on other parameters such as weight, volume, or power. To establish such an allocation in a meaningful way in the present case would require considerably greater total system definition than is attainable within the present Phase A study. Moreover, as discussed in Sections C and D of this chapter, the concept of reliability per se is not strictly applicable to maintained systems.

The design reference SSM 1-year reliability point estimate is 0.98408 (Table VIII-1); this number results, for the most part, from design margins, redundant paths arising from functional requirements, and the critical-function, single-point failure (SPF) protection criterion. Figure VIII-1 illustrates the SSM reliability decay. Redundancy beyond that required by the SPF criterion is applied only to the following equipment blocks:

TABLE VIII-1. LST SSM RELIABILITY POINT ESTIMATE SUMMARY

Subsystem	Reliability	
	1 Year	2 Years
Attitude Control (ACS)	0.98795	0.93344
Electrical Power (EPS)	0.99801	0.98520
Communications and Data Handling (C&DHS)	0.99807	0.99191
SSM	0.98408	0.91218

1. Transponders (XPDRs).

2. Reference gyro assembly (RGA).

3. Electrical batteries.

4. Computer memory sizing.

5. Voltage regulators.

The XPDRs chosen (min-mod Apollo and Earth Resources Technology Satellite) represent existing equipment. Other choices, while offering some reliability and mass advantages, would entail a significant cost penalty. With regard to choices of existing equipment, the question of hardware availability during the procurement time frame must be recognized. Some RGA redundancy is necessary to meet any reasonable reliability goal and since the dodecahedral RGA is used in the HEAO spacecraft, it is considered to be existing equipment. An increase in RGA redundancy would incur significant penalities. The batteries represent an unknown reliability (Subsection 3), and the present system sizing corresponds to system requirements. Thus, a reduction of battery capacity or number is not indicated. The cost and mass impacts of varying computer memory size are minor. Therefore, while the redundancy shown reflects more than SPF protection, this is justifiable,

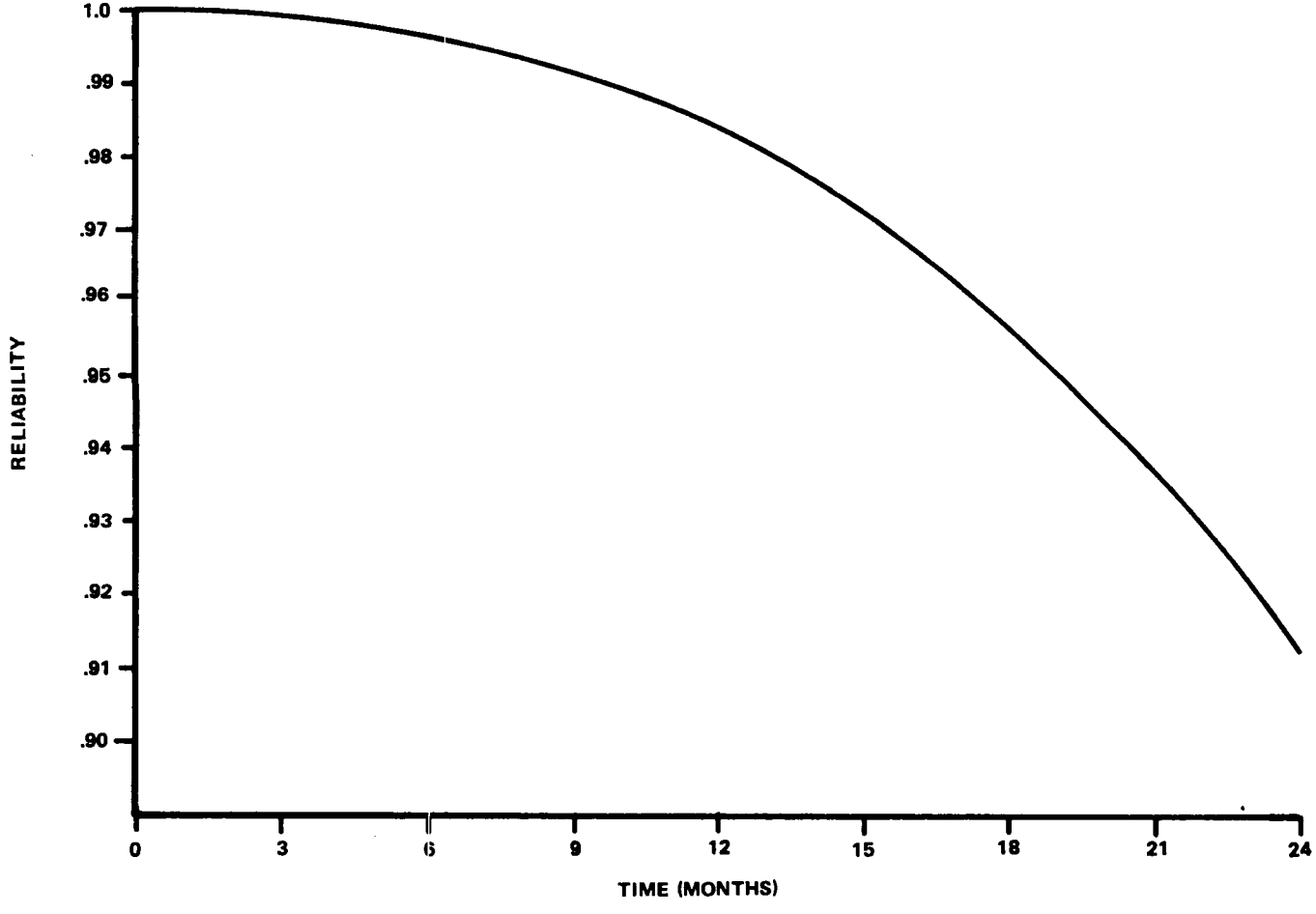

Figure VIII-1. LST SSM reliability curve.

particularly since memory size requirements are "soft." The indicated redundancy for the regulator is a minimum of 4 and a maximum of 6 — a 7.3 kg difference. Since this is a high failure rate item, the additional redundancy is reasonable.

Failure rates used in this exercise are given in Table VIII-2. A listing of specific vendor equipment is provided, where possible, to document failure rate sources; this listing does not necessarily indicate equipment selection preferences. Since these failure rates represent presently achieved values, they are in most cases conservative estimates for the SSM equipment selection time frame. Failure rate reductions of 10:1 and 4:1 for standby status of electronic equipment have been used where appropriate. The code $[n/(\ell + m)]^b$ is used to describe redundant assemblies; b is the number of identical serial blocks within the assembly and, within each block, n is the number of identical elements required for success, ℓ is the number of online elements, and m is the number of standby elements.

2. Attitude Control System. The ACS dependency diagram is shown as Figure VIII-2.

A number of RGA configurations were evaluated against the following considerations:

1. During the performance of certain experiments which are interrupted by occultation, the LST must maintain its two-axis inertial pointing orientation within a 30 arc sec (half-angle) cone. Failure to meet this requirement results in a degraded mode, as discussed in Section C. Based on a worst-case occultation period of 36 min, the RGA must meet the accuracy requirements satisfied by an orthogonal triad of gyros with a random drift rate of 0.005 degree/hour (1σ).

2. In normal operation, it is highly desirable that the LST shall be capable of fault detection by voting the information from redundant operating gyros.

These requirements imply consideration of two physical RGA configurations. The dodecahedral configuration consists of six gyros whose input axes are normal to six of the faces of a regular dodecahedron (Fig. VIII-3). The second configuration, called the orthogonal configuration, is obtained by augmenting a conventional orthogonal triad with a standby gyro on each axis. This latter configuration has the reliability code $[1/(1 + 1)]^3$, and the resulting reliability curve is shown in Figure VIII-4.

TABLE VIII-2. LST SSM FAILURE RATE DATA

Equipment	Failure Rate (PPMH)[a]	Source	Remarks
Wide Angle Sun Sensor (WASS)	0.692	GAC[b]	BDX 1818787
WASS Electronics	0.68	GAC	BDX
Fixed-Head Star Tracker (FHST) and Electronics	4.411	TRW[c]	ITT Breadboard
Inertial Rate-Integrating Gyro	5.0	TRW	Nortonics GI-K7G
Gyro Electronics	10.0	TRW	
Digital Processor Assembly (DPA)	—	—	See Figure VIII-7
DPA Power Supply	3.252	CDC[d]	
Transfer Assembly (TA)	5.957	TRW	Corrected for DPA power supply
Magnetometer (per axis)	0.3	GAC	Dalmo-Victor
Magnetic Coil	0.4	BECO[c]	Dalmo-Victor
Coil Driver Electronics	0.702	BECO	Parts Count
Control Moment Gyro (CMG)	—	—	See Figure VIII-6
Regulator	11.1	MSFC	ATM
Electrical Control Assembly (ECA)	3.643	BECO	Parts Count
Electrical Distribution Unit (EDU)	0.538	BECO	Parts Count

TABLE VIII-2. (Concluded)

Equipment	Failure Rate (PPMH)[a]	Source	Remarks
Antenna	0.13	TRW	Antenna failure rate assumed similar to HEAO program antenna
Pulse-Modulated Receiver	15.51	Motorola	
Frequency-Modulated Receiver	10.4	Motorola	
Pulse-Modulated Transmitter	9.595	Motorola	
Frequency-Modulated Exciter/Transmitter	7.415	Motorola	
Phase Shift Keyed (PSK) Demodulator	1.788	TRW	
Frequency Multiplexer	1.147	TRW	
Format Generator	5.0	GAC	
Read-Only-Memory (ROM)	0.28	S&E-QUAL[f]	
Pulse Code Modulator (PCM) Encoder	9.0	GAC	
Remote Decoder	1.8	GAC	

a. PPMH = parts per million hours
b. Grumman Aerospace Corporation
c. TRW Systems, Inc.
d. Control Data Corporation
e. Teledyne-Brown Engineering Co.
f. Quality and Reliability Assurance Laboratory, MSFC

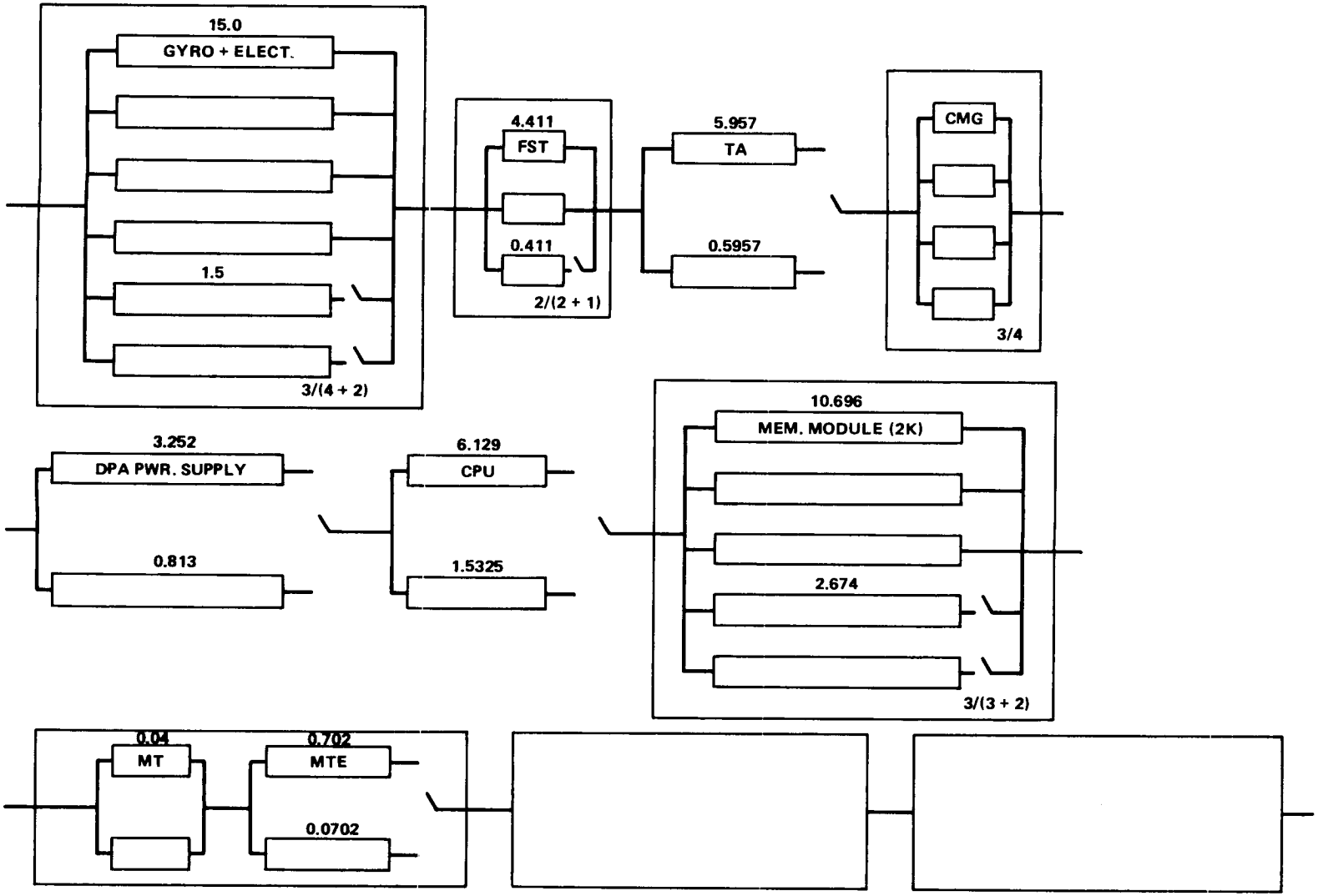

Figure VIII-2. ACS dependency diagram.

The orthogonal configuration has certain important disadvantages. When its 1-year reliability of 0.97419 is combined with the reliabilities of other system elements, the 0.95 1-year SSM reliability goal becomes difficult to meet without introducing excessive redundancy at other points. The consequence of failure in this case is that three-axis attitude information is no longer available, implying that no scientific data can be taken. Thus, a further consequence of this failure is a decision to commit to a Shuttle maintenance flight. A second disadvantage is the fact that voting fault detection, but not isolation, is not feasible unless all six gyros are kept on line. In this case, the reliability code becomes $(1/2)^3$, and the resulting reliability curve is shown in Figure VIII-4 from which it can be seen that the reliability drops still further.

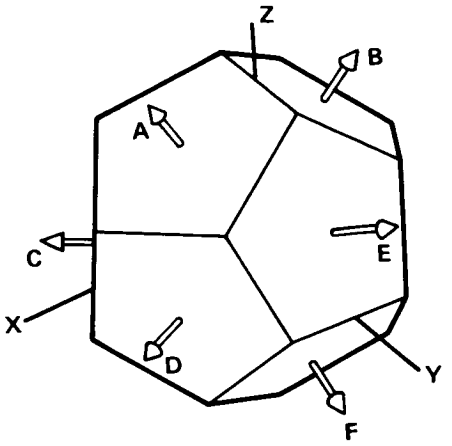

Figure VIII-3. Dodecahedral RGA geometry.

The most straightforward operation of the dodecahedral configuration is obtained by operating all six gyros. The corresponding reliability curve is that marked with the code 3/6 in Figure VIII-4. To realize the greatest reliability benefits from this configuration, however, only four gyros are kept on line with two on standby. Since only three gyros are required to provide three-axis attitude information, the applicable reliability curve is that coded by 3/(4 + 2) in Figure VIII-4. As can be seen, this configuration is superior to both possibilities for the orthogonal configuration. The dodecahedral configuration can provide voting fault detection so long as at least four gyros are kept on line (more than four would also give isolation). Thus, the curve marked 4/(4 + 2) gives the probability for voting fault detection, but not isolation.

A slight modification of the "four on line" approach maximizes the probability of meeting the accuracy requirement. In fact, the requirement is not quite so stringent as stated above. It is sufficient that the accuracy described be attained only about the pitch (y) and yaw (z) axes, and this can be done with any combination of five or six gyros and with six of the possible 15 four-gyro combinations. With the gyro labeled as in Figure VIII-3 these latter combinations are: ABEF; BCEF; ACEF; ADEF; BDEF; and CDEF. Figure VIII-5 illustrates one tentative concept for maximizing the probability of satisfying the accuracy requirement.

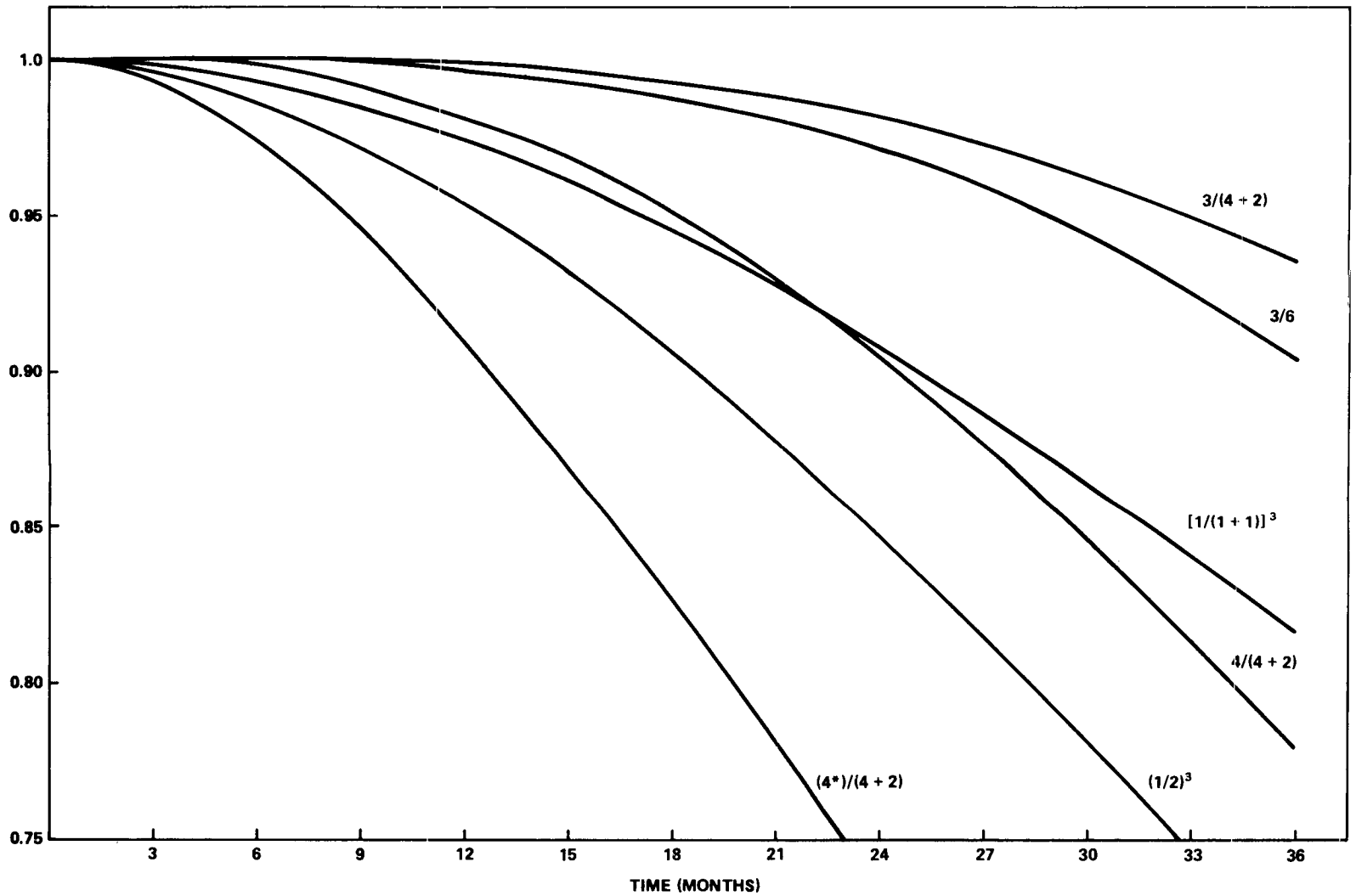

Figure VIII-4. Candidate RGA reliability comparisons.

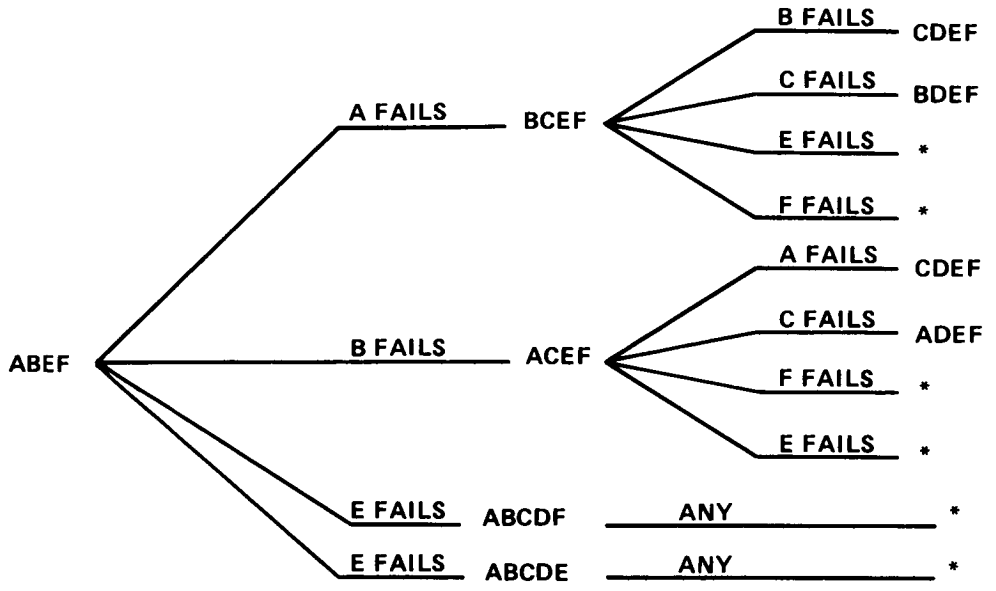

Figure VIII-5. Dodecahedral RGA operational concept.

Initially the four gyros ABEF are on line. When the corresponding parity equations[1] detect a failure occurrence, the failure may be isolated directly from the parity equation by bringing gyro C on line. This procedure can be implemented on board or, since the predominant gyro failure mode is a gradual drift out of specified performance, on the ground. It is assumed that the gyro internal states (wheel speed, temperature, etc.) will also be transmitted to the ground to complement the parity equations. In either case, the failed gyro data are ignored by the onboard strapdown algorithm and the failed gyro turned off on ground command. If, for example, gyro A had failed, the new operating combination would be BCEF and the second failure could be isolated by bringing gyro D on line. If the first failure had been gyro E, then gyro D would also be brought on line, and the operating combination would be ABCDF. This brief discussion should serve to explain the operating concept. Although there is some arbitrariness in the choices made, all choices lead to the same numerical reliability result; namely,

$$R(t) = \sum_{i=0}^{7} p_i(t) \quad ,$$

1. Gilmore, J. P.: A Non-Orthogonal Gyro Configuration. MIT Master of Science Thesis, 1967.

where

$$p_0(t) = e^{-(4\lambda + 2\lambda')t} \quad ,$$

$$P_1(t) = 2 \frac{P_s \lambda}{\lambda'} (e^{\lambda' t} - 1) P_0 \quad ,$$

$$P_2(t) = 2(e^{\lambda' t} - 1) P_0 \quad ,$$

$$P_3(t) = \frac{2 P_s^2 \lambda}{\lambda - 2\lambda'} (P_0 - e^{-5\lambda t}) \quad ,$$

$$P_4(t) = P_1^2(t)/4P_0(t)$$

$$P_5(t) = \frac{P_s \lambda}{\lambda'} \left[\left(\frac{P_s \lambda}{\lambda'} + 1 \right) (1 - e^{\lambda' t})^2 + (1 - P_s)(e^{2\lambda' t} - 1) \right] P_0 \quad ,$$

$$P_6(t) = \frac{3P_s \lambda}{2\lambda'} (1 - e^{\lambda' t}) P_0 \quad ,$$

and

$$P_7(t) = (1 - e^{\lambda' t}) P_0 \quad ,$$

with P_s being the gyro startup probability, λ the online failure rate, and λ' the standby failure rate. The results of calculations with these formulas ($P_s = 1$) are plotted in Figure VIII-4 and coded by $(4^*)/(4 + 2)$. The sensitivity of this curve to small variations about the value $P_s = 0.9995$ is negligible. It should be emphasized that the consequence of failing to meet the accuracy requirement about the pitch and yaw axis is merely the degraded mode discussed in Section C.

A typical single-gimbal control moment gyro (SGCMG) dependency diagram, showing the failure rates used, is given in Figure VIII-6. These failure rates are applicable to one version of the Bendix MA-500 SGCMG, assuming an orbital environment and an ambient temperature of 30°C. Similar failure rates will apply to other SGCMGs with the same momentum capabilities. Satisfactory steering laws have recently been developed for configurations of three and four operating SGCMGs, so that the minimum number to be considered is four, which provides the required single-point failure protection. The configurations to be considered are then 3/4, 3/(3 + 1), 3/5, 3/(3 + 2), etc. The reliability numerics for the first three of these are given in Table VIII-3. The numerics for the 3/(3 + 1) configuration were generated using an equivalent failure rate computed from the corresponding SGCMG unit reliability. Although this technique is of dubious accuracy, the results are in accord with the intuitive expectation that the 3/(3 + 1) configuration should be intermediate between the 3/4 and 3/5 configurations.

When the reliabilities of the remaining system elements are considered, the data of Table VIII-3 do not support a requirement for a fifth SGCMG. The choice between the 3/4 and 3/(3 + 1) configurations was made on the basis of other than reliability considerations. The 3/(3 + 1) configuration is slightly more reliable and has a slightly smaller power requirement than the 3/4 configuration. In addition, since the case of three operational SGCMGs must be considered as a degraded case of the 3/4 configuration, use of the 3/4 configuration implies the development and implementation of either two steering laws or a single steering law applicable to both three and four operational SGCMGs. The selection of the 3/4 configuration for the design reference was made on the basis of its greater momentum capability. Further steering law developments could reverse this choice.

A block diagram of an internally redundant CDC 469 is shown in Figure VIII-7. For computational purposes, this is simplified as shown in the ACS dependency diagram (Fig. VIII-2). The failure rates are as follows:

Central Processor Unit (CPU)	5.827 PPMH
Switches A/B	0.308 PPMH
Memory Module (2K)	10.124 PPMH
Switches C/D	0.572 PPMH
Power Supply	3.252 PPMH

Preliminary memory estimates require a 6K word memory. One of the extra two 2K word memory modules allows for possible memory requirement growth and the second provides single-point failure protection. The reliability code is 3/(3 + 2). The code for the power supply is 1/(1 + 1).

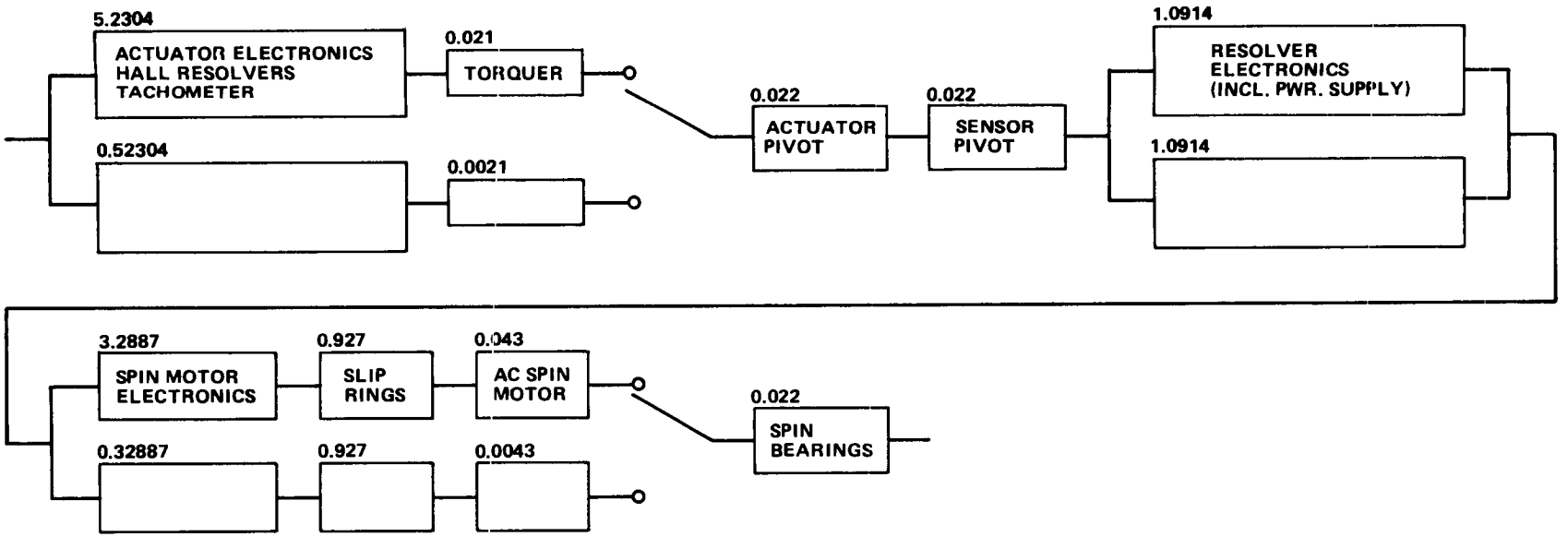

Figure VIII-6. SGCMG dependency diagram.

TABLE VIII-3. NUMERICAL RELIABILITY COMPARISON OF CANDIDATE SGCMG CONFIGURATIONS

Time, Months	Unit Reliability	3/4	3/(3 + 1)	3/5
3	0.99972	>0.99999	>0.99999	>0.99999
6	0.99918	0.99999	>0.99999	>0.99999
9	0.99837	0.99998	0.99999	>0.99999
12	0.99732	0.99995	0.99997	>0.99999
15	0.99602	0.99990	0.99993	>0.99999
18	0.99448	0.99982	0.99986	>0.99999
21	0.99270	0.99968	0.99975	>0.99999
24	0.99070	0.99949	0.99960	0.99999

Two of the three fixed star trackers (FSTs) provide three-axis attitude information over 95 percent of the celestial sphere. With all three FSTs unfailed, this coverage increases to 99 percent. Thus, the effect of the first FST failure is a minor capability degradation. With the second failure, the capability for updating the reference gyros is lost, and guide stars cannot be brought into the field-of-view of the fine guidance sensor. The applicable reliability code is then $2/(2 + 1)$, since only two FSTs need be on line simultaneously. A duty cycle of 100 percent has been assumed for the online FSTs. The failure rate of 4.411 PPMH is based on a TRW piece-part count for the HEAO Phase C/D proposal.

Six magnetic torquers (MTs) are included in the design reference to accommodate worst-case gravity gradient torques. As failures occur, a degraded capability will exist so long as at least one MT is unfailed on each of the three orthogonal axes. Thus, the redundancy shown arises, not from the SPF criterion, but from capability improvement. The reliability code for the MTs is therefore $(1/2)^3$. The failure rate of 0.04 PPMH is the estimate for the Orbiting Astronomical Observatory (OAO) magnetic coils. All sources consulted agreed that the coil size should not have a significant effect on the failure rate. Two sets of magnetic torquer electronics (MTE), one on line,

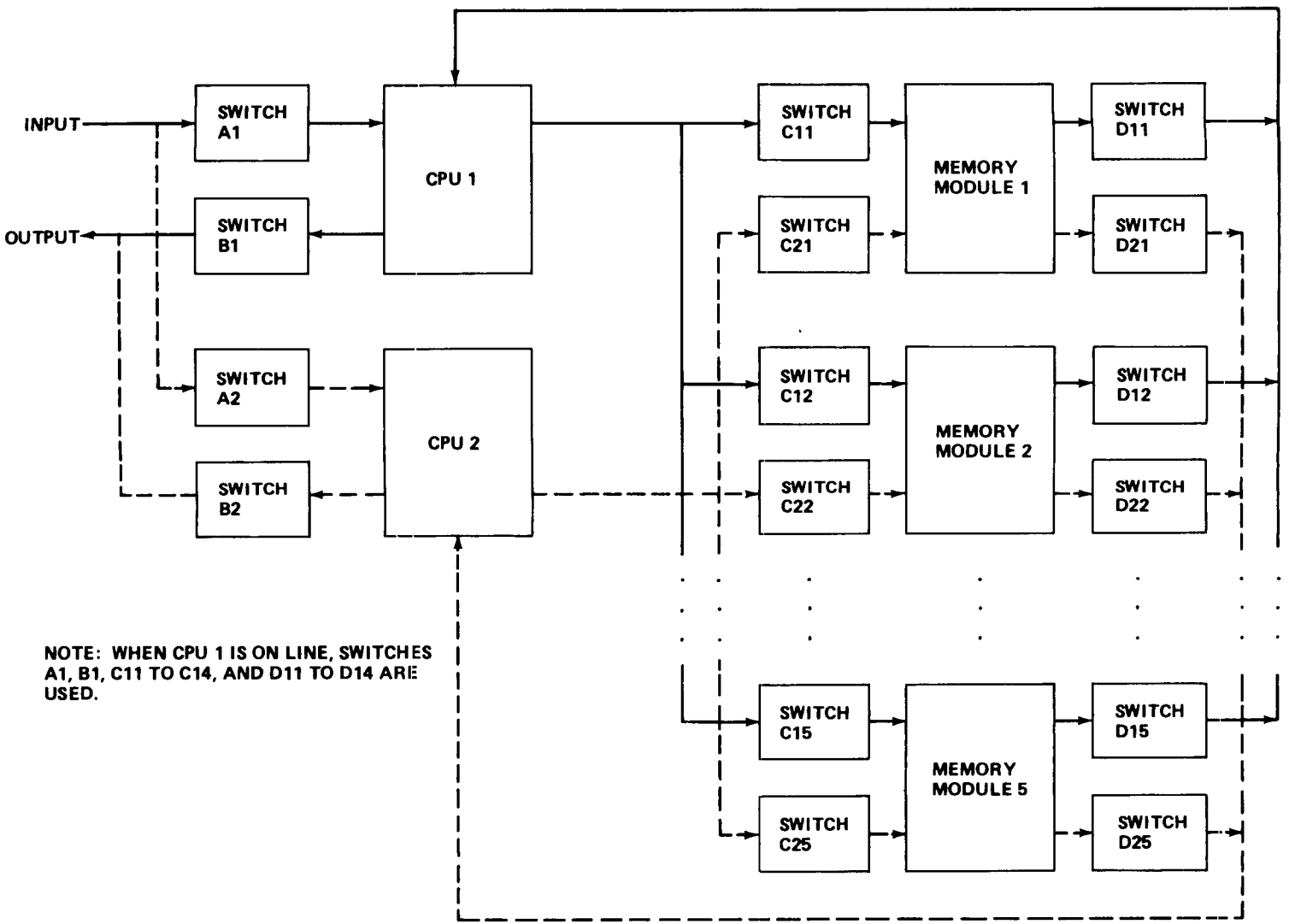

Figure VIII-7. Block diagram of internally redundant CDC 469 computer.

are provided for each axis. Either set is capable of controlling the two MTs dedicated to that axis. The failure rate of 0.702 PPMH was derived from a BECO piece-part count. The reliability code for the MTE is then $[1/(1 + 1)]^3$.

The onboard magnetometer senses the ambient magnetic field and is designed as a $[1/(1 + 1)]^3$ reliability configuration. With a 0.3-PPMH failure rate for each of the sensing elements, a high reliability was computed for this unit. However, since ground computation of the field is a feasible alternative/backup, the magnetometer is not shown as an essential system element.

The LST transfer assembly is assumed similar to that proposed for HEAO, although unique to the LST. The failure rate shown has been compensated for the DPA power supply, which is treated separately.

The three wide angle sun sensors dedicated to the ACS are used for the sun acquisition mode and the emergency attitude hold mode. The duty cycle is essentially zero and the components themselves are highly reliable. Only one is required, although the sun acquisition mode is simplified by having one sensor aligned with the +Z-axis and a second with the -Z-axis.

The RCS and its electronics also have a negligible duty cycle and are included in the design reference to back up catastrophic failures and to enable recovery from other failures. Table VIII-4 summarizes the ACS reliability calculations.

TABLE VIII-4. ACS RELIABILITY SUMMARY

Assembly	1-Year Reliability
RGA	0.99827
FST	0.99702
TA	0.99855
DPA (Processor, Memory, and Power Supply)	0.99416
CMG	0.99996
MT	0.99999
MTE	0.99994
ACS	0.98795

3. Electrical System. The electrical power system contains two elements for which no satisfactory quantitative reliability assessment can be given: solar panels and batteries.

For all but the simplest academic examples of solar arrays, the number of cells, solder joints, interconnects, blocking diodes, etc., is so large, and these are arranged in such a complex manner, that the applicable reliability models defy analysis by deterministic methods. This system complexity arises in part from the nature of solar arrays and in part from the desire to avoid single-point failures. In a typical solar panel, for example, there are no single-point failures and few instances of simple dual redundancy. Multiple electrical paths are the rule rather than the exception. This extreme use of redundant paths is sufficient to preclude practical deterministic models. One technique used in the past for solar power system reliability prediction has been the assumption of a solar cell failure rate, and organization of the solar panel in a standard series-parallel reliability model involving only the cells. Data accumulated from the Skylab and Apollo Telescope Mount (ATM) solar panel tests indicate that this approach is grossly inadequate. Moreover, the usual objective of a reliability analysis is an estimate of the probability that the system analyzed will operate satisfactorily over a given time interval. A more satisfactory objective, particularly in the LST context, would be an estimate of the density function of the power output, with time as a parameter. These considerations indicate that only a statistical modeling technique such as Monte Carlo could produce useful results.

To accomplish this objective, considerable data must be accumulated. The power degradation effects of incident sunlight angle, temperature, and accumulated radiation dosage have been reasonably well quantified. Other data, however, are scanty and subject to extreme variability. There are several reasons for this. Testing of solar arrays has generally been confined to some form of acceptance testing; visual and radiographic inspection and a very limited amount of environmental testing to eliminate obvious design and manufacturing flaws. The primary factor, apart from those already mentioned, leading to power degradation is component breakage resulting from thermal cycling. Since this breakage is random in occurrence, only test data can provide the statistical information required to assess its effects. Unfortunately, this information has been observed to vary widely according to design, manufacturer, and date of manufacture. Since the fabrication process is largely a manual one, this is to be expected. One additional problem is that solar cells must be placed in operation without the considerable burn-in process usually employed, and must therefore suffer from infant mortality of components while in operation. Acceptance testing can eliminate only the most obvious infant mortality effects.

A number of attempts were made to arrive at a credible battery reliability estimate. As a result, it was found that the six-battery configuration of the design reference is a potential reliability problem. Since the estimates obtained varied widely, the battery reliability numerics were not factored into either the EPS or SSM reliability totals.

Assuming an exponential failure distribution with the 1.527-PPMH cell failure rate used in the ATM primary power supply reliability analysis, a 1-year reliability of 0.944 was calculated assuming three of the batteries were required. This is the number of batteries required for the nominal power profile. Additional batteries are required to reduce the depth of discharge (DOD), which extends the battery system life. Six batteries are required to supply the power demands for an off-sun pointing spectrometer slit orientation mode requirement. One battery can provide the power required for the emergency attitude hold mode.

The sources consulted to obtain a more realistic battery reliability model essentially agreed that a normal distribution for cell life expectancy could lead to a better estimate of the battery reliability, although the assumption of a predominately "short" cell failure mode would still introduce a considerable pessimism. With this distribution,

$$\text{Prob}(L \geq t) = \frac{1}{\sqrt{2\pi}\, s} \int_t^\infty \exp\left[-\frac{(u - m)^2}{2s^2}\right] du = \text{erfc}\left(\frac{t - m}{\sqrt{2}\, s}\right),$$

where L is the cell life, m is its mean, and s is its standard deviation. The reliability of a 24-cell battery is then

$$R(t) = \text{Prob}(L \geq t)^{24} \quad .$$

The Boeing Company (TBC) has estimated $\sigma/m = 0.28$, regardless of operating temperature and DOD.

Figure VIII-8 illustrates the dispersion in mean cell life estimates. The straight line curves at 0, 10, and 25°C were provided by The Boeing Company. The remaining curves at 0, 25, and 40°C were generated at MSFC. In Figure VIII-9 the mean cell life is plotted versus temperature (quadratic curve fit). Note that the MSFC data predict an optimum operating temperature

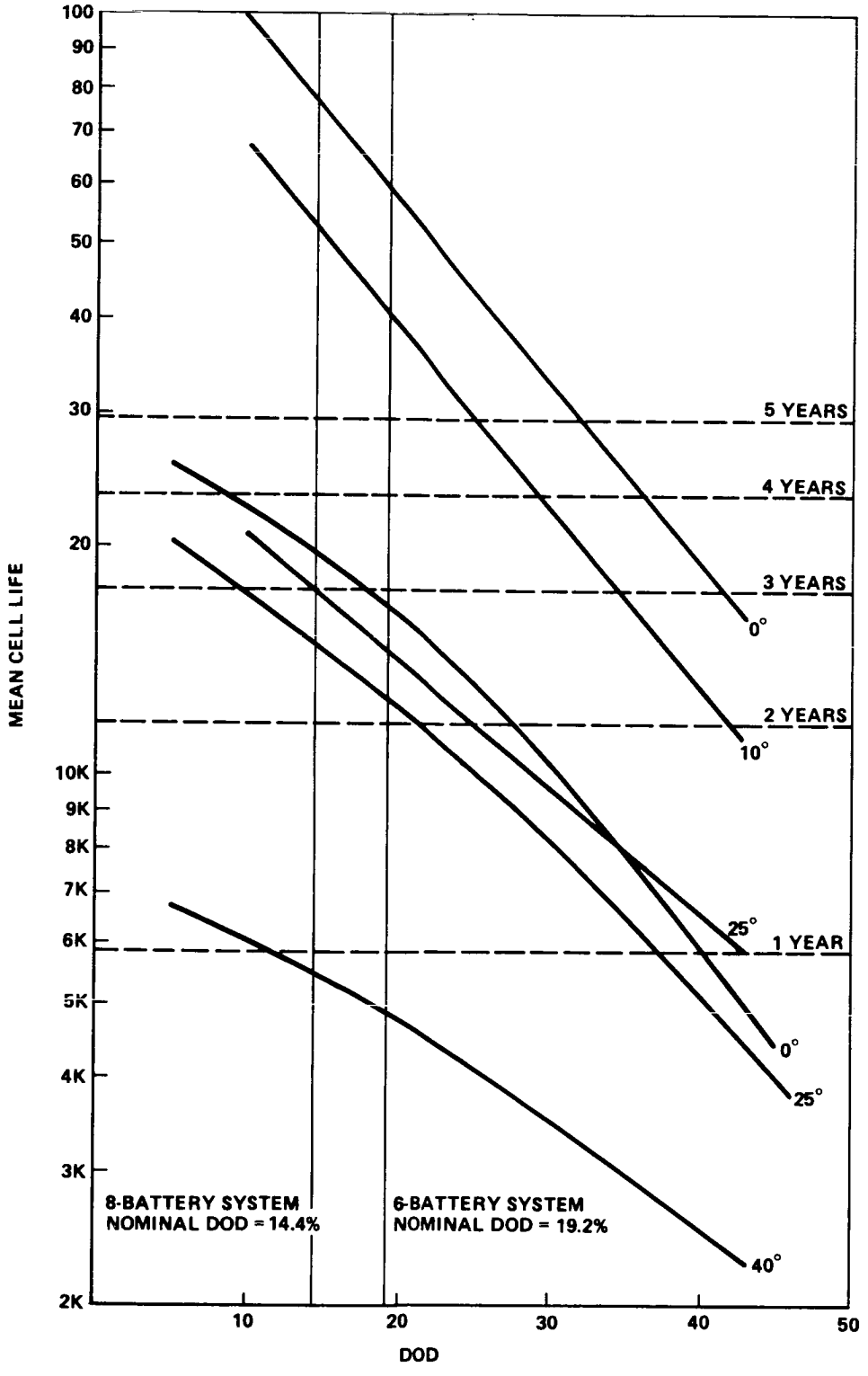

Figure VIII-8. 20 A-h NiCd cells mean cycle life, 1.5-hour cells.

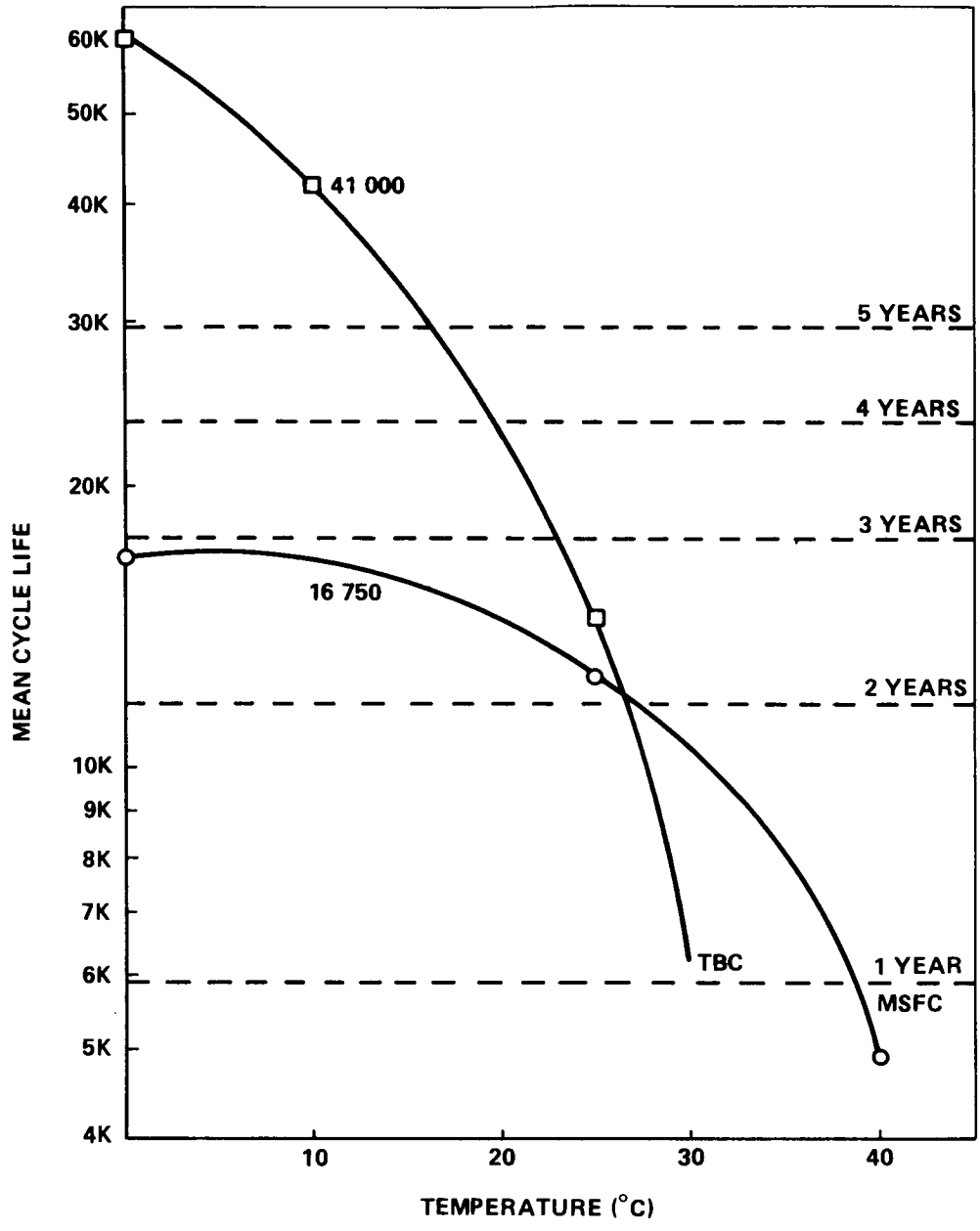

Figure VIII-9. Mean cell life versus temperature at 19.2-percent DOD.

in the range of 0 to 10°C, which is in agreement with experiment experience. In Figure VIII-10, the battery reliability obtained with the MSFC data (P (BATT)), the probability of no battery failure (P(O)), and the binomial probability of survival of three of six batteries (P(3/6) are plotted. The binomial formula is optimistic in this case since load-sharing effects are ignored.

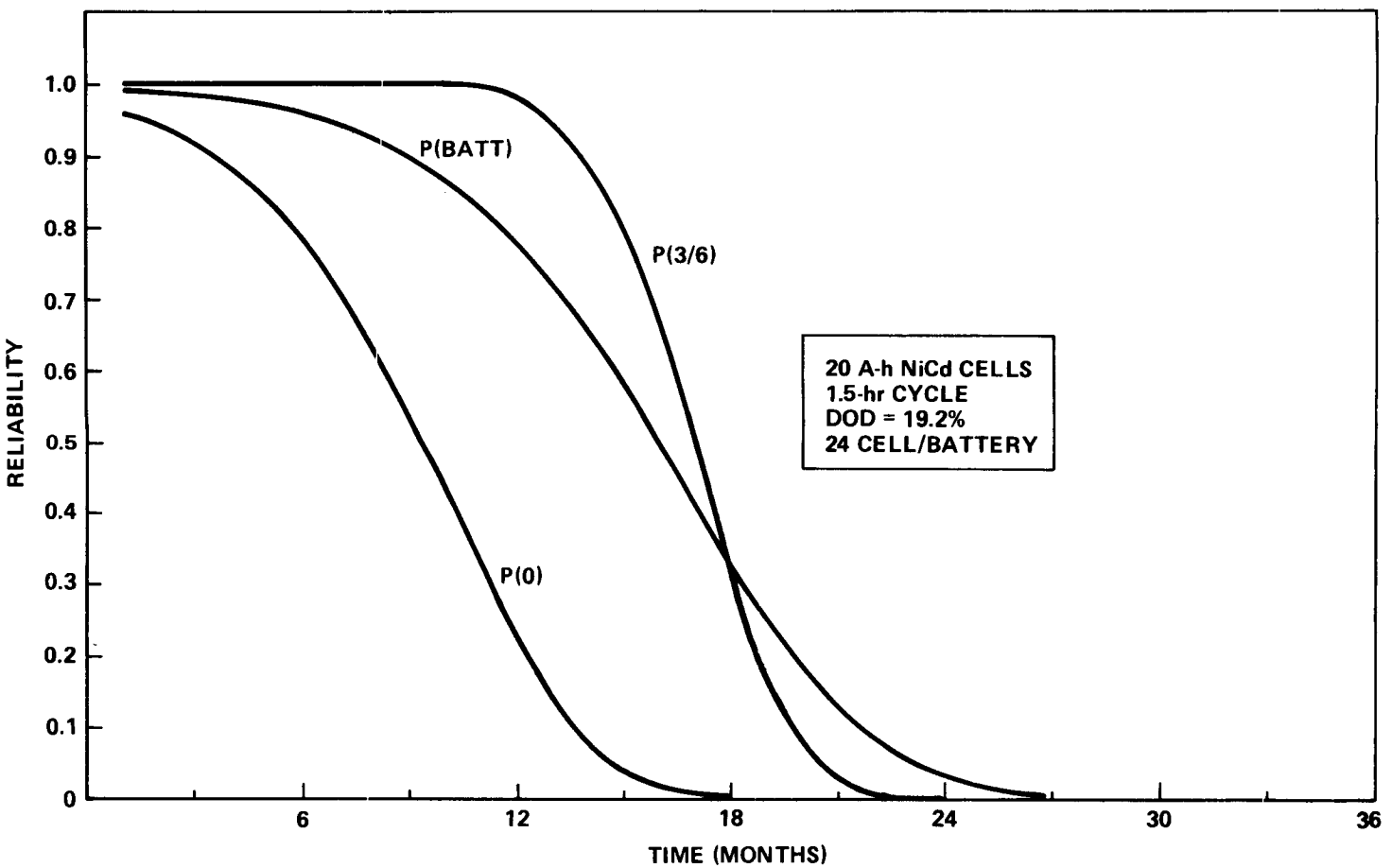

Figure VIII-10. Six-battery system reliability (MSFC data).

The corresponding reliabilities obtained with the Boeing data are plotted in Figure VIII-11. As can be seen from these curves, the battery system useful life lies in the range of 9 to 24 months.

The same exercise was repeated for an eight-battery system and the results are plotted in Figures VIII-12, VIII-13, and VIII-14. Keeping in mind the variation in the data and the optimism of the binomial calculation, Figures VIII-13 and VIII-14 indicate only that an eight-battery system is more reliable and that a potential for battery failure after 1 year still exists.

Three of the six regulators are sufficient to handle the nominal power profiles. The additional regulators are included to bring the reliability numbers up and to provide SPF protection. One regulator is sufficient for the emergency attitude hold mode.

The use of dual ECAs and EDUs provides SPF protection. The EPS dependency diagram is shown in Figure VIII-15 and the reliability numerics are given in Table VIII-5.

4. Communications and Data Handling System. A simplified functional diagram of the LST communications system is shown in Figure VIII-16, where the equipment required for three links is identified. Note that although the frequency-modulated exciter/transmitter is intended primarily for experimental television, it can also be used for spacecraft and other experiment data. This diagram is expanded to the C&DHS dependency diagram (Fig. VIII-17), where redundancy is also shown. Apart from the redundancy imposed by the SPF criterion, the choice of the Apollo Block II unified S-band equipment (USBE) transponder and ERTS transponder (arising from the choice for existing equipment to minimize cost) creates additional redundancy. Note that one receiver is "on" for each antenna, so that a single receiver failure does not destroy the command uplink. The probability of two simultaneous receiver failures during one loss-of-contact period, one in each transponder, is negligible. (The command uplink can be accomplished through either path, with the strongest signal path being the one used.)

Since the triplexers are simply tuned metal cavities, there is no discernible failure mode, which accounts for their absence from the dependency diagram.

The data acquisition system allows housekeeping data to be transmitted via the spacecraft downlink either in real time from the data acquisition units (DAU) or as stored data from the tape recorders. These data can then

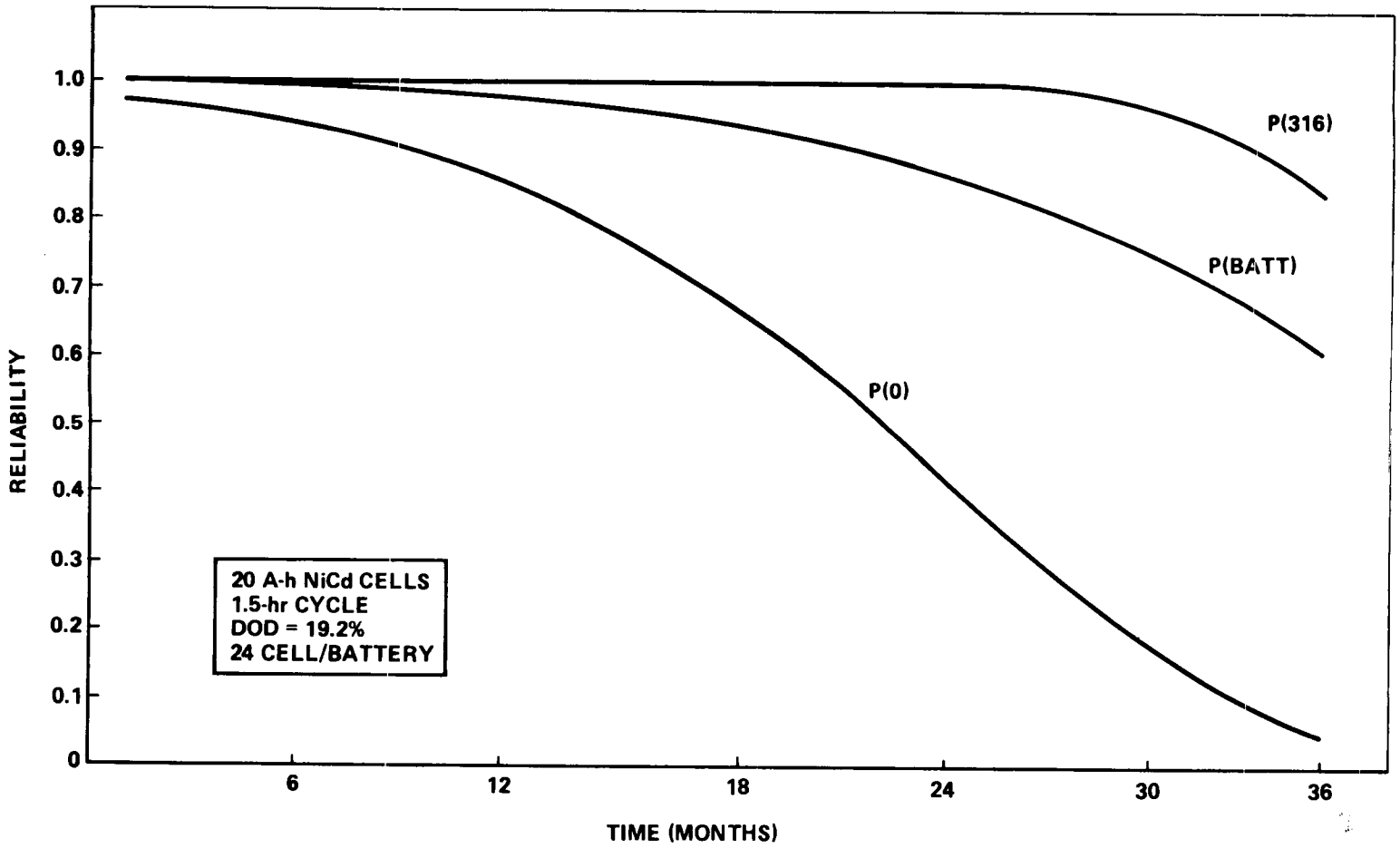

Figure VIII-11. Six-battery system reliability (TBC data).

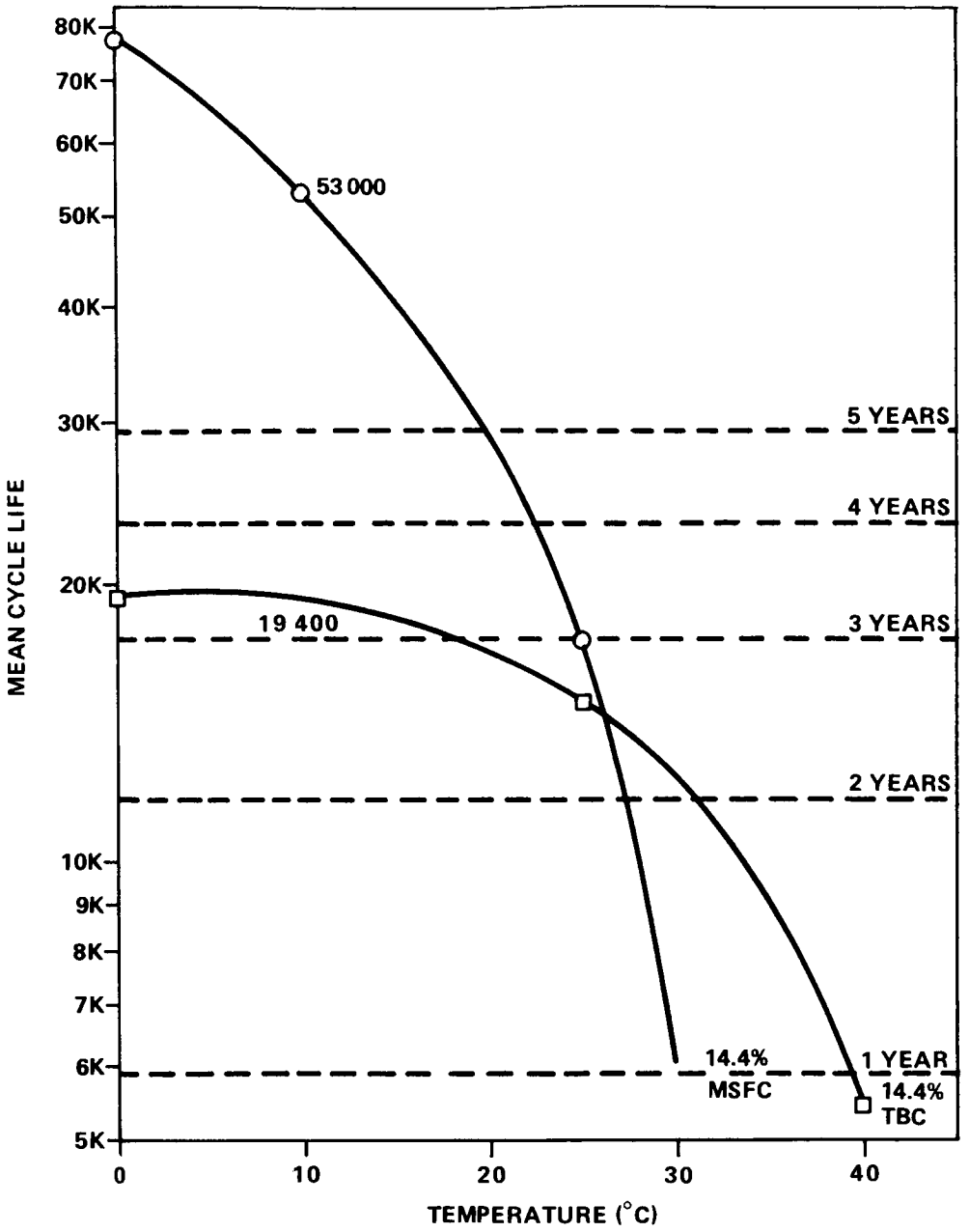

Figure VIII-12. Mean cell life versus temperature at 14.4-percent DOD.

be correlated with the experiment data or used to monitor and detect/isolate equipment failures. The probability of a large number of DAUs failing is vanishingly small, and isolated failures will not imperil successful LST

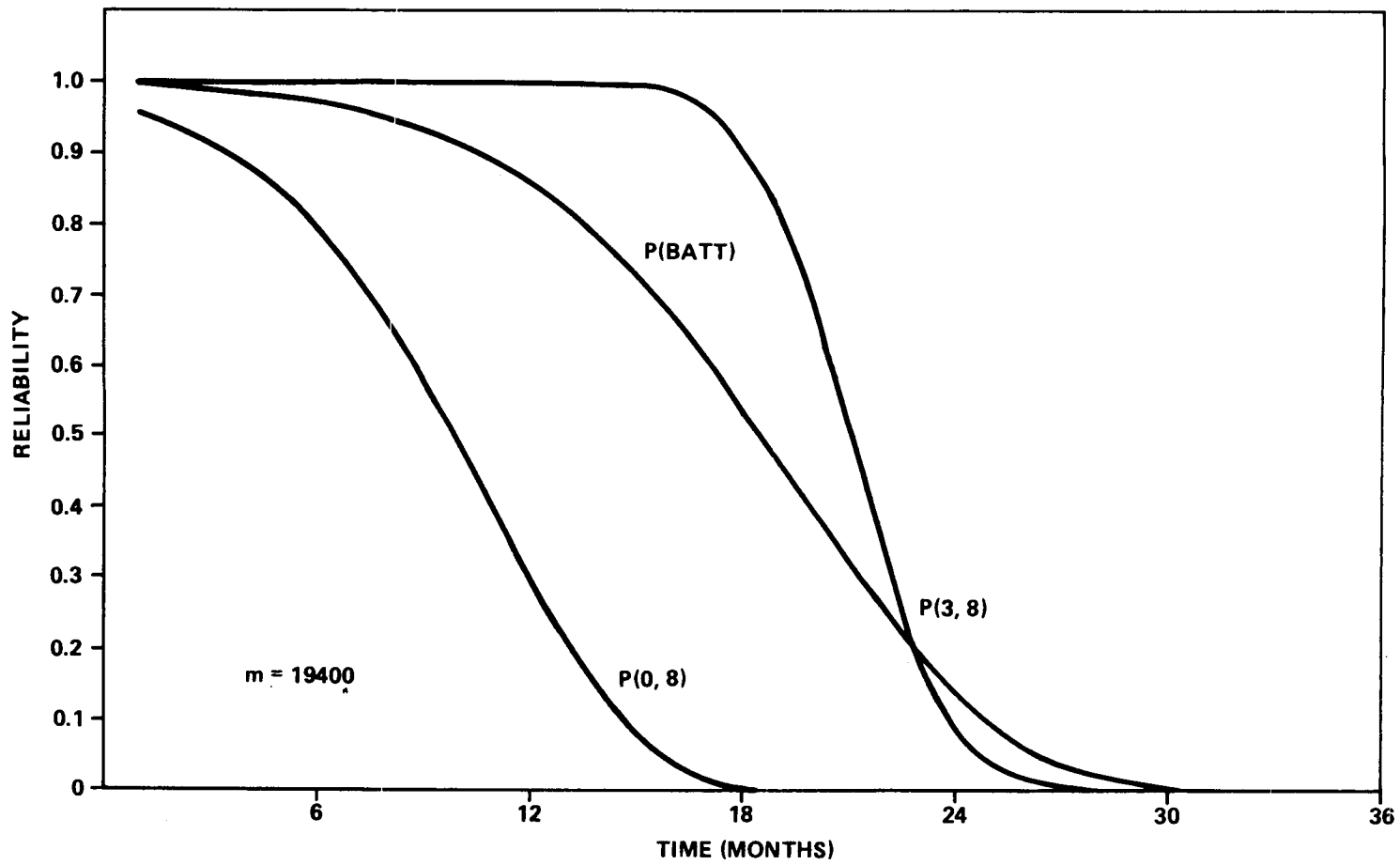

Figure VIII-13. Eight-battery system reliability (MSFC data).

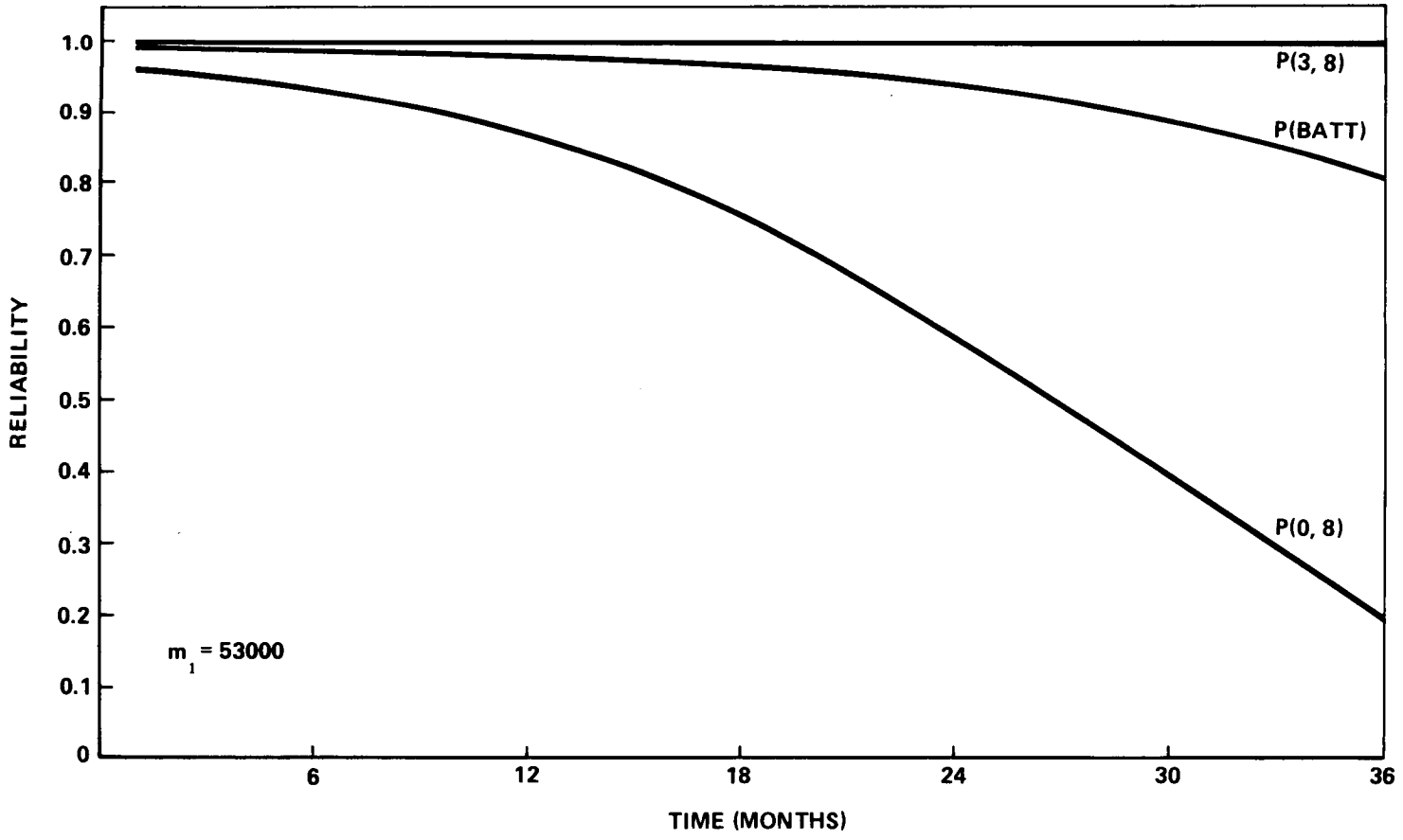

Figure VIII-14. Eight-battery system reliability (TBC data).

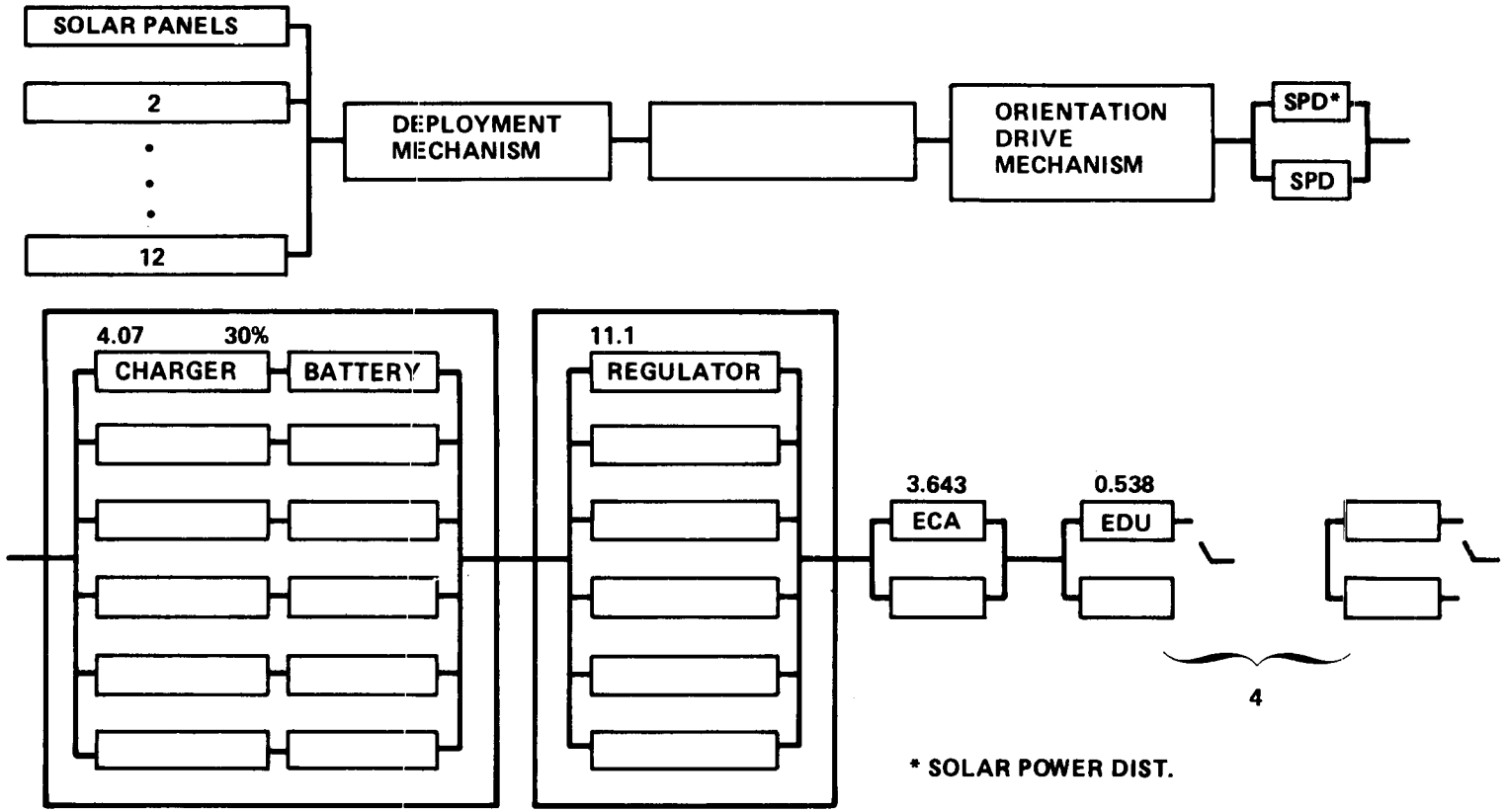

Figure VIII-15. EPS dependency diagram.

TABLE VIII-5. EPS 1-YEAR RELIABILITY SUMMARY

Regulators	0.99905
ECAs	0.99901
EDUs	0.99995
EPS	0.99801

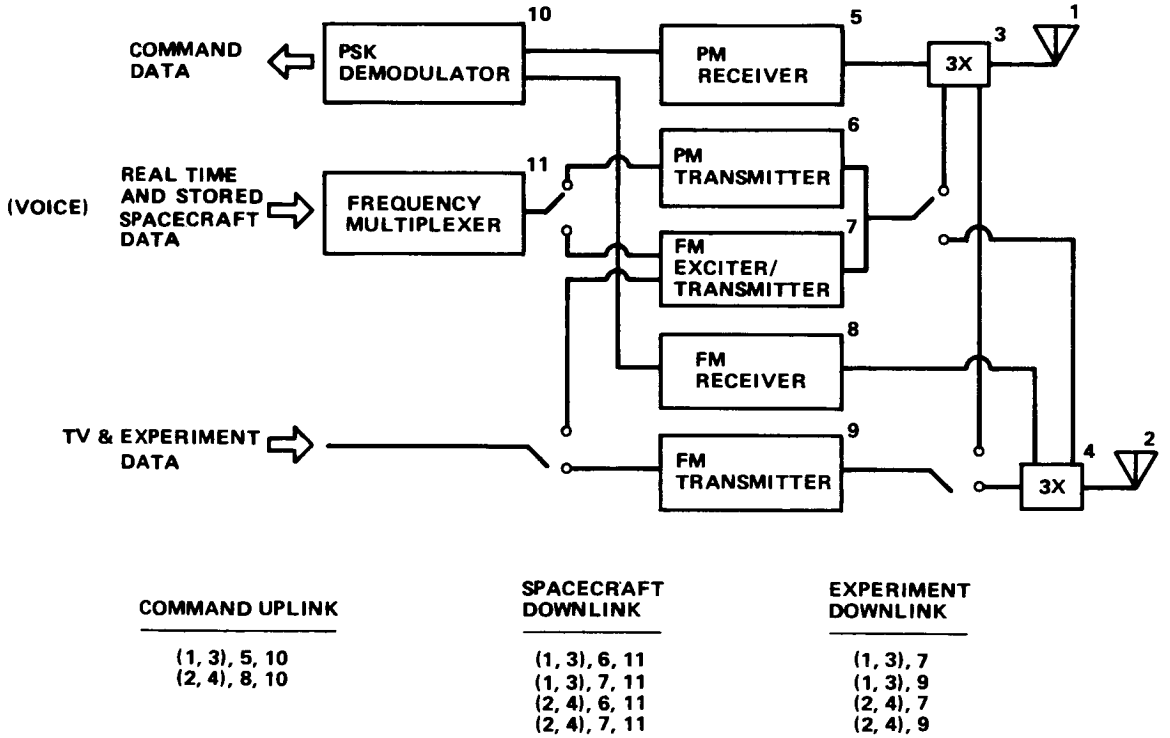

Figure VIII-16. LST communications functional diagram.

operation. Accordingly, the DAUs are not included in the dependency diagram. Similarly, the tape recorders are omitted since real time data should be sufficient for system monitoring and since there does not appear to be a critical need to correlate experiment and spacecraft data.

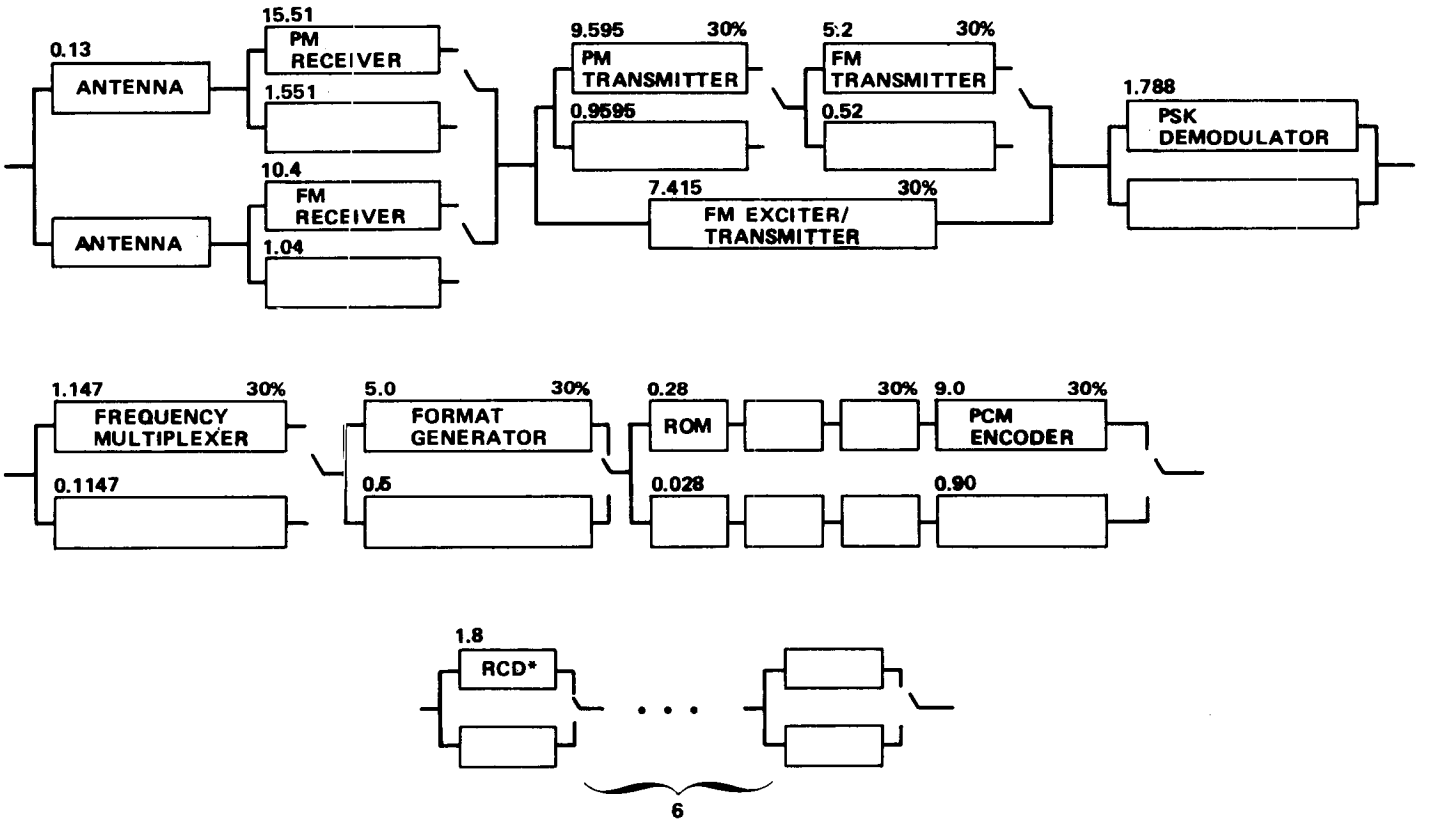

*REMOTE COMMAND DECODER
NOT INCLUDED: COMMAND PROCESSOR AND MEMORY, DIGITAL ACQUISITION UNITS, TAPE RECORDERS.

Figure VIII-17. LST C&DHS dependency diagram.

The command memory requirement estimate currently stands at 4096 words of plated wire memory. Dual redundancy is applied to both the command memory and command processor. Since a real time command mode exists, the memory and processor do not appear in the dependency diagram.

Six remote decoders have been identified as essential for the simplex system. Dual redundancy has been used, however, not only for these but for the others also since a simple OR circuit can prevent the issuance of a faulty command. Alternately, fault isolation can be provided by test commands. This is discussed further in Section D.

Letting P_A denote the antenna reliability and P_1 and P_2 the reliabilities of the pulse-modulated (PM) and frequency-modulated (FM) receivers, respectively, the reliability of the antenna/receiver block is computed from the formula

$$R = P_A P_1 + P_2 (1 - P_A P_1) \quad ,$$

where P_1 , P_2 , and P_3 denote the reliabilities of the PM and FM transmitters and the FM exciter/transmitter, respectively. In both cases, the reliability code for P_1 and P_2 is $1/(1 + 1)$. Table VIII-6 summarizes the results of the C&DHS reliability calculations.

TABLE VIII-6. C&DHS 1-YEAR RELIABILITY SUMMARY

Antenna/Receiver Block	0.99994
Transmitter Block	0.99998
PSK Demodulator	0.99976
Frequency Multiplexer	0.99999
Format Generator	0.99983
PCM Encoder and ROMs	0.99937
Remote Decoders	0.99919
C&DHS	0.99807

B. LST Checkout and Fault Isolation

1. General. An important consideration in the design of the LST SSM subsystems is the elimination of critical-function, single-point failures — often termed "hardcore." This dictates functional redundancy throughout all active system areas. In general, conventional masking techniques, such as triple modular redundancy (TMR), are avoided because of their uneconomical equipment, power, weight, and volume implementation requirements. However, masking schemes that are economically implemented, such as error detection/correction encoding and TMR for the status register configuration control circuitry, can be used where warranted, as detailed in the following paragraphs.

Most frequently, where masking is not used, functional redundancy is achieved by what is commonly called "standby sparing" redundancy. This type redundancy has the greatest potential for economical, long-lived unmaintained systems if they are carefully designed, because a minimum amount of functional equipment is required for system success and advantage may be taken of lower power-off failure rates. However, two outstanding pitfalls that must be scrupulously avoided at all phases of the design are: (1) the design of the reconfiguration switches and their controls must be continuously scrutinized to preclude inordinate amounts of implementation hardware and introduction of potential SPFs into the system, and (2) the fault-detection/isolation schemes throughout the system must be virtually infallible if sparing techniques are to truly enhance rather than reduce system effectiveness.

In view of these pitfalls and constraints, the LST SSM systems are designed to have:

1. Highest priority ground override control of system configuration.

2. Onboard autonomous control where the implementation penalties are reasonable.

3. Onboard checking circuit data transmitted to ground control centers at each opportunity for communications between the ground stations and the LST.

The fault detection/isolation features that determine the system partitioning occur at natural boundaries where the number of lines to be switched (for system reconfiguration) are at a minimum, and fault detection/isolation can be uniquely tailored to the particular type of functional equipment.

Where appropriate, power switching with diode isolation is used because of the economies in circuitry afforded by this type reconfiguration switching. The major sensors and effectors of the attitude sensing and control system (ASCS) are digital readin and readout devices. Thus, a troublesome central analog signal-dominated complex of multiplexers, decoders, scaling amplifiers, converters, and sample-hold amplifiers is eliminated. The replacement simplified digital signal switching circuitry provides a more naturally partitioned system and minimizes problems of line noise and long term calibration. The fault detection, isolation, reconfiguration, and recovery implementation are significantly facilitated by this design.

The built-in test equipment (BITE) signals from the primary ACS sensors, the third electrode and temperature signals from the electrical power system, and other signals associated with redundancy management functions, rather than being primary mission critical signals, may be handled in a standard manner. Thus, these types of signals may enter and leave the transfer assemblies as analog signals when most convenient. The transfer assemblies would then contain a complex containing analog-to-digital (A/D) and digital-to-analog (D/A) converters, analog multiplexers, scaling and drive amplifiers, and sample-and-hold circuits.

2. Switchable Interfaces. The design of the reconfiguration switches, as previously mentioned, is especially crucial if SPFs are not to be introduced into the system and if the amount of switch implementation circuitry is to be minimal. Interface switches fundamentally must be designed so that there is no fanout from the switching elements. This assures that a failure in the switches affects, at most, one functional receiving module. Functionally then, the switches are uniquely associated with their associated receiving modules, and the failure rate of a switch may be combined with the failure rate of the receiving module with which it is associated.

On the other hand, the switch control circuitry cannot be uniquely associated with elements of the functional hardware. If this control circuitry is made orders of magnitude more reliable than the remainder of the functional hardware, then the failure probability of the control circuitry is relatively negligible and may be neglected in the quantitative analysis.

The system configuration control in the LST system resides in status registers. These status registers are triple modular redundant to afford the requisite reliability. The functional logic for a typical switch is shown in Figure VIII-18. Two identical receiving modules, designated RCVR1 and 2, are connected through appropriate switching logic under control of

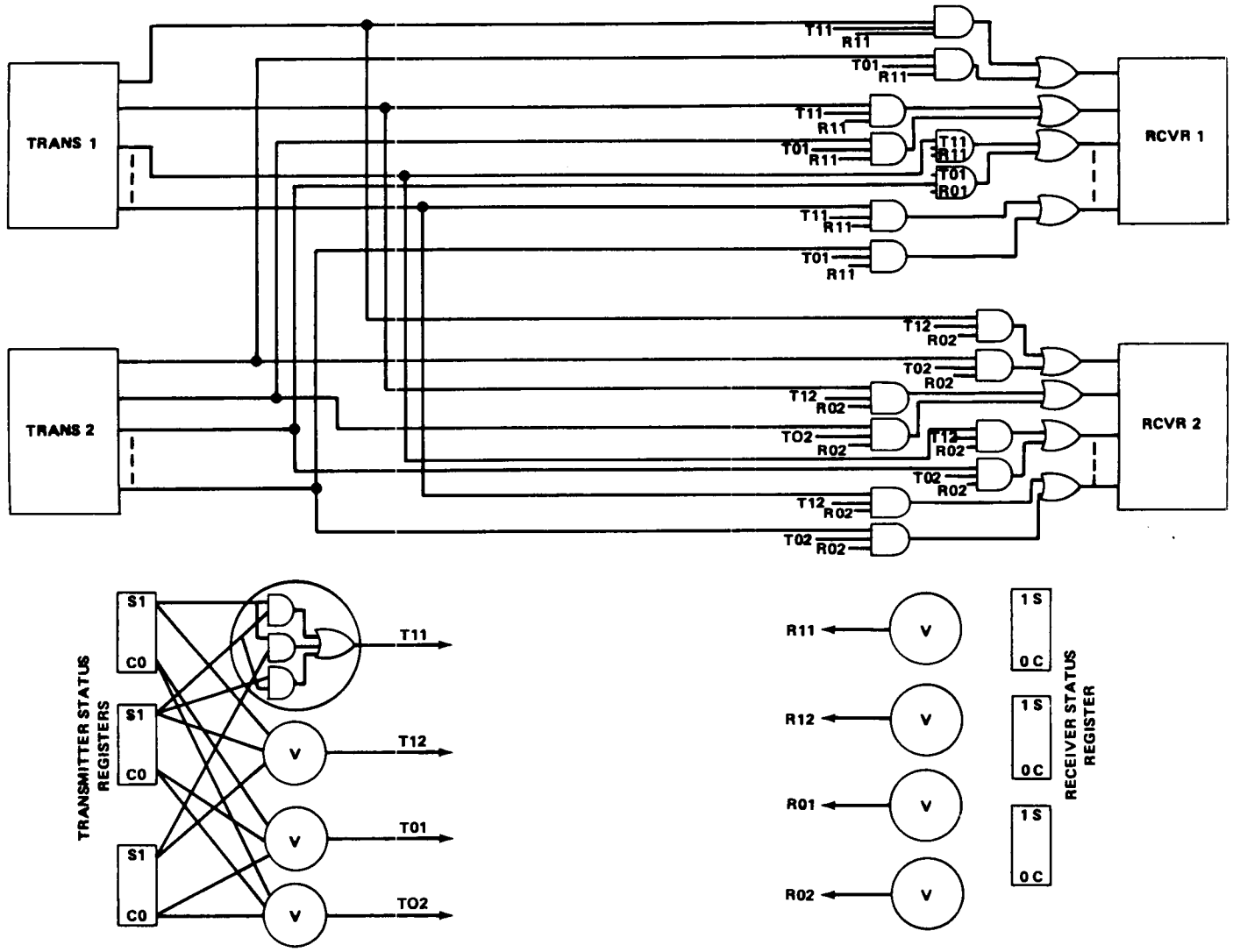

Figure VIII-18. Typical module-to-module status register controlled switching interface.

triple modular redundant status registers designated TRANSMITTER status and RECEIVER STATUS respectively. The design is such that only one of the two transmitter modules is connected to only one of the two receiver modules. There is no fanout of the switching logic; therefore, failure of a switch element affects, at most, the operation of one receiving module.

Referring to the transmitter status registers, three identical S-C flip-flops under normal conditions are set such that the 1 output is up (that is at the 1 level) and the 0 outputs of the flip-flops are down (that is at the 0 level).

There are four majority vote circuits (depicted as circles) associated with each status register. Two voters vote the 1 output of the three flip-flops, and two vote the 0 outputs of the flip-flops. This duality precludes the voters as single failure points. It is straightforward to design similar switching interfaces for interconnecting larger numbers of transmitting and/or receiving modules along the same principles.

3. Status Register Control. Figure VIII-19 shows the functional schematic logic for control of the status registers. The dual redundant command decoders control the triplicate flip-flops. Two lines from each decoder control a mode flip-flop such that if the flip-flop is set in the automatic mode, then the onboard fault detection equipment can control the status registers which in turn control the interface configuration. If the mode flip-flop is set to the manual mode, then only ground command signals can control the status registers. For this purpose, two additional lines, one for the Set and one for the Clear input of the associated status register, are used to set the interface configuration. The onboard fault detection signals are present at the input to the AND gates but are not effective unless the auto mode is set in the mode flip-flop.

4. Digital Processor Assembly. The digital processor assembly consists of two CPUs plus a shared memory with associated memory translators. Onboard fault detection/isolation for the CPUs is by means of the built-in hardware and software self-test equipment coupled with an external window timeout device. Fault detection and isolation for the memory array is by means of error encoding of the words stored in the memory. The memory translator translates from the error correction encoding in the memory to the byte parity encoding in the CPU and vice versa. Fault detection/isolation for the memory translators is by means of self-testing, self-checking circuitry.

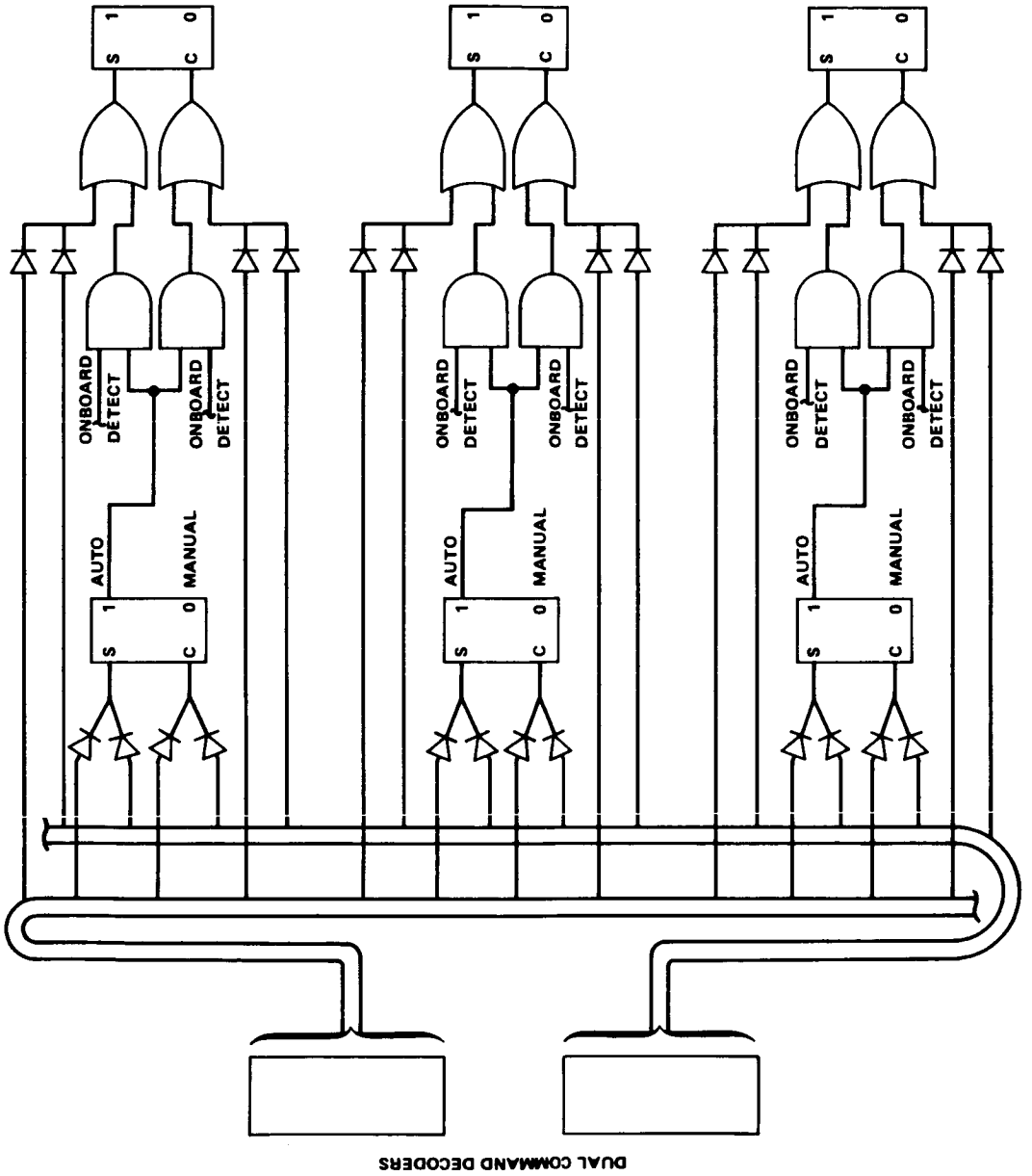

Figure VIII-19. Configuration control of status registers.

The CDC-469 computer was chosen for the design reference as "existing" equipment, for HEAO commonality, and to provide a source of quantitative failure rate data. Certain advantages would accrue, however, from the choice of a processor which has fault-tolerance features incorporated into its design. The MSFC-developed Space Ultrareliable Modular Computer (SUMC) has been under development for several years in the MSFC Astrionics Laboratory. Several breadboard models were built to verify the concepts. Currently prototypes are under construction by RCA and IBM. The SUMC will be available as a space-qualified off-the-shelf processor for operation in the 1975 time frame.

The microprogram control store of the SUMC provides essential capability for processor self-testing as well as capabilities for checking and control of peripherals. The SUMC is a state-of-the-art processor in large scale integration (LSI) and packaging technologies.

An extensive qualification program has been and will continue to be conducted in all phases of the development. This coupled with the flexible modular design will result in a space-qualified, highly reliable off-the-shelf processor for a broad spectrum of space applications.

a. CPU Checking. In addition to the built-in hardware checks, the choice of such a processor would enable the CPU to be checked by a comprehensive self-test microprogram. Periodically and frequently, the digital computer assembly, which is at the time on line, will go into a self-test mode. The self-test mode will verify the integrity of the memory, the CPU, and the input/output (I/O) subsections. Failure of either the CPU or the I/O indicated during the testing of either unit will result in failure to set a discrete out to the window timer. The window timer is located in the transfer assembly and will be described in conjunction with that subsystem. For the purposes of this discussion it is sufficient to say that failure to set the discrete will cause switchover to the alternate CPU during periods in which the system is in the auto mode. When the system is in the manual mode, a proper indication of a test failure will be set. The CPU hardware is comprised mainly of registers, an arithmetic logic unit (ALU), and control circuitry that initiates the proper sequences of information transfer within the CPU in response to the programmed instructions. The control circuitry would account for more than half of the total CPU circuitry. Proper functioning of the ALU and the registers is virtually essential for proper functioning of the CPU. Tests for these portions of the CPU are relatively straightforward. Verification of the integrity of the control circuitry, however, is not so straightforward. It is in this area of the CPU that there exists a potential for major improvements in self-test techniques over predecessor programs.

Figure VIII-20 will serve to illustrate the difficulties of verifying the integrity of complex logic arrays such as in the CPU control circuitry. It also serves to illustrate why the basic design of the ASCS processor must be inherently checkable. A testable design is not a retrofit. It must be included in the basic processor design.

The square in Figure VIII-20 represents a complex multiinput, multioutput array. Two interior logic gates within the array are shown with their input lines; 1, 2, and 3. The problem is to verify the integrity of the OR gate when one has control only over the input patterns on lines 1, 2, and 3, and can only sense the output of the AND gate. The eight possible 0-1 patterns that can appear on interior lines 1, 2, and 3 together with the corresponding correct outputs of the OR and AND gates are listed in Figure VIII-20.

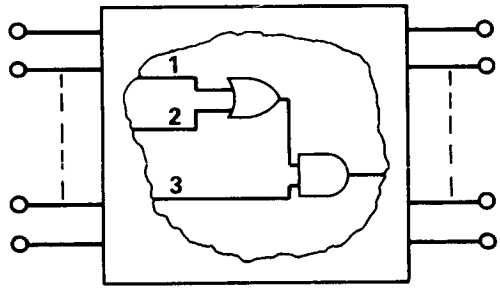

LATENT FAULTS

HARDWARE ANALOGY

1	2	3			
0	0	0	0	0	
0	0	1	0	0	SA1
0	1	0	1	0	
0	1	1	1	1	SA0
1	0	0	1	0	
1	0	1	1	1	SA0
1	1	0	1	0	
1	1	1	1	1	SA0

Figure VIII-20. Logic verification implementation schematic.

Assume for a moment that the output of the OR gate is stuck at one (S-A-1). Only one of the eight input patterns would cause the output of the AND gate to be influenced by this fault; that is, the fault could only be detected by this one pattern. Three patterns would be effective for detecting an S-A-0 condition of the OR gate.

As the complexity of the logic is increased, the number of input patterns necessary to verify the functional integrity of the total logic increases very rapidly. It is imperative then to analyze the logic and determine the minimal set of input patterns necessary to verify the functional integrity.

The CPU self-test microprogram can be structured to operate each logic element in the CPU in both logic states, at least once during the course of the routine, thus verifying the integrity of the entire CPU.

The extensive CPU testing on LST is possible because of the disparity in processor speed and processing speed requirements. The processor speed can be approximately three times the speed required to run the operational programs. Thus, 50 percent of the computer time may be used for system COFI if necessary.

Once or more during each self-test loop, a discrete bit is set if there has been no detected failure. This discrete bit (OK reset) is used to set a countdown counter to its all 1s value. The counter then proceeds to decrement toward zero. If another OK reset pulse does not reset the counter before it reaches zero, a CPU failure is indicated. The above operation of the decrementing counter handles both CPU self-test detected failures and failures that cause the program to branch to a wrong location and wander unpredictably. Another type failure is that which causes the self-test program to erroneously branch into a tight loop that includes issuing of the OK reset. This is handled by the window logic on the timer. Once the timer is reset to the all 1s position, another OK reset occurring before the window will have the same effect as the timer reaching the all 0s position — a failure indication. The functional logic of the window reset timer, which is located in the transfer assembly, is shown in Figure VIII-21.

b. Memory System Fault Detection/Isolation. Memory system fault detection, isolation, and recovery are achieved by means of error correction and coding with self-checking circuitry for selected portions of the system. The organization is such that any single fault may be tolerated. Extension to withstand any number of single faults (not simultaneous) is straightforward if deemed necessary. The memory technology will be nonvolatile, nondestructive readout technology, probably either plated wire or

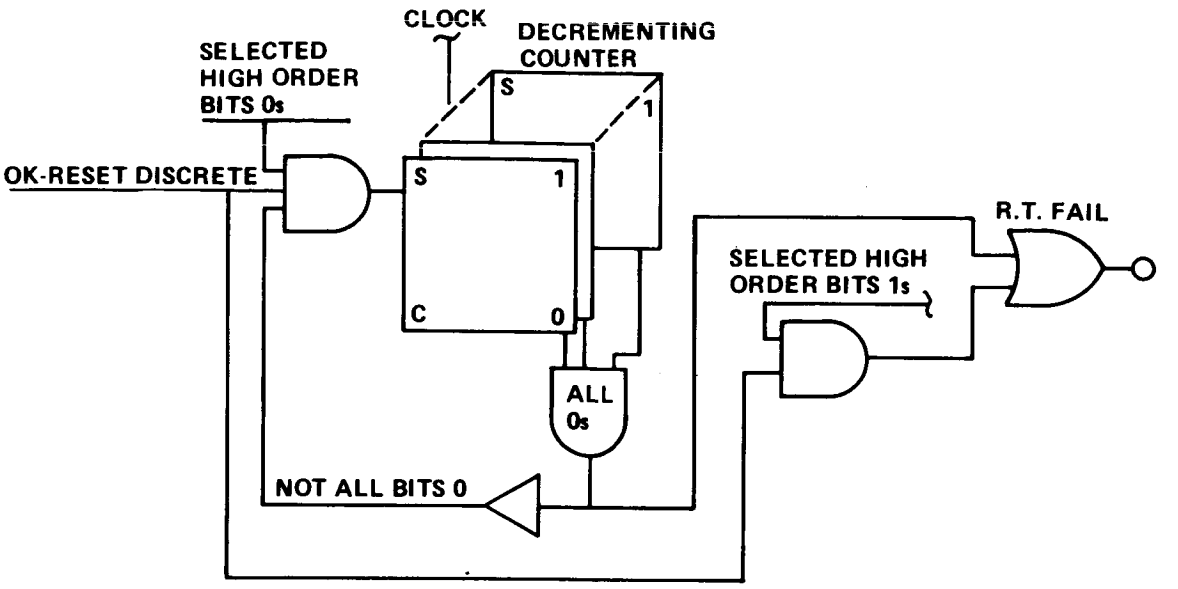

Figure VIII-21. Window reset timer functional logic schematic.

monolithic. Several independent memory modules, the exact number is not presently specified, contribute to each word read from the memory. Redundant bits forming a part of each word enable identification and correction of errant bits in each word readout. Recovery from both transient and hard failures is facilitated by the memory organization. Since the memory system is shared by the CPUs, the fault recovery problems associated with dedicated memory CPUs are largely circumvented. Referring to Figure VIII-22 for purposes of explanation, the memory system is composed of several independent basic operating modules (BOMs). A device called a translator is interposed between the memory and the CPU. The purpose of the translator is to translate between the code used for the stored data and the code that is accepted by the CPUs. Words stored in the memory are encoded in an error-correcting code referred to herein as a single BOM correct, double BOM detect (SbEC/DbED) encoding. Words read from the memory are comprised of bits from all the BOMs; that is, each BOM contributes one or more bits to each word, thus any failure in the BOM can affect only those bits in the word that the BOM contributes. Because of the encoding, the translator can determine which BOM has failed and correct the bits such that the output to the CPU is a correct word encoded with conventional byte parity encoding normally accepted by the CPU. Also, the same circuitry in the translator translates

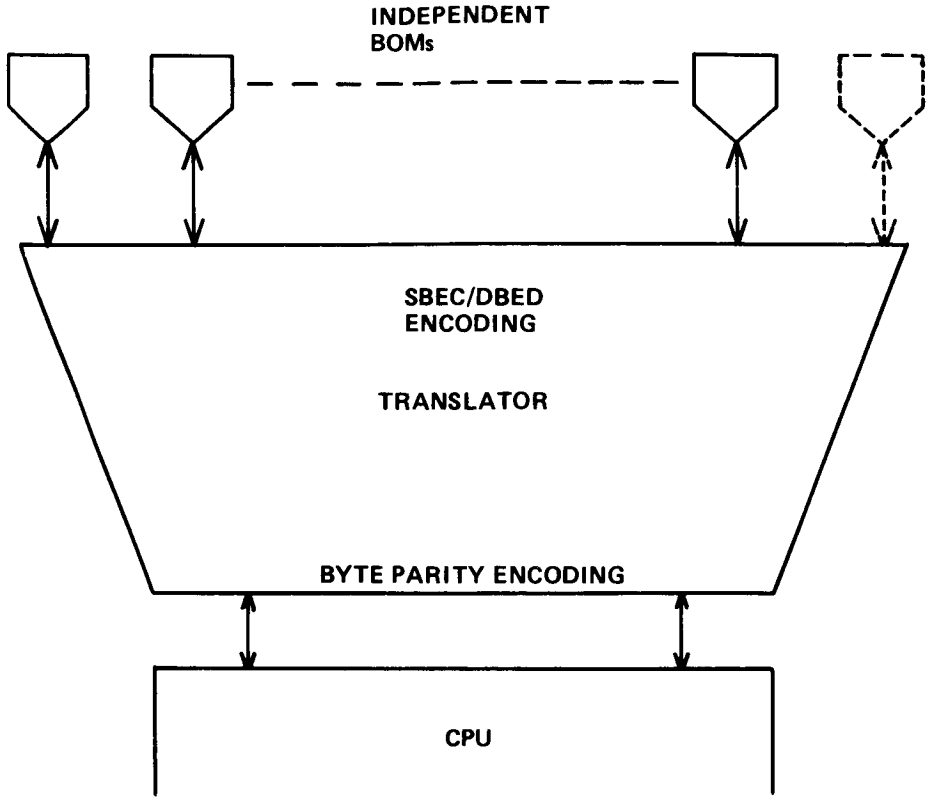

Figure VIII-22. Memory system organization schematic.

from the CPU encoding to the error correction encoding before the word is stored in the memory. The BOM width, that is the number of bits that each BOM contributes to the word readout, will be highly technology dependent. If the memory technology is monolithic, it is probable that each BOM will contribute only one bit to the word. If the technology is plated wire, it is probable that a BOM width of four bits will be more cost effective. The error encoding for the single bit per BOM can be a conventional Hamming encoding. The encoding for greater BOM widths would be of the more recently introduced b-adjacent error correction codes. The translator will be designed to be self-checking; that is, a single circuit failure in the translator will not produce an erroneous output without simultaneously indicating a failure. Figure VIII-23 illustrates the implementation of the fault tolerant memory system with two translators. The BOMs can feed either of the two translators as determined by the voted outputs of the status register. Each translator contains checking circuitry such that if the translator fails, an erroneous indication is given simultaneously with the production of the information out. In the event that the two checking signal lines from either translator have an even parity output,

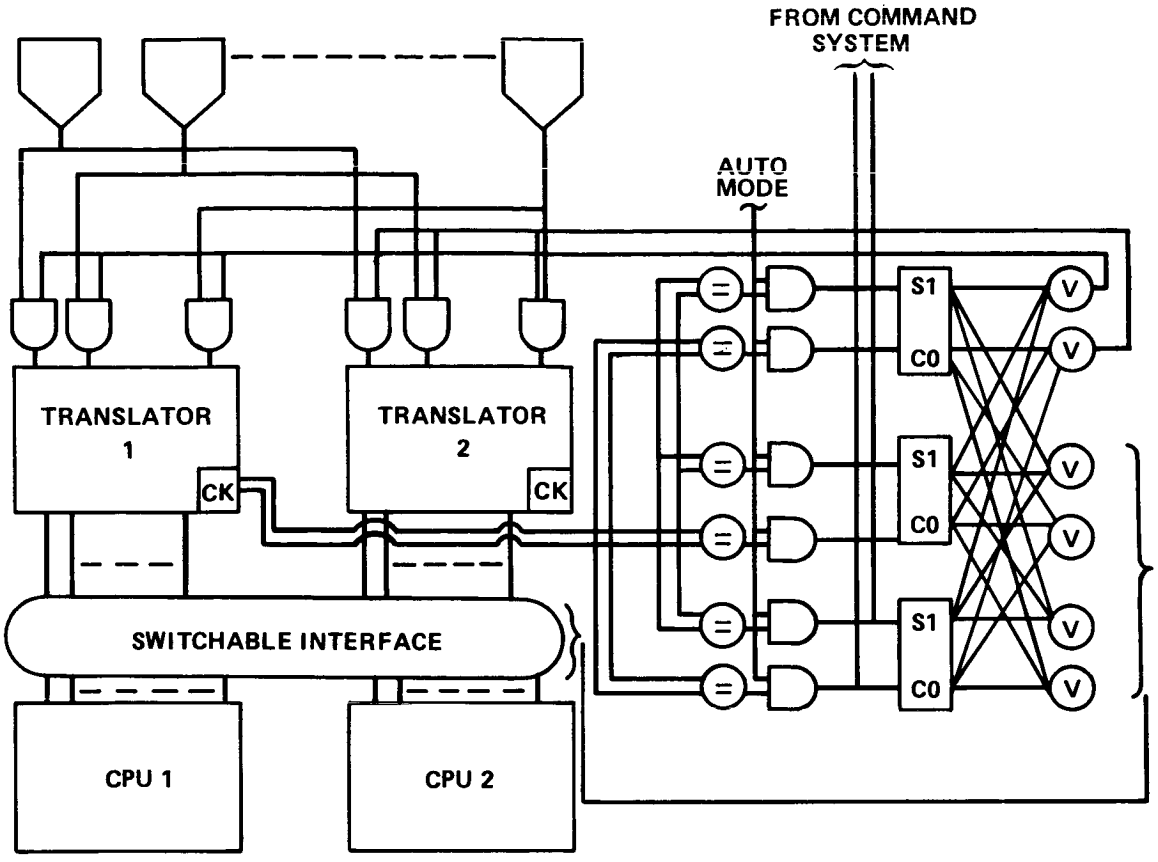

Figure VIII-23. Fault tolerant memory system with two translators.

this is an indication of a failure in that translator. The signal pairs are routed to equivalence function circuits denoted by the circle with an equal sign inside. If the system is in auto mode, the flip-flop status registers will be reset such that the alternate translator is operational. This is under control of the voted outputs of the status registers. The switchable interface interposed between the translators and the CPUs is essentially the same as that shown in Figure VIII-18.

c. Memory Organization Control and Fault Detection/Isolation. As part of the digital processor assembly self-test, every location in memory will be verified for proper operation. A rapid and efficient means for accomplishing this is by means of a complement check. In this check, the contents of each location, no matter what they may be, are read out and stored in a register. This value is then complemented and restored. The restored value

is next read out, and the original contents are compared by either an exclusive OR logical operation or an equals logical operation. If the exclusive OR operation is used, all positions should indicate a 1 from the exclusive OR. If the equal compare is used, all positions should indicate a 0. Any bit position or positions that do not agree with these criteria are faulty; therefore, the logic compare word with any faulty positions is incorrect. The time required for testing all memory words would be less than 1 sec. In the event that time constraints of the operational program do not allow complete memory testing on each self-test cycle, then fractional portions of successive sections of memory might be tested on successive self-test cycles with little loss of reliability. A retry capability for the memory will be incorporated to distinguish between transient and hard failures. Whenever an error is indicated in a word read out from memory by the translator, a retry will be initiated. If on retry the location is read correctly, then the retried word will be issued to the CPU. If on retry the location still indicates a failure, the failure will be corrected and the word issued to the CPU if the indication is a single failure; that is, a single BOM failure. If the indication is that the failure is a multiple failure that is not correctable directly by the translator, then a software routine will be entered. First, the routine will determine if the indication of the translator is a double BOM failure; then the store and read complement and compare with the original word test will be initiated. This test will then indicate the errant bits, and they may be corrected by a straightforward routine. In the event that the translator indicated greater than a two-BOM failure, the word is not correctable. In some situations, a checkpoint rollback procedure may be used to recover; in other situations this may not be feasible. An attitude hold or sun-point maneuver may be necessary until the next ground contact, where the situation is flagged by means of the command downlink system and ground isolation reconfiguration will be used. When any digital processor assembly failure is indicated from which onboard recovery may not be effective, the system is put into a hold mode or a sun acquisition mode until such time as ground contact can be made and reconfiguration and recovery can be effected from the ground.

5. Transfer Assembly. The transfer assembly serves as the interface between the sensors and actuators and the digital processor assembly. It contains such things as the up-down counters for the rate gyros, the window timeout for the digital processor assembly, the configuration control status registers, the amplifiers for controlling the magnetic torquers, and the discrete drivers for the reaction control system engines. In general, the various portions of the transfer assembly are functionally independent. It is for this reason that the transfer assembly is not reconfigured as a unit, but rather portions of the transfer assembly are reconfigured as their associated external

equipment or they themselves fail. Data from the sensors are transmitted to the transfer assembly in digital form. The rate gyros transmit the delta-V information as a pulsatile train, and an up-down counter in the transfer assembly dedicated to each of the rate gyros accumulates these pulses. Other sensors, in general, will have built-in conversion equipment and will encode the information in a gray code with attached parity check-bit for transmission to the transfer assembly. Sensor information comes to the transfer assembly in serial form, high-order bit first. The serial input of the digital processor assembly I/Os will have a simple translator to translate the gray encoded information to signed binary information. A standard instruction in the CPU then converts the signed binary information to two's complement binary for storage in the memory and ultimate utilization in calculations. A straightforward implementation of the communications between sensors and the transfer assembly would be to have two wires, one to indicate to the sensor when it should transmit the serial data along the second wire. Figure VIII-24 depicts the functional layout of the input sensor to the CPU interface. Readout of the devices is effected in any sequence by the CPU in command sending an address to its device address register. The address decoder then selects the line corresponding to the address and commands the particular device to begin a serial readout of the contents of its register. The serial data are then transmitted to the data input multiplexer, which has also selected the corresponding line to the addressed device. The data then pass through the multiplexer directly into the CPU serial data register. It is significant that no physical switches are required in this portion of the system; since, in the event of failure of a sensor, the CPU can simply neglect addressing this device. Alternatively, the device could be read if it was desired to maintain a fixed sequence, and the data simply could be ignored in the software. The serial data device on each sensor will have a command line from the address decoder associated with each CPU and a data transmission line to each CPU input multiplexer. Diode isolation will be used to preclude a short in address decoder number 1, for example, causing address decoder number 2 to be unable to access a particular sensor. Similarly, diode isolation will be used on the data output lines of each sensor device. The implementation in Figure VIII-24 is shown only for the up-down counter of rate gyro number 1; however, it is understood to be applicable to the devices on all the remaining sensors. Functionally, the address decoder and the input multiplexer are dedicated to a CPU and therefore form a part of that CPU.

a. Transfer Assembly Outputs. Figure VIII-25 depicts the functional logic of the output portions of the transfer assembly. Commencing from the top, each CPU has a reset time pulse to indicate that its hardware, firmware, and software self-checks have all indicated good health in the

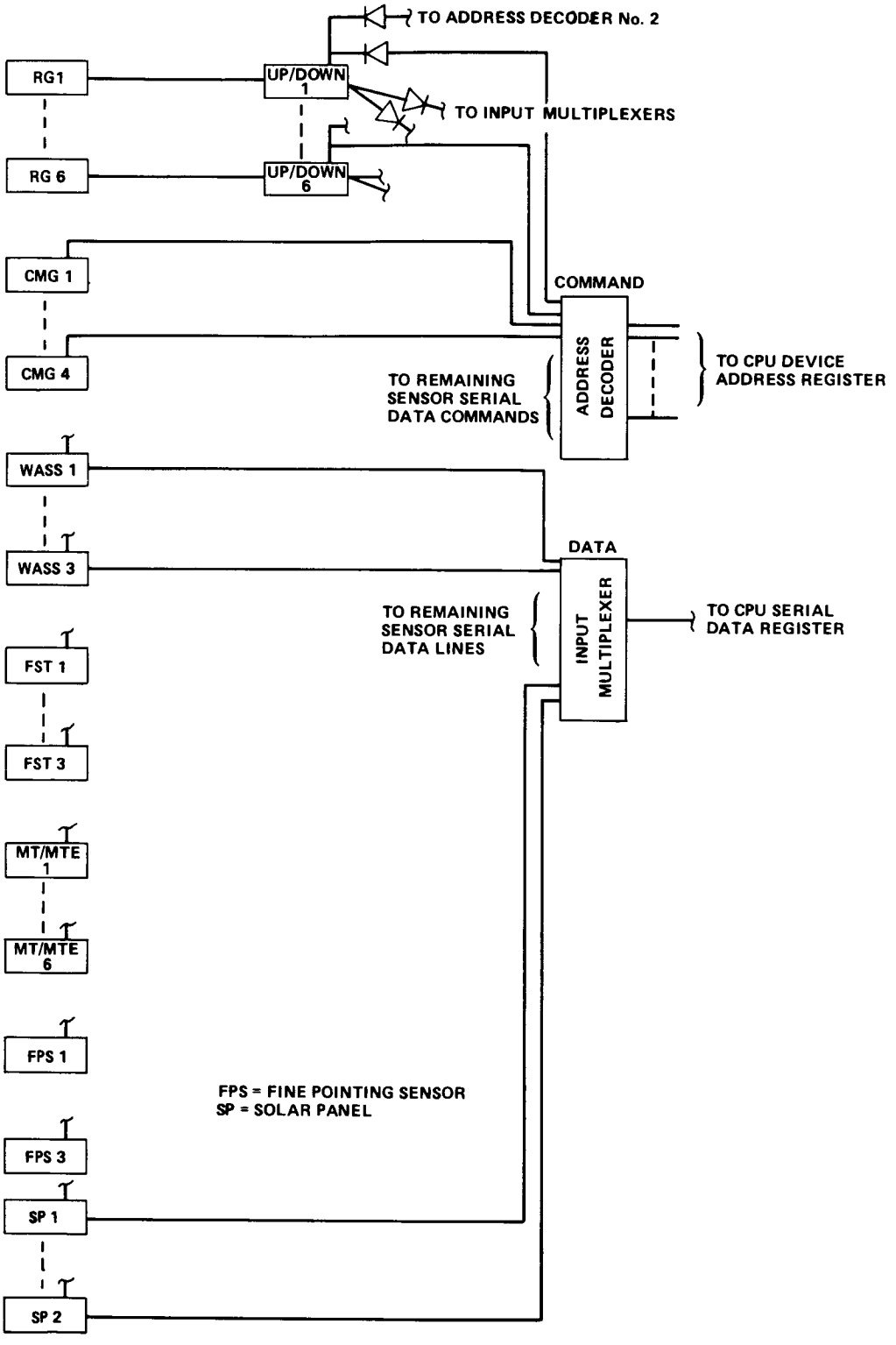

Figure VIII-24. Transfer assembly sensor input functional layout.

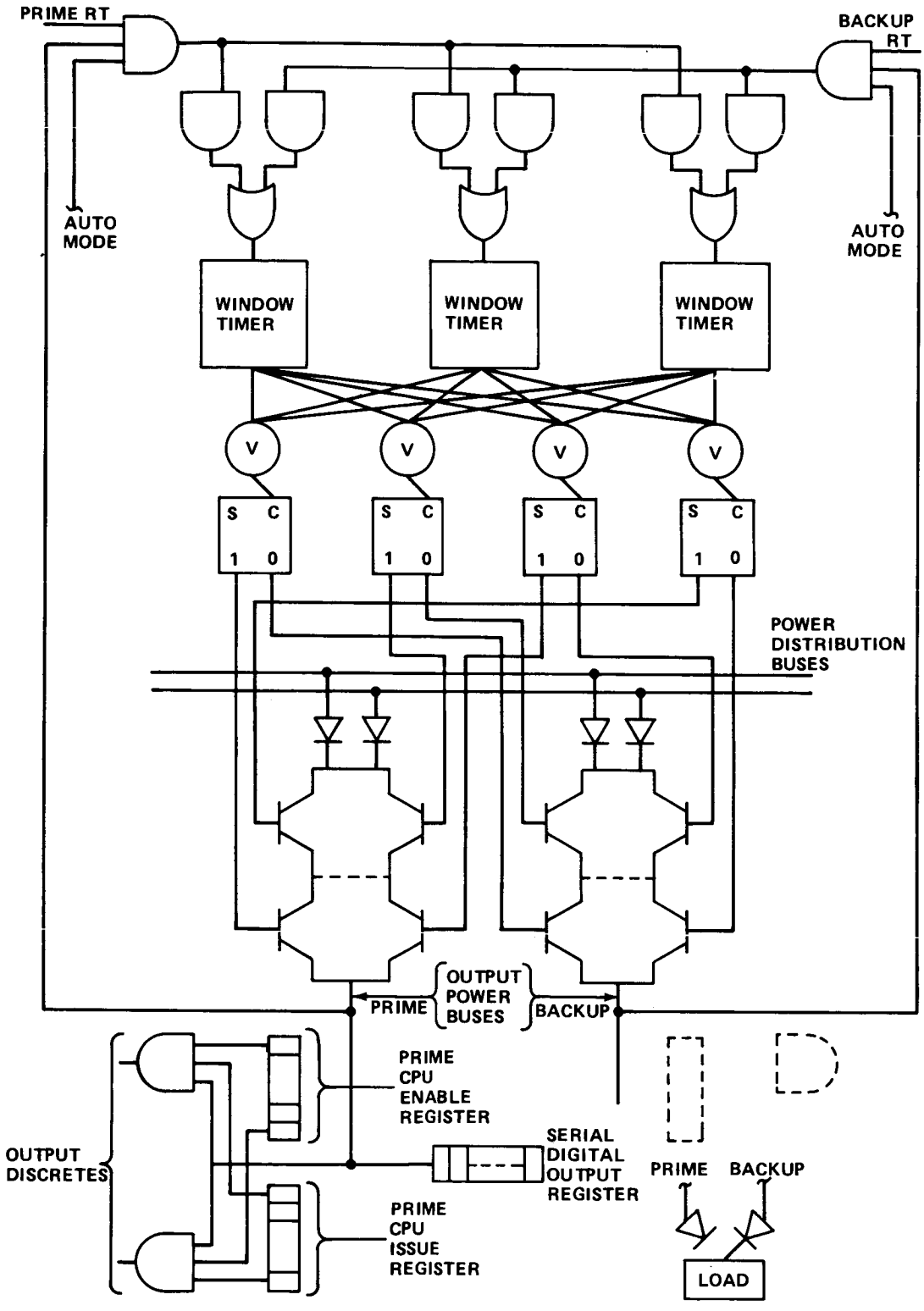

Figure VIII-25. Transfer assembly outputs.

self-test mode. The window timer is only effective when the system is in the automatic mode. Conventional circuitry not shown in Figure VIII-25 could be added to the voters such that they are effective only in the auto mode. Failure to properly reset two or more of the window timers will cause the flip-flops following the voters to move to the clear or reset state. In the normal set state of the flip-flops, the quad redundant switch on the left is effective and enables power to the output section of the transfer assembly for the prime CPU. If the flip-flops are in the reset state, power is switched from the prime CPU output to the backup CPU output; thus a CPU, in the event of failure, is effectively eliminated from having any effect on the system. These power switches are made quad redundant to eliminate single failure points in the switch. Assuming for the moment that the prime CPU is in control, the method of handling discretes is shown. There are two discrete registers; one is a discrete enable register and the second is a discrete issue register. A one-bit in the corresponding position of each of these registers is necessary to issue any particular discrete. The discrete enable register is set by the CPU program just prior to the self-test mode. The discrete issue register is set just subsequent to the self-test routine. Thus, the discretes are not, indeed, issued until a very recent self-test health check is completed satisfactorily. Handling of the outputs from the backup CPU is similar to that of the prime. At the receiver load, both the prime and the backup signals are combined, such that either the prime or the backup functioning can actuate the load. Short circuits upstream from the load ahead of the isolating diodes preclude one line shorting and disabling the other line from actuating the load.

b. Transfer Assembly Redundancy Management Input/Output. In addition to the communications between the ASCS primary sensors and effectors with the transfer assembly and digital processor assembly, there are similar communication requirements of the latter assemblies with other points of the system. Certain onboard redundancy management functions are to be controlled by the ACS processor when the system is placed in the auto mode.

6. Reference Gyros. The strapdown references gyros for the inertial reference system will utilize six reference gyros mounted with their sensitive axes perpendicular to the faces of a regular dodechaedron. This configuration has advantages in regard to accuracy and failure detection. During regular operation, four reference gyros will be active and two will be powered-down in standby status to take advantage of the lower failure rate in standby status and the savings in power. The primary means of failure detection is by comparison of the outputs of the four rate gyros. So-called parity equations for combinations of any four rate gyros may be written which under ideal

alignment and operations equal zero. Practical threshold levels will have to be determined that allow for normal instrument variations, alignment errors, and computational precision. Out-of-tolerance conditions in any one of the four may then be detected as a solution to the equation exceeding the allowable threshold value. To isolate the recalcitrant unit, a fifth gyro will have to be powered-up. Diagnostic computations to identify this unit will then be computed. Included in the computations is a health status matrix. The elements of the matrix for the active units are set to one. The elements of the matrix for the inactive units, whether it be because they are intentionally in standby or because they have been identified as failed units, are set to zero, thus effecting a software switch. To maintain configuration control is a straightforward matter.

Up to two failures may be detected and isolated by observations of the outputs of the reference gyros alone with this technique. A third failure may be detected; however, it cannot be isolated without additional information. This additional information will be obtained by means of the built-in test equipment of the reference gyros. Additionally, the built-in test equipment will be used to augment the primary failure detection means. During each computational minor loop, after the most recent information is read from the gyros but prior to utilizing this information in computation, the health status will be determined. If the information from one of the reference gyros is unacceptable, one of two alternatives can be used. The first is: if mission constraints allow a standby gyro to be powered-up, locate the defective unit, reread the remaining four good units, and utilize these values in the computations. With this alternative, there is essentially no system recovery problem. In the event the particular phase of the mission places constraints where this is impractical, the last good values are still available and could be saved — the computations performed, including the bad unit, until such time as it can be identified. Having identified the unit, it is then relatively straightforward to calculate the present rates from the checkpoint restart and the deviations of the three good units. Of course, if another means such as the BITE indications are sufficient to identify the bad unit, then the powering-up of the standby and diagnostic calculations also could be precluded.

7. Control Moment Gyros. Several methods of failure detection for any one of the four control moment gyros (CMGs) may be used. The first test is a measurement of the resolver reference voltage. A deviation greater than a predetermined allowable variation indicates a failure of the CMG resolver and consequently of the CMG. A second test of the CMG is a comparison of the integral of the drive command over any period of time with the gimbal angle change over the same period of time to verify their correspondence. A third

failure detection test for the CMGs is to compare the vehicle attitude, and attitude changes corresponding to the commands to the CMG as measured by the rate gyro assembly. Upon detection of a CMG failure by any or all of the above methods, system recovery must be effected by first withholding any subsequent rate commands to the CMGs and by exchanging momentum of the failed CMG with the remaining good CMGs so that vehicle attitude may be maintained with a three-CMG control law. The momentum exchange can be accomplished utilizing the three-CMG control law but is only initiated by ground command.

8. Wide-Angle Sun Sensors. The fault detection on the wide-angle sun sensors is primarily by means of comparison consistency checks between sun sensors and internal consistency checks of individual sun sensors. The redundant pair of sun sensors oriented along the plus Z vehicle axis can be compared with one another for fault detection. Fault isolation may be done on this pair by internal consistency checks, and recovery entails primarily a software switch to ignore the data from the failed cell and turn off the power to its associated electronics. For the wide-angle sun sensor oriented along the minus Z-axis, internal consistency checks together with reasonableness tests of the vehicle attitude, known from the vehicle attitude computations, may be used to detect and isolate a failed cell. For the two wide-angle sun sensors mounted one each on the solar panels, internal consistency checks plus correlation with the solar power impinging on the solar array may be used to detect and isolate failures. Recovery, again, consists of a software switch together with power turnoff of the electronics associated with the failed cell.

9. Fixed Star Trackers. The three fixed star trackers oriented in the Y-Z plane — one collinear with the minus Z-axis and the remaining two, one at +45 and one at -45 degrees, with the minus Z-axis — are redundant in the sense that any two of the three may be used to establish the reference plane for vehicle orientation. However, the 6-degree fields-of-view of the trackers do not coincide or overlap. Thus, instantaneous comparisons of their outputs are not useful for failure detection. Detection of catastrophic failures when in the tracking mode is rather straightforward in that the indication would be a dramatic increase in one or both of the output access signals without a corresponding indication of the vehicle attitude control system. Slow drift failures may be detected when all three trackers are locked on separate stars. The drift of the outputs of one tracker relative to the corresponding axes of the other two would be manifest as a significant difference in drift rate of the faulted tracker. For the case when only two of the three trackers are locked on a star, the failure detection might revert to comparison with the fine pointing signal from the scientific instrument package (SIP) or a ground analysis of the picture quality data being received indicating the drift condition.

10. Three-Axis Magnetometers. The pair of three-axis magnetometers may have failure detection by means of comparing the corresponding axis outputs of the magnetometers. Resolution of any discrepancy may be done by noting the vehicle attitude effects in response to specific torquing signals and noting which magnetometer most correctly models these effects.

11. Communications and Data Handling System.

a. Command Subsystem. Fault detection, isolation, and recovery in the command subsystem are largely dependent upon verification by means of the downlink that the commands transmitted in the uplink channel were, indeed, obeyed. Real-time response is not of paramount importance for this purpose. At each opportunity for earth-to-spacecraft communications, the system status is transmitted from the spacecraft by means of the downlink command system. The system configuration may be changed in response to commands up-linked from the ground station. A subsequent transmittal of system status will then reveal whether the spacecraft has, indeed, responded correctly to the commands. In the event that it has not, a systematic sequence of commands from earth may be used to isolate the faulted unit. Sufficient redundancy is incorporated that the system may withstand any single failure and recovery may be effected. Two independent transponder systems are used: one is a modified Apollo transponder which is dual-redundant in that it contains two transmitters and two receivers; the second transponder, likewise, is dual-redundant being a modified ERTS transponder with dual transmitters and receivers. For command receivers in the uplink mode, one receiver in each of the two transponders is powered on. The ERTS receiver is connected to one antenna and the Apollo transponder receiver is connected to the second. Signals from both receivers are channeled through the electronic switch assembly to the dual PSK demodulator. The PSK demodulator assembly selects the channel with the strongest automatic gain control (AGC) signal and sends a switching signal to the antenna's switch so that subsequent transmissions will be routed to the antenna receiving the strongest signal from the ground.

To detect interference noise that constitutes failures in the uplink information channel, an information bit is derived from five subbits which are transmitted. Since there are 32 combinations of 5 bits, there are 32 combinations from which to choose the 0 and 1 command representations. For example, the subbit code for data 1 may be chosen as 11010; and the subbit code for a data 0 may be chosen as the complement or 00101. There are other possibilities also such as a different encoding for the address bits to the decoders in order that confusion may not arise between address bits and data bits. Only prewired, valid combinations of bits are accepted; otherwise an

error is flagged. The outputs from the dual PSK demodulators, each receiving signals from a separate receiver, are compared, and if they agree, the command is issued. In the event of discompare, the command is not issued and an error message is reported to the ground. The mode is automatically set to enable either (or both) channels to receive and issue commands. Ground analysis of the error message will determine the faulty channel. The next uplink will be directed to the good channel to reconfigure the system and switch out the faulty channel.

b. Command Decoders. Command decoders are used with a prime and standby spare type of operation. Each decoder has an 8-bit input that is decoded to one of 256 output lines. A status register controlled switchable interface is used to direct the command signal to the online decoder. Outputs of the dual decoders are diode ORed to the points at which the lines are directed. Failure detection of the decoders is by means of a parity check as shown in Figure VIII-26 with backup being by ground control. Ground analysis of the cause of failure, and reconfiguration requirements to circumvent the failure should be greatly augmented by circuits such as the decoder checking circuit when they can be economically implemented. Figure VIII-26 shows the decoder detection scheme. The outputs of all lines which should be activated by even parity inputs are ORed together as are the second group of output lines that should be activated by even parity inputs. In the event an erroneous output condition is detected by the checking circuit, a flip-flop associated with the particular failed command decoder is set and the status is transmitted on the subsequent health transmission.

c. Command Processor. It is desirable to have certain commands initiated by the ground issued and executed at a time when the spacecraft does not have ground communication contact. The command processor has the capability to accept and store commands from the ground and to issue the command at a predetermined later time. The processor consists, basically, of a memory that is read in cycles and a real-time clock. Part of each stored command consists of a time-tag which specifies the time when the command is to be executed. As the memory is cycled, the real-time clock is compared with the successive commands being read from the memory; and, when there is a correspondence between the real time and the time tag, the command is output to the command bus.

The clocking circuitry consists of three crystal-controlled, phase-locked oscillators with individual associated shaping circuitry. After shaping the individual channel, square waves may be voted with conventional voting circuitry. Also, the various subdivided clock pulses can be voted in a

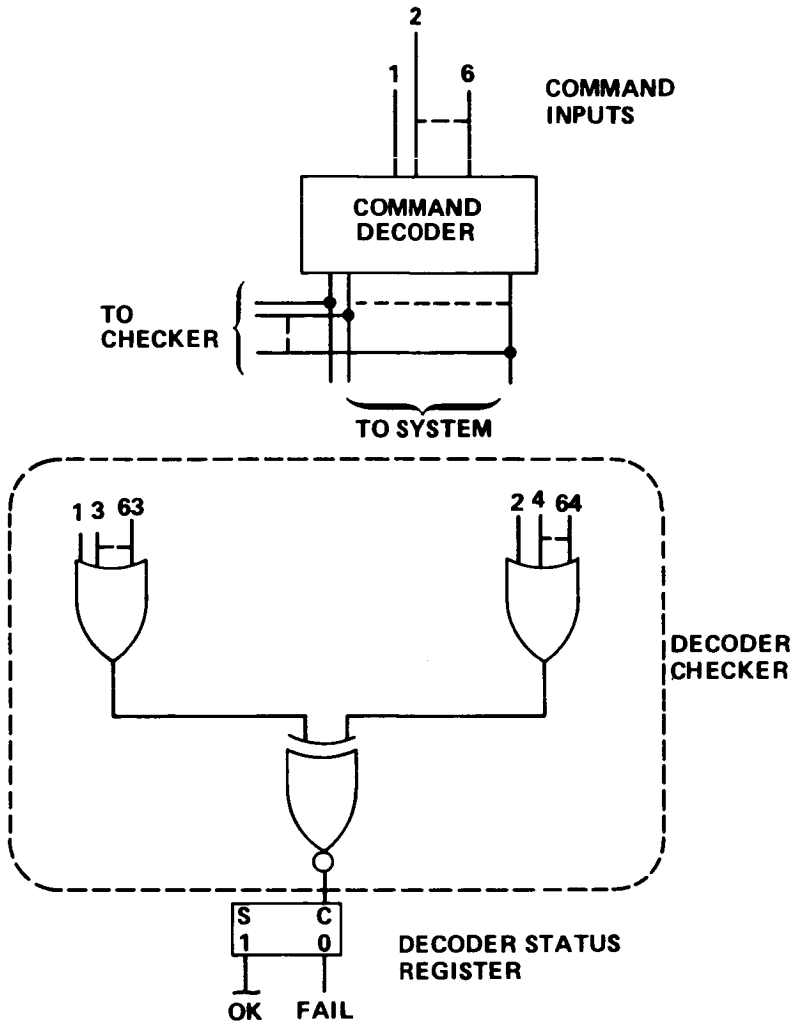

Figure VIII-26. Command decoder checker.

TMR fashion; thus, triplicate redundant clocking signals used throughout the communications and data handling subsystem are distributed over triplicated buses. Units which require these clocking pulses are served by voting the three signals as clocking inputs to the using devices. The memory for the command processor is a nondestructive readout read-write memory. The memory is organized with error encoding redundant bits similar to the ACS computer. Associated with the memory is a self-testing translator. The translator, at this time, is not specified as having a backup because the entire delay command capability is not essential to experiment and mission success.

12. Electrical System. Fault tolerance in the electrical system is obtained by means of diode isolation throughout the system and reconfiguration switching. The system is partitioned to a very high level such that there are a multitude of successful states to circumvent all single failures and a large variety of multiple failures. Figure VIII-27 is a schematic of the system. It may be seen that there are 12 solar arrays, 6 on each of 2 solar wings. Each panel has a dual output which is switchable and may be diode-isolated. Each output from each wing is dot ORed to common primary buses in the solar power distributor. There are two solar power distributors with six panels connected to each of their primary buses. There is also an alternate primary bus in each solar power distributor to which the second array outputs are connected. The corresponding primary buses and alternate primary buses in the solar distributors may be connected through a switch to each other. Each primary bus is connected through switches to three battery-charger combinations. All six charger-battery combinations can receive power from any of the four primary power buses via crossties between solar power distributors and between the electrical control assemblies.

Following the solar power distributors and battery-charger combinations are two identical ECAs. These each contain a main battery bus and an alternate battery bus. The main battery bus in each of the two ECAs is fed by three charger-battery units through diodes and switches. The main battery buses are also connected through switches to the corresponding channel primary buses in the solar power distributors. The alternate battery buses, one each in each of the two ECAs, is fed by the alternate outputs of the three battery-charger units through diodes and switches. The alternate battery buses are also connected through switches to the corresponding channel alternate primary buses in the solar power distributors. Three regulators may receive input power from either the main battery bus or the alternate battery bus in the corresponding ECA. Dual outputs from each of the three regulators are dot ORed through switches to a main and an alternate distribution bus in the ECA. Diode isolation is not required on the output of the regulators because of the design. A finite equivalent impedance in the output of each regulator and feedback enables regulating the share of the load that each regulator contributes. The main and alternate distribution buses then feed eight EDUs through appropriate switches. In turn, the EDUs supply the various loads throughout the system. The capacities of the regulators are such that any three of the six are capable of supplying the total system requirements.

Fault Detection and Isolation. Throughout the system, the voltage and current parameters of the buses and the various types of modules supplying the buses are continuously monitored for fault detection and power

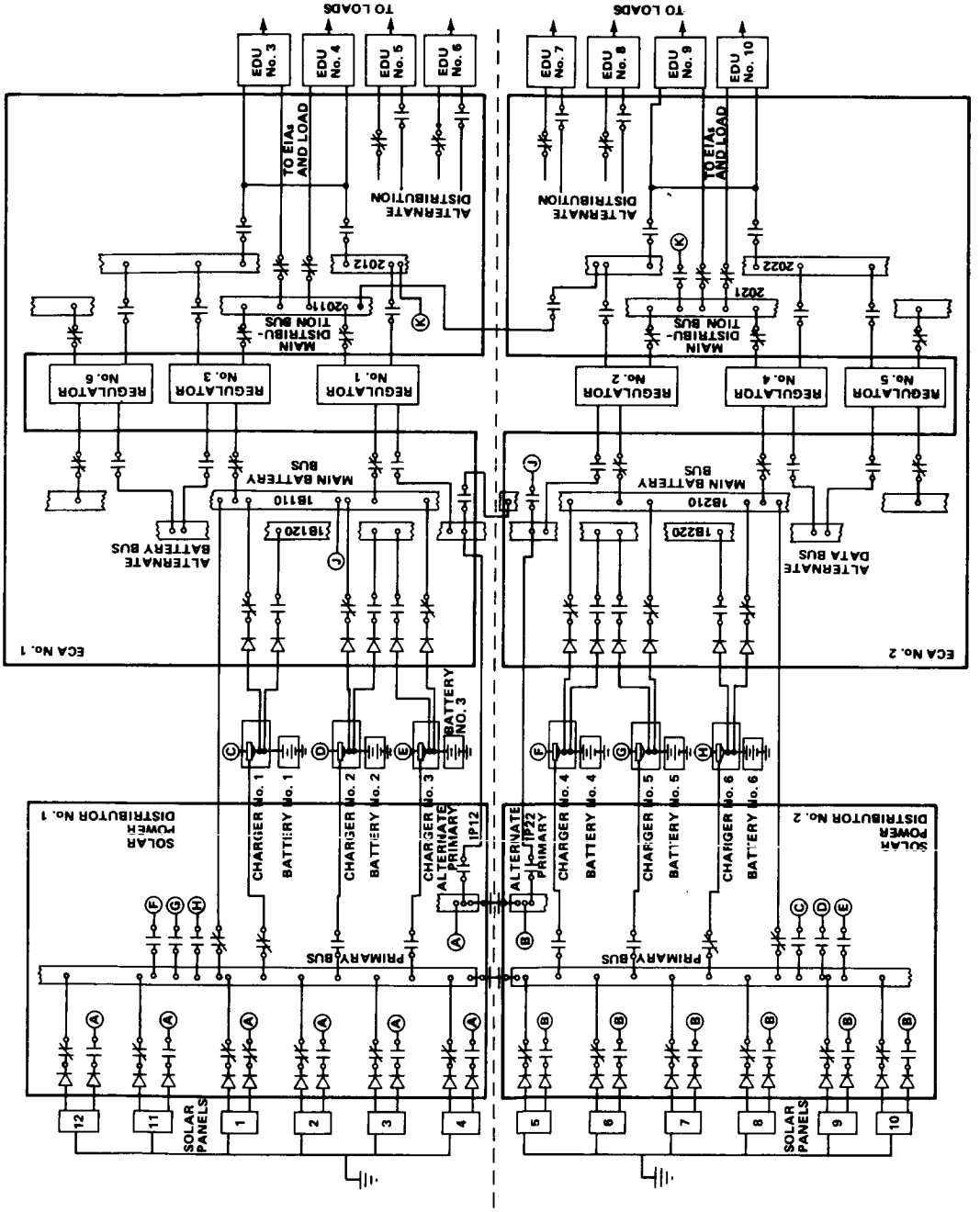

Figure VIII-27. LST electrical system.

control. The solar arrays themselves are additionally monitored from the ground by measurements of their I-V characteristics. Temperatures of the solar arrays, as well as other components in the system, are measured to detect incipient and occurred faults. The various test points and parameters within the electrical power system are continually being monitored by the DAUs allocated to the electrical system. The power management switches that control the configuration of the system are controlled from signals received from command decoders. The decoders are addressed and controlled from the ground through the radio-frequency (RF) command uplink. The ground also has override control of automatic protective switching.

13. Software Estimates. The onboard redundancy management software is estimated to require a few more than 2000 16-bit locations. Table VIII-7 is a breakdown of this estimate.

The rate gyro routine has been written at the MIT Draper Laboratory. The CMG and sun sensor routines are written for the Skylab program. The remaining estimates are based on assumed complexity.

The electrical system redundancy management estimate is assumed to implement a keep-alive algorithm to circumvent system faults until the next ground communication opportunity. Optimum reconfiguration for the degraded mode system operation is assumed to be uplinked from the ground via the command system. Also, an upgraded electrical system redundancy management algorithm is assumed to be uplinked to the ACS processor.

No onboard redundancy management is postulated for the C&DHS system.

TABLE VIII-7. MEMORY SIZE ESTIMATES

ACS	Memory Words
Rate Gyro Failure Isolation and Adaptation	800
CMG	575
Acquisition Sun Sensors	170
Magnetometers	170
Star Trackers	225
Magnetic Torquers	75
	2015
Electrical System	250
	2265

C. Degraded Mode Assessment

A study of the design reference reveals a considerable measure of fault-tolerance; i.e., a large number of failures can occur with no significant impact on the system capability. This is particularly true in the SSM and optical telescope assembly (OTA). Since the SIP instrument failures are, for the most part, independent, a given instrument failure will affect only the operation of that instrument. The most noticeable exception is the slit jaw camera that operates in conjunction with certain other instruments and whose failures would decrease the usefulness of those instrument outputs.

The most important credible degraded modes in the SSM are discussed below.

Failure of the command processor or memory would result in loss of the stored command capability. Hence, redundancy has been applied to these system elements, since a real-time only command execution capability would greatly decrease the information output of the LST.

Failure of one or more electrical batteries would effectively eliminate the present capability for one orbit of off-sun pointing to satisfy a spectrometer slit orientation requirement and would also necessitate experiment scheduling to minimize the power demands and conserve battery system life. Alternatively, so long as three batteries are unfailed, the nominal loads could be satisfied, but this might result in a shorter maintenance interval.

As described previously, the reference gyro assembly must provide attitude information about the pitch and yaw axes with accuracy at least equivalent to an orthogonal triad with gyros aligned along these axes. This is based upon a desire to avoid a target reacquisition sequence, with the attendant possibility of locking onto the wrong guide stars. The time estimated for completion of the reacquisition sequence, including maneuvering and settling time, is approximately 5 min. With gyros having a random drift of 0.005 degree/hour (1σ) and with a maximum occultation time of 35.5 min, the gyro combinations described in Section A.2 will permit the guide stars to remain within the coarse field of the fine guidance sensor. Since observations can be continued with up to three gyro failures, albeit with greater difficulty, these failures constitute a degraded mode of operation.

D. Future Effort: The Reliability and Maintainability Problem

Once the decision had been made to launch the LST using the Shuttle, there arose the problem of effectively utilizing the Shuttle maintenance capability to achieve a feasible low cost design. While considerable emphasis has been placed on this capability, there is a dearth of techniques useful to the hardware designer. For the first time, the maintenance mode, policy, and level form an integral part of the hardware design problem.

The "mode" is simply the method by which maintenance is to be accomplished. For the LST, three maintenance modes were considered: (1) pressurized, shirtsleeve, on-orbit maintenance; (2) unpressurized (manipulator) maintenance; and (3) ground maintenance using the Shuttle retrieval capability. The option of a Shuttle-launched, expendable LST was also considered. For the design reference, the pressurized mode, with ground return backup capability, was selected. The qualitative and economic reasons for this selection are discussed in Chapter VII. "Policy" is the term used to describe the frequency of maintenance actions or, what amounts to the same thing, the criteria used to determine maintenance actions. These criteria can be called maintenance action initiation decision rules. Two policies were considered for the LST: scheduled maintenance at fixed intervals, and random, or unscheduled, maintenance. The latter is a "fix when failed using the Shuttle as available" approach. Shuttle availability is discussed in Chapter VIII. For these policies, the interval length or interval length statistics can be varied by changing the decision rules or the hardware characteristics. At the present time, the random maintenance policy appears to offer the greatest potential for cost savings.

Early in the Phase A study, it became obvious that the traditional reliability techniques were inadequate to answer the questions raised by the Shuttle maintenance capability. As an example of this inadequacy, consider the SSM spares problem. Table VIII-8 lists 21 different replaceable items having a total volumetric requirement of 2.299 m^3. Due to lifetime problems, it was assumed that the batteries and tape recorders would be replaced during every maintenance action. The expected, or average, spares volume for a maintenance flight occurring at 1 year was calculated to be 0.414 m^3 (these are "raw" volumes; i.e., no allowance is made for packaging, tools, test equipment, contamination control equipment, etc.). However, this single number is not very informative. Note that the volume of a single CMG is approximately 0.461 m^3. Accordingly, a crude attempt was made to estimate the reasonable spares volume requirement. Table VIII-9 gives the results.

TABLE VIII-8. LST SPARES PROBLEM

Item	No. Units	Unit Vol. (L)	Total Vol. (L)	Expected Spares Vol. (L)
1 RGA	1	11.70	11.70	6.38
2 FST	3	5.31	15.93	0.60
3 TA	2	7.63	15.26	2.87
4 DPA (8K memory)	2	5.05	10.11	1.18
5 CMG	4	460.97	1843.88	255.36
6 Magnetometer	2	4.10	8.19	0.06
7 MTE	1	2.10	2.10	0.04
8 RCS Electronics	2	14.45	28.91	0.08
9 Battery Charger	6	9.44	56.63	0.74
10 Regulator	6	7.21	43.26	4.01
11 ECA	2	14.68	29.37	0.92
12 EDU	8	1.18	9.44	0.04
13 Transponder-Apollo	1	19.69	19.69	2.50
14 Transponder-ERTS	1	10.23	10.23	1.17
15 Baseband Unit	1	2.29	2.29	0.08
16 Data Control Unit	1	2.48	2.48	0.10
17 Remote Decoder	16	2.48	39.64	0.62
18 DAU	28	0.13	3.60	0.04
19 Format Generator	2	4.96	9.91	0.43
Subtotals (m^3)			2.163	0.278
20 Batteries	6	20.19	121.13	121.13
21 Tape Recorders	3	7.35	15.05	15.05
Totals (m^3)			2.299	0.414

TABLES VIII-9. LST SPARES PROBLEM

Item	Unit Vol. (L)	No. Spares	Total Vol. (L)	"Renewal" Probability	No. Spares	Total Vol. (L)	"Renewal" Probability	No. Spares	Total Vol. (L)	"Renewal" Probability
1 RGA (1)	11.70	0	0	0.57565	1	11.70	1	1	11.70	1
2 FST (3)	5.31	0	0	0.92220	0	0	0.92220	1	5.31	0.99702
3 TA (2)	7.63	0	0	0.91501	0	0	0.91501	1	7.63	0.99662
4 DPA, 8K memory (2)	5.05	0	0	0.51251	1	5.05	0.91929	2	10.10	1
5 CMG (4)	460.97	0	0	0.55086	1	460.97	0.90507	2	921.94	0.99048
6 Magnetometer (2)	4.10	0	0	0.99136	0	0	0.99136	0	0	0.99136
7 MTE (1)	2.10	0	0	0.97990	0	0	0.97990	1	2.10	1
8 BCS Electronics (2)	14.45	0	0	0.99430	0	0	0.99430	0	0	0.99430
9 Battery Charger (6)	9.44	0	0	0.92385	0	0	0.92385	1	9.44	0.99751
10 Regulator (6)	7.21	0	0	0.55777	1	7.21	0.89977	2	14.42	0.98353
11 ECA (2)	14.68	0	0	0.93813	0	0	0.93813	1	14.68	0.99901
12 EDU (8)	1.18	0	0	0.96297	0	0	0.96297	1	1.18	0.99939
13 Transponder-Apollo (1)	19.69	0	0	0.82235	0	0	0.82235	1	19.69	1
14 Transponder-ERTS (1)	10.23	0	0	0.88541	0	0	0.88541	1	10.23	1
15 Baseband Unit (1)	2.29	0	0	0.96457	0	0	0.96457	1	2.29	1
16 Data Control Unit (1)	2.48	0	0	0.96027	0	0	0.96027	1	2.48	1
17 Remote Decoder (16)	2.48	0	0	0.77689	1	2.48	0.97458	2	4.96	0.99816
18 DAU (28)	0.13	0	0	0.74488	1	0.13	0.96543	2	0.26	0.99691
19 Format Generator (2)	4.96	0	0	0.95293	0	0	0.95293	1	4.96	0.99898
Subtotals (m^3)			0	0.02293		0.488	0.30794		1.043	0.94460
20 Batteries	20.19	6	121.13	1	6	121.13	1	6	121.13	1
21 Tape Recorders	7.35	3	15.05	1	3	15.05	1	3	15.05	1
Totals (m^3)			0.136	0.02293		0.624	0.30794		1.180	0.94460

It was first assumed that only batteries and tape recorders would be replaced; 0.136 m^3 was required, but the SSM then had only about a 2-percent probability of being "as good as new." Spares were then allowed for those items least likely to be "as good as new." The volumetric requirement rose to 0.624 m^3 and the "renewal" probability to about 31 percent. Further spares raised the volume to 1.180 m^3 and the renewal probability to about 94 percent. This analysis is misleading in that ground diagnostics of the telemetered spacecraft data would, in actual practice, define the spares kit. Accordingly, the "spares" shown in these two tables more nearly describe the inventory from which the kit would be drawn. A second point to be noted is that it is not essential that a given maintenance action restore the spacecraft to a "new" condition.

The spares problem, either in the volumetric context just described or reformulated in terms of maintenance action duration statistics, is typical of the problems raised by the Shuttle maintenance capability. Problems relating to the number of maintenance actions required, Shuttle availability, and program cost statistics are other examples.

CHAPTER IX. CONCLUSIONS

CHAPTER IX. CONCLUSIONS

The results of the Phase A study indicate that a 3 m optical telescope can be operated in low earth orbit for 5 or more years. The telescope support requirements can be provided by onboard systems to provide near-diffraction-limited optical performance. The LST spacecraft may be launched by either the Shuttle (primary) or the Titan IIIE/Orbit Adjust System (OAS) (alternate) vehicle. Specific conclusions are categorized as follows:

1. Configuration.

a. The reference design support systems module (SSM) configuration is compatible with either a Shuttle or Titan launch. The docking structure blends easily into the reference design SSM. However, either launch requires that the SSM be provided with fittings for a Shuttle recovery. The Shuttle launch/recovery in turn requires a pallet or cradle to adapt the SSM to the Shuttle payload bay and to avoid inducing loads into the LST from Shuttle flexing. Conical adapters are required for the Titan launch to adapt the SSM and the fairing to the OAS kick stage. One cone provides support for the aerodynamic fairing while another provides the primary LST/OAS load path.

b. The arrangement of support system components provides adequate clearance for astronaut maintenance of the LST in a shirtsleeve environment. The arrangement also is thermally compatible with the SSM radiating surface area and solar orientation and is adequate for the reference design thermal control system.

2. Structures

a. The reference design SSM is a conventional pressurized cylindrical structure of simple aerospace skin/stringer construction, although several other standard aerospace structural design techniques, i.e., "isogrid," honeycomb, integrally stiffened panels, etc., might easily be substituted. Conventional materials such as aluminum alloys in standard gages with standard fasteners will provide a satisfactory pressure shell with an adequate factor of safety. The meteoroid protection shield is easily integrated into the reference design structure or other standard aerospace structures and is compatible with the reference design thermal control system.

b. The reference design solar array is structurally adequate; however, alternate structures provide design leeway and may be preferred for other than structural requirements.

c. No significant disturbance to telescope pointing is caused by oscillation of the solar array following reorientation of the spacecraft.

d. Dynamic deflections of the spacecraft structure caused by control moment gyro (CMG) disturbances (rotor unbalance) are not structurally significant.

3. Thermal Control

a. A passive thermal control design is feasible for the SSM.

b. Louvers will be required to control the battery temperatures within their prescribed limits.

c. Approximately 250 watts will be required for heaters to control the temperature of the pressure bulkhead of the SSM during pressurized on-orbit maintenance.

d. The system allows substantial changes in systems design and power requirements.

e. The SSM thermal control design utilizes either existing materials and hardware or those which will be developed before their requirement for the LST program. This represents a low-cost R&D effort.

f. The system allows for easy component maintenance and replacement.

4. Electrical System

a. The electrical power system is designed for an orbital average power of 1500 watts at the 5 year end-of-mission conditions.

b. The LST average power requirement is 1283 watts and the peak is 1785 watts. This gives design margins of 217 and 915 watts for the average and peak powers.

c. The energy storage requirement for the docked operations is 1024 watt-hours for the maximum occultation period and an average power of 1500 watts. This will be provided by six nickel cadmium 30 Ah batteries. Depth of discharge will be limited to 19 percent to provide a lifetime in excess of 2 years.

d. The use of phase change material within the solar array substrate can reduce the range of solar array temperatures from 135 to 43°C. This will increase the reliability of cell interconnections; however, power output will be increased by only about six percent. The mass penalty would be 91 kg.

e. The number of consecutive orbits that the spacecraft may be oriented in a nonoptimum solar panel illumination attitude for polarization measurements depends on the location of the target, the degree of freedom in roll, and the installed battery capacity. If a slit rotation of ±45 degrees is satisfactory, the reference electrical power subsystem (EPS) has the capability to sustain several orbits for all pointing directions. If a ±90 degree slit rotation is required, the reference EPS cannot sustain a full orbit for about 30 percent of the celestial sphere targets. An additional battery is required for full sphere coverage for one complete orbit if ±90 degree roll is necessary.

f. The low mass, high performance battery concept is based on proposed standardized cells and assemblies for future payloads.

g. The solar array reference design, based on conventional solar panels, can satisfy the LST requirements. However, it is a high mass approach and its storage, deployment, and retraction are complex; in addition, it is not a good candidate for in-space maintenance. The alternate flexible roll-out arrays have much more attractive mass, deployment, retraction, and maintenance characteristics. Further study is recommended to determine whether the alternates would be cost effective.

5. Communications and Data Handling

a. The communications and data handling (C&DH) system utilizes state-of-the-art hardware to provide a flexible data system.

b. Two dual data transponders, one for high-speed scientific data and one for slower-speed engineering data, utilized with two conical spiral antennas, provide a communications link with the Space Tracking and Data Acquisition Network (STADAN) stations.

c. The data system is capable of taking a single frame of data from a 50 mm by 50 mm target format with 60 cycle/mm resolution and transmitting it to ground at a rate of 1 m bit/sec within 10 min.

d. A mass memory storage alternative for storing scientific data is circumvented by utilizing secondary electron conduction (SEC) vidicon tubes with a storage capability of up to several hours.

e. The data relay satellite could permit real-time observations should it become available for LST use.

f. The command system can distribute both real-time and stored commands to eight addressable decoders, each with a command repertoire to 256 commands.

g. Both status and diagnostic data can be gathered from 28 data acquisition units placed throughout the LST.

h. Capability for a flexible scientific observational program has been provided by permitting arbitrary instrument sequencing through either uplink commands or onboard control.

i. The scientific instrument controller provides maximum flexibility in the event of a change in the instrument complement.

6. Attitude Control System

a. The design reference attitude control system (ACS) used in conjunction with the optical telescope assembly (OTA) fine guidance system (FGS) will satisfy the LST pointing requirements.

b. Tip and tilt positioning of the secondary mirror in response to FGS star tracker outputs is required to maintain the 0.005 arc sec pointing stability.

c. The reference gyro assembly (RGA) can provide the sensing functions to maintain the line of sight (LOS) excursions within the limits of the FGS coarse fields-of-view during guide star occultation periods.

d. Sensor noise (RGA and FGS) will be one of the primary factors limiting the body-pointing capability of the LST.

e. CMG gimbal component nonlinearities are a source of pointing instability but the effects can be minimized by mechanical design of the CMG and by electronic design of the gimbal and vehicle control loops.

f. CMG-generated disturbance torques, when propagated through the structure to critical optical components, create pointing errors. The effects can be reduced by shock mounts and rotor speed timing.

g. The four-skewed single-gimbal (SG) CMG configuration selected for the LST reference design permits continuous experiment data gathering without desaturation for 6.2 orbits (4.4 orbits with three CMG operations) under worst case environmental disturbances.

h. One CMG of the four-skewed configuration can fail and normal operations be continued without performance degradation.

i. The vehicle inertias can become much larger and more unfavorable without impacting the momentum exchange system.

j. The magnetic torquer system used for momentum management of the CMGs produces magnetic fields in the support systems module (SSM)/ scientific instrument package (SIP) area which are an order of magnitude less than the earth's magnetic field. Therefore, no additional shielding is required for magnetically sensitive instruments over that normally required to shield the earth's field.

k. Gyro hangup (ghu) detection and avoidance are not required for the design reference ACS CMGs using the magnetic torquer system for desaturation.

l. The reaction control system (RCS) raises the confidence level for mission success by providing a standby actuator system for abnormal situations such as Shuttle misdock and by providing an emergency backup system for short-time use during major ACS component failures.

7. Maintainability

a. The selected maintenance concept is unscheduled, on-orbit, manned maintenance using the Shuttle orbiter for support.

b. Equipment will be replaced only when required because of failure or degradation or for scientific update.

c. Unscheduled maintenance allows for reduction in design lifetime of equipment from a previous goal of 2.5 years to some shorter time.

d. The maintenance mission will share Shuttle flights with other payloads to reduce costs.

e. The LST may be returned to earth for major maintenance when dictated by complexity of repair or for major upgrading of optical or instrument systems.

8. Reliability

a. The SSM 1 year reliability goal was set at 0.95. The current one year point estimate is 0.98408; however, this does not include the reliability estimates for batteries or the solar array.

b. The 1-year reliability estimate for the OTA is 0.9631.

c. The probability estimate for no maintenance requirement for the SIP for 1 year is 0.79336.

9. Contamination Control

a. The contamination level in the LST during orbital maintenance is controlled to a 10 000-class particulate level in the SIP, to a 100 000-class particulate level in the SSM volume about the SIP, and to a 15 ppm maximum level of trace contaminants.

b. To achieve these contamination levels, ducting and high efficiency particulate air (HEPA) filters are located on the LST. A trace contamination control loop, environmental control equipment, and power sources are located in the orbiter support volume.

c. Existing equipment has been selected for the components of the contamination control system to minimize costs.

APPENDIX A. LST CONTAMINATION CONTROL

TABLE OF CONTENTS

TABLE OF CONTENTS (Concluded)

LIST OF ILLUSTRATIONS

LIST OF TABLES

APPENDIX A

LST CONTAMINATION CONTROL

The LST, in its present configuration, may be launched with either the Space Shuttle or the Titan launch vehicle. Space Shuttle launch is used as the design reference in this study. Current concepts provide for maintenance visits to the LST by the Space Shuttle either on an as-needed or periodic basis and for retrieval by the Space Shuttle for refurbishment if required. One of the on-orbit maintenance modes considered involves pressurizing the support systems module (SSM) of the LST which contains the instrumentation. The SSM would be pressurized to 1 atm to provide a shirtsleeve environment (with clean-suits) for the two-man maintenance crew which will enter the SSM and replace faulty components as required. This exposes the sensitive LST instruments to another potential source of contamination.

The LST mission concept outlined above presents numerous problems of contamination control. Both high-resolution imagery and faint-source detection are goals of the mission and the optical instruments on board, particularly those operating in the ultraviolet spectral region, are highly sensitive to degradation by contamination.

The purpose of this study, which is reported in detail in Reference A-1, is to investigate sources of contamination which represent a threat to the LST or its mission, to determine the effects of such contamination, and to identify and evaluate the effectiveness of potential countermeasures.

When an LST contamination control design concept was developed, an attempt was made to define the problem within the framework of available information. LST contamination control equipment design concepts were then developed based on work done for other systems. It became evident very quickly that the levels of tolerable contamination desired for the LST and the levels of contamination production predicted for manned, general scientific spacecraft missions were not amenable within reasonable flight equipment weight and power limits. Tradeoff studies were performed to evaluate equipment impacts as a function of contamination control levels. The contamination control equipment concepts derived represent achievable designs for reasonable contamination control provided that all equipment is thoroughly cleaned, baked out, and designed for minimum contamination production in orbit. The equipment cannot function effectively with careless design or lax operational procedures.

As the susceptibility of the LST to various contaminants and realistic contaminant production rates is more confidently defined, a relief in the rigidity of contamination control procedures and LST contamination control system design specifications may result. Uncertainty usually produces more severe specifications.

A. Requirements

Contamination control must be involved in all aspects of LST activity. It must be permitted to influence concept definition and development from a design and operational viewpoint since contamination has the potential of nullifying LST usefulness. Some of the elements of LST activity which must be strongly influenced by and which may be used in achieving effective contamination control aboard the orbiting LST are:

1. Design.
2. Selection of Materials.
3. Environmental Control.
4. Scheduling of Events.
5. Cleaning.
6. Special Manufacturing Processes.
7. Compensatory Measures.
8. Verification.
9. Configuration Management.
10. Personnel Indoctrination.

These elements are dependent and overlap; therefore, each influences the other. The possible impact of each element is illustrated by the methods, considerations, and approaches to achieve effective LST contamination control discussed in Reference A-1.

1. Design for Contamination Control. Control of LST contamination should begin with the basic design concept of the spacecraft. By regarding contamination as a design parameter at the outset, numerous problems of

contamination control may be circumvented. Figure A-1 illustrates some potential sources of contaminants during orbital operations which must be considered during the design phase. These potential sources are categorized as follows by type of device and expected mode of contamination:

1. Drive Motors (lubricants, field coil insulation).

    a. Aperture drive.

    b. Mirror drive.

    c. Sunshade deployment mechanism.

    d. Pressure bulkhead drive.

    e. Solar panel drive.

2. Thermal Coatings and Paints (outgas, flaking).

    a. Exterior of sunshade, white paint, S13G.

    b. Optical Telescope Assembly (OTA) exterior, white paint, S13G.

    c. SSM exterior, zinc orthotitanate.

    d. OTA interior and light baffles, Cat-a-Lac black.

    e. SSM interior, Cat-a-Lac white paint.

3. OTA graphite epoxy structure (outgassing, absorbs moisture).

4. Wiring Harnesses and Electromechanical Assemblies (Outgassing, Adsorption of Secondary Contamination).

5. Internal Insulation. (Represents a large surface area subject to adsorption of trace contaminants.)

6. Reaction Control System (RCS) Thrusters (should be clean, inert gas type).

7. Tape Recorders (typical of wear particle generators, must be sealed to contain contaminant).

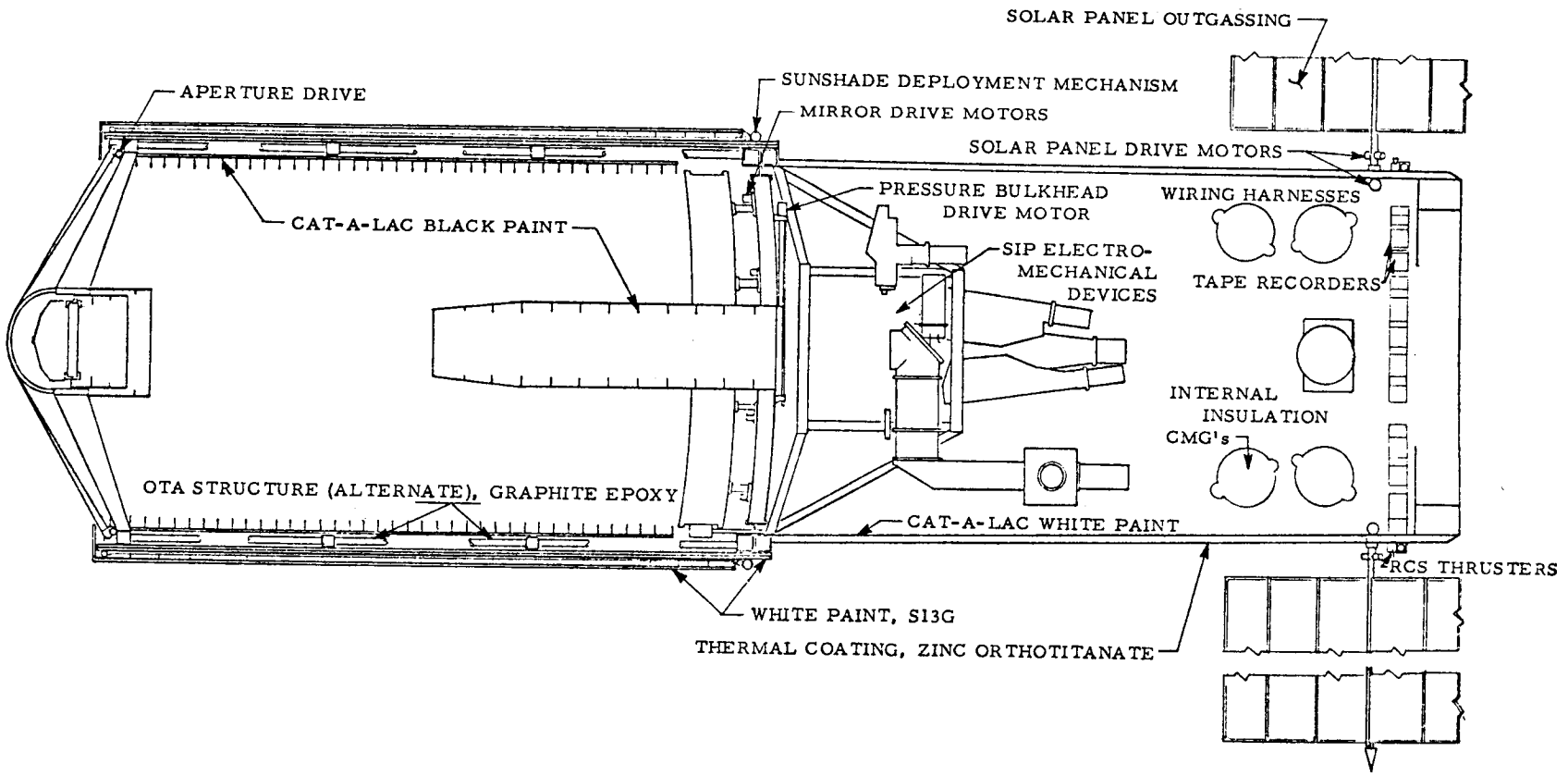

Figure A-1. Potential contaminant sources in orbital operation.

8. Scientific Instrument Package (SIP) Electromechanical Devices (lubricants, wear particles, insulation outgassing). (An asterisk indicates that one device is used for several instruments.)

a. Fine guidance assembly.

b. Echelle spectrographs (2).

(1) Slit width selector*.

(2) Collimating mirror position control*.

c. Czerny-Turner spectrograph (axial).

(1) Slit width control*.

(2) Collimating mirror position control*.

(3) Grating selector.

d. f/12 field camera — filter wheel.

e. f/96 cameras (3).

(1) Flip mirror position selector.

(2) Filter wheel.

f. Wadsworth spectrograph — slit width selector.

g. Czerny-Turner Spectrograph (radial) — slit width control.

h. Fourier Interferometer — field-of-view opening control.

Of course, some of these sources are also sensitive to contamination or degenerate in performance as they produce contamination. An example of the latter is the thermal coatings. An example of the former is the graphite epoxy which absorbs moisture so that it changes dimensions approximately 25 μm/m in going from 0 to 25 percent humidity (soak).

2. Nonparticulate Contaminants. Many of the potentially harmful contaminants are nonparticulates. These gases, vapors, and moisture-transported contaminants must be controlled to an acceptable level. The

definition of an acceptable level is difficult without a knowledge of the physical and chemical characteristics of the materials used throughout the LST and a detailed knowledge of the physical and chemical characteristics of contaminants produced by the LST and its environment. An attempt has been made to define acceptable concentrations during pressurized on-orbit maintenance from the point of view of "no deposit — no contamination." That is, there is a critical contaminant concentration during the maintenance period, at standard temperature and pressure of air, below which the evaporation rate exceeds the deposition rate for that potential contaminant. Theoretically, that contaminant would not deposit on any surface if held below the critical concentration. However, if the contaminant hits a cold surface it may well condense on that surface, particularly if it is water soluble and is suspended in the humid air provided for crew comfort.

Since chemisorbed materials will deposit to a monolayer for virtually any concentration other than zero, the only practical means for controlling such contaminants is not to allow them within the LST support volume. For some materials this can be feasible. For biological products such control is, of course, impossible. The contamination control subsystem must be designed to keep low vapor pressure compounds to concentrations which do not provide molecular incidence rates greater than approximately 5×10^{14} molecules cm^{-2} sec^{-1}. For vapor pressures greater than 10^{-2} mm Hg, molecular incidence rates of 10^{18} molecules cm^{-2} sec^{-1} can be allowed. For very high vapor pressure compounds, permanent deposition is not a problem. However, if these compounds are not controlled, cloud obscurement of the LST becomes a problem. For this reason, it is considered advisable to control these high vapor pressure contaminants actively rather than to vent the contaminants in the vicinity of optical experiment packages.

Without detailed descriptions of the materials used in the servicing vehicle LST support volume as well as the surface areas of those materials (and recent environmental history to evaluate contaminant adsorption), it is difficult to determine the types and quantities of nonparticulate contaminants to be expected. Trace contaminants from biological sources will be present. If only materials from the Apollo Telescope Mount (ATM) approved list or a more stringent LST approved materials specification are used on the LST and within the "clean" LST support volume aboard the on-orbit maintenance support vehicle, contaminants from nonbiological sources should be materially reduced. Effective control within those limits indicated as necessary by preliminary analysis will require sharp curtailment or elimination of nonbiological contaminant production. The only available experience factor for nonbiological contaminant production was that assumed for the Space Station prototype (SSP) study [A-2] based on spacecraft simulation studies for missions

similar to the LST on-orbit pressurized maintenance concept. Calculations indicate that excessive contamination control equipment would be necessary to control these to LST specifications.

In summary, the production of biological contaminants to be controlled totals about 5.5 g/day plus about 2.5 g/day of nonbiological ammonia. Of this total, about 4.5 g/day of ammonia will be produced along with approximately 3.5 g/day of contaminants requiring the catalytic oxidizer for removal (including 1.2 g/day of methane in a total of about 2.2 g/day of hydrocarbons). The production of sorbable contaminants was estimated at 75 g/day.

The reference design contamination control subsystem was designed to control ammonia concentrations to 2.8 parts per million (ppm) or less, sorbable intermediate vapor pressure and low vapor pressure contaminants to 10 ppm (10^{18} molecules cm^{-2} sec^{-1}), and hard-to-oxidize high vapor pressure contaminants, including methane, to 15 ppm or less.

3. Particulate Contaminants. Contamination of sensitive surfaces by particulate matter is a type of problem that is common to all spacecraft and one particularly difficult to prevent, especially for large spacecraft. Particulate contamination may occur at any stage in the life of the spacecraft and consists of the deposition on spacecraft surfaces of small particles of dust, soil, lint, skin, and the like. Primary and secondary forms of particulate contamination may be distinguished. Primary contamination occurs when the sensitive surfaces of the spacecraft such as thermal control and optical surfaces become contaminated directly by particulate matter from sources external to the spacecraft. In secondary contamination, an insensitive spacecraft surface collects particles initially and these are later dislodged by vibration of air currents and are deposited on sensitive surfaces as contaminants.

In the design of a particulate control concept, the class 350 (10 000) specification was used for sensitive areas with class 3500 (100 000) acceptable for the support volume and less sensitive areas. The design endeavors to put the clean air just out of the filters into the sensitive areas, forcing particulates from these areas to less sensitive areas. A tradeoff of hardware penalties versus particulate cleanliness level led to a compromise system which could be used for small particle control by installing a filtration system to eliminate the smaller particles.

Particulate contamination may be reduced to an acceptable level by filtering all air introduced into critical areas and maintaining a controlled

flow of air so that entrained particles will be continuously moved from the more critical to the less critical system. With this method, all the air going into a critical area is cleaned by high efficiency particulate air (HEPA) filters. The air is pumped from a more contaminated area, filtered, and allowed to flow back after ventilation of the critical area with "clean" air. An open loop system which pumps air from outside the contamination control or "clean" area may be used.

B. Contamination Control System (CCS) Reference Design

The removal of nonparticulate contaminants in the vapor and gaseous state must be accomplished by thorough (near 100 percent) removal of all such undesirable contaminants from a portion of the airflow to reduce the concentration of these contaminants to an acceptable level. Processing the entire flow required for particulate control would be prohibitive in terms of pressure drop (fan power) and size of the sorbent beds and/or oxidizers required. To an extent, this implies open loops with smaller flow rates; however, the nonparticulate contaminant production rates characteristic of manned spacecraft do not allow control of these contaminants to an LST acceptable level for the entire servicing vehicle without excessive equipment weight and power penalties. It is therefore necessary to provide a separate, controlled volume with principal contamination activities (food, waste management, equipment outgassing) isolated from the LST nonparticulate contamination control loop. This implies a sealed volume whose environmental control and life support system (EC/LSS) can be isolated from that of the main cabin area of the support vehicle. In this sense, a closed loop system to limit contaminant production to manageable proportions is required.

The criticality of contamination effects on LST performance indicates a need for class 350 (10 000 English System) overall cleanliness for the LST, at least class 3500 (100 000) for the vehicle servicing the LST, and positive pressure forcing flow out of the LST. The objectives of the following analysis were first to determine the costs of the class 350 (10 000) requirement in terms of power, occupied volume and mass, and then to arrive at a recommended particulate control system.

1. The Particulate Control System. Table A-1 indicates that the cost of class 350 (10 000) particulate cleanliness is relatively great and yet class 3500 (100 000) conditions may not be sufficient for the sensitive instruments of the SIP. It was reasoned that a significant amount of cleandown capability could be achieved, above the class 3500 (100 000) level, by enclosing the SIP

and diverting flow through it to establish a positive pressure purge. A savings in mass and power would also be realized over the class 350 (10 000) system, while class 350 (10 000) conditions could hopefully be approximated within the SIP cowling. Thus, such a particulate control system design was evolved and is presented herein as the recommended system for inclusion in the overall contamination control system (CCS) design.

TABLE A-1. MASS AND POWER SUMMARY FOR LST CONTAMINATION CONTROL SYSTEM CLEANLINESS CLASS TRADE STUDY

Cleanliness Class	Mass [kg (lb)]			Power (W)		
	Support Vehicle	LST	Total	Support Vehicle	LST	Total
350 (10 000)	250 (549)	113 (248)	362 (797)	2674	0	2674
3500 (100 000)	219 (481)	13.2 (29)	232 (510)	824	0	824

Figures A-2 and A-3 are schematic diagrams of the system, designated class 350/3500 (10 000/100 000), showing the filtering equipment and ductwork installed in the SSM. This "hybrid" system was sized to supply the distribution manifold a sufficient volumetric flow rate to maintain class 3500 (100 000) cleanliness within the cabin and provide, in addition, a stream of filtered air to the cowled SIP, by means of a pressure-actuated flow diverter. When an instrument is removed for servicing and the integrity of the cowling is interrupted, the SIP flow would increase to provide at least a 0.5 m/sec (100 fpm) outflow.

A mass and power breakdown for the recommended system is given in Tables A-2 and A-3. Mass and power savings of 40 and 65 percent, respectively, have been gained over the class 350 (10 000) system design (not including the clean-work station and separate support volume filtering equipment penalties).

Nonparticulate contamination control requires the removal of atmospheric contaminants to maintain concentrations at an acceptable low level.

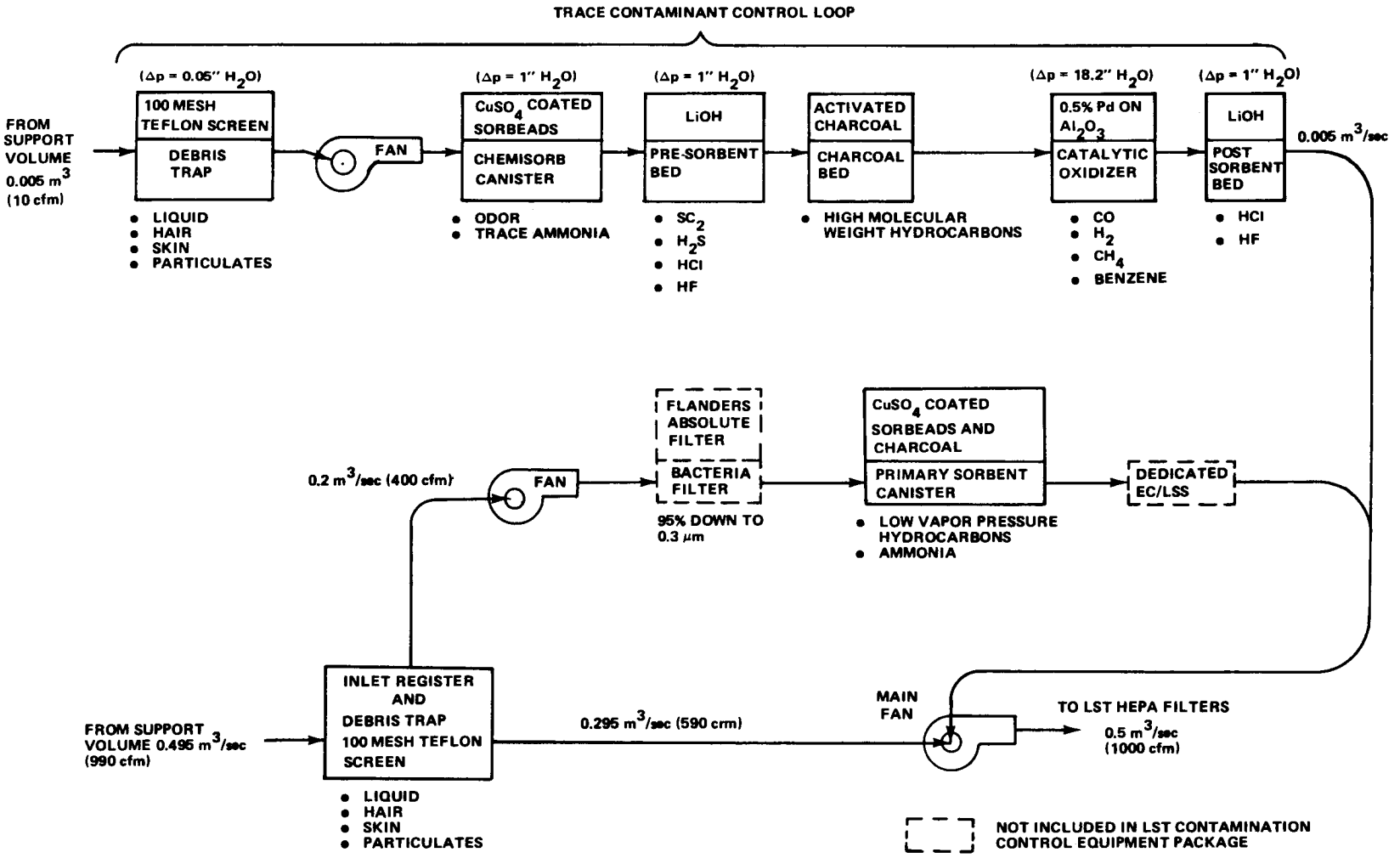

Figure A-2. Contamination control system for class 350/3500 (10 000/100 000) LST.

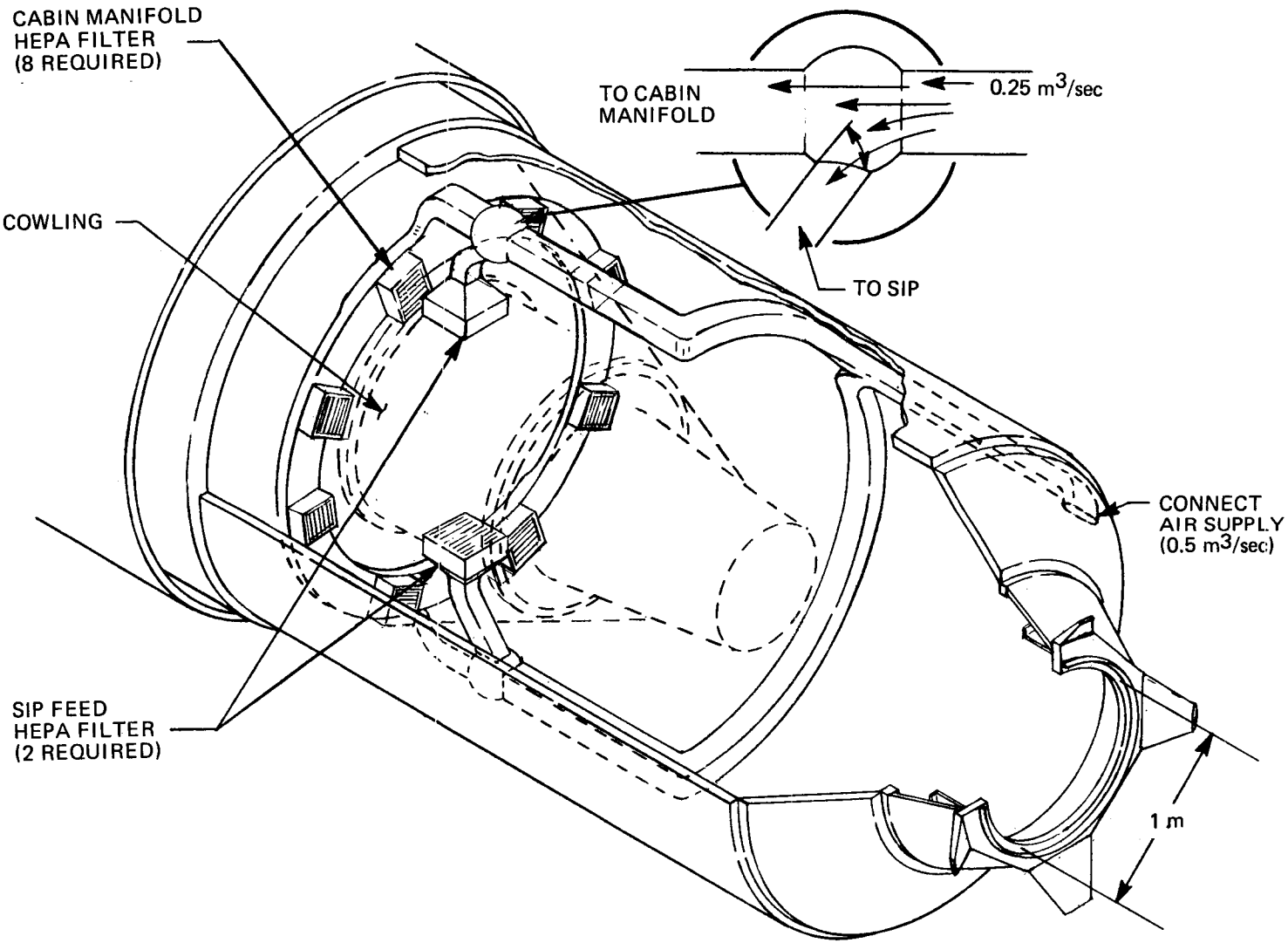

Figure A-3. Class 350/3500 (10 000/100 000) LST contamination control system layout (hybrid version).

TABLE A-2. LST CONTAMINATION CONTROL SYSTEM MASS AND POWER BREAKDOWN: ONBOARD REQUIREMENTS FOR CLASS 350/3500 (10 000/100 000) LST

Item	No. of Units	Unit Mass (kg)	Total Average Power (W)	Total Mass [kg (lb)]	Total Average Power (W)	Size (mm)	Remarks
Ducting	1	12.8	—	12.8 (28)	—	150 × 150 × 0.005	15 m length; unit weight of 0.85 kg/m
Miscellaneous Fittings	—	—	—	1.8 (4)	—	—	Ductwork Support Straps, etc.
Quick-Disconnect Joint	1	0.9	—	0.9 (2)	—	150 Inside Diameter	Plug-In for Air Supply
HEPA Filters (Cabin Manifold)	8	1.4	—	11.2 (25)	—	300 × 300 × 150	Cabin Manifold 0.0675 m^3/sec (135 cfm) Capacity
HEPA Filters (SIP Feed)	2	1.8	—	3.6 (8)	—	350 × 350 × 150	SIP Inlet; 0.1 m^3/sec (200 cfm) Capacity
Total				30.3 (67)	0		

TABLE A-3. LST CONTAMINATION CONTROL SYSTEM MASS AND POWER BREAKDOWN: SUPPORT REQUIREMENTS FOR CLASS 350/3500 (10 000/100 000) LST

Item	No. of Units	Unit Mass (kg)	Unit Average Power (W)	Total Mass [kg (lb)]	Total Average Power (W)	Size (mm)	Remarks
Miscellaneous Ducting and Fittings	—	--	—	11.4 (25)	—	—	Includes approx. 150 × 150 × 0.005 mm of ducting
Quick-Disconnect Joint	1	2.3	—	2.3 (5.1)	—	150 ID	
Contamination Control Equipment Package	—	--	—	150 (330.4)	874	650 × 670 × 1170	(See Table A-4 for package details.)
Total				≈164 (362)	874		

2. The Nonparticulate Control System. Assuming that nonbiological contaminant production will be held to negligible proportions by materials selection, bakeout, and cleaning techniques, the major concern of the contamination control system equipment is with the biologicals. Those trace contaminants specified for control in the Shuttle are listed in Table A-4 with the production of the two-man LST maintenance crew (rather than the entire four-man Shuttle crew), principal method of control, flow rate of the principal control method, and minimum concentration $C_{(\infty)}$ achievable at that flow rate.

a. Removal Methods. The chemical removal of trace contaminants may be broken down into several groups which indicate possible control methods:

1. Ammonia. A small molecule cannot be readily sorbed by charcoal. It can be oxidized but the oxidation products are not easily removable. Ammonia can be easily sorbed by an acidic sorbent or dissolved in water.

2. Hydrogen, Carbon Monoxide, and Methane. Small molecules which cannot be readily sorbed but can be oxidized.

3. Hydrazine Derivatives such as Mono-Methyl Hydrazine and Dimethyl Hydrazine. Can be removed by acid compounds and are soluble in water. (Molecules easily dissolved in water such as hydrogen sulphide, sulphur dioxide, hydrogen chloride, and hydrogen fluoride, can also be removed by molecular sieve, silica gel, and LiOH, Li_2CO_3.

4. Acids. In general, these can be readily sorbed by highly basic compounds such as LiOH or Li_2CO_3 and generally can be dissolved in water.

5. Organic Compounds. May all be potentially oxidized but those products of combustion other than CO_2 and H_2O should be sorbed before leaving the contaminant control section. Some are soluble in water.

A detailed analysis of the contaminant list (Table A-4) defined the process rates required for each of the contaminants. The contaminants are listed with the design flow rate, primary removal mechanism, and the resulting limiting concentration, $C_{(\infty)}$ in parts per million.

TABLE A-4. PERFORMANCE OF CONTAMINATION CONTROL EQUIPMENT ON BIOLOGICALLY PRODUCED CONTAMINANTS (SHUTTLE SPECIFICATIONS)

Contaminant	Biological Production Rate[a] (gm/day)	Possible Methods of Control[b]	Flow Rate (m^3/sec)	Limiting Concentration $C_{(\infty)}$ (PPM)
Acetone	0.001	Charcoal W.S.	0.2	4.7×10^{-5}
Acetaldehyde	0.0004	Charcoal W.S.	0.2	1.9×10^{-5}
Ammonia	2	W.S. Sorbeads	0.2	0.1
n-Butyl Alcohol	0.006	Charcoal, C/O	5×10^{-3}	0.01
Carbon Monoxide	0.0324	C/O	5×10^{-3}	0.06
Ethyl Alcohol	0.02	Charcoal, W.S.	0.2	9.4×10^{-4}
Hydrogen	0.10	C/O	5×10^{-3}	0.19
Hydrogen Sulfide	0.000116	Charcoal, W.S.	0.2	5.4×10^{-6}
Indole	0.2	Charcoal, W.S. (hot), C/O	5×10^{-3}	0.37
Methyl Alcohol	0.02	Charcoal, W.S.	0.2	9.4×10^{-4}
Methane	1.2	C/O	5×10^{-3}	2.24
Methyl Mercaptan	0.0556	W.S., C/O	5×10^{-3}	0.104
Phenol	0.7565	Charcoal, C/O, W.S.	0.2	0.035
Propyl Mercaptan (-n)	0.0556	Charcoal, C/O	5×10^{-3}	0.104
Pyruvic Acid	0.7565	LiOH, C/O, W.S.	0.2	0.035
Skatol	0.0556	Charcoal, C/O	5×10^{-3}	0.104
Caprylic Acid	0.0556	C/O, LiOH	0.2	2.6×10^{-3}
Ethyl Mercaptan	0.0556	C/O, Charcoal	0.2	2.6×10^{-3}
Propyl Mercaptan (-iso)	0.0556	Charcoal, C/O	5×10^{-3}	0.104
Valeric Acid	0.0556	LiOH, C/O	5×10^{-3}	0.104

a. Based on two-man LST maintenance crew only, not including entire (four-man) Shuttle crew.

b. Principal method of control is underlined, W.S. means water soluble and C/O, catalytic oxidizer.

b. Flow Requirements and Cleandown Capability. Given an initial concentration C_0 a production rate P, an efficiency per pass of η and a flow rate F, we may calculate the concentration in terms of characteristic emptying time $T = V/\eta F$ and $C_{(\infty)} = P/\eta F$.

$$C_{(t)} = (C_0 - C_{(\infty)}) \exp\left(-\frac{t}{T}\right) + C_{(\infty)} \qquad \text{(A-1)}$$

or normalizing to t/T and $C/C_{(\infty)}$,

$$\frac{C_{(t)}}{C_{(\infty)}} = \left(\frac{C_0}{C_{(\infty)}} - 1\right) \exp(-t/T) + 1 \quad . \qquad \text{(A-2)}$$

This normalization allows the plotting of the ratio of the concentration as a function of time $C_{(t)}$ to the limiting concentration $C_{(\infty)} = P/\eta F$, versus time in units of the characteristic emptying time T or t/T. A series of curves for different ratios of the $C_0/C_{(\infty)}$ is shown in Figure A-4. With this parametric presentation it is possible to select any volume, flow rate, contaminant production rate, and initial concentration and determine the time to "clean down" to a predetermined concentration $C_{(t)}$. If we assume the Shuttle air is in the control volume at the start, an initial concentration equal to the maximum allowable concentration (MAC) for manned occupancy is possible in the worst case. To facilitate cleandown, the control volume will be kept vacant, so $P = 0$ is assumed. The MAC of those hydrocarbon contaminants primarily controlled by the catalytic oxidizer is 1355.5 ppm (of which 1060.8 ppm is methane). Since $P = 0$, $C_{(\infty)} = P/\eta F = 0$, and $C_0 = 1355.5$ ppm, then $C_{(3T)} = 0.05\ (1355.5) = 67.7$ ppm in 5 hours if $V = 28.23\ m^3$ ($1000\ ft^3$) and $C_{(6T)} = 0.05\ (67.7) = 3.4$ ppm in 10 hours.

Figure A-5 is a plot of normalized cleandown time t/T as a function of initial concentration C_0 to various final concentrations $C_{(t)}$ with various values $C_{(\infty)} = P/\eta F$ which correspond to given production rates.

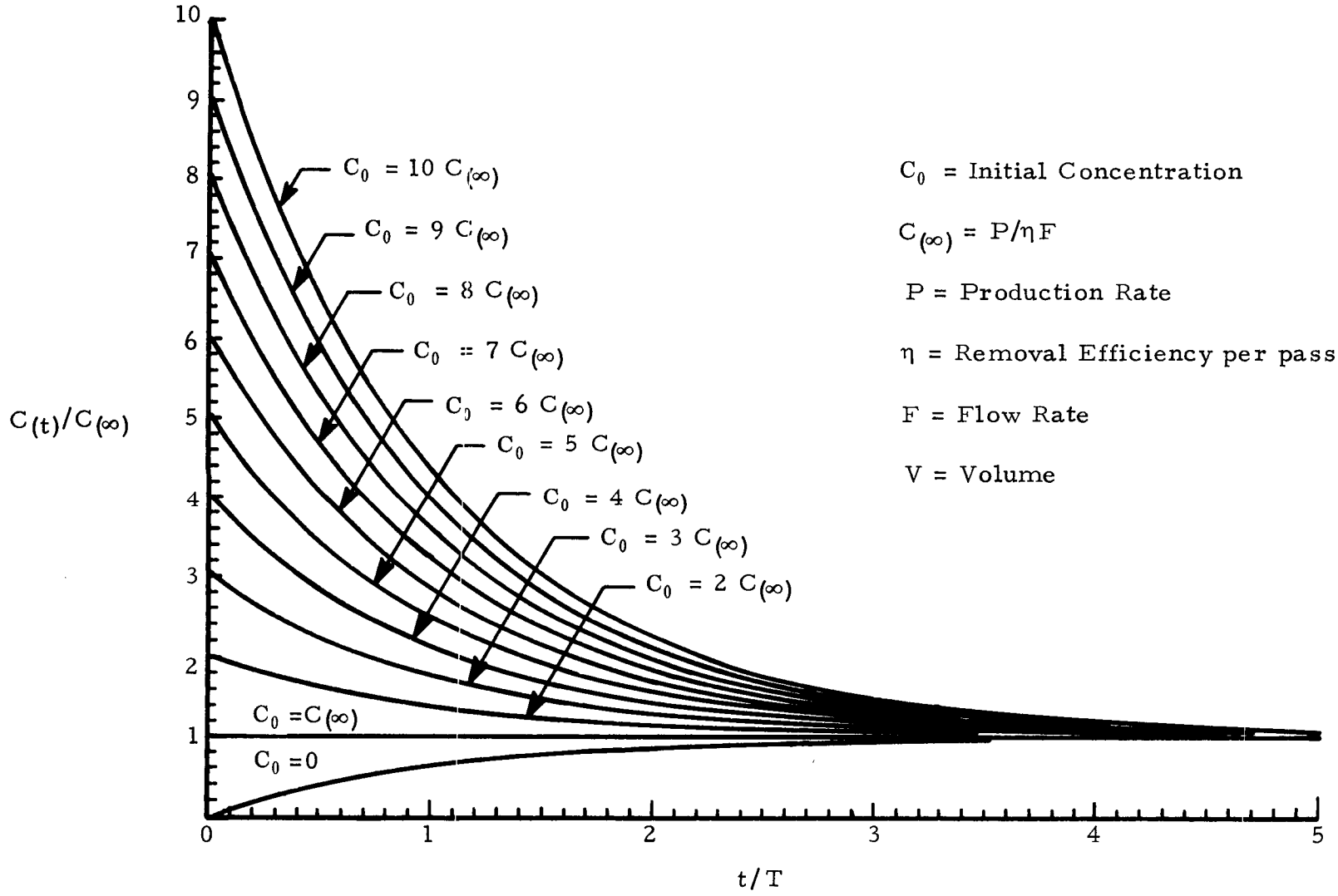

Figure A-4. Normalized concentration $C_{(t)}/C_{(\infty)}$ variation with time t in multiples of characteristic emptying time, $T = V/\eta F$.

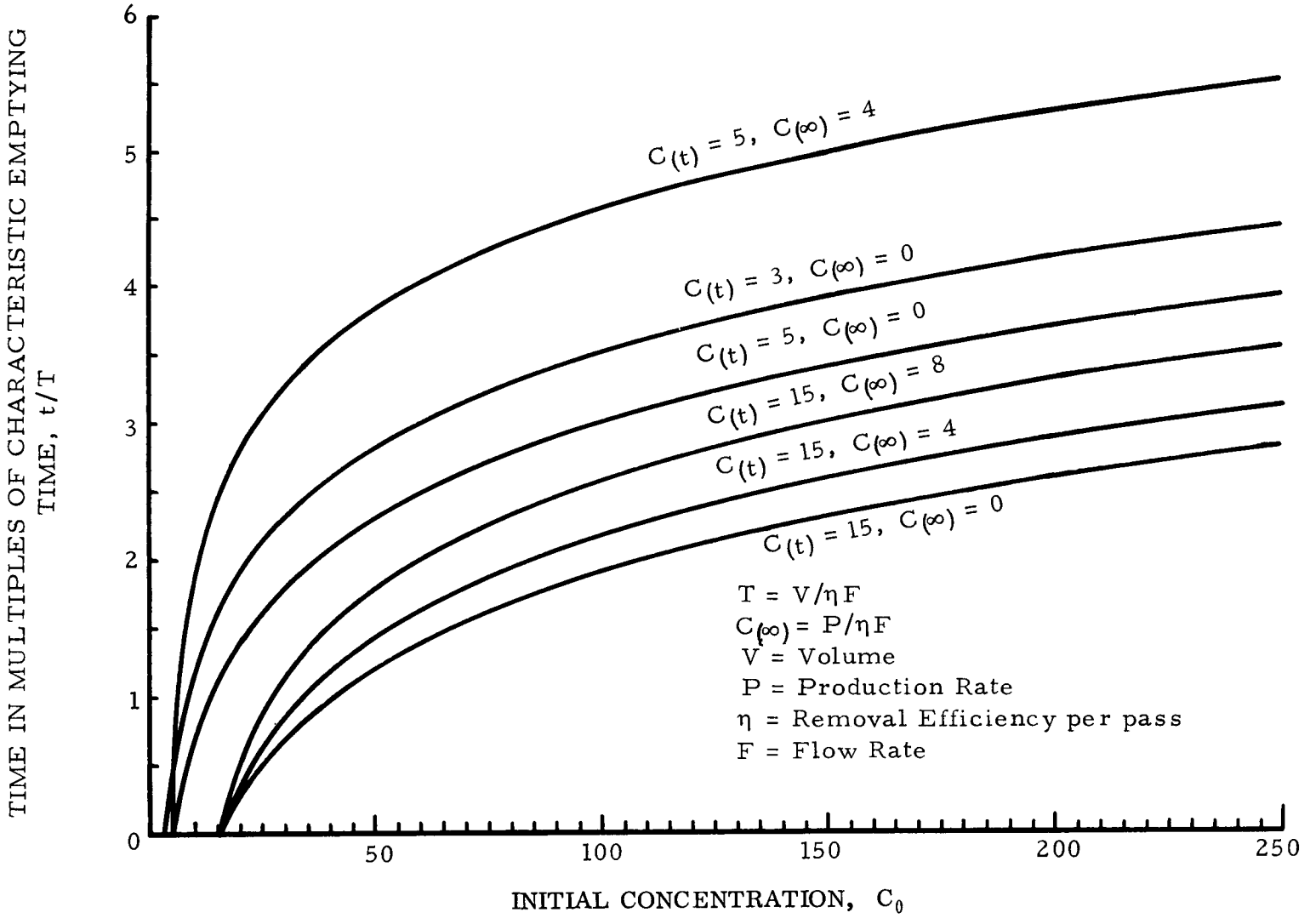

Figure A-5. Cleandown time to various concentrations $C_{(t)}$ for given ratios of production rate to effective flow rate $P/\eta F$ as a function of initial concentration C_0.

If $C_{(\infty)}$ is in parts per million (ppm), P is g/day and F is 5×10^{-3} m^3/sec (10 cfm) with $\eta = 0.99$, $C_{(\infty)}$ (ppm) ≈ 2 P (g/day).

c. Equipment Functional Description. Primary ammonia control is accomplished by the use of $CuSO_4$ coated sorbeads in the primary sorbent bed (Fig. A-6). This material provides the best weight efficiency of the candidate materials surveyed (sorbeads, regenerated charcoal, acid-impregnated charcoal).

The primary control of intermediate and low vapor pressure hydrocarbons is to be accomplished by the use of activated charcoal, which is to be placed in the main sorbent bed along with the $CuSO_4$ coated sorbeads for space efficiency. Since the hydrocarbons require a considerably higher flow rate, the ammonia control will be more than adequate. The flow rate for this loop was set at 0.2 m^3/sec (400 cfm), which allows a safety factor of four. This loop has been designed into an integrated LST contamination control package concept (Fig. A-6); however, it should interface directly with an EC/LSS loop dedicated to the LST and its support volume. The dedicated EC/LSS loop is necessary to limit contaminant production to controllable levels. Such interfacing will also allow for the control of water-soluble contaminants in the temperature and humidity control subsystem without the need of a separate contamination control subsystem. Acid vapor and CO_2 control will be accomplished by the EC/LSS subsystem LiOH canisters.

The high vapor pressure contaminants will be controlled by the utilization of a 5×10^{-3} m^3/sec (10 cfm) catalytic oxidizer (Fig. A-6), which is required for control of hydrogen, carbon monoxide, and methane. The catalytic oxidizer cleans up the high vapor pressure compounds by oxidizing those compounds. Consequently, an LiOH post-sorbent bed is included downstream from the catalytic oxidizer to remove the oxidizer residue. To minimize the load on the catalytic oxidizer, a secondary sorbent canister containing $CuSO_4$ sorbeads and charcoal and an LiOH presorbent canister identical with the postsorbent LiOH canister is included upstream from the catalytic oxidizer.

A Flanders absolute filter for dust and bacteria is normally a part of EC/LSS systems. Because it is assumed that the 0.2 m^3/sec (400 cfm) loop will interface with the LSS, a better location for the filter might be ahead of the primary sorbent canister; however, this filter is not included in the integrated package.

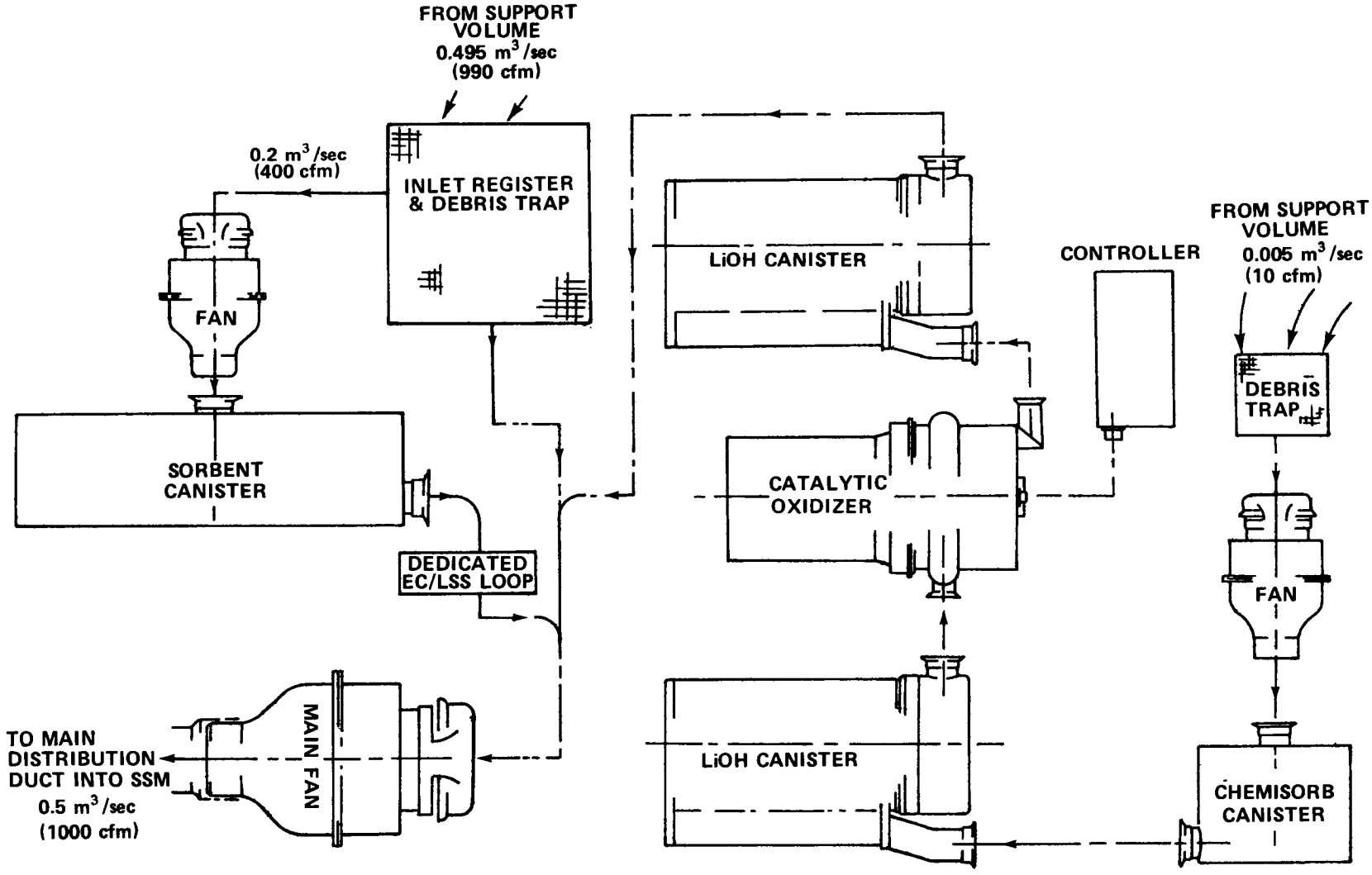

Figure A-6. Contamination control equipment package for class 350/3500 (10 000/100 000) LST.

3. Contamination Control Support Equipment Packaging. An integrated package of those elements of the LST contamination control equipment to be placed aboard the support vehicle was assembled to determine the overall dimensions and volume required (Fig. A-7). An attempt was made to use a quasi-portable CCS scheme by taking the equipment package into the LST SSM. Although the equipment will clear the 1 m hatch, the procedure is not recommended because it ignores the dependency of the CCS on a dedicated (isolated) loop of the EC/LSS of the support vehicle and may also cramp the available volume in the SSM. It also is not considered good practice to locate the operating equipment of the system within the volume of air upon which it is operating.

The dimensions, weight, and power required for the LST contamination control equipment package are summarized in Table A-5.

C. Summary of Equipment Functions and Procedures

1. On-Board Equipment. The equipment recommended for installation aboard the LST to provide a class 350/3500 (10 000/100 000) particulate cleanliness and control of hydrocarbons to less than 15 ppm within the SIP/SSM is listed in Table A-2 and illustrated in Figure A-3. The design philosophy of this concept is to supply clean air from the support vehicle with nonparticulate contaminants removed. This air is routed through an umbilical connected by the crew through the open hatch to the ductwork installed in the SSM of the LST and thence through HEPA filters to the SIP and the forward end of the SSM. The idea is to provide the cleanest air to the most sensitive parts and have it flow outward to less sensitive regions. Airflow through the SIP is governed by valves which control the pressure so that approximately 0.5 m/sec (100 ft/min) flow through any opening in the SIP cowling.

2. Support Equipment. The equipment required aboard the support vehicle to service the recommended contamination control concept is listed in Tables A-3 and A-5 and illustrated in Figures A-2, A-6 and A-7. In addition to the equipment listed, a volume with an individually controlled clean environment sealed off from the contamination of the support vehicle is required for spares and work space for two scientist-astronauts. This space should be directly accessible to the docked and pressurized LST during maintenance operations and provided a plenum for the backflow of HEPA filtered air from the SIP and SSM. To this volume will be connected the inlets of the contamination control equipment package which will, in turn, be interconnected with a separate dedicated EC/LSS loop operating independently from the support vehicle (Shuttle) EC/LSS during LST maintenance. The

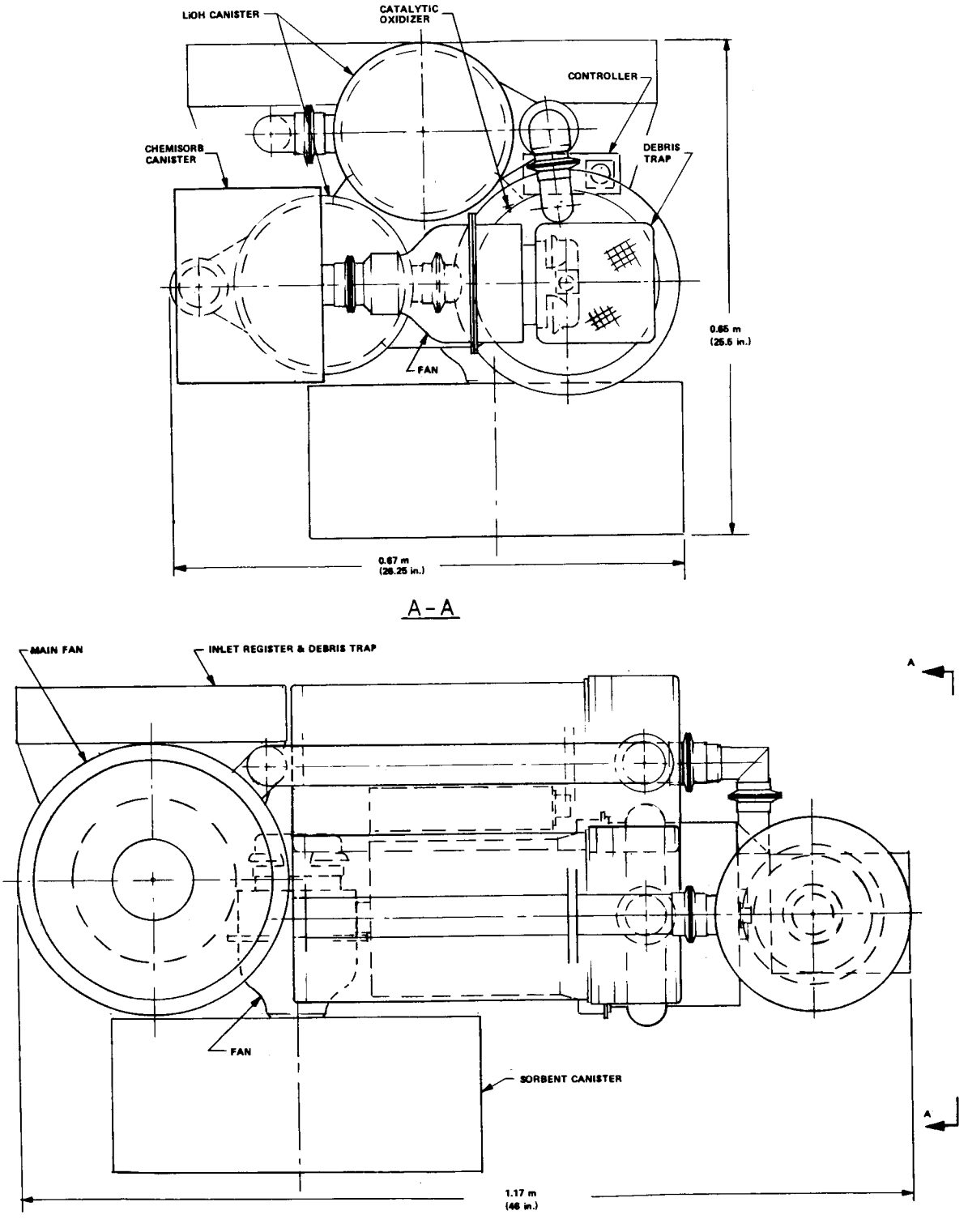

Figure A-7. LST contamination control equipment package.

TABLE A-5. LST SUPPORT VEHICLE CONTAMINATION CONTROL EQUIPMENT PACKAGE MASS AND POWER BREAKDOWN

Item	No. of Units	Unit Mass (kg)	Unit Average Power (W)	Total Mass [kg (lbm)]	Total Average Power (W)	Size (mm)	Remarks
Main Fan	1	18.1	400	18.1 (40.0)	400	356 diam. × 305 long	0.6 m^3/sec (1300 cfm) $\Delta P = 1.7$ N/cm^2 (2.5 in. H_2O)
Debris Filter	1	3.6	0	3.6 (8.0)	0	430 × 430	
Fan	1	5.9	87	5.9 (13.0)	87		0.005 m^3/sec (10 cfm)
Debris Filter	1	0.5	0	0.5 (1.0)	0	150 × 150	0.005 m^3/sec loop
Chemisorb Canister	1	2.3	0	2.3 (5.0)	0	250 diam. × 280 long	0.005 m^3/sec loop
Presorbent Canister	1	10.5	0	10.5 (23)	0	356 diam. × 500 long	0.005 m^3/sec loop
Charcoal Bed	1	36.5	0	36.5 (80.0)	0	610 diam. × 125 long	0.005 m^3/sec loop
Catalytic Oxidizer	1	24.5	300	24.5 (54.0)	300	178 diam. × 250 long	0.005 m^3/sec loop
Postsorbent Canister	1	10.5	0	10.5 (23)	0	356 diam. × 500 long	0.005 m^3/sec loop
Fan	1	5.9	87	5.9 (13.0)	87		0.20 m^3/sec (400 cfm)
Primary Sorbent Canister	1	18.1	0	18.1 (40.0)	0	610 diam. × 787 long	0.20 m^3/sec loop
Packaging	1	13.6	0	13.6 (30.0)	0	650 × 670 × 1170	
Total				150 (330 lbm)	874	650 × 670 × 1170	

sealing off of the control volume may be accomplished by an air-supported fabric which maintains a proper cleanliness/airflow barrier without imposing safety problems such as emergency egress, etc., which might accrue with hard structure.

3. Procedures. Contamination control with minimum equipment requires that the LST maintenance operation start clean, keep cleaning, and stay clean during the operation and after termination. It is expected that the LST will be remotely commanded to close the OTA aperture doors and the pressure bulkhead door between the main mirror and the SIP prior to docking with the Shuttle. After docking, the SSM/SIP will be pressurized with clean air from tanks aboard the Shuttle.

Some of this same clean air might also be used to expand the folded fabric "control volume" surrounding and sealing in the LST spares. This volume would then occupy a larger portion of the Shuttle crew compartment. A slight overpressure would allow the two scientist-astronauts to enter, in "clean suits," through a zippered access door to airlock. Note that this clean volume is not a shirt-sleeve environment. It requires clean suits such as those used in ground-based clean rooms.

The maintenance crew would proceed through the Shuttle airlock, open the outer Shuttle hatch, then the LST hatch. The CCS umbilical would be pulled through the hatch and connected to the LST ductwork before flow through the umbilical was allowed. The flow of clean air, once established, would come from the SIP and the forward end of the SSM out through the hatch and airlock into the control volume in the Shuttle. From there it would be recycled through the dedicated EC/LSS loop and the contamination control equipment.

This concept provides free access between the Shuttle-provided LST Clean Control Volume and the LST-pressurized SSM/SIP for the maintenance crew. After performing a checkout, replacement, and recheck of the LST equipment as needed, the maintenance crew would withdraw as "cleanly" as possible. One aspect of contamination control during this part of the operation concerns debris trapped by the HEPA filters located in the SSM. To remove the filters would contaminate the SSM; to leave them open into the ducts during evacuation might also permit the debris to migrate through the filters or out of the ducts. Some provision will have to be made to seal them off from both sides before evacuation of the SSM.

With the completion of required activities aboard the LST, the maintenance crew would withdraw, close the LST hatch, the Shuttle airlock

hatch, depressurize the LST, and disengage from the LST. After the Shuttle is sufficiently far away, the LST pressure bulkhead and aperture doors may be remotely commanded to open.

Aboard the Shuttle, the control volume may be evacuated and collapsed around the spares cabinets to occupy a minimum of space and the LST dedicated EC/LSS loop may be switched back to the main Shuttle EC/LSS function.

The degree to which many of the special contamination control procedures and equipment will be needed is a function of what degree of basic contamination control is provided aboard the servicing vehicle (the Shuttle).

D. Contamination Control for Prelaunch, Launch, and Retrieval

These problems were addressed primarily as a purge/vent system definition and description, subject to the general requirements given as follows:

1. The primary purpose of the purge system is to prevent penetration of the LST or its internal sensitive areas by gaseous or gas-borne contaminants. The pressure differential and resulting weight flow rate required to satisfy this purpose were established in the following environments: ground, shuttle cargo bay, and orbit. Purge flow should not be required during ascent ventdown.

2. Purge flow will be needed during both ground operations and descent and retrieval operations. These requirements necessitate the presence of purge flow distribution and overboard vent management hardware onboard the flight vehicle. To minimize the complexity of both systems and operations, ground purge operations should utilize the flight hardware wherever possible, provided that LST flight weight and reliability are not compromised. In addition, some purge flow will be required before Shuttle arrival and after Shuttle departure to prevent penetration by Shuttle propellant effluents; thus, completely autonomous operation upon remote command appears necessary. An examination of relative operating times reveals that autonomous operation involves relatively little gas; this in turn suggests that the great majority of purge gas can be stored externally to the LST and delivered through supply lines, umbilicals, or quick-disconnects. Only the small purge gas capacity required during autonomous operation would need to be carried onboard the LST.

3. A single, preferably passive purge gas is desired in order to be compatible both with systems simplicity and safety philosophy during ascent and descent. However, a purge with clean air is necessary during ground operations to allow manned access for component installation, checkout, or removal. This latter requirement coupled with the desire to use flight purge hardware during ground operations suggests that dry nitrogen be chosen as a purge gas. The fluid flow properties of dry air and dry nitrogen are sufficiently similar to allow a system designed for nitrogen to perform adequately well when operated with air. In addition, the fact that the design reference RCS approach is cold nitrogen gas offers the possibility of sharing components or even tankage space, provided that the autonomous purge requirement is small enough and that no major reliability penalty occurs.

4. The primary purposes of the vent system are to manage the overboard disposal of the purge gas during purge flow and of the internal atmosphere during ascent to orbit in such a way that the design pressure differential is not exceeded. Neither the forward aperture doors nor the aft SSM closure are pressure doors; both are limited to the maximum Δp they may tolerate. The reference design Δp is 0.07 N/cm^2 (0.1 psig) while the maximum for this study will be 0.7 N/cm^2 (1.0 psig). Furthermore, both closures are assumed to have a gas leakage area of 0.025 cm^2 per linear cm (0.01 $in.^2/in.$) of perimeter. (This is also the maximum leakage area for this study.)

5. From a contamination control standpoint, the portion of the OTA containing the primary mirror and the portion of the SSM containing the SIP are the most sensitive of the LST. Further, the presence of potential contamination sources in the subsystems area of the SSM (wiring harness, equipment, etc.) suggests the desirability of designing the vent system to direct purge flow away from the sensitive area. Thus, two vent locations appear to be desirable: toward the rear of the SSM and toward the front of the OTA. The design reference purge/vent approach will be two separate systems, one for the SSM and one for the OTA. During operation the pressure door in the forward SSM bulkhead will be closed.

The ambient pressure trace for shuttle-launched LST ascent is presented in Figure A-8. A descent pressure trace (Fig. A-9) was constructed from Reference A-3 and a Manned Spacecraft Center Internal Note.[1] These were assumed to be the existing conditions within the cargo bay for this investigation.

---

1. A Representative Reentry and Landing Trajectory for the Space Shuttle Orbiter. MSC Internal Note 72-FM-197, Manned Spacecraft Center, NASA, Houston, Tex., Aug. 17, 1971, p. 16.

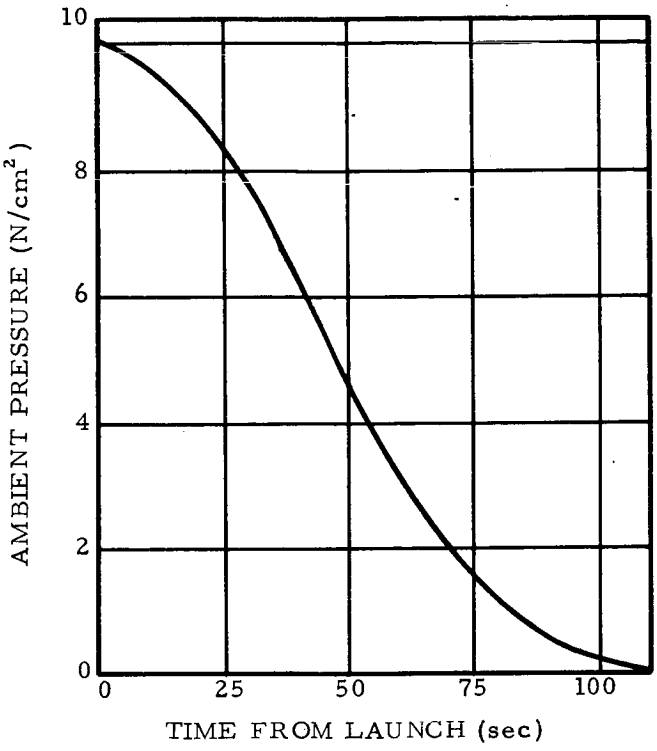

Figure A-8. Cargo bay ambient pressure history for LST ascent venting analysis.

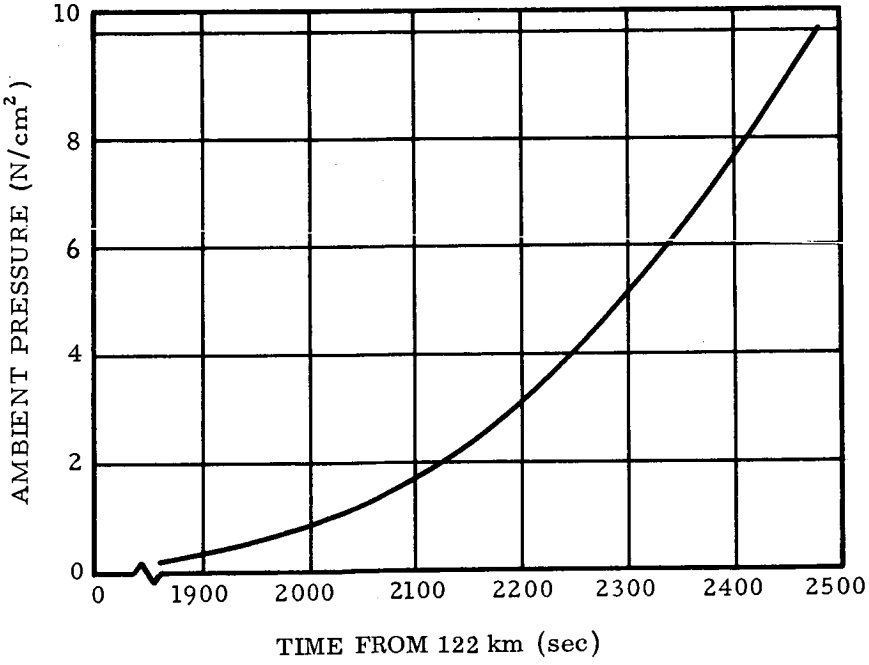

Figure A-9. Cargo bay ambient pressure history for LST descent purge analysis.

1. Steady-State Requirements. For ground and on-orbit operations a slight, positive pressure differential is needed to prevent penetration by gaseous or gas-borne contaminants. In an effort to keep the calculations at a manageable level of accuracy for this brief analysis and not try the capabilities of state-of-the-art pressure sensors in the preliminary design stage, a minimum allowable pressure differential was arbitrarily set at 0.007 N/cm^2 (0.01 psig). The important steady-state relationships for both ground and on-orbit operations were evaluated at this minimum allowable pressure differential, and are given in Table A-6.

TABLE A-6. OTA, SSM STEADY-STATE RELATIONSHIPS DURING GROUND SUPPORT AND ON-ORBIT OPERATIONS

	Operation Mode					
	Ground Support			On-Orbit		
Component	OTA	SSM	Total	OTA	SSM	Total
Component Volume [m^3 (ft^3)]	47.35 (1672)	42.62 (1505)	89.97 (3177)	47.35 (1672)	42.62 (1505)	89.97 (3177)
Baseline Leakage Area [cm^2 (in.^{2})]	88.07 (18.65)	8.13 (1.26)	96.20 (14.91)	88.07 (18.65)	8.13 (1.26)	96.20 (14.91)
GN_2 to Pressurize (at Δp = 0.007 N/cm^2) [kg (lb)]	58.97 (130)	53.07 (117)	112.04 (247)	0.0402 (0.0887)	0.0362 (0.0799)	0.0764 (0.1686)
Steady-State Leakage Rate [kg/hr (lb/hr)]	254 (560)	23.59 (52)	277.59 (612)	3.09 (6.81)	0.29 (0.64)	3.38 (7.45)

2. Ascent Ventdown Analysis. A computerized procedure was developed to determine the LST interior-to-ambient pressure differential during ascent and descent, given the ambient pressure traces and assuming an isentropic expansion process within the LST interior. A series of runs was then conducted to determine the additional vent area required to limit the maximum Δp during ascent to the 0.07 N/cm^2 (0.1 psig) design value while holding minimum Δp above the arbitrary 0.007 N/cm^2 (0.01 psig) design value. In this analysis the total flow area (leakage plus vent) was assumed

to be open at launch, thus requiring "makeup" purge flow during the first portion of ascent to maintain the minimum Δp. The results of this parametric analysis are shown in Figure A-10.

3. Purge Requirements Analysis. A timeline for a typical Shuttle-launched-and-retrieved LST mission was constructed from Reference A-4 and two internal communications[2] and the purge gas requirements were estimated by source for each mission phase. The mission model is presented in Table A-7, with the purge gas sources identified as follows:

1. GSE — supplied by Ground Support Equipment.

2. ORB — supplied by the Shuttle orbiter.

3. LST — stored onboard the LST.

The prelaunch and postlanding estimates are based on the steady-state requirement calculations. All prelaunch purge was assumed to be provided by GSE through an umbilical connection penetrating the orbiter cargo bay. At liftoff the GSE umbilical would fall away and any necessary "makeup" purge during ascent would be supplied by ORB. During postlanding operations ORB must supply purge until the GSE umbilical can be reconnected, which should be accomplished as soon as possible to minimize the orbiter weight penalty.

An LST autonomous purge is needed only when the spacecraft is in the vicinity of the orbiter and the ORB unbilical has been disconnected. This occurs when the LST is released to pursue its mission and when it is retrieved for servicing. No purge is required during LST orbital operations.

Using the previously described computer program and the descent pressure trace of Figure A-9, the required purge flow from initiation of the Shuttle reentry at 122 km (400 000 ft) to landing was calculated. All vents were assumed closed with only the baseline leakage area allowing purge escape. The pressurization flow was sized to afford the baseline minimum Δp for this study, 0.007 N/cm^2 (0.01 psig). The results show that during

2. D. Stewart, Large Space Telescope Ground Operations Timelines, and Powered Flight and On-Orbit Operations for Shuttle/LST Mission with Recoverable Second Stage Engines, internal correspondence to J. Heyer, Program Development Directorate, Marshall Space Flight Center, NASA, Huntsville, Ala., Aug. 4, 1972.

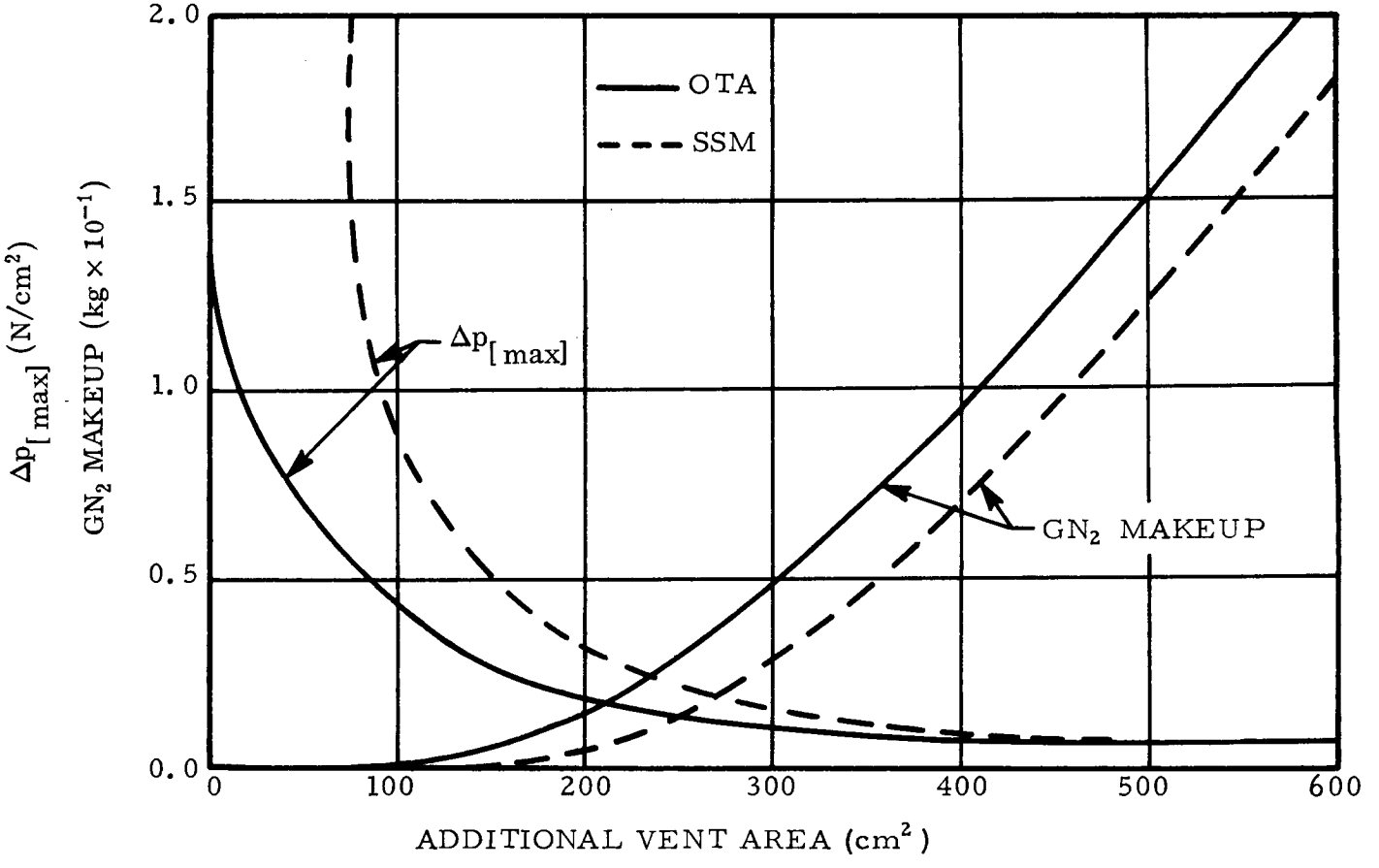

Figure A-10. Ascent venting history: maximum Δp during ascent and GN_2 makeup to hold minimum Δp vs baseline leakage area plus additional vent area open at launch.

TABLE A-7. PURGE REQUIREMENTS BY SOURCE PER TIMELINE ENTRY FOR CONCEPTUAL SHUTTLE-LAUNCHED-AND-RETRIEVED LST MISSION

Phase	Event Description	Start (hr:min)	Stop (hr:min)	Event Time (hr)	Flow Rate [kg/hr (lb/hr)]	Purge Requirements Total mass [kg (lb)]		
						GSE	ORB	LST
Prelaunch	Transfer LST from clean to Mating/Checkout Facility	0:00	2:00	2.0	277.6 (612)	555 (1 224)	0	0
	Load into orbiter cargo bay	2:00	8:00	6.0	277.6 (612)	1 666 (3 672)	0	0
	Checkout & prepare for transfer	8:00	29:00	21.0	277.6 (612)	5 830 (12 852)	0	0
	Transfer from MCF to Vertical Assembly Building	29:00	31:00	2.0	277.6 (612)	555 (1 224)	0	0
	Orbiter prepare & mate	31:00	83:00	52.0	277.6 (612)	14 435 (31 824)	0	0
	Transfer Shuttle to pad	83:00	89:00	6.0	277.6 (612)	1 666 (3 672)	0	0
	Prelaunch preparation	89:00	112:00	23.0	277.6 (612)	6 385 (14 076)	0	0
	Cabin closeout & cargo service	112:00	120:00	8.0	277.6 (612)	2 221 (4 896)	0	0
	Countdown preparation & countdown	120:00	136:00	16.0	277.6 (612)	4 442 (9 792)	0	0
	Prelaunch Totals	0:00	136:00	136.0	—	37 755 (83 232)	0	0
Ascent/ Checkout	Liftoff & ascent to 611 km orbit	136:00	142:08	6.1	277.6 ~ 3.37 (612 ~ 7.43)	0	23 (51)	0
	LST systems checkout	142:08	143:45	1.6	3.37 (7.43)	0	5 (12)	0
	Start LST autonomous purge; deploy LST & service; separate orbiter & depart for remote checkout operations	143:45	144:45	1.0	3.37 (7.43)	0	0	4 (8)
	LST remote checkout	144:45	302:00	157.3	0	0	0	0
	Ascent/checkout totals	136:00	302:00	166.0	—	0	28 (63)	4 (8)
Mission	LST mission	—	—	—	—	0	0	0
Checkout/ Descent	Orbiter approach & dock	0:00	2:00	2.0	3.37 (7.43)	0	0	7 (15)
	Checkout & descent preparation	2:00	4:00	2.0	3.37 (7.43)	0	7 (15)	0
	Descent & landing	4:00	4:42	0.70	3.37 ~ 277.6 (7.43 ~ 612)	0	140 (309)	0
	Checkout/descent totals	0:00	4:42	4.7	—	0	147 (324)	7 (15)
Postlanding	Postlanding operations	4:42	5:02	0.3	277.6 (612)	0	83 (184)	0
	GSE hookup	5:02	5:04	0.03	277.6 (612)	0	17 (37)	0
	Orbiter safing & transport to MCF	5:04	15:32	10.5	277.6 (612)	2 905 (6 405)	0	0
	Transfer LST from cargo bay to transport trailer	15:32	23:37	8.1	277.6 (612)	2 248 (4 957)	0	0
	Transport LST to clean room	23:37	25:37	2.0	277.6 (612)	555 (1 224)	0	0
	Postlanding totals	4:42	25:37	20.9	—	5 708 (12 586)	100 (221)	0
Total	Mission Totals	—	—	—	—	43 463 (94 818)	275 (608)	11 (23)

descent approximately 88.5 kg (195 lb) and 51.7 kg (114 lb) of GN_2 are required for the OTA and SSM, respectively, and 140.2 kg (309 lb) of GN_2 total. This purge would be supplied by ORB through an umbilical connection at a controlled flow rate.

4. "Clean Bag" Concept. Table A-7 shows that, because of the large leakage area, a prohibitive amount of purge is required during periods that the LST is out of a clean room on the ground. As a solution to this and other problems, a contamination control bag (clean bag) has been proposed which, because of its much smaller leakage area, would greatly reduce purge leakage.

Before leaving the clean room after final integration, the LST would be enclosed in a clean bag and pressurized with purge gas for prelaunch preparations. During ascent the bag would allow ventdown through Δp-actuated vent holes. When the LST is retrieved a new clean bag could be installed and deployed prior to reentry and the spacecraft would remain in the clean bag during postlanding operations and transport back to the clean facility. Thus, the clean bag and its deployment/retraction mechanism would be completely portable and provide sealed access to support points for transfer operations. Prior to installation of the LST in the Shuttle cargo bay, the clean bag deployment/retraction canister could be supported by an LST transport/handling fixture or by attachment to the LST itself so that it could be detached after installation in the Shuttle.

Figure A-11 shows a conceptual design for the clean bag system placed in the cargo bay. The design employs Velcro tape to hold the bag in position and draw the bag toward the bag canister for retraction; the bag is stowed in a lap-folded position (see detail). Deployment could be accomplished by moving the drive motors forward of the stowed bag or by use of the orbiter's manipulators, if available. The bag end is attached to a rigid ring containing a seal; the ring travels on three guide cables during deployment/retraction and helps hold the bag in position to keep it from abrading the LST exterior. There is a seal around the LST support points (see detail in Fig. A-11). A flexible boot containing a coil spring is attached to the LST surrounding the support point and a soft pressure seal is maintained around the bag penetration. When the LST is held by the support points the spring would be compressed, and the simple shear force caused by tension on the bag would overcome the soft seal when the bag was retracted.

The perimeter along the bag's seals is calculated at 742 cm (292 in.). Applying the same leakage area factor 0.025 cm^2/cm (0.01 $in.^2/in.$), the total leakage area would be 18.55 cm^2 (2.92 $in.^2$), as compared with

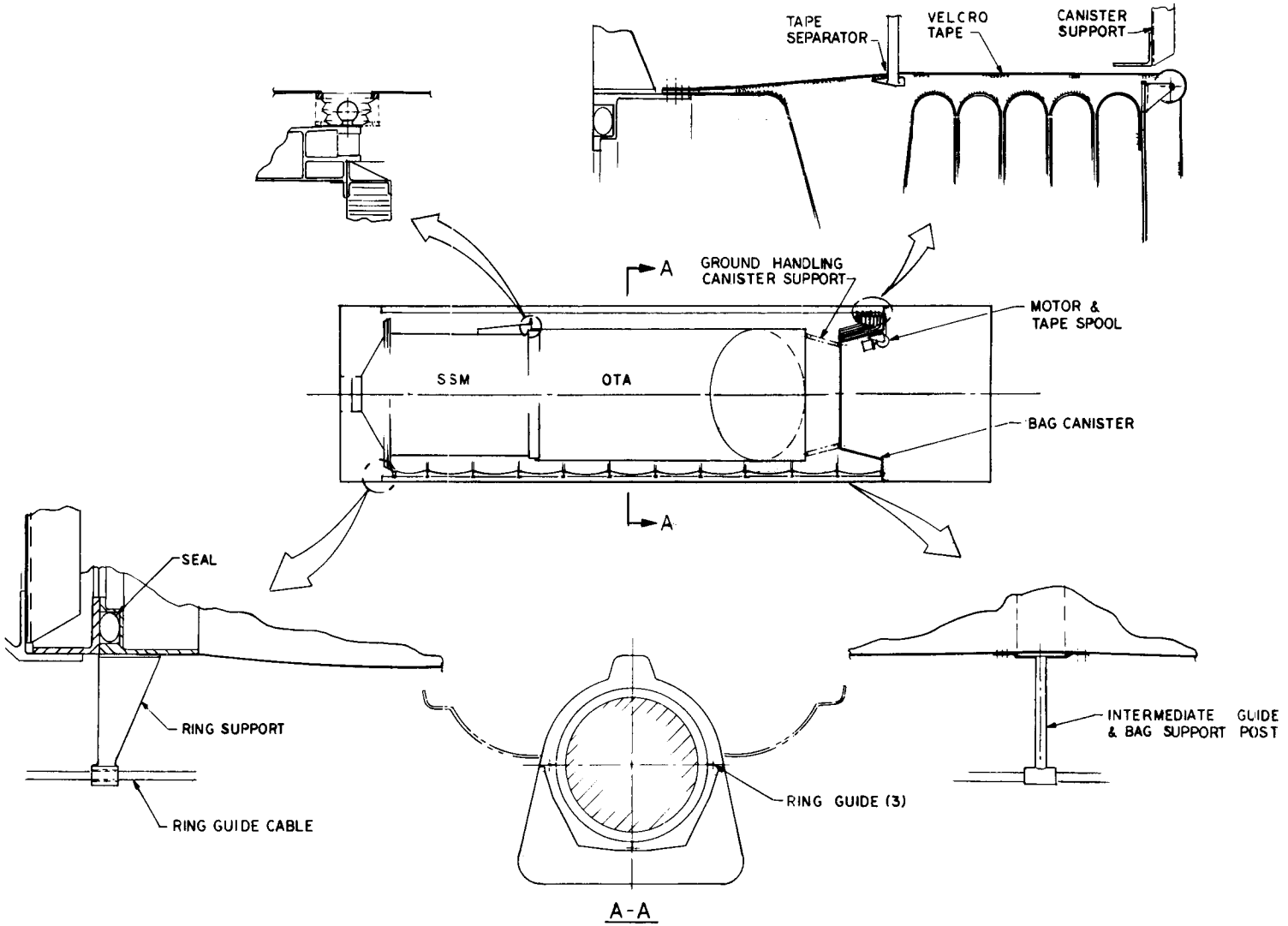

Figure A-11. Contamination control "clean bag" system concept: lap-folded stowage.

96.20 cm^2 (14.91 $in.^2$) for the unprotected vehicle. The steady state leakage rates are directly proportional to the leakage area, so the amount of purge required from the GSE (Table A-7) would be reduced by a factor of five. Additionally, the orbiter requirements during steady-state operations (ground and on-orbit) would be cut by the same factor and further savings would be realized during descent. Of course, a better seal might be available which could reduce the leakage area even more.

Two other possible advantages occur through utilization of the clean bag: Δp-actuated vent holes may be used during ascent ventdown so that no makeup purge is required of the orbiter and because of the relative size of the LST, the clean bag should be adequate for the handling of most other anticipated Shuttle payloads.

5. Vent System Recommendations. Sufficient vent area may be available to the OTA through utilization of the aperture doors in a spring-loaded mode but the large vent area required for the SSM threatens to compromise the simplicity of the vent system and the performance of other SSM systems. It may be possible, however, to alleviate the problem by redesigning the aft SSM closure to withstand the large Δp incurred with no vent area (the pressure door between the OTA and SSM is currently capable of withstanding SSM pressurization for manned maintenance) or to provide additional vent area as needed in the hatch. SSM relief via the pressure door behind the primary mirror is not desirable because it involves flow through the contamination-sensitive SIP.

6. Purge System Recommendations. A NASA Technical Memorandum now in preparation[3] describes the baseline RCS for the LST as a pressure-regulated system utilizing nitrogen gas. Currently the RCS nitrogen tank is sized for a 19.5 kg (43 lb) capacity, including a 50 percent contingency factor and allowance for residual pressurant. Since Table A-7 indicates that only 10.4 kg (23 lb) of nitrogen need be carried onboard the LST, it appears technically feasible to share tankage with the RCS. The onboard system must be capable of autonomous purge upon remote command for maintenance operations. Quick-disconnecting umbilical connections must be provided for purge supply from the Shuttle orbiter and ground support sources when available and a regulating system will be required to control the LST internal pressure with respect to the ambient.

3. William B. Price, Phase A LST Reaction Control System Design for the Large Space Telescope (LST), NASA Technical Memorandum, Marshall Space Flight Center, Huntsville, Ala., to be published.

It is recommended that mission scheduling be structured to allow the LST to remain in a clean room as late as possible in the prelaunch timeline and compel it to be returned to a clean environment immediately after orbiter landing. The design of the orbiter's onboard purge supply system and the necessary GSE will depend largely on the amount of purge required of each source. The clean bag concept should minimize purge requirements during ground operations and may possibly aid in ascent ventdown by eliminating the need for makeup.

E. Contamination Control During Ground Operations

The LST is basically composed of three assemblies. These are the OTA, the SIP, and the SSM. The manufacture, handling, transport, etc., of the major components of each of the assemblies are considered from a contamination standpoint during their integration to form the assembly. The handling, transport, etc., of each assembly are similarly considered during their integration to form the LST. Finally, the disposition of the LST in regard to contamination control is traced to the launch operation.

Before being brought into a clean room, parts and subsystems are precleaned by wiping, flushing, and scrubbing to remove dirt, fouling, etc., acquired in the fabrication and manufacturing processes.

The prevention of damage to the part or subsystem is the governing principle determing the temperature-time bakeout profile for a given part or subsystem.

The systems possessing complex geometry are, in general, vacuumed in addition to flushing in the final cleaning process.

1. LST Integration. In a class 350 (10 000) clean room, the OTA and SIP structures are mated and aligned. The SIP contamination control ducts are assembled to the SIP structure and the HEPA filters installed. The ducting is connected to a fan which takes air from the clean room in which the LST is being assembled and pumps it through the ducting system to create positive purge flow through the SIP.

a. SIP Assembly. Once clean purge flow is established, the optical instruments and SSM interface hardware are assembled to the SIP structure. The SSM interface hardware to be installed in the SIP consists of such equipment as remote data acquisition units, remote command decoders,

power distributors, and data bus terminals. The optical instruments are aligned. Similarly, the star trackers are installed and aligned on the SIP structure.

b. SSM Assembly. Independently, the SSM structure, GN_2 thruster system, gyros, attitude control system (ACS) equipment, sun sensors, SSM contamination control ducts, batteries, tape recorders, electronics, electrical, communications, and data management equipment are assembled together in a class 350 (10 000) clean environment.

c. OTA, SIP, and SSM Mating. The SIP duct fan is disconnected and the SSM assembly is integrated with the OTA/SIP assembly and the OTA sunshade. The sunshade is cleaned by methods similar to the cleaning of other large similarly manufactured structures. Another option is to assemble it to the OTA during OTA assembly. The fan is reconnected to the SSM duct which feeds the SIP system and clean flow within the SSM is established. Then alignment and integral tests are performed.

The partially assembled spacecraft is placed in a clean bag (see section D-4 of this Appendix) so that it can be transported out of the clean room. While the partially assembled LST is being transferred between testing stations, it is necessary to purge the SSM by forcing GN_2 or clean air through the ducting and HEPA filters in the SSM. It should be noted that whenever and wherever this purge system is operated, there must be a source of purge gas, umbilical connections to the clean bag, blowers, and a power source to operate the purge system, as indicated in section D).

d. Solar Vacuum Tests. The LST is taken into a solar-environmental test chamber, which is at least class 350 (10 000) clean. This facility must admit a cylindrical shape approximately 19 m (60 ft) long and 6 m (17 ft) in diameter. The clean enclosure is removed and the thermal-vacuum tests are performed.

Upon completion of these tests, the LST is enclosed in the portable clean room or clean container and transported back to the class 350 (10 000) clean room. The clean enclosure is removed and laminar flow is reestablished through the SIP/SSM.

e. Final Assembly and Launch Preparation. The solar panels and solar panel deployment mechanism are integrated and then assembled to the LST. A final integral test is performed on all systems. Next, the SIP/SSM purge flow blower fan is disconnected, the HEPA filters are replaced, and the LST is placed in the clean bag transport assembly.

A controlled temperature GN_2 or clean air purge and pressurization system is installed so as to maintain a purge of the LST/clean bag system. This system should provide a positive gage pressure of GN_2 inside the clean bag from this point until the LST autonomous purge system is activated for Shuttle release.

The LST is transported to and mated with the Shuttle orbiter. The electrical, GN_2, or clean air purge and temperature control umbilical connection is made to the payload for use during launch operations.

2. Ground Support Contamination Control Systems and Facilities. The following is a summary of the ground support systems and facilities needed for LST contamination control:

1. Facilities.

a. Class 350 (10 000) clean room capable of containing either the integrated LST or the SSM and OTA at the same time, along with ancillary equipment, to be used for LST integration. Vertical laminar flow design, estimated size 20 m long by 10 m wide by 10 m high (66 ft by 33 ft by 33 ft), estimated volumetric flow rate 100 m^3/sec (210 000 cfm), and estimated fan power 60 kW (80 hp). Must include nonparticulate CCS.

b. Class 350 (10 000) clean room capable of containing either the OTA or the SSM, along with ancillary equipment, for final component integration. Vertical laminar flow design, estimated size 10 m long by 10 m wide by 10 m high (33 ft by 33 ft by 33ft), estimated volumetric flow rate 50 m^3/sec (110 000 cfm), and estimated fan power 30 kW (40 hp). It must include nonparticulate contaminant control.

2. GSE.

a. Cradles and/or supports capable of supporting the OTA, SSM, and LST during assembly.

b. Dynamic dehumidifiers.

c. Dry GN_2 purge system with umbilical connections to clean bag transport assembly.

d. Gas leak rate test equipment.

e. Handling equipment capable of lifting LST/clean bag transport assembly: estimated capacity 11 000 kg (25 000 lb).

f. Portable class 350 (10 000) clean room capable of containing the LST. Estimated size 16 m long by 5 m wide by 6 m high (50 ft by 16 ft by 20 ft), estimated volumetric flow rate 40 m^3/sec (85 000 cfm), and estimated fan power 25 kW (34 hp). It must also include nonparticulate contaminant control.

g. Portable class 350 (10 000) clean room with nonparticulate contaminant control capable of containing the OTA. Estimated size 7 m long by 5 m wide by 6 m high (23 ft by 16 ft by 20 ft), estimated volumetric flow rate 20 m^3/sec (42 500 cfm), and estimated fan power 12 kW (16 hp).

F. Conclusions and Recommendations

Available analytical and empirical evidence indicates that contamination can have a marked effect on LST performance. Experience gained on other programs is continually reemphasizing both the need for and the difficulty of improved contamination control.

To obtain effective contamination control without undue program impact, it is recommended that:

1. Tolerable limits to likely contaminants be established for all LST equipment.

2. An overall LST contamination control specification be established.

3. An LST acceptable materials list and stricter qualification criteria be a part of the design specification.

4. A "traceable environment" specification be imposed as a verification technique to assure contamination control.

5. The list of known spacecraft contaminants (Table I, Reference A-1) be reviewed and revised to more accurately reflect Shuttle/LST production rates, LST tolerance levels, and possible control mechanisms.

6. The LST contamination control system for on-orbit maintenance be designed to work with the Shuttle EC/LSS system either as an impact on that system or as a supplemental kit to augment it for LST on-orbit maintenance.

7. A purge and vent system using an in-flight clean bag for the LST be incorporated in the design.

8. Manufacturing, assembly, prelaunch and refurbishment operations strictly adhere to contamination control requirements.

9. In-flight operations be designed to minimize the LST contamination potential.

The contamination control procedures and equipment described in this report would assure adequate control; however, a better definition of contaminant production and susceptibility could reduce the required measures.

REFERENCES

A-1. Chafin, J. M.: Large Space Telescope Contamination Control. Report ASD-PD-1668, Brown Engineering Co., Huntsville, Ala., November 1972.

A-2. Space Station Prototype, Contaminant Removal Subsystem. Delta Preliminary Design Package, SSP Document nos. A40, A41, A42, Hamilton-Standard Div. of United Aircraft Corp., Windsor Locks, Conn., 1971.

A-3. Dubin, Maurice; Sissenwine, Norman; and Wexler, Harry; eds: U.S. Standard Atmosphere, 1962. National Aeronautics and Space Administration, Washington, D.C., December 1962.

A-4. Space Shuttle Launch Operations Center Study. TR-1078-1, Kennedy Space Center, NASA, Cape Kennedy, Fla., Dec. 1, 1971, p. B-7/8.

APPENDIX B
SCIENTIFIC DATA GATHERING EFFICIENCY ANALYSIS

APPENDIX B

SCIENTIFIC DATA GATHERING EFFICIENCY ANALYSIS

An important consideration in the overall use of the LST is the amount of scientific data that can be gathered by the system. With data storage capability limited to the target of the SEC vidicons, a possible reduction in data gathering efficiency can arise when the SEC targets become saturated, no ground contact is available for data transmission, and a celestial source is available for viewing.

To examine this situation, a computer simulation was devised for the operations of the f/96 camera system to estimate the scientific data gathering efficiency as a function of target integration time with system storage as a variable parameter. Four cases were examined: a single camera, two cameras, three cameras, and three cameras plus a tape recorder.

In the simulation, the equations of motion of a vehicle in earth orbit were examined at 1 sec intervals. At each second the computer was checked for visibility of a given celestial target and RF contact with a ground station (the six tracking stations discussed as design reference for the project were used in the simulation). If a given star was available for viewing, a counter was incremented representing the gathering of light by a camera. When a camera counter became full, representing tube target saturation, another camera counter was incremented if available. When no cameras were available for intergration, a counter representing wasted time was incremented. Integration times for several stars were varied by changing the limits of the camera counters. When a star became occulted, the dead time counter was activated until the star could be reacquired. If ground contact was established and a camera counter was full, this single camera counter was reset to zero.

The efficiency for each of the four cases in question was computed as a function of integration time needed to obtain tube target saturation. The following equation was used to compute system efficiency:

$$\frac{(\text{Total Time}) - (\text{Dead Time})}{(\text{Total Time})} \times 100\% = \text{Efficiency} .$$

Figure B-1 presents the results of this simulation. The jagged nature of the curves is a result of two constraints placed upon the simulation: (1) No counter could be reset to zero until it had reached saturation and (2) a counter could only be reset to zero when enough ground contact time existed for total frame transmission, i.e., if camera saturation was attained during the later portion of a ground contact period the camera must wait until the next ground station was acquired for data transmission so that sufficient time would be available for total frame transmission. These curves show that the simulated system's efficiency is proportional to the required integration times for the various celestial targets. For the case of two or three cameras, 100 percent efficiency could be reached at approximately 1 hour integration. Three cameras and a tape recorder approach 100 percent for integration times of 15 min or longer.

The conclusion that can be drawn from this simulation is that even a one-camera system can operate efficiently when being used strictly for dim sources. The problem now becomes one of mission definition. Will the LST's prime mission be the observation of bright objects or will it be more concerned with higher magnitude sources? Once this is determined the system efficiency can be evaluated.

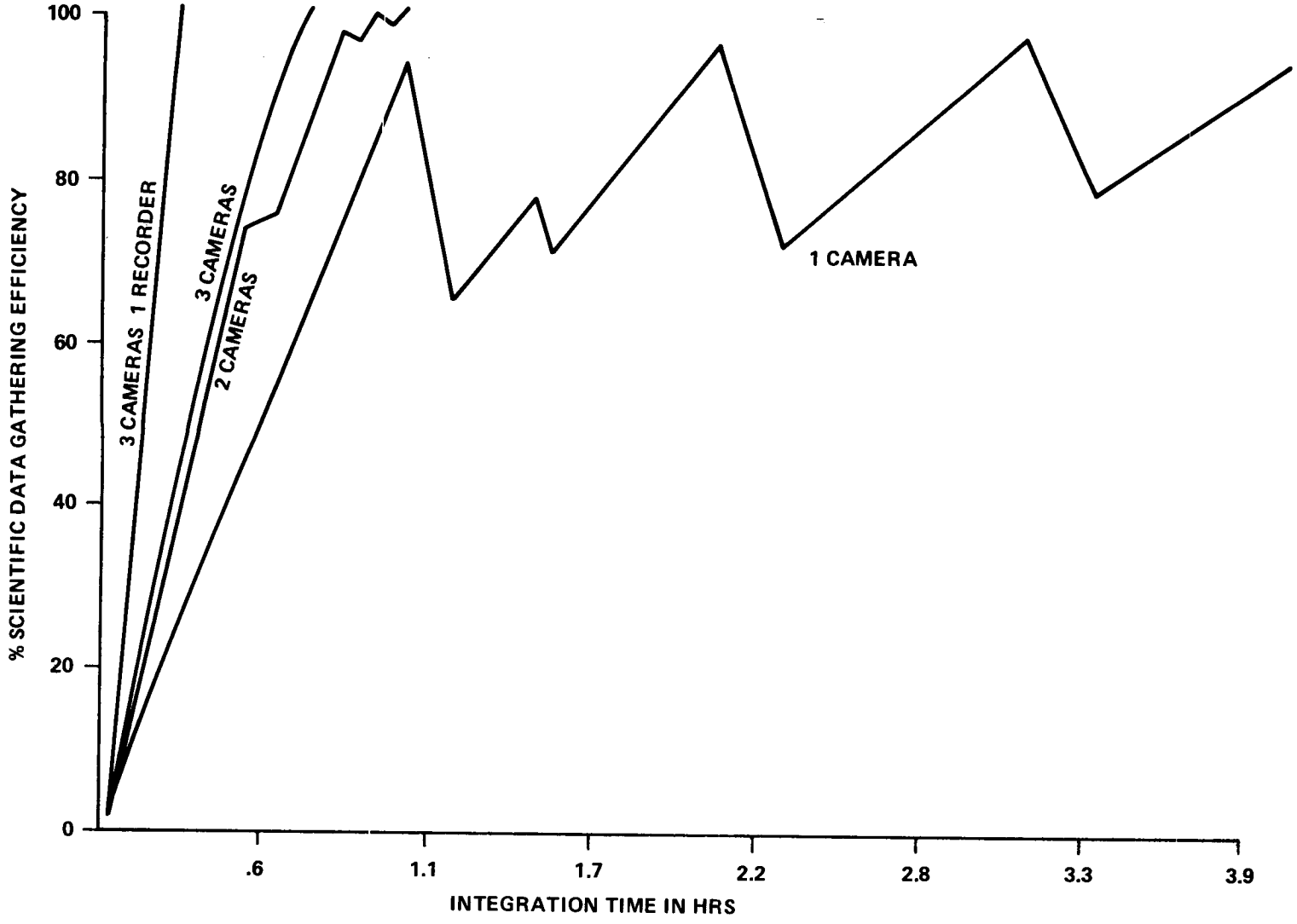

Figure B-1. Scientific data gathering efficiency.

APPENDIX C
DERIVATION OF OPTIMUM READOUT BANDWIDTH FOR PREAMPLIFIER OF SEC VIDICON

APPENDIX C

DERIVATION OF OPTIMUM READOUT BANDWIDTH FOR PREAMPLIFIER OF SEC VIDICON

The optimum readout time of an SEC vidicon is a function of the tube's preamplifier since this is the dominant noise source of the SEC. The first impression is that the preamplifier's bandwidth, input impedance, and gain should be examined to determine noise characteristics. This would be true if the tube were used strictly for high illumination. However, where the system is used for photon counting or low-light-level slow scan, the preamplifier's bias resistor and the shunt capacitance of the leads from the SEC to the amplifier become very important.

The Field Effect Transistor (FET) amplifier with its high input impedance, low noise, and wide bandwidth makes it an ideal candidate for this application. Its low voltage gain, however, requires additional stages of amplification. The first stage of amplification establishes the noise characteristics. Since the charge due to stored electrons on each resolution element of the SEC vidicon will be quite small, the shot noise within the FET must certainly be considered. In addition, the thermal noise of the bias resistor is increased by the gain of the amplifier and must also be accounted for in the noise calculations. To determine the operating frequency at which the total noise contribution of the preamplifier is minimal, expressions must be found for both shot noise and thermal (Johnson) noise in terms of readout frequency.

Shot noise in the FET occurs as a result of the granular or particle nature of the electron flow. The total instantaneous current I_b in Figure C-1 represents the current in the channel, while I_{dc} is the average over a large interval of time. The mean square variations about I_{dc} are defined by

$$\overline{i^2} \equiv \overline{(I_b - I_{dc})^2}$$

$$= \frac{1}{\Delta t} \int_0^{\Delta t} (I_b - I_{dc})^2 \, dt$$

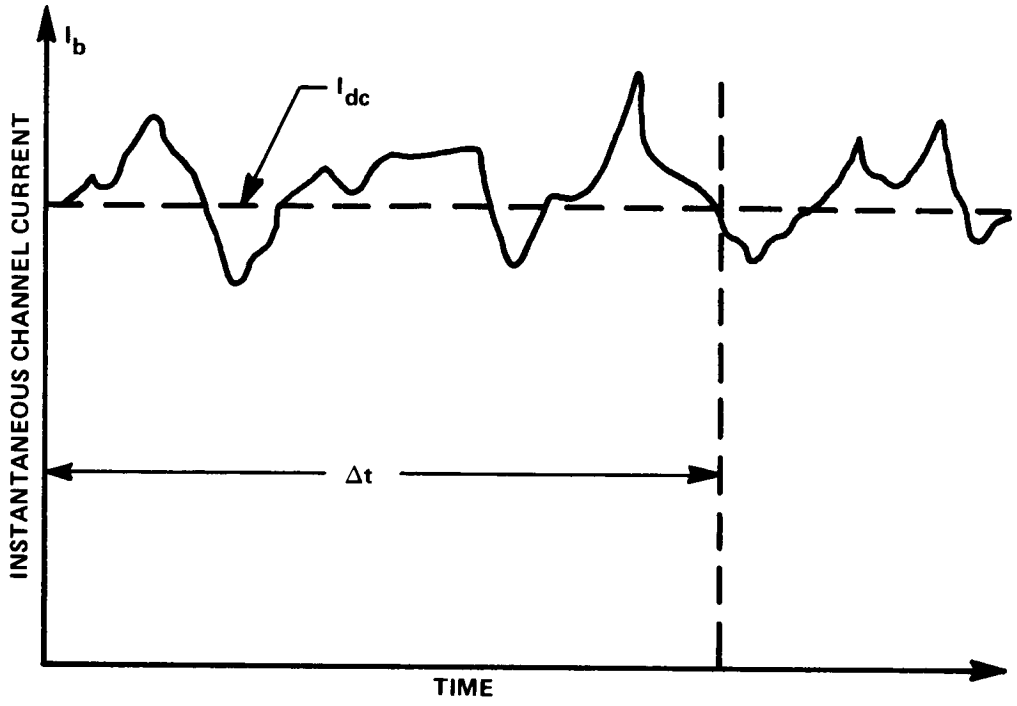

Figure C-1. Instantaneous channel current in an FET.

where Δt is dwell time of readout beam on any given resolution element. The interval Δt is very much larger than the transient time of an electron through the channel of an FET. In his book Information Transmission Modulation and Noise, Schwartz shows how the integral above can be expanded in a Fourier series regardless of the shape of the noise pulse. If the consideration is for low frequencies where $\Delta f \ll 1/\tau$ (note τ is the transient time through the channel), the mean square deviation in the load current is found to be

$$\overline{i^2} = 2 \frac{Nq_e}{\Delta t} q_e \Delta f \quad .$$

Substituting

$$I_{dc} = \frac{Nq_e}{\Delta t}$$

and

$$\Delta t \equiv \frac{1}{2\Delta f}$$

yields the root mean square (rms) deviation in the load current due to shot noise in terms of dwell time and drain current,

$$\sqrt{\frac{I_{dc}\, q_e}{\Delta t}} = \sqrt{\overline{i^2}} \quad .$$

This is the result of the internal noise of the FET on the output signal. In order to combine the effects of this shot noise current with the thermal noise of the input bias resistor, the above equation must be referred to the input of the FET.

The current in the output due to the gate voltage for the circuit in Figure C-2 is

$$I = g_m E_g$$

where g_m is the transconductance of the FET and E_g is gate voltage. Then the rms noise voltage referred to the input of the FET is

$$\sqrt{\frac{I_{dc}\, q_e}{\Delta t}} = g_m E_g \quad .$$

The noise voltage in terms of the number of electrons on the input capacitor is given as

$$E_g = \frac{N_c\, q_e}{C} \quad .$$

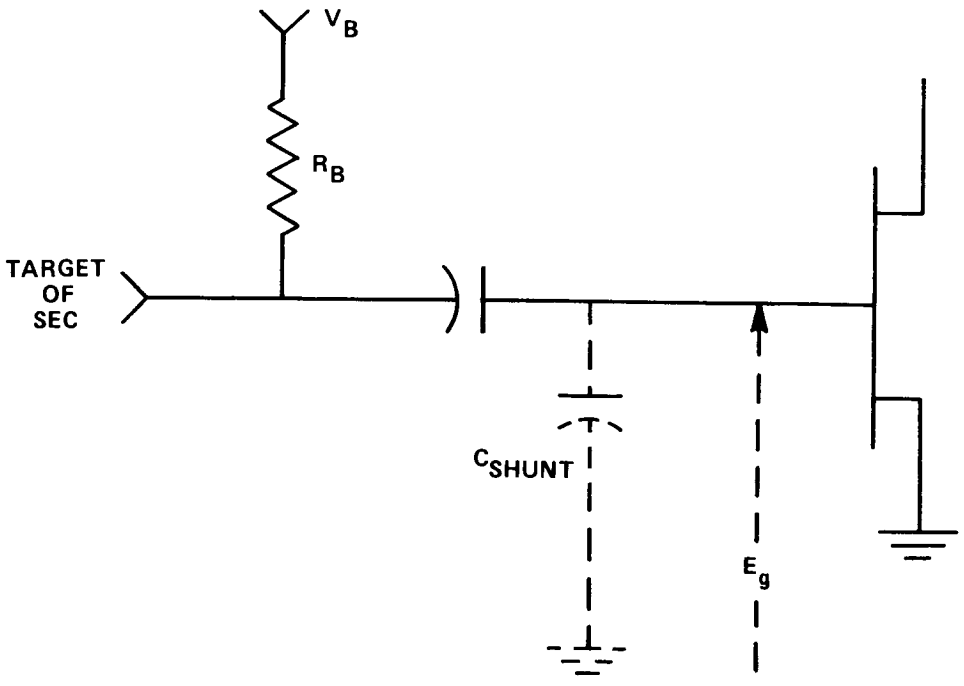

Figure C-2. FET preamplifier stage used with SEC vidicon.

Now, the equation of the FET noise in terms of noise electrons in the input, N_c, of the FET is

$$\sqrt{\frac{I_{dc}\, q_e}{\Delta t}} = \frac{g_m\, N_c\, q_e}{C} \quad .$$

Solving for N_c yields

$$N_c = \frac{C}{g_m} \sqrt{\frac{I_{dc}}{q_e\, \Delta t}} \quad .$$

This says the rms value of shot noise electron during the dwell time on a pixel in the SEC vidicon is a function of current through the FET, the total capacitance

in the input, and the transconductance of the FET. Translating this into noise electrons/half cycle yields

$$N_c = \frac{C}{g_m} \sqrt{\frac{2 \Delta f I_{dc}}{q_e}} \quad .$$

With an expression for shot noise now defined, attention will be focused upon the thermal noise of the input bias resistor.

H. Nyquist demonstrated that a resistor could be considered the source of spontaneous fluctuation voltages with mean-squared valve

$$\overline{v^2} = 4 KTR \Delta f$$

where T is temperature in degrees Kelvin of the resistor, R is the resistance in ohms, K is the Boltzmann constant (1.38×10^{-23} joule/°K), and Δf is the frequency bandwidth. Using Ohm's law this equation can be rewritten to yield the rms value of thermal noise current in a resistor:

$$\sqrt{\overline{i_r^2}} = \sqrt{\frac{4 KT \Delta f}{R}} \quad .$$

Substituting an equivalent equation for current in terms of electrons,

$$i_r = \frac{N_r q_e}{\Delta t}$$

where N_r represents rms thermal noise electrons and Δt is the dwell time of the readout beam in the SEC on a single pixel given by $\Delta t = 1/2\Delta f$ yields

$$2 N_r q_e \Delta f = \sqrt{\frac{4 KT \Delta f}{R}} \quad .$$

Solving for N_r, one obtains the root mean square value of thermal noise electron due to the resistor in the gate circuit:

$$N_r = \sqrt{\frac{KT}{\Delta f\, R\, q_e^2}} \quad .$$

The thermal noise of the bias resistor combined with the shot noise of the FET provides an expression for the total noise effect of the preamplifier for an SEC vidicon:

$$N_a = \sqrt{\frac{KT}{\Delta f\, R\, q_e^2} + \frac{2\, I_{dc}\, \Delta f\, (C)^2}{q_e\, (g_m)^2}} \quad .$$

Two things should be noted from this expression:

1. The bias resistor should be as large as practical.

2. The shunt capacitance of the lead should be as small as possible.

A curve of this equation indicates that an optimum frequency for minimum noise in the output exists (see Figure C-3). The minimum point on the curve can be found by differentiating the above expression for preamplifier noise (electrons per half cycle) with respect to frequency (Δf) and setting the resultant equation equal to zero. This procedure yields the following expression for Δf:

$$\Delta f = \sqrt{\frac{KT\, g_m^2}{2\, I_{dc}\, R\, q_e\, C^2}} \quad .$$

The following are some realistic values for the components of an FET amplifier:

$T = 260^\circ K.$

$R = 2 \times 10^8$ ohms.

$I = 7 \times 10^{-3}$ amperes (typical).

$g_m = 13.4 \times 10^{-3}$ amperes/volt (typical).

$C = 40 \times 10^{-12}$ (measured for second amplifier).

$K = 1.362 \times 10^{-23}$ joules/°K.

$q_e = 1.6 \times 10^{-19}$ coulombs/electron.

Substituting these values in the above equation results in an optimum frequency on the order of 30 kHz.

Earlier in this report the sampling rate and encoding levels were developed. If 30 kHz is used as upper frequency limit, the bit rate can be determined as follows:

Bit Rate = (4 samples/cycle) (8 bits/sample) (30×10^3 Hz)

= 960×10^3 bits/sec.

If one assumes 10 bits encoding, the bit rate would be slightly higher:

Bit Rate = (4 samples/cycle) (10 bit/sample) (30×10^3 Hz)

= 1.2×10^6 bits/sec.

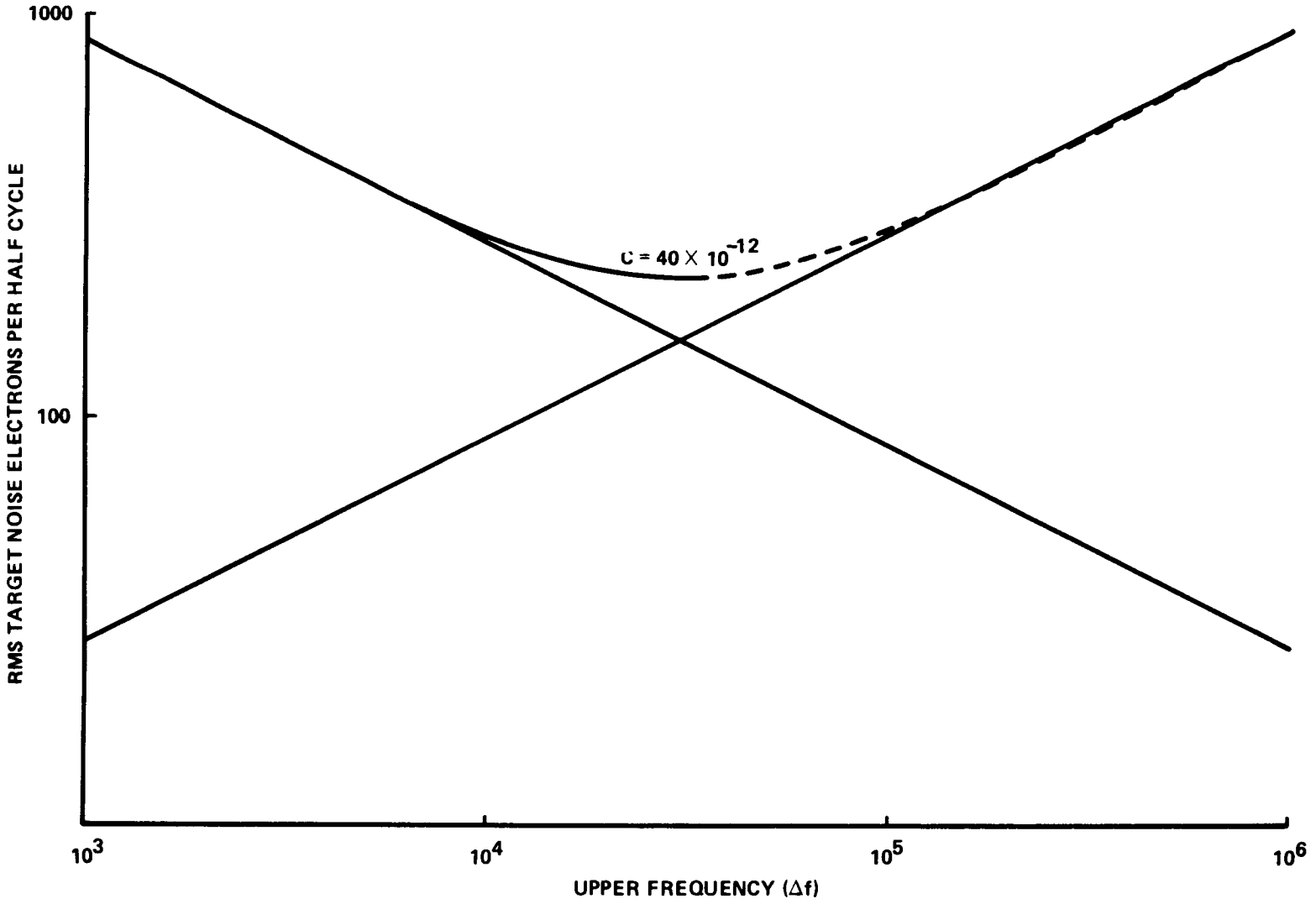

Figure C-3. SEC preamplifier noise performance with frequency.

APPROVAL

LARGE SPACE TELESCOPE
PHASE A FINAL REPORT

Volume V — Support Systems Module

By Program Development

The information in this report has been reviewed for security classification. Review of any information concerning department of Defense or Atomic Energy Commission programs has been made by the MSFC Security Classification Officer. This report, in its entirety, has been determined to be unclassified.

This document has also been reviewed and approved for technical accuracy.

FRED E. DIGESU
Chief, Electronics and Control Division
Preliminary Design Office

ERICH E. COERNER
Director, Preliminary Design Office

HERMAN P. GIEROW
Director, Mission and Payload
Planning Office

JAMES A. DOWNEY
Manager, LST Task Team

JAMES T. MURPHY
Director, Program Development

MSFC—RSA, Ala

DISTRIBUTION

INTERNAL

DIR
Dr. Petrone

DEP-T
Dr. Lucas

AD-S
Dr. Stuhlinger

PD-DIR
Mr. Murphy
Mr. Jean
Dr. Mrazek

PD-LST
Mr. Downey
Dr. O'Dell
Mr. McCulloch
Mr. Olivier (8)
Mr. Heyer (8)
Mr. Hamilton
Mr. Perry
Mr. Nelson (6)
Mr. Ealy
Mr. Conway
Mr. Teuber

PD-PL
Mr. Huff

PD-MP
Mr. Gierow (3)
Mr. Emanuel
Mr. Bradford

PD-PP
Mr. Sneed (3)

PD-SL
Mr. Trott

PD-DO
Mr. Goerner
Mr. Marshall
Mr. Laue
Mrs. Kozub
Mr. Darwin
Mr. Butler
Mr. Blumrich
Mr. Colley
Mr. Love
Mr. Nixon
Mr. Fritz
Mr. Mordan
Mr. Goldsby
Mr. Burton
Mr. French
Mr. Fults
Mr. Kromis
Mr. Digesu (10)
Mr. Fikes
Mr. Schultz
Mr. Davis
Mr. Green
Dr. Steincamp
Mr. Sanders
Mr. W. Price
Mr. Boehme

PD-DO (Cont'd)
Mr. Rood
Mr. Arsement
Mr. Reed

SS-H
Dr. Speer
Mr. Fichtner
Mr. Dailey
Mr. Shields
Mr. Wiesenmaier
Mr. Carlile

SP-EM
Mr. Harden
Dr. Thomason

MO
Mr. Kurtz (2)

S&E-DIR
Dr. Weidner
Mr. Richard

S&E-S&P
Mr. Vreuls (2)

S&E-R
Dr. Johnson

S&E-AERO
Dr. Geissler
Mr. Horn
Mr. Dahm (2)
Mr. Baker (3)
Mr. Lindberg (3)
Dr. Lovingood (5)

S&E-ASTR
Mr. Moore
Mr. Horton
Mr. Powell
Mr. Mack (3)
Mr. Barr (8)
Mr. Hosenthien (3)
Mr. Wojtalik (3)
Mr. Swearingen (3)
Mr. Taylor (3)
Mr. Boehm (3)
Mr. Aden (3)
Mr. Dugan (3)
Mr. Justice
Mr. Counter
Mr. Zurasky
Mr. Shearer
Dr. Clarke
Mr. Tutt
Mr. Golley

S&E-ASTN
Mr. Heimburg
Mr. Kingsbury
Mr. Kroll (2)
Mr. Isbell (2)
Mr. Sterett (2)
Mr. Paul (2)
Mr. Connor (2)
Mr. Swinghamer (2)

S&E-SSL
Dr. Haeussermann
Dr. Naumann (2)
Dr. Decher
Dr. Sieber (2)
Mr. Snoddy (2)

A&PS-MS-D
Mr. Garrett

A&PS-MS-I
Mr. Ziak

A&PS-MS-IP
Mr. Ledbetter (2)

A&PS-MS-IL
Miss Robertson (8)

A&PS-MS-H
Mr. Akens

A&PS-PAT
Mr. Wofford

A&PS-TU (6)

EXTERNAL

NASA Headquarters
MH/Mr. Donlan (Vol I only)
MK/Mr. Culbertson (Vol I only)
MTL/Mr. Armstrong (Vol I only)
SG/Dr. Nancy Roman (Vol I only)
SG/Mr. Aucremanne (3 complete sets plus 10 of Vol I)
WX/Mr. Krueger (3 complete sets plus 6 of Vol I)

Goddard Space Flight Center
Code 604/Mr. Meese (80)

Johnson Space Center
LP/Mr. Heberlig
LP/Mr. Battey
ER-4/Mr. Davis
ER-4/Mr. Hirasaki
ER-4/Mr. Casey

Kennedy Space Center
FP-B/Mr. McCoy
LL-OPN-2/Mr. Sheppard
FP-B/Mr. Engle
FP-B/Mr. Bailey

Dr. Herbert Flicker
L-DOT TA-35
Los Alamos Scientific Lab
Los Alamos, N. W. 87544

Dr. Robert E. Danielson
Princeton University Observatory
Peyton Hall
Princeton, N.J. 08540

Scientific and Technical
Information Facility
College Park, Maryland 20740
Attn: NASA Representative (S-AK/RKT) (25)